Methods in Cell Biology

VOLUME 61

Mitosis and Meiosis

Edited by

Conly L. Rieder

Prepared under the Auspices of the American Society for Cell Biology

Methods in Cell Biology

VOLUME 61
Mitosis and Meiosis

Series Editors

Leslie Wilson
Department of Biological Sciences
University of California, Santa Barbara
Santa Barbara, California

Paul Matsudaira
Whitehead Institute for Biomedical Research and
Department of Biology
Massachusetts Institute of Technology
Cambridge, Massachusetts

Methods in Cell Biology

Prepared under the Auspices of the American Society for Cell Biology

VOLUME 61

Mitosis and Meiosis

Edited by

Conly L. Rieder

Division of Molecular Medicine
Wadsworth Center
Albany, New York

ACADEMIC PRESS

San Diego London Boston New York Sydney Tokyo Toronto

Cover photograph (paperback edition only): Newt lung epithelial cell in prometaphase of mitosis. In this example, three fluorescent probes were used to reveal different components of the cell. The image shows the replicated chromosomes (blue) in various stages of attaching to the forming bipolar mitotic apparatus or "spindle" (yellow). At the time the cell was fixed, some of the chromosomes were only attached to one of the two spindle poles, while the others had already attached to both poles and were positioned near the spindle equator. The spindle is surrounded by keratin filaments (red) that prohibit other components of the cell from invading the region containing this structure as it forms. Courtesy of Conly L. Reider and Cindy Hughes, Wadsworth Center, New York State Department of Health, Albany, New York.

This book is printed on acid-free paper. ♾

Academic Press
a division of Harcourt Brace & Company
525 B Street, Suite 1900, San Diego, California 92101-4495, USA
http://www.apnet.com

Academic Press
24-28 Oval Road, London NW1 7DX, UK
http://www.hbuk.co.uk/ap/

International Standard Book Number: 0-12-544163-0 (hb)
International Standard Book Number: 0-12-588540-7 (pb)

PRINTED IN THE UNITED STATES OF AMERICA
98 99 00 01 02 03 EB 9 8 7 6 5 4 3 2 1

CONTENTS

CONTRIBUTORS

Numbers in parentheses indicate the pages on which the authors' contributions begin.

Bruce M. Alberts (1), National Academy of Sciences, Washington, DC 20418
Dale L. Beach (369), Department of Biology, University of North Carolina at Chapel Hill, Chapel Hill, North Carolina 27599
Kerry S. Bloom (369), Department of Biology, University of North Carolina at Chapel Hill, Chapel Hill, North Carolina 27599
Michael Bornens (13), Section de Recherche, Institut Curie, UMR-144/CNRS, Biologie du Cycle Cellulaire et de la Motilite, 75248 Paris Cedex 05, France
William R. Brinkley (57), Department of Cell Biology, Baylor College of Medicine, Houston, Texas 77030
Grisel Cassels (297), Division of Molecular Medicine, Wadsworth Center, New York State Department of Health, Albany, New York 12201
Arshad Desai (155,385), Department of Cell Biology, Harvard Medical School, Boston, Massachusetts
Kathy Ensrud (233), Department of Cell Biology and Neuroanatomy, University of Minnesota, Minneapolis, Minnesota 55455
Margarete M. S. Heck (317), Institute of Cell and Molecular Biology, University of Edinburgh, Edinburgh EH9 3JR, United Kingdom
Peter K. Hepler (413), Department of Biology and the Plant Biology Graduate Program, University of Massachusetts, Amherst, Massachusetts 01003
Edward H. Hinchcliffe (439), Department of Cell Biology, University of Massachusetts Medical Center, Shrewsbury Campus, Shrewsbury, Massachusetts 01655
Tony Hyman (137,145), Cell Biology Program, EMBL, Heidelberg D-69117, Germany
Mary Ann Jordan (267), Department of Molecular, Cellular, and Developmental Biology, University of California at Santa Barbara, Santa Barbara, California 93106
Ken Kaplan (145), Department of Biology, Massachusetts Institute of Technology, Cambridge, Massachusetts 02139
Ryoko Kuriyama (233), Department of Cell Biology and Neuroanatomy, University of Minnesota, Minneapolis, Minnesota 55455
Paul Maddox (369), Department of Biology, University of North Carolina at Chapel Hill, Chapel Hill, North Carolina 27599
Michael Marko (81), Division of Molecular Medicine, Wadsworth Center, New York State Department of Health, Albany, New York 12201
Bruce F. McEwen (81), Division of Molecular Medicine, Wadsworth Center, New York State Department of Health, Albany, New York 12201; and Department of Biomedical Sciences, State University of New York, Albany, New York 12222
Frederick J. Miller (439), Department of Cell Biology, University of Massachusetts Medical Center, Shrewsbury Campus, Shrewsbury, Massachusetts 01655

Timothy J. Mitchison (385), Department of Cellular and Molecular Pharmacology, University of California at San Francisco, San Francisco, California 94143

Michelle Moritz (1), Department of Biochemistry and Biophysics, University of California, San Francisco, San Francisco, California 94143

Mohammed Moudjou (13), Unité de Virologie et Immunologie Moleculaire, Centre de Recherche de Jouy en Josas, Institut National de la Recherche Agronomique, 78352 Jouy en Josas Cedex, France

Andrew Murray (385), Department of Physiology, University of California at San Francisco, San Francisco, California 94143

R. Bruce Nicklas (209), DCMB Zoology, Duke University, Durham, North Carolina 27708

Berl R. Oakley (317), Department of Molecular Genetics, Ohio State University, Columbus, Ohio 43210

Rudolf Oldenbourg (175), Marine Biology Laboratory, Woods Hole, Massachusetts 02543

Robert E. Palazzo (35), Department of Biochemistry, Cell, and Molecular Biology, The University of Kansas, Lawrence, Kansas 66045; and Marine Biological Laboratory, Woods Hole, Massachusetts 02543

Conly L. Rieder (297), Division of Molecular Medicine, Wadsworth Center, New York State Department of Health, Albany, New York, 12201; Department of Biomedical Sciences, State University of New York, Albany, New York 12222; and Marine Biology Laboratory, Woods Hole, Massachusetts 02543

Edward D. Salmon (155,369), Department of Biology, University of North Carolina at Chapel Hill, Chapel Hill, North Carolina 27599

Fedor Severin (145), Cell Biology Program, EMBL, Heidelberg D-69117, Germany

Sidney L. Shaw (369), HHMI Long Laboratory, Department of Biology, Stanford University, Stanford, California 94305

Greenfield Sluder (439), Department of Cell Biology, University of Massachusetts Medical Center, Shrewsbury Campus, Shrewsbury, Massachusetts 01655

Peter Sorger (145), Department of Biology, Massachusetts Institute of Technology, Cambridge, Massachusetts 02139

Kevin F. Sullivan (113), Department of Cell Biology, The Scripps Research Institute, La Jolla, California 92037

William Theurkauf (317), Department of Biochemistry and Cell Biology, State University of New York at Stony Brook, Stony Brook, New York 11794

A. Van Hooser (57), Department of Cell Biology, Baylor College of Medicine, Houston, Texas 77030

Aline H. Valster (413), Department of Biology and the Plant Biology Graduate Program, University of Massachusetts, Amherst, Massachusetts 01003

Jacalyn M. Vogel (35), Department of Biochemistry, Cell, and Molecular Biology, The University of Kansas, Lawrence, Kansas 66045; and Marine Biological Laboratory, Woods Hole, Massachusetts 02543

Jan W. Vos (413), Department of Biology and the Plant Biology Graduate Program, University of Massachusetts, Amherst, Massachusetts 01003

Patricia Wadsworth (219), Department of Biology, Merril Science Center, University of Massachusetts, Amherst, Massachusetts 01003

Mike Wagenbach (245), Department of Physiology and Biophysics, University of Washington School of Medicine, Seattle, Washington 98195

Claire E. Walczak (385), Department of Cellular and Molecular Pharmacology, University of California at San Francisco, San Francisco, California 94143

Clare Waterman-Storer (155), Department of Biology, University of North Carolina at Chapel Hill, Chapel Hill, North Carolina 27599

Leslie Wilson (267), Department of Molecular, Cellular, and Developmental Biology, University of California at Santa Barbara, Santa Barbara, California 93106

Torsten Wittmann (137), Cell Biology Program, EMBL, Heidelberg D-69117, Germany

Linda Wordeman (245), Department of Physiology and Biophysics, University of Washington School of Medicine, Seattle, Washington 98195

Elaine Yeh (369), Department of Biology, University of North Carolina at Chapel Hill, Chapel Hill, North Carolina 27599

Dahong Zhang (209), DCMB Zoology, Duke University, Durham, North Carolina 27708

This Page Intentionally Left Blank

PREFACE

This volume consists of 22 chapters that detail many of the systems and methods currently used to study mitosis and meiosis in organisms from yeast to humans. Both of these related processes involve the transient formation of a highly dynamic structure, known as the spindle, that functions to equally segregate the replicated chromosome during the division of somatic cells (mitosis) and gametes (meiosis). In essence, the spindle is a complex machine that coverts chemical energy into mechanical work in a highly controlled fashion, and important strides have been made over the past decade in understanding how this machine forms and functions to generate and transmit the mitotic forces. The old axiom "necessity is the mother of invention" is especially true in the area of mitosis/meiosis research, where the ability to test and refine increasingly sophisticated hypotheses relies on the development of new, or the creative modifications of existing, methods and tools.

I am lucky that so many colleagues readily agreed to take the time to contribute to this volume. I thank them for their efforts and hope they approve of the final result. Throughout this endeavor I was assisted by Ms. Cathy Kahler, who deserves a special thanks, especially for her pleasant tenacity in reminding the authors of their deadlines. I am also grateful to Ms. Susan Nowogrodzki for her encouragement and editorial assistance. Finally, it was a pleasure to work with Ms. Jennifer Wrenn and Ms. Kay Sasser of Academic Press—both are courteous and responsible professionals with a great sense of humor.

Conly L. Rieder

This Page Intentionally Left Blank

CHAPTER 1

Isolation of Centrosomes from *Drosophila* Embryos

Michelle Moritz* **and Bruce M. Alberts†**

* Department of Biochemistry and Biophysics
University of California, San Francisco
San Francisco, California 94143-0448

† National Academy of Sciences
Washington, DC 20418

I. Introduction

Although the importance of the centrosome as the main microtubule-organizing center of animal cells has been recognized for many years, a detailed understanding of its components and activities has been out of reach, mainly because of the difficulty in obtaining large quantities of centrosomes for study. Recently, however, several protocols have been developed (some of which are described in this volume) that allow the isolation of relatively large numbers of centrosomes from calf thymus, budding yeast, *Drosophila* embryos, and oocytes of the clam, *Spisula* (see Chapter 3) (Palazzo *et al.*, 1988; Komesli *et al.*, 1989;

METHODS IN CELL BIOLOGY, VOL. 61

0091-679X/99 $30.00

Rout and Kilmartin, 1990; Moritz *et al.*, 1995a). The ability to isolate large quantities of functional centrosomes is useful not only for the study of the microtubule-organizing center itself but also for generating focused arrays of microtubules *in vitro* that can then be used to study microtubule dynamics (e.g., Mitchison and Kirschner, 1984a; Belmont *et al.*, 1990), the movement of motor proteins, and kinetochore–microtubule interactions (e.g., Mitchison and Kirschner, 1985).

Here we describe a protocol for the isolation of large quantities of centrosomes from early *Drosophila* embryos and two protocols for assaying the microtubule-nucleating activity of the isolated centrosomes. These centrosomes display a robust microtubule nucleation activity *in vitro,* each one generating an array of hundreds of microtubules. Perhaps because they are embryonic and must drive the rapid divisions that occur at this stage of development, these centrosomes have a large amount of pericentriolar material compared to isolated mammalian centrosomes. Other advantages of using *Drosophila* embryos as a source of centrosomes include the ease of obtaining multigram quantities of embryos in a few hours, the potential for isolating centrosomes from mutant fly stocks, the ability to employ genetics and the unique cell biological properties of live embryos in studying any new proteins identified, and the low cost of maintaining large populations of flies.

The yield of active centrosomes from this preparation is typically $1–5 \times 10^7$ per sucrose gradient, from the equivalent of 2 g of embryos. Approximately 5 μg of protein is found in the peak fraction (0.5 ml). Assuming that there is an average of 2500 centrosomes in a *Drosophila* embryo, and that an embryo is 9.5 μg, we estimate this to be an approximately 10% yield. The purification is estimated to be ~1000-fold, based on the number of centrosomes per milligram of protein in the starting extract compared to the same in the peak centrosome fraction. More than 90% of the centrosomes isolated are competent to nucleate microtubules, as determined by comparing the number of asters formed to the number of organelles staining with an antibody against γ-tubulin in a given microscope field.

II. Isolation of Centrosomes from *Drosophila* Embryos

This procedure involves making an extract from precellularized embryos, removing nuclei by low-speed centrifugation, and then isolation of centrosomes on sucrose step gradients.

A. Buffers, Solutions, and Special Equipment

Guanosine 5′-triphosphate (GTP), protease inhibitors and phenylmethylsulfonyl fluoride (PMSF) (purchased from Sigma Chemical Co., St. Louis, MO) are added to solutions just before use. Ultrapure sucrose (ICN Biomedicals, Aurora, OH) is used in all solutions.

1. Buffers and Solutions

Egg wash: 0.03% Triton-X-100, 0.04% NaCl

50% Bleach in dH_2O

5× BRB80: 400 m*M* K-Pipes (pH 6.8), 5 m*M* $MgCl_2$, 5 m*M* Na_2EGTA

Protease inhibitor stock: 10 m*M* benzamidine–HCl, 0.1 mg/ml phenanthroline, 1 mg/ml aprotinin, 1 mg/ml leupeptin, 1 mg/ml pepstatin A. Dissolve (will not dissolve completely) in ethanol (high grade, 200 proof) and store at −20°C. Vortex before removing an aliquot.

100 m*M* PMSF: Dissolve in isopropanol, store at −20°C in the dark. Must be heated to 37°C to redissolve after storage.

0.5 *M* GTP stock: 0.5 *M* GTP (Sigma Chemical Co., Cat. No. G5881) in 1× BRB80. Store at −20°C in small aliquots.

Homogenization buffer: 1× BRB80, 100 m*M* KCl, 14% sucrose (weight/volume), 1:100 protease inhibitor stock, 1 m*M* PMSF.

70% Sucrose solution: 70% sucrose (weight/volume), 1× BRB80, 100 m*M* KCl (add GTP to 1 m*M* for use in the step gradient cushion, but there is no need to add GTP to the 70% sucrose solution that will be used to bring the low-speed supernatant to 50% sucrose).

55% Sucrose solution: 55% sucrose (weight/volume), 1× BRB80, 100 m*M* KCl, 1 m*M* GTP.

2. Special Equipment

Population cages for the collection of multigram quantities of embryos.

Two sieves: Fisher Scientific USA Standard Sieves, one No. 18 (1-mm mesh) and one No. 140 (106-μm mesh), are needed.

A rubber spatula or paintbrush for freeing embryos from collection trays.

A Wheaton overhead stirrer to which a pestle from a Dounce homogenizer may be attached.

A 55-ml Dounce homogenizer with medium-tight fitting Teflon pestle and a glass mortar.

Miracloth (Calbiochem, La Jolla, CA).

An SW28 rotor (Beckman, Palo Alto, CA).

An HB-4 rotor (Sorvall, Newtown, CT) or equivalent.

A rack to hold microfuge tubes that has been marked at the 0.5-ml level (place a tube in the rack with 0.5 ml liquid in it, then draw a line across the side of the rack indicating the 0.5-ml level).

B. Preparation of Embryo Extract

We maintain nine population cages (dimensions: 12 × 12 × 12 in.) from which multigram quantities of embryos may be collected. We collect the embryos on

flat trays (8.5 × 10 in.) of cornmeal–molasses food with a petri dish full of yeast paste set on top. A 3.5-hr collection from all nine cages typically yields 10–20 g of embryos at 25°C. We generally find that the more embryos we obtain, the better the yield of centrosomes, but one should theoretically be able to isolate centrosomes from as little as 2 g of embryos. It may be possible to scale the entire preparation down so that small numbers of centrosomes may be isolated on, for example, 5-ml gradients. We have not attempted this ourselves.

1. Collect embryos from population cages for 3.5 hr. In our cages, this length of collection enriches for embryos between nuclear cycles 8 and 13 (precellularization). The length of this collection should be optimized for the collection environment used. We have successfully used 12-hr collections as well, but in terms of obtaining the cleanest possible preparation of centrosomes, it is probably best to minimize the extraneous tissue by using younger embryos. In addition, during the rapid, early nuclear divisions in the embryo, the centrosomes are less likely to be attached to the nuclear envelope.

2. Rinse the embryos onto a sieve (we use two stacked sieves: the top sieve removes contaminating adult flies, and the bottom sieve collects the embryos) using egg wash in a squirt bottle and a rubber spatula or paintbrush to release the embryos from the food.

3. Dechorionate the embryos by incubating in 50% bleach in dH_2O for 2 min. Rinse in dH_2O until the embryos no longer smell of bleach. Blot the embryos dry with paper towels and weigh them.

The following steps should be performed at 4°C. Our homogenizer is set up in the cold room.

4. Dounce homogenize (five passes) the embryos in 5 vol. (weight/volume) homogenization buffer.

5. Filter the homogenate twice through Miracloth that has been previously moistened with homogenization buffer. The Miracloth removes large debris and any unhomogenized embryos. Wetting the Miracloth first helps the extract flow more quickly through it.

6. Centrifuge twice at 1500*g* for 10 min (3000 rpm in an HB-4 rotor) to pellet nuclei, some yolk, and debris. Aspirate the lipid layer at the top and discard the pellet. The low-speed supernatant typically contains ~75 mg/ml protein. At this point, one may proceed with the purification, or the extract may be frozen in liquid nitrogen and stored for months at −80°C. A minimum of 65–70 ml (this corresponds to 13 or 14 g of embryos) of low-speed supernatant is needed to complete the purification (assuming that all six buckets in an SW28 rotor will be used). If this amount is not available, fewer gradients may be run.

C. Isolation of Centrosomes on Sucrose Gradients

1. Prepare six sucrose step gradients in 35-ml tubes for a Beckman SW28 rotor:
   a. Pour a 3-ml 70% sucrose solution + 1 m*M* GTP cushion.
   b. Layer 4 ml 55% sucrose solution + 1 m*M* GTP on top of the 70% cushion.

2. Make the extract 50% sucrose by adding 1.8 vol 70% sucrose solution. Also add 20% Triton X-100 to a final concentration of 0.1–0.5% (for one gradient, mix 10.7 ml of low-speed supernatant with 19.3 ml 70% sucrose solution and 0.15–0.75 ml 20% Triton X-100).

We have found that the amount of Triton X-100 added affects the protein composition of the centrosome fraction (Fig. 1). γ-Tubulin is highly enriched in the peak centrosome-containing fractions regardless of the detergent concentration; however, the centrosomal proteins CP60 and CP190 (Kellogg and Alberts, 1992) are more highly enriched in centrosomes at a lower (0.1%) detergent concentration. These differences in composition of the centrosomes under the two isolation conditions do not affect the gross appearance of the centrosomes in the electron microscope, and they do not appear to affect the ability of the centrosomes to nucleate microtubules (data not shown).

3. Load 30 ml of the mixture of extract/sucrose/Triton onto each step gradient and centrifuge for 1.5 hr at 27,000 rpm in a Beckman SW28 rotor (acceleration and deceleration settings of 7). Thus, the equivalent of 2 g of embryos is loaded on each gradient.

4. Collect one 1-ml fraction and seven 0.5-ml fractions from the bottom of the gradients. Rather than using a fraction collector, we find it easiest to use the following setup: To puncture the bottom of the tube, use an 18-gauge needle that has been pushed through a rubber stopper so that ~0.8 cm of the sharp end protrudes; set the stopper with its needle on a microfuge tube rack with the blunt end of the needle in one of the holes of the rack. The stopper acts as a bumper so that the tube may be punctured without disturbing the gradient. Then collect fractions by hand in the cold room, allowing them to drip into graduated microfuge tubes in a rack with markings for 0.5 ml. Most centrosomes are usually found in fractions 3 and 4, near the 70–55% sucrose boundary. Sometimes centrosomes are found in fractions 5 and 6 as well. The centrosomes are stable for a day or two on ice or can be frozen in small aliquots in liquid nitrogen and stored at −80°C indefinitely with little loss of activity.

It may be possible to purify the centrosomes further by running the centrosome-containing fractions from these step gradients on a second gradient. We have investigated this approach to a very limited extent and found that active centrosomes were recoverable, but many were lost in the subsequent purification steps.

III. Assays for Microtubule Nucleation by Isolated Centrosomes

Once the centrosomes have been sedimented on sucrose gradients, the gradient fractions must be assayed for microtubule nucleation in order to localize the centrosomes and confirm their activity. We have used two assays to determine activity, as explained below.

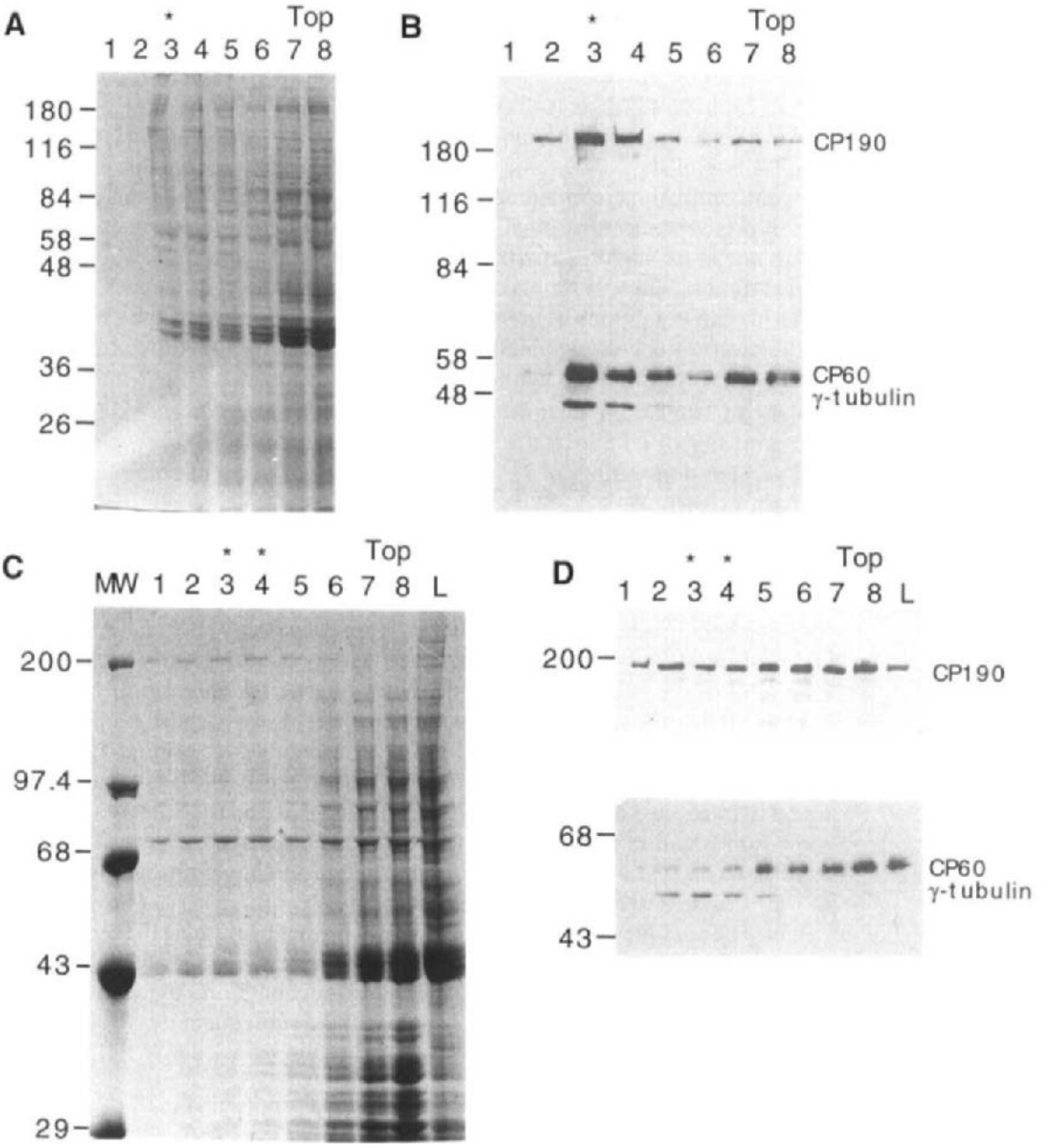

Fig. 1 Protein profiles across centrosome gradients. Molecular weight markers are indicated on the left of each panel. Fraction numbers are at the top. *Asterisks* mark gradient fractions containing the most centrosomes, as determined by aster formation. L, gradient load. (A) Coomassie-stained gel of proteins from fractions of a centrosome gradient containing 0.1% Triton X-100. Approximately 20 μg protein were loaded per lane, except in lane 1, in which ~30 μl of fraction 1 were loaded.

A. Buffers, Solutions, and Special Equipment

1. Buffers and Solutions

5× BRB80: 400 m*M* K-Pipes (pH 6.8), 5 m*M* MgCl2, 5 m*M* Na_2EGTA.

Bovine brain tubulin (at a concentration of at least 10 mg/ml) in BRB80.

Optional: rhodamine-labeled tubulin (at least 10 mg/ml) in BRB80.

30% glycerol in 1× BRB80.

1% glutaraldehyde (50% stock, electron microscopy grade, Ted Pella, Redding, CA) in BRB80; prepare fresh just before use.

Methanol at −20°C.

Mounting medium: 80% glycerol in PBS (10 m*M* Na_2HPO_4, 1.8 m*M* KH_2PO_4, 136 m*M* NaCl, 2.6 m*M* KCl, pH 7.2) + 1 mg/ml *p*-phenylenediamine. Store in the dark at −20 or −80°C.

Tubulin dilution buffer (TDB): 1× BRB80, 10% glycerol, 1 m*M* GTP.

TDB wash: TDB + 10 mg/ml bovine serum albumin (Fraction V, A-7906, Sigma Chemical Co.).

2. Special Equipment

At least eight 15-ml Corex tubes that have been modified to hold a coverslip in the bottom, plus a tool for removing the coverslip (see Evans *et al.,* 1985, for details on making these).

Acid-washed 12-mm round coverslips: We prepare large batches of these by incubating the coverslips in a large glass beaker with 1*N* HCl at 65°C for 4 hr to overnight with occasional swirling. Rinse the coverslips extensively in dH_2O, until the pH is neutral (check with pH paper). Dry the coverslips by laying them out on a large piece of filter paper or in a drying oven. Be careful not to let lint or dust collect on them. After drying, store the coverslips in a large petri dish.

The peak fraction (*) contained ~2 × 10^6 centrosomes. Fractions 1 and 2 contained virtually none. Fractions 4–6 contained ~10^4–10^5 centrosomes. (B) Immunoblot corresponding to gel in A. The blot was probed with antisera against CP190, CP60, and γ-tubulin, revealing that these proteins are enriched in fraction 3, which contains the most centrosomes. (C) Coomassie-stained gel of proteins from fractions of a centrosome gradient containing 0.5% Triton X-100. Because of the small amount of protein in each fraction, like fractions from three gradients were combined, diluted into 60 m*M* Tris pH 6.8, 50 m*M* NaCl, 50 μg/ml insulin carrier protein, and concentrated. One half of the protein obtained from fractions 1–5 was loaded. Approximately 20 μg protein from fractions 6–10 was loaded. The peak fractions (*) contained ~1 × 10^7 centrosomes. Fractions 1,2, and 5–8 contained ~10^4–10^6 centrosomes. (D) Immunoblots corresponding to gel in C. The blots were probed with antisera against CP60 and γ-tubulin or CP190 (reproduced from *The Journal of Cell Biology,* 1995, **130**, 1149–1159 by copyright permission of the The Rockefeller University Press).

B. Aster Spin-Down Assay

This assay is based on one published by Mitchison and Kirschner (1984b), and involves incubating centrosomes in solution with pure tubulin at a subcritical concentration so that microtubules polymerize only when nucleated by the centrosomes. Any resulting asters are sedimented onto coverslips using specially modified centrifuge tubes, which are made from 15-ml Corex tubes as described in Evans *et al.* (1985). The asters can then be viewed on the coverslips using a fluorescence microscope.

1. Prepare as many tubes for sedimenting asters as there are fractions to be tested: Place an acid-washed coverslip on top of the removable disk in the bottom of each modified 15-ml Corex tube. Pipet a 5-ml cushion of 30% sucrose in BRB80 into each tube, tapping out air bubbles so that the removable disks and coverslips rest flatly in the bottoms of the tubes. Keep the tubes on ice until ready to use.

2. Mix 4 μl sucrose gradient fraction + tubulin (final concentration 2 or 3 mg/ml) on ice. Our tubulin stocks are usually 10–15 mg/ml in BRB80, so we simply add 1 or 2 μl of tubulin to 4 μl of gradient fraction. It should be possible to do this reaction in larger volumes, but keep in mind that about half of the centrosomes lose their activity with a twofold dilution out of the sucrose. If the sucrose concentration is maintained, the centrosomes are more stable. We use a mixture of unlabeled and rhodamine-labeled bovine brain tubulin so that the resulting asters can be visualized directly on a fluorescence microscope. Alternatively, unlabeled tubulin may be used, followed by immunofluorescence using an antibody against tubulin. Tubulin is purified from bovine brain as described in Mitchison and Kirschner (1984b) and labeled with rhodamine as described in Hyman *et al.* (1991).

3. Incubate the mixture of centrosomes and tubulin for 10 min in a water bath held at 29°C.

4. Fix by adding 10 vol of room-temperature 1% glutaraldehyde in 1× BRB80 for at least 3 min at room temperature, then layer the mixture on top of the glycerol cushion in a prepared tube. (Once the asters have been fixed for 3 min, they can be placed onto this 4°C cushion).

5. Centrifuge at 12,000 rpm for 10 min in an HB-4 rotor at 4°C (23,300*g*).

6. Place the tubes on ice. Aspirate to remove approximately 1 ml at the top of the cushion and rinse it two or three times with 1 ml of 1× BRB80 before aspirating the rest of the cushion. (This washing step is optional. It merely removes the glutaraldehyde and any rhodamine-labeled tubulin left unincorporated into asters, thereby giving a lower background fluorescence on the coverslip).

7. While the coverslip is still in the tube, add enough −20°C methanol to cover it (~1 ml) and incubate for 3 min on ice.

8. Remove the coverslip from the tube using a tool made from a straightened paper clip (Evans, 1985), and carefully blot away any liquid and invert onto a

small drop of mounting medium on a slide. We mount in 80% glycerol in PBS + 1 mg/ml *p*-phenylenediamine, but any medium should work. View on a fluorescence microscope with a 100× objective. A typical field of asters is shown in Fig. 2. The number of centrosomes in a preparation is estimated from the number of asters counted in 50 microscope fields: We calculate that there are ~6944 fields (100× objective) on a 12-mm round coverslip. Therefore, the yield of centrosomes can be calculated from

$$\frac{\dfrac{\text{Average No. centrosomes}}{\text{field}} \times 6944 \text{ fields}}{\text{Reaction volume (in ml)}} = \frac{\text{No. centrosomes}}{\text{ml}}$$

This aster spin-down protocol may be used for preparing centrosomes for electron microscopy as well. Simply replace the glass coverslips with plastic ones cut from Thermonox (Ted Pella), sediment the asters onto them, fix and stain for electron microscopy, and invert the coverslips onto epon (or resin of choice). The Thermonox may be peeled off the top of the block once the resin has hardened.

C. The On-Glass Microtubule Nucleation Assay

Alternatively, a less quantitative method for assaying centrosome function that does not require sedimentation of the asters onto coverslips may be used. This assay takes advantage of the natural "stickiness" of the centrosomes; the centrosomes are allowed to stick to coverslips, and then microtubules are grown from them *in situ* (Fig. 3):

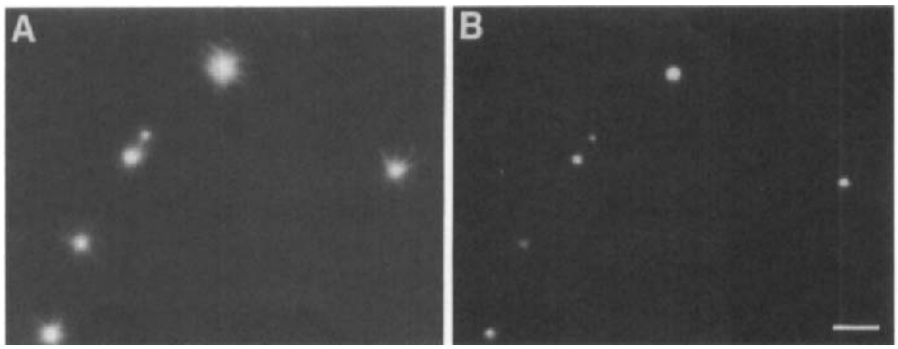

Fig. 2 Fluorescence microscopy of isolated centrosomes with regrown asters. (A) A typical field of isolated centrosomes on which microtubules have been regrown using rhodamine-labeled tubulin. These asters were regrown and sedimented onto coverslips as described in the first assay in the text. (B) Immunolocalization of γ-tubulin on the asters shown in A. Immunofluorescence using an antibody against γ-tubulin was carried out after sedimentation of the regrown asters onto coverslips. Scale bar = 10 μm (reproduced from The Journal of Cell Biology, 1995, **130**, 1149–1159 by copyright permission of The Rockefeller University Press).

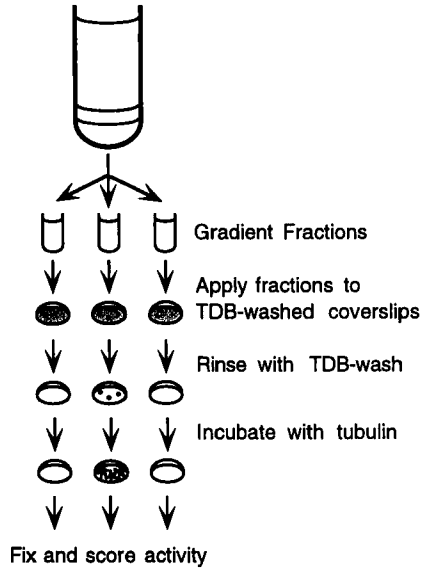

Fig. 3 Schematic of the second assay for centrosome function described in the text. Aliquots of gradient fractions are applied to coverslips and incubated so that centrosomes may bind. The coverslips are washed and then incubated with rhodamine-labeled tubulin so that any centrosomes present may nucleate microtubule growth. Any resulting asters are fixed and viewed in the fluorescence microscope.

1. Place a large petri dish (13.5-cm diameter) on a flat support in a 29°C water bath. Cover the bottom of the dish with a piece of Parafilm and place some wetted Kimwipes around the edge of the dish to keep it moist inside. Place as many acid-washed (1 mg/ml polylysine coating optional) 12-mm round glass coverslips as there are fractions to be tested on the Parafilm. Keep the lid on the dish during incubations. Work quickly so that the coverslips do not dry out.

2. Coat the coverslips with ~60 μl of TDB wash. Incubate for 5 min at 29°C. Aspirate away the wash.

3. Pipet at least 10 μl of each fraction to be tested onto a coverslip. Incubate for 5 min at 29°C.

4. Wash briefly with 3 × 60 μl 29°C TDB wash, removing the buffer by aspiration.

5. Pipet on 25 μl 2.5–3 mg/ml tubulin in TDB (can be a mixture of unlabeled and fluorescently labeled tubulin, or use immunofluorescence to detect the microtubules). Incubate for 10 min at 29°C.

6. Aspirate away the tubulin and fix by pipeting on 60 μl 29°C 1% glutaraldehyde in 1× BRB80. Incubate for 3 min at 29°C.

7. Move the dish to the benchtop and fix again by pipeting on 60 μl −20°C methanol. Incubate for 3 min. Aspirate and then blot away any remaining liquid

before mounting on a small drop of mounting medium on a slide. View in the fluorescence microscope.

IV. Conclusions

The ability to isolate large quantities of centrosomes has allowed recent exciting advances in our understanding of this microtubule-organizing center. For example, we now know that the microtubule-nucleating sites within the pericentriolar material are highly conserved, ring-shaped, γ-tubulin-containing structures that appear to serve as templates for microtubule growth (Moritz *et al.,* 1995a,b; Vogel *et al.,* 1997). Great progress has also been made in understanding the structure and constituents of the spindle pole body, the yeast centrosome counterpart (Rout and Kilmartin, 1991; Bullitt *et al.,* 1997). With the recent advances in identifying proteins in bands on polyacrylamide gels using mass spectrometry and peptide sequencing, our knowledge of centrosome/spindle pole body constituents should increase dramatically in the coming years. It is hoped that this will allow us to decipher the many mysteries that remain concerning this interesting and complicated organelle.

Acknowledgments

Many thanks to Tim Mitchison for useful discussions while developing these protocols and to John Sisson, Karen Oegema, and Sally Cudmore for helpful comments on the manuscript.

References

Belmont, L. D., Hyman, A. A., Sawin, K. E., and Mitchison, T. J. (1990). Real-time visualization of cell cycle-dependent changes in microtubule dynamics in cytoplasmic extracts. *Cell* **62,** 579–589.

Bullitt, E., Rout, M. P., Kilmartin, J. V., and Akey, C. W. (1997). The yeast spindle pole body is assembled around a central crystal of Spc42p. *Cell* **89,** 1077–1086.

Evans, L., Mitchison, T., and Kirschner, M. (1985). Influence of the centrosome on the structure of nucleated microtubules. *J. Cell Biol.* **100,** 1185–1191.

Hyman, A., Drechsel, D., Kellogg, D., Salser, S., Sawin, K., Steffen, P., Wordeman, L., and Mitchison, T. (1991). Preparation of modified tubulins. *Methods Enzymol.* **196,** 478–487.

Kellogg, D. R., and Alberts, B. M. (1992). Purification of a multiprotein complex containing centrosomal proteins from the Drosophila embryo by chromatography with low-affinity polyclonal antibodies. *Mol. Biol. Cell* **3,** 1–11.

Komesli, S., Tournier, F., Paintrand, M., Margolis, R. L., Job, D., and Bornens, M. (1989). Mass isolation of calf thymus centrosomes: Identification of a specific configuration. *J. Cell Biol.* **109,** 2869–2878.

Mitchison, T. J., and Kirschner, M. W. (1984a). Dynamic instability of microtubule growth. *Nature* **312,** 237–242.

Mitchison, T. J., and Kirschner, M. W. (1984b). Microtubule assembly nucleated by isolated centrosomes. *Nature* **312,** 232–237.

Mitchison, T. J., and Kirschner, M. W. (1985). Properties of the kinetochore in vitro. II. Microtubule capture and ATP-dependent translocation. *J. Cell Biol.* **101,** 766–777.

Moritz, M., Braunfeld, M. B., Fung, J. C., Sedat, J. W., Alberts, B. M., and Agard, D. A. (1995a). Three-dimensional structural characterization of centrosomes from early *Drosophila* embryos. *J. Cell Biol.* **130,** 1149–1159.

Moritz, M., Braunfeld, M. B., Sedat, J. W., Alberts, B. M., and Agard, D. A. (1995b). Microtubule nucleation by γ-tubulin-containing rings in the centrosome. *Nature* **378,** 638–640.

Palazzo, R. E., Brawley, J. B., and Rebhun, L. I. (1988). Spontaneous aster formation in cytoplasmic extracts from eggs of the surf clam. *Zool. Sci.* **5,** 603–611.

Rout, M. P., and Kilmartin, J. V. (1990). Components of the yeast spindle and spindle pole body. *J. Cell Biol.* **111,** 1913–1917.

Rout, M. P., and Kilmartin, J. V. (1991). Yeast spindle pole body components. *Cold Spring Harbor Symp. Quant. Biol.* **56,** 687–691.

Vogel, J. M., Stearns, T., Rieder, C. L., and Palazzo, R. E. (1997). Centrosomes isolated from *Spisula solidissima* oocytes contain rings and an unusual stoichiometric ratio of alpha/beta tubulin. *J. Cell Biol.* **137,** 193–202.

CHAPTER 2

Studying the Composition and Function of Centrosomes in Vertebrates

Michel Bornens* **and Mohammed Moudjou†**

* Section de Recherche
Institut Curie
UMR-144/CNRS
Biologie du Cycle Cellulaire et de la Motilité
75248 Paris Cedex 05, France

† Unité de Virologie et Immunologie Moleculaire
Centre de Recherche de Jouy en Josas
Institut National de la Recherche Agronomique
78352 Jouy en Josas Cedex, France

METHODS IN CELL BIOLOGY, VOL. 61

0091-679X/99 $30.00

I. Introduction

The centrosome is the microtubule organizing center of animal cells. During cell division, the duplication and segregation of centrosomes dictate the bipolarity of the mitotic spindle and thus determine the plane of the cleavage furrow. The centrosome is composed of two centrioles tightly associated with a matrix, the so-called pericentriolar material, which consists of a complex thin filament network. In addition, two sets of appendages surround the mother centriole (Paintrand *et al.,* 1992). The centrosome is an intriguing single copy organelle, the reproduction mechanism of which is still unknown. Hence, there is a precise control over centrosome number and coordination of its activities with other cell cycle events. The importance of centrosome as a central organizer during cell division was recognized in the early days of cell biology (Wilson, 1928). Despite its critical role in several cellular processes, our knowledge of the centrosome organelle was, until the past decade, largely based on ultrastructural descriptions and to a lesser extent on functional and biochemical studies. A major barrier has been the difficulty in isolating sufficient quantities of pure centrosomes for such studies. Isolation of this single-copy organelle, which was pioneered by Blackburn *et al.* (1978; for a review, see Bornens, 1992) has been critical for the determination of its overall structural organization and of its biochemical and functional properties. Other strategies such as genetic approaches (Huang, 1990; Kilmartin, 1994; Snyder, 1994) or microtubule affinity columns (Kellogg *et al.,* 1989), as well as the use of autoimmune sera (Doxsey *et al.,* 1994; Gosti-Testu *et al.,* 1986) have also contributed to the identification of centrosomal components. Finally, genuine centrosomal components have been identified by serendipity (Bouckson-Castaing *et al.,* 1996a).

Molecular characterization of centrosomal components is progressing and significant advances can be expected in the near future because a great conservation among divergent organisms of the main centrosome-associated functions, and thus of the centrosomal components, can be expected. The function and the precise localization of the majority of these components represent a promising field of investigation. During the past decade, several methods for centrosome isolation have been described. Different starting materials, including cultured animal cells (Mitchison and Kirschner, 1984; Bornens *et al.,* 1987), animal tissues (Komesli *et al.,* 1989; Lange and Gull, 1995, 1996), *Drosophila* embryos (Moritz *et al.,* 1995a), marine eggs (Vogel *et al.,* 1997), and fungi (Rout and Kilmartin, 1990), have been used. All these procedures have provided a necessary step for the biochemical, structural, and functional characterization of the centrosome. The aim of this chapter is to provide a brief overview of these methods and to discuss the results and limitations of these approaches. It will then deal with the more recent use of evolutionary conservation to identify essential centrosomal components. Finally, we discuss what the past can teach us for future studies of this unique organelle.

II. Isolation of Centrosomes from Animal Cells

A. Cultured Cells

Here, we detail the isolation procedure for centrosomes from human lymphoblastic cultured cells. It is essentially as described elsewhere (Moudjou and Bornens, 1998), except that we have critically assessed the requirement for pretreating cells with microtubule and microfilament drugs and concluded that the use of the drug cytochalasin D (an expensive drug) is not necessary.

1. Materials

1. *Cell wash solutions:* Tris-buffered saline (TBS) buffer (20 m*M* Tris–HCl, pH 7.4, 150 m*M* NaCl) and TBS 1/10 buffer diluted 10-fold containing 8% (w/v) sucrose
2. *Lysis buffer:* 1 m*M* Hepes (pH 7.2), 0.5% NP40, 0.5 m*M* $MgCl_2$, 0.1% β-mercaptoethanol, protease inhibitors (leupeptin, pepstatin, and aprotinin) at 1 μg/ml each, and 1 m*M* of phenylmethylsulphonyl fluoride (PMSF)
3. *1 M Pipes (pH 7.2)* stock solution
4. *DNase I* 1 mg/ml in double-distilled water (from Boehringer)
5. *Sucrose gradient buffer:* 10 m*M* Pipes (pH 7.2), 0.1% Triton X-100, and 0.1% β-mercaptoethanol
6. *Sucrose solutions:* sucrose 70% (w/w), sucrose 60% (w/w), sucrose 50% (w/w), and sucrose 40% (w/w), all made in gradient buffer

All solutions must be filtred through a 0.22-μm filter, except for sucrose solutions, which must be sterilized with an autoclave at 105°C.

2. Procedure

1. The human lymphoblastic KE37 cells are cultured in suspension in RPMI 1640 medium supplemented with 7% of fetal calf serum (FCS) at 37°C and 5% CO_2. Exponentially growing cells (8×10^5 to 1×10^6 cells/ml) are incubated for 1 hr with 2×10^{-7} M nocodazole at 37°C.

2. Cells, classically from 1 to 3 liters, are washed by rapid centrifugation and resuspended at 4°C once with half of the initial volume of TBS buffer and a second time with half volume of TBS 1/10 8% sucrose buffer. All the following steps should be carried out at 4°C unless otherwise indicated.

3. Resuspend cells in 20 ml of TBS 1/10 8% sucrose buffer before lysis, and then add the lysis buffer to obtain a concentration of 1×10^7 cells per milliliter. Resuspend cells four or five times with a 10-ml pipe. Pellet the swollen nuclei, chromatin aggregates, and unlysed cells at 2500*g* (3500 rpm) for 10 min.

4. Filter the lysis supernatant through a nylon mesh into a 250-ml Nalgene tube and add concentrated solutions of 1 *M* Hepes and DNase I at 1 mg/ml to

make a final concentration of 10 m*M* and 1 μg/ml of each component, respectively. Let the suspension sit for 30 min.

5. Centrifuge the lysis supernatant on 10 ml of 60% sucrose cushion at 10,000*g* (7500 rpm) for 30 min in a J2-21M/E Beckman centrifuge equipped with the JS 7.5 rotor.

6. During centrifugation, prepare a discontinuous sucrose gradient in 38 ml SW28 Beckman ultraclear tube, containing from the bottom 5, 3, and 3 ml of 70, 50, and 40% sucrose solutions, respectively. After centrosomes are concentrated on the 60% sucrose cushion by the previous centrifugation, remove the supernatant until only about 25–30 ml remain in the bottom of the 250-ml Nalgene tube.

7. Resuspend centrosomes by pipeting followed by brief vortexing and fill the SW28 Beckman tube with this sample (which is now in about 20–25% sucrose). Centrifuge at 40,000*g* (25,000 rpm) for 1 hr in the ultracentrifuge Beckman L8.50B equipped with the SW28 rotor.

8. Place the SW28 tube on the Density Gradient Fractionator (ISCO): Optimally, the tube is clamped in the ISCO apparatus, perforated at the bottom with a two-hole needle, and 14 fractions of 0.5 ml each are manually recovered from the bottom into 1.5-ml Eppendorf tubes. Other systems of fractionating the sucrose gradient are also suitable.

9. Remove 10 μl from each fraction for monitoring the preparation (see below). The fractions are flash frozen in liquid nitrogen and conserved at −80°C for several months with little loss of activity.

3. Immunofluorescence Analysis of Sucrose Gradient Fractions

1. Disperse 10 μl of fractions 4–13 in their corresponding 15-ml Corex tubes filled with 3 ml of 10 m*M* Pipes (pH 7.2) buffer and containing a special Plexiglas adapter and 12-mm clean round coverslips as described by Evans *et al.* (1985). Centrifuge them at 20,000*g* (10,000 rpm) for 10 min with JS 13.1 rotor in a Beckman J2-21M/E centrifuge. Fractions 5–7 contain the major part of centrosomes loaded on the sucrose gradient.

2. After centrifugation, remove the Pipes buffer from the tubes, place the coverslips in a coverslip-holder box, and immerse them in methanol at −20°C for 6 min. All the following steps take place at room temperature.

3. Rinse three times the coverslips with PBS–0.1% Tween 20 buffer and place them in a chamber suitable for the immunofluorescence experiments with coverslips. Apply a mixture of polyclonal anti-centrosome and monoclonal anti-tubulin antibodies at the correct dilution on samples during 30 min.

4. Rinse the coverlips three times with PBS–0.1% Tween 20 buffer and add the corresponding mixture of secondary antibodies for 30 min.

5. Rinse coverslips with PBS–Tween 20 buffer and place them in ethanol for 2 min. When coverslips are dry, mount them on a drop of solution for fluorescence

mounting with media placed on microscope slides. An example of centrosomal staining is shown in Fig. 1a.

B. Animal Tissue

Thymus is the main animal tissue used to isolate centrosomes. This starting material can provide abundant and enriched preparations of centrosomes from a simplified isolation procedure because thymocytes have a very low cytoplasm to nucleus ratio. Both calf (Komesli *et al.*, 1989) and lamb thymus (Lange and Gull, 1995) have been used successfully because they provide a considerable

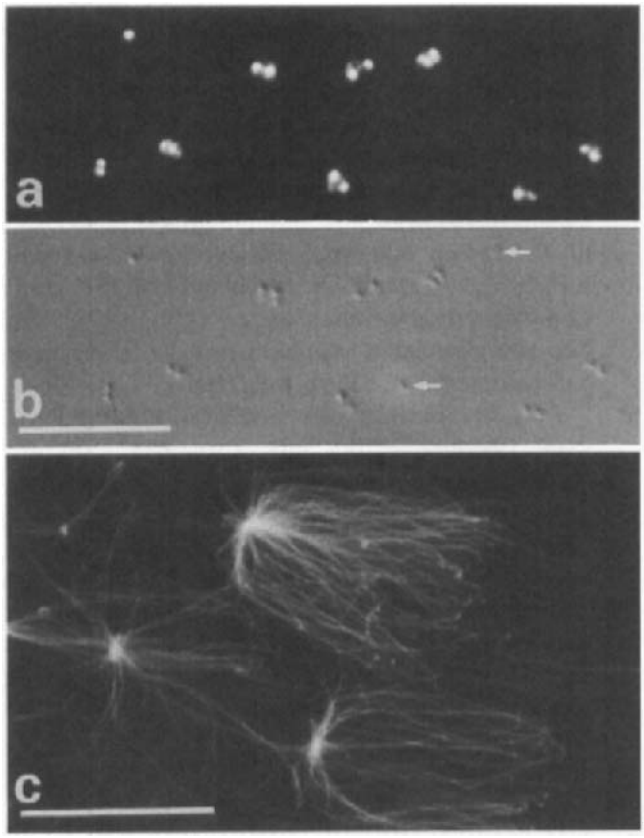

Fig. 1 Centrosomes isolated from KE37 cells are stained with a monoclonal anticentriole antibody, revealed with rhodamine-conjugated goat anti-mouse as secondary antibody (a). Centrosomes are recovered in their native configuration as a pair of centrioles. Differential interference contrast observation of the same field (b) shows a minimal number of unstained structures (arrows). Functional assay of isolated centrosomes show that they are competent to nucleate microtubules from purified tubulin (c). Microtubules are stained with an anti-α-tubulin antibody. Scale bars = 10 μm.

amount of thymocytes, which compensate the low yield of centrosome isolation. Rat and mouse thymus have been also used (Tournier *et al.*, 1991a).

C. Comments and Pitfalls

The yield of centrosome preparation from lymphoblastic KE37 cells varies between 15 and 30%. It can be significantly increased when small numbers of cells are processed: The concentration step on 60% sucrose can be eliminated and the lysis supernatant directly sedimented on the sucrose gradient (Bornens *et al.*, 1987). The method described here can be adapted to other cell types, although it must be optimized for each case. Centrosomes have been isolated in this way from human and bovine peripheral lymphocytes (Tournier *et al.*, 1989, 1991a).

Mass isolation of centrosomes has been obtained using animal tissue such as thymocytes (Komesli *et al.*, 1989; Lange and Gull 1995, 1996). In this case, drug pretreatment to disassemble microfilaments was not used. We have extended this to cultured lymphoblastic cells: Pretreatment with cytochalasin D is unnecessary. This significantly reduces the cost of centrosome preparations. In contrast, nocodazole pretreatment must be maintained to obtain a good yield of optimally cleaned centrosomes. This might appear paradoxical since preparations are made at 4°C, which is a very efficient condition to disassemble microtubules from KE37. The explanation is probably that *in vivo* microtubule disassembly has important repercussions on the actin system; for example, most of myosin II becomes associated with the cortical actin (Bornens *et al.*, 1989) and thus favors centrosome release during cell lysis.

Recently, centrosomes have been isolated from *Drosophila* embryos (Moritz *et al.*, 1995a) and from *Spisula solidissima* oocytes (Vogel *et al.*, 1997). In both methods, centrosomes were isolated from lysates by sucrose gradient velocity sedimentation using a modification of the original procedures described by Mitchison and Kirschner (1984) and Bornens *et al.*, (1987). The fractions were assayed for centrosome content using their ability to nucleate microtubules from pure brain tubulin dimer. We have, for comparison, summarized in Table I the data concerning the yield, protein content, and purification fold (calculated as the ratio of the protein content in the first homogenate to that of the centrosome preparation for an equivalent number of centrosomes) in isolation procedures from published work.

III. Preparation of Immunological Probes from Isolated Centrosomes

A. Preparation of the Immunogen

One approach to characterize centrosomal antigens begins with the production of antibodies (Kuriyama, 1992; see Chapter 13). Monoclonal antibodies have

Table I
Comparison of Centrosome Isolation Efficiency from Different Sources

Cell type or tissue	Protein content	Yield (%)	Purification factor
Cultured lymphoblastic cells[a]	2–3 μg/1.10^8 centrosomes	15–50 (see comments)	2000
Animal tissues (thymus)[b]	3–4 μg/1.10^8 centrosomes	10	Undetermined
Drosophila melanogaster[c]	5 μg/1–5.10^7 centrosomes (from 2g embryos)	10	1000
Spisula solidissima[d]	53 μg/1–2.10^7 centrosomes (from 2–3 ml of crude homogenate)	68	2500
Saccharomyces cerevisiae[e]	1 μg/4.10^7 SPB	45	600

[a] Bornens *et al.* (1987).
[b] Komesli *et al.* (1989).
[c] Moritz *et al.* (1995a).
[d] Vogel *et al.* (1997).
[e] Rout and Kilmartin (1990).

been produced in our laboratory using human centrosomes as immunogen (Bailly *et al.*, 1988). The specificities of the antibodies depended on the preparation of the immunogen: Centrosome preparations were injected either native or after denaturation by 0.1% sodium dodecyl sulfate (SDS). Only in the latter case did we obtained anti-centriole specificities (Fig. 1a), whereas with native centrosomes, most of the antibodies were reacting with PCM components.

Other immunogens have been used which led to anti-centrosome antibodies, including mitotic cell extract (Davis *et al.*, 1983), sea urchin and Chinese hamster ovary mitotic spindles (Kuriyama and Borisy, 1985; Kuriyama, 1992), and quail ciliated cortices (Klotz *et al.*, 1986).

Antibodies against spindle pole body components have also been produced using enriched SPB fractions and proteins separated on SDS–PAGE gels. Bands recognized on gels were cut out and used as immunogens to produce both polyclonal and monoclonal antibodies in mice (Rout and Kilmartin, 1990).

Another indirect strategy for the production of immunological probes is microtubule affinity chromatography (Kellogg *et al.*, 1989). Taxol-stabilized microtubules were coupled to a solid matrix and proteins from extracts that bind microtubules were eluted using different conditions. Antibodies were produced against individual polypeptides after separation by gel electrophoresis. This method, used with extract from *Drosophila* embryos and from yeast, has allowed the identification of a few centrosomal proteins in *Drosophila* (CP60 and CP190; Kellogg and Alberts, 1992) and only of microtubule-associated proteins in yeast (Barnes *et al.*, 1992).

B. Results and Limitations

In most cases, antibodies were screened according to their immunocytochemical labeling. Although rapid and highly sensitive, this screen has to be coupled to immunoblotting screening of centrosomal and total cellular proteins. Indeed, a frequent outcome in monoclonal antibody production using either centrosomes or mitotic spindles as immunogen is the obtainment of antibodies which work perfectly by immunofluorescence but do not recognize any antigen by immunoblotting.

Different categories of monoclonal antibodies have been consistently obtained. Some of them have been shown to decorate the centrosome during all stages of the cell cycle and others in a cell cycle-dependent manner. In addition, several antibodies showed staining of centrosomes and other cellular organelles (Buendia *et al.*, 1990; Perret *et al.*, 1995). One can indeed also obtain specificities against cell compartments located in the vicinity of the centrosome, such as Golgi apparatus (Jasmin *et al.*, 1989), which are tightly associated with the centrosome boundary *in situ* (Perret *et al.*, 1995) and are present in the centrosome-enriched fractions.

Another important approach in identifying centrosomal proteins has been to take advantage of the existence of autoimmune sera which, for unknown reasons, are directed against the centrosome. The most extensively used are the human autoimmune serum 5051 (Calarco-Gillam *et al.*, 1983) and the spontaneous rabbit serum 0013 (Gosti-Testu *et al.*, 1986). The 5051 human serum has led to the identification and molecular characterization of the centrosomal matrix component pericentrin (Doxsey *et al.*, 1994), and the rabbit 0013 serum has been shown to recognize the high-molecular-weight AKAP350 centrosomal-specific antigen (Keryer *et al.*, 1993). The latter is also recognized by the monoclonal antibody CTR453. The presence of spontaneous anti-centrosome specificities in rabbit sera is frequent: During the production of an anti-γ-tubulin antibody (Moudjou *et al.*, 1996), we noted that preimmune sera of 12 of 12 rabbits already possessed an anti-centrosomal activity as judged by immunofluorescence. Thus, affinity purification of specific immunoglobulins should be systematically done. In any case, a direct biochemical demonstration of the association of an antigen to the centrosome is necessary before any conclusion can be drawn.

IV. Ultrastructural Analysis of Isolated Centrosomes

A. Structural Preservation of Isolated Centrosomes

The isolation of centrosomes has led to several new observations concerning the nature and the organization of both the centrioles and the centrosomal matrix and has indicated the role of divalent cations in the whole organization of the centrosome (Paintrand *et al.*, 1992). Isolated centrosomes maintain their paired configuration and look, to a large extent, like those observed *in situ*, provided divalent cations are not removed by chelating agents from the isolation buffer.

We recently compared the structure of extemporaneously isolated centrosomes (not frozen after isolation) with those which have been stored in high sucrose concentration at −80°C for several weeks or months. Slight modifications in the structure were produced by freezing and thawing, the diameter of each centriole being slightly increased by this treatment. Accordingly, we observed a definite difference in the accessibility of some centrosomal antigens to their antibodies: This is the case for CTR453 (Bailly *et al.,* 1988) which, even after methanol fixation at −20°C, stains weakly the freshly made centrosomes, whereas it gives a strong signal on centrosomes which have been frozen once.

B. The Centriole Pair and the Centrosomal Matrix

Serial sections of isolated centrosomes have revealed a complex structure in the lumen of centrioles at their distal half. Consistent with numerous *in situ* observations, no detectable material was present in the proximal lumen of centrioles using the available contrasting agents. One of the recurrent debates about centrosomes from animal cells is the role of centrioles. Recently, we have shown that centriolar tubulin, and mainly α-tubulin, is highly polyglutamylated in non-neuronal cells (Bobinnec *et al.,* 1998). HeLa cells loaded with anti-polyglutamylated tubulin monoclonal antibody show a transient disassembly of centrioles which eventually leads to the total disorganization of the centrosome (Bobinnec *et al.,* 1995). This result suggests that the centriole pair is essential for the structural integrity of the centrosome in animal cells.

The centrosomal matrix, often described as an amorphous material, is likely to be organized about the ninefold symmetry of centrioles, around their proximal part. This matrix is likely to be dynamic (Baron and Salisbury, 1992; Moudjou and Bornens, 1992). Its distribution around centrioles varies during the cell cycle and is sensitive to the concentration of Ca^{2+}. Mild denaturing conditions, such as 3 or 4 *M* urea or 0.5 *M* KI, can be efficient to extract most of the centriolar components. However, ultrastructural observations of the remnant structure after treatment with such agents showed that the overall shape of the centrosome is maintained: The centrosomal matrix appears as linking two empty and roughly cylindrical structures (Klotz *et al.,* 1990; Paintrand *et al.,* 1992). This material is organized by the interconnection of very thin filaments. The possibility that this structure actually represents a unique continuous structure, on which other centrosomal components would be anchored, cannot be eliminated. The protein profile of a 8 *M* urea-treated matrix is much simpler than that of the nontreated centrosome preparations (Klotz *et al.,* 1990; Moudjou *et al.,* 1991) but the individual proteins remain to be identified.

Recently, computational tomography reconstitution of centrosomes isolated from *Drosophila* embryos (Moritz *et al.,* 1995a) and from *S. solidissima* oocytes (Vogel *et al.,* 1997) has shown the presence of structures organized in a ring-like shape reminiscent of the γ-tubulin-containing ring complexes isolated from *Xenopus* egg extracts (Zheng *et al.,* 1995). However, the anchorage of these

ring structures within the pericentrosomal matrix is not yet known. The human homolog of the yeast Spc110p (Kilmartin and Goh, 1996) is one of the candidates for such a role (Tassin *et al.*, 1997). Indeed, it has been recently reported that the yeast microtubule nucleating heterotrimeric complex, containing tub4p (the yeast γ-tubulin), Spc98p, and Spc97p, binds to the spindle pole body via an interaction with Spc110p (Knop and Schiebel, 1997).

C. Immunolocalization of Centrosomal Antigens

1. Preembedding

1. Sediment about 2×10^7 centrosomes onto a glass coverslip as described in Section II,A.

2. Fix the centrosomes by incubating the coverslip with 0.5% glutaraldehyde in 10 m*M* K-Pipes buffer (pH 7.2) for 10 min, and wash them three times with the K-Pipes buffer.

3. Incubate coverslips for 20 min with 1 mg/ml of $NaBH_4$ freshly prepared in the K-Pipes buffer to reduce free amino groups of glutaraldehyde.

4. Rinse the coverslips for 3 × 10 min with TBS buffer (20 m*M* Tris–HCl, pH 7.2, 150 m*M* NaCl) containing 0.1% BSA, and incubate centrosomes with the primary antibody(ies) diluted in TBS–BSA buffer for 1 hr at room temperature.

5. Rinse the coverslips for 3 × 10 min with TBS–BSA buffer, and incubate centrosomes with the corresponding secondary antibody(ies) coupled to colloidal gold particles of a given size (G5, G10, or G15).

6. Wash the coverslips three times with TBS–BSA buffer and postfix the centrosomes with 2.5% glutaraldehyde in 0.1 *M* cacodylate buffer for 1 hr. Rinse the coverslips with cacodylate buffer and incubate them for 1 hr with solution containing 1% osmium tetroxide and 0.5% tannic acid.

7. Incubate the coverslips with ethanol (50% 2 × 5 min, 70% 2 × 5 min) for progressive dehydratation and stain the sample with 0.5% uranyl acetate made in 70% ethanol before embedding in Epon.

8. After polymerization, dissociate the Epon block from the coverslips by hot/cold shocks alternately using boiling water and liquid nitrogen. Section the sample parallel to the coverslip contacting the surface and observe in the electron microscope.

2. Postembedding

1. Sediment centrosomes onto glass coverslips as described in Section II,A.

2. Fix the centrosomes for 1 min with 1.25% glutaraldehyde in 0.1 *M* cacodylate buffer containing 4% low molecular galloyl glucose (LMGG) and for 29 min in 0.125% glutaraldehyde in 0.1 *M* cacodylate buffer containing 4% LMGG and 4% sucrose.

3. Rinse the coverslips once with 0.1 *M* cacodylate buffer containing 4% sucrose and once with K-Pipes buffer. Neutralize the glutaraldehyde by 3 × 10 min incubation in 1 mg/ml NaBH4 prepared in K-Pipes buffer followed by a last rinse in the K-Pipes buffer alone.

4. Incubate the coverslips with ethanol (50% 2 × 5 min, 70% 2 × 5 min) for progressive dehydratation, and embed centrosomes in a mixture of LR–White/ethanol at a ratio of 2/1 for 30 min and pure LR–White for 3 hr at room temperature with three changes. Let polymerize for 48 hr at 54°C. Alternatively, centrosomes can be prefixed according to Burgess *et al.,* (1991) and embedded in the hydrophile resin, Unicryl, according to Scala *et al.,* (1992). In this case, polymerization is carried out at 55°C for 48 hr instead of using UV light.

5. Dissociate the coverslips from the polymerized resin by hot/cold shocks alternately using boiling water and liquid nitrogen. Make sections parallel to the coverslip surface and place them onto nickel grids for incubation with the antibodies.

6. Incubate both LR–White or Unicryl sections first with a blocking solution containing unlabeled secondary serum diluted 10-fold in TBS–BSA–Tw buffer (TBS, pH 7.2, containing 0.2% BSA and 0.2% Tween 20) for 10 min. This is done by placing the section-supporting grids on a small drop of the buffer. This method is used during the following step.

7. Incubate sections with the primary antibodies diluted in TBS–BSA–Tw buffer for 90 min at room temperature. Rinse grids for 4 or 5 min with TBS–BSA–Tw buffer and incubate the sections with the secondary antibodies diluted 20-fold in TBS–BSA–Tw buffer. Sections are observed with an electron microscope after 4- or 5-min washes with TBS–BSA–Tw buffer and double contrast with uranyl acetate and lead citrate.

3. Results and Comments

The major drawback of the preembedding technique is that it restricts immunolocalization to accessible antigens, i.e., to the more peripheral. For example, we have never succeeded in localizing the prominent microtubule triplets using several anti-tubulin antibodies. The immunolocalization of γ-tubulin was first assayed by preembedding experiments (Stearns *et al.,* 1991) and a localization restricted to the periphery of the centrosomal matrix was described. Postembedding techniques have allowed specific staining of centriolar antigens, including microtubules, using different anti-α/β-tubulin antibodies (Moudjou *et al.,* 1996; Bobinnec *et al.,* 1998) and have demonstrated that γ-tubulin has a preferential localization close to the centrioles (Moudjou *et al.,* 1996), in agreement with many studies by immunofluorescence *in situ.*

However, a centrosomal protein, centrin has been successfully immunolocalized by both post- and preembedding techniques. Centrin is accumulated within the distal lumen of centrioles (Paoletti *et al.,* 1996), suggesting an easy access to

intraluminal antigens. Thus, as for any other organelle, caution should be taken when immunolocalizing antigens at the ultrastructural level. This is even more true for the centrosome, which has a particularly complex architecture. A rigorous localization of centrosomal antigens should involve postembedding techniques and an analysis by complete serial sectioning. Computational tomography might represent an alternative to serial sectioning (Moritz *et al.*, 1995b).

V. Biochemical Composition of Centrosomes

A. Direct Analysis of Isolated Centrosome Preparations

Isolated centrosomes from human lymphoblastic KE37 cells have been analyzed for their protein content by SDS–PAGE. This was achieved using preferably a 6–15% polyacrylamide gel gradient in order to resolve proteins ranging from 14 to 400 kDa molecular weight (MW). Silver staining of a monodimentional gel of isolated centrosomes shows that there are about 10 major polypeptides and approximately 50 minor ones. Between 1×10^7 and 2×10^7 enriched centrosomes are necessary to obtain a protein profile such as the one shown in Fig. 2, in which genuine centrosomal proteins can be observed. For example, the highest component in terms of MW observed in the 1D analysis on Fig. 2 (asterisk) is highly enriched in centrosome preparations and has been shown to be a very good RII-binding protein; thus, it was called AKAP350 (*a kinase anchoring protein*; Keryer *et al.*, 1993). To see it by Coomassie blue staining, i.e., to have about 0.5 μg of protein, requires 10^8 centrosomes. Among the major proteins present in such preparations, several are likely to be contaminants, however. We have identified a few of the major components, indicated on the 2D profile of Fig. 2, either by specific antibodies or by microsequencing. Such proteins are, by increasing MW, G3PDH, actin, α/β-tubulins, Tcp1, hsp70, hsp90, and HsEg5. Except for α/β-tubulins and AKAP350 protein, which are definitely true centrosomal components because they are intrinsic components of the centriole barrels and the centrosomal matrix, respectively, there is no clear demonstration that the other major polypeptides represent centrosomal components.

Two-dimensional gel analysis shows that about 150 minor spots can be visualized after silver staining. It also shows that keratin contamination (the two horizontal silver-stained bands spanning the complete width of the gel at about 60 kDa) is always a concern when one works with small amount of proteins. Extremely stringent cleaning of all the glassware and the use of gloves are necessary to diminish contamination. A large 2D gel, such as the one shown in Fig. 2, requires about 4×10^7 centrosomes. However, the use of 2D minigel system from Biorad also gives excellent results with half the number of centrosomes (see Fig. 1 in Moudjou *et al.*, 1996).

B. Evolutionary Conservation

The centrosome organelle can vary considerably in shape, size, or structure among divergent organisms. However, in all cases, it ensures a main function,

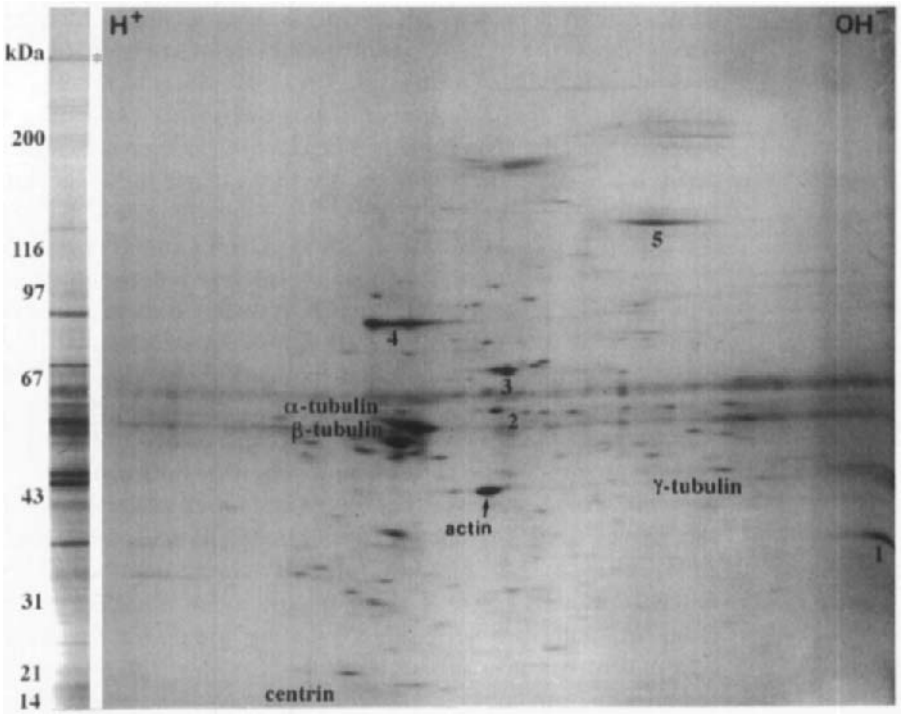

Fig. 2 The mono- and two-dimensional electrophoretic protein profile of centrosome preparations. As expected, α- and β-tubulin are prominent centrosomal components, reflecting the presence of the centriole pair as a conspicuous compartment in the centrosome organelle. γ-Tubulin and centrin are important markers of the centrosome *in vivo*. Centrosome-associated centrin is confined within the distal lumen of each centriole and γ-tubulin is distributed in the pericentriolar matrix but is often closely associated with centrioles. However, the centrosome-associated fraction of both proteins is a minor part of the total cellular content. The high-molecular-weight component observed in 1D corresponds to AKAP350, a genuine centrosomal component. It is too insoluble to be correctly electrofocused. Actin (arrow) is always an abundant component in the preparations. The meaning of such an abundance must still be clarified. This is also the case for other major proteins, including G3PDH (1), Tcp1 (2), hsp70 (3), hsp90 (4), and HsEg5 (5).

the control of the nucleation of microtubules, and undergoes a duplication process once per cell division cycle. That such properties are apparently maintained among divergent species suggests that functional protein complexes are also conserved. This is the case for γ-tubulin (Oakley, 1992), which has been discovered in a genetic screen for revertants of β-tubulin mutation in *Aspergillus nidulans* and has been involved in microtubule nucleation (for review, see Erickson and Stoeffer, 1996; Pereira and Schiebel, 1997). Homologs are present in all centrosomes tested so far. Other examples of fungi SPB components have been identified in the human system using evolutionary conservation, either using cross-reacting antibodies or sequence conservation. Monoclonal antibodies directed against the yeast Spc110p (Kilmartin and Goh, 1996) have been shown

to react with a protein specifically located at the centrosome of animal cells which, in the case of human centrosomes, seems to be involved in the microtubule nucleating activity (Tassin *et al.,* 1997). However, screening expression libraries did not allow the detection of a positive clone, suggesting that the protein is indeed a very rare component. The alternative approach, which is now becoming powerful, is to use database expressed sequence tags. Recently, primers derived from a human expressed sequence tags matching SPC98 (Geisseler *et al.,* 1996) were used to clone the human Spc98 cDNA (Tassin *et al.,* 1998). This study has shown that the human Spc98p, like γ-tubulin, is concentrated at the centrosome, although a large fraction is found in cytosolic complexes. Sucrose gradient sedimentation of the cytosolic fraction, in conjunction with immunoprecipitation experiments have demonstrated that both γ-tubulin and HsSpc98p are in the same complex. It has also been demonstrated that inactive centrosomes from *Xenopus* sperm cells contain comparable amounts of Spc98p and γ-tubulin than active human somatic centrosomes. These results contrast with early reports in *Xenopus* which proposed that the essential step of the activation reaction is the γ-tubulin recruitment from egg cytoplasm (Felix *et al.,* 1994; Stearns and Kirschner, 1994). These authors have put forward the idea that the centrosome is assembled at fertilization by a type of complementation in which the centriole pair, inherited from the male gamete, binds nucleating components from the female gamete. Sperm centrosomes, although inactive for microtubule nucleation, do not differ apparently from active somatic centrosomes with respect to the presence of both Spc98p and γ-tubulin and also of all the other centrosomal components which have been examined, such as centrin, CTR2611 antigen (Felix *et al.,* 1994), and pericentrin (Doxsey *et al.,* 1994; Stearns and Kirschner, 1994). Thus, the classical view, according to which the centrosome organelle is paternally inherited and fertilization triggers a switch in its activity, is likely to be correct.

With a similar approach, the human homolog (HsCEN3) of the yeast CDC31 gene product has been cloned and shown to be localized within the centrioles of human cells (Middendorp *et al.,* 1997). Because the CDC31 gene product is involved in the duplication of SPB (Baum *et al.,* 1986, 1988), HsCEN3 represents the first candidate for which molecular and immunological probes are now available to design experiments for unraveling the duplication mechanism of the centrosome.

All these results show that the combination of studies from genetically tractable organisms with studies on centrosomes from animal cells will rapidly increase our understanding of the molecular mechanisms underlying the main functions of this organelle. Serendipity may also contribute to this understanding: It is by serendipity that ninein was discovered.

C. What Is a Genuine Centrosomal Component?

Attempts to classify proteins that are associated transiently or permanently to the centrosome have been made (Kimble and Kuriyama, 1992; Kalt and

Schliwa, 1993). Cell fractionation and centrosome isolation are necessary to correctly estimate the cellular distribution of proteins which have been localized at the centrosome by cytological methods. A genuine centrosomal protein should be present in a detectable amount only in highly enriched centrosome preparations. Few proteins fulfill this criteria: AKAP350 (Gosti-Testu *et al.,* 1986; Keryer *et al.,* 1993), pericentrin (Doxsey *et al.,* 1994), ninein (Bouckson-Castaing *et al.,* 1996a), the human homolog of Spc110 (Tassin *et al.,* 1997), and probably cenexin (Lange and Gull, 1995). The predicted amino acid sequence is known only for pericentrin and ninein. The pericentrin sequence does not contain any predictive information or relatedness to known proteins, except for the presence of a large coiled coil domain. The ninein sequence is more informative: Ninein contains as many as nine distinct domains, including a highly basic domain which can be alternatively spliced, an EF-hand calcium binding site, a PEST sequence, a GTP binding site, four leucine zipper domains within a large coiled coil domain, and a basic domain at the COOH-terminal end.

However, functionally important centrosome-associated proteins, such as γ-tubulin and centrin, have been shown to be involved in a cytoplasmic pool which exceeds by far the centrosome-associated fraction (Moudjou *et al.,* 1996; Paoletti *et al.,* 1996). Recently, the human homolog of Spc98p has been shown to be both concentrated in the centrosome and to participate in a large and more diluted cytoplasmic pool (see section V,B). The significance of such pools is not understood.

VI. Functional Assays of Isolated Centrosomes

A. Microtubule Nucleating Activity

Isolated centrosomes are tested for their capacity to nucleate microtubules from purified tubulin, using the procedure described by Mitchison and Kirschner (1984).

1. Solutions

1. Purified brain tubulin solution at 2.5 mg/ml
2. RG2 buffer: 80 m*M* Pipes (pH 6.8), 1 m*M* $MgCl_2$, and 1 m*M* EGTA
3. RG1 buffer: RG2 buffer + 1 m*M* GTP
4. Glutaraldehyde: 1% (v/v) made in RG2 buffer
5. Glycerol; 25% (v/v) solution in RG2 buffer
6. Triton X-100: 1% (v/v) solution made in RG2 buffer

2. Steps

1. Mix 50 μl of tubulin solution, 5 μl of centrosomes (between 2 to 5×10^5 centrosomes), and 10 μl of RG1 buffer at 4°C, and then place the mixture at 37°C for 8 min.

2. Add 200 μl of the 1% glutaraldehyde solution, and place the tube at 25°C for 3 min.

3. Place the tube on ice and add 1 ml of RG2 cold buffer.

4. Prepare 15-ml Corex tubes with corresponding adapters and glass coverslips (Evans *et al.*, 1985). Fill them with 5 ml of the 25% glycerol solution. Overlay this solution with the nucleated microtubule sample and sediment the asters at 20,000*g* (10,000 rpm) for 10 min with the JS 13.1 rotor in a Beckman J2-21M/E centrifuge at 4°C.

5. Aspire 1 ml from the top of the Corex tube and replace it with 1 ml of the 1% Triton X-100 solution.

6. Remove all of the glycerol solution to leave just the 1 ml of the Triton X-100 solution over the coverslip and recover the latter from the Corex tube. Classically, an immunofluorescence experiment (see Section II) is run to detect the centrosomes and microtubule asters. An example of asters stained with anti-α-tubulin antibody is shown in Fig. 1c.

3. Comments

This test is routinely used to determine whether an antibody directed against a centrosomal component blocks the nucleation of microtubules. It must be completed by independent experiments. Negative results with an antibody do not eliminate the participation of the antigen in the nucleating reaction. Positive results could reflect a simple steric hindrance effect by the antigen–immunoglobulin complex close to the nucleating sites. Further experiments, such as microinjection of antibodies into the cell and overexpression or depletion of the protein or of mutated forms, must be carried out in parallel before any firm conclusion can be reached.

B. Centrosome Biogenesis

Centrosome biogenesis involves several distinct aspects, including the turnover of individual centrosomal components, the assembly of a new centrosome during each cell cycle through a duplication mechanism, and the coupling between this duplication and the progression of the cell division cycle.

The pathenogenetic assay in *Xenopus* eggs represents the most established and reliable system to study centrosome duplication *in vivo*. Frog eggs are unable to assemble a centrosome from its elements in the absence of a preexisting centrosome. A striking feature of this system is that centrosome assembly from egg precursor components can be triggered by a centrosome from heterologous species (Tournier and Bornens, 1994). This emphasizes the great functional conservation of the centrosome duplication mechanisms among divergent species.

1. The Parthenogenetic Assay in *Xenopus* Eggs

Solutions

1. 2% cystein (pH 7.8) solution

2. MMR buffer: 5 m*M* Hepes (pH 7.4), 0.1 *M* NaCl, 2 m*M* KCl, 1 m*M* $MgSO_4$, 2 m*M* $CaCl_2$, 0.1 m*M* EDTA

3. K-Pipes buffer: 10 m*M* Pipes (ph 7) with KOH

Steps

1. Dejelly unfertilized eggs from *Xenopus laevis* with 2% cystein solution.

2. Wash dejellied eggs three times in MMR buffer.

3. Microinject eggs, incubated in MMR–5% Ficoll 400 (Sigma), using a nanoject system (Drummond). Centrosomes are diluted in K-Pipes buffer and injected at different dilutions. In a typical experiment, three dilutions are tested on batches of 30–50 eggs per dilution: <1, 1–2, and 10 centrosomes are injected per egg in 50 nl of diluting buffer.

4. Score blastulas 3 and 5 hr after injection (Tournier *et al.*, 1989, 1991a).

C. Comments

Turnover must be established for individual centrosomal components because they may indeed each have a specific type of turnover. Centriole tubulin has been shown, for example, to slowly turn over (Kochanski and Borisy, 1990) at about 10% per generation cycle. By contrast, centrin 1 or 2, when overexpressed in human cells, suggests that the cytoplasmic pool of centrins is in rapid equilibrium with the centrosomal one (Middendorp, 1998). The example of ninein suggests another scenario: When overexpressed, ninein, which is a genuine centrosomal protein, accumulates steadily at the centrosome, where it can form a pericentriolar aggregate as large as the nucleus itself. How is this protein turned over? Apparently in a cyclic manner by a proteolytic destruction at the end of mitosis (Bouckson-Castaing *et al.*, 1996b).

VII. Prospects

A. What Does the Past Teach Us?

A biochemical approach of the centrosome duplication pathway requires an efficient assay. Indeed, extracts from amphibian or marine eggs are likely to provide the only systems in which this aim can be reached. An efficient and reliable *in vitro* assay for centrosome duplication will be invaluable as a tool for studying the molecular mechanisms underlying centrosome duplication. Previous attempts have been reported (Tournier *et al.*, 1991b; Palazzo *et al.*, 1992), but they have limitations. An efficient system should possess a few minimal features to be reliable: first, a simple way to monitor centrosome duplication. Because centrioles are indeed indicative of the reproductive capacity of centrosomes (Sluder and Rieder, 1985), they are good markers for the progression of centrosome duplication. However, the parental and daughter centrioles during centrosome duplication must be distinguished unambiguously. Second, initiation of

procentriole bud formation must be distinguished from procentriole elongation itself. This implies that one is able to start with centrosomes from synchronized cells, in which procentriole budding has not been initiated. Third, the scoring method must be simple enough so that the fate of a great number of centrosomes can be followed in each independent experiment.

It is hoped that such a system might be designed in the near future. It will be complementary of, and should benefit from, genetic approaches in suitable systems such as yeasts, *Drosophila,* or *Caenorhabditis elegans.*

The past decade of centrosome studies has taught us how the identification of new centrosomal components can benefit from the combination of genetic, molecular, and biochemical strategies and from the functional conservation of centrosomal components among divergent species.

The recent advances in computational tomography at the ultrastructural level represent a promising approach for building a resolutive 3D reconstruction of the major structural components of the isolated centrosome which is still missing. Attempts toward this goal have been reported (Moritz *et al.,* 1995a; Vogel *et al.,* 1997; see Chapters 1 and 3). Coupled with an immunolocalization of the major genuine centrosomal proteins, this should lead to a novel vision of the centrosome organelle and to a description of the duplication process at the structural level.

Finally, genome sequencing of several model organisms, coupled with the now available highly sensitive mass spectroscopy techniques, should provide an unprecedented wealth of data. Such an approach has been pioneered by Kilmartin *et al.,* (1997) with the budding yeast SPB.

B. Studying Centrosome Functions *in Vivo*

GFP-tagged centrosomal proteins will certainly represent powerful tools in the near future. One may anticipate the discovery of as yet unsuspected properties of the centrosome organelle dynamics *in vivo.* Already γ-tubulin from *Dictyostelium discoideum* (Ueda *et al.,* 1997) or from vertebrates (Khodjakov *et al.,* 1997), mouse ninein (V. Bouckson-Castaing and M. Bornens, unpublished data), and human centrin (White and Salisbury 1997; Y. Abraham, M. Piel, and M. Bornens, unpublished data) have been observed *in vivo.* Centrin is a particularly exquisite tool for observing the centrosome behavior *in vivo* in that it concentrates rapidly in the distal lumen of each centriole. Thus, it provides a means to follow individual centrioles and their mutual movements in a centrosome and a unique approach to describe the whole duplication process in a precise manner during the cell division cycle.

This approach has also been used recently to show that calmodulin associates with the SPB in both *Saccharomyces cerevisiae* and *Schizosacharomyces pombe* (Moser *et al.,* 1997). One can expect the approach to be developed further in the near future. It should lead to significant advances in the description and understanding of the cell cycle-dependent behavior of many regulatory proteins

(Bailly *et al.*, 1989; Lane and Nigg, 1997) that have been reported to transiently associate with the centrosome.

Note added in proof. For work on the human Spc98 cDNA (see Section V,B), see also S. M. Murphy, L. Urbani, and T. Stearns, 1998, *J. Cell Biol.* **141,** 663–674, and O. C. Martin, R. N. Gunawardane, A. Iwamatsu, and Y. Zheng, 1998, *J. Cell Biol.* **141,** 675–687.

References

Bailly, E., Berges, J., Bordes, N., Celati, C., and Bornens, M. (1988). Analysis of centrosomal components with monoclonal antibodies. *In* "European Symposium on the Structure and Functions of the Cytoskeleton, Lyon, France." J. Libbey Eurotex, Montrouge, FR.

Bailly, E., Dorée, M., Nurse, P., and Bornens, M. (1989). p34cdc2 is located in both the nucleus and cytoplasm; Part is centrosomally associated at G2/M and enters vesicles at anaphase. *EMBO J.* **8,** 3985–3995.

Barnes, G., Louie, A., and Botstein, D. (1992). Yeast proteins associated with microtubules *in vitro* and *in vivo*. *Mol. Biol. Cell.* **3,** 29–47.

Baron, A. T., and Salisbury, J. L. (1992). Role of centrin in spindle pole dynamics. *In* "The Centrosome" (V. T. Kalnins, ed.), pp. 167–195. Academic Press, New York.

Baum, P., Fulong, C., and Byers, B. (1986). Yeast gene required for spindle pole body duplication: Homology of its gene product with Ca^{++}-binding proteins. *Proc. Natl. Acad. Sci. USA* **83,** 5512–5516.

Baum, P., Ying, C., Goetsch, L., and Byers, B. (1988). A yeast gene essential for regulation of spindle pole duplication. *Mol. Cell Biol.* **8,** 5386–5397.

Blackburn, G. R., Barreau, M. D., and Dewey, W. C. (1978). Partial purification of centrosomes from Chinese hamster ovary cells. *Exp. Cell Res.* **113,** 183–187.

Bobinnec, Y., Moudjou, M., Mir, L., Eddé, B., and Bornens, M. (1995). A role for centrioles in centrosome organization. *Mol. Biol. Cell Suppl.* **6,** 41a.

Bobinnec, Y., Moudjou, M., Fouquet, J. P., Desbruyères, E., Eddé, B., and Bornens, M. (1998). Glutamylation of centriole and cytoplasmic tubulin in proliferating non-neuronal cells. *Cell Motil. Cytoskel.,* **39,** 223–232.

Bornens, M. (1992). Structure and functions of isolated centrosomes. *In* "The Centrosome" (V. T. Kalnins, Ed.), pp. 1–43. Academic Press, New York.

Bornens, M., Paintrand, M., Berges, J., Marty, M. C., and Karsenti, E. (1987). Structural and chemical characterization of isolated centrosomes. *Cell Motil. Cytoskel.* **8,** 238–249.

Bornens, M., Paintrand, M., and Celati, C. (1989). The cortical microfilament system of lymphoblasts displays a periodic oscillatory activity in the absence of microtubules: Implication for cell polarity. *J. Cell Biol.* **109,** 1071–1083.

Bouckson-Castaing, V., Moudjou, M., Ferguson, J. P., Mucklow, S., Belkaid, Y., Milon, G., and Crocker, P. R. (1996a). Molecular characterization of Ninein, a new coiled-coil protein of the centrosome that binds spindle microtubules at mitosis. *J. Cell Sci.* **109,** 179–190.

Bouckson-Castaing, V., Tassin, A. M., and Bornens, M. (1996b). Functionnal domains of a new centrosomal protein. *Mol. Biol. Cell Suppl.* **7,** 206a.

Buendia, B., Antony, C., Verde, F., and Karsenti, E. (1990). A centrosomal antigen localized on intermediate filaments and mitotic spindle poles. *J. Cell Sci.* **97,** 259–271.

Burgess, S. A., Carter, D. A., Dover, S. D., and Woolley, D. M. (1991). The inner dynein arm complex: Compatible images from freeze-etch and thin sections methods of microscopy. *J. Cell Sci.* **100,** 319–328.

Calarco-Gillam, P. D., Siebert, M., Hubble, R., Mitchison, T. J., and Kirschner, M. W. (1983). Centrosome development in early mouse embryos as defined by an autoantibody against pericentriolar material. *Cell* **80,** 2926–2930.

Davis, F. M., Tsao, T. Y., Fowler, S. K., and Rao, P. N. (1983). Monoclonal antibodies to mitotic cells. *Proc. Natl. Acad. Sci. USA* **80,** 2926–2930.

Doxsey, S. J., Stein, P., Evans, L., Calarco, P. D., and Kirschner, M. W. (1994). Pericentrin, a highly conserved centrosome protein involved in microtubule organization. *Cell* **76,** 639–650.

Erickson, H. P., and Stoeffer, D. (1996). Protofilaments and rings, two conformations of the tubulin family conserved from bacterial FtsZ to alpha/beta and gamma tubulin. *J. Cell Biol.* **135,** 5–8.

Evans, L., Mitchison, T. J., and Kirschner, M. W. (1985). Influence of the centrosome on the structure of nucleated microtubules. *J. Cell Biol.* **100,** 1185.

Felix, M. A., Antony, C., Wright, M., and Maro, B. (1994). Centrosome assembly *in vitro*: Role of γ-tubulin recruitement in *Xenopus* sperm aster formation. *J. Cell Biol.* **124,** 19–31.

Geisseler, S., Pereira, G., Spang, A., Knop, M., Soues, S., Kilmartin, J., and Schiebel, E. (1996). The spindle pole body component Spc98p interacts with the gamma-tubulin-like Tub4p of *Saccharomyces cerevisiae* at the sites of microtubule attachment. *EMBO J.* **15,** 3899–3911.

Gosti-Testu, F., Marty, M.-C., Berges, J., Maunoury, R., and Bornens, M. (1986). Identification of centrosomal proteins in human lymphoblastic cell line. *EMBO J.* **5,** 2245–2250.

Huang, B. (1990). Genetics and biochemistry of centrosomes and spindle poles. *Curr. Opin. Cell Biol.* **2,** 28–32.

Jasmin, B., Cartaud, J., Bornens, M., and Changeux, J. P. (1989). Golgi apparatus in chick skeletal muscle: Changes in its distribution during end plate development and after denervation. *Proc. Natl. Acad. Sci. USA* **86,** 7218–7222.

Kalt, A., and Schliwa, M. (1993). Molecular components of the centrosome. *Trends Cell Biol.* **3,** 118–128.

Kellogg, D. R., and Alberts, B. M. (1992). Purification of a multiprotein complex containing centrosomal proteins from the *Drosophila* embryo by chromatography with low affinity antibodies. *Mol. Biol. Cell* **3,** 1–11.

Kellogg, D. R., Field, C. M., and Alberts, B. M. (1989). Identification of microtubule-associated proteins in the centrosome, spindle, and kinetochore of the early *Drosophila* embryo. *J. Cell Biol.* **109,** 2977–2991.

Keryer, G., Rios, R. M., Landmark, B. F., Skalhegg, B., Lohmann, S. M., and M. Bornens. (1993). A high-affinity binding protein for the regulatory subunit of cAMP-dependent protein kinase II in the centrosome of human cells. *Exp. Cell Res.* **204,** 230–240.

Khodjakov, A., Cole, R. W., and Rieder, C. L. (1997). A synergy of technologies: Combining laser microsurgery with green fluorescent tagging. *Cell. Motil. Cytoskel.* **38,** 311–317.

Kilmartin, J. V. (1994). Genetic and molecular approaches to spindle function and chromosome segregation in eukaryotic microorganisms. *Curr. Opin. Cell Biol.* **6,** 50–54.

Kilmartin, J. V., and Goh, P. Y. (1996). Spc110p: Assembly properties and role in the connection of nuclear microtubules to the yeast spindle pole body. *EMBO J.* **15,** 4592–4602.

Kilmartin, J. V. *et al.* (1997). Paper presented at the Santa Cruz, CA. Fifth ASCB/EMBO Joint Meeting on Centrosomes and Spindle Pole Bodies, August 23–27, 1997.

Kimble, M., and Kuriyama, R. (1992). Functional components of microtubule-organizing center. *Int. Rev. Cytol.* **136,** 1–50.

Klotz, C., Bordes, N., Laine, M. C., Sandoz, D., and Bornens, M. (1986). A protein of 175,000 daltons associated with striated rootlets in ciliated epithelia, as revealed by a monoclonal antibody. *Cell Motil. Cytoskel.* **6,** 56–67.

Klotz, C., Dabauvale, M. C., Paintrand, M., Weber, V., Bornens, M., and Karsenti, E. (1990). Parthogenesis in *Xenopus* eggs requires centrosomal integrity. *J. Cell Biol.* **110,** 405–415.

Knop, M., and Schiebel, E. (1997). Spc98p and Spc97p of yeast γ-tubulin complex mediate binding to the spindle pole body *via* their interaction with Spc110. *EMBO J.* **16,** 6985–6995.

Kochanski, R. S., and Borisy, G. G. (1990). Mode of centriole duplication and distribution. *J. Cell Biol.* **109,** 1599–1605.

Komesli, S., Tournier, F., Paintrand, M., Margolis, R. L., Job, D., and Bornens, M. (1989). Mass isolation of calf thymus centrosomes: The identification of a specific configuration. *J. Cell Biol.* **109,** 2869–2878.

Kuriyama, R. (1992). Monoclonal antibodies to microtubule-organizing center antigens. *In* "The Centrosome" V. T. Kalnins, (Ed.), pp. 131–165. Academic Press, New York.

Kuriyama, R., and Borisy, G. G. (1985). Identification of molecular components of the centrosphere in the mitotic spindle of sea urchin eggs. *J. Cell Biol.* **101,** 524–530.

Lane, H. A., and Nigg, E. A. (1997). Cell cycle control: Polo-like kinases join the outer circle. *Trends Cell Biol.* **7,** 63–68.

Lange, B. M. H., and Gull, K. (1995). A molecular marker for centriole maturation in the mammalian cell cycle. *J. Cell Biol.* **130,** 919–927.

Lange, B. M. H., and Gull, K. (1996). A structural study of isolated mammalian centrioles using negative staining electron microscopy. *J. Struc. Biol.* **117,** 222–226.

Middendorp, S. (1998). Caractérisation et analyse fonctionnelle des centrines humaines. Thèse de l'université Paris 6.

Middendorp, S., Paoletti, A., Schiebel, E., and Bornens, M. (1997). Identification of a new mammalian centrin gene, more closely related to *Saccharomyces cerevisiae* CDC31 gene. *Proc. Natl. Acad. Sci. USA* **94,** 9141–9146.

Mitchison, T. J., and Kirschner, M. W. (1984). Microtubule assembly nucleated by isolated centrosomes. *Nature* **312,** 232–237.

Moritz, M., Braunfield, M. B., Fung, J. C., Sedat, J. W., and Alberts, B. A. (1995a). Three dimensional characterization of centrosome from early *Drosophila* embryos. *J. Cell Biol.* **130,** 1149–1159.

Moritz, M., Braunfield, M. B., Sedat, J. W., Alberts, B. A., and Agard, D. A. (1995b). Microtubule nucleation by γ-tubulin-containing rings in the centrosome. *Nature* **378,** 638–640.

Moser, M. J., Flory, M. R., and Davis, T. N. (1997). Calmodulin localizes to the spindle pole body of *Schizosacharomyces pombe* and performs an essential function in chromosome segregation. *J. Cell Sci.* **110,** 1805–1812.

Moudjou, M., and Bornens, M. (1992). Method of centrosome a dynamic structure? *Comp. Ren. Acad. Sci. Paris* **315,** 527–534.

Moudjou, M., and Bornens, M. (1998). Method of centrosome isolation from cultured animal cells. *In* "Cell Biology: A Laboratory Handbook" (J. E. Celis, Ed.), vol. 2, 2nd ed., pp. 111–119. Academic Press, London.

Moudjou, M., Paintrand, M., Vigues, B., and Bornens, M. (1991). A human centrosomal protein is immunologically related to basal body-associated proteins from lower eucaryotes and is involved in the nucleation of microtubules. *J. Cell Biol.* **115,** 129–140.

Moudjou, M., Bordes, N., Paintrand, M., and Bornens, M. (1996). γ-Tubulin in mammalian cells: The centrosomal and the cytosolic forms. *J. Cell Sci.* **109,** 875–887.

Oakley, B. R. (1992). γ-Tubulin: The microtubule organizer. *Trends Cell Biol.* **2,** 1–5.

Paintrand, M., Moudjou, M., Delacroix, H., and Bornens, M. (1992). Centrosome organization and centriole architecture: Their sensitivity to divalent cations. *J. Struct. Biol.* **108,** 107–128.

Palazzo, R. E., Vaisberg, E., Cole, R. W., and Rieder, C. (1992). Centriole duplication in lysates of *Spisula solidissima* oocytes. *Science* **256,** 219–221.

Paoletti, A., Moudjou, M., Paintrand, M., Samlisbury, J. L., and Bornens, M. (1996). Most of centrin in animal cells is not centrosome-associated and centrosomal centrin is confined to the distal lumen of centrioles. *J. Cell Sci.* **109,** 3089–3102.

Pereira, G., and Schiebel, E. (1997). Centrosome–microtubule nucleation. *J. Cell Sci.* **110,** 295–300.

Perret, E., Moudjou, M., Geraud, M. L., Derancourt, J., Soyer-Gobillard, M. O., and Bornens, M. (1995). Identification of protein from the hsp70 family constitutively associated with the centrosome from dinoflagellate to human cells. *J. Cell Sci.* **108,** 711–725.

Rout, M. P., and Kilmartin, J. V. (1990). Components of the yeast spindle and spindle pole body. *J. Cell Biol.* **11,** 1913–1927.

Scala, C., Cenacchi, G., Ferrari, C., Pasquinelli, G., Preda, P., and Manara, G. C. (1992). A new acrylic resin formulation: A useful tool for histological, ultrastructural and immunocytochemical investigations. *J. Histochem. Cytochem.* **40,** 1799–1804.

Sluder, G., and Rieder, C. L. (1985). Centriole number and the reproductive capacity of spindle poles. *J. Cell Biol.* **100,** 887–896.

Snyder, M. (1994). The spindle pole body of yeast. *Chromosoma* **103,** 369–380.

Stearns, T., and Kirschner, M. W. (1994). *In vitro* reconstitution of centrosome assembly and function: The central role of γ-tubulin. *Cell* **76,** 623–637.

Stearns, T., Evans, L., and Kirschner, M. (1991). γ-Tubulin is a highly conserved component of the centrosome. *Cell* **65,** 825–836.

Tassin, A. M., Celati, C., Moudjou, M., and Bornens, M. (1998). *J. Cell Biol.* **141,** 689–701.

Tassin, A. M., Celati, C., Paintrand, M., and Bornens, M. (1997). Identification of an Spc110p-related protein in vertebrates. *J. Cell Sci.* **110,** 2533–2545.

Tournier, F., and Bornens, M. (1994). Cell cycle regulation of centrosome function. *In* "Microtubules" (J. Hyams, Ed.), pp. 303–324. Wiley–Liss, New York.

Tournier, F., Karsenti, E., and Bornens, M. (1989). Parthenogenesis in *Xenopus* eggs injected with centrosomes from synchronized human lymphoid cells. *Dev. Biol.* **136,** 321–329.

Tournier, F., Komesli, S., Paintrand, M., Job, D., and Bornens, M. (1991a). The intercentriolar linkage is critical for the ability of heterologous centrosomes to induce parthenogenesis in *Xenopus*. *J. Cell Biol.* **113,** 1361–1369.

Tournier, F., Cyrklaff, M., Karsenti, E., and Bornens, M. (1991b). Centrosome competent for parthenogenesis in *Xenopus* eggs support budding in cell-free extracts. *Proc. Natl. Acad. Sci. USA* **88,** 9929–9933.

Ueda, M., Gräf, R., MacWilliams, H. K., Schliwa, M., and Euteneuer, U. (1997). Centrosome positioning and directionality of cell movements. *Proc. Natl. Acad. Sci. USA* **94,** 9674–9678.

Vogel, J. M., Stearns, T., Rieder, C. L., and Palazzo, R. E. (1997). Centrosomes isolated from *Spisula solidissima* oocytes contain rings and an unusual stochiometric ratio of α/β tubulin. *J. Cell Biol.* **137,** 193–202.

White, R. A., and Salisbury, J. L. (1997). Paper presented at the Fifth ASCB/EMBO Joint Meeting on Centrosomes and Spindle Pole Bodies, August 23–27, Santa Cruz, CA.

Wilson, E. B. (1928). "The Cell in Development and Heredity," 3rd ed. Macmillian, New York.

Zheng, Y., Wong, M. L., Alberts, B., and Mitchison, T. (1995). Nucleation of microtubule assembly by a γ-tubulin-containing ring complex. *Nature* **378,** 578–583.

CHAPTER 3

Isolation of Centrosomes from *Spisula solidissima* Oocytes

Robert E. Palazzo and Jacalyn M. Vogel

Department of Biochemistry, Cell, and Molecular Biology
The University of Kansas
Lawrence, Kansas 66045; and
Marine Biological Laboratory
Woods Hole, Massachusetts 02543

METHODS IN CELL BIOLOGY, VOL. 61

0091-679X/99 $30.00

I. Introduction

Most animal cells contain a single centrosome that functions as the major microtubule organizing center. As such, this organelle is essential for maintaining the organization of cell cytoplasm, and it must duplicate prior to cell division because two centrosomes are required to form the bipolar microtubule array (the mitotic/meiotic apparatus) needed for chromosome segregation. Despite their significance, however, surprisingly little is known about the molecular composition of centrosomes and the mechanisms by which they assemble and duplicate. This lack of information can be ascribed largely to the fact that it has been difficult, until recently, to isolate sufficient quantities of centrosomes for direct biochemical analyses. However, in recent years, methods have been developed for the bulk isolation of centrosomes from a variety of organisms, including mammalian cultured cells (Mitchison and Kirschner, 1984, 1986; Bornens *et al.,* 1987), *Drosophila* embryos (Moritz *et al.,* 1995a), yeast (spindle-pole bodies: Rout and Kilmartin, 1990), and clam oocytes (Vogel *et al.,* 1997). In this chapter we describe methods perfected in our laboratory for the isolation of centrosomes from oocytes of the marine surf clam, *Spisula solidissima.*

A number of unique properties have made marine eggs and embryos long-favored model systems for studies on cell replication. These properties include *e.g.,* (i) the ability to easily isolate large quantities of eggs and oocytes from marine organisms; (ii) the exceptional clarity of marine oocytes which, in turn, allows observation of dynamic structural events in real time; (iii) the rapid rate at which fertilized marine zygotes undergo cell division; (iv) the natural synchrony of division in a large population of fertilized eggs; and, importantly, (v) the fact that the marine oocytes are often naturally arrested at a specific point in the cell cycle until fertilized or artificially activated.

The *S. solidissima* oocyte system described here possesses many of these features and has proven useful for the relatively large-scale isolation of centrosomes from one specific time point in the meiotic cycle (Palazzo *et al.,* 1988, 1992; Vogel *et al.,* 1997). The oocytes in *Spisula* are arrested in late prophase of meiosis I and can be easily activated en mass by simply elevating the potassium concentration of the surrounding seawater (Allen, 1953). Once activated, the oocytes proceed synchronously through a number of critical cell cycle events, including centrosome assembly, germinal vesicle (nuclear envelope) breakdown, and assembly of the meiosis I spindle. Remarkably, all these events are completed within *15 min* after oocyte activation. Here we describe methods for preparing lysates and obtaining functional centrosomes from oocytes 4 min after they have been activated. Importantly, these lysates can be stored frozen at −80°C with no apparent loss in the centrosome's ability to organize microtubules into astral arrays. We routinely prepare lysates during the summer months when clams are gravid and store them frozen for experimentation throughout the year.

Centrosomes are isolated from *Spisula* lysates by sucrose density gradient centrifugation using simple step gradients (Vogel *et al.,* 1997) patterned after a

procedure first described by Mitchison and Kirschner (1984, 1986). In this method, individual gradient fractions are tested for centrosome content using a functional reconstitution assay that is based on the ability of centrosomes to nucleate radial (astral) arrays of microtubules when incubated in microtubule protein (tubulin). Because *Spisula* centrosomes are so large (approximately 2 μm diameter; see Vogel *et al.*, 1997), and because their microtubule nucleation potential is so high, the asters formed in association with *Spisula* centrosomes are highly birefringent. As a result, their presence and numbers can be easily monitored in eggs and lysates, and also during various stages of the isolation procedure, with a relatively inexpensive polarized light microscope equipped with a 100-W, or preferably a 200-W, mercury arc lamp for a light source (Optiquip, Inc., Highland Mills, NY).

II. Obtaining Organisms

In our laboratory we use the surf clam (*S. solidissima*) to obtain centrosomes and centrosome-containing lysates. By contrast, we normally use oocytes from the sea urchin (*Strongylocentrotus purpuratus*) to obtain the tubulin that we will subsequently use to assay for centrosomes during various stages in the preparation of *Spisula* centrosomes.

Surf clams are found along the northeastern coast of the United States. These organisms are commercially fished from the coast of New Foundland, Canada, down to the northern coast of North Carolina. Clams are found on sandy bottoms in shallow water and can be collected at low tide, or they can be collected by scuba diving in deeper water. Ripe animals can be obtained during the summer from May to September (Schechter, 1941; Allen, 1953). Organisms are collected and maintained in constant-flow seawater aquaria and can be ordered from the Marine Resources Center of the Marine Biological Laboratory, Woods Hole, Massachusetts.

Adult *S. pupuratus* can be obtained from a number of commercial vendors, including Marinus, Inc. (Long Beach, CA). Generally, these organisms are gravid from late November to June. Once received, they can be used immediately or maintained in artificial seawater at 15°C for months before use.

III. Isolation and Activation of *Spisula solidissima* Oocytes

A. Clam Dissection and Preparation of Oocytes

1. Materials and Equipment

4–6 ripe clams
Clam knife (or flat blade spatula)
Filtered seawater or artificial seawater

Cheesecloth
Beakers: 250 ml and 2 or 3 liter
Scissors
Phase-contrast microscope
Polarized light microscope

2. Procedure

The procedures described are patterned after those of Allen (1953) and Costello and Henley (1971).

1. Open clams by inserting the clam knife between the siphon and the overlying clam shell. Cut the adductor muscles by running the blade along the inside of the shell. The bulk of the animal, which lies beneath the gills and contains the gonad, is removed and the sex of the animal determined. To sex the animal, touch the gonad with a clean, rinsed, and wet clam knife. The gametes will quickly spread along the blade of the knife. Oocytes spread as tiny particles which can be distinguished, whereas sperm generally spreads as a creamy substance with no particulate nature. Female gonads are often, but not always, pink in color, whereas male gonads are generally white. Alternatively, animals can be sexed before dissection by inserting a sterile 20-gauge hypodermic needle attached to a syringe near the hinge region of the shell. Drawing fluid with the syringe allows the removal of a small volume of gametes for analysis. Whatever the collection method, accurate sexing can be achieved by removing a small drop of gonadal fluid, dropping it onto a glass slide, and observing with a microscope. Oocytes appear as 55-μm-diameter spheres which contain a large germinal vesicle of approximately 25 μm diameter (Fig. 1A). Sperm appear as phase-dense heads associated with long flagella that swim rapidly through the medium. Once the animal is sexed, female gonads can be dissected by first trimming off the gill tissue and then excising the gonadal tissue such that it falls into a 200-ml beaker. Care should be taken to avoid contamination with liver, intestine, and other components of the gut which lie beneath and in close association with the gonad (Costello and Henley, 1971).

2. Dissected gonads are minced into a slurry with scissors. The slurry is transferred to a 1.0-liter beaker and filtered seawater is added to 500–700 ml. The

Fig. 1 Artificial activation of *Spisula* oocytes. Polarized light microscopy of oocytes. Oocytes arrested at prophase of meiosis I contain a large germinal vesicle (A). Within 8–10 min after treatment with KCl, germinal vesicles break down and two asters are visible in each oocyte (B). By 15 min after KCl activation a meiosis I spindle assembles and migrates to the oocyte cortex by 20–25 min (C). By 35 min after KCl treatment, the spindle disappears and oocytes extrude a polar body indicating the completion of meiosis I (D).

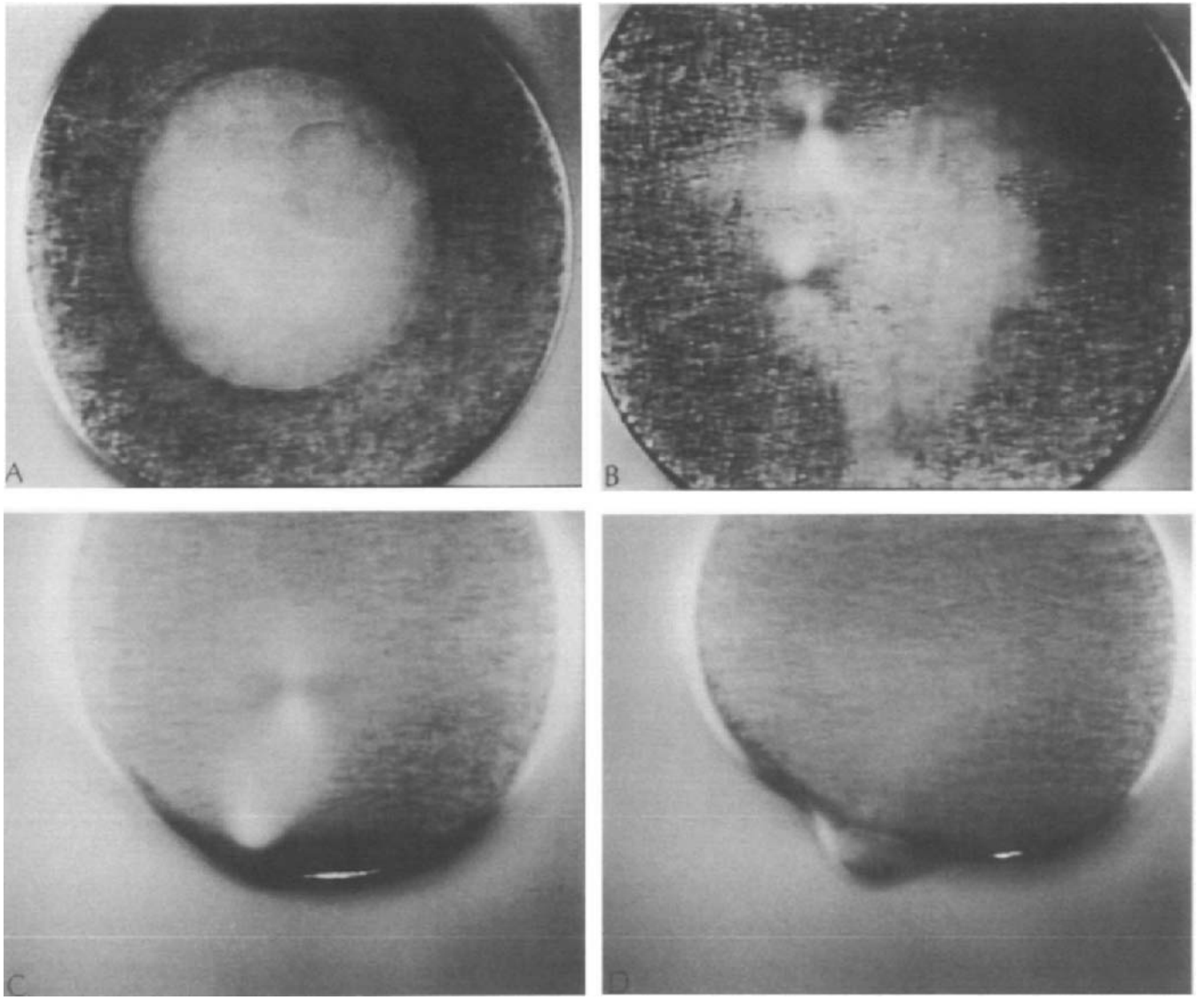
A
B
C
D

suspension is stirred vigorously by hand, and released oocytes are collected by pouring the suspension through several layers of cheesecloth that was previously rinsed with seawater. Oocytes will pass through the cheesecloth and are thus separated from unwanted gonadal tissue. Oocytes will settle out of solution quickly and can be washed by decanting the supernatant and resuspending in filtered seawater. A minimum of three washes by rounds of resuspension and settling are recommended (Allen, 1953).

3. Comments

Depending on the need, gonads can be dissected from a number of females and pooled. As much as 50 ml (approximately 50–70 g) of gonad can be prepared from a single female, which can yield as much as 30–35 g of pure oocytes. However, more typically a single ripe female contains 20–40 g of gonad which yields about 10–20 ml (10–20 g) of unpacked oocytes. The procedures described in this chapter are based on preparations that require 20 ml of packed (1000*g* pelleted) oocytes as starting material. Taking into account seasonal and clam-to-clam variability, this quantity can usually be obtained from the dissection of two to four females.

B. Test for Oocyte Activation

When viewed with a phase-contrast or polarized light microscope, washed, oocytes contain a large germinal vesicle (Fig. 1A). If oocytes do not contain germinal vesicles, they were activated during the dissection and washing procedures. This is rare, but it could result from sperm contamination or from other unknown causes. Thus, it is wise to first observe the oocytes to make certain that more than 99% of them contain germinal vesicles and to test them for a normal activation response before proceeding (Allen, 1953). A simple procedure to test for oocyte activation follows.

1. Materials and Equipment

Oocyte suspension
0.5 *M* KCl stock (room temperature)
Seawater
Polarized light microscope

2. Procedure

1. Resuspend an aliquot of washed oocytes to a final oocyte:seawater concentration of 1–5%. Take 860 μl of this suspension and add 140 μl of 0.5 *M* KCl (Allen, 1953). Shake gently at room temperature (22°C) for 7 or 8 min.

2. Place a drop of the KCl-activated oocyte suspension onto a glass slide and cover with a coverslip lined with silicone grease, or some other support, since the pressure of the coverslip can rupture the oocytes.

3. Observe with a polarized light microscope. Within 8–10 min after activation, the germinal vesicle should begin to break down and disappear [germinal vesicle breakdown (GVBD) (Fig. 1B)]. By 10–12 min after KCl addition, GVBD should have occurred, and two asters should be visible in each oocyte (Fig. 1B). By 15 min, all oocytes should contain a birefringent meiosis I spindle (Fig. 1C). By 30–35 min after activation, spindles disappear and a polar body should form on the surface of each oocyte (Fig. 1D).

3. Comments

For the preparation of lysates, asters, and centrosomes described later, it is necessary only to observe KCl-induced GVBD. However, if the timing of GVBD is asynchronous in the oocyte culture, or if >90% of oocytes do not contain spindles by 15 min after KCl activation, it will likely affect the yield of centrosomes. If oocytes respond to KCl treatment by undergoing GVBD and spindle assembly by 15 min, continue with the preparations.

IV. Preparation of Oocyte Lysates

A. Materials and Equipment

20 ml of oocyte pellets (1000*g* pellet)

Clinical centrifuge

Disposable centrifuge tubes (50 ml)

Filtered seawater or artificial seawater (200 ml)

Graduated cylinders (200 ml and 50 ml)

250-ml beaker

Magnetic stir plate and stir bar

0.5 *M* KCl (28 ml; store at room temperature)

Glycerol/phosphate buffer [1.0 *M* glycerol, 10 m*M* NaH_2PO_4, pH 8.0 (250 ml; store at room temperature)]

Aster buffer [20 m*M* Pipes, 100 m*M* NaCl, 5 m*M* $MgSO_4$, pH 7.2 (200 ml; ice cold)]

p5000 Eppendorf Pipetman

Polycarbonate centrifuge tubes (30–40 ml)

Hexylene glycol (Kodak, Rochester, NY)

Super-speed centrifuge (capable of generating 10,000–39,000*g* forces)

Swinging bucket rotor (e.g., Beckman JS13.1)

Polarized light microscope
Phase-contrast microscope

B. Procedure

Oocyte lysates are prepared by modification of the procedures described by Palazzo *et al.* (1988) and Vogel *et al.* (1997).

1. Oocytes are activated by addition of KCl to a 10% oocyte:seawater suspension. Oocytes are first concentrated into pellets by centrifugation at 1000*g* for approximately 30 sec.

2. Twenty milliliters of oocyte pellet is resuspended to a final volume of 172 ml by adding filtered or artificial seawater. The suspension is transferred to a 250-ml beaker and stirred gently. While stirring, 28 ml of 0.5 *M* KCl is added and the suspension is incubated with continuous stirring at 22°C for 4 min.

3. After the 4-min incubation period, the tough vitelline coat which prohibits oocyte lysis is removed by treating with a buffered solution of glycerol and sodium phosphate (Rebhun and Sharpless, 1964; Palazzo *et al.*, 1988). The 200-ml oocyte : seawater : KCl suspension is aliquoted equally into four 50-ml disposable centrifuge tubes and oocytes are pelleted in a clinical centrifuge at top speed for approximately 30 sec. The supernatant is quickly decanted, and oocyte pellets are resuspended in 8–10 vol of glycerol/phosphate buffer and incubated for a total time of 1.0 min. Removal of the vitelline layer can be observed with a phase-contrast microscope as a phase-dense material that progressively lifts from the surface of the oocytes.

4. After 1-min incubation in the glycerol/phosphate buffer, oocytes are pelleted again with a clinical centrifuge. The supernatant is decanted, and the pellets are quickly resuspended in 8–10 vol of ice-cold aster buffer and quickly centrifuged at top speed with a clinical centrifuge for 30–60 sec. At this point in the preparation, oocytes are delicate and will lyse in aster buffer, so it is crucial that oocytes are resuspended and centrifugation is begun as quickly as possible to minimize the time in aster buffer. It is not unusual to lose the preparation due to oocyte lysis at this step. Once centrifuged into a pellet, oocytes remain stable until lysed by shearing as described below.

5. Following centrifugation, the supernatant is aspirated, leaving a dry oocyte pellet which is placed on ice.

6. Oocytes are lysed by mechanical shearing. Dry oocyte pellets are triturated vigorously on ice using a p5000 Eppendorf Pipetman set at a 3.5-ml volume to avoid suction of the viscous oocyte/lysate pellet into the pipetman. Generally, 50–60 vigorous pumps with the pipetman are needed to lyse oocytes completely. Alternatively, oocytes can be vortexed to lyse the cells, but it is not clear what effect this has on the final yield of centrosomes. Lysis with a pipetman is the preferred method.

7. To clarify lysates, lysed oocyte pellets are pooled into a 30-ml polycarbonate centrifuge tube, triturated again to mix the various batches thoroughly, and centrifuged at 8000–10,000*g* using a swinging bucket rotor at 2–4°C for 15 min. Centrifugation should result in three layers: an upper lipid layer, a clarified middle layer, and a pellet. The clarified middle layer and the lipid layer are collected on ice, and triturated vigorously again to resuspend, and the centrifugation is repeated. If the first centrifugation does not result in separation, then the top 75% of the lysate mixture is collected, triturated, and centrifuged again. Again, centrifugation should result in the separation of the lysate into a pellet, a clarified middle layer, and an overlying lipid layer. The clarified middle layer is collected and kept on ice. Starting with 20 ml of packed oocytes, this preparation generally yields 10–12 ml of clarified lysate.

8. Once collected, the clarified lysate is tested for aster formation. To gauge the number of asters and centrosomes per unit volume of lysate, 48.5 μl of clarified lysate is added to 1.5 μl of hexylene glycol and mixed thoroughly by pipeting. Hexylene glycol at a final concentration of 3% promotes the polymerization of microtubules from microtubule organizing centers and is used to augment the birefringence of asters (Palazzo *et al.*, 1988) such that they are easily detectable with a polarized light microscope (Fig. 3A). After mixing, a small aliquot of the sample is dropped onto a glass slide, covered with a coverslip, warmed to room temperature, and observed with a polarized light microscope. Within 5–7 min after warming, using a 10 or 20× pol lens, bright birefringent asters should be visible (Fig. 3A). Asters can be counted using a standard hemacytometer and the number of asters per unit volume is determined. Although preparations are highly variable, the concentration is generally in the range of 2–4 × 10^6 asters/ml of lysate.

9. Lysates can be used immediately for experiments or aliquoted at desired volumes, snap frozen in liquid nitrogen, and stored at −80°C until further use. Frozen-stored lysates retain the ability to assemble asters for more than 6 years.

V. Preparation of Microtubule Protein

The preparation of microtubule protein is needed to assay sucrose gradient fractions for centrosome content (described later). We use sea urchin microtubule protein, rather than conventional brain tubulin, because it can polymerize into microtubules at room temperature and at significantly lower protein concentrations (Suprenant and Foltz-Dagget, 1995). Similar methods to those described for the preparation of microtubule protein from sea urchin eggs can be used to prepare microtubule protein from clam oocytes and lysates. However, since clam oocytes are a valuable source of centrosomes, we do not normally sacrifice this material for preparation of microtubule protein. Thus, sea urchin egg tubulin serves our purposes well and allows the dedication of clam oocyte materials for centrosome preparations.

A. Materials and Equipment

Sea urchin eggs (*S. purpuratus*; approximately 100 ml of settled eggs) or oocyte lysate (10 ml minimum)

Assembly buffer [100 m*M* Pipes, 4 m*M* EGTA, 1 m*M* $MgSO_4$ (pH 7.2)]

Reassembly buffer [RAB: 100 m*M* Pipes, 1 m*M* EGTA, 5 m*M* $MgSO_4$ (pH 6.9), with GTP added to 2.0 m*M*]

GTP (100 m*M* stock in H_2O; stored at −20°C)

DTT (500 m*M* stock in DMSO; stored at −20°C)

Coomassie Plus Protein Assay Kit (Pierce Chemical, Rockford, IL)

PMSF (100 m*M* stock in DMSO; store at −20°C)

Leupeptin (10 mg/ml stock in H_2O; store at −20°C)

Super-speed centrifuge with rotor (capable of generating 39,000*g* force)

B. Preparation of Sea Urchin Microtubule Protein

Sea urchin microtubule protein is prepared by successive rounds of microtubule assembly/disassembly according to the methods of Suprenant and Marsh (1987). For bulk preparations, generally 100–150 ml of settled sea urchin eggs is used as starting material. Following two cycles of assembly/disassembly, aspirated-dry pellets of twice-cycled microtubule protein are stored at −80°C and further processed as described by Palazzo *et al.* (1991). For final preparation of microtubule protein to be used to assay centrosome content in the procedures described later, twice-cycled pellets are thawed in ice-cold reassembly buffer, triturated into solution, and incubated on ice with intermittent trituration for 30 min. The solution is centrifuged at 39,000*g* at 4°C for 30 min to clarify. The supernatant is collected on ice and the protein concentration determined using a Coomassie Plus Assay Kit. Once the protein concentration is known, the sample is diluted by addition of reassembly buffer to a concentration of 2.0 mg/ml, aliquoted in 0.1 or 0.2 ml volumes, and snap frozen in liquid nitrogen for storage at −80°C. For use in the functional assays described later, aliquots of microtubule protein are thawed on ice, diluted to 0.7 mg/ml with reassembly buffer, and centrifuged at 39,000*g* for 30 min at 4°C to clarify. The supernatants are collected and kept on ice until use.

C. Preparation of *Spisula* Oocyte Microtubule Protein

If necessary, microtubule protein can also be prepared from clam oocyte lysates. Briefly, lysates are thawed on ice and diluted by addition of 0.8 vol of assembly buffer. In addition, DTT, GTP, PMSF, and leupeptin are added to final concentrations of 1.0 m*M*, 1.0 m*M*, 0.2 m*M*, and 10 μg/ml, respectively. The diluted lysate is resuspended on ice by pipeting and centrifuged at 39,000*g* for 30 min at 4°C to clarify. The supernatant is collected and cycled microtubule

protein prepared as previously described by Suprenant and Marsh (1987) for sea urchin preparations (as described previously). Three times-cycled *Spisula* microtubule protein is prepared and aliquoted for use in centrosome isolation procedures as described under Section V,A for the preparation of sea urchin microtubule protein.

VI. Isolation of Centrosomes from Activated Oocyte Lysates

Centrosomes are isolated from lysates by sucrose-density gradient centrifugation. A maximum of six gradients per centrifuge can be run simultaneously. For each gradient described, 2.0 ml of lysate is used. Increasing the volume of lysate per gradient results in lower centrosome yield, probably due to centrosome sticking which distorts the gradient and interferes with separation. Thus, a maximum number of centrosomes can be loaded on gradients for optimum yield. The procedure involves further clarification of lysate, followed by dilution into a large volume of 48% sucrose, loading and centrifugation, collection, and finally the assay of gradient fractions for centrosome content. Isolated centrosome fractions can be used immediately or stored at −80°C for future use. A general outline for centrifugation, fraction collection, and storage is shown in Fig. 2. Samples must be kept cold at all times during the procedure unless otherwise stated.

A. Materials and Equipment

Lysates from activated oocytes (2.0 ml per gradient: generally six gradients are run simultaneously)

Buffer and sucrose stocks

a. PEM buffer [5 m*M* Pipes, 1 m*M* EGTA, 1 m*M* $MgSO_4$ (pH 7.2)]
b. Sucrose stocks: 66, 52.5, and 48% (w/v) in PEM using ultracentrifugation grade or higher purity sucrose. Sucrose concentration is determined by use of hand-held refractometers (Fisher Scientific, Pittsburgh, PA)
c. RAB
d. Aster buffer

Microtubule protein (sea urchin or *Spisula*): diluted to 0.7 mg/ml in RAB

Ultracentrifugation tubes (30 ml)

Ultracentrifuge

Swinging bucket rotor (30-ml centrifuge tube capacity, e.g., Beckman SW28)

Hemacytometer

B. Procedure

1. For each gradient to be run, remove 2.0 ml of lysate is removed from −80°C and thawed on ice. Add 0.6 vol (1.2 ml) of ice-cold aster buffer and mix gently,

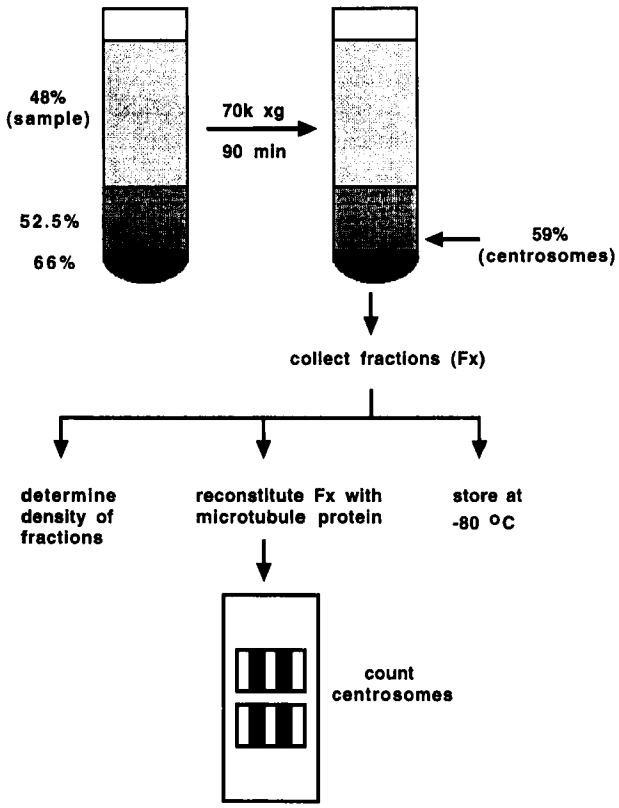

Fig. 2 Schematic representation of centrosome isolation procedure. Sucrose step gradients are used to isolate centrosomes from activated oocyte lysates. Clarified lysate (2.0 ml) is diluted in 48% sucrose buffer (20 ml final volume), loaded onto a gradient consisting of 3.0 ml of 66% sucrose and 5.0 ml of 52.5% sucrose, and centrifuged at 70,000*g* for 90 min at 4°C. Fractions (1.0 ml) are collected from the bottom. Sucrose density of fractions is determined with the use of hand-held refractometers. Centrosomes are recovered in the 58–60% sucrose fraction, which represents the 52.5–66% sucrose interface. Aliquots from fractions are reconstituted with microtubule protein and loaded into a hemacytometer. Asters are then observed and counted with a polarized light microscope. Fractions containing centrosomes are mixed, aliquoted in desired volumes, and snap frozen in liquid nitrogen. Isolated centrosomes can be stored at −80°C with no apparent loss in their ability to nucleate microtubules into astral arrays.

but thoroughly, with a pipetman. Centrifuge at 3300*g* for 10 min at 4°C using a swinging bucket rotor. Centrifugation results in a clarified supernatant and a pellet which varies in size from prep to prep.

2. The supernatant is collected, the volume is determined, and the supernatant is transferred to a 50-ml tube. Two volumes of 66% sucrose is added to the supernatant and the solution is brought to 20 ml final volume by addition of 48% sucrose stock. The solutions are mixed by inverting the tube.

3. Sucrose gradients are set up by transferring 3.0 ml of 66% sucrose to the bottom of a 30-ml ultracentrifuge tube. This step is overlayed with 5 ml of 52.5% sucrose, making certain that a sharp line is maintained at the interface between the two sucrose densities. The 52.5% step is then gently overlayed with the 20-ml sample prepared previously (now 48% sucrose sample). Throughout this procedure it is important to maintain a sharp interface between each sucrose step.

4. The loaded gradients are inserted into the holders of a swinging bucket ultracentrifuge rotor. If necessary, 48% sucrose is added to balance the tubes. The gradients are centrifuged at 70,000*g* for 90 min at 4°C.

5. Sucrose gradient fractions are collected at 4°C, preferably in a cold room. Fractions are collected by piercing the bottom of the gradient-containing centrifuge tube with a 20-gauge syringe needle and 1.0-ml fractions are collected drop by drop in 1.5-ml Eppendorf tubes. Typically, the first 10 fractions are collected, but the centrosomes are usually found in the first 3–6 fractions. To disperse the contents evenly, each fraction is thoroughly mixed with a p1000 pipetman, using pipete tips with a cut end to widen the bore of the tip. The refractive index of each fraction, indicative of the sucrose density, is determined using hand-held refractometers (Fisher Scientific). Gradient fractions are kept on ice at all times.

6. Sucrose gradient fractions are tested for centrosome content using a functional reconstitution assay. In this assay, aliquots of fractions are diluted into tubulin containing media, warmed to room temperature, and mixtures assayed for aster formation using a polarized light microscope (Fig. 3C). The number of asters is indicative of the number of centrosomes present. Thus, by counting the number of asters per unit volume using a hemacytometer (Fig. 3), and taking into account the various dilutions at each step of the assay, one can extrapolate the number of centrosomes/ml in each sucrose gradient fraction. For this procedure 10-μl aliquots are removed from each fraction, mixed with 40 μl of 0.7 mg/ml cycled sea urchin or clam tubulin in reassembly buffer containing 2.0 m*M* GTP, and warmed to room temperature. Aliquots are dropped onto glass slides, covered with coverslips, and observed with a polarized light microscope using a low-power objective (10 or 20×). Within 10–20 min after warming, asters should be visible in samples prepared using the 58–60% sucrose gradient fractions (Fig. 3C). If 1-ml fractions are collected accurately, the major centrosome-containing fraction usually corresponds to fraction No. 3, and sometimes fractions Nos. 3 and 4, from each centrifuge tube (Fig. 3B). Asters may be found in samples corresponding to trailing gradient fractions, but the concentration will be far lower (Fig. 3B). If the gradients are assembled and fractions collected carefully, the peak centrosome-containing fraction will consistently be the 58–60% sucrose fraction (No. 3; Fig. 3B).

7. The number of asters per unit volume is calculated with a hemacytometer observed with a polarized light microscope (Figs. 2 and 3). Although use of the hemacytometer results in a degraded image, because of the high birefringence, asters can still be visualized. The concentration of asters will vary from sample to sample.

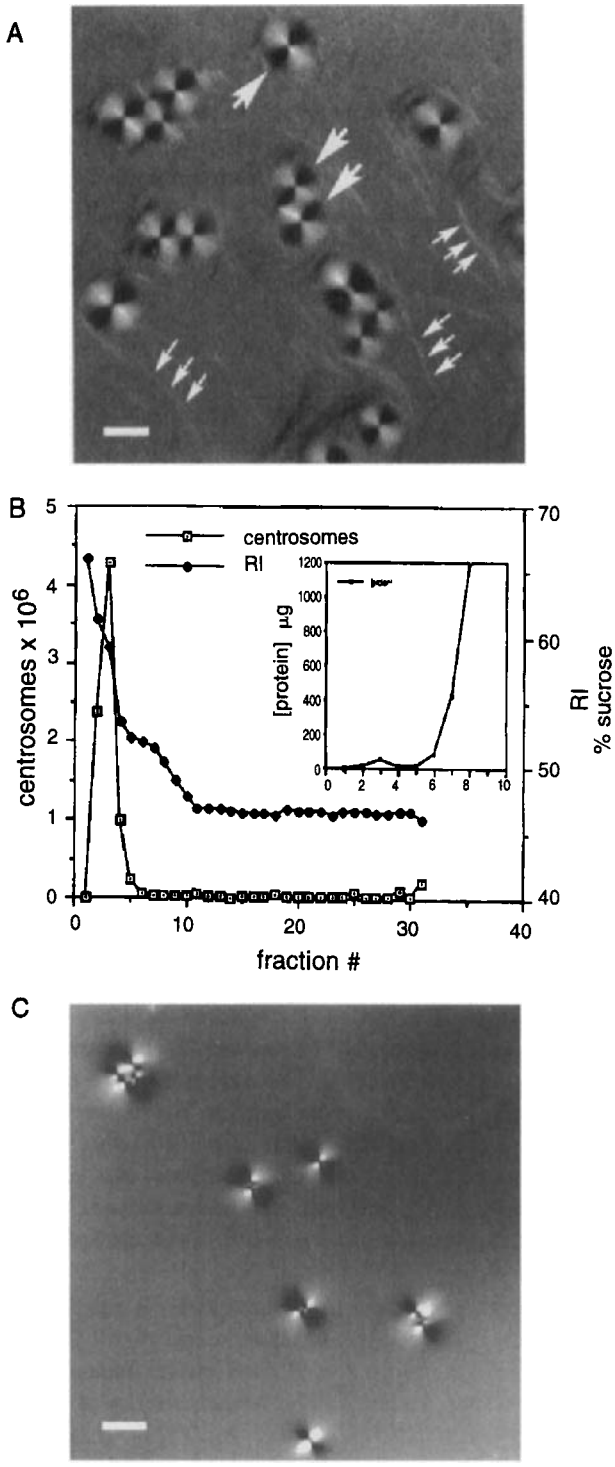
A
B
centrosomes
RI
centrosomes x 10^6
[protein] µg
RI
% sucrose
fraction #
C

8. The peak centrosome-containing fractions obtained from multiple gradients are pooled, mixed gently but thoroughly on ice with a p1000 pipetman, and used immediately. Alternatively, centrosome-containing fractions can be aliquoted in desired volumes, drop frozen in liquid nitrogen, and stored at −80°C. Isolated centrosomes frozen in 55–60% sucrose can be stored at −80°C for years with little or no loss in their ability to nucleate microtubules and assemble asters.

VII. Immunofluorescence of Centrosomes and Asters

The procedures detailed here are adapted from those described by Mitchison and Kirschner (1984, 1986). For a complete description of the design of the modified centrifuge tubes ("spin tubes") used to centrifuge and attach centrosomes and asters to coverslips, see Mitchison and Kirschner (1986). When viewed by immunofluorescence microscopy using anti-tubulin antibodies, *Spisula* asters appear as large radial arrays of microtubules emanating from a defined center (Fig. 4).

A. Preparation of Elvanol Mounting Medium

Elvanol is a mounting medium used to mount coverslips for immunofluorescence analysis. This medium polymerizes and hardens to give a permanent mounting for the sample. In addition, it contains 1,4-diazobicyclo-[2,2,2]-octane (DABCO), which serves to reduce photobleaching and preserves the fluorescent signal. Once prepared, Elvanol is stored at −20°C and can be thawed, aliquots can be removed for use, and the stock can be refrozen many times.

1. Materials

0.2 *M* Tris buffer, pH 6.5 (12 ml)
Polyvinyl alcohol (2.4 g: average MW 30–70 × 10^3)

Fig. 3 Isolation of centrosomes from activated oocyte lysates. Polarized light microscopy of asters assembled in lysates (A) and asters assembled by reconstitution of sucrose density gradient fractions with microtubule protein (C). Lysates prepared from activated oocytes contain an abundance of asters (A). Addition of hexylene glycol to a final concentration of 3% results in augmentation of aster birefringence (large arrows in A). Hexylene glycol treatment also induces the polymerization of microtubules in the background (small arrows in A). Sucrose density gradient fractions are assayed for centrosome content based on their ability to form asters when introduced into media which contains microtubule protein (C). Aster formation correlates with fraction No. 3 (58–60% sucrose) when fractions are collected from the bottom of the gradient (B). Fraction No. 3 contains relatively little protein when compared to other fractions in the gradient (insert in B) indicating an enrichment for centrosome protein. Scale bars = 10 μm.

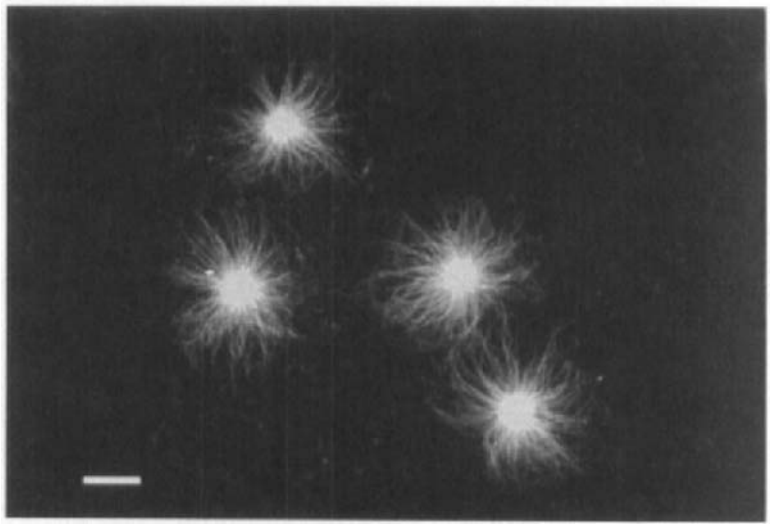

Fig. 4 Immunofluorescence microscopy of asters. Asters, assembled in lysates or in defined media using sucrose gradient fractions which contain centrosomes reconstituted with microtubule protein, are composed of a radial array of microtubules emanating from a dense core. Scale bar = 10 μm.

Glycerol (6.0 g)
H_2O (6.0 ml)
DABCO

2. Procedure

1. Mix and stir the first four ingredients thoroughly (leaving out the DABCO) and incubate for 1 hr at room temperature.
2. Incubate in a water bath at 50°C and continue stirring until all ingredients are dissolved.
3. Clarify the solution by centrifugation at 5000*g* at 22°C for 15 min.
4. Collect the clarified gel–supernatant, add DABCO to 2.5%, and mix into solution.
5. Aliquot as 0.5 ml and store at −20°C.

B. Immunofluorescence of Asters Assembled in Clarified *Spisula* Oocyte Lysate

1. Materials

Spisula oocyte lysate (20 μl per sample)
Aster isolation buffer [AIB: 20 m*M* MES, 1.0 m*M* EGTA, 1.0 m*M* $MgSO_4$, (pH 6.5), 1.0% Triton-X 100 or NP-40]

Fixation solution (AIB buffer containing 1% glutaraldehyde)

Phosphate-buffered saline (PBS)

30% glycerol in PBS

Polylysine–coated 22-mm round coverslips (Bellco Glass, Inc., Vineland, NJ)

Spin tubes (centrifuge tubes prepared and assembled according to the methods of Mitchison and Kirschner, 1986)

Methanol at −20°C

Reducing solution [$NaBH_4$ (10 mg/ml in PBS)]

PBS/bovine serum albumin (BSA) solution (5% BSA in PBS. Carnation nonfat dry milk can be used as an inexpensive substitute for BSA)

Mouse anti-tubulin primary antibody (DMIB, Sigma)

Rhodamine- or florescein-conjugated rabbit anti-mouse secondary antibody

Elvanol mounting medium

Clean glass slides

Superspeed centrifuge and swinging bucket rotor (capable of 12,000*g* forces, e.g., Beckman JS13.1 rotor)

Fluorescence microscope

2. Procedure

1. Remove lysate from −80°C and thaw on ice. For each sample to be prepared for immunofluorescence, incubate 20 μl of lysate at 24°C for 5 min.

2. Dilute the sample by addition of 180 μl of aster isolation buffer rapidly followed by the addition of 3.0 ml of fixation solution. Incubate at room temperature for 3–5 min and then transfer to ice for an additional 10 min.

3. Assemble spin tubes mounted with polylysine-coated coverslips (Mitchison and Kirschner, 1986). Adhere the coverslip to mount with a drop of PBS, drop the coverslip–mount assembly into the spin tube, and overlay with 2.0 ml of 30% glycerol in PBS. Overlay the 30% glycerol cushion with 1.5 ml of fixed sample.

4. Centrifuge at 12,000*g* using a swinging bucket rotor for 15 min at 22°C.

5. Remove coverslips from the spin tubes (Mitchison and Kirschner, 1984, 1986), transfer into methanol at −20°C, and incubate for 5–10 min. Be certain to keep track of the sample side of the coverslip so that the following treatments are all done on the sample side rather than the back of the coverslip.

6. Transfer the coverslip to PBS and wash three times by exchange of PBS solutions. For this purpose, a series of 1-ml drops of PBS are dropped onto a flattened sheet of Parafilm. This allows washing by simply transferring coverslips from one drop to another.

7. Transfer each coverslip to a 2- or 3-ml drop of reducing solution on Parafilm. Incubate for 10–15 min, occasionally tapping the coverslip with forceps to release

bubbles that form on the surface. Remember which side of the coverslip the sample is on.

8. Wash three times with PBS and incubate in blocking solution (PBS/5% BSA) for 20–30 min.

9. Place a 20-μl drop of blocking solution containing the appropriate dilution of primary antibody (e.g., DMIB mouse anti-β-tubulin) onto a flattened sheet of Parafilm. Invert the coverslip, sample side down, onto the drop allowing the antibody solution to spread under the coverslip. Incubate for 30 min at room temperature.

10. Again, wash three times with PBS and invert the coverslip onto a 20-μl drop of secondary antibody solution. Incubate for 30 min at room temperature.

11. Wash five times with PBS, and incubate in the last wash while preparing to mount the coverslip.

12. To mount the coverslip, place a drop of Elvanol (20–30 μl) onto the center of a clean glass slide. Remove the coverslip from the final PBS wash, drain the remaining solution by touching the edge of the coverslip with a paper towel or Kimwipe, and gently lower the coverslip, sample-side down, onto the Elvanol while allowing the Elvanol to slowly spread under the coverslip. Doing this slowly and carefully avoids the formation of air bubbles under the coverslip.

13. Incubate the mounted sample at room temperature, in the dark, overnight to harden the Elvanol. After the Elvanol has hardened samples can be stored in the dark at 4°C. Observe samples with a fluorescent microscope.

C. Immunofluorescence of Asters Reconstituted *in Vitro*

1. For each sample coverslip to be prepared, remove 10 μl of sucrose gradient purified centrosomes and 40 μl of sea urchin (or clam) microtubule protein from −80°C (see section V) and thaw on ice.

2. Dilute the microtubule protein to 0.5 mg/ml by adding reassembly buffer containing 2.0 m*M* GTP.

3. Mix 10 μl of the sucrose gradient fraction with 10 μl of diluted microtubule protein and incubate at room temperature for 20–30 min.

4. Dilute the sample with 3.0 ml of fixation solution and incubate for 3–5 min at room temperature and an additional 10 min on ice.

5. Follow precisely steps 3–13 in (Section VII,B,2).

VIII. Electron Microscopy of Asters and Centrosomes

1. Prepare, fix, and pellet asters and centrosomes:

a. For preparation of asters from clarified oocyte lysates, warm 100 μl of thawed lysate to room temperature, dilute into aster isolation buffer, and fix

with glutaraldehyde as previously described (see Section VII,B). Centrifuge at 1000–3000*g* for 10 min at room temperature, aspirate supernatant, and proceed, beginning with step 2 below.

b. For preparation of asters reconstituted *in vitro,* mix 100 μl of centrosome fraction with 400 μl of microtubule protein, incubate for 30 min at room temperature, and fix with glutaraldehyde as described under Section VII,C (steps 1–4). Centrifuge at 1000–3000*g* for 10 min, aspirate supernatant, and proceed, beginning with step 2 below.

c. For preparation of isolated centrosomes, take the peak sucrose gradient fractions (58–60% gradient fraction; see Section VI,B steps 4–7) and dilute into 2 vol of PEM buffer containing 1% glutaraldehyde (final concentration). Incubate samples for 3–5 min at room temperature and an additional 10 min on ice. Concentrate centrosomes into a loose pellet by centrifugation at 70,000*g* for 30 min at 4°C. Carefully remove the supernatant so as to leave the pellet, which may not be visible, at the bottom of the centrifuge tube. While aspirating, leave a little fluid covering the bottom of the tube to be certain that the pellet is not removed. Often the centrosome pellet is invisible at this point. Proceed, beginning with step 2.

2. To the pellets carefully add a small volume of 1% OsO_4:H_2O to postfix, and incubate on ice for 10–30 min.

3. Remove the OsO_4, dehydrate, embed, section, and analyze as previously described (Palazzo *et al.,* 1988, 1992; Rieder *et al.,* 1985).

A. Comments

When analyzed by electron microscopy, asters assembled in lysates or those assembled using isolated centrosomes reconstituted with microtubule protein all contain a single centriole surrounded by pericentriolar material (Palazzo *et al.,* 1988, 1992). Electron microscope (EM) analysis of isolated centrosomes revealed that centrosomes isolated from oocytes as described are very homogeneous (Vogel *et al.,* 1997). Each centrosome is approximately 2 μm in diameter and composed of a single centriole surrounded by dense pericentriolar material (Fig. 5). Intermediate voltage EM tomography studies of these preparations have revealed that the pericentriolar material is studded with 25-nm diameter "ring" structures (Vogel *et al.,* 1997) first identified in isolated *Drosophila* centrosomes and thought to be required for microtubule nucleation (Moritz *et al.,* 1995b).

IX. Summary

We have described methods for the preparation of lysates and isolation of centrosomes from parthenogenetically activated oocytes of the surf clam, *S. solidissima.* Although oocyte availability is seasonal, between June and August

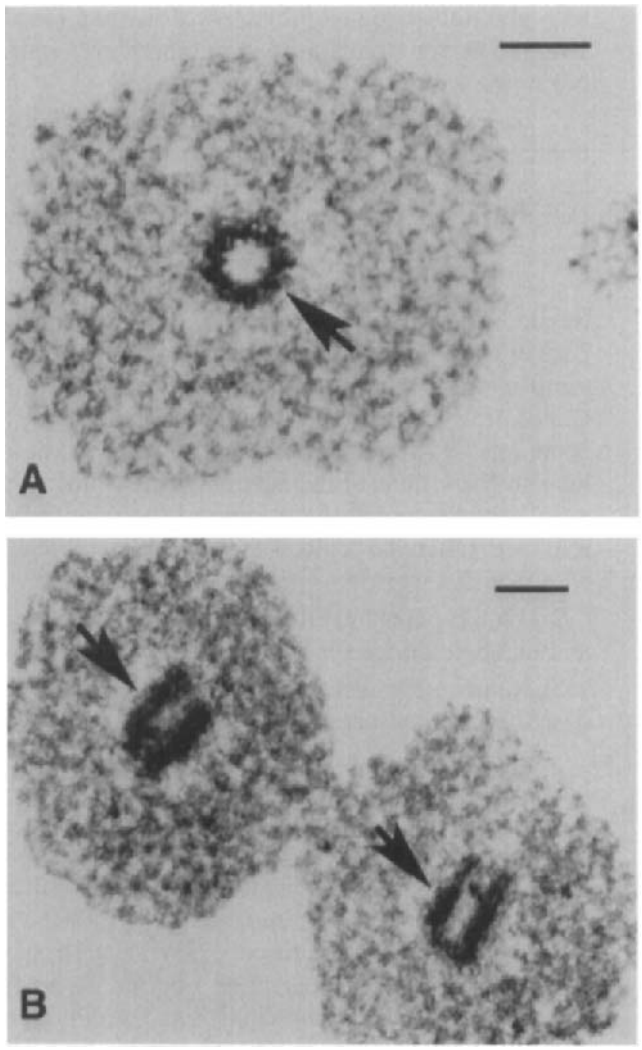

Fig. 5 High-voltage electron microscopy (HVEM) of 25-μm-thick sections through isolated *Spisula* centrosomes reveals that each is composed of a single centriole (arrows) which is surrounded by an extensive cloud of pericentriolar material. (A) Cross section and (B) lateral section through centrioles. Scale bars = 0.2 μm.

as much as 2 liters of lysate can be generated by a single person. Since lysate can be stored frozen at −80°C with no apparent loss in centrosome-dependent microtubule nucleation, this is a convenient system for year-round experimentation. On average, per milliliter of frozen-stored lysate, 2 or 3 $\times$ 10^6 centrosomes can be obtained at 3000- or 4000-fold purification by sucrose-density gradient centrifugation. Centrosome fractions typically contain 6.0 $\times$ 10^{-12} g of protein

per centrosome (Vogel *et al.*, 1997) and 140–200 μg of protein is usually obtained from a single run involving six sucrose-density gradients (12 ml of lysate). One person can easily run three preparations in a day, and thus 420–600 μg of centrosome protein could be prepared daily. Therefore, based on the effort of one individual, as much as 20–40 mg of centrosome protein could be prepared per year. Another convenient feature of the system is that once centrosomes are isolated, they can be stored in high sucrose media at −80°C for years with little or no loss in microtubule nucleation potential.

Once isolated, centrosomes can be used for protein analysis, ultrastructural studies, or in functional reconstitution assays (Vogel, 1997). In addition, these preparations offer the isolation of sufficient quantities of centrosome proteins to be used as antigens for generating centrosome-specific antibodies or for obtaining protein sequence for the purpose of antibody production or the design of oligonucleotide primers for isolating cDNA fragments coding for centrosome proteins. Thus, the preparations described offer a biochemical approach for defining centrosome composition. The methods described for immunofluorescence analysis of asters assembled in lysates offer rapid and convenient preparations for screening antibodies for centrosome localization and specificity. Finally, the ability to prepare large quantities of homogeneous centrosomes should enhance ultrastructural studies since many centrosomes can be sectioned and analyzed simultaneously by EM, avoiding the problem of having to hunt through sections of single cells to find a single centrosome for analysis. In addition, colloidal gold localization studies, using antibodies and EM to pinpoint the relative location of individual proteins, could be carried out on populations of centrosomes in the same preparation simultaneously, thus drastically expanding the quantity of data gathered.

In conclusion, the clam oocyte system described here offers the potential for a combined structural and biochemical approach for identification of novel centrosome proteins and elucidation of the molecular basis of microtubule nucleation, centrosome assembly, and centrosome function.

Acknowledgments

The authors thank Dr. Raymond Stephens for his advice, support, and encouragement during the development of these procedures. In addition, we thank Clay Lyddane, G. Osorio, and Xingyong Wu for assistance with centrosome preparations, EM, fluorescence microscopy, and manuscript preparation. Special thanks to Dr. Conly Rieder and the Wadsworth Center for continuous support and collaborations which made the structural analysis of centrosomes possible. This work was supported in part by National Institutes of Health Grant NIH-GM43264, The American Cancer Society Grant JFRA-314, and the Robert Day Allen Fellowship of the Marine Biological Laboratory (R. E. Palazzo), the Ida Hyde Scholarship (J. M. Vogel), NIH Grant GM40198 (C. L. Rieder), and National Science Foundation Grants BIR 9219043 and RR 01219 awarded by the Biomedical Research Technology Program, National Center for Research Resources (Department of Health and Human Resources/Public Health Service) to support the Wadsworth Center's Biological Microscopy and Image Reconstruction Facility as a National Biotechnological Resource.

References

Allen, R. D. (1953). Fertilization and artificial activation in the egg of the surf clam *Spisula solidissima*. *Biol. Bull.* **105,** 213–219.

Bornens, M., Paintrand, M., Berges, J., Marty, M. C., and Karsenti, E. (1987). Structural and chemical characterization of isolated centrosomes. *Cell Motil. Cytoskel.* **8,** 238–249.

Costello, D. P., and Henley, C. (1971). "Methods for Obtaining and Handling Marine Eggs and Embryos." Marine Biological Laboratory, Woods Hole, MA.

Mitchison, T. J., and Kirschner, M. (1984). Microtubule assembly nucleated by isolated centrosomes. *Nature* (*London*) **312,** 232–237.

Mitchison, T. J., and Kirschner, M. (1986). Isolation of mammalian centrosomes. *Methods Enzymol.* **134,** 261–268.

Moritz, M., Braunfield, M. B., Fung, J. C., Sedat, J. W., Alberts, B. M., and Agard, D. A. (1995a). Three-dimensional structural characterization of centrosomes from early *Drosophila* embryos. *J. Cell Biol.* **130,** 1149–1159.

Moritz, M., Braunfield, M. B., Sedat, J. W., Alberts, B. M., and Agard, D. A. (1995b). Microtubule nucleation by γ-tubulin containing rings in the centrosome. *Nature* (*London*) **378,** 638–640.

Palazzo, R. E., Brawley, J. B., and Rebhun, L. I. (1988). Spontaneous aster formation in cytoplasmic extracts from eggs of the surf clam. *Zool. Sci.* (*Tokyo*) **5,** 603–611.

Palazzo, R. E., Lutz, D. A., and Rebhun, L. I. (1991). Reactivation of isolated mitotic apparatus: Metaphase versus anaphase spindles. *Cell. Motil. Cytoskel.* **18,** 304–318.

Palazzo, R. E., Vaisberg, E., Cole, R. W., and Rieder, C. L. (1992). Centriole duplication in lysates of *Spisula solidissima* oocytes. *Science* (*Washington, DC*) **256,** 219–221.

Rebhun, L. I., and Sharpless, T. K. (1964). Isolation of spindles from the surf clam *Spisula solidissima*. *J. Cell Biol.* **22,** 488–491.

Rieder, C. L., Rupp, G., and Bowser, S. S. (1985). Electron microscopy of semithick sections: Advantages for biomedical research. *J. Electron Microsc. Technol.* **2,** 11–28.

Rout, M. P., and Kilmartin, J. V. (1990). Components of the yeast spindle and spindle pole body. *J. Cell. Biol.* **111,** 1913–1927.

Schechter, V. (1941). Experimental studies upon the egg cells of the clam, *Mactra solidissima,* with special reference to longevity. *J. Exp. Zool.* **86,** 461–477.

Suprenant, K. A., and Foltz-Dagget, M. A. (1995). Sea urchin microtubules. *Curr. Topics Dev. Biol.* **31,** 65–99.

Suprenant, K. A., and Marsh, J. C. (1987). Temperature and pH govern the self-assembly of microtubules from unfertilized sea urchin egg extracts. *J. Cell. Sci.* **87,** 71–84.

Vogel, J. M., Stearns, T., Rieder, C. L., and Palazzo, R. E. (1997). Centrosomes isolated from *Spisula solidissima* oocytes contain rings and an unusual stoichiometric ratio of α/β tubulin. *J. Cell Biol.* **137,** 193–202.

CHAPTER 4

Methods for *in Situ* Localization of Proteins and DNA in the Centromere–Kinetochore Complex

A. Van Hooser and William R. Brinkley

Department of Cell Biology
Baylor College of Medicine
Houston, Texas 77030

I. Introduction

Centromeres are heterochromatin-rich loci located at the primary constriction of most eukaryotic chromosomes. These complex arrays of DNA and protein

METHODS IN CELL BIOLOGY, VOL. 61

0091-679X/99 $30.00

are essential for sister chromatid attachment, kinetochore organization, and chromosome movement on spindles during mitosis and meiosis (Brinkley *et al.*, 1992). Recent molecular studies indicate that the greater centromere or centromere–kinetochore complex (Zinkowski *et al.*, 1991) may be involved in a variety of more subtle mitotic functions, including the signaling and integration of complex chromosome behavior on the mitotic spindle (Gorbsky, 1997; Sullivan, 1998). Recently, we demonstrated that the centromere is a principal site for the initiation of chromosome condensation at the onset of mitosis (He and Brinkley, 1996; Hendzel *et al.*, 1997).

Centromeres were long known as impenetrable "black boxes" on chromosomes that defied structural and molecular analysis due to the lack of reagents available to detect specific DNA sequences or proteins within the region. Although the centromere stains intensely with some chromatin dyes, a Giemsa staining technique called C-banding, described by Pardue and Gall (1970), provided the first specific information on DNA composition. C-banding takes advantage of the highly compact, repetitive nature of DNA contained within most eukaryotic centromeres. Its specificity is thought to depend on the differential denaturation and renaturation properties of DNA in methanol–acetic acid-fixed chromosome preparations. The highly repetitive base sequences composing centromeric DNA will anneal more rapidly after denaturation and subsequently stain more intensely with Giemsa than the nonrepetitive DNA of other chromosomal regions (Waring and Britten, 1966; Britten and Kohne, 1968; Mace *et al.*, 1972).

Electron microscopy first opened the door for structural analysis of the centromere, revealing a trilaminar plate-like structure at the kinetochore of most eukaryotic chromosomes. Thin sections of cells fixed in glutaraldehyde and osmium revealed a dense outer plate, a lightly stained middle layer, and a dense inner layer juxtaposed to the centromeric chromatin (Brinkley and Stubblefield, 1966; Jokelainen, 1967). A prominent "fuzzy coat" or corona exists along the surface of the outer plate, to which microtubules become attached at prometaphase. Although very little was known of the molecular composition of the centromere–kinetochore complex, early studies suggested that the structure was largely proteinaceous. Tubulin was found to be associated with the kinetochore (Pepper and Brinkley, 1977), and ribonucleoprotein was detected using Bernard's uranyl acetate–EDTA staining procedure (Rieder, 1979a,b).

The technique of indirect immunofluorescence ushered in the era of immunocytochemistry and opened the way for *in situ* localization of both rare and common proteins in eukaryotic cells. Still in widespread use, this procedure was of historical significance in the characterization of the cytoskeleton and mitotic apparatus (Lazarides and Weber, 1974; Fuller *et al.*, 1975; Brinkley *et al.*, 1975). Indirect immunofluorescence was first used effectively to detect centromeres of eukaryotic chromosomes by Tan and coworkers (Moroi *et al.*, 1980) following their important discovery of human autoantibodies in the serum of patients with the CREST (calcinosis, Raynaud's phenomenon, esophageal dysmotility, sclerodactyly, and telangiectasia) variant of scleroderma. Their studies clearly showed discrete

CREST staining in the centromeres of human metaphase chromosomes and identified centromeric domains in interphase nuclei (Fig. 1, see color plate). Subsequently, Brenner *et al.* (1981) demonstrated specific staining along the surface of the centromere and concluded that CREST antiserum recognized a zone that corresponded to the kinetochore in PtK1 rat kangaroo cells. These investigators further demonstrated a direct correlation between the number of fluorescent spots in the interphase nuclei and the diploid chromosome number. Using CREST staining in combination with BrdU labeling, they showed that the fluorescent spots doubled during the late stages of S phase, concomitant with the replication of centromeric DNA. The centromere, once accentuated only by primitive, nonspecific staining reagents, was opened to structural and molecular analysis by the discovery of scleroderma CREST antiserum. In the following sections, we describe the most commonly used methods for centromere/kinetochore analysis using this antiserum.

II. *In Situ* Localization of Proteins: Indirect Immunofluorescence

The techniques of indirect immunofluorescence are established, reliable, and relatively easy to accomplish. The only specialized equipment needed is an epifluorescence microscope, equipped with an appropriate set of quartz objectives, exciter and barrier filters, and a standard or digital camera for photomicroscopy. Of course, the more advanced digital equipment one can access, such as cooled charge couple device color cameras, confocal or deconvolution microscopes, and image analysis software, dye sublimation printers, the greater the latitude of image acquisition. The procedures described in the following section have been used by our laboratory for many years and give consistently reliable results.

A. Collection, Titering, and Storage of CREST Antisera

The most available source of human autoantisera can be found in patients treated in rheumatism and arthritis clinics. We were successful in collecting CREST autoantiserum from blood samples of patients admitted to the Comprehensive Arthritis Center at University Hospital, University of Alabama at Birmingham, as well as from arthritis patients of physicians at Baylor College of Medicine. Although anti-centromere autoantibodies are most frequently found in the serum of patients with the CREST variant of scleroderma (Moroi *et al.*, 1980), autoantibodies are also found in some patients with Raynaud's phenomenon. Before collecting blood samples, it is necessary to solicit the participation of the physician in charge and to complete all patient consent forms and other legal documents required by the hospital and/or granting agency. The physicians or their appointees collect blood samples from arm veinipuncture, and the sam-

ples are allowed to sit at room temperature (RT) overnight to facilitate clotting. Subsequently, the plasma is removed with a small syringe or carefully decanted into conical tubes for storage at −80°C until use. The antiserum should be titered by dilution in TBS-T (see buffered solutions in Section II,E). We have obtained best results with CREST antiserum diluted 1:500 to 1:1000, but even greater dilutions may be possible with some antisera. Testing is done by indirect immunofluorescence using tissue culture cells, as described in Section II,E. The titer that gives crisp centromere staining with minimal background is selected.

B. Cell Culture Conditions

We use a variety of mammalian tissue culture cells in our studies. For *in situ* staining, cells are maintained in a humidified 37°C incubator with a 5% CO_2 atmosphere. Cell cultures are grown in any number of suitable culture media. We have used the following with excellent results: McCoy's 5A (Gibco Laboratories, Grand Island, NY) medium supplemented with 10% CPSR-4 (Sigma Chemical Co., St. Louis, MO), Ham's F-10 medium supplemented with 15% FBS (Gibco Laboratories), DMEM supplemented with 10% FBS (Gibco Laboratories), and OptiMEM supplemented with 4% FBS (Gibco Laboratories). All growth media are supplemented with 1% penicillin and 1% streptomycin (Gibco Laboratories). Almost every laboratory has slightly modified conditions for cell culture. The main requirement for centromere/kinetochore staining is that the cell monolayers are contiguous, not overgrown or overlapping, and remain reasonably flat. If you wish to observe mitotic cells, it is, of course, essential to select growth conditions that favor cells entering mitosis. Cultures should be given fresh medium the day prior to harvest. For some experiments, it may be necessary to add a mitotic inhibitor, such as 0.1 μg/ml Colcemid (Gibco Laboratories) or 0.1 μg/ml nocodazole (Sigma Chemical Co.), to arrest cells in mitosis.

C. Mitotic Shake-Off

Tissue culture cells tend to round during mitosis. Cells arrested with mitotic inhibitors can be selectively detached from cell monolayers by lightly tapping the sides of tissue culture flasks. Detached cells are then pelleted in a centrifuge at 1000*g* for 5 min, resuspended in PBS (0.14 *M* NaCl, 2.5 m*M* KCl, 8 m*M* Na_2HPO_4, 1.6 m*M* KH_2PO_4, pH 7.4), and pelleted a second time. When experiments call for the collection of cells that have not been exposed to arresting agents, mitotic cells can be selectively detached by lightly tapping the tissue culture flask during brief, sequential rinses in PBS and 0.03% EDTA in Puck's saline. Both rinses are added to the aspirated medium in a conical tube and pelleted in a centrifuge at 1000*g* for 5 min. At this point, cells may be swollen briefly (<15 min) in hypotonic solution (75 m*M* KCl containing multiple protease inhibitors) at 37°C to improve the visualization of metaphase chromosomes (Fig. 2, see color plate).

D. Cytocentrifugation

It is often necessary to carry out immunofluorescence on cells that have been detached from monolayers or grown in suspensions, rounded cells such as blood samples, or lysed cell extracts. Cytocentrifugation flattens cells onto coverslips and enables one to obtain improved images of objects such as chromosomes and mitotic spindles. We have obtained excellent results with a Cytospin 3 cytocentrifuge (Shandon Instruments, Inc., Pittsburgh, PA). Cell pellets are resuspended in 1 or 2 ml of PBS (see Section II,E) providing a final concentration of about 1×10^6 cells per milliliter. It may be necessary to adjust the concentration of cells or cell extract so as to obtain a thin monolayer without overcrowding or piling up objects on the slide. Approximately 100 μl of the cell suspension is pipetted into a cytocentrifuge cup and spun through an aperture in a porous card onto acid-etched and/or poly-amino acid-coated coverslips at speeds from 800 to 2000 rpm for 2 min. The coverslips are then removed and immediately processed, as described later. If cytocentrifuged material tends to wash off during the immunostaining process, the preparation may be coated with a thin layer of parlodian or colloidin before processing. However, this is usually not necessary when using etched, poly-amino acid-coated slides or coverslips.

E. Staining of Cell Monolayers

Reagents

1. Buffered solutions: The amount of each reagent needed will vary, depending on whether you use 13-mm round coverslips in 24-well trays (250 μl per well), 11 × 22-mm coverslips in small Coplin jars (5 ml per jar), 75 × 25-mm glass slides in large Coplin jars (50 ml per jar), etc.

   PBS (0.14 *M* NaCl, 2.5 m*M* KCl, 8 m*M* Na_2HPO_4, 1.6 m*M* KH_2PO_4, pH 7.4).

   PEM [80 m*M* K-PIPES (pH 6.8), 5 m*M* EGTA (pH 7.0), 2 m*M* $MgCl_2$].

   TBS-T [20 m*M* Tris–HCl, (pH 7.6), 137 m*M* NaCl, 0.1% Tween-20].

2. Permeabilization solution

   0.5% Triton X-100 in PEM: To preserve the cytoskeleton and nuclear matrix while extracting soluble proteins, we recommend the use of 0.5% Triton X-100 in CSK [10 m*M* PIPES (pH 6.8), 100 m*M* NaCl, 300 m*M* sucrose, 3 m*M* $MgCl_2$, 1 m*M* EGTA] containing 4 m*M* vanadryl riboside complex (VRC) and multiple protease inhibitors [1.2 m*M* phenylmethylsulfonyl fluoride (PMSF), and 1 μg/ml each of aprotinin, leupeptin, antipain, and pepstatin]. Prepare immediately before use and keep on ice. Make a 1:20 dilution of 10% stock Triton X-100.

3. Fixative

   3.7% formaldehyde, diluted in PEM from 16% ultrapure electron microscope (EM)-grade formaldehyde (Polysciences, Inc., Warrington, PA) or freshly prepared from paraformaldehyde.

4. Blocking agent

   5 g dry milk per 100 ml of TBS-T.

5. Antibodies

   CREST antisera is diluted 1:500 to 1:1000 in TBS-T.

   Fluorophore-conjugated anti-human IgG(H+L) secondary antibodies (Pierce Chemicals) are diluted 1:500 in TBS-T.

6. Counterstains

   DNA is counterstained with 0.1 μg/ml 4′,6-diamidino-2-phenylin-dole (DAPI), 0.5 μg/ml propidium iodide, 1 μg/ml Hoechst 33258, or 10 μg/ml ethidium bromide, diluted in 1 × TBS-T.

Protocol

1. Cells are grown on or cytospun (800 rpm, 2 min) onto acid-etched and/or poly-amino acid-coated glass coverslips.

2. Transfer coverslips to a multiwell tissue culture tray or to Coplin jars containing cold PBS. Keep on ice.

3. Rinse coverslips with cold PEM.

4. To better visualize chromosomes and centromeres, soluble proteins may be extracted prior to fixation with 0.5% Triton X-100 in PEM or CSK (see above) for 2 min at 4°C. This step is omitted for whole cell preparations. Rinse cells briefly in fresh, cold PEM.

5. Preparations are fixed in 3.7% formaldehyde in PEM for 40 min at 4°C.

6. Rinse coverslips three times in PEM, 5 min each while on rotator.

7. Whole cell preparations are permeabilized postfixation with 0.5% Triton X-100 in PEM for 30 min at RT. This step is optional if cells were extracted prior to fixation. Some cells require more permeabilization than do others. Rinse cells three times in PEM for 2 min.

8. Incubate samples in 5% milk in TBS-T for at least 30 min at RT or overnight at 4°C to block nonspecific staining.

9. Without rinsing, incubate primary antibodies, diluted in TBS-T, on preparations for 30–60 min at 37°C in a humid chamber.

10. The samples are then rinsed three times in TBS-T for 5 min each.

11. Block in 5% milk and TBS-T for 10 min at RT. Do not rinse.

12. Protect samples from light during all remaining steps. Fluorophore-conjugated secondary antibodies (see Section II,F), diluted in TBS-T, are incubated with samples for 30–60 min at 37°C in a humid chamber.

13. The samples are then rinsed three times in TBS-T for 5 min at RT.

14. DNA is counterstained with DAPI, propidium iodide, Hoechst 33258, or ethidium bromide for 15–45 sec at RT.

15. Rinse samples three times in TBS-T, 2 min each.

16. Coverslips are mounted onto glass slides using Vectashield antifade medium (Vector Laboratories, Inc., Burlingame, CA) or 1 mg/ml *p*-phenylenedia-

mine in a 1:10 (v/v) mixture of PBS:glycerol, pH 8.0 (Johnson and Nogueira Araujo, 1981).

17. Seal coverslips with nail polish. Stained preparations should be examined and images captured immediately for best results. Slides may be stored at 4°C for a few weeks in a light-tight box.

F. Double- and Triple-Staining Techniques

When examining the centromere or kinetochore, it is often necessary to use double- and triple-staining techniques to examine multiple antigens, such as motors, microtubules, and chromatin in the same preparation. This can be readily accomplished by carefully selecting combinations of primary and secondary antibodies conjugated to a variety of fluorescent tags, such as fluorescein isothiocyanate (FITC) (excitation/emission = 494/518 nm), tetramethylrhodamine isothiocyanate (TRITC) (552/570 nm), and Texas Red (TXRD) (595/615 nm) (Molecular Probes, Inc.). In applying combinatory immunofluorescence, it is critical to avoid antibody cross-reaction. For example, if you wish to stain both the centromere and mitotic spindle in the same preparation, you would use CREST antisera primary antibody, followed by FITC-labeled goat anti-human secondary antibody, and then apply anti-tubulin primary antibody from a different organism, such as mouse, followed by TXRD-labeled sheep anti-mouse secondary antibody. In actual practice, we stain first with a mixture of the two primary antibodies, followed by a mixture of the two secondary antibodies. Chromatin can be enhanced with an appropriate counterstain, such as DAPI (ex/em = 358/461 nm), propidium iodide (535/617 nm), bis-benzimide (Hoechst 33258) (352/461 nm), or ethidium bromide (518/605 nm). With the proper selection of activating filters, you may view multiple antigens in the same sample. If you wish to produce a single image with multiple fluorescent probes, you must use image processing software to merge the collected data (as shown in Fig. 2).

III. *In Situ* Localization of Proteins: Immunogold EM

Reagents (Fig. 3)

1. Buffered solutions

   PBS (0.14 *M* NaCl, 2.5 m*M* KCl, 8 m*M* Na_2HPO_4, 1.6 m*M* KH_2PO_4, pH 7.4).

   PEM [80 m*M* K-PIPES (pH 6.8), 5 m*M* EGTA (pH 7.0), 2 m*M* $MgCl_2$].

   TBS-1 [10 m*M* Tris (pH 7.7), 150 m*M* NaCl, 3 m*M* KCl, 1.5 m*M* $MgCl_2$, 0.05% Tween-20, 0.1% BSA, 0.2% glycine] (Nickerson *et al.*, 1990).

   TBS-2 [20 m*M* Tris (pH 8.2), 140 m*M* NaCl, 0.1% BSA] (Nickerson *et al.*, 1990).

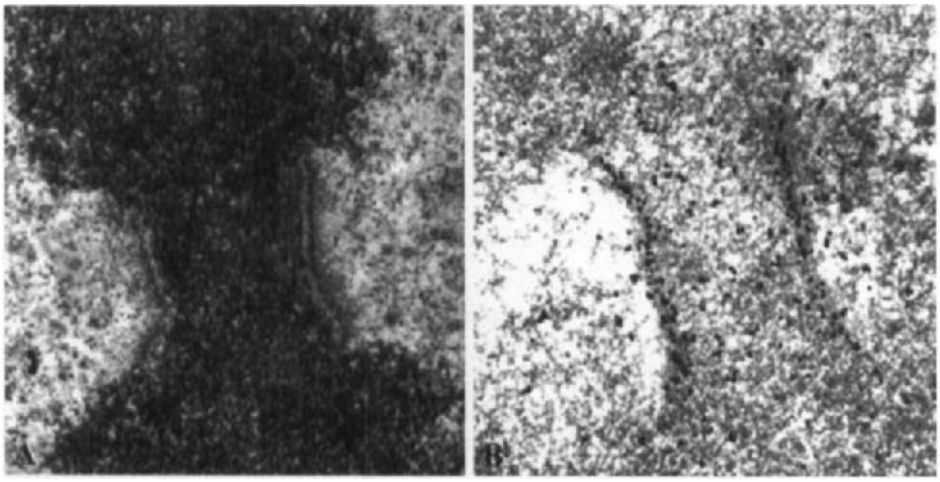

Fig. 3 (A and B) Indian muntjac chromosomes observed by EM. Prior to fixation, the chromosome in B was swollen in hypotonic solution and does not display the trilaminar kinetochore plate morphology seen along each chromatid in A. Centromere–kinetochore antigens were detected in preparation B using SH-CREST autoantiserum and immunogold labeling according to the protocol given in Section III. Thin sections were made using an RMC 6000 ultramicrotome, collected on copper mesh grids, and stained with uranyl acetate and Reynold's lead citrate. Electron micrographs were captured on a Hitachi H-7000 electron microscope operated at 75 kV.

0.1 *M* cacodylate, diluted in ddH_2O from a 0.2 *M* stock (Electron Microscopy Sciences, Ft. Washington, PA).

2. Permeabilization solution

   0.5% Triton X-100 in PEM. Make a 1 : 20 dilution of 10% stock Triton X-100.

3. Fixatives

   3.7% formaldehyde (diluted from 16% ultrapure EM-grade formaldehyde; Polysciences, Inc.) in PEM containing 0.1% glutaraldehyde (diluted from 25% ultrapure EM grade; Polysciences, Inc.).

   1% glutaraldehyde diluted from 25% ultrapure EM grade (Polysciences, Inc.) in 0.1 *M* sodium cacodylate (pH 7.4).

   1% osmium tetroxide (OsO_4) (Electron Microscopy Sciences) in 0.1 *M* sodium cacodylate (pH 7.4).

4. Reducing agent

   PEM + 1 mg/ml sodium borohydrate ($NaBH_4$), freshly prepared. To a tube containing preweighed sodium borohydrate, slowly add the appropriate amount of PEM buffer to bring the final concentration to 1 mg/ml. This reducing agent eliminates reactive aldehydes after fixation.

5. Blocking agent

   5% heat-inactivated normal goat serum (NGS) in TBS-1.

6. Antibodies

CREST antisera is diluted 1:500 to 1:1000 in TBS-1.

Colloidal gold-conjugated (5, 10, or 12 nm diameter) anti-human IgG(H+L) secondary antibody (Amersham Life Science, Inc.) is diluted 1:5 in TBS-2.

Protocol

1. Cells are harvested by mitotic shake-off (see Section II) and cytospun (800 rpm, 2 min) onto poly-amino acid-coated Thermanox coverslips (Nunc, Inc., Naperville, IL). This provides a highly concentrated monolayer of mitotic cells within a small area for ease of sectioning. Alternatively, cells can be grown and processed in Contur Permanox tissue culture dishes (Miles Scientific, Naperville, IL).

2. Transfer coverslips to a multiwell tissue culture tray or to Coplin jars containing cold PBS. Keep on ice.

3. Rinse coverslips with cold PEM.

4. Cells should be permeabilized prior to fixation to allow greater accessibility of the colloidal gold immunoprobes to intracellular antigens. Permeabilization and extraction is achieved by treating preparations with 0.5% Triton X-100 in PEM or CSK for 2 min at 4°C. Some cell types require longer exposures. To preserve the cytoskeleton and nuclear matrix while extracting soluble proteins, we recommend the use of 0.5% Triton X-100 in CSK [10 m*M* PIPES, (pH 6.8), 100 m*M* NaCl, 300 m*M* sucrose, 3 m*M* $MgCl_2$, 1 m*M* EGTA] containing 4 m*M* VRC and multiple protease inhibitors (1.2 m*M* PMSF and 1 μg/ml each of aprotinin, leupeptin, antipain, and pepstatin). Prepare immediately before use and keep on ice.

5. Rinse briefly in fresh, cold PEM.

6. Preparations are fixed in 3.7% paraformaldehyde and PEM containing 0.1% glutaraldehyde for 40 min at 4°C.

7. Remove fixative and wash coverslips three times with PEM, 5 min each on a rotator. Do not remove the last PEM wash until your are ready to perform the next step.

8. Quench in $NaBH_4$ and PEM as follows: Gently mix the freshly prepared $NaBH_4$ and PEM by pipetting in and out. It may be difficult to pipette accurately because of the air bubbles formed. Immerse the coverslips and place on a rotator for 5 min.

9. Repeat the above step with fresh $NaBH_4$.

10. Rinse coverslips three times in PEM, 5 min each while on rotator.

11. Nonspecific binding of antibodies is blocked with 5% NGS in TBS-1 for at least 30 min at RT or overnight at 4°C.

12. Without rinsing, the cells are incubated for 2 hr at 37°C in CREST antiserum diluted in TBS-1.

13. The samples are then washed three times in TBS-1, 5 min each.

14. Block in 5% NGS for 10 min.

15. Without rinsing, incubate preparations for 1 hr at 37°C with gold-conjugated anti-human secondary antibody, diluted in TBS-2.

16. The preparations are then washed three times for 5 min in TBS-2.

17. Postfix cells with 1% glutaraldehyde in 0.1 *M* sodium cacodylate for 5 min. This and the remaining steps are done at RT.

18. Follow with three 5-min washes in 0.1 *M* sodium cacodylate.

19. The samples are then fixed for 10–15 min in 1% OsO_4 in 0.1 *M* sodium cacodylate.

20. Wash coverslips extensively in ddH_2O.

21. The samples are then dehydrated in a graded series of ethanols: 5 min in 30, 50, 70, 90, and 100%.

22. Infiltrate overnight with Spurr's resin (Spurr, 1969).

23. Cell monolayers are flat embedded according to the procedure of Brinkley and Chang (1973).

24. Thin sections are made using an ultramicrotome and collected on copper mesh grids.

25. Contrast briefly (5 min each) with uranyl acetate and Reynolds' lead citrate (Reynolds, 1963).

IV. Fluorescent *in Situ* Hybridization Using DNA Satellite Probes

Perhaps one of the most powerful tools in cell and molecular biology to be developed in this century is the technique of fluorescent *in situ* hybridization (FISH), used for detecting specific nucleic acid sequences in cells (John *et al.*, 1969; Lawrence *et al.*, 1988). Used widely for mapping DNA on metaphase chromosomes, this method is especially useful for the analysis of centromeric DNA. The centromeres of higher eukaryotes are composed of highly repetitive, noncoding DNA sequences. In humans and other primates, the centromere consists of a tandem series of 171-bp monomeric repeats, arranged in higher-order families known as α-satellite or alphoid DNA (Wevrick *et al.*, 1992; Haaf and Willard, 1992). By synthesizing probes from cloned fragments of alphoid DNA, it is possible to localize these sequences in the centromeres of specific human chromosomes using FISH. It is also possible to use a combination of FISH and indirect immunofluorescence to localize both DNA and protein in the same centromere (Fig. 4, see color plate; the method for combination staining is given in Section V). The technique for FISH that we use routinely is described below. Before you begin, it is helpful to prepare the following stock and working solutions:

Reagents

PBS (0.14 *M* NaCl, 2.5 m*M* KCl, 8 m*M* Na_2HPO_4, 1.6 m*M* KH_2PO_4, pH 7.4).

PBD (PBS + 0.1% Tween-20).

0.5% Triton X-100 in PBS.

20× SSC (1× SSC = 0.15 *M* NaCl, 15 m*M* sodium citrate, pH 7.0). Dilutions of 4×, 2×, and 0.5–0.75× will be needed.

4× and 2× SSC containing 0.1% Tween-20.

2.5–3% formaldehyde in PBS. Dilute 16% ultrapure EM-grade formaldehyde (Polysciences, Inc.) or freshly prepare from paraformaldehyde.

Carnoy's fixative (3:1 methanol:glacial acetic acid).

70% formamide + 2× SSC [dilute 100% formamide (Gibco Laboratories) and 20× SSC, pH 7.0].

70, 85, and 100% ethanol series.

Satellite DNA probes prepared by nick translating centromeric DNA with biotin-labeled dNTPs (Langer *et al.*, 1981). Digoxigenin-labeled deoxynucleotide oligomers also give excellent results.

Fluorophore-conjugated avidin (Vector Laboratories, Inc.) is diluted 1:200 in 4× SSC containing 1% BSA,

Fluorophore-conjugated anti-avidin antibody (Vector Laboratories, Inc.) is diluted 1:500 in 1× PBD.

Or, fluorophore-conjugated sheep anti-digoxigenin antibody (Oncor, Inc., Gaithersburg, MD), diluted 1:100 in 1× PBD,

And, fluorophore-conjugated rabbit anti-sheep antibody (Oncor, Inc.), diluted 1:500 in 1× PBD.

DNA is counterstained with 0.1 μg/ml DAPI, 0.5 μg/ml propidium iodide, 1 μg/ml Hoechst 33258, or 10 μg/ml ethidium bromide, diluted in 1× PBD.

Protocol

Denaturation

1. Cells are grown on or cytospun (800 rpm, 2 min) onto acid-etched and/or poly-amino acid-coated glass coverslips (as described in Section II).
2. Transfer coverslips to Coplin jars containing cold PBS. Keep on ice.
3. Cells are permeabilized prior to fixation with 0.5% Triton X-100 in PBS for 1 min.
4. Rinse briefly in fresh, cold PBS.
5. Preparations are fixed in 2.5–3% formaldehyde and PBS for 15 min on ice.
6. Remove fixative and wash coverslips three times with ddH_2O, 5 min each.
7. The cells are then fixed in freshly prepared Carnoy's fixative for 20 min at RT.

8. Dehydrate samples in a graded series of ethanols: 70, 85, and 100%, 2 min each at RT.

9. The coverslips are allowed to air-dry and should be stored at −20°C with desiccant for a few days.

10. Preparations are denatured in 70% formamide, 2× SSC (pH 7.0) for 9 min at 79°C (place Coplin jar in a water bath).

11. The coverslips are immediately placed in 70% ethanol at −20°C for 2 min, moved to 85% ethanol at −20°C for 2 min, and finally to 100% ethanol at −20°C for 2 min.

12. Air dry the preparations and immediately begin hybridization.

Probe Preparation

13. 50 ng of probe is suspended in 13 μl of deionized formamide with 10 μg of sheared salmon sperm DNA (Sigma Chemical Co.) and 15 μg of *Escherichia coli* tRNA (Boehringer–Mannheim Biochemicals, Indianapolis, IN).

14. The probe is then denatured at 70°C for 5 min and immediately put on ice.

15. 7 μl of hybridization buffer is added to the probe so that the final hybridization solution consists of 65% formamide, 2× SSC, 10% dextran sulfate, and 1% BSA.

Hybridization

16. Each coverslip is inverted onto 20 μl of hybridization solution on parafilm and incubated at 37°C overnight in a humidified chamber.

17. Samples are then rinsed in 0.75× (or 0.5×) SSC for 5 min at 72°C.

Detection

18. Protect samples from light during all remaining steps. Hybridization of biotinylated probes is detected by incubating fluorophore-conjugated avidin on samples for 30–60 min at RT. See step 20 for digoxigenin-labeled probes.

19. The preparations are rinsed in 2× and 4× SSC containing 0.1% Tween-20 at RT, 10 min each. Skip to step 21.

20. When using digoxigenin-labeled probes, hybridization is detected by incubating samples with fluorophore-conjugated anti-digoxigenin antibody for 15 min at 37°C.

21. The preparations are rinsed three times in PBD, 5 min each.

22. DNA is counterstained with DAPI, propidium iodide, Hoechst 33258, or ethidium bromide for 15–45 sec at RT.

23. Rinse samples three times in PBD, 2 min each.

24. Coverslips are mounted onto glass slides using Vectashield antifade medium (Vector Laboratories, Inc.) or 1 mg/ml *p*-phenylenediamine in a 1:10 (v/v) mixture of PBS:glycerol (pH 8.0).

25. Seal coverslips with nail polish. Stained preparations should be examined and images captured immediately for best results. Slides may be stored at 4°C for a few weeks in a light-tight box.

Signal amplification

26. Peel the nail polish off and soak the slides in PBD until the coverslip moves freely.

27. Remove coverslips and rinse them thoroughly in PBD at RT.

28. Incubate avidin-labeled samples for 15 min at 37°C with fluorophore-conjugated anti-avidin antibody. Complete steps 21–25.

29. Amplification of digoxigenin-conjugated probes is achieved by incubating samples with rabbit anti-sheep antibody at 37°C for 15 min.

30. Rinse three times 5 min in PBD at RT.

31. Incubate with fluorophore-labeled anti-rabbit antibody for 15 min at 37°C.

32. Complete steps 21–25.

V. Combination Staining: DNA/Protein

Reagents

PBS (0.14 *M* NaCl, 2.5 m*M* KCl, 8 m*M* Na_2HPO_4, 1.6 m*M* KH_2PO_4, pH 7.4).

PBD (PBS + 0.1% Tween-20).

PEM [80 m*M* K-PIPES (pH 6.8), 5 m*M* EGTA (pH 7.0), 2 m*M* $MgCl_2$].

0.5% Triton X-100 in PEM.

20× SSC (1× SSC = 0.15 *M* NaCl, 15 m*M* sodium citrate, pH 7.0). Dilutions of 4×, 2×, and 0.5–0.75× will be needed.

4× and 2× SSC containing 0.1% Tween-20.

0.5–1.5% and 2.5–3% formaldehyde in PEM. Dilute 16% ultrapure EM-grade formaldehyde (Polysciences, Inc.) or freshly prepare from paraformaldehyde.

Carnoy's fixative (3:1 methanol:glacial acetic acid).

70% formamide + 2× SSC [dilute 100% formamide (Gibco Laboratories) and 20× SSC, pH 7.0].

70, 85, and 100% ethanol series.

Satellite DNA probes prepared by nick translating centromeric DNA with biotin-labeled dNTPs (Langer *et al.,* 1981). Digoxigenin-labeled deoxynucleotide oligomers also give excellent results.

Fluorophore-conjugated avidin (Vector Laboratories, Inc.) is diluted 1:200 in 4× SSC containing 1% BSA,

And fluorophore-conjugated anti-avidin antibody (Vector Laboratories, Inc.) is diluted 1:500 in 1× PBD.

Or, fluorophore-conjugated sheep anti-digoxigenin antibody (Oncor, Inc.), diluted 1:100 in 1× PBD.

And fluorophore-conjugated rabbit anti-sheep antibody (Oncor, Inc.), diluted 1:500 in 1× PBD.

CREST antisera is diluted 1:500 to 1:1000 in PBD.

Fluorophore-conjugated anti-human IgG(H+L) secondary antibodies (Pierce Chemicals) are diluted 1:500 in PBD.

DNA is counterstained with 0.1 μg/ml DAPI, 0.5 μg/ml propidium iodide, 1 μg/ml Hoechst 33258, or 10 μg/ml ethidium bromide, diluted in 1× PBD.

Protocol

Immunostaining

1. Cells are grown on or cytospun (800 rpm, 2 min) onto acid-etched and/or poly-amino acid-coated glass coverslips (as described in Section II).
2. Transfer coverslips to Coplin jars containing cold PBS. Keep on ice.
3. Rinse slides with cold PEM.
4. Cells are permeabilized prior to fixation with 0.5% Triton X-100 in PEM or CSK for 1 min on ice. Rinse briefly in fresh, cold PEM. To preserve the cytoskeleton and nuclear matrix while extracting soluble proteins, we recommend the use of 0.5% Triton X-100 in CSK [10 m*M* PIPES (pH 6.8), 100 m*M* NaCl, 300 m*M* sucrose, 3 m*M* $MgCl_2$, 1 m*M* EGTA] containing 4 m*M* VRC and multiple protease inhibitors (1.2 m*M* PMSF and 1 μg/ml each of aprotinin, leupeptin, antipain, and pepstatin). Prepare immediately before use and keep on ice.
5. Preparations are fixed in 0.5–1.5% formaldehyde, PEM for 15 min on ice.
6. Wash coverslips three times in PEM, 5 min each on a rotator.
7. Primary antibodies in PBD are incubated on preparations for 30–60 min at 37°C in a humid chamber.
8. The samples are then rinsed three times in PBD, 5 min each.
9. *Protect samples from light during all remaining steps.* Labeled secondary antibodies in PBD are incubated with samples for 30–60 min at 37°C in a humid chamber.
10. The coverslips are rinsed in PBD and PEM for 5 min each at RT.
11. Fix samples in 2.5–3% formaldehyde, PEM for 15 min at RT.
12. Wash coverslips three times with ddH_2O, 5 min each.

Denaturation

13. The cells are fixed in freshly prepared Carnoy's fixative for 20 min at RT.
14. Dehydrate samples in a graded series of ethanols: 70, 85, and 100%, 2 min each at RT.
15. The coverslips are then allowed to air-dry and should be stored at −20°C with desiccant for a few days.

16. Preparations are denatured in 70% formamide, 2× SSC (pH 7.0) for 9 min at 78 or 79°C (place Coplin jar in a water bath).

17. The coverslips are immediately placed in 70% ethanol at −20°C for 2 min and moved to 85% ethanol at −20°C for 2 min, and finally to 100% ethanol at −20°C for 2 min.

18. After air-drying the coverslips, immediately begin hybridization.

Probe preparation

19. Suspend 50 ng of probe in 13 μl of deionized formamide with 10 μg of sheared salmon sperm DNA (Sigma Chemical Co.) and 15 μg of *E. coli* tRNA (Boehringer–Mannheim Biochemicals).

20. The probe is then denatured at 70°C for 5 min and immediately put on ice.

21. Prior to hybridization, 7 μl of hybridization buffer is added to the probe so that the final hybridization solution consists of 65% formamide, 2× SSC, 10% dextran sulfate, and 1% BSA.

Hybridization

22. Each coverslip is inverted onto 20 μl of hybridization solution on parafilm and incubated at 37°C overnight in a humidified chamber.

23. Samples are then rinsed in 0.5–0.75× SSC for 5 min at 72°C.

Detection

24. Hybridization of biotinylated probes is detected by incubating fluorophore-conjugated avidin on samples for 30–60 min at RT. See step 26 for digoxigenin-labeled probes.

25. The preparations are rinsed in 2× and 4× SSC containing 0.1% Tween-20 at RT, 10 min each. Skip to step 27.

26. When using digoxigenin-labeled probes, hybridization is detected by incubating samples with fluorophore-conjugated anti-digoxigenin antibody for 15 min at 37°C.

27. The preparations are rinsed three times in PBD, 5 min each.

28. DNA is counterstained with DAPI, propidium iodide, Hoechst 33258, or ethidium bromide for 15–45 sec at RT.

29. Rinse samples three times in PBD, 2 min each.

30. Coverslips are mounted onto glass slides using Vectashield antifade medium (Vector Laboratories, Inc.) or 1 mg/ml *p*-phenylenediamine in a 1:10 (v/v) mixture of PBS:glycerol, pH 8.0.

31. Seal coverslips with nail polish. Stained preparations should be examined and images captured immediately for best results. Slides may be stored at 4°C for a few weeks in a light-tight box.

Signal amplification

32. Peel the nail polish off and soak the slides in 1× PBD until the coverslip moves freely.

33. Rinse the coverslips thoroughly in 1× PBD at RT.

34. Incubate avidin-labeled samples for 15 min at 37°C with fluorophore-conjugated anti-avidin antibody. Complete steps 27–31.

35. Amplification of digoxigenin-conjugated probes is achieved by incubating samples with rabbit anti-sheep antibody at 37°C for 15 min.

36. Rinse three times for 5 min in 1× PBD at RT.

37. Incubate with fluorophore-labeled anti-rabbit antibody for 15 min at 37°C.

38. Complete steps 27–31.

VI. Specialized Techniques

The intact centromere is arranged as a series of repetitive subunits, folded tightly into a dense array of heterochromatin, often making it a difficult region of the chromosome to analyze by standard fluorescent staining techniques. A number of specialized techniques have been developed by our laboratory and others to make the centromere–kinetochore complex more accessible to structural and molecular analysis.

A. Centromere Fragmentation in Mitotic Cells with Unreplicated Genomes

In the late 1980s, we discovered that the centromere could be fragmented into small functional subunits that retain their capacity to capture microtubules and become aligned on the metaphase plate (Fig. 5, see color plate). This phenomenon is produced *in situ* by exposing cells to caffeine that have been arrested at the G_1/S phase boundary with hydroxyurea (Brinkley *et al.*, 1988). By an unknown mechanism, cells treated under these conditions circumvent the DNA replication checkpoint and enter mitosis prematurely without progressing through S phase (Schlegel and Pardee, 1986; Hartwell and Weinert, 1989). Such cells display a highly fragmented genome, consisting of small chromosome fragments scattered throughout the cytoplasm (Ishida *et al.*, 1985).

Recently, we identified two types of centromere fragments in these mitotic cells with unreplicated genomes (MUGs): those that display kinetochore plates [centromere–kinetochore fragments (CFKs); Wise and Brinkley, 1997] and those that lack kinetochores. The CFKs are CREST-positive and undergo attachment to the spindle (Fig. 5), whereas those that lack kinetochores are CREST-negative and lack the capacity to attach and undergo movements. The latter can only be detected by FISH, using selected α-satellite DNA probes (D. He and B. R. Brinkley, manuscript in preparation). For details on the structure and movement of CKFs in MUGs, as well as interpretations of their relationship to centromere structure and function, readers are referred to earlier publications (Zinkowski *et al.*, 1991; Christy *et al.*, 1995; Wise and Brinkley, 1997). Although MUGs

represent highly perturbed cells that have been subjected to catastrophic conditions, much can still be learned about the structure and behavior of the eukaryotic centromere–kinetochore complex from this unique model.

In our hands, the MUG technique works only on certain mammalian cell types (rodents and muntjac deer) and is only useful for human chromosomes in rodent × human somatic cell hybrids. Although conditions may vary with different cell cultures, we have obtained excellent results with Chinese hamster ovary (CHO) cells. In this procedure, cell cultures are first arrested at G_0 by growing them until confluent and allowing them to undergo contact inhibition in nutrient-depleted medium. The cultures are then rinsed and replated to a density of 1×10^6 cells/28 mm^2 flask and incubated in serum-free medium for 66 hr at 37°C (Ashihara and Baserga, 1979; O'Keefe *et al.,* 1992). Cultures synchronized in G_0 should lack rounded mitotic cells when examined under the phase contrast microscope. The cells are then incubated in fresh, serum-containing medium for 4 hr, allowing progression into the G_1 phase of the cell cycle. Subsequent incubation in 2 m*M* hydroxyurea (HU) for 16–20 hr results in the arrest of cells at the G_1/S boundary of the cell cycle. Fresh medium is added containing 2 m*M* HU plus 5 m*M* caffeine, and the cells are cultured for an additional 2–6 hr. In order to increase the mitotic index, MUGs may be arrested in mitosis with 0.1 μg/ml Colcemid (Gibco Laboratories) concurrent to caffeine treatment. MUGs are selectively harvested by mitotic shake-off (described in Section II), cytocentrifuged onto coverslips, and processed according to given protocols.

B. Cloning Centromere DNA from MUGs

In many ways the MUG procedure utilizes the living cell to achieve the first step in isolating centromere fragments for *in vitro* analysis. We have adapted this procedure to facilitate the isolation and cloning of DNA from the centromere fragments of CHO cells (Ouspenski and Brinkley, 1993). The schematic shown in Fig. 6a illustrates the basic procedure that utilizes several previously described probes and techniques in a novel way to isolate a chromosome-specific centromere DNA sequence. The isolation of functional centromeric fragments involves three steps: (i) *in vivo* chromosome fragmentation, (ii) isolation of total chromosome fragments, and (iii) immunoprecipitation of the centromere fragments using antibodies from scleroderma CREST antiserum. After following the MUG procedure described in Section VI, A, we (as stated in Ouspenski and Brinkley, 1993)

> adapted the polyamine chromosome isolation procedure of Gasser and Laemmli (1987) for the isolation of dispersed mitotic chromatin. The strategy of the method is to homogenize hypotonically swollen cells in a buffer that stabilizes the compact structure of mitotic chromatin, and then to fractionate the lysate by rate-zonal and isopycnic centrifugations. Centrifugation through a glycerol gradient as the first step allowed the separation of fine chromatin particles from unlysed cells, nuclei, whole chromosomes and chromatin aggregates (which sedimented into the lower part of the gradient) and soluble proteins (which remained in the supernatant).

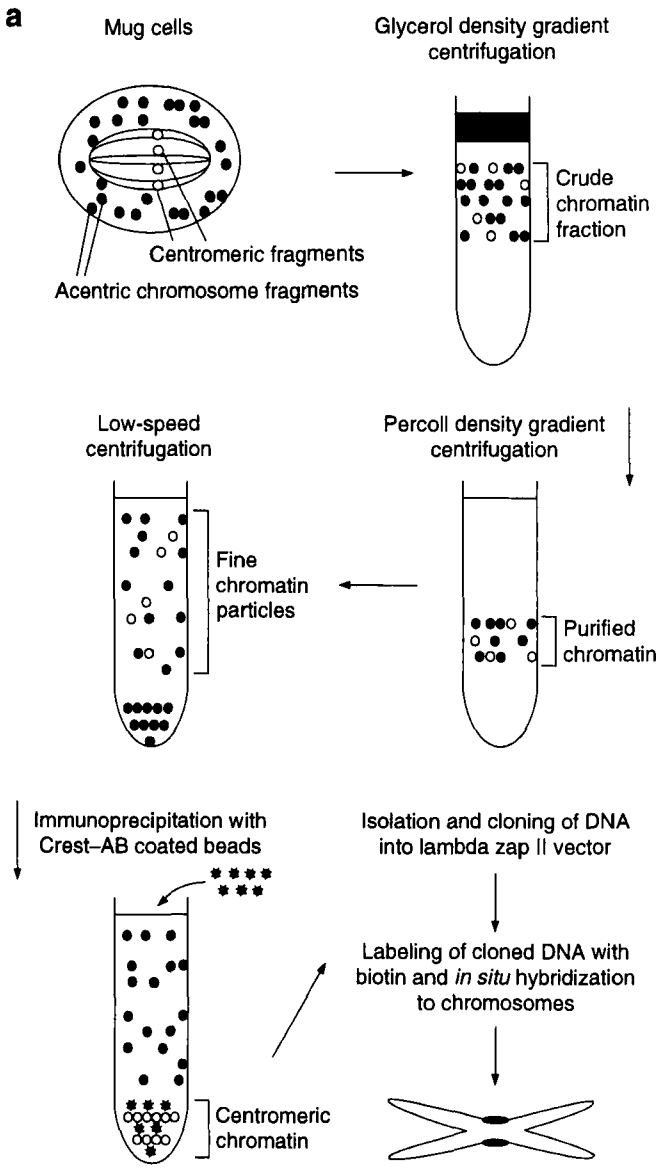

Fig. 6 (a) Isolation of functional centromeric fragments involving three steps: (i) *in vivo* chromosome fragmentation, (ii) isolation of total chromosome fragments, and (iii) immunoprecipitation of the centromere fragments using antibodies from scleroderma CREST antiserum (see Section VI,B) (reproduced by permission from Ouspenski and Brinkley, 1993, and by the Company of Biologists Limited).

> The chromatin was purified further by "banding" in an isopycnic gradient of Percoll, resulting in a preparation that was essentially free of cytoskeletal debris, as determined by microscopic observation. (p. 362)

The technical details of chromatin isolation, immunoaffinity purification of centromere fragments, and DNA cloning analysis are beyond the scope of this chapter and may be found in the original paper. To validate the specificity of the procedure, a randomly selected clone was labeled by nick translation with biotin-11-dUTP and hybridized to CHO chromosomes using the FISH procedure described in Section IV. Localization was observed exclusively at the centromere of chromosome 1 (Fig. 6b, see color plate). Further analysis of this and other clones is under way.

C. Centromere Stretching

The tightly compacted centromere–kinetochore complex can be relaxed considerably, allowing the application of immunofluorescence, immunogold EM, or FISH to evaluate the organization of this complicated structure. This technique was inspired by earlier work, which showed that metaphase chromosomes can be microscopically identified and examined in much greater detail after mild hypotonic treatment (Fig. 2), a procedure that revolutionized the field of cytogenetics (Hsu, 1952; Tjio and Levan, 1956). Using a modified procedure developed in our laboratory, one can stretch or extend the centromere in such a way as to uncoil its structure and better resolve the repetitive pattern of DNA and proteins (Zinkowski *et al.,* 1991; Haaf and Ward, 1994a).

In one procedure, cells are harvested by mitotic shake-off (described in Section II) and suspended in 1 or 2 ml of PBS, containing a protease inhibitor cocktail [0.1 m*M* PMSF and 1 μg/ml each of chymostatin, leupeptin, antipain, and pepstatin (P-CLAP)], for a final concentration of about 1×10^6 cells per milliliter. The cells are then lysed by forcing the suspension through a 26-gauge syringe three times. Approximately 100 μl of the lysed cell preparation is added to a cytocentrifuge cup, and the chromosomes and cell debris are spun onto acid-etched and/or poly-amino acid-coated slides or coverslips using a Cytospin cytocentrifuge (Shandon Instruments, Inc.) at 800–1200 rpm for 2 min. The preparations are promptly removed and processed according to the given protocols.

In a second procedure, hypotonic stretching of chromosomes is achieved by incubating mitotic cells (harvested by shake-off) or cell lysates (from the previous procedure) in 75 m*M* KCl containing P-CLAP for 5–15 min. The preparations are then spun onto coverslips using a cytocentrifuge at 2000 rpm for 2 min with high acceleration. Generally, short exposures to hypotonic solution produce swollen chromosomes, whereas longer exposures improve the centromere stretching process. Chromosomes generally stretch poorly in the center of the cell spot (usually the most crowded area), whereas chromosomes along the outer perimeter are maximally stretched. This produces a gradient in centromere distension that is often useful in structural interpretations (Fig. 7, see color plate).

Centromere stretching may be facilitated by growing cells in the presence of nonintercalating DNA-binding agents, such as Hoechst 33258 or DAPI, which induce the undercondensation of chromatin, especially heterochromatin, by unknown mechanisms (Hilwig and Gropp, 1973; Rocchi *et al.*, 1979). For example, human cells are grown in the presence of 100 μg/ml DAPI for 16–18 hr prior to metaphase arrest in order to facilitate centromere stretching. The cytidine analogs 5-azacytidine and 5-azadeoxycytidine also induce undercondensation, most likely by inhibiting DNA methylation (Jones and Taylor, 1980; Schmid *et al.*, 1983). In a comparative study using a variety of treatments, the overall length of human chromosomes was greatest after treatment with 5-azacytidine following a fluorodeoxyuridine (FUdR)/uridine metabolic block (Jeppesen *et al.*, 1992). Cell cultures are synchronized in 0.1 μM FUdR and 1 μM uridine for 13 hr. The block is then removed by adding thymidine to a final concentration of 10 μM, at which time 5-azacytidine is added to 0.37 μM. Cells are harvested 5 hr after treatment and processed according to the previously discussed hypotonic procedure.

The degree of centromere stretching produced by these procedures can range from zero in some chromosomes to maximum centromere stretching of 20 times their normal metaphase length in the same preparation. In a study of muntjac chromosomes, we found that centromeres were stretched about 11- or 12-fold on average (Zinkowski *et al.*, 1991). Interphase chromatin, including chromatin in prekinetochores, may be stretched to a much greater degree. It should be pointed out, however, that this procedure has certain limitations and, by its nature, produces considerable artifact and perturbation of structure. Careful controls must be followed, and interpretations must be made with caution. Hypotonic swelling of mammalian cells leads to the loss of kinetochore plate morphology as well as the disruption of microtubules, centrioles, and centrosomes (Brinkley *et al.*, 1980; Ris and Witt, 1981). However, if the period of hypotonic swelling is brief (under 15 min), the damage can be reversed by returning the cells to an isotonic tissue culture environment (Brinkley *et al.*, 1980). Under these conditions, cell viability will not be adversely affected.

With these caveats in mind, much can be learned about chromatin organization from centromere stretching experiments. Using a combination of immunofluorescence and FISH (see Section V) on the same stretched preparations, we discovered several new features of the centromere–kinetochore complex. Prior to stretching, CREST staining reveals a single plate or band along the outer surface of the centromere. Immunogold EM images show that most of the CREST antigens are subjacent to the inner kinetochore plate and totally excluded from the outer plate. After stretching, a series of punctate, CREST-positive segments become increasingly separated by unstained regions, producing the beads-on-a-string appearance (Zinkowski *et al.*, 1991) seen in Fig. 7. When stretched human chromosomes are stained with a combination of CREST immunofluorescence and FISH using a consensus α-satellite probe, one can see that the repetitive subunits are connected by a continuous fiber of α-satellite DNA (Haaf and Ward, 1994a; D. He and B. R. Brinkley, manuscript in preparation). Haaf and Ward

(1994a,b) noted DNA resolution of around 10 kb/μm and concluded that such preparations were extremely useful for long-range mapping research of both interphase and metaphase chromatin.

D. Frozen Sections

The study of centromere–kinetochores in whole tissues is difficult because one must resort to sectioning. Standard paraffin sections can be used if the cells are properly fixed and deparaffinized prior to staining, but they are still of limited value due to section thickness. We have obtained excellent results using a cryomicrotome to cut thick (up to 50 μm) frozen (−80°C) sections of tissues dissected from experimental animals. The frozen sections are mounted on precoated slides (Fisher Scientific, Pittsburgh, PA), permeabilized with 0.5% Triton X-100 for 3 min, and fixed in 3.7% formaldehyde in PBS for 15 min at room temperature. The sections are stained by standard procedures (refer to Section II) using a combination of CREST immunofluorescence for 3 hr at 37°C, detected by fluorophore-conjugated secondary antibody, and nucleic acid counterstaining. Sections are examined by confocal microscopy [in our case, using a Molecular Dynamics (Sunnyvale, CA) Multiprobe 2001 laser scanning confocal microscope] and images are collected at 0.2–5.0 μm steps. Three-dimensional projections are then rendered using an appropriate software package (ImageSpace by Molecular Dynamics). Examples of centromere staining in rat mammary gland tissues are shown in Fig. 8 (see color plate).

E. Centromere–Kinetochores of Plant Chromosomes

The centromere and kinetochore of many plant chromosomes, like those of animal chromosomes, are confined to a single focus. Those of other plant species may be diffuse or polycentric in their distribution along the chromosomes. Relatively little is known about the molecular composition of plant centromeres, largely due to the fact that human anticentromere autoantibodies have had limited application. A clear exception is found in an antiserum designated EK, collected from a patient with the CREST variant of scleroderma. EK-CREST stains both prekinetochores in interphase nuclei and centromeres on metaphase chromosomes of the higher plant *Haemanthus katherinae* Bak and the spiderwort plant *Tradescantia virginiana* (Mole-Bajer *et al.*, 1990; Wolniak and Larsen, 1992). In western blots using *Haemanthus* cell extracts, EK-CREST predominantly recognizes two bands of 65 and 135 kDa. In human (HeLa) cell extracts, EK-CREST recognizes bands of 52, 80, and 110 kDa as well as two or three minor bands between 140 and 200 kDa. Other CREST antisera in our collection fail to stain the centromere of plant chromosomes.

1. Protocol for CREST Immunofluorescence

Endosperm cells are spun onto clean glass microscope slides at 1500 rpm for 3 min using a cytocentrifuge (see Section II). The preparations are permeabilized

and fixed in 100% methanol at −20°C for 7 min and then rinsed and rehydrated twice in PBS, 5 min each. The slide preparations are incubated in CREST antiserum, diluted 1:20 in PBS, for 30 min in a humidified 37°C incubator. After three 5-min rinses in PBS, the preparations are incubated in 1:20 FITC-conjugated goat anti-human IgG (Boehringer–Mannheim Biochemicals) for 30 min at 37°C. The preparations are rinsed for 5 min in PBS, counterstained for DNA in PBS containing 10 μg/ml Hoechst 33258 (Sigma Chemical Co.), and rinsed again for 5 min in PBS. The slides are overlaid with 50 μl of mounting medium [1 mg/ml *p*-phenylenediamine in a 1:10 (v/v) mixture of PBS:glycerol], and a coverslip is applied. Preparations may be examined using a standard fluorescence microscope.

2. Protocol for Silver Enhancement

Excellent contrast and resolution of the centromere can be obtained by brightfield microscopy using the silver enhancement procedure. Cells are fixed as described previously and incubated with CREST antiserum at a 1:5 to 1:10 dilution overnight at room temperature. The preparations are incubated with 5 nm immunogold for 6 hr. Immunogold silver-enhanced staining is then accomplished by the method of Hoefsmit *et al.* (1986), as modified for *Haemanthus* by Mole-Bajer *et al.* (1990). Preparations are embedded in Permount (Fisher Scientific), a mounting medium that matches the refractive index of chromosomes and nuclei fixed with methanol. A glass coverslip is placed over the cellular material prior to examination with brightfield optics.

Acknowledgments

We thank L. Zhong for contributing technical expertise throughout the writing of the manuscript. Appreciation is also extended to M. G. Mancini and C. P. Schultz for technical assistance, to B. Ledlie for secretarial assistance, and to M. A. Mancini and I. Ouspenski for helpful suggestions. These studies were supported in part by Grants CA41424 and CA64255 from the National Institutes of Health to BRB and Grant DAMD17-94-J-4253 from the Department of the Army to J. Rosen.

References

Ashihara, T., and Baserga, R. (1979). Cell synchronization. *Methods Enzymol.* **58**, 248–262.

Brenner, S., Pepper, D., Berns, M. W., Tan, E., and Brinkley, B. R. (1981). Kinetochore structure, duplication, and distribution in mammalian cells: Analysis by human autoantibodies from scleroderma patients. *J. Cell Biol.* **91**, 95–102.

Brinkley, B. R., and Chang, J. P. (1973). Embedding *in situ*. *In* "Tissue Culture: Methods and Applications," pp. 438–443. Academic Press, New York.

Brinkley, B. R., and Stubblefield, E. (1966). The fine structure of the kinetochore of a mammalian cell *in vitro*. *Chromosoma* **19**, 28–43.

Brinkley, B. R., Fuller, G. M., and Highfield, D. P. (1975). Cytoplasmic microtubules in normal and transformed cells in culture: Analysis by tubulin antibody immunofluorescence. *Proc. Natl. Acad. Sci. USA* **72**, 4981–4985.

Brinkley, B. R., Cox, S. M., and Pepper, D. A. (1980). Structure of the mitotic apparatus and chromosomes after hypotonic treatment of mammalian cells *in vitro*. *Cytogenet. Cell Genet.* **26**, 165–174.

Brinkley, B. R., Zinkowski, R. P., Mollon, W. L., Davis, F. M., Pisegna, M. A., Pershouse, M., and Rao, P. N. (1988). Movement and segregation of kinetochores experimentally detached from mammalian chromosomes. *Nature* **336**, 251–254.

Brinkley, B. R., Ouspenski, I., and Zinkowski, R. P. (1992). Structure and molecular organization of the centromere–kinetochore complex. *Trends Cell Biol.* **2**, 15–21.

Britten, R. J., and Kohne, D. E. (1968). Repeated sequences in DNA. Hundreds of thousands of copies of DNA sequences have been incorporated into the genomes of higher organisms. *Science* **161**, 529–540.

Christy, C. S., Deden, M., and Snyder, J. A. (1995). Localization of kinetochore fragments isolated from single chromatids in mitotic CHO cells. *Protoplasma* **186**, 193–200.

Fuller, G. M., Brinkley, B. R., and Boughter, J. M. (1975). Immunofluorescence of mitotic spindles by using monospecific antibody against bovine brain tubulin. *Science* **187**, 948–950.

Gasser, S. M., and Laemmli, U. K. (1987). Improved methods for the isolation of individual and clustered mitotic chromosomes. *Exp. Cell Res.* **173**, 85–98.

Gorbsky, G. J. (1997). Cell cycle checkpoints: Arresting progress in mitosis. *Bioessays* **19**, 193–197.

Haaf, T., and Ward, D. C. (1994a). Structural analysis of alpha-satellite DNA and centromere proteins using extended chromatin and chromosomes. *Hum. Mol. Genet.* **3**, 697–709.

Haaf, T., and Ward, D. C. (1994b). High resolution ordering of YAC contigs using extended chromatin and chromosomes. *Hum. Mol. Genet.* **3**, 629–633.

Haaf, T., and Willard, H. F. (1992). Organization, polymorphism, and molecular cytogenetics of chromosome-specific alpha-satellite DNA from the centromere of chromosome 2. *Genomics* **13**, 122–128.

Hartwell, L. H., and Weinert, T. A. (1989). Checkpoints: Controls that ensure the order of cell cycle events. *Science* **246**, 629–634.

He, D., and Brinkley, B. R. (1996). Structure and dynamic organization of centromeres/prekinetochores in the nucleus of mammalian cells. *J. Cell Sci.* **109**, 2693–2704.

Hendzel, M. J., Yi, W., Mancini, M. A., Van Hooser, A., Ranalli, T., Brinkley, B. R., Bazett-Jones, D. P., and Allis, C. D. (1997). Mitosis-specific phosphorylation of histone H3 initiates primarily within pericentromeric heterochromatin during G_2 and spreads in an ordered fashion coincident with mitotic chromosome condensation. *Chromosoma* **106**, 348–360.

Hilwig, I., and Gropp, A. (1973). Decondensation of constitutive heterochromatin in L. cell chromosomes by a benzimidazole compound ("33258 Hoechst"). *Exp. Cell Res.* **81**, 474–477.

Hoefsmit, E. C., Korn, C., Blijleven, N., and Ploem, J. S. (1986). Light microscopical detection of single 5 and 20 nm gold particles used for immunolabelling of plasma membrane antigens with silver enhancement and reflection contrast. *J. Microsc.* **143**, 161–169.

Hsu, T. C. (1952). Mammalian chromosomes *in vitro*. I. The karyotype of man. *J. Heredity* **43**, 167–172.

Ishida, R., Kozaki, M., and Takahashi, T. (1985). Caffeine alone causes DNA damage in Chinese hamster ovary cells. *Cell Struct. Funct.* **10**, 405–409.

Jeppesen, P., Mitchell, A., Turner, B., and Perry, P. (1992). Antibodies to defined histone epitopes reveal variations in chromatin conformation and underacetylation of centric heterochromatin in human metaphase chromosomes. *Chromosoma* **101**, 322–332.

John, H. A., Birnstiel, M. L., and Jones, K. W. (1969). "RNA–DNA hybrids at the cytological level. *Nature* **223**, 582–587.

Johnson, G. D., and Nogueira Araujo, G. M. D. C. (1981). A simple method of reducing the fading of immunofluorescence during microscopy. *J. Immunol. Methods* **43**, 349–350.

Jokelainen, P. T. (1967). The ultrastructure and spatial organization of the metaphase kinetochore in mitotic rat cells. *J. Ultrastruct. Res.* **19**, 19–44.

Jones, P. A., and Taylor, S. M. (1980). Cellular differentiation, cytidine analogs and DNA methylation. *Cell* **20**, 85–93.

Langer, P. R., Waldrop, A. A., and Ward, D. C. (1981). Enzymatic synthesis of biotin labeled polynucleotides: Novel nucleic acid affinity probes. *Proc. Natl. Acad. Sci. USA* **78**, 6633–6637.

Lawrence, J. B., Villnave, C. A., and Singer, R. H. (1988). Sensitive, high-resolution chromatin and chromosome mapping *in situ:* Presence and orientation of two closely integrated copies of EBV in a lymphoma line. *Cell* **52**, 51–61.

Lazarides, E., and Weber, K. (1974). Actin antibody: The specific visualization of actin filaments in non-muscle cells. *Proc. Natl. Acad. Sci. USA* **71**, 2268–2272.

Mace, M. L., Jr., Tevethia, S. S., and Brinkley, B. R. (1972). Differential immunofluorescence labeling of chromosomes with antisera for single stand DNA. *Exp. Cell Res.* **75**, 521–523.

Mole-Bajer, J., Bajer, A. S., Zinkowski, R. P., Balczon, R. D., and Brinkley, B. R. (1990). Autoantibodies from a patient with scleroderma CREST recognized kinetochores of the higher plant *Haemanthus. Proc. Natl. Acad. Sci. USA* **87**, 3599–3603.

Moroi, Y., Peebles, C., Fritzler, M. J., Steigerwald, J., and Tan, E. M. (1980). Autoantibody to centromere (kinetochore) in scleroderma sera. *Proc. Natl. Acad. Sci. USA* **77**, 1627–1631.

Nickerson, J. A., Krockmalnic, G., He, D., and Penman, S. (1990). Immunolocalization in three dimensions: Immunogold staining of cytoskeletal and nuclear matrix proteins in resinless electron microscopy sections. *Proc. Natl. Acad. Sci. USA* **87**, 2259–2263.

O'Keefe, R. T., Henderson, S. C., and Spector, D. L. (1992). Dynamic organization of DNA replication in mammalian cell nuclei: Spatially and temporally defined replication of chromosome-specific α-satellite DNA sequences. *J. Cell Biol.* **116**, 1095–1110.

Ouspenski, I. I., and Brinkley, B. R. (1993). Centromeric DNA cloned from functional kinetochore fragments in mitotic cells with unreplicated genomes. *J. Cell Sci.* **105**, 359–367.

Pardue, M. L., and Gall, J. G. (1970). Chromosomal localization of mouse satellite DNA. *Science* **168**, 1356–1358.

Pepper, D. A., and Brinkley, B. R. (1977). Localization of tubulin in the mitotic apparatus of mammalian cells by immunofluorescence and immunoelectron microscopy. *Chromosoma* **60**, 223–235.

Reynolds, E. S. (1963). The use of lead citrate of high pH as an electron-opaque stain in electron microscopy. *J. Cell Biol.* **17**, 208–212.

Rieder, C. L. (1979a). Ribonucleoprotein staining of centrioles and kinetochores in newt lung cell spindles. *J. Cell Biol.* **80**, 1–9.

Rieder, C. L. (1979b). Localization of ribonucleoprotein in the trilaminar kinetochore of Ptk1. *J. Ultrastruct. Res.* **66**, 109–119.

Ris, H., and Witt, P. L. (1981). Structure of the mammalian kinetochore. *Chromosoma* **82**, 153–170.

Rocchi, A., Di Castro, M., and Prantera, G. (1979). Effects of DAPI on human leukocytes *in vitro. Cytogenet. Cell Genet.* **23**, 250–254.

Schlegel, R., and Pardee, A. B. (1986). Caffeine-induced uncoupling of mitosis from the completion of DNA replication in mammalian cells. *Science* **232**, 1264–1266.

Schmid, M., Grunert, D., Haaf, T., and Engel, W. (1983). A direct demonstration of somatically paired heterochromatin of human chromosomes. *Cytogenet. Cell Genet.* **36**, 554–561.

Spurr, A. R. (1969). A low-viscosity epoxy resin embedding medium for electron microscopy. *J. Ultrastruct. Res.* **26**, 31–43.

Sullivan, K. F. (1998). A moveable feast: The centromere/kinetochore complex in cell division. *In* "Mechanisms of Cell Division: Frontiers in Molecular Biology" (S. Endow and D. Glover, Eds.). Oxford University Press, Oxford, England.

Tjio, J. H., and Levan, A. (1956). The chromosome number of man. *Hereditas* **42**, 1–6.

Waring, M., and Britten, R. J. (1966). Nucleotide sequence repetition: A rapidly reassociating fraction of mouse DNA. *Science* **154**, 791–794.

Wevrick, R., Willard, V. P., and Willard, H. F. (1992). Structure of DNA near long tandem arrays of alpha satellite DNA at the centromere of human chromosome 7. *Genomics* **14**, 912–923.

Wise, D. A., and Brinkley, B. R. (1997). Mitosis in cells with unreplicated genomes (MUGs): Spindle assembly and behavior of centromere fragments. *Cell Motil. Cytoskel.* **36**, 291–302.

Wolniak, S. M., and Larsen, P. M. (1992). Changes in the metaphase transit times and the pattern of sister chromatid separation in stamen hair cells of *Tradescantia* after treatment with protein phosphatase inhibitors. *J. Cell Sci.* **102**, 691–715.

Zinkowski, R. P., Meyne, J., and Brinkley, B. R. (1991). The centromere–kinetochore complex: A repeat subunit model. *J. Cell Biol.* **113**, 1091–1110.

CHAPTER 5

Three-Dimensional Transmission Electron Microscopy and Its Application to Mitosis Research

Bruce F. McEwen*,† and Michael Marko*

* Division of Molecular Medicine
Wadsworth Center
New York State Department of Health
Albany, New York 12201-0509

† Department of Biomedical Sciences
State University of New York
Albany, New York 12222

METHODS IN CELL BIOLOGY, VOL. 61

0091-679X/99 $30.00

I. Introduction

The overall goal of mitosis research is to achieve a molecular understanding of the complex mechanisms responsible for the proper segregation of the genome and cytoplasm during cell division. During the past decade, molecular and genetic techniques have made striking progress in identifying several protein components required for mitosis (For recent reviews see Elledge, 1998; Hyman and Karsenti, 1996; Merdes and Cleveland, 1997; Nicklas, 1997; Pennisi, 1998; Rudner and Murray, 1996; Waters and Salmon, 1997; Yen and Schaar, 1996). However, a complete molecular understanding also requires knowing how these individual proteins are arranged in the mitotic apparatus. Various forms of light microscopy have succeeded in providing a general picture of where different components are located, but the resolving power of electron microscopy is needed to achieve an appreciation of the molecular architecture that enables the mitotic apparatus to generate and control chromosome movements.

The primary challenge of transmission electron microscopy is that it provides a translucent (i.e., "x-ray") view of the specimen rather than the surface view we are accustomed to seeing in everyday life. While this has the advantage of enabling the user to see inside the specimen, it has the disadvantage that features from different levels within the specimen overlap and create a confusing image. In quantitative terms, the image produced by a transmission electron microscope (TEM) is a two-dimensional (2D) projection of the 3D specimen (see Fig. 1A for a simplified illustration). Potentially the same problem exists with light microscopy except that the relatively shallow depth of field of this instrument, compared to typical specimen thicknesses, restricts the amount of in-focus information that is visible. Furthermore, out-of-focus contributions can be eliminated either by computational (i.e., deconvolution) or mechanical/optical (i.e., confocal) methods. A 3D image can then be computed by collecting images at different focal planes and stacking them into a 3D volume. Thus far, it has not been possible to use such "optical sectioning" methods with TEM.

Traditionally, the projection problem of electron microscopy has been circumvented by embedding the specimen into plastic and cutting sections so thin (i.e., 0.05–0.1 μm thick) that they contain relatively little depth information. This strategy also solves the problem of limited electron penetrating power at conventional accelerating voltages. Serial thin sections can then be stacked into a 3D volume, or analyzed sequentially, to provide depth information. Although this procedure is labor-intensive, it is feasible and extremely effective as long as the specimen is not so large that several hundreds of serial sections must be cut.

Electron tomography has emerged as another effective method for obtaining 3D information from TEM (Frank, 1995; Koster *et al.,* 1997). In tomography, a 3D image is computed from a single thicker section by recording a series of 2D images of the specimen at different tilt angles relative to the electron beam (Crowther *et al.,* 1970; Hoppe, 1972). The 2D projections comprising such a tilt

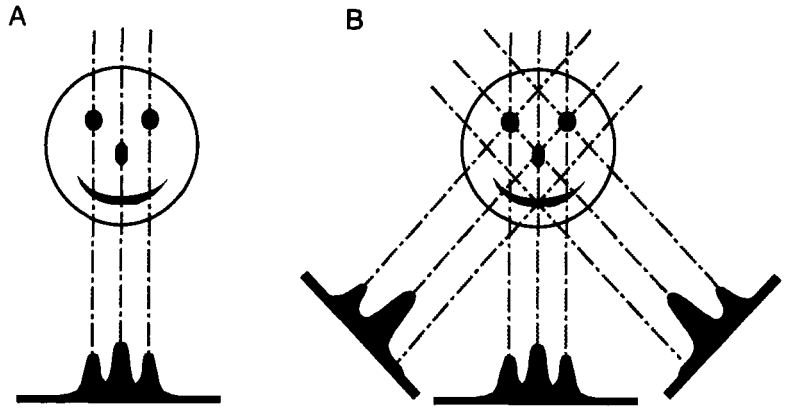

Fig. 1 Illustration of projection and reconstruction via back projection. (A) Projection of a 2D image onto a 1D line. The broken lines indicate selected projection rays. In transmission imaging, the projection rays also indicate the path taken by photons, electrons, etc. The graph along the solid line indicates the amount of specimen mass traversed by electrons that reach each point in the projection image (note that the actual number of electrons reaching the film is inversely proportional to the specimen mass traversed by the beam). Peaks of mass are recorded where the beam goes through the "eyes," "nose," and "mouth" of the face. (B) Projection from different directions. Note that the shape of the projected mass plot changes with the direction of projection, i.e., at the angle of the tilted projections some rays traverse both an eye and the nose. For reconstruction via back projection, the mass recorded at each point in the projection image is smeared uniformly along the projection ray. Such "backprojection rays," arising from areas of high recorded mass in different tilt views, intersect and reinforce one another at the locations of the main features in the image. In this way the 2D image is "reconstructed" from a series of 1D projections.

series are then "backprojected" into a 3D volume as illustrated in Fig. 1B. Essentially the same approach is used in medical imaging procedures such as computerized axial tomography and magnetic resonance imaging. The term *tomography* literally means visualization of slices, which derives from the fact that individual 2D slices can be computed and viewed independently of the rest of the 3D volume.

Sometimes sufficient 3D information can be obtained without computing a tomographic reconstruction simply by viewing stereo pairs or the images of a tilt series in rapid enough succession to become a "3D movie." This approach often works for relatively simple specimens that are not crowded with overlapping features, but structures in the mitotic apparatus are generally too complex to analyze via stereo pairs. For example, in a preliminary study to determine the number of microtubules on sister kinetochores fully contained within a 0.50-μm-thick section, we detected only 10 and 12 kinetochore microtubules via tracing stereo pairs and 23 and 28 kinetochore microtubules via electron tomography (McEwen *et al.*, 1995b).

In this chapter we describe the basic methodology involved in computing and analyzing 3D reconstructions via electron tomography and serial thin sections.

Examples are provided from recent studies applying these techniques to mitosis research.

II. Resolution and Choosing between Tomography and Serial Sections

When embarking upon an investigation of 3D ultrastructure the first practical question facing the investigator is whether to use electron tomography or serial section analysis. The main two factors to be considered are the required resolution, especially in the depth dimension, and whether or not the full structure must be analyzed in each 3D reconstruction. For example, if the question is how many microtubules are attached to a kinetochore then the whole kinetochore must be analyzed (McEwen *et al.,* 1997), but if one is interested in how individual microtubules interact with the kinetochore plate, then a portion of the plate can be analyzed in greater detail (McEwen and Heagle, 1997). Generally, it is much easier to study the whole structure via serial section analysis because it is difficult to ensure that an organelle such as the kinetochore is completely contained within a single 0.5 or 1.0-μm-thick plastic section. On the other hand, tomography provides much higher resolution in the depth dimension and is therefore the preferred approach for studies requiring fine detail.

The resolution of a serial section reconstruction in the depth dimension can be no better than twice the section thickness. There is a general misconception that resolution in the depth dimension is equal to the section thickness, but digital sampling theory tells us that resolution is never better than twice the sampling size (i.e., twice the section thickness). This is illustrated in Fig. 2, in which it can be seen that to resolve a string of small spheres, 40 nm in diameter and spaced 80 nm apart, one must collect sections every 40 nm so that one sees the spaces between the spheres. If one collects 80-nm-thick sections there will be one sphere per section which will appear as a solid line in the 3D reconstruction. Thus, 80-nm resolution requires cutting 40-nm-thick sections.

Since serial sections are seldom cut thinner than about 50 nm, resolution is generally limited to 100 nm in the depth dimension. There are preliminary reports that serial sections can be cut as thin as 10 nm, which could yield 20-nm resolution (e.g., Mastronarde *et al.,* 1997a). However, this is still less that the 5- to 10-nm resolution that is routinely obtained via electron tomography. Furthermore, it is questionable whether it will ever be feasible to cut the several hundreds of consecutive serial super-thin sections required to track through enough of the mitotic spindle to find the organelle of interest.

Although depth resolution is limited in serial section reconstructions, the x–y resolution is high, being restricted only by the specimen preparation. In some cases, good x–y resolution enables answering the questions at hand, even though depth resolution is limited. For example, the arrangement of spindle microtubules (MTs) was reconstructed with high accuracy in PtK_1 cells by sectioning in the

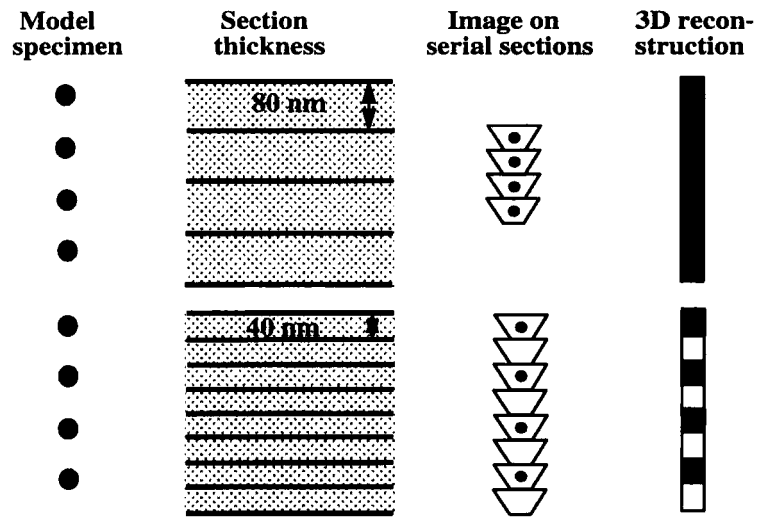

Fig. 2 Illustration showing that the limit of depth resolution for a serial section reconstruction is twice the section thickness. For a specimen consisting of a string of globular units spaced 80 nm apart, one must cut sections at 40-nm thickness to see the "gap" between units. Since resolution is defined as the limit of how close two points can come and still be resolved as two, the resolution limit of a serial section reconstruction is twice the section thickness. Note that if the globular units are touching each other, like beads on a string, then even thinner sections may be required to resolve the beads as separate entities.

axial direction (McDonald *et al.*, 1992). Since MTs are long and fairly straight, high depth (z) resolution was not required for following individual MTs, but the high x–y resolution was needed for their accurate placement.

For tomography, resolution is determined by the object size and the number of tilt views collected (Crowther *et al.*, 1970):

$$d = \alpha D/N \tag{1}$$

where d is the resolution (in nm), α is the angular tilt range (in radians), D is the diameter of the reconstructed object and N is the number of views collected in the tilt series. For plastic sections this can be expressed in terms of section thickness (Radermacher, 1992):

$$d = \pi aT/180\cos\theta_{\max} \tag{2}$$

where a is the tilt angle interval (in degrees). T is the section thickess (in nm), and $\theta_{\max}$ is the maximum tilt angle (usually 60° or 70°). Thus,

$$d = 0.035\ aT \text{ at } \theta_{\max} = 60° \tag{3a}$$

and

$$d = 0.052\ aT \text{ at } \theta_{\max} = 70° \tag{3b}$$

For a 250-nm-thick section, a 1° tilt angle interval, and 60° maximum tilt angle, the calculated resolution is 8.7 nm. In principle, resolution can be increased to the desired level simply by collecting more images (i.e., larger value for N in Eq. [1] and a smaller value for a in Eqs. [2] and [3]). In practice, tilt angle intervals less than 1 or 2° are seldom used due to file handling considerations and limits to the accuracy of electron microscope tilt stages. Higher resolution can also be achieved by cutting thinner sections, as long as the section is thick enough to provide useful depth information in the 3D reconstruction.

We emphasize that, as for light microscopy, resolution limit is not the same as detection limit. Thus, features finer than the resolution calculated by Eq. [3] are frequently detected without difficulty, particularly when they have a high contrast relative to the surrounding matrix. Examples include mitochondrial cristae (Mannella *et al.,* 1997), mineralization crystals (Landis *et al.,* 1993), selectively stained Golgi (Ellisman *et al.,* 1990), and selectively stained dendrites (Wilson *et al.,* 1992).

Furthermore, the resolution given by Eqs. [1]–[3] is a conservative estimate, with the actual resolution frequently being better. This is because Eq. [1] was formulated for an object that is uniformly solid. In the previous examples, however, the features of interest consist of more heavily stained objects that are sparsely distributed within a lighter staining matrix. For such specimens, the object diameter, D, used in Eq. [1] should be the diameter of individual objects rather than being derived from the total section thickness, as in Eq. [2]. On the other hand, Eqs. [2] and [3] accurately describe the resolution obtained for reconstructions of samples such as the kinetochore that uniformly fill the section thickness (McEwen *et al.,* 1993).

A potential disadvantage of tomography is that with conventional TEMs, image quality deteriorates rapidly at higher tilt angles for specimens thicker than approximately 0.10 μm. For this reason, tomography often requires a high or intermediate voltage electron microscope (HVEM or IVEM) with an accelerating voltage of about 1.0 MV or 200–400 kV, respectively. These microscopes are capable of recording quality images (i.e., with insignificant amounts of multiple scattering and chromatic aberrations) for specimens between 0.2 and 2.0 μm in thickness (e.g., King *et al.,* 1980; Soto *et al.,* 1994; Wilson *et al.,* 1992).

Since it is easier to follow a complete structure in serial sections and higher resolution is obtained with tomography, it would seem logical to combine the two techniques. Although there are reports of using serial section tomography (Soto *et al.,* 1994), in our experience it has not been feasible to trace fine features across the boundaries of serial tomographic reconstructions. The problem most likely stems from the fact that plastic sections lose 20–50% of their thickness upon exposure to the electron beam (Luther *et al.,* 1988). The nature of this mass loss is poorly characterized, but van Marle *et al.* (1995) present evidence suggesting that mass is lost from section surfaces. This contradicts an earlier report of uniform shrinkage throughout the section (Bennett, 1974) but is consistent with the fact that in most reconstructions the spacings and dimensions of

well-known structures, such as MTs, are not significantly flattened in the depth dimension. In addition, the top and bottom surfaces of tomographic reconstructions are generally of poorer quality than the rest of the volume, as expected for surface collapse (McEwen *et al.*, 1986; Frank *et al.*, 1987). These observations suggest that mass loss must be avoided if serial electron tomography is to be generally useful.

Nevertheless, it is advisable to cut serial sections in preparation for tomography so that one can find structures of interest, such as centrosomes and kinetochores, especially if the cell has been followed via video light microscopy (e.g., McEwen and Heagle, 1997). In addition, if the section thickness is at least 250 nm, then serial sections can be quickly and conveniently surveyed via phase-contrast light microscopy.

III. Electron Tomography

A. Specimen Preparation and Fiducial Markers

It goes without saying that the resolving power of tomography is of little value when applied to a poorly fixed and/or poorly stained specimen. Thus, all the usual care and consideration need to be applied when preparing sectioned material for electron tomography. One can also greatly improve resolution and feature detection in tomographic reconstructions by selectively staining features of particular interest to give them higher contrast than the rest of the specimen. Thus, neurons injected with the horseradish peroxidase (Wilson *et al.*, 1992) and Golgi impregnated with osmium (Ellisman *et al.*, 1990; Soto *et al.*, 1994) were reconstructed with good spatial resolution in 2.0-μm-thick sections. One recent application used photoconversion of BODIPY–ceramide to an osmiophilic reaction product that selectively stained the trans-Golgi network (Ladinsky *et al.*, 1994). This approach has obvious potential for determining the locations of specific spindle proteins via electron tomography, especially if green fluorescent tags with efficient photoconversion can be developed.

For conventional plastic sections, specimen preparation undoubtedly limits the meaningful resolution of tomographic reconstructions. For example, subunit structure that is readily apparent in negatively stained MTs is not visible in plastic sections, even when stained en bloc with tannic acid and uranyl acetate. However, negatively stained specimens often become distorted when drying down on the support film, which limits the interpretations that can be made. Frozen–hydrated specimens, prepared by rapid-freezing methods (Dubochet *et al.*, 1988; Ruiz *et al.*, 1994), avoid most of the collapse and drying artifacts that plague conventional preparations but, until recently, the extreme radiation sensitivity of frozen–hydrated specimens has precluded attempts to collect a tomographic tilt series. Cryoelectron tomography has now become feasible (Dierksen *et al.*, 1995; Grimm *et al.*, 1997, 1998) due to the development of improved data collection methods (Koster *et al.*, 1992, 1997; Dierksen *et al.*, 1992; Rath *et al.*, 1997) and a renewed

appreciation for the principle of dose fractionation (McEwen *et al.,* 1995a). Unfortunately, most components of the mitotic apparatus are too large or delicate to be isolated and imaged intact via cryoelectron microscopy. An alternative approach is to cryosection mitotic cells that have been rapidly frozen via high-pressure freezing, but these methods are still extremely challenging and unreliable (Michel *et al.,* 1992; Ruiz *et al.,* 1994; Erk *et al.,* 1998). Currently, the best compromise is freeze substitution (i.e., permeating the specimen with organic solvents and fixatives at low temperatures immediately after cryofixation; Moor, 1987; Dahl and Staehelin, 1989; Hippe-Sanwald, 1993; McDonald, 1994; Erk *et al.,* 1998). Preliminary reports of high-pressure frozen/freeze-substituted kinetochores from PtK_1 cells indicate improved preservation of the kinetochore and enhanced contrast of MTs (Mastronarde *et al.,* 1997b).

The images of a tomographic tilt series must be aligned to one another before computing the 3D reconstruction. The preferred way to accomplish this is by using gold particles as fiducial markers (Berriman *et al.,* 1984; Lawrence, 1992). Colloidal gold is applied to the Formvar support film, on the side opposite the sections, by incubation with approximately 10 μl of colloidal gold solution for 5–10 min. The amount of gold that sticks to the section surface can be controlled with reasonable consistency by using freshly prepared Formvar (within a few days of preparation), by making colloidal gold solutions rather than relying on commercial products (Frens, 1973; Slot and Geuze, 1985), and by carefully wicking the grid at the end of the incubation to leave a thin sheen on the surface. However, even with these precautions it is still advisable to incubate gold solutions on test grids (Formvar-coated grids without sections) for varying amounts of time in order to ensure getting the optimal amount of gold on the grid (i.e., 15–25 particles evenly distributed in a field of view equivalent to the area to be used for a single tomographic reconstruction). Some laboratories enhance gold binding by applying polylysine to the section surface prior to the colloidal gold solution.

The size of colloidal gold used depends on the section thickness, the magnification to be used, and the nature of the background material. For kinetochores in 250-nm-thick sections, we generally use 25 nm gold and image the kinetochore at 8000–12000× magnification. For thicker sections, it is often necessary to use 40 nm gold because the chromatin is relatively densely staining, and smaller gold particles will be hard to identify if they overlap with chromosomes at high tilt angles. On the other hand, for thinner sections, or regions of the cell without such a dense background, 10- to 15-nm gold particles are sufficiently large, especially when working at higher magnifications.

B. Instrumentation Requirements and Limitations Imposed by Specimen Geometry

It is much easier to record a suitable tomographic tilt series if the electron microscope has an accurate, motorized tilt stage that is reasonably eucentric and equipped with a digital angular readout. The stage should be able to tilt at least

to ±60° without occluding the central part of the specimen grid. For this reason, it is best if the specimen of interest is located away from the edges of the grid. It is also preferable that the microscope be an IVEM or HVEM because tomography is generally used with thicker specimens, and the effective specimen thickness increases dramatically at higher tilt angles. For those in institutions without suitable instrumentation, we strongly recommend collecting data at an electron microscopy center that routinely uses electron tomography. In the United States there are national resource centers at the Wadsworth Center in Albany, New York (Dr. C. L. Rieder, director), the University of Colorado in Boulder, Colorado (Dr. J. R. McIntosh, director), and the University of California San Diego, San Diego, California (Dr. M. Ellisman, director) that have suitable equipment and expertise to assist the user in collecting data sets from biological specimens. The laboratories of Dr. D. Agard (University of California San Francisco), Dr. W. Baumiester (Max Planck Institute Martinsried, Germany), and Dr. A. Belmont (University of Illinois, Urbana) also have extensive equipment and expertise for electron tomography.

In electron tomography, specimen geometry places important limitations on data collection. Most TEM specimens have an infinite slab geometry, i.e., the planar dimensions are effectively infinite because they are so much greater than the section thickness (usually more than 1000× greater; Fig. 3; Barnard *et al.*, 1992). For this reason, and because of the specimen support grid, it is generally not possible to collect tilt images over the full 180° angular range (collecting a 360° tilt range is unnecessary for complete coverage because 2D projections collected 180° apart provide identical information). Often the specimen rod will occlude the sample between 60 and 70°, thus limiting the total tilt range to ±70°. Even with specially designed tilt stages and an HVEM, it is seldom possible to record quality data beyond 70° tilt due to overlap with other objects in the section and image degradation resulting from the increased path length of the electron beam through the section (Fig. 3). For example, the path length of the electron beam is twice the section thickness at 60°, three times the section thickness at 70°, and thereafter rapidly increases to effectively infinite length at 90°.

The limited tilt range produces a wedge of missing data in the tilt series, i.e., a wedge of space that is not sampled by the tilt series (Fig. 4). This missing angular information causes a distortion in the reconstruction known as the elongation factor (Frank and Radermacher, 1986; Fig. 5). The missing wedge also causes anisotropic resolution in the reconstruction with the result that when linear elements, such as MTs, are oriented perpendicular to the tilt axis they fade and are often lost to view (Penczek *et al.*, 1995; Mastronarde, 1997). These difficulties can be partially alleviated by using a conical tilting scheme. Conical tilting reduces the missing wedge to a missing cone (Fig. 4B) and thereby reduces the amount of elongation and produces resolution that is isotropic in the planar dimensions (Frank and Radermacher, 1986; Radermacher, 1988). Unfortunately, conical tilting requires recording approximately 2.5 times as many images, with all images taken at high tilt where focusing is more difficult and image quality likely to

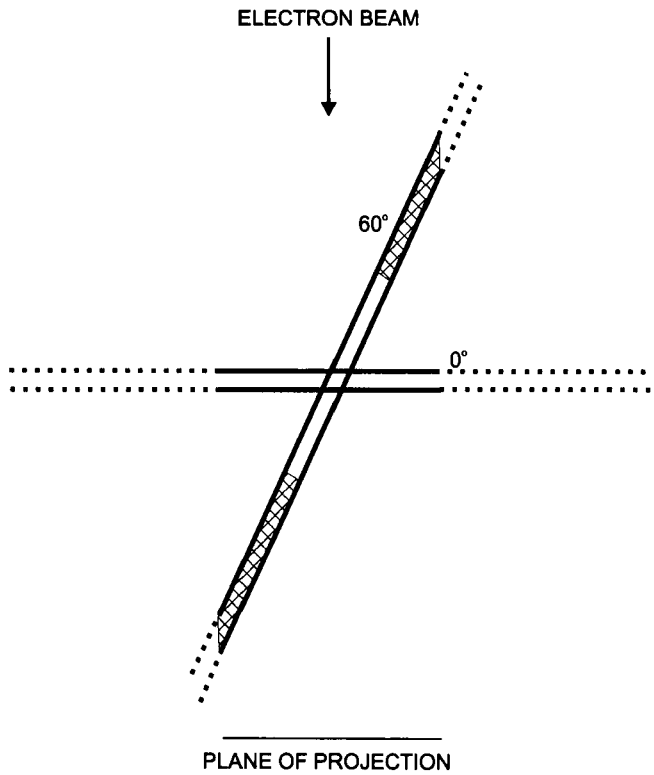

Fig. 3 Illustration of the infinite-slab geometry typical of electron microscope specimens. Arrow indicates the direction of the electron beam, whereas the plane of projection indicates the area where the image is recorded. The direction of the tilt axis is perpendicular to the plane of the figure. The solid lines depict the region of the specimen that is in the viewing area at the indicated tilt angles. Hatched area of the specimen denotes material that is in the viewing area at 60° tilt but not at 0° tilt. This material only causes a problem in areas of the specimen where the electron beam passes through both hatched and clear regions. This area of overlap is small as long as the tilt angle is not >60°, and the length of the viewing area is 5–10 times the specimen thickness, as in the illustration. If the length of the viewing area and specimen thickness are more nearly equal, then a significant portion of the 3D reconstruction will be affected by the artifact. Above 60°, the area of overlap increases rapidly with increased tilt angle, as does the path length of the electron beam. For these reasons, quality data are rarely obtained above 70° tilt (reproduced with permission from McEwen and Heagle, 1997).

suffer from an increased beam path. As an alternative, Penczek *et al.* (1995) introduced a double-tilt scheme that combines two orthogonal single-axis tilt series (Fig. 6) and reduces the missing wedge to a missing pyramid. This scheme provides most of the advantages of the conical scheme (i.e., near isotropic resolution and reduced elongation factor) without requiring special tilt-stage design or recording all images at high tilt angles (Penczek *et al.*, 1995; Mastronarde, 1997).

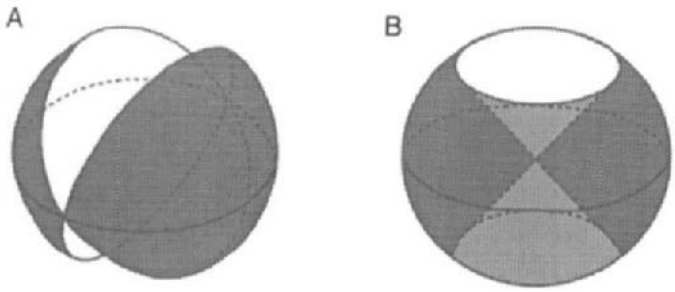

Fig. 4 Illustration of the tilt range limitations imposed by specimen geometry. (A) For single-axis tilting, the angular range depicted by the unshaded, wedge-shaped region of the sphere is inaccessible due to specimen geometry (see Fig. 3 and text). (B) For conical tilting, the inaccessible tilt range forms a cone. Distortion due to missing angular information is more severe for single-axis tilting because the unsampled area is both larger and asymmetric (see text).

Fig. 5 A single slice from a tomographic reconstruction viewed along the tilt axis. The boundaries of the specimen are clear in the depth dimension, although individual features are hard to discern in this view. The light feature is a gold particle that is oblong due to the missing angular range (see Figs. 3 and 4). Since gold particles have a high mass density, they are white in the 3D reconstruction (see text). The dark shadows on either side of the gold particle are also caused by the missing angular information (Frank and Radermacher, 1986). The large streaks on the right edge of the reconstruction are caused by a wraparound that is introduced into the tilt series images during alignment (see Fig. 6). Scale bar = 0.25 μm.

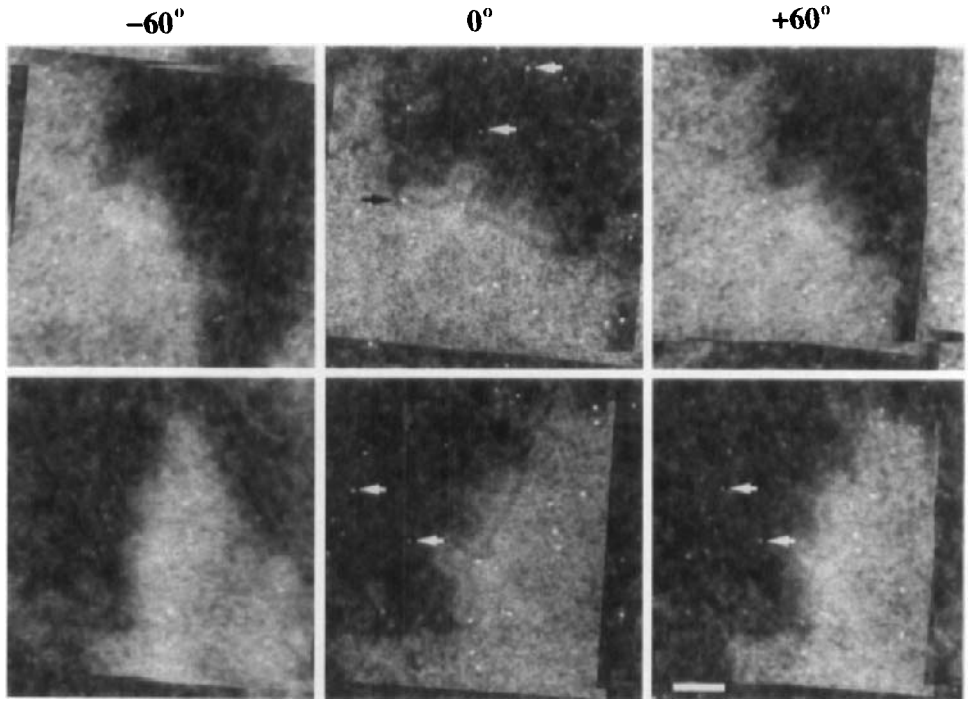

Fig. 6 Digitized electron micrographs from a double-tilt series. The wraparound effect in the images is the result of applying the alignment parameters to shift and rotate individual images. Images from the untilted and ±60° tilts are indicated for both the reference and orthogonal tilt series. Arrows indicate examples of colloidal gold particles that are in all the views. Scale bar = 0.25 μm.

C. Collecting a Double-Tilt Series and Minimizing Electron Dose

Before recording a double-tilt series, the structure of interest is located and checked to ensure that it has an appropriate distribution of colloidal gold particles and the ability to reach high tilt angles before occlusion occurs. There should be at least 4, ideally 8–12, suitable gold particles in the specimen area intended for tomographic reconstruction. Suitable gold particles are those evenly arranged around the structure of interest and well separated from the other gold particles or very dense areas of the specimen. If a particular sample is unique or relatively rare (i.e., a kinetochore followed by video light microscopy up to the point of fixation; McEwen and Heagle, 1997), more gold can be added to the section, if necessary. While that may mean adding a layer of fresh Formvar to ensure that the gold will stick, the extra Formvar is generally not a problem when using an IVEM or HVEM. Although occlusion can sometimes be avoided by moving the grid in the specimen holder, the best way to avoid occlusion is to carefully mount sections singly or as short ribbons in the center of slot or 100–200 mesh grids.

Relatively low magnifications are generally used for electron tomography. If the images are being recorded on film, 6000–30,000× will suffice for most applications. If the images are being recorded directly on a charge coupled device (CCD) camera, the magnification should be chosen to give the desired pixel size in the digitized image. Since digital cameras take the image from a different location in the microscope column than film cameras, magnification at the level of the digital camera needs to be accurately calibrated. The image magnification on a CCD camera should be adjusted so that, in the untilted view, the area of the specimen that is reconstructed is slightly larger than the area of interest. With film, one can be more generous in the extra area included within the recorded image. The extra area enables the user to trim away part of the edges of the reconstruction where artifacts accumulate due to wraparound in individual images of the tilt series after alignment (Fig. 6). The edges of the 3D reconstruction can also be affected by features that are outside the reconstructed area (in the 2D projection image) at low tilt angles but overlap with it at higher tilt angles (Figs. 1 and 3).

Before starting to collect the tilt series, the goniometer should be adjusted to the eucentric height. This adjustment places the tilt axis within the specimen plane, rather than above or below the plane, and thereby minimizes the amount of refocusing and sample chasing required between tilt images. Generally, it is advisable to start at one extreme of the tilt range (usually between −60 and −70°) and collect images at 1 or 2° angular intervals until reaching the other extreme of the tilt range (usually between 60 and 70°). The extremes of the tilt range are defined either by specimen occlusion or by stops in the goniometer that prevent the tilted specimen holder from running into other microscope components. Note that in this tilt scheme the untilted, or 0°, view is collected in the middle of the series. Starting at high tilt angle can be confusing for the novice user because the specimen is highly foreshortened in the direction perpendicular to the tilt axis (Fig. 6). Therefore, we recommend that the sample be tilted from 0° to the starting angle at low magnifications, keeping track of the desired area as the specimen is being tilted (most motorized stages tilt the specimen slowly enough to be followed).

Some tilt schemes vary the tilt angle interval based on geometric considerations that indicate a finer increment is required at high tilt angles (Olins *et al.*, 1989; Radermacher, 1992; Grimm *et al.*, 1998). However, simulations of the same data set reconstructed with fixed and variable tilt angle intervals indicate that the fixed interval schemes perform slightly better (Mastronarde, 1997). For simplicity, we recommend using the fixed angular interval scheme until the more complex schemes are further refined.

During data collection, the operator often has to recenter and refocus the specimen after changing the tilt angle. The amount of adjustment required depends on the eucentricity of the stage and how well it was adjusted before starting the tilt series. Some stages require focus adjustment only every 5–10° and very

little translational adjustment, but many tilt stages require significant adjustments between successive 1 or 2° angular intervals.

Effort should be made to minimize the total electron dose given to the specimen during data collection. Although embedded specimens are relatively insensitive to radiation damage, plastic sections do shrink in the electron beam, losing 25–50% of their original thickness (Luther *et al.,* 1988; Luther, 1992). In contrast, changes within the plane of the sections are relatively minor. The loss of section thickness is biphasic, with the initial phase being a large and rapid loss of 20–25% of the original sections thickness within a few seconds at the electron dose required for normal screen viewing. The slower phase is much more gradual and many images can be recorded with little additional shrinkage. The usual strategy, therefore, is to allow the sample to sit in the electron beam for 5–15 min to ensure the initial thinning is complete and that the specimen has stabilized. The actual tilt series is then recorded with as little additional electron dose as possible to minimize any further distortion (i.e., the primary consideration is that the specimen does not change while recording the tilt series).

There are a number of strategies for minimizing electron dose while recording the tilt series (e.g., Dierksen *et al.,* 1993; Koster *et al.,* 1993). The most straightforward is to focus and adjust x–y translations in an area of the specimen adjacent to the object of interest. The object of interest is then shifted into the electron beam only for the duration of image recording. It is important that shifting between exposure and focusing areas be along the tilt axis; otherwise, high-tilt images will be severely out of focus. Modern TEMs are often equipped with low-dose imaging kits that employ a double-deflection system to produce a rapid electronic shift between the two areas. This obviates the need to physically translate the specimen. With direct digital recording, focusing and recentering can be accomplished automatically, either off sample or directly on the sample at a low electron dose (Koster *et al.,* 1993; Dierksen *et al.,* 1993). An additional advantage of the CCD camera is that it provides immediate feedback about the quality of each image.

After recording the first tilt series, the specimen grid is rotated by 90°, and the second tilt series is recorded. If the specimen stage does not have a tilt/rotation holder, the specimen holder must be taken out of the microscope and the grid rotated by hand. For slot grids, the orientation of the slot can be used to estimate 90° with sufficient accuracy (the exact relative orientation of the two tilt series will be computed later as described below). For mesh grids, we advise putting a small guide mark on the rim of the copper grid with a super-fine Sharpie pen. Since the same specimen area has to be relocated after rotation, it is important to note landmark features after recording the first tilt series. This is done by following the specimen at lower magnification (preferably in the low-magnification mode if available) when returning to the untilted view, and then noting key features in the surrounding area. For example, if there is more than one section on the grid, the operator should know which section, and which area

of the section, contains the structure of interest. From there, it is usually easy to re-find the mitotic cell.

D. Digitization and Determining Pixel Size

If the tilt series has been recorded on film, the data must be scanned into digital form before a tomographic reconstruction can be computed. Ideally, one would use a high-quality, near video-rate CCD camera with few chip defects, low spatial distortion, 1024 × 1024 spatial resolution, and 12- to 14-bit gray scale resolution. However, such cameras are expensive. Since sensitivity is not an issue for film scanning, the CCD chip does not have to be cooled. High-resolution tube-type video cameras can also be used, and 8–10 bits gray scale is adequate if the scale and black level can be adjusted to make full use of the available dynamic range (e.g., Hindus, 1992; McEwen and Heagle, 1997). It is advisable to mount the camera on a copy stand so that the pixel size (size of the picture elements) can be adjusted by varying the camera height. Interchangeable 50- and 105-mm lenses and an extension ring enable us to adjust the pixel size over a five- or six-fold range (approximately 10–60 μm on the film).

The pixel size is chosen to exceed the resolution limit imposed by the angular interval used for recording the tilt series. Theoretically, digital resolution is equal to twice the pixel size, but in tomography there are a number of interpolation steps used during the rotational and translational alignments that precede computing the reconstruction. For this reason it is advisable to make the pixel size one-third to one-fourth the desired resolution (McEwen *et al.,* 1986). On the other hand, if the pixel size is too small, too many pixels are required to represent the full image and storage and data handling become a problem, even for modern workstations and multigigabyte hard drives. A pixel size of 1.0–3 nm is suitable for most studies in mitotic systems. Knowing the pixel size makes it convenient to compute magnifications, identify features, and draw scale bars at all subsequent steps, e.g., if the pixel size is 2 nm, a 0.10-μm scale bar is 50 pixels long and MT diameters will be 12 or 13 pixels.

The pixel size is measured before scanning by imaging a clear plastic ruler placed on the film plane of the camera. Pixel size at the film plane is then equal to the distance scanned on the ruler divided by the number of pixels in the width dimension of the image. Pixel size on the specimen is the pixel size on the film plane divided by the microscope magnification. Thus, if 10 mm on the ruler equals 500 pixels in the scanned image, the pixel size at the film plane is 20 μm, and if the microscope magnification was 10,000×, then the pixel size on the specimen is 2 nm.

For direct digital recording, the pixel size of the specimen is simply the element size of the CCD chip divided by the microscope magnification, as calibrated for the CCD camera. Most CCD chips used for digital electron microscopy have an element size of 24 μm, but frequently the image is binned (i.e., averaging of four neighboring pixels to create a new pixel) to correct for image imperfections

introduced by the scintillator that detects electrons and its coupling to the CCD chip that detects photons from the scintillator. Thus, the element size is 24 μm for an unbinned image, 48 μm for a binned image, and magnifications of 12,000 or 24,000× are required to achieve a 2-nm pixel size on the specimen.

E. Alignment and Mass Normalization of the Tilt Series

After digitization, the images of a tilt series must be aligned relative to one another, and the precise tilt axis direction computed, so that the back-projection algorithm places all the image density into its proper location in the reconstruction volume (Fig. 1B). Random misalignment causes loss of resolution in proportion to the extent of the errors. Systematic misalignments, such as incorrect placement of the tilt axis, causes distortions in the reconstruction (e.g., so that a spherical gold particle appears "C-shaped" in cross section).

The most straightforward method of alignment is to use the colloidal gold particles as fiducial markers. The tilt series is recorded so that the same 8–12 (minimum of 4) gold particles are present in each image of the tilt series (this requires some care because markers move relative to the underlying specimen as the section is tilted). Marker coordinates are then manually located using a cursor and appropriate graphics software. Automated procedures for finding gold particles have also been described (Fung *et al.*, 1996; Mastronarde, 1997). The 2D coordinates of all the markers on a given image of the tilt series are stored in a single text file that is identified with that image. Corresponding text files from all the tilt images serve as the input for algorithms that iteratively compute rotation, translation, and scale-change parameters for each image of the tilt series and 3D coordinates for each marker (Lawrence, 1992; Penczek *et al.*, 1995). During each round of iteration the algorithms seek to minimize the positional error between actual and computed marker locations on all images of the tilt series.

For alignment of a double-tilt data set, each single-axis tilt series is first aligned independently, using the same gold particles as fiducial markers in both tilt series (Fig. 6). Then the two tilt series are aligned to one another using the 3D coordinates computed for the fiducial markers in each data set during the independent alignment (Penczek *et al.*, 1995). Alternatively, tomographic reconstructions can be computed independently from each of the two single-axis data sets and the 3D reconstruction volumes aligned and merged (Mastronarde, 1997).

Markerless alignment schemes have been developed for specimen preparations where it is difficult to add colloidal gold (Liu *et al.*, 1995; Owen and Landis, 1996). To date, only a few successful applications of these schemes have been reported (e.g., Bullitt *et al.*, 1997) and, in our experience, these schemes are not as reliable as using fiducial markers. For this reason, and because it is not clear how well markerless alignment will work on double-tilt data sets, we recommend using fiducial markers whenever possible.

Technically, the tilt series should be normalized before computing the tomographic reconstruction so that gray-scale values have the same correlation to mass density on the different images of the tilt series. In addition, one should take the negative log of the recorded electron density to compute mass density (Hawkes, 1992), preceded by taking the negative log of the film density, if the tilt series has been recorded on film (i.e., take the double-negative log of film density to compute mass density). In practice, many investigators do not bother with mass normalization, or even computing negative log values, because computing mass normalization is not straightforward (due to variable illumination levels and the nature of most specimens) and because experience shows that the quality of the reconstruction is not very sensitive to the exact values used for mass density. The reason for the lack of sensitivity is probably because staining gives fairly high contrast to the objects of interest, and because most studies require boundary information rather than actual mass densities. Nevertheless, a number of "bootstrap" normalization schemes have been developed (e.g., McEwen *et al.*, 1986; Koster *et al.*, 1993; Grimm *et al.*, 1998), and these may become important for applications of tomography to unstained specimens in which precise mass density becomes more important.

F. Computing the 3D Reconstruction

Although computation of the reconstruction lies at the heart of the tomographic reconstruction procedure and is the most sophisticated and computationally intensive step, it is also the step that is most transparent to the user. In most software packages the user simply submits the aligned, normalized images and waits for the reconstruction. The computation actually has two steps: weighting and back projection. The weighting function is applied in Fourier space (i.e., to the Fourier transform) and it corrects for the fact that the tilt series gives more weight to low-resolution components of the image (Frank and Radermacher, 1986). Thus, application of the weighting function affects individual images in a similar fashion to high-pass filtration. Although weighting can be applied to the 3D reconstruction volume, it usually is quicker to weight the input images. For a single-axis tilt series, R^* weighting, in which components of the Fourier transform are simply multiplied by their Fourier radius, is the most commonly used weighting function. For back projection using a double-tilt series, a general weighting function must be used (Radermacher, 1988; Penczek *et al.*, 1995). If, however, the two tilt series are combined after computing independent 3D reconstruction, R^* weighting can be used during the reconstructions steps and common Fourier components averaged when combining the two 3D reconstructions (Mastronarde, 1997).

Since tomographic reconstructions of moderate size volumes (i.e., $900 \times 900 \times 200$ voxels) can take several hours to compute, it is advisable to first compute a small test volume to check for alignment error and to ensure adequate depth dimension has been allotted for the reconstruction (usually specified as

an input parameter for the reconstruction program). This is easy to do for single-axis data sets because most algorithms compute the reconstruction one slice at a time along the tilt axis, enabling the user to specify which slice or slices to compute (hence the origin of the term tomography or viewing slices). One such slice is shown in Fig. 5. Notice that the reconstruction is well-defined against the background, the top and bottom boundaries of the specimen are clearly visible, and features in the volume are crisp, although still hard to identify. The gold particle is oblong, rather than circular, due to the missing wedge. The dark shadows on either side of the gold particle are also caused by the missing wedge (Frank and Radermacher, 1986) but they are not nearly so noticeable for other features in the reconstruction (gold particles have a particularly high mass density). If the tilt series had been systematically misaligned, relative to the tilt axis, the gold particle would be C-shaped or otherwise distorted.

IV. Serial Section Reconstruction

A. Background

Serial thin section methods for TEM are well established and have played a key role in initial ultrastructural characterizations of the mitotic apparatus (e.g., Brinkley and Cartwright, 1971; McIntosh and Landis, 1971; Roos, 1973; Rieder, 1981). These methods continue to play an important role in mitosis research as illustrated by the recent use of serial thin sections to investigate the length and number of kinetochore MTs in kinetochore fibers (McDonald *et al.*, 1992), the ultrastructure of yeast spindles (Ding *et al.*, 1993), and how variations in kinetochore MT number are correlated to control of chromosome motion (McEwen *et al.*, 1997).

Detailed protocols for flat embedding and serial sectioning of mitotic cells can be found elsewhere in this book. Here we briefly describe methods for stacking serial sections into a 3D volume and analysis of the results. We also present a comparison of 3D reconstructions created from serial thin sections, serial thick sections traced via stereo viewing, and electron tomography.

B. Sectioning

The first step is to decide how thick to cut the sections. As mentioned earlier, the z resolution of the reconstruction will be best with the thinnest sections but the best possible z resolution may not be needed to answer the biological question. If good depth resolution is needed, but the specimen is large, there are two alternatives to cutting numerous very thin sections. One alternative is to make serial tomographic reconstructions from thick sections but, as discussed previously the loss of material from section surfaces leaves gaps in the final structure. The other alternative is to use stereo viewing to trace contours on multiple levels of thick sections. With this approach, the depth resolution in each section is not

as good as with tomography because the number of levels traced in each section depends on visual depth acuity, which in turn depends on the visibility of structures in the stereo view. Nevertheless, resolution is approximately equivalent to tracing conventional serial thin sections, and tracing thicker sections is more practical both because fewer sections are required and because sections that are at least 0.25 μm thick can be rapidly prescanned via phase contrast light microscopy (Rieder *et al.*, 1985). However, as mentioned previously stereo viewing works poorly for thicker sections that are densely packed with structures, and any method using section thicknesses more than approximately 0.20 μm should employ an IVEM or HVEM.

C. Aligning and Stacking Serial Thin Sections

Strictly speaking, proper alignment of serial sections requires some form of fiducial marks that are consistently located throughout the serial section series. Fiducial markers can be introduced by using a laser to drill holes into the specimen before sectioning (Bron *et al.*, 1990). Alternatively, the block can be trimmed with at least two adjacent edges perpendicular to the block face instead of being beveled as is the usual practice. This means that on every section, the area of interest will be located at the same position relative to the two perpendicular edges.

In practice, successive sections are usually aligned simply by matching the contours traced on the previous section with the image of the current section. For serial thick sections traced in stereo, structures from the top surface of the current section are aligned with contours from the bottom surface of the previous section. Although such markerless alignment schemes can be plagued by twisting or shifting distortions of the object through the 3D reconstruction (Russ, 1992), in most studies this modest amount of distortion is tolerable because the purpose is to determine structural relationships in the sample rather than the precise overall shape. In this regard, prior knowledge of the typical overall shape of the sample (e.g., from light microscopy) often aids in keeping the alignment reasonable.

Although serial section reconstructions are normally based on traced contours of the structures of interest, continuous-density volumes can also be constructed by stacking up aligned sets of images from very thin sections (Bron *et al.*, 1990). In either case, the depth dimension has to be stretched to make the scales the same in all directions. Reconstruction can then be visualized in the same way as a tomographic volume.

V. Analysis and Display of 3D Reconstructions

A. Slice Viewing

In tomography, the 3D structural relationships of the specimen can often be appreciated and interpreted by simply looking carefully at sequential slices

through the 3D reconstruction. In many cases, this will suffice to answer the biological question at hand. Normally, the slices are only 1 voxel (volume element) thick, although sequential slices are sometimes averaged to reduce the total number. A tomographic volume can be sliced along any desired axis, with the most common ones being along the original direction of the electron beam (for the untilted specimen), along the tilt axis, and along the axis orthogonal to these two. Generally, slices from a tomographic volume are much thinner than can be cut by a microtome, and the detail visible on a slice is always much better than that seen in any one of the tilt images that went into the reconstruction (i.e., compare Fig. 6 and Fig. 7, see color plate).

Before analyzing the slices, some simple image processing is usually done to enhance visibility of the structure of interest. As a minimum, the contrast and brightness should be optimally adjusted using techniques that operate on the histogram of the image, e.g., histogram stretching if the image is has low contrast and histogram equalization if contrast is too great or the dynamic range is too high. In some cases, the image is filtered to enhance or decrease the sharpness of edges and fine features. Although it is preferable for these operations to be performed on the 3D volume as a whole, it is usually satisfactory to do them on the individual slices. Many low-cost or free software packages are available which are capable of this kind of image processing (Carragher and Smith, 1996).

The best way to view slices is to move along a chosen axis at any desired speed, stopping or reversing direction at will. This process is aided by software packages that hold the entire volume in memory and show the slices very quickly, even from three axes at once. A simpler alternative is to take all the slices along a desired axis from the volume and make them into a "movie," which can be played with one of the movie or video players available on most computers.

Unlike tomographic slices, the contrast of serial sections usually varies, so image processing must be "customized" for each section. As with tomographic volumes, movies are a convenient way to view successive images of an aligned stack of serial sections. Sometimes this movie is all that is required for the user to interpret the 3D structure. Several serial thin sections can also be stacked and looked at stereoscopically to provide a 3D view. This is done in the same way as for confocal light microscopy, i.e., the slices are copied into two parallel stacks of images in which each successive image in depth is offset in x by a defined increment. The stereo pair is formed by making a projection image through each stack (van der Voort *et al.*, 1985). Serial thick sections must be recorded in stereo at the outset to enable stereo tracing.

Often it is advantageous to cut out a 3D window, containing a particular region of interest, rather than looking at slices from the whole volume. Besides saving computer space, this provides a way to do side-by-side comparisons of different parts of the volume or of successive slices through the volume. For example, in Fig. 8 a kinetochore present in nine successive serial sections is presented in one view as a gallery of small windows from each electron micrograph.

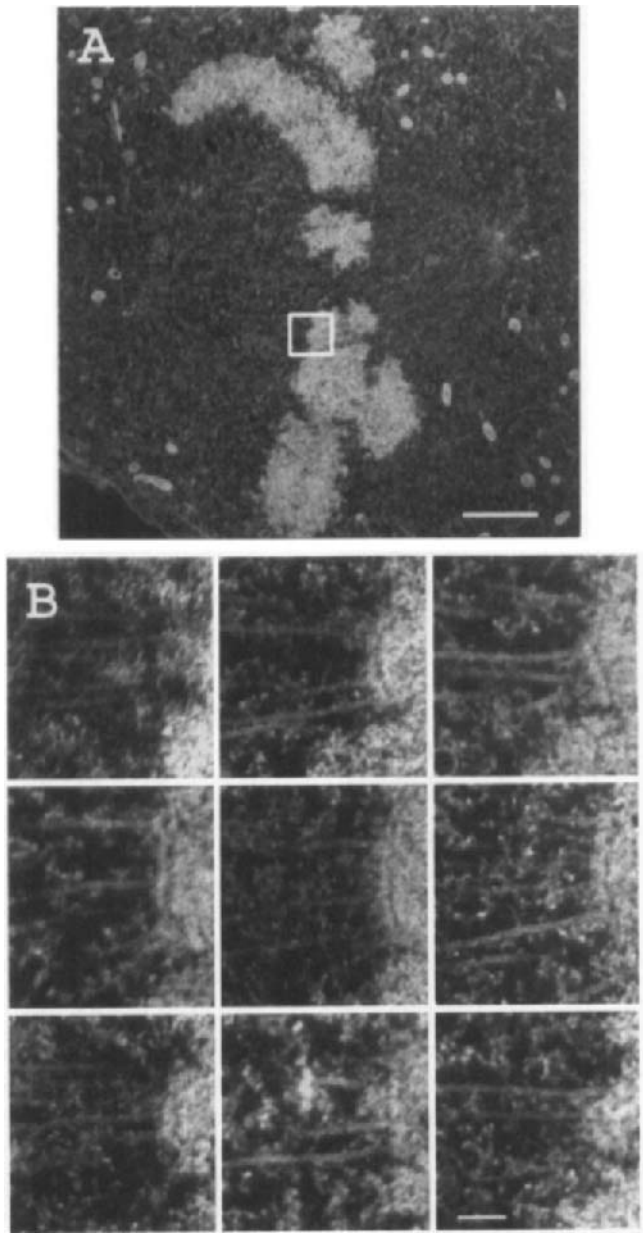

Fig. 8 Using multiple small windows for comparative display. (A) Full area recorded from a single serial thin section of a metaphase PtK_1 cell. In this study, electron micrographs were recorded with sufficiently low magnification to include all of the mitotic spindle. Small windows, such as the one indicated by the white box, were subsequently scanned at higher magnification for analysis of single kinetochores. (B) The kinetochore indicated by the box in A followed through nine serial sections. A total of 28 kMTs were detected on this kinetochore. Scale bars: A, 2 μm; B, 0.20 μm (adapted with permission from McEwen *et al.*, 1997).

B. Segmentation

Although someone very familiar with the sample being examined can often interpret all that is necessary just by viewing slices, presenting the data to others usually requires a simplified model that clearly demonstrates the points of interest. Some form of modeling is also required for quantitative analysis. The first step in modeling is usually segmentation, which is the separating, isolating, or accentuating objects of interest within the volume.

Segmentation can be done automatically or interactively. The automatic approach requires that the voxels which make up, or outline, the object of interest share some distinctive characteristics. The most common defining characteristics are gray-scale values and proximity to other voxels of like density. For example, if all voxels of the object fall within a density range that does not overlap the density range of voxels in the rest of the volume, the object can be automatically segmented simply by specifying the appropriate density thresholds. If there is some overlap in density range with other voxels in the volume, the object can still be automatically segmented if the surface voxels of the object are in a narrow density range and are all contiguous (or at least contiguous within a defined distance range).

Unfortunately, such conditions rarely occur in conventionally stained electron micrographs. More commonly, objects in electron micrographs are distinguished by their textures. For example, in most electron micrographs kinetochores do not have a distinctive brightness level or even a clear border. Rather, kinetochores are distinguished by their more compact structures compared to chromatin (Fig. 7, see color plate). In other imaging fields sophisticated automatic segmentation techniques have been developed, including texture identification and intelligent 3D detection of interfaces (Jain, 1989; Russ, 1992), but these methods have not yet been adapted for electron microscopy.

Interactive segmentation relies on human pattern recognition to trace the object of interest. Although this tracing can sometimes be semiautomated (e.g., McDonald *et al.,* 1992; Mastronarde *et al.,* 1993), it usually requires manually drawing lines or indicating points using a cursor. For example, we recently segmented kinetochores and kMTs by drawing a contour around each object on all the tomographic slices in which they were visible (Fig. 7, see color plate). Although several objects can be traced simultaneously on each slice, we traced kinetochores and kMTs in separate steps because kinetochores were easier to follow after a smoothing filtration, whereas kMTs were easier to follow after edge enhancement (compare Figs. 7B and 7C). In most studies tracings on successive slices are stacked for subsequent rendering or analysis (e.g., Figs. 9B and 10, see color plate). Several software packages are available for tracing on 2D images including Sterecon, which we distribute (Marko and Leith, 1996).

A special feature of Sterecon, is tracing in 3D, which enables tracing stereo pairs of thicker serial sections. This in turn allows the user to track a structure over several micrometers of depth without cutting an unwieldy number of serial

thin sections (Rieder *et al.,* 1985; Parsons *et al.,* 1991). Using stereo viewing and a 3D cursor, linear structures such as spindle MTs can be traced as 3D lines, whereas larger structures, such as chromosomes and kinetochores, can be traced as parallel planes in the 3D volume. The advantage of this approach is that the 3D structure is apparent during tracing.

Serial thin sections and tomographic volumes can also be traced in stereo by creating two stacks of slices, with slices in each set being progressively translated in a direction perpendicular to the tilt axis. This method is helpful for segmenting objects in serial sections since the poor depth resolution (Fig. 2) often results in uncertainties about structural continuity that are partially alleviated by stereo tracing. Stereo tracing also helps maintain structural continuity for tomography volumes. However, since tomographic reconstructions are generally too complex to appreciate as a whole via stereo viewing, 3D tracing has to be done on subvolumes. Normally these subvolumes are overlapping "thick" slices along the original axis of the electron beam. The maximum number of depth contours that can be drawn for a given subvolume is equal to the number of 1-voxel-thick slices in the subvolume.

The sets of stacked contours created by any of the previous methods form the boundaries of the individual objects in the segmented volume. For this reason, the contour stacks can be used as masks to create continuous-density subvolumes that either include or exclude the voxels bounded by the contours. Contours are also commonly used directly for creating models and/or for making quantitative length, volume, or surface area measurements. Examples of quantitative length measurements are shown in Fig. 9 (see color plate).

Recently, an interactive volume editor called Tinkerbell has been developed at the Wadsworth Center (Li *et al.,* 1997). This system uses a 3D cursor of adjustable shape and size to cut out desired regions of a rendered volume that is viewed in stereo. The cutout volumes are moved to another window, which accumulates a collection of segmented objects that retain the same spatial relationships they had in the original volume. This gives the same result as masking from contours, but in a more direct way. With the relatively large volumes used in mitosis research, this system works best on a high-end Silicon Graphics workstation equipped with a Reality Engine.

C. Modeling and Rendering from Contours

Stacks of contours, created for each individual object of interest in the segmentation processes described previously enable the reconstructed volume to be displayed with any combination of these objects (e.g., Figs. 9A, 9B, 10A, and 10B, see color plate). This in turn allows interrelationships between objects to be clearly seen without the confusion that arises from trying to view too many features at one time. Viewing is also facilitated by making surface models from the contour stacks using a process called *tiling.* Tiling is the creation of small polygonal surfaces, usually triangles, between defined 3D points on the surface

of a segmented volume (Figs. 10E and 10F). The 3D points are called *nodes.* Each node often has an associated normal that is used to control the shading and lighting parameters that are subsequently applied to the surface representation. Tiled surfaces can be smoothed to reduce the effect of tracing artifacts (Figs. 10C and 10D).

When the stacked contours are used directly, tiling simply involves connecting points between contours of adjacent depth planes (e.g., Fig. 10E). Software packages such as MOVIE.BYU (Christiansen and Sederberg, 1978) are able to create tiled surfaces from contours semiautomatically. With serial section reconstructions, the contours are often widely spaced along the sectioning direction. Since the shape of successive contours can vary considerably, intervention by the user is sometimes necessary to ensure that depth connections are correct. With tomographic volumes, the shape of adjacent depth contours does not vary greatly and tiling is usually automatic.

Since the volume produced by electron tomography is continuous, contours segmenting an object can be drawn on every voxel in depth. When such a contour stack is filled, the resulting binary volume can be tiled using an algorithm such as marching cubes (Lorensen and Cline, 1987). The major difference between using MOVIE.BYU and marching cubes is that the former draws tiles that connect discrete points on adjacent contours, whereas the latter uses an algorithm to decide where to place tiles along a more or less continuous surface. Marching cubes usually produces smaller polygons, and thereby a more detailed surface, than MOVIE.BYU (compare Figs. 10E vs 10F and 10C vs 10D). Tracing artifacts are also more prominent, but these can be mitigated by filtering (blurring) the binary volume or smoothing the polygons. Marching cubes software is readily available as shareware or from workstation vendors.

Surface rendering of tiled models has proven to be a versatile method for displaying both electron tomographic and serial section reconstructions. Rendering refers to using parameters such as color, transparency, shininess, and shadow to depict a surface created by tiling or other methods. Rendering also allows textures or patterns to be mapped onto the surface. Each of the several segmented objects from the original reconstruction can be rendered with different sets of these parameters (e.g., kinetochore and MTs in Fig. 9B). Thus, when any desired collection of objects are combined into a scene, they can be easily distinguished from each other. The group of selected objects can be rotated and viewed from any direction and cut by arbitrary clipping planes to reveal interior objects in cross section. Video animations can be made to show the features of interest in a dynamic and attractive way.

D. Rendering from Continuous-Density Volumes

When traced contours are used as a mask (see Section V,B), the segmented reconstruction volumes retain all of their 3D density information, unlike the solid-object binary volumes created from contour stacks. These continuous-density

volumes can be either surface or volume rendered and combined in scenes as previously described. In general, the full reconstruction volume cannot be effectively rendered without prior segmentation (see Section V,B).

Surface rendering of continuous-density volumes can be accomplished by a shading algorithm (e.g., Radermacher and Frank, 1984), by algorithms such as marching cubes, or by controlling the opacity of the volume during volume rendering to show only the surface. In all cases, the location of the surface can be controlled by setting a threshold density value for the surface voxels of the object. Smoothing can also be applied, along with shading as a depth cue. Surface rendering of continuous volumes has the potential for giving a more faithful representation of the actual surface of an object than the rendering of a surface from stacked contours. However, care should be taken during the segmentation process that the contours drawn are smooth and accurate. Otherwise, objects of interest acquire a step-like appearance on their edges.

Volume rendering is a display method that can retain the translucent quality of the reconstruction, showing the 3D structure within an object (Fig. 11A). The procedure involves projection through the volume using a specified opacity to control image translucence. Each density value in the histogram of the volume is assigned an opacity value. Thus, volume rendering can be used for segmenting objects within a volume, but only in special cases in which the objects to be segmented have high contrast (see Section V,B). More commonly, volume rendering is used to give a view of the internal 3D structure of a segmented object. The internal 3D structure can only be appreciated by either a stereo pair image or by combining several views to form a rotation movie, which gives the appearance of seeing a "3D electron micrograph." When the opacity is set to its maximum value (i.e., 1.0; Fig. 11B), the result is a surface view similar to that produced by the shaded surface algorithm of Radermacher and Frank (1984). Software for volume rendering is available from vendors catering to applications in confocal light microscopy and medical tomography.

VI. Software Packages

A number of laboratories have developed extensive software packages for electron microscopy that include the required programs for computing tomographic reconstructions. These packages are generally available at nominal cost. At the Wadsworth Center we use SPIDER, which has been developed over several years by Joachim Frank and colleagues and distributed worldwide (Frank *et al.*, 1996). For tracing contours on both tomographic reconstructions and serial sections we use Sterecon, which has the capability of tracing with a stereo cursor (Marko and Leith, 1996). Various software packages for electron microscopy are featured in a recent issue of the *Journal of Structural Biology*, which is a valuable resource for those considering acquiring the capacity to compute and analyze tomographic reconstructions (Carragher and Smith, 1996).

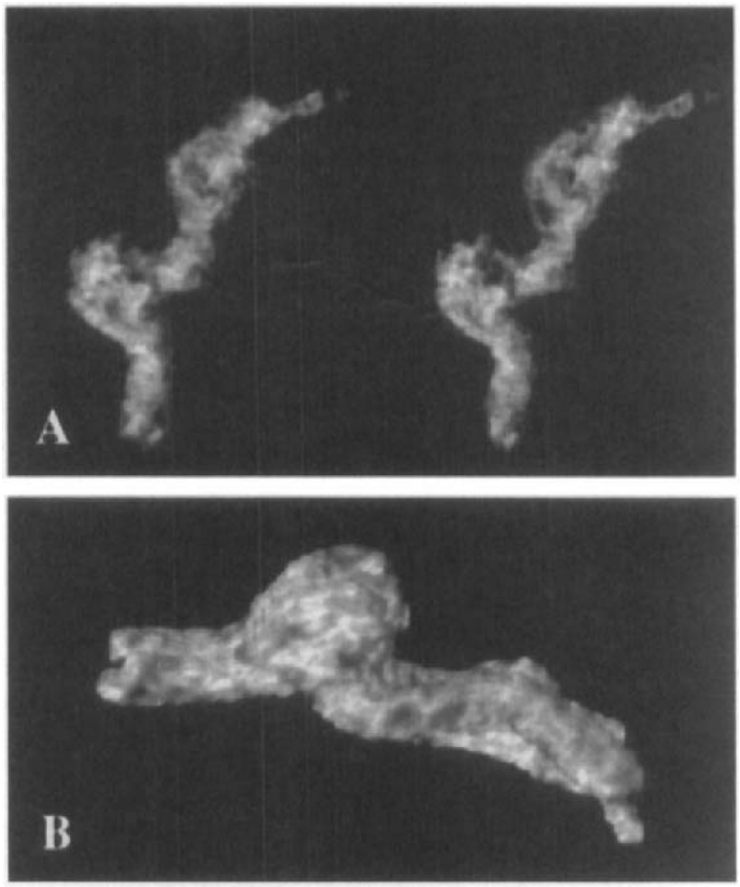

Fig. 11 Renderings of a segmented continuous-density volumes of the kinetochore shown in Fig. 7, 9, and 10. (A) Volume rendering showing internal 3D structure. The Stereo pair is meant to be viewed with a pocket stereoscope or by converging the eyes. The opacity was adjusted to give an indication of the surface as well as the internal structure. The mask used to segment this volume is represented by the rendering shown in Fig. 10D. (B) Volume rendering showing a surface view. In this case, the opacity was set to full value (i.e., 1.0) to block internal visibility and provide a surface view. This volume was segmented using the new Tinkerbell utility created at the Wadsworth Center (see text).

VII. Summary and Conclusions

Transmission electron microscopy produces images that are projections of the original object, with the consequence that features from different depths of the specimen overlap and give a confusing image. This problem is overcome by reconstructing the object in 3D from a series of 2D views using either serial thin section reconstruction or electron tomography. In the serial section approach,

the series of 2D views is generated from images of successive serial sections cut thin enough to be effectively 2D slices of the specimen. For electron tomography the series of 2D views is generated by tilting a single, usually thicker, section in the electron beam. Resolution in the depth dimension is limited to twice the section thickness for serial section reconstruction and is determined by the number of tilt views collected (i.e., by the fineness of the angular interval between successive tilt views) for electron tomography. Both methods produce distorted 3D reconstructions because of missing material and alignment difficulties in the case of serial sections and the limited angular tilt range in the case of electron tomography. However, techniques have evolved for minimizing and circumventing these distortions and, as long as the user is aware of the limitations, misinterpretations can be avoided.

Since electron tomography provides better resolution (generally 5–20 nm), it is the method of choice for determining detailed structural interactions such as the depth of kinetochore MT penetration into the kinetochore outer plate. On the other hand, serial section reconstruction is more effective for projects that require tracking through a complete object in the specimen, such as counting the number of kinetochore MTs on each kinetochore. If the project requires finding a relatively small object in a large specimen (e.g., finding centrioles in an oocyte), then it is sometimes advantageous to cut thicker plastic sections and analyze them via stereo viewing. The mitotic spindle, however, is generally too complex to be analyzed via stereo viewing. Currently, collapse of plastic sections in the electron beam limits the utility of serial section electron tomography.

Once a 3D reconstruction is completed it must be analyzed with the 2D medium of the screen on a computer monitor. The easiest approach is usually to walk through the 3D reconstruction volume slice by slice. However, in order to appreciate 3D interactions, and to communicate the results to others, it is generally necessary to segment key components from the rest of the volume and use modeling and rendering techniques. Rendered surface views can easily be color coded and provided with a number of depth cues to simulate the surface viewing encountered in everyday life. In some instances, it is useful to look through a smaller portion of the reconstruction volume with "X-ray vision." This can accomplished by using volume rendering to create a series of semitransparent views from different tilt angles.

Acknowledgments

We thank Drs. Ardean Leith, Alex Khodjakov, Michael Koonce, and Carmen Mannella for helpful comments on the manuscript. We also thank Karolyn Buttle for information about applying colloidal gold to plastic sections and Drs. Paul Penczek, Joachim Frank, and Conly Rieder for many stimulating conversations. BFM receives support from NSF Grant MCB9420772 and NIH Grant RR01219. MM is supported by New York State through the Wadsworth Center. The BMIRR Facility is supported by NIH Grant RR01219, awarded by the Biomedical Research Technology Program. Original work in this chapter also uses the Modeling for Biological Complexity Facility funded by NSF Grant BIR

9219043 (to J. Frank) and the video light microscopy and electron microscopy core facilities of the Wadsworth Center.

References

Barnard, D. P., Turner, J. N., Frank, J., and McEwen, B. F. (1992). A 360° single-axis tilt stage for the high-voltage electron microscope. *J Microsc.* **167,** 39–48.

Bennett, P. (1974). Decrease in section thickness on exposure to the electron beam: The use of tilted sections in estimating the amount of shrinkage. *J. Cell Sci.* **15,** 693–701.

Berriman, J., Bryan, R. K., Freeman, R., and Leonard, K. R. (1984). Methods for specimen thickness determination in electron microscopy. *Ultramicroscopy* **13,** 351–364.

Brinkley, B. R., and Cartwright, J. (1971). Ultrastructural analysis of mitotic spindle elongation in mammalian cells in vitro. *J. Cell Biol.* **50,** 416–431.

Bron, C., Gremillet, P., Launay, D., Jourlin, M., Gautschi, H. P., Baechi, H. P., and Schuepbach, J. (1990). Three dimensional microscopy of an entire cell. *J. Microsc.* **157,** 115–126.

Bullitt, E., Rout, M. P., Kilmartin, J. V., and Akey, C. W. (1997). The yeast spindle pole body is assembled around a central crystal of Spc42p. *Cell* **89,** 1077–1086.

Carragher, B., and Smith, P. R. (1996). Advances in computational image processing for microscopy. *J. Struct. Biol.* **116,** 2–8.

Christiansen, H. W., and Sederberg, T. W. (1978). Conversion of complex contour line definitions into polygonal element mosaics. *Computer Graphics* **12,** 187–192.

Crowther, R. A., DeRosier, D. J., and Klug, A. (1970). The reconstruction of a three-dimensional structure from its projections and its application to electron microscopy. *Proc. R. Soc. London A* **317,** 319–340.

Dahl, R., and Staehelin, L. A. (1989). High-pressure freezing for the preservation of biological structure: Theory and practice. *J. Electron Microsc. Tech.* **48,** 103–106.

Dierksen, K., Typke, D., Hegerl, R., Koster, A. J., and Baumeister, W. (1992). Towards automatic electron tomography. *Ultramicroscopy* **40,** 71–87.

Dierksen, K., Typke, D., Hegerl, R., and Baumeister, W. (1993). Towards automatic electron tomography II. Implementation of autofocus and low-dose procedures. *Ultramicroscopy* **49,** 109–120.

Dierksen, K., Typke, D., Hegerl, R., Waltz, J, Sackmann, E., and Baumeister, W. (1995). Three-dimensional structure of lipid vesicles embedded in vitreous ice and investigated by automatic electron tomography. *Biophys. J.* **68,** 1416–1422.

Ding, R., McDonald, K. L., and McIntosh, J. R. (1993). Three-dimensional reconstruction and analysis of mitotic spindles from the yeast, *Schizosaccharomyces pombe. J. Cell Biol.* **120,** 141–151.

Dubochet, J., Adrian, M., Chang, J.-J., Homo, J.-C., Lepault, J., McDowall, A. W., and Schultz, P. (1988). Cryo-electron microscopy of vitrified specimens. *Q. Rev. Biophys.* **21,** 129–288.

Elledge, S. J. (1998). Mitotic arrest: Mad2 prevents sleepy from waking up the APC. *Science* **279,** 999–1000.

Ellisman, M. H., Lindsey, J. D., Carragher, B. O., Kiyonaga, S. H., McEwen, L. R., and McEwen, B. F. (1990). Three-dimensional tomographic reconstructions of components of the Golgi apparatus imaged by selective staining and high voltage electron microscopy. *J. Cell Biol.* **111,** 199a.

Erk, I., Nicolas, G., Caroff, A., and LePaul, J. (1998). Electron microscopy of frozen biological objects: A study using cryosectioning and cryosubstitution. *J. Microsc.* **189,** 236–248.

Frank, J. (1995). Approaches to large-scale structures. *Curr. Opin. Struct. Biol.* **5,** 194–201.

Frank, J., and Radermacher, M. (1986). Three-dimensional reconstruction of non-periodic macromolecular assemblies from electron micrographs. *In* "Advanced Techniques in Biological Electron Microscopy" (J. Koehler, Ed.), pp. 1–72. Springer-Verlag, Berlin.

Frank, J., McEwen, B. F., Radermacher, M., Turner, J. N., and Rieder, C. L. (1987). Three-dimensional tomographic reconstruction in high-voltage electron microscopy. *J. Electron Microsc. Tech.* **6,** 193–205.

Frank, J., Radermacher, M., Penczek, P., Zhu, J., Li, Y., Ladjadj, M., and Leith, A. (1996). SPIDER and WEB: Processing and visualization of images in 3D electron microscopy and related fields. *J. Struct. Biol.* **116,** 190–199.

Frens, G. (1973). Controlled nucleation for the regulation of the particle size in mono-dispersed gold solutions. *Nature Phys. Sci.* **241,** 20–22.

Fung, J. C., Liu, W., De Ruijter, W. J., Chen, H., Abbey, C. K., Sedat, J. W., and Agard, D. A. (1996). Toward fully automated high-resolution electron tomography. *J. Struct. Biol.* **116,** 181–189.

Grimm, R., Bärmann, M., Häckl, W., Typke, D., Sackmann, E., and Baumeister, W. (1997). Energy-filtered electron tomography of ice-embedded actin and vesicles. *Biophys. J.* **72,** 482–489.

Grimm, R., Singh, H., Rachel, R., Typke, D., Zillig, W., and Baumeister, W. (1998). Electron tomography of ice-embedded prokaryotic cells. *Biophys. J.* **74,** 1013–1042.

Hawkes, P. W. (1992). The electron microscope as a structure projector. *In* "Electron Tomography" (J. Frank, Ed.), pp. 17–38. Plenum, New York.

Hindus, L. A. (1992). 2K images from a 1K camera: High resolution at lower costs. *Adv. Imaging* **7,** 52–53.

Hippe-Sanwald, S. (1993). Impact of freeze substitution on biological electron microscopy. *Microsc. Res. Tech.* **24,** 400–422.

Hoppe, W. (1972). Dreidimensional abbildende Elektronenmikroskope. *Z. Naturforsch.* **27a,** 919–929.

Hyman, A. A., and Karsenti, E. (1996). Morphological properties of microtubule assembly/disassembly in mitosis and related movements. *Cell* **84,** 401–410.

Jain, A. K. (1989). "Fundamentals of Digital Image Processing." Prentice-Hall, Englewood Cliffs, NJ.

Khodjakov, A., Cole, R. W., McEwen, B. F., Buttle, K. F., and Rieder, C. L. (1997). Chromosome fragments possessing only one kinetochore can congress to the spindle equator. *J. Cell Biol.* **136,** 229–240.

King, M. V., Parsons, D. F., Turner, J. N., Chang, B. B., and Ratkowski, J. (1980). Progress in applying the high-voltage electron microscope to biomedical research. *Cell Biophys.* **2,** 1–95.

Koster, A. J., Chen, H., Sedat J. W., and Agard, D. A. (1992). Automated microscopy for electron tomography. *Ultramicroscopy* **46,** 207–227.

Koster, A. J., Braunfeld, M. B., Fung, J. C., Abbey, C. K., Han, K. F., Liu, W., Chen, H., Sedat, J. W., and Agard, D. A. (1993). Towards automatic three dimensional imaging of large biological structures using intermediate voltage electron microscopy. *MSA Bull.* **23,** 176–188.

Koster, A. J., Grimm, R., Typke, D., Hegerl, R., Stoschek, A., Walz, J., and Baumeister, W. (1997). Perspective of molecular and cellular electron tomography. *J. Struct. Biol.* **120,** 276–308.

Ladinsky, M. S., Kremer, J. R., Furcinitti, P. S., McIntosh, J. R., and Howell, K. E. (1994). HVEM tomography of the *trans*-Golgi network: Structural insights and identification of a lace-like coat. *J. Cell Biol.* **127,** 29–38.

Landis, W. J., Song, M. J., Leith, A., McEwen, L., and McEwen, B. F. (1993). Mineral and organic matrix interaction in normally calcifying tendon visualized in three dimensions by high voltage electron microscope tomography and graphic image reconstruction. *J. Struct. Biol.* **110,** 39–54.

Lawrence, M. C. (1992). Least-squares method of alignment using markers. *In* "Electron Tomography" (J. Frank, Ed.), pp. 197–204. Plenum, New York.

Li, Y.-H., Leith, A., and Frank, J. (1997). Tinkerbell—A tool for interactive segmentation of 3D data. *J. Struct. Biol.* **120,** 266–275.

Liu, Y., Penczek, P. A., McEwen, B. F., and Frank, J. (1995). A marker-free alignment method for electron tomography. *Ultramicroscopy* **58,** 393–402.

Lorensen, W. E., and Cline, H. E. (1987). Marching cubes: A high resolution surface construction algorithm. *Computer Graphics* **21,** 163–169.

Luther, P. K. (1992). Sample shrinkage and radiation damage. *In* "Electron Tomography" (J. Frank, Ed.), pp. 39–60. Plenum, New York.

Luther, P. K., Lawrence, M. C., and Crowther, R. A. (1988). A method for monitoring the collapse of plastic sections as a function of electron dose. *Ultramicroscopy* **24,** 7–18.

Mannella, C. A., Marko, M., and Buttle, K. (1997). Reconsidering mitochondrial structure: New views of an old organelle. *TIBS* **22,** 37–38.

Marko, M., and Leith, A. (1996). Sterecon-three-dimensional reconstructions from stereoscopic contouring. *J. Struct. Biol.* **116,** 93–98.

Mastronarde, D. N. (1997). Dual-axis tomography: An approach with alignment methods that preserve resolution. *J. Struct. Biol.* **120,** 343–352.

Mastronarde, D. N., McDonald, K. L., Ding, R., and McIntosh, J. R. (1993). Interpolar spindle microtubules in PtK cells. *J. Cell Biol.* **123,** 1475–1489.

Mastronarde, D. N., Ladinsky, M. S., and McIntosh, J. R. (1997a). Super-thin sectioning for high-resolution 3-D reconstruction of cellular structures. *In* "Proceedings of Microscopy and Microanalysis 1997" (G. W. Bailey, R. V. W. Dimlich, K. B. Alexander, J. J. McCarthy, and T. P. Pretlow, Eds.), pp. 221–222. Springer, New York.

Mastronarde, D. N., Morphew, M. K., and McIntosh, J. R. (1997b). HVEM tomography of PtK cells shows that the plus ends of kinetochore microtubules flare outward in prometaphase, metaphase, and anaphase. *Mol. Biol. Cell.* **8,** 171a.

McDonald, K. L. (1994). Electron microscopy and EM immunocytochemistry. *Methods Cell Biol.* **44,** 411–444.

McDonald, K. L., O'Toole, E. T., Mastronarde, D. N., and McIntosh, J. R. (1992). Kinetochore microtubules in PtK cells. *J. Cell Biol.* **118,** 369–383.

McEwen, B. F., and Heagle, A. B. (1997). Electron microscopic tomography: A tool for probing the structure and function of subcellular components. *J. Imaging Syst. Technol.* **8,** 175–187.

McEwen, B. F., Radermacher, M., Rieder, C. L., and Frank, J. (1986). Tomographic three-dimensional reconstruction of cilia ultrastructure from thick sections. *Proc. Natl. Acad. Sci. USA* **83,** 9040–9044.

McEwen, B. F., Arena, J., Frank, J., and Rieder, C. L. (1993). Structure of the colcemid-treated PtK_1 kinetochore outer plate as determined by high voltage electron microscopic tomography. *J. Cell Biol.* **120,** 301–312.

McEwen, B. F., Downing, K. H., and Glaeser, R. M. (1995a). The relevance of dose-fractionation in tomography of radiation-sensitive specimens. *Ultramicroscopy* **60,** 357–373.

McEwen, B. F., Osorio, G., Cole, R., and Rieder, C. L. (1995b). Same-cell correlative video light microscopy/electron microscopy tomography: An approach to understanding kinetochore behavior during mitosis. *In* "Proceedings of Microscopy and Microanalysis 1995" (G. W. Bailey, M. Ellisman, R. A. Hennigar, and N. J. Zaluzec, Eds.), pp. 744–745. Jones & Begell, New York.

McEwen, B. F., Heagle, A. B., Cassels, G. O., Buttle, K. F., and Rieder, C. L. (1997). Kinetochore-fiber maturation in PtK_1 cells and its implications for the mechanisms of chromosome congression and anaphase onset. *J. Cell Biol.* **137,** 1567–1580.

McEwen, B. F., Ding, Y., and Heagle, A. B. (1998). Relevance of kinetochore size and microtubule binding capacity for stable chromosome attachment during mitosis in PtK_1 cells. *Chromosome Res.* **6,** 123–132.

McIntosh, J. R., and Landis, S. C. (1971). The distribution of spindle microtubules during mitosis in cultured human cells. *J. Cell Biol.* **49,** 468–497.

Merdes, A., and Cleveland, D. (1997). Pathways of spindle pole formation: Different mechanisms, conserved components. *J. Cell Biol.* **138,** 953–956.

Michel, M., Hillmann, T., and Müller, M. (1992). Diamonds are a cryosectioner's best friend. *J. Microsc.* **166,** 43–56.

Moor, H. (1987). Theory and practice of high pressure freezing. *In* "Cryotechniques in Biological Electron Microscopy" (R. A. Steinbrecht and K. Zierold, Eds.), pp. 175–191. Springer-Verlag, Berlin.

Nicklas, R. B. (1997). How cells get the right chromosomes. *Science* **275,** 632–638.

Olins, A. L., Olins, D. E., Levy, H. A., Margle, S. M., Tinnel, E. P., and Durfee, R. C. (1989). Tomographic reconstruction from energy-filtered images of thick biological sections. *J. Microsc.* **154,** 257–265.

Owen, C. H., and Landis, W. H. (1996). Alignment of electron tomographic series by correlation without the use of gold particles. *Ultramicroscopy* **63,** 27–38.

Parsons, D. F., Marko, M., and Leith, A. (1991). Organelle rearrangement and cell column changes during "squeezing invasion" of peritoneal elastic lamina by targeted murine breast carcinoma cells. *Tissue Cell* **23,** 293–305.

Penczek, P., Marko, M., Buttle, K., and Frank, J. (1995). Double-tilt electron tomography. *Ultramicroscopy* **60,** 393–410.

Pennisi, E. (1998). Cell division gatekeepers identified. *Science* **279,** 477–478.

Radermacher, M. (1988). Three-dimensional reconstruction of single particles from random and nonrandom tilt series. *J. Electron Microsc. Tech.* **9,** 359–394.

Radermacher, M. (1992). Weighted back-projection methods. *In* "Electron Tomography" (J. Frank, Ed.), pp. 91–115. Plenum, New York.

Radermacher, M., and Frank, J. (1984). Representation of three-dimensionally reconstructed objects in electron microscopy by surfaces of equal density. *J. Microsc.* **136,** 77–85.

Rath, B. K., Marko, M., Radermacher, M., and Frank, J. (1997). Low-dose automated electron tomography: A recent implementation. *J. Struct. Biol.* **120,** 210–218.

Rieder, C. L. (1981). Thick and thin serial sectioning for the three-dimensional reconstruction of biological ultrastructure. *Methods Cell Biol.* **22,** 215–249.

Rieder, C. L. (1982). The formation, structure, and composition of the mammalian kinetochore and kinetochore fiber. *Int. Rev. Cytol.* **79,** 1–58.

Rieder, C. L. (1990). Formation of the astral mitotic spindle: Ultrastructural basis for the centrosome–kinetochore interaction. *Electron Microsc. Rev.* **3,** 269–300.

Rieder, C. L., Rupp, G., and Bowser, S. S. (1985). Electron microscopy of semithick sections: Advantages for biomedical research. *J. Electron Microsc. Tech.* **2,** 11–28.

Roos, U.-P. (1973). Light and electron microscopy of rat kangaroo cells in mitosis. II. Kinetochore structure and function. *Chromosoma* **41,** 195–220.

Rudner, A. D., and Murray, A. W. (1996). The spindle assembly checkpoint. *Curr. Opin. Cell Biol.* **8,** 773–780.

Ruiz, T., Erk, I., and Lepault, J. (1994). Electron cryo-microscopy of vitrified biological specimens: Towards high spatial and temporal resolution. *Biol Cell* **80,** 203–210.

Russ, J. C. (1992). "The Image-Processing Handbook." CRC Press, Boca Raton, FL.

Slot, J., and Geuze, H. (1985). Sizing of protein A-gold probes for immunoelectron microscopy. *J. Cell Biol.* **90,** 533–536.

Soto, G. E., Young, S. J., Martone, M. E., Deerinck, T. J., Lamont, S., Carragher, B. O., Hama, K., and Ellisman, M. H. (1994). Serial section electron tomography: A method for three-dimensional reconstructions of large structures. *NeuroImage* **1,** 230–243.

van der Voort, H. T. M., Brakenhoff, G. J., Valkenburg, J. A. C., and Nanninga, N. (1985). Design and use of computer controlled confocal microscope for biological applications. *Scanning* **7,** 66–78.

van Marle, J., Dietrich, A., Jonges, K., Jonges, R., DeMoor, E., Vink, A., Boon, P., and van Veen, H. (1995). EM-tomography of section collapse, a non-linear phenomenon. *Microsc. Res. Tech.* **31,** 311–316.

Waters, J. C., and Salmon, E. D. (1997). Pathways of spindle assembly. *Curr. Opin. Cell Biol.* **9,** 37–43.

Wilson, C. J., Mastronarde, D. N., McEwen, B. F., and Frank, J. (1992). Measurement of neuronal surface area using high voltage electron microscope tomography. *NeuroImage* **1,** 11–22.

Yen, T. J., and Schaar, B. T. (1996). Kinetochore function: Molecular motors, switches, and gates. *Curr. Opin. Cell Biol.* **8,** 381–388.

This Page Intentionally Left Blank

CHAPTER 6

Enlightening Mitosis: Construction and Expression of Green Fluorescent Fusion Proteins

Kevin F. Sullivan

Department of Cell Biology
The Scripps Research Institute
La Jolla, California 92037

METHODS IN CELL BIOLOGY, VOL. 61

0091-679X/99 $30.00

I. Introduction: Visualizing the Molecular Anatomy of the Spindle

The study of mitosis began with the microscope and direct visualization of cell division remains a fundamental tool in dissecting the mechanisms of spindle function. In particular, methods for observing and recording the dynamic behavior of the cell during mitosis have shaped our thinking about spindle function and molecular mechanisms, from the dynamic equilibrium of spindle fibers to the dynamic instability of individual microtubules. Advanced imaging modes in light microscopy, in particular differential interference contrast, provide remarkable resolution of spindle components. Fluorescence microscopy has extended these methods to allow direct observation of specific molecular components of the spindle. Until recently such observations have been limited to components of the spindle that could be purified and chemically labeled with a fluorochrome, such as tubulin, or for which specific vital stains were available, such as DNA (Leslie *et al.,* 1984; Hiraoka *et al.,* 1991). The introduction of green fluorescent protein (GFP) fusion protein technology (Chalfie *et al.,* 1994; Wang and Hazelrigg, 1994) has erased these limitations and promises to yield unprecedented access to the molecular details of mitotic processes through fluorescence microscopy. In this chapter we will discuss the properties of GFP as a fluorochrome and strategies for constructing functional biofluorescent probes and for the expression of GFP chimeras in cells. Methods for fluorescence microscopy of live mitotic cells are discussed in other chapters in this volume.

II. Fluorescence Properties of GFP

GFP was identified in the jellyfish *Aequoria victoria,* in which it is thought to serve as a cofactor for the Ca^{2+}-sensitive luminescent enzyme aequorin, enhancing the product release step in the photoreaction cycle by acting as a resonant energy transfer acceptor for aequorin (Prasher, 1995). At the atomic level, GFP has been described as a molecular "can of paint" because of a remarkable curved 11-stranded β-sheet structure that forms a cylinder enclosing a single α-helix within its lumen (Fig. 1, see color plate) (Ormo *et al.,* 1996). The fluorochrome is made from three contiguous residues in the center of the helix, Ser65-Tyr66-Gly67, that undergo a spontaneous cyclization reaction followed by oxidation to form a cyclic tripeptide with an extended aromatic ring structure, characteristic of more familiar fluorochrome dyes (Cody *et al.,* 1993). The photostability of GFP is thought to be due to the tight packing of the fluorochrome within the protein core, which shields it from solvent and from reactive oxygen species responsible for photobleaching. The high stability of GFP fluorescence contributes significantly to its practical utility in live cell microscopy applications.

The fluorescence spectrum of GFP is obviously the key functional property of the protein and has turned out to be remarkably mutable, leading to the

generation of several useful spectral variants of GFP (Heim and Tsien, 1996; Rizzuto *et al.*, 1996; Heim *et al.*, 1994). Wild-type GFP is maximally excited in the near UV (396 nm) and possesses a secondary excitation peak at 475 nm. Emission at 508 nm produces the characteristic bright green color. This has been a starting point for several mutational strategies designed to enhance the utility of GFP in a variety of biological systems. The resulting mutated gene products can be classified into three types: spectral mutants, stability mutants, and transcript mutants.

A. Spectral Mutations

The search for novel fluorescent forms of GFP generated by mutagenic strategies was immediately fruitful (Heim and Tsien, 1996; Heim *et al.*, 1995; Yang *et al.*, 1996b). These experiments have led to rapid development of a growing "rainbow" of available GFP derivatives (Table I). The most useful of these is the bright green mutant S65T, in which Ser65 of the fluorochrome has been replaced with Thr. The mutation simplifies the GFP absorption spectrum, abolishing the UV absorption peak, and increases the extinction coefficient of the blue absorption peak at 489 nm. This and other GFP mutants are referred to as red-shifted mutants due to an increase in excitation frequency relative to the wild-type protein. Emission frequency (511 nm) and quantum yield (0.68) are essentially unchanged, resulting in a protein that is approximately sixfold brighter than the wild-type protein excited at 475 nm (Heim *et al.*, 1995).

Of major interest to cell biologists is the development of fluorescent proteins with distinctive emission spectra to provide the ability to do multicolor fluorescence (Rizzuto *et al.*, 1996) and fluorescence resonance energy transfer experiments to analyze intermolecular interactions *in vivo* (Miyawaki *et al.*, 1997). Four useful classes of mutation have been described and these are detailed in Table I (Heim and Tsien, 1996; Miyawaki *et al.*, 1997). A "yellow" mutant with an emission maximum at 527 nm is the brightest GFP derivative yet obtained but due to spectral overlap is probably not useful in conjunction with green GFP fluorochromes (Miyawaki *et al.*, 1997). Blue-emitting and cyan-emitting (emission maxima ca. 445 and 475 nm) have been reported and applied to cellular localization (Rizzuto *et al.*, 1996). These forms are much dimmer than GFP, however, and can be difficult to detect with typical fluorescence microscopes. A useful variant, GFP-uv, provides a complement to the blue-excited S65T, possessing only the ultraviolet excitation peak at 395 nm (Crameri *et al.*, 1998). Although this mutant fluoresces at essentially the same wavelength as GFP-S65T, the distinctive excitation spectra should allow these to be easily distinguished for two-color microscopy.

B. Thermostability and Folding Mutations

A key feature of GFP is the rate and extent of protein folding and chromophore formation, which does not take place optimally at 37°C for the wild-type protein

Table I
GFP Variants[a]

Class	Variant	Fluorochrome mutations	Other mutations		Excitation	Emission	Extinction coefficient ($\times 10^3$)	Quantum yield	Reference	Vendor
Green	WT				395 (475)	508	21	0.77	1	A
	S65T	S65T			489	511	39.2	0.66	1	A
	EGFP	S65T	F64L	Thermostable	488	507	NA	NA	2	A
	Emerald	S65T	F64L, S72A, N149K, M153T, I167T, H231L	Thermostable	484	508	57.5	0.68	3	B
	GFP-A		V163A, S175G	Thermostable	395 (475)	508	NA	NA	4	
	GFPuv		F99S, M153T, V163A		395	509	NA	NA	5	A
	Sapphire		S72A, Y145F, T203I, H231L	Thermostable	395	511	29	0.64	5	B
Blue	P4-3	Y66H	Y145F		381	445	14	0.38	1	
	eBFP	S65T, Y66H	F64L, Y145F	Thermostable	380	440	37	NA	6	A
	qBFP	NA	NA		395	450	NA	NA	7	C
Cyan	W7	Y66W	N146I, M153T, V163A, N212K		433 (453)	475 (501)	18	0.67	1	
	W2	Y66W	123V, Y145H, H148R, M153T, V163A, N212K		433 (453)	480	10	0.72	1	
Yellow	C10/eYFP	S65G	V68L, S72A, T203Y		513	527	36.5	NA	8	A
	Topaz	S65G	S72A, K79R, T203Y, H231L	Thermostable	514	527	94.5	0.6	3	B

[a] Listed are several of the most useful spectral and stability variants of GFP, along with their spectral properties where known. References: 1, Heim and Tsien (1996); 2, Cormack *et al.* (1996); 3, Packard Instruments documentation; 4, Siemering *et al.* (1996); 5, Cormier *et al.* (1996); 6, Miyawaki *et al.* (1997); 7, Quantum biotechnologies, Inc. documentation; 8, Ormo *et al.* (1996). Vendors: A, Clontech Laboratories, Inc., Palo Alto, CA; B, Packard Instrument Co., Meriden, CT; C, Quantum Biotechnologies, Inc., Montreal, Canada. NA, not available.

(Siemering *et al.*, 1996). Many early workers reported no or low fluorescence yield with wild-type GFP in cells cultured at 37°C, which could be compensated by growth at lower temperatures. A careful screen for "bright" mutants of GFP revealed a class of mutations that enhance the folding and stability of the protein at 37°C (Siemering *et al.*, 1996; Cormack *et al.*, 1996). These different mutations are additive to a certain extent, presumably approaching maximal protein stability. The rate of posttranslational chromophore formation was previously reported to be quite slow, with a time constant on the order of hours (Heim *et al.*, 1994). Renaturation studies of bacterially expressed GFP-S65T, however, revealed that oxidation is the rate-limiting step in acquisition of fluorescence (Reid and Flynn, 1997). Measurement of the rate of GFP-S65T oxidation in yeast indicates that the time constant for this reaction is only about 6 min at 37°C and 18 min for the thermostable mutant GFPA (Siemering *et al.*, 1996). The rate of chromophore formation, although perhaps a limitation in rapid pulse-labeling experiments, should not be an issue for analysis of proteins in mitosis.

C. Transcript Mutations

A second type of limitation for GFP expression in exogenous systems has been mRNA stability or translational efficiency. The discovery that WT-GFP transcripts contained a cryptic intron that severely limited expression in plants, and the recovery of expression by mutating this site, provided the most striking example (Haseloff *et al.*, 1997). Modifications to match the codon usage of mammalian cells (Yang *et al.*, 1996a), plants (Rouwendal *et al.*, 1997), and yeast (Cormack *et al.*, 1997) have been reported to improve expression in these systems.

D. Which GFP to Use?

The array of available GFP mutants begs the question: Which GFP is best for a particular application? Fortunately, this is easily answered for most experiments. The bright green S65T variant coupled with enhanced folding mutations is ideal for most single-probe experiments (Cormack *et al.*, 1996; Siemering *et al.*, 1996). This and other enhanced GFP mutants are commercially available as mammalian fusion protein expression vectors (Clontech, Palo Alto, CA; Quantum Biotechnologies, Montreal, Canada). The humanized GFP coding sequence in these vectors is ideal for expression in a wide variety of mammalian species. Because its excitation and emission spectra are quite similar to fluorescein, special filters are not required for efficient visualization of S65T derivatives. Similarly, these GFP derivatives are ideal for confocal microscopy because they are very efficiently excited by the 488-nm argon laser line.

For dual-receptor experiments, the second GFP of choice is an enhanced blue derivative because this provides the best spectral resolution from GFP (Rizzuto *et al.*, 1996). Commercially available eBFP genes are available from

Clontech and Quantum. From both spectral properties and our experience, eBFP is significantly dimmer than eGFP. Thus, while compatible with many filter sets designed for DAPI or Cascade Blue detection, effective use of the BFP derivatives will require careful selection of optimal filter sets for fluorescence microscopy.

III. Strategies for Constructing Fusion Proteins

GFP is a fairly large tag to add to a protein at 28 kDa (238 amino acids). Nevertheless, it has proven effective in more cases than not. Fusions with both the N and C termini of GFP have been performed successfully. The properties of the target protein should dictate the choice of which end to fuse to GFP, and in cases in which there is no strong bias, it is prudent to try both. Addition of a few linker amino acids between GFP and the fusion target is also a good idea. In the case of commercial fusion vectors, the polylinker sequence can provide this linker (showing that the sequence often does not matter).

For construction of fusion proteins, PCR is used to amplify the DNA fragment(s) to be cloned. Some of the important considerations in designing the PCR experiment are discussed later. The method used in our lab has been optimized for high efficiency in accurate synthesis and recovery of PCR products for subsequent cloning into expression vectors. We often also use PCR to construct the fusion itself prior to expression vector cloning, using a method called recombinant PCR.

A. Primers

Primers for fusion fragment generation typically contain three elements: target priming sequence, spacer codons, and restriction site(s) (Fig. 2A). We generally use a 15-bp sequence that is 100% complementary to the target gene as the 3′ or priming end of the oligonucleotide (hatched regions in Fig. 2A). This should avoid heavily (>70%) G + C-rich sequences and secondary structure as much as possible and terminate with a G or a C at the 3′ end for most efficient priming. The spacer codon segment contains an in-frame sequence designed to place a flexible linkage between GFP and the fusion partner, if necessary. This is generally a glycine- and alanine-rich peptide sequence 5–10 residues long. We have used the sequence GGSGST, which is part of a natural linker sequence that links the DNA-binding domain of CENP-B to the C-terminal portions of the molecule (Shelby *et al.*, 1996; Sullivan and Glass, 1991). Extending an Ala linker to 10 residues improved the properties of an actin–GFP fusion in yeast (Doyle and Botstein, 1996). Primers also generally contain a restriction site(s) that will be used to fuse with GFP and clone into the expression vector. Ideally, two unique restriction sites compatible with the target vector are used to allow

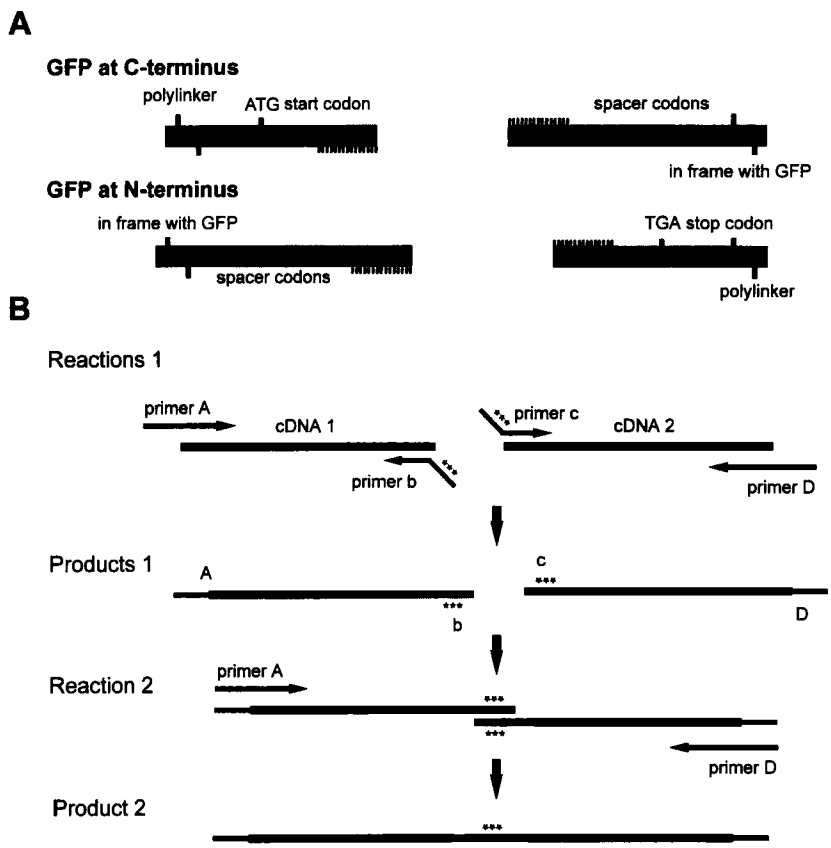

Fig. 2 Primer design and PCR strategies for constructing fusion proteins. (A) General structure of primers used for amplifying cDNAs for fusion to GFP in a typical protein expression vector. Each primer pair contains a pair of restriction enzyme recognition sites, denoted "polylinker" and "in frame with GFP." Ideally, these correspond to two different restriction endonucleases to facilitate directional cloning of PCR products. For fusions with GFP at the C terminus of the experimental protein, the 5′ primer must contain an effective start codon and the 3′ primer often includes a set of 5–10 codons comprising a spacer region to allow independent folding of the experimental protein and GFP. This can often be omitted if using a protein expression vector that contains an extensive polylinker since it can be used as a spacer. For fusions with GFP at the N terminus of the experimental protein, the 5′ primer contains the in frame with GFP restriction site and spacer codons, whereas the 3′ primer contains a stop codon for proper translation termination. (B) Strategy for recombinant PCR, showing a diagrammatic representation of the recombinant PCR strategy described in the text.

directional cloning. An open reading frame must be maintained across the fusion site itself. The organization of the primers differs depending on whether GFP will be fused at the C terminus or the N terminus of the target gene. For C-terminal GFP, the 5′ or top primer must contain an initiator codon, which may be that endogenous to the transcript, and the 3′ or bottom primer contains the

linker and GFP fusion site. For N-terminal GFP, the 5′ primer contains the GFP fusion site and linker sequence, whereas the 3′ primer must contain a stop codon to terminate translation properly. Primers are diluted in TE (10 m*M* Tris, 1 m*M* EDTA, pH 8.0) to 10-μm working stocks. These can be stored at 4°C for up to 1 year or at −20°C indefinitely.

B. Template

Most often, a plasmid containing a cDNA of the fusion target protein is available. In these cases, we use a large excess of template DNA (5 μg/ml) compared with a more typical analytical PCR where the template DNA is present in small quantities. The logic behind this is that with a high template concentration the input DNA will be used as the actual template during much of the PCR reaction, as opposed to synthetic PCR products. This should minimize the possibility of amplifying mutated sequences and increase the fidelity of the PCR. Keep in mind that the goal is not so much to amplify the DNA per se but rather to add the primer sequences to your gene.

C. DNA Polymerase

Taq DNA polymerase is the standard polymerase used for DNA synthesis in PCR. It is available from several suppliers including Gibco-BRL, Promega, and Qiagen; most of our work has been done with native Taq from Promega. One issue in using PCR to make protein constructs for expression is the fidelity of enzymatic DNA replication *in vitro.* Taq polymerase has been reported to have a reduced fidelity compared with more traditional DNA polymerases such as T7 and Klenow. Our approach to the issue of fidelity has been to use a mixture of Taq with Pfu DNA polymerase, a higher fidelity enzyme (Stratagene, Inc., La Jolla, CA) as originally described in a method for "extended" PCR (Barnes, 1994). Taq and Pfu are mixed in a ratio of 8:1 units and stored at −20°C. We generally use this within 1 week; for longer periods, aliquots should be stored at −70°C. In practice, there are several high-quality thermostable DNA polymerases and polymerase mixtures available from a variety of commercial sources and any of these should suffice. However, note that it is prudent to sequence DNA fragments constructed by PCR. In our experience with this method, we observe a mutational frequency of ~1 per 2000-bp sequenced.

D. Cloning PCR Fragments

The most straightforward completion of the fusion construction is to digest the PCR fragment(s) with restriction enzymes and ligate them directly into a GFP fusion vector. If PCR fragments are to be cloned directly after restriction digestion, it is necessary to extend the 5′ ends of the PCR primers to minimize end effects on restriction enzyme activities. Usually two to four additional 5′

nucleotides are included to "buffer" the end. New England Biolabs (Beverly, MA) provides a useful table in their catalog showing efficiencies of cleavage close to DNA ends for several restriction enzymes.

We have found that PCR fragments are often difficult to digest with certain restriction enzymes and the resulting efficiency of ligation to the fusion protein vector is extremely low. To circumvent this difficulty, we often recover fragments by TA cloning (Invitrogen, Carlsbad, CA) as described later. This method results in highly efficient product recovery: We have never failed to clone a PCR product with a single ligation and transformation reaction using the TA approach.

E. PCR Protocol

1. Working on ice, prepare a 25-μl reaction containing
   2.5 μl primer 1, 1 μM final concentration
   2.5 μl primer 2, 1 μM final concentration
   2.5 μl 10× PCR buffer obtained from manufacturer
   2.5 μl 10× dNTP stock, 1.0 mM each dNTP
   Template: up to 125 ng of plasmid DNA, 1 μg of genomic DNA or cDNA
   0.5 U Taq : Pfu mix, 8 : 1 unit ratio
   H_2O to 25 μl.
2. Cover with oil if necessary.
3. Execute 20 PCR cycles:
   1 × 2 min at 95°C
   20 × (30 sec at 95°C, 60 sec at 50°C, 90 sec at 72°C)
   1 × 10 min at 72°C.
4. Analyze the product by agarose gel electrophoresis. If it is a clean reaction without side products, the PCR reaction product can be used directly for TA cloning. If the fragment will be digested for direct cloning into the expression vector, or if there are additional bands besides the desired product, it is advisable to gel purify the correct fragment before proceeding.
5. Perform ligation to TA vector: 1–2.5 μl PCR reaction from step 3 or 5–10 ng of purified DNA fragment is ligated to the TA vector according to the manufacturers instructions. Ligate 4 hr to overnight.
6. Transform ligation mixture into *Escherichia coli* and plate on kanamycin selective plates.
7. Isolate miniprep DNA from TA colonies and digest with the restriction enzymes to be used for GFP fusion vector cloning to verify recovery of the correct fragment. Gel purify the insert from the TA clone miniprep DNA.
8. Ligate fusion insert with GFP fusion protein vector after appropriate restriction digestion. Transform into *E. coli,* pick colonies, and identify an appropriate recombinant. Miniprep DNA prepared with commercial kits is generally suitable

for transfection using the methods discussed later. Once a properly constructed plasmid has been verified, we prepare a "midi prep" of DNA (~250 μg) purified using Qiagen columns (Qiagen, Chatsworth, CA).

F. Recombinant PCR

The principle behind recombinant PCR is simple: Two DNA fragments with overlapping termini are constructed in a first round of PCR and then fused together in a second round by forcing them to act as primers for each other (Fig. 2B). In practice, the experiment requires a set of four primers to be constructed. Two of these, the outer primers A and D in Fig. 2B, correspond to the termini of the ultimate DNA fragment that is being assembled. The other two, b and c, provide primers for the first-round PCR and incorporate a segment of overlap common to both fragments. These first-round products are synthesized and gel purified for use in the second PCR reaction. In the second PCR reaction, 100–200 ng of each first-round fragment is combined to form the template in a standard PCR reaction using only the outer primers A and D. Since each fragment can hybridize to only one of these primers, a full template molecule can only be formed by the two first-round products acting as templates for each other, resulting in synthesis of a full-length molecule in the Taq polymerase extension reaction. Once such a molecule is formed, it is subject to normal amplification with the oligonucleotide primers in the reaction. The availability of good expression vectors designed for protein fusion may limit the necessity for this type of approach in general. We have used it extensively for construction of mutated proteins and it has proven a simple and reliable approach for fusing DNA molecules without the introduction of artificial restriction sites. Although most of our experience is with bimolecular recombinant PCR, we have used as many as three fragments in this type of reaction, successfully constructing the desired tripartite DNA molecule.

G. Assessing DNA Sequence Fidelity

The issue of DNA sequence fidelity after PCR is an important one. If a GFP fusion protein fails to localize or has an unexpected biological activity it is important to know whether the sequence of the fusion protein is correct. There are two approaches to this. The first is a "wait and see" approach in which fusion constructs are assayed for fluorescence and localization in animal cells after cloning into appropriate expression vectors. If the GFP fusion protein is well behaved, the precise sequence of the protein may be a moot point. The second is a "let's make sure" approach in which PCR products are sequenced before use. We have generally used the latter approach, sequencing a set of four TA clones prior to assembly of the GFP expression construct.

H. Cloning Vectors

The target vector for fusion protein constructs must be designed for expression in the cell type under study. Most convenient from a design and use standpoint

are the excellent set of GFP expression vectors available commercially from Clontech and Quantum Biotechnologies (discussed previously). For virtually all vertebrate cell types, vectors based on the CMV immediate early promoter are efficiently expressed and these are available from numerous sources. For regulated gene expression, we have used the tetracycline-regulated vector system designed by Gossen and Bujard (1992).

IV. Expression in Mammalian Cells

The methods for labeling cellular structures with GFP encompass the technologies for expression of exogenous genes in experimental systems. Protocols for transient transfection, optimization of transfection efficiency, and selection of stable transformants that are used in our laboratory are detailed.

A. Transient Transfection

The endpoint of a GFP expression experiment is generally visualization on the microscope. Thus, it is convenient to plate cells directly on glass coverslips prior to transfection. We use 12-mm No. 1.5 coverslips (Belco Technology, Vineland, NJ) for standard observations methods. These coverslips fit easily into standard 24-well dishes with a 15-mm well diameter. A convenient 4-well plate that fits these coverslips can be obtained from Nunc Incorporated (Naperville, IL, catalog No. 176740). For live cell observation we use a Dvorak–Stotler chamber that houses 24.5-mm No. 1.5 coverslips (Lucas-Highland Co., Chantilly, VA). These fit the standard 35-mm 6-well dish format. Coverslips are acid washed prior to use.

Acid washing coverslips

1. In a fume hood, put ~200 ml of 12*N* HCl into a clean 500-ml beaker. You may want to prerinse the beaker with HCl.
2. Remove coverslips from the box and place onto a piece of weighing paper or into a weigh boat. Slowly pour coverslips into the beaker of HCl. Carefully swirl the beaker to mix the coverslips around a bit. Cover the beaker with foil and let stand overnight.
3. Decant HCl into appropriate disposal vessel and replace with distilled water.
4. Gently swirl beaker to wash coverslips.
5. Decant and replace distilled water.
6. Bring to boil and hold for ~10 min.
7. Pour off water, let cool for ~5 min, add distilled water, and boil again for ~10 min.
8. Decant water and wash twice with distilled water, swirling gently to mix coverslips.

9. Decant water and replace with 95% ethanol. Wash three times in ethanol.
10. Before the ethanol washes, spread several large Kim-Wipes or paper towels in tissue culture hood and sterilize under the UV lamp. We generally irradiate for ~10 min.
11. In sterile tissue culture hood, pour coverslips out onto a large Kim-Wipe or paper towel.
12. Using two sets of forceps to manipulate coverslips, separate them onto the Kim-Wipes to dry. This prevents them from sticking together as they dry.
13. Place coverslips into a tissue culture dish and store covered in the hood.

Several methods are available for transfecting populations of mammalian cells: cationic lipid-mediated transfection, the calcium phosphate method, electroporation, and microinjection. We routinely use lipid-mediated transfection and detail our protocol later. This method generally yields 20–80% transfectants with easily transfected cells (HeLa, U2OS, Cos, Indian muntjac fibroblasts, and mouse L cells). The calcium phosphate transfection method is methodologically similar and the reagents are easily prepared or can be obtained from a variety of vendors (Chen and Okayama, 1987). Lipid-mediated transfection generally yields higher transfection efficiencies than the calcium phosphate method in our hands, but it can be more toxic to cells and hence it is useful to titrate effective reagent amounts as described later. Another potential drawback that we have observed is the formation of a red to orange autofluorescent material in some cell types after lipid-mediated transfection. We suspect that this may represent products formed as the cell attempts to metabolize the unnatural lipids, and it usually appears as "blotches" of red fluorescent material in the cytoplasm. Nevertheless, the simplicity and efficiency of lipid-mediated transfection make it worthwhile to try to work around this problem if it appears, e.g., by extraction of cells prior to fixation.

Optimization of transfection efficiencies with cationic lipids requires titration of three codependent variables: DNA concentration, lipid concentration, and cell density. The procedure described later has been optimized for HeLa cells using Lipofectamine (Gibco-BRL). In practice, this protocol works well with a number of mammalian cell lines. Other lipid-mediated transfection reagents may perform differently and require optimization. We present a simple approach for titrating lipid-mediated transfections later.

A word on cell plating densities and conditions is in order. Transfection with Lipofectamine is most efficient with higher cell densities—ca. 70–80% confluence at the time of transfection. In our hands, a confluent HeLa cell culture yields about $1–1.25 \times 10^5$ cells/cm^2. If mitotic cells are to be observed directly, either live or after fixation alone, it is sufficient to plate cells at a density of $\sim 5 \times 10^4$ cells/cm^2 the afternoon before transfection is to be carried out. If cells are to be processed for immunofluorescence, retention of mitotic cells on the coverslips through the processing can become a significant issue. We have found that mitotic

cells adhere much more efficiently if they have grown on the coverslip for 2 or 3 days prior to transfection. Accordingly, cells are plated at a density of 1 or 2×10^4 cells/cm^2 2 or 3 days before transfection and allowed to approach ~70–80% confluence by growth on glass.

1. Transfection with Lipofectamine

This is a stringent protocol we have developed to optimize viability of cells during the transient transfection. The following procedure is scaled for 12-mm coverslips in a 15-mm tissue culture dish, equivalent to a single well in a standard 24-well plate or 4-well Nunc plate. Table II provides conversions for other scales.

Preparation of cells

1. Working in the tissue culture hood, put a drop of sterile PBS into each well to be plated for transfection.

2. Using sterile forceps, place a coverslip into each well. Press to the bottom of the dish. This causes the coverslip to adhere to the bottom of the dish, minimizing medium flow underneath the coverslip and restricting cells to the top surface of the glass.

3. Trypsinize cells from a 50–80% confluent plate by washing twice with PBS followed by application of 2 ml trypsin–EDTA solution (0.05% trypsin, 0.53 m*M* EDTA; Gibco, 25300-013). Incubate the cells for 5–10 min at room temperature, tapping the dish occasionally to observe cell detachment. Once cells are detached, quench the trypsin by addition of 8 ml complete medium containing 10% FBS. Pipette cells up and down a few times to disperse aggregates and wash the surface of the dish. Count cells using a hemocytometer.

4. Prepare a suspension of 2.5×10^4 cells/ml, if transfecting the next day, or $0.5–1 \times 10^4$ cells/ml if transfecting on Day 3, as discussed previously. By plating cells at low concentration, a large column of medium is delivered to the well, reducing the tendency of cells to accumulate in the center of the well due to the "vortex" current created during pipetting.

5. Pipette 2 ml of cell suspension to each well. Pipette straight down into the well to avoid creating a vortex current.

6. Replace cells in the incubator and allow to grow overnight to 3 days.

Transfection

7. For each transfection to be performed dilute 25 ng of DNA into 25 μl of serum-free medium in a sterile Eppendorf tube.

8. In a separate tube, dilute 1.5 μl of Lipofectamine into 25 μl of serum-free medium. For multiple transfections, prepare a single batch of Lipofectamine in medium and aliquot into each DNA tube.

9. Add 25 μl of diluted Lipofectamine to the 25 μl DNA sample and mix gently; Do not vortex.

10. Incubate DNA–Lipofectamine mixture at room temperature for 30 min (15 min to 1 hr is ok).

11. Dilute DNA–Lipofectamine solution(s) to 250 μl by addition of 200 μl serum-free medium.

12. Retrieve cells from the incubator and wash twice with serum-free medium or PBS.

13. Add 250 μl transfection reaction mixture to each coverslip.

14. Return to 37°C incubator for 5 or 6 hr.

15. Aspirate transfection reaction mixture off of cells, wash twice with serum-free medium or PBS, and then add 1 ml complete medium. Alternatively, the wells may simply be supplemented with 1 ml complete medium. This may increase transfection efficiencies at a cost of higher rates of cell loss.

16. Incubate in 37°C incubator overnight.

17. Next day, aspirate medium, wash twice in PBS, and replace medium. Incubate cells an additional 24–48 hr prior to analysis.

18. Process coverslips for microscopy. In our experience GFP derivatives are stable to fixation in formaldehyde up to 4% or in methanol at −20°C. For quick visualization, coverslips can simply be inverted onto a slide and washed with distilled water to remove medium salts. We use an aspirator with a 2-μl disposable pipette tip to remove excess medium and draw off water as it is carefully applied to the coverslip. Cells mounted directly begin to disintegrate after 20–30 min, but this is ample time to evaluate expression and localization of GFP fusion proteins.

While gene expression can be detected as early as 4 or 5 hr following addition of DNA to the cells, mitotic cells are not observed for at least 18–24 hr after transfection with CENP-B-GFP. By analysis of HeLa cells transfected with a GFP expression plasmid at early times after transfection, we have recently discovered that the earliest detectable transfectants almost always occur in pairs (Fig. 3). In this experiment, about 90% (110/121) of cells that express detectable levels of GFP possess a nearest-neighbor GFP-positive cell and many of these are clearly connected by a cytoplasmic bridge. This experiment demonstrates that gene expression from transfected DNA occurs shortly after mitosis. We interpret this to indicate that the transfected DNA does not gain access to the nucleus until mitosis, when the nuclear envelope is broken down, and that expression begins promptly in early G_1. We are not aware of other studies that have identified the mechanism of DNA transfer into the nucleus following transfection or whether this effect is specific for lipofected DNA. It does, however, have important implications for workers using transient transfection to study mitosis: The minimal time for detection of transfected mitotic cells is a complete cell cycle.

B. Titering Transfection Reagents

Transfection efficiency is a product of three codependent variables and although the conditions discussed previously are a good starting point, if transient

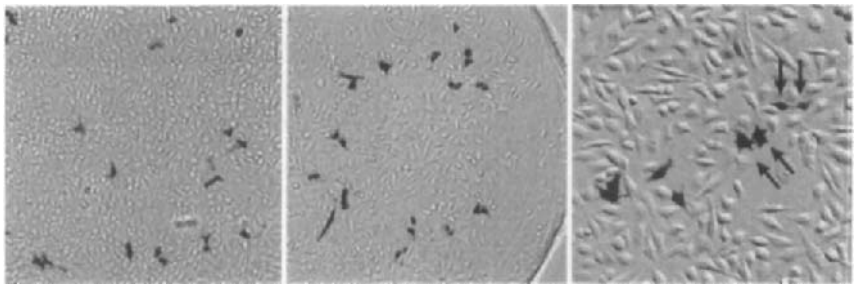

Fig. 3 DNA expression does not occur until very soon after mitosis. Shown are representative low power fields of cells observed 5 or 6 hr after transfection with pEGFP-N1 (Clontech). Virtually all (>90%) of GFP-expressing cells (black) occur in pairs, as detailed in higher magnification image in the right panel (arrows). We interpret this to show that tranfected DNA gains access to the nucleus only during mitosis, when the nuclear envelop is absent.

transfection is to be used as a routine tool it is a good idea to titrate DNA, lipid, and cell concentrations. This experiment is very easily performed if an inverted fluorescence microscope is available. It is more cumbersome if processed on coverslips, but the ease of detection of GFP minimizes the effort required to work up the samples.

A day prior to transfection, seed a 24-well dish at two concentrations of cells. For HeLa cells, prepare two cell suspensions: 25 ml each of cells at 1.5×10^4/ml and 3×10^4/ml. Pipette 2 ml of the low concentration into each well of the left half of the plate (3×4 wells) and similarly on the right half for the higher concentration. These cell densities correspond to approximately 30–40% and 60–80% confluence on the day of transfection.

1. Pipette 200 μl of serum-free DMEM into each of four sterile polypropylene microcentrifuge tubes. Add 4, 8, 12, and 16 μl, respectively, of lipofectamine into each tube. These will correspond to 0.5, 1, 1.5, and 2 μl, respectively, of lipid in the transformation reaction.

2. Pipette 250 μl of serum-free DMEM into each of three sterile polypropylene microcentrifuge tubes. Add 5, 10, and 20 μl, respectively, of a 200 μg/ml solution of pEGFP or comparable GFP expression plasmid into each tube. These will correspond to 125, 250, and 500 ng of DNA in the transformation reactions, respectively.

3. Combine 50 μl of Lipofectamine dilution and 50 μl of DNA dilution in a set of sterile microcentrifuge tubes to create a 3×4 grid as shown in Fig. 4. Incubate 30 min at room temperature.

4. Add 0.45 ml of prewarmed serum-free DMEM to each solution of DNA–lipid complex.

5. Retrieve the 24-well dish from the incubator, aspirate medium, and wash twice with PBS.

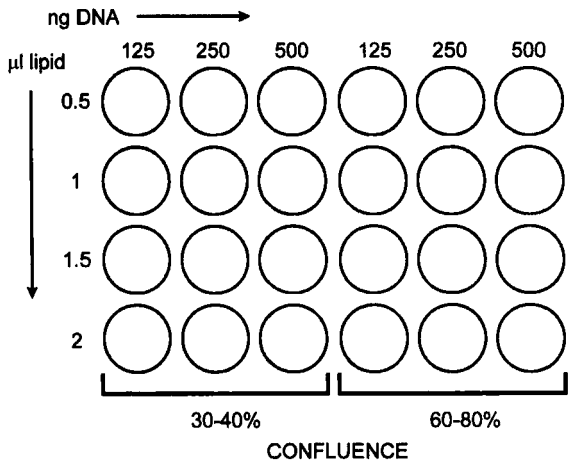

Fig. 4 Optimizing transfection efficiency with cationic lipid reagents. The grid represents a standard 24-well tissue culture plate. To titrate DNA:lipid ratios on cultures of two different cell densities, cells are plated at 30–40% and at 60–80% confluence on each half of the plate. DNA stock solutions and stock lipid dilutions are prepared as described in the text and complexes are delivered to the plate following the grid as illustrated. Each row represents a single lipid concentration complexed with differing amounts of DNA, whereas each column represents a single DNA concentration complexed with increasing amounts of lipid. It is fairly easy to scan the grid 1 or 2 days after transfection to determine optimal levels of cells, DNA, and lipid.

6. Aspirate PBS and pipette 250 μl of each transfection solution into corresponding wells at the two cell dilutions. Process a single row at a time to prevent cells from drying out.

7. Return plate to incubator once all the wells have received transfection solution. Incubate and wash following the protocol detailed previously.

8. After 24–36 hr, assay transfection efficiency by fluorescence microscopy. If an inverted microscope is available, simply remove medium and replace with PBS (to avoid background due to medium autofluorescence). Otherwise, fix coverslips in 2% formaldehyde at room temperature or in −20°C MeOH. Rinse in distilled water and mount on slides.

9. Assay each reaction by viewing through standard fluorescein filters and counting the number of fluorescent cells in several fields. In practice, a rapid scan of the dish or slides will reveal the reactions near optimum and these can be quantitated by cell counting, if necessary. Note that viewing through long working distance optics in the plastic dish will tend to yield an underestimate of the absolute level of transfection. Nevertheless, the relative efficacy of transfection across the reaction panel can be accurately assessed.

C. Stable Transfection

The process of isolating stably transfected cell lines involves selecting the small population of cells that integrate the transfected plasmid into the genome after

a standard transfection protocol. We typically use lipid-mediated transfection to introduce plasmids, but calcium phosphate works just as well.

Transformation

1. Set up transfection(s) in 35-mm dishes/6-well plate. Plate 3–6 × 10^5 cells per well the day before the transfection.

2. Perform transfection as described for coverslips, but scale up for 35-mm dishes as shown in Table II, e.g., use 1 μg of DNA and 6 μl of Lipofectamine per dish in a total volume of 1 ml serum-free medium.

3. Incubate transfected cells for 2 days at 37°C.

4. After 2 days, remove plates and wash cells twice with warm PBS. Collect cells by trypsinization, using 0.5 ml 0.05% trypsin–EDTA solution per 35-mm dish/well. When cells have detached, stop trypsin by addition of 5 ml complete medium and collect cells by gentle elutriation with the pipette.

5. Prepare two 150-mm tissue culture dishes by addition of 20 ml of complete medium. Innoculate one dish with 1 ml and the other dish with the remaining 4 ml of transfected cell suspension. Swirl gently to distribute cells evenly in the dishes.

6. Place the plates in the incubator at 37°C for 2 days.

Selection

7. After 2 days, remove medium and replace with selective medium. The selective medium depends on the selectable marker present on the expression plasmid or cotransfected marker plasmid, and the concentration of selecting drug depends on the susceptibility of untransformed cells to killing by the drug. We have primarily used selection with G418 (neo^r) and have found 0.4–0.8 mg/ml to be generally effective. Puromycin resistance is another, more economical

Table II
Scale Factors for Transfection Experiments

Culture vessel	Diameter (mm)	Area (cm^3)	DNA	Lipid	SFM diluent	Standard medium (ml)	Cells (HeLa) at confluence
24-well plate	15	2.5	250 ng/25 μl	1.5 μl/25 μl	200 μl	0.5	2.5 × 10^5
6-well plate	35	9.6	1 μg/100 μl	6 μl/100 μl	800 μl	2.0	1 × 10^6
4-well plate	60	28	2 μg/200 μl	12 μl/200 μl	1.6 ml	4.0	3 × 10^6
100-mm dish	100	78	5 μg/500 μl	30 μl/500 μl	4.0 ml	10	1 × 10^7

Note. These parameters are necessary for scaling lipid-mediated transfection reagents to different culture sizes. Listed are the diameter and surface area of different standard-sized cultured plates and dishes. DNA indicates the amount of DNA/volume of serum-free medium required for each reaction and, similarly, lipid refers to the amount of cationic lipid reagent/volume of serum-free medium required. These reagents are mixed and allowed to complex as described in the text and then diluted with the indicated amount of serum-free medium (SFM) diluent prior to application to washed cells on the dish. Also listed is the amount of medium used for standard culture conditions and the number of HeLa cells we typically obtain at confluence.

selectable marker, with effective killing concentrations on the order of 25–50 μg/ml (de la Luna *et al.*, 1988). It is advisable to titrate the amount of drug required to just kill a lawn of cells in preliminary experiments.

8. Return plates to the incubator and change medium every 2–4 days. Colonies should become apparent after ~1 week and should reach a size sufficient for picking after 2 or 3 weeks.

G418 and, to a lesser extent, puromycin, kill cells slowly, over the course of a week to 10 days. If the majority of cells have not been killed after a week, we increase the concentration of selecting drug by 1.5 to 2-fold. Increase drug concentration again after an additional 3 or 4 days if the "lawn" of cells has not died.

Picking colonies

9. Colonies are picked using cloning cylinders, short segments of 0.25-in. i.d. borosilicate tubing with polished ends, available from Belco (Stock No. 2090-00608). Prior to use, cloning cylinders are acid washed as for coverslips. Clean cloning cylinders are placed in a beaker, covered with foil, and autoclaved.

10. To pick colonies, the cloning cylinder is placed over the colony to serve as a well for a small amount of trypsin–EDTA solution. In order to form a seal against the dish, one end of the cylinder is coated lightly with vacuum grease. We use Dow Corning high vacuum grease, a silicone grease commonly available in laboratories. A small dollop of grease is placed in foil, wrapped, and autoclaved. We autoclave grease freshly each time because it appears that cytotoxic materials are generated with repeated autoclaving.

Take a sterile 100-mm tissue culture dish in the hood and with an ethanol-washed gloved finger, spread a small amount of grease in a thin layer over the inside of the lid of the dish. Try to make a uniform layer, covering most of the surface of the lid. The thickness of the layer should be such that the cloning cylinder will seat firmly when pushed into the grease layer but not extrude grease into the lumen of the cylinder. Place a grid of cloning cylinders into the lid, seating each firmly in the grease. About 25–30 cylinders will fit in each dish. Invert the bottom of the dish over the lid to cover the cylinders. They can be stored indefinitely in this manner.

11. Before picking clones it is important to identify them and mark them on the dish. If an inverted microscope is available, it should be possible to identify fluorescent colonies directly by visual inspection. If not, colonies are to be picked at random. Hold the dish up and look for the pale light scattering spots that correspond to colonies. Mark colonies with a black marker.

12. Prepare 24-well plates by pipetting 1 ml of prewarmed selective medium into each well.

13. Aspirate medium and wash dishes twice with PBS. Process only one dish at a time.

14. Aspirate PBS. Apply cloning cylinders over colonies, taking care to center the cylinder on the colony. Working quickly, place cylinders over each colony

to be picked. It is best to limit the time spent on this step to 2 or 3 min lest the dish dry out. We have found that 12–15 colonies are about the most we care to pick from a single dish. Too much time in this step reduces viability of resultant clones.

15. Pipette 50 μl of 0.05% trypsin–EDTA solution into each cylinder. Take care to deliver it down the side of the cylinder or else there is a tendency to form a bubble and kill the underlying colony by drying.

16. After ~5 min, remove colony by pipetting trypsin up and down with a micropipette and inoculate a single well of the 24-well dish.

17. Allow colonies to grow. Assay by fluorescence microscopy if an inverted scope is available. Otherwise, when cells have reached near confluence, trypsinize and replate 90% in a 6-well dish to expand. Plate the remaining 10% on a coverslip in a 24-well dish to assay by fluorescence microscopy when it is sufficiently grown.

18. Expand positive colonies to 10-cm dishes. When near confluence, trypsinize and plate three dishes at one-tenth dilution. Freeze the remainer as 5 aliquots. This is first-generation stock. When the three new dishes are near confluence, trypsinize and freeze two plates in 5 aliquots each. This provides 10 aliquots of second-generation stock. The third plate provides cells for experimental use and seeding of plates for a third-generation stock, which we generally store as 10 aliquots. It is important to use as many of the early passage cells as possible for frozen stocks. Stable transformants often lose gene expression after several passages or become unsuitably heterogeneous in terms of gene expression. Having sufficient early passage stocks can be the difference between a stable reagent system and a temporarily available cell line.

This is the traditional method for obtaining cloned stable cell lines. One advantage of this approach is that it automatically selects for clones with levels of expression of the GFP fusion protein that are compatible with cell growth and division. Nevertheless, an alternative approach is available for isolation of GFP-expressing transformants: fluorescence-activated cell sorting (FACS) (Long *et al.*, 1997; Lybarger *et al.*, 1996). While we have not used this method, it should be considered an important option for experiments with GFP. One caveat with this method is that one should examine cells across a wide range of GFP expression levels in order to identify populations that have sufficient expression for analysis without overexpression.

D. Verifying the GFP Fusion Protein

It is crucial to verify the activity and localization of GFP fusion proteins within cells prior to using them for analysis. For proteins whose localization is known, GFP fusion derivatives can be directly assessed by microscopy and immunostaining with appropriate marker antibodies (Fig. 5). If the protein under study has not previously been localized within the cell, it is important to verify that the GFP fusion protein properly reflects the distribution of the normal protein. This

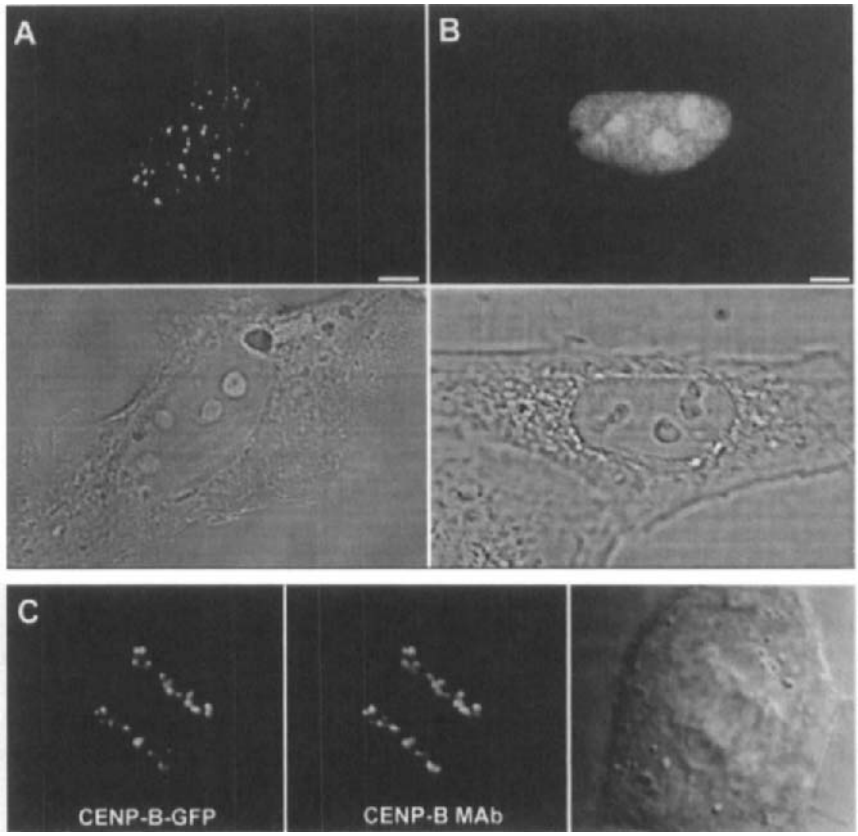

Fig. 5 Verifying the function of GFP fusion proteins. Data shown are for CENP-B-GFP expressed in humans cells. The centromeric localization of CENP-B-GFP fusion constructed with wild-type CENP-B DNA-binding domain (A) is contrasted with the essentially uniform nucleoplasmic distribution of a fusion constructed with a mutated form of CENP-B that fails to bind DNA in *in vitro* assays (B). This experiment shows that the targeting properties of the CENP-B-GFP fusion protein are a consequence of the DNA binding activity of the protein. (C) CENP-B-GFP (left) is colocalized with endogenous GFP, detected with a monoclonal antibody reactive with a C-terminal epitope absent from the fusion protein (center). This cell is executing anaphase, demonstrating at a qualitative level that the presence of the fusion protein does not disrupt the process under study.

can be done by immunofluorescence or using a complementary protein construct that has been tagged by an independent method, such as addition of a small peptide epitope. Ultimately, this is a crucial point because we have seen gross mislocalization of GFP fusions constructed from small proteins, such as CENP-A (Sullivan *et al.*, 1994) and caltractin (Lee and Huang, 1993), in our laboratory. At a functional level, the GFP fusion protein will presumably be the starting point for studies of mitosis in living cells. Using transient transfections, it is possible to assess whether the GFP fusion is compatible with mitosis by determin-

ing whether the proportion of mitotic cells in the transformed population is normal and whether cells at all stages of mitosis can be observed. Live cell imaging using techniques discussed in other chapters of this book can be used to more completely assess the behavior of mitotic cells in the presence of the GFP fusion protein (Shelby *et al.*, 1996).

In addition to using GFP fusion proteins as noninvasive labeling reagents, GFP can also be added to mutated genes that exert a dominant-negative effect on mitotic processes. Schaar *et al.* (1997) demonstrated this application of GFP for analysis of CENP-E, a kinetochore-associated kinesin-related protein. The advantage of constructing biofluorescent dominant-negative mutant proteins is that transfected cells can be readily identified for phenotypic analysis, thus ameliorating one of the classic shortcomings of transient transfection technology for examination of events at the single cell level. This logic can be extended to the application of GFP alone as a cotransfected marker for transient experiments, allowing unambiguous observation of cells transfected with experimental gene constructs or direct selection of the transfected cell population by FACS, as mentioned previously.

By reducing fluorescent protein labeling technology to the universal technology of molecular biology, GFP has made experiments that were simply not possible as little as 5 years ago relatively simple. Perhaps more important, GFP has sent a new generation of people to the microscope and a complementary group to the molecular biology bench—it is hoped to stimulate the intellectual cross-fertilization that will be necessary to understand the molecular basis of mitosis.

Acknowledgments

Thanks to Richard D. Shelby for outstanding technical assistance in developing the methods described here. Work in the author's laboratory is supported by a grant from the National Institute of General Medical Sciences.

References

Barnes, W. M. (1994). PCR amplification of up to 35-kb DNA with high fidelity and high yield from lambda bacteriophage templates. *Proc. Natl. Acad. Sci. USA* **91,** 2216–2220.

Chalfie, M., Tu, Y., Euskirchen, G., Ward, W. W., and Prasher, D. C. (1994). Green fluorescent protein as a marker for gene expression. *Science* **263,** 802–805.

Chen, C., and Okayama, H. (1987). High-efficiency transformation of mammalian cells by plasmid DNA. *Mol. Cell Biol.* **7,** 2745–2752.

Cody, C. W., Prasher, D. C., Westler, W. M., Prendergast, F. G., and Ward, W. W. (1993). Chemical structure of the hexapeptide chromophore of the Aequorea green-fluorescent protein. *Biochemistry* **32,** 1212–1218.

Cormack, B. P., Valdivia, R. H., and Falkow, S. (1996). FACS-optimized mutants of the green fluorescent protein (GFP). *Gene* **173,** 33–38.

Cormack, B. P., Bertram, G., Egerton, M., Gow, N. A., Falkow, S., and Brown, A. J. (1997). Yeast-enhanced green fluorescent protein (yEGFP) a reporter of gene expression in Candida albicans. *Microbiology* **143,** 303–311.

Crameri, A., Whitehorn, E. A., Tate, E., and Stemmer, W. P. C. (1998). Improved green fluorescent protein by molecular evolution using DNA shuffling. *Nature Biotechnol.* **14,** 315–319.

de la Luna, S., Soria, I., Pulido, D., Ortin, J., and Jimenez, A. (1988). Efficient transformation of mammalian cells with constructs containing a puromycin-resistance marker. *Gene* **62,** 121–126.

Doyle, T., and Botstein, D. (1996). Movement of yeast cortical actin cytoskeleton visualized in vivo. *Proc. Natl. Acad. Sci. USA* **93,** 3886–3891.

Gossen, M., and Bujard, H. (1992). Tight control of gene expression in mammalian cells by tetracycline-responsive promoters. *Proc. Natl. Acad. Sci. USA* **89,** 5547–5551.

Haseloff, J., Siemering, K. R., Prasher, D. C., and Hodge, S. (1997). Removal of a cryptic intron and subcellular localization of green fluorescent protein are required to mark transgenic Arabidopsis plants brightly. *Proc. Natl. Acad. Sci. USA* **94,** 2122–2127.

Heim, R., and Tsien, R. Y. (1996). Engineering green fluorescent protein for improved brightness, longer wavelenghts and fluorescence resonance energy transfer. *Curr. Biol.* **6,** 178–182.

Heim, R., Prasher, D. C., and Tsien, R. Y. (1994). Wavelength mutations and posttranslational autoxidation of green fluorescent protein. *Proc. Natl. Acad. Sci. USA* **91,** 12501–12504.

Heim, R., Cubitt, A. B., and Tsien, R. Y. (1995). Improved green fluorescence. *Nature* **373,** 663–664.

Hiraoka, Y., Swedlow, J. R., Paddy, M. R., Agard, D. A., and Sedat, J. W. (1991). Three-dimensional multiple-wavelength fluorescence microscopy for the structural analysis of biological phenomena. *Semin. Cell Biol.* **2,** 153–165. [Review]

Lee, V. D., and Huang, B. (1993). Molecular cloning and centrosomal localization of human caltractin. *Proc. Natl. Acad. Sci. USA* **90,** 11039–11043.

Leslie, R. J., Saxton, W. M., Mitchison, T. J., Neighbors, B., Salmon, E. D., and McIntosh, J. R. (1984). Assembly properties of fluorescein-labeled tubulin in vitro before and after fluorescence bleaching. *J. Cell Biol.* **99,** 2146–2156.

Long, Q., Meng, A., Wang, H., Jessen, J. R., Farrell, M. J., and Lin, S. (1997). GATA-1 expression pattern can be recapitulated in living transgenic zebrafish using GFP reporter gene. *Development* **124,** 4105–4111.

Lybarger, L., Dempsey, D., Franek, K. J., and Chervenak, R. (1996). Rapid generation and flow cytometric analysis of stable GFP-expressing cells. *Cytometry* **25,** 211–220.

Miyawaki, A., Llopis, J., Heim, R., McCaffery, J. M., Adams, J. A., Ikura, M., and Tsien, R. Y. (1997). Fluorescent indicators for Ca^{2+} based on green fluorescent proteins and calmodulin. *Nature* **388,** 882–887.

Ormo, M., Cubitt, A. B., Kallio, K., Gross, L. A., Tsien, R. Y., and Remington, S. J. (1996). Crystal structure of the Aequorea victoria green fluorescent protein. *Science* **273,** 1392–1395.

Prasher, D. C. (1995). Using GFP to see the light. *Trends Genet.* **11,** 320–323.

Reid, B. G., and Flynn, G. C. (1997). Chromophore formation in green fluorescent protein. *Biochemistry* **36,** 6786–6791.

Rizzuto, R., Brini, M., De, G. F., Rossi, R., Heim, R., Tsien, R. Y., and Pozzan (1996). Double labelling of subcellular structures with organelle-targeted GFP mutants in vivo. *Curr. Biol.* **6,** 183–188.

Rouwendal, G. J., Mendes, O., Wolbert, E. J., and Douwe, D. B. (1997). Enhanced expression in tobacco of the gene encoding green fluorescent protein by modification of its codon usage. *Plant Mol. Biol.* **33,** 989–999.

Schaar, B. T., Chan, G. K., Maddox, P., Salmon, E. D., and Yen, T. J. (1997). CENP-E function at kinetochores is essential for chromosome alignment. *J. Cell Biol.* **139,** 1373–1382.

Shelby, R. D., Hahn, K. M., and Sullivan, K. F. (1996). Dynamic elastic behavior of alpha-satellite DNA domains visualized in situ in living human cells. *J. Cell Biol.* **135,** 545–557.

Siemering, K. R., Golbik, R., Sever, R., and Haseloff, J. (1996). Mutations that suppress the thermosensitivity of green fluorescent protein. *Curr. Biol.* **6,** 1653–1663.

Sullivan, K. F., and Glass, C. A. (1991). CENP-B is a highly conserved mammalian centromere protein with homology to the helix–loop–helix family of proteins. *Chromosoma* **100,** 360–370.

Sullivan, K. F., Hechenberger, M., and Masri, K. (1994). Human CENP-A contains a histone H3 related histone fold domain that is required for targeting to the centromere. *J. Cell Biol.* **127,** 581–592.

Wang, S., and Hazelrigg, T. (1994). Implications for bcd mRNA localization from spatial distribution of exu protein in Drosophila oogenesis. *Nature* **369,** 400–403.

Yang, T. T., Cheng, L., and Kain, S. R. (1996a). Optimized codon usage and chromophore mutations provide enhanced sensitivity with the green fluorescent protein. *Nucleic Acids Res.* **24,** 4592–4593.

Yang, T. T., Kain, S. R., Kitts, P., Kondepudi, A., Yang, M. M., and Youvan, D. C. (1996b). Dual color microscopic imagery of cells expressing the green fluorescent protein and a red-shifted variant. *Gene* **173,** 19–23.

This Page Intentionally Left Blank

CHAPTER 7

Recombinant p50/Dynamitin as a Tool to Examine the Role of Dynactin in Intracellular Processes

Torsten Wittmann and Tony Hyman

Cell Biology Program
EMBL
Heidelberg D-69117, Germany

I. Introduction

Dynein is a minus-end-directed motor responsible for many intracellular functions. Traditionally it has been difficult to interfere with dynein function and thus test its role in intracellular organization. It has become clear that most dynein functions in cytoplasmic organization are mediated through dynactin, a complex of proteins which appears to target dynein to different intracellular locations and regulate its function. Thus, a simple way of disrupting dynactin function would be to prevent dynein localization and therefore to disrupt its specific functions. Recently, such a tool has been described: the overexpression of one of the components of dynactin, p50/dynamitin. When overexpressed in cells by transfection, p50/dynamitin has been shown to disrupt the dynactin complex (Echeverri *et al.*, 1996) and therefore the function of dynein in spindle

METHODS IN CELL BIOLOGY, VOL. 61

0091-679X/99 $30.00

assembly and Golgi organization (Burkhardt *et al.*, 1997). While this is a valuable tool, in many systems it is not possible to transfect cells.

Here we describe a simple two-step method for the production of large amounts of active p50/dynamitin in bacteria using ammonium sulfate precipitation and subsequent anion-exchange chromatography. We show that the recombinant protein disrupts the dynactin complex in *Xenopus* egg extracts. Expressed p50/dynamitin has been used to block spindle pole assembly in *Xenopus* egg extracts (Wittmann *et al.*, 1998) and rearrangement of microtubules during neuronal differentiation (Ahmad *et al.*, 1998). Microinjection of p50/dynamitin also leads to the dispersion of the Golgi apparatus in mammalian as well as *Xenopus* tissue culture cells (Ahmad *et al.*, 1998; Nathalie Le Bot, personal communication).

II. Production of Recombinant p50/Dynamitin

A. Solutions

Phosphate-buffered saline (PBS): 137 m*M* NaCl, 2.7 m*M* KCl, 4.3 m*M* Na_2HPO_4, and 1.4 m*M* KH_2PO_4 (pH 7.4).

Lysis buffer: PBS containing 1 m*M* ethylene glycol-bis(β-aminoethyl ether)-*N,N,N',N'*-tetraacetic acid (EGTA), 1 m*M* ethylenediaminetetraacetic acid (EDTA), 0.1% 2-mercaptoethanol, 10 μg/ml leupeptin, aprotinin, pepstatin, and 1 m*M* phenylmethylsulfonyl fluoride (PMSF). PMSF should be added just before use from a stock solution in an anhydrous solvent (e.g., absolute ethanol) stored at −20°C.

Mono Q buffer: 40 m*M* bis-tris propane, pH 7.0, 10% glycerol, 1 m*M* EDTA, 1 m*M* dithiothreitol (DTT), and 0.01% Tween 20.

B. Procedure

1. The full-length p50/dynamitin cDNA was cloned into a T7 expression vector (Way *et al.*, 1990) by PCR. For protein expression this plasmid is transformed into BL21(DE3)pLysS *Escherichia coli* cells (Studier, 1991) and an overnight culture grown at 37°C in LB medium supplemented with 100 μg/ml ampicillin and 25 μg/ml chloramphenicol. The next morning the bacteria are diluted 1:8 into fresh LB medium containing antibiotics and grown to an OD_{600} of 0.4–0.6 at 20°C. Protein expression is induced by addition of 0.1 m*M* isopropylthio-β-galactoside (IPTG) and the bacteria are grown overnight at 20°C. We sometimes observed that expression of p50/dynamitin was induced before the addition of IPTG leading to a very slow growth of the bacteria. However, this did not seem to affect the high level of expression. We also keep a glycerol stock of the BL21 strain overexpressing p50/dynamitin without any reduction of the expression level.

2. The bacteria are harvested by centrifugation (5000*g*, 30 min, 4°C), resuspended in a small volume of PBS and centrifuged again, and the bacterial pellet is frozen in liquid nitrogen. The pellet can be stored at −70°C for several months.

3. All subsequent steps are carried out at 4°C. The bacterial pellet (from 1 liter of culture) is thawed and resuspended in 10 ml of lysis buffer. We lysed the bacteria either by sonication (three times 30 sec in the presence of 1 mg/ml lysozyme) or by using a French press with comparable results. If the extract appears to be very viscous due to DNA contamination, 10 μg/ml DNAse I can be added followed by an incubation on ice for a few minutes. The extract is then diluted to 20 ml with lysis buffer and precleared by centrifugation for 15 min at 30,000*g* at 4°C (Fig. 1, lane 1).

4. The precleared extract is filled in a beaker and placed in an ice bath on a magnetic stirring plate. While stirring the extract, finely ground ammonium sulfate powder is added slowly to a saturation of 20% (2.12 g ammonium sulfate for 20 ml of extract). The incubation on ice is continued with slight agitation for approximately 1 hr and the precipitate recovered by centrifugation for 10 min at 20,000*g* at 4°C. Under these conditions most of the p50/dynamitin is recovered in the precipitate, whereas most bacterial proteins remain soluble (Fig. 1, lane 2).

5. The ammonium sulfate pellet is then redissolved in 40 ml Mono Q buffer containing protease inhibitors for 30 min at 4°C with slight agitation. This volume of buffer sufficiently reduces the salt concentration to allow binding of p50/dynamitin to the Mono Q resin. Remaining particulate material is removed by centrifugation for 10 min at 30,000*g* at 4°C and subsequent filtration through a Millipore low-protein-binding filter unit.

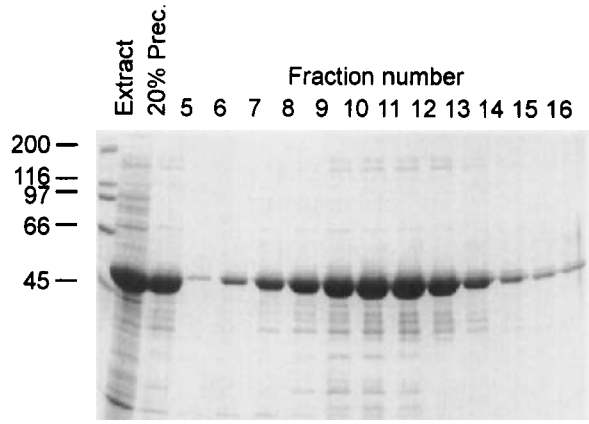

Fig. 1 Purification of bacterially expressed p50/dynamitin. Coomassie-stained 10% SDS–PAGE of precleared extract, 20% ammonium sulfate precipitate, and fractions of the Mono Q chromatography (0.5-μl aliquots of the fractions indicated were loaded on the gel). Fraction 10 contained about 12 mg/ml protein. The molecular mass of marker proteins is indicated on the left.

6. Typically, per run 20 ml of this protein solution is applied to a 1-ml Mono Q FPLC column (Pharmacia) equilibrated in Mono Q buffer. Use of more than this amount tends to overload the column and a substantial amount of protein is lost in the flowthrough. The column is washed extensively until the OD_{280} returns to zero and the column is eluted with a 20-ml linear gradient of 0–500 m*M* KCl in Mono Q buffer. One-milliliter fractions are collected. The peak of p50/dynamitin elutes at around 200 m*M* KCl (Fig. 1). The Mono Q peak fractions usually contain more than 10 mg/ml p50/dynamitin making further concentration unnecessary for most applications. If necessary, p50/dynamitin can be further purified on a Superose 12 gel filtration column.

III. Disruption of the Dynactin Complex by p50/Dynamitin in *Xenopus* Egg Extracts

When p50/dynamitin is overexpressed in tissue culture cells, this leads to the dissociation of the dynactin complex (Echeverri *et al.*, 1996). This has been demonstrated by analysis of the sedimentation behavior of different components of the dynactin complex in p50/dynamitin overexpressing cells. The most dramatic effect is observed for the $p150^{Glued}$ subunit of the dynactin complex, which normally sediments at around 18S together with other dynactin subunits but is shifted to 9S upon overexpression of p50/dynamitin. We used *Xenopus* egg extract to examine whether addition of the bacterially expressed p50/dynamitin would have the same effect and to test whether the recombinant protein is active.

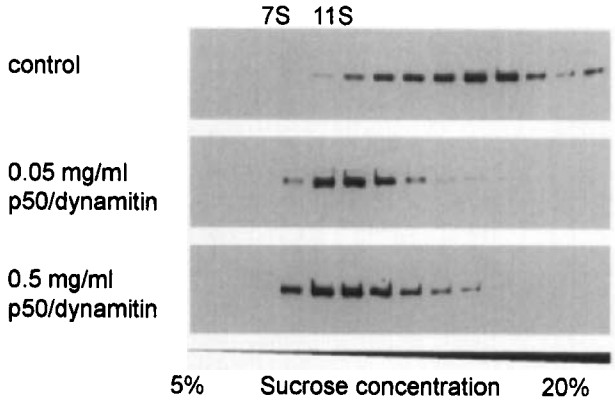

Fig. 2 Sedimentation analysis of the $p150^{Glued}$ dynactin subunit after addition of p50/dynamitin to *Xenopus* egg extract. The indicated amounts of Mono Q fraction 10 were added to 150,000*g* CSF-arrested *Xenopus* egg extract and subjected to 5–20% sucrose density gradient sedimentation. Two microliters of Mono Q buffer was added to the control reaction. The peak positions of two marker proteins are indicated on top (aldolase, 7.35 S; catalase, 11.3 S).

CSF-arrested *Xenopus* egg extract (Murray, 1991) was centrifuged for 60 min at 150,000*g* at 4°C. The high-speed cytosol (50 μl) was supplemented with p50/dynamitin and incubated for 30 min at 20°C. The reactions were then diluted with 200 μl CSF-XB (10 m*M* K-Hepes, pH 7.7, 50 m*M* sucrose, 100 m*M* KCl, 2 m*M* $MgCl_2$, 0.1 m*M* $CaCl_2$, and 5 m*M* EGTA) containing 1 m*M* DTT and protease inhibitors and layered on top of a 4.8-ml 5–20% sucrose gradient in CSF-XB containing 1 m*M* DTT and protease inhibitors. The gradients were centrifuged at 100,000*g* (28,000 rpm in a Beckman SW50.1 rotor) at 4°C for 18 hr. We collected and analyzed 350-μl fractions by Western blotting probed with an antibody against $p150^{Glued}$ (Fig. 2). We observed the same sedimentation

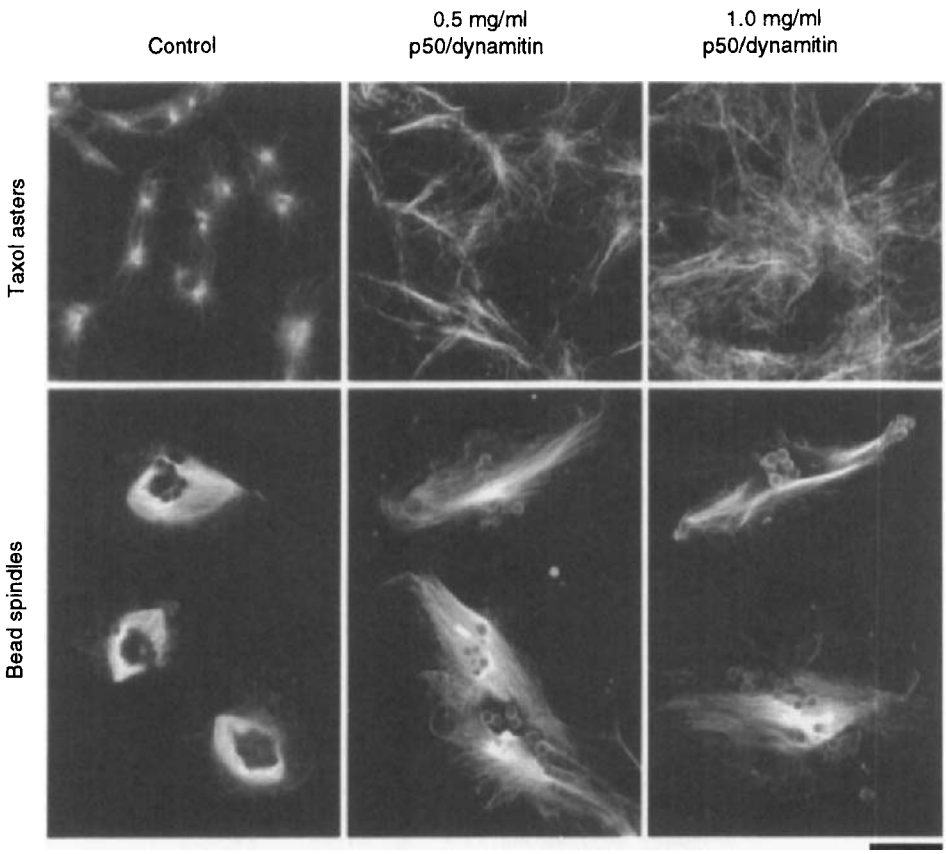

Fig. 3 Effect of p50/dynamitin on mitotic spindle poles. p50/dynamitin was added to 20 μl CSF-arrested *Xenopus* egg extract as indicated. An equivalent amount of Mono Q buffer was added to the control reaction. Microtubules were visualized by the addition of 0.2 mg/ml rhodaminated tubulin (Hyman *et al.*, 1991). Taxol asters were assembled by the addition of 1 μ*M* taxol (paclitaxel, Molecular Probes) and incubation for 30 min at 20°C. Bead spindles were assembled according to Heald *et al.*, (1996) for 60–90 min at 20°C. The reactions were fixed with 1 ml BRB80 (80 m*M* K-Pipes, pH 6.8, 1 m*M* EGTA, and 1 m*M* $MgCl_2$) containing 10% glycerol, 0.25% glutaraldehyde, 1 m*M* GTP, and 0.1% Triton X-100 and centrifuged on coverslips according to Sawin and Mitchison (1991). Scale bar = 20 μm.

pattern for p150^{Glued} as previously reported, even at rather low concentrations of exogenously added p50/dynamitin (0.05 mg/ml).

IV. Disruption of Spindle Poles Using p50/Dynamitin

In the absence of centrosomes, spindles can form in mitotic *Xenopus* egg extracts by self-organization of microtubules into poles. We have shown that this is due to cytoplasmic dynein using an antibody, m70.1, against the dynein intermediate chain (Heald *et al.*, 1996). Cytoplasmic dynein is also required for the formation of mitotic asters in the absence of centrosomes when microtubules are stabilized by taxol (Verde *et al.*, 1991).

To determine whether the dynactin complex was required for the formation of spindle poles, we added p50/dynamitin (0.5 and 1.0 mg/ml) to mitotic *Xenopus* egg extracts and then induced the assembly of taxol asters or bead spindles. We found that taxol-stabilized microtubules fail to organize into asters in the presence of p50/dynamitin. Bead spindles showed a phenotype similar to what has been observed upon addition of the m70.1 antibody (Fig. 3). Arrays of microtubules formed around the beads but they failed to form focused poles. This indicates that a dynein–dynactin interaction is required for spindle pole formation in *Xenopus* egg extracts. However, the concentration of p50/dynamitin required to observe a phenotypic effect in concentrated *Xenopus* egg extract appeared to be about 10 times higher compared to that of the biochemical dynactin disruption assay described previously.

Acknowledgments

We thank Christophe J. Echeverri for the original p50/dynamitin clone, Michael Way for help with subcloning, Trina Schroer for the p150^{Glued} antibody, and Rebecca Heald for her help with the bead spindles. T. W. is an EMBL predoctoral fellow.

References

Ahmad, F. J., Echeverri, C. J., Vallee, R. B., and Baas, P. W. (1998). Cytoplasmic dynein and dynactin are required for the transport of microtubules into the axon. *J. Cell Biol.* **140,** 391–401.

Burkhardt, J. K., Echeverri, C. J., Nilsson, T., and Vallee, R. B. (1997). Overexpression of the dynamitin (p50) subunit of the dynactin complex disrupts dynein-dependent maintenance of membrane organelle distribution. *J. Cell Biol.* **139,** 469–484.

Echeverri, C. J., Paschal, B. M., Vaughan, K. T., and Vallee, R. B. (1996). Molecular characterization of the 50-kD subunit of dynactin reveals function for the complex in chromosome alignment and spindle organization during mitosis. *J. Cell Biol.* **132,** 617–633.

Heald, R., Tournebize, R., Blank, T., Sandaltzopoulos, R., Becker, P., Hyman, A., and Karsenti, E. (1996). Self-organization of microtubules into bipolar spindles around artificial chromosomes in *Xenopus* egg extracts. *Nature* **382,** 420–425.

Hyman, A. A., Drechsel, D., Kellogg, D., Salser, S., Sawin, K., Steffen, P., Wordeman, L., and Mitchison, T. J. (1991). Preparation of modified tubulins. *Methods Enzymol.* **196,** 478–485.

Murray, A. W. (1991). Cell cycle extracts. *Methods in Cell Biol.* **36,** 581–605.

Sawin, K. E., and Mitchison, T. J. (1991). Mitotic spindle assembly by two different pathways in vitro. *J. Cell Biol.* **112,** 925–940.

Studier, F. W. (1991). Use of bacteriophage T7 lysozyme to improve an inducible T7 expression system. *J. Mol. Biol.* **219,** 37–44.

Verde, F., Berrez, J. M., Antony, C., and Karsenti, E. (1991). Taxol-induced microtubule asters in mitotic extracts of *Xenopus* eggs: Requirement for phosphorylated factors and cytoplasmic dynein. *J. Cell Biol.* **112,** 1177–1187.

Way, M., Pope, B., Gooch, J., Hawkins, M., and Weeds, A. G. (1990). Identification of a region in segment 1 of gelsolin critical for actin binding. *EMBO J.* **9,** 4103–4109.

Wittmann, T., Boleti, H., Antony, C., Karsenti, E., and Vernos, I. (1998). Localization of the kinesin-like protein Xklp2 to spindle poles requires a leucine zipper, a microtubule-associated protein, and dynein. *J. Cell Biol.,* in press.

This Page Intentionally Left Blank

CHAPTER 8

In Vitro Assays for Studying *Saccharomyces cerevisiae* Kinetochore Activity

Fedor Severin,[*] Ken Kaplan,[†] Peter Sorger,[†] and Tony Hyman[*]

[*] Cell Biology Program
EMBL
Meyerhofstrasse 1
Heidelberg D-69117, Germany

[†] Department of Biology
Massachusetts Institute of Technology
Cambridge, Massachusetts 02139

I. Introduction

Kinetochores are complexes which are required for faithful chromosome segregation: They link centromeric DNA to microtubules of mitotic spindles. Due to its high complexity in higher eukaryote, kinetochore function is best studied in the

METHODS IN CELL BIOLOGY, VOL. 61

0091-679X/99 $30.00

budding yeast *Saccharomyces cerevisiae.* The centromeric DNA in *S. cerevisiae* is only 125 bp and is present in one copy per chromosome. It has been shown that mutations in centromere sequences prevent chromosome segregation (Hyman and Sorger, 1995) and prevent the binding of a kinetochore complex to chromosome 3 centromere (CEN3) *in vitro* (Kingsbury and Koshland, 1991; Lechner and Carbon, 1991; Ng and Carbon, 1987; Sorger *et al.,* 1994, 1995). These findings allowed the development of two assays to monitor kinetochore function *in vitro.* The first assay is a bead-binding assay for studying the interaction of *S. cerevisiae* kinetochores with microtubules *in vitro.* In this assay either wild-type CEN3 or CEN3 with the 3-bp deletion is attached to fluorescent beads. The beads are incubated with yeast extract in the presence of nonspecific carrier DNA and added to microtubules. While the beads with wild-type CEN3 bind to microtubules, the beads carrying CEN3 with 3-bp deletion fail to interact with microtubules. The second assay is a band shift assay for studying the interaction of the kinetochore complex with the CEN3. In this chapter we describe the methods for both of these techniques.

II. Microtubule-Binding Assays for *S. cerevisiae* Kinetochores

A. Preparation of CEN3 Beads

1. Making the DNA

1. For a basic bead-binding assay, amplify two sequences by PCR using a 5′ primer biotin-CCACCAGTAAACGTTTC and a 3′ primer GTACAAATAAGTCACATGATGATATTTG (Sorger *et al.,* 1994). Use the following plasmids; wild-type CEN3 (plasmid PRN505) (Ng and Carbon, 1987) and CEN3 with a 3-bp deletion in the central CCG (plasmid PSF137) (Sorger *et al.,* 1994). To make 300 pmol of each fragment use the following Mastermix for the PCR reaction:

500 μl 10× PCR buffer (Perkin–Elmer, Foster City, CA) 15 m*M* $MgCl_2$, 500 m*M* KCl, 100 m*M* Tris–HCl (pH 8.3), 0.01% gelatin

40 μl of 25 m*M* dNTPs

100 μl of each primer initial concn 100 pmol.

200 μl of 50 m*M* $MgCl_2$

3810 μl H_20

Split the mix in two equal parts and to each add 125 μl of plasmid (initial concn on approximately 5 μg/ml) and 25 μl of taq polymerase (Amplitaq, Perkin–Elmer). Run PCR for 35 amplification cycles (15 sec at 94°C, 15 sec at 56°C, and 15 sec at 72°C) on GeneAmp PCR System 2400 (Perkin–Elmer).

2. Purify the PCR products on a 1-ml MonoQ column (Pharmacia LKB Biotechnology, Piscataway, NJ) using FPLC system (Pharmacia). Load pooled reac-

tions onto the column equilibrated with TE (10 m*M* Tris–HCl, 1 m*M* EDTA, pH 7.5), wash with 400 m*M* NaCl in TE for 5 column volumes, and elute the DNA with 20 ml 400 m*M*–1 *M* linear gradient of NaCl in TE. The flow rate is 0.5 ml/min. Collect 0.5-ml fractions. The product elutes in fractions 19–21 and the amount of both wild-type and 3-bp-del DNA is 330 pmol.

2. Coupling of CEN DNA to Beads

Prepare the beads as follows:

1. Make biotin–BSA by reaction of BSA with NHS–biotin (Molecular Probes, Eugene, OR, No. B-1606). Dissolve 1 g of BSA in 20 ml of 50 m*M* K-Pipes (pH 7.5). Dissolve 57 mg of NHS–biotin in 1 ml of DMSO. Mix and leave at room temperature for 1 h. Add 1 ml of 1 *M* lysine dissolved in the same Pipes buffer to stop the coupling reaction.

2. Separate biotin–BSA from free biotin on P10 desalting column (BioRad Labs, Hercules, CA). Use a column 10 times bigger than the volume of the load. Collect the peak of the protein (not the trailing fractions) and confirm the presence of biotinylated protein using rhodamine–HABA: Biotin displaces rhodamine from the HABA, thus indicating the presence of the biotinylated protein (Molecular Probes, biotin-labeling kit, No. F-2610; see the instructions provided with the kit).

3. Add 1 ml of biotin–BSA and 0.125 ml of 1 *M* sulfo-NHS (Pierce, Rockford, IL) dissolved in 50 m*M* K-Pipes (pH 7.0) to 1 ml of 0.2-μm beads (carboxylate modified, Molecular Probes) at 4°C. Then bring the tube to room temperature and add 5 mg of 1-ethyl-3-(3-dimethylaminopropil carbomide (EDAC; Sigma Chemical Co., St. Louis, MO) at 1-h intervals for 4 hr while shaking on a time shaker, 5 sec every minute. After the last EDAC addition add 0.1 ml of 1 *M* lysine to stop the reaction.

4. Spin the BSA beads down at 4°C in the Eppendorf centrifuge (14,000 rpm for 10 min), resuspend in the same volume of 0.5 *M* NaCl in 50 m*M* K-Pipes (pH 7.0), spin again, wash again in 100 m*M* K-Pipes (pH 7.0), and finally resuspend in 2 ml of 100 m*M* K-Pipes (pH 7.0). The beads can be stored at 4°C with Na-Azide.

5. Count the number of BSA beads per milliliter under the microscope. Adjust the concentration to 1.2×10^{12} beads/ml.

6. Add 50 μl of beads to 50 μl of 100 m*M* K-Pipes (pH 7.0) and 1 m*M* EDTA. Add 1 mg of streptavidin (Molecular Probes) dissolved in 50 μl of the same buffer. Agitate the mixture for 1 h at 4°C.

7. Dilute the beads with 150 μl of the same buffer and centrifuge in TLX-55 rotor at 20,000 rpm onto 100-μl cushion containing 100 m*M* K-Pipes (pH 7.0), 1 m*M* EDTA, and 20% glycerol for 10 min.

8. Resuspend the bead pellet in 300 μl of 100 m*M* Pipes 1, m*M* EDTA and 500 m*M* NaCl (pH 7.0), and sonicate with a tip sonicator until the beads become monodispersed. To avoid heating perform the sonication on ice with short (0.5-sec) pulses. Spin the beads again under the same conditions and resuspend in 300 μl of 100 m*M* Pipes and 1 m*M* EDTA (pH 7.0).

9. Sonicate the beads to make them monodispersed and dilute to a concentration 5×10^7 beads/μl with the same buffer. At this stage split the beads into two equal volumes and add either wild-type or 3-bp-del biotinylated DNA to each tube at the molar ratio 1000 DNA molecules/bead. Incubate the beads at 4°C overnight with agitation.

10. Spin the beads in the Eppendorf centrifuge at 14,000 rpm for 5 min and resuspend in 300 μl of 50 m*M* Hepes (pH 8.0), 1 m*M* EDTA, and 500 m*M* NaCl. Sonicate to disperse the bead aggregates. After the next spin (5 min at 14,000 rpm) resuspend the beads in 50 m*M* Hepes (pH 8.0), 1 m*M* EDTA, and 50% glycerol buffer.

11. Sonicate the beads and adjust to the concentration of 3×10^7 beads/μl.

B. Preparation of Carrier DNA

Prepare the carrier DNA from commercial DNA from salmon testis by sonication.

1. Dissolve 1 g of salmon sperm DNA (Sigma, No. D-1626) in 0.5 liters of TE. Sonicate with a tip sonicator—0.1-sec pulses every second for 24 hr. Keep solutions on ice and stirring on a magnetic stirrer to avoid heating.

2. Check the average length of the DNA fragments by running a sample of sonicated DNA on 2% agarose gel. The length should be approximately 200 bp. If the fragments are not short enough, continue sonication.

3. Add 1.25 liters of ethanol and 50 ml of 2.5 NaAc (pH 5.5) to precipitate the DNA. Keep the mixture on ice for 20 min, then spin in J-6B rotor (5000 rpm for 20 min).

4. Resuspend the DNA pellet in 50 ml of TE. Split between two 50-ml Falcon tubes. Add 25 ml of phenol to each Falcon tube and then vortex.

5. Separate the layers by centrifugation at 4000 rpm for 5 min (Megafuge 10R, Heraeus, South Plainfield, NJ). Collect the DNA (top layer).

6. Extract the DNA with chloroform twice. Use the same procedure as for phenol extraction.

7. Collect the DNA (the volume will be about 40 ml). Precipitate the DNA with ethanol: +2.5 vol of ethanol, +1/10 vol of 2.5 *M* NaAc, 20 min. on ice, spin in a Megafuge at 4000 rpm for 20 min.

8. Finally, resuspend the DNA in TE and adjust to the concentration of 10 mg/ml. Store frozen at −20°C.

C. Preparation of Microtubules

1. Preparation of Polarity-Marked Microtubules

Make all solutions in BRB80 [80 m*M* potassium Pipes (pH 6.8), 1 m*M* $MgCl_2$, and 1 m*M* EGTA]. Prepare and label tubulin with rhodamine and with Oregon green (Molecular Probes) as described (Hyman *et al.*, 1991). Polarity-marked microtubules can be prepared in three ways. To study the total binding of microtubules of kinetochores prepare taxol-stabilized polarity-marked microtubules as described in Howard and Hyman (1993). First, polymerize short, rhodamine-labeled microtubules in the presence of nonhydrolyzable GTP analog, GMPCPP. The commercial source of GMPCPP is not available and must be synthesized (Hyman *et al.*, 1992). Dilute the formed brightly labeled microtubules into lightly labeled tubulin at a concentration of tubulin below the critical concentration for nucleation. Polymerization mostly occurs at the plus ends of the preexisting microtubules. Then stabilize microtubules in taxol.

1. Polymerize 5 μl of bright microtubules in the presence of GMPCPP (10 μM rhodamine-labeled tubulin and 0.2 m*M* GMPCPP) at 37°C for 10–15 min.
2. Add 40 μl of dimly labeled tubulin (2μM rhodamine tubulin, 20 μM unlabeled tubulin, 1 m*M* GTP) to the microtubules. Allow the microtubules to grow for 15 min and then stabilize by the addition of 150 μl of 10 μM taxol.
3. Spin microtubules at 50,000 rpm for 5 min in TLA 100 rotor and resuspended in 50 μl of 10 μM taxol in BRB80.

2. Preparation of Capped Microtubules

To study the interaction of kinetochores with GDP versus GTP types of microtubule lattices, make the capped microtubules as described in Severin *et al.* (1997).

1. Add 1 μM of Oregon green tubulin to 0.5 m*M* GMPCPP in BRB80 at 37°C. Typical volume is 5 μl.
2. Add 1 μM Oregon green tubulin to the mixture every 30 min for 2 or 3 hr. This creates GMPCPP microtubules with an average length of 6.5 μm. We confirmed that GMPCPP was not hydrolyzed using the method of Field *et al.* (1996).
3. Preincubate 20 μl of 0.1 m*M* GTP, 10 μM tubulin, and 5 μM rhodamine tubulin in BRB80 for 10 min on ice and prewarm for 30 sec at 37°C. Add 2 μl of the Oregon green microtubules to the mixture and allow GTP tubulin to polymerize for 20 min. Under these conditions more than 90% of the GMPCPP microtubules nucleate GTP microtubules.
4. Preincubate 40 μl of 0.5 μM Oregon green tubulin and 0.5 m*M* GMPCPP in BRB80 on ice for 10 min, prewarm at 37°C for 1 min, and then mix with 0.5 μl of the GMPCPP–GTP microtubules, giving a final GTP concentration of 1 μM and GMPCPP concentration of 500 μM.

5. Add 0.5 μM of Oregon green tubulin after 1 hr of incubation at 37°C and leave at 37°C for 30 min.

Microtubules are stable only for a few hours at room temperature.

3. Preparation of GMPCPP Polarity-Marked Microtubules

To study the binding of kinetochores to the ends of microtubules versus the microtubules lattice, prepare GMPCPP-stabilized microtubules as described in Severin *et al.* (1997).

1. Add 1 μM Oregon green tubulin to 0.5 mM GMPCPP at 37°C. Add 1 μM Oregon green tubulin to the mixture every 30 min for 3 or 4 hr.

2. Mix 2 μl of the Oregon green microtubules with 20 μl of 0.3 μM tubulin, 0.2 μM rhodamine tubulin, and 0.5 mM GMPCPP. Incubate the mixture at 37°C for 30 min. Add 0.3 μM of unlabeled tubulin and 0.2 μM of rhodamine tubulin every 30 min during 3 or 4 hr. Because tubulin grows approximately three times faster from the plus end compared to the minus end (Walker *et al.*, 1988), the red segments at the minus ends of the microtubules are visibly shorter then the red segments at the plus ends.

We confirmed the polarity of the microtubules in a kinesin-gliding assay. The coverslip was coated with bovine brain kinesin and GMPCPP microtubules were added. Because kinesin is a plus-end directed motor, the microtubules were moving with their short red segments (which correspond to the minus ends) leading.

D. Preparation of Yeast Extracts

Prepare whole cell extracts from cells grown at 30°C in 0.5–1 l of YPD medium to a density of 2–5 $\times$ 10^7 cells/ml.

1. Pellet the cells by centrifugation in J-6B centrifuge (Beckman) at 4000 rpm for 5 min.

2. Wash cells once by pelting in 50 ml of water in a Falcon tube (Megafuge 10R, Heraeus), weight, and then resuspend in the same weight of two times breakage buffer [200 mM β-glycerophosphate, 100 mM bis–tris propane (pH 7.0), 400 mM KCl, 10 mM EDTA, 10 mM EGTA, and 20% glycerol] with protease inhibitors (final concentrations: 1 mM phenylmethylsulfony fluoride and 10 μg/ml each of pepstatin, leupeptin, and chymostatin).

3. Freeze the cells by dripping the cell suspension in a 50-ml Falcon tube filled with liquid nitrogen.

4. Fragment the cells with porcelain mortar and pestle cooled in liquid nitrogen. It takes 100 pestle strokes to break more than 50% of the cells.

5. Remove the cell debris by centrifugation at 15,000*g* for 30 min. Typical protein concentration in extracts is 30–40 mg/ml. Freeze the extracts in liquid nitrogen and store at −70°C in aliquots.

E. Microtubule-Binding Assays

1. Add 15–200 μg of yeast extract to a 30-μl reaction containing 3×10^7 beads and 10 μg of sonicated salmon sperm DNA in bead-binding buffer [10 m*M* Hepes (pH 8.0), 6 m*M* $MgCl_2$, and 10 % glycerol and adjusted to a final KCl concentration of 150 m*M*].

2. After 30–40 min of incubation at room temperature, take the samples and dilute 1:1 into antifade solution. Antifade contains 40 m*M* KPipes (pH 6.8), 3.5 m*M* $MgCl_2$, 0.1% 2-mercaptoethanol, 1.5 mg/ml casein, 0.1 mg/ml catalase, 0.1 mg/ml glucose oxidase, 10 m*M* glucose, and 10 μ*M* taxol.

3. Perfuse the polarity-marked microtubules into a 5-μl chamber and allow to adsorb for 5 min. Perfuse 6 μl of 3 mg/ml casein into a chamber followed by 6 μl of the bead-binding reaction diluted into antifade.

4. We observe the chambers with a Zeiss Axioskop microscope and a 63× PlanApo 1.4 NA lens. This gives the best field size for counting statistics. A 100× lens gives a higher resolution image of the actual binding event. Count the number of beads/field bound to microtubules in a coverslip focal plane.

To study the binding of the beads to GDP versus GTP parts of microtubules, mix 2 μl of the bead-binding reaction with 2 μl of the capped microtubules. Incubate the mixture for 5 min at room temperature dilute with 40 μl of BRB80, and then observe with a Zeiss Axioskop microscope and a 63× PlanApo 1.4 lens using Colour Cool View camera (Photonic Sciences, East Sussex, UK). To avoid bias, photograph all microtubules containing a bead. To examine which color to which the beads were bound, split the colors into the three components of the RGB signal.

To study the binding of the beads to the microtubule ends versus microtubule lattice, mix 1 μl of the GMPCPP microtubules with 10 μl of the kinetochore beads, allowed to bind for 5 min, then dilute with 200 μl of BRB80 and observe in the same way.

III. Band Shift Assay for the Kinetochore Complex

A. CEN3 Probe Isolation

1. The DNA probe for measuring kinetochore binding *in vitro* consists of an 89-bp fragment from the CEN3 sequence of *S. cerevisiae* and is synthesized by PCR. Probe sequences: 5' TAT TAG TGT ATT TGA TTT CCG AAA GTT AAA AAA GAA ATA GTA AGA AAT ATA TAT TTC ATT GAA TGG

ATA TAT GAA ACG TTT ACT GGT GG 3'. However, it is possible to use as little as 56 bps from this region to detect the kinetochore complex formation (Espelin *et al.*, 1997).

2. Following amplification, the PCR product is purified using anion-exchange column chromatography as described previously.

B. Labeling of CEN3 DNA by T4 DNA Kinase

1. Radiolabeled probe sufficient for approximately 100 reactions is prepared as follows: 7.50 pmol of purified probe DNA is added to a 20-μl reaction in 1× T4 polynucleotide kinase buffer [70 m*M* Tris–HCl (pH 7.6), 10 m*M* $MgCl_2$, and 5 m*M* DTT], 150 μCi of γ-^{32}P-ATP (6000 Ci/mmol; New England BioLabs, Beverly, MA), and 10 units of T4 polynucleotide kinase (New England BioLabs).

2. The reaction is incubated at 37°C for 3 hr.

3. Following the addition of 30 μl TE [10 m*M* Tris–HCl (pH 8.0) and 1 mM EDTA] reactions are terminated by phenol extraction and purification over a G-50 sepharose spin column. A yield of 50% is typically recovered and the probe is brought to a final concentration of 40 fmol/μl with TE. A successful labeling is judged to have a $>0.5 \times 10^5$ cpms/μl (Cherenkof counts).

C. Band Shift Gels

1. Kinetochore band shift products are resolved by PAGE using the Hoefer (San Francisco, CA) SE 600 series standard cooled dual gel. These gels are maintained at a more constant temperature due to the buffer surrounding the gel plates (no extra cooling is typically required), giving rise to more consistent results. However, band shift products can be adequately resolved using standard electrophoresis equipment if a cooled apparatus is not available.

2. For a single band shift gel (16 × 20 × 0.1 cm), a 30% solution of acrylamide/bis (29:1) is diluted to 4% in 1× gel running buffer (0.29 *M* glycine and 0.045 *M* Tris base) and is polymerized by adding 40 μl of ammonium persulfate (20%) and 20 μl of TEMED.

3. After polymerization, band shift gels are prerun for approximately 1 hr before loading reactions in 1× gel running buffer.

D. Kinetochore-Binding Reaction

1. The kinetochore-binding reaction is performed in 1× binding buffer [10 m*M* Hepes (pH 8.0), 6 m*M* $MgCl_2$, and 10% glycerol] with 40 fmol of CEN3 DNA probe in a final volume of 30 μl. Kinetochore binding to CEN3 DNA is extremely sensitive to salt concentrations; therefore, binding reactions are adjusted to a final concentration of 150 m*M* KCl after addition of an extract.

2. To reduce nonspecific binding of proteins to probe DNA, 2.5 μg of sheared salmon sperm testes DNA (ssDNA) is added as a nonspecific carrier DNA. Since the extent of shearing varies with each preparation, we empirically determine the optimal amount of ssDNA for each preparation. To demonstrate CEN-specific binding, excess cold wild-type or mutant CEN DNA (64× molar excess to radiolabeled probe) can be added at the start of the reaction (Espelin *et al.*, 1997). Under these conditions, kinetochore complex binding is easily detected with 40 μg of yeast extract. Reactions are assembled and then incubated at room temperature for 40 min. A small amount of bromophenol blue tracking dye, diluted in 1X binding buffer, is added prior to loading reactions on the prerun band shift gel. Gels are run at 300V, removed when the tracking dye reaches the bottom, and then dried on Whatman 3M paper before exposing to film or using a Phosphorimager (Molecular Dynamics). Screen to detect the radiolabeled DNA.

References

Espelin, C. W., Kaplan, K. B., and Sorger, P. K. (1997). Probing the architecture of a simple kinetochore using DNA–protein crosslinking. *J. Cell Biol.* **139,** 1383–1396.

Field, C. M., Ai-Awar, O., Rosenblatt, J., Wong, M. L., Alberts, B., and Mitchison, T. J. (1996). A purified Drosophilla septin complex forms filaments and exhibits GTPase activity. *J. Cell Biol.* **133,** 605–616.

Howard, J., and Hyman, A. A. (1993). Preparation of marked microtubules for the assay of the polarity of microtubule-based motors by fluorescence microscopy. *Methods Cell Biol.* **39,** 105–113.

Hyman, A. A., and Sorger, P. K. (1995). Structure and function of kinetochores in budding yeast. *Annu. Rev. Cell Dev. Biol.* **11,** 471–495.

Hyman, A. A., Drexel, D., Kellog, D., Salser, S., Sawin, K., Steffen, P., Wordeman, L., and Mitchison, T. J. (1991). Preparation of modified tubulins. *Methods Enzymol.* **196,** 478–485.

Hyman, A. A., Salser, S., Drechsel, D. N., Unwin, N., and Mitchison, T. J. (1992). Role of GTP hydrolysis in microtubule dynamics: Information from a slowly hydrolyzable analogue, GMPCPP. *Mol. Biol. Cell.* **3,** 1155–1167.

Kingsbury, J., and Koshland, D. (1991). Centromere-dependent binding of yeast minichromosomes to microtubules *in vitro*. *Cell* **66,** 483–495.

Lechner, J., and Carbon, J. (1991). A 240kd multisubunit protein complex, CBF3, is a major component of the budding yeast centromere. *Cell* **64,** 717–726.

Ng, R., and Carbon, J. (1987). Mutational and *in vitro* protein-binding studies on centromere DNA from *Saccharomyces cerevisiae*. *Mol. Cell Biol.* **7,** 4522–4534.

Severin, F. F., Sorger, P. K., and Hyman, A. A. (1997). Kinetochores distinguish GTP from GDP forms of the microtubule lattice. *Nature* **388,** 888–891.

Sorger, P. K., Severin, F. F., and Hyman, A. A. (1994). Factors required for the binding of reassembled yeast kinetochores to microtubules in vitro. *J. Cell Biol.* **127,** 995–1008.

Sorger, P. K., Doheny, K. F., Hieter, P., Kopski, K. M., Huffaker, T. C., and Hyman, A. A. (1995). Two genes required for the binding of an essential Saccharomyces cerevisiae kinetochore complex to DNA. *Proc. Natl. Acad. Sci. USA* **92,** 12026–12030.

Walker, R. A., O'Brien, E. T., Pryer, N. K., Sobeiro, M. F., Voter, W. A., Erickson, H. P., and Salmon, E. D. (1988). Dynamic instability of individual microtubules analysed by video light microscopy: Rate constants and transition frequencies. *J. Cell Biol.* **107,** 1437–1448.

This Page Intentionally Left Blank

CHAPTER 9

Fluorescent Speckle Microscopy of Spindle Microtubule Assembly and Motility in Living Cells

Clare Waterman-Storer,* Arshad Desai,† and E. D. Salmon*

*Department of Biology
University of North Carolina at Chapel Hill
Chapel Hill, North Carolina 27599

†Department of Cell Biology
Harvard Medical School
Boston, Massachusetts

METHODS IN CELL BIOLOGY, VOL. 61

0091-679X/99 $30.00

I. Introduction

We have found that fluorescent speckle microscopy can reveal many features about the assembly dynamics and movement of microtubules in the tissue cell interphase cytoplasmic microtubule complex and the mitotic spindle (Waterman-Storer and Salmon, 1997, 1998; Waterman-Storer *et al.*, 1998a). In this method, contrast is created by assembly with a very small fraction of fluorescently labeled tubulin subunits. Random variation in association creates a non-uniform fluorescent "speckle" pattern during microtubule growth. Fluorescent speckle images of microtubles are recorded using conventional wide-field fluorescence microscopy and digital imaging with a sensitive, low noise, cooled charge coupled device (CCD) camera (Salmon *et al.*, 1998). Speckle imaging can also be employed to examine the assembly dynamics and motility of actin filament arrays in cells and the binding and release of microtubule associated proteins (MAPs) on the microtubule lattice (Waterman-Storer *et al.*, 1998a). In principle, the method can be combined with high-resolution techiques for tracking chromosomes and kinetochores (Skibbens *et al.*, 1993; Salmon *et al.*, 1994; Khodjakov and Rieder, 1996) to yield information about the relative motions of kinetochores and their kinetochore microtubules.

In this chapter, we introduce the principles of the fluorescent speckle microscopy method for microtubules and then briefly describe the features of a digital imaging system that are important for speckle image recording and analysis with other optical modes such as phase contrast or vital staining with DNA dyes such as the blue fluorescent Hoescht or DAPI to record chromosome position. Applications of the method are presented for measuring microtubule movements in tissue cell spindles and asters (Waterman-Storer *et al.*, 1998a) and in spindles reassembled *in vitro* in cytoplasmic extracts of *Xenopus* eggs (Murray *et al.*, 1995b; Desai *et al.*, 1998). We are in the very early stages in the development of fluorescent speckle microscopy and the following procedures represent our initial experience.

II. Principles of the Fluorescence Speckle Method for Microtubules

Microtubules dynamically assemble in cells from a cytoplasmic pool of α/β-tubulin dimers (Inoué and Salmon, 1995; Desai and Mitchison, 1997). Each tubulin dimer is about 8 nm long $\times$ 5 nm wide. Dimers are oriented head to tail

at 8 nm spacing along the 13 protofilaments which comprise the 25-nm diameter cylindrical wall of a microtubule (Fig. 1) There are 1625 dimers per 1 μm of microtubule length. Microtubules grow by dimer association with their ends. In cells, the minus end is often attached to the centrosome or spindle pole complexes (Waters and Salmon, 1997), whereas the plus end is oriented away from the centrosome or pole toward the cell surface in the asters and toward the chromosomes in the spindle. The plus end is the primary site of growth. In living cells, microtubule plus ends grow at a velocity of 5–15 μm/min, corresponding to 135–400 dimers/s association. The plus ends often exhibit dynamic instability (Inoué and Salmon, 1995; Desai and Mitchison, 1997), abruptly switching from growth to shortening at similar or faster velocities for many micrometers before switching back to growth or depolymerizing back to the nucleation centers at the centrosome or spindle poles.

The resolution of microtubules in the light microscope depends on the wavelength of light (Inoué and Spring, 1997). Resolution, r, in wide-field fluorescence microscopy is given by:

$$r = 0.61\ \lambda/\mathrm{NA}_{\mathrm{obj}} \quad (1)$$

where λ is its wavelength of light and $\mathrm{NA}_{\mathrm{obj}}$ is the numerical aperture of the objective. For example, resolution is about 0.27 nm for the 620-nm fluorescence from tubulins conjugated to X-rhodamine fluorophore. Thus, at this wavelength, the fluorescent distribution along images of microtubules depends on variations in the number of fluorescent tubulin subunits at intervals of about 0.27 μm (Fig. 1).

Analysis of the assembly of purified tubulins *in vitro* (Waterman-Storer and Salmon, 1998) has shown that fluorescent speckles are generated by the normal stochastic association of fluorescently labeled and unlabeled tubulin dimers with growing microtubule ends (Fig. 1). Each time a dimer is added to 1 of the 13

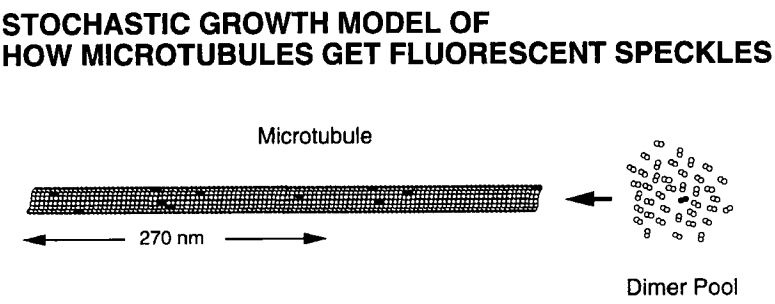

Fig. 1 A stochastic growth model for the origin of the fluorescent speckle distribution in light micrographs of microtubules grown from a tubulin pool containing a small fraction of labeled dimers. The model assumes that microtubule growth occurs by stochastic tubulin dimer association at the ends of the protofilaments in the microtubule cylindrical wall (only 7 of the 13 protofilaments are shown) (reproduced with permission from Waterman-Storer and Salmon, 1998, from *Biophys. J.*, 1998, in press, by copyright permission of The Rockefeller University Press).

protofilaments at the growing end, the probability that it will be a dimer with a fluorophore depends directly on the fraction (f) of labeled dimers in the tubulin pool. For example, if $f = 1\%$, then each time a dimer is added to a microtubule end there is a 1 in 100 chance it will have bound fluorophore. Over many micrometers of microtubule growth, the mean number (M) of fluorescent dimers per N dimers in 0.27 μm, the limit of resolution, is

$$M = fN \tag{2}$$

and $M = 4.4$ when $f = 1\%$ of $N = 440$ dimers. The speckle pattern is produced by variations from the mean. The standard deviation (SD) from the mean for a stochastic process is given by

$$SD = (Nf(1\text{-}f))^{0.5} \tag{3}$$

which is approximately the square root of the mean for small values of the fraction of labeled tubulin. For a mean value of 4.4, SD = 2.15. We define contrast (C) of the fluorescent speckle distribution along a microtubule by the ratio of the standard deviation of the fluctuations to the mean fluorescence:

$$C = \mathrm{SD}/M \tag{4}$$

and $C = 2.15/4.4 = 0.49$ for a 1% fraction of labeled tubulin.

A high SD relative to the mean for stochastic growth at small fractions of labeled tubulin provides an explanation of how microtubules get fluorescent speckles (Fig. 2). Contrast measured for microtubules assembled *in vitro* with various fractions of tubulin conjugated to X-rhodamine (average stoichiometry 1:1 fit to a first approximation were in agreement with theoretical simulations based on the stochastic incorporation model described previously (Fig. 2; Waterman-Storer and Salmon, 1998). As is shown in Fig. 2, the contrast of fluorscent speckles is low above 5–10% of labeled tubulin, but it rises rapidly for lower fractions.

Variation in the number of fluorophores per labeled tubulin subunit has not yet been considered. The previous analysis also does not consider the effects of background fluorescence in the imaging system and effects due to unincorporated labeled dimers on speckle contrast. However, as the fraction, f, of fluorescently labeled tubulin decreases, background fluorescence also decreases, giving higher measured speckle contrast in the microscope images.

For the spindle speckle imaging described later, we estimate that the fraction of labeled tubulin is about 0.4% or less. Thus, the speckles represent only a few fluorophores at these low fractions of labeled tubulin (Fig. 2) and a sensitive high-resolution imaging system and methods to retard photobleaching are needed.

III. Specimen Methods

A. Purification and Tubulin Labeling

We labeled purified porcine brain tubulin with X-rhodamine with a stoichiometry of approximately one fluorophore:one dimer as described by Waterman-

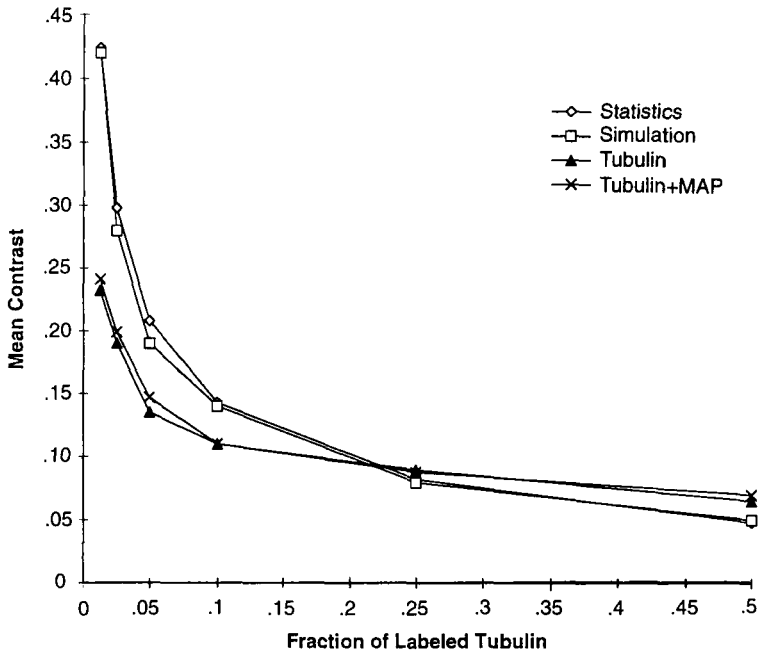

Fig. 2 Mean speckle contrast for microtubules assembled *in vitro* and for simulated microtubules depends on the fraction of labeled tubulin. Microtubules were assembled *in vitro* from pure tubulin and pure tubulin in the presence of 0.4 mg/ml porcine brain MAPs as a function of the fraction of labeled tubulin dimers. Each *in vitro* data point represents the average contrast of 10 microtubules. The simulated microtubule values represent the average from 5 microtubules for each fraction of labeled tubulin. See Waterman-Storer and Salmon (1998) for details about the simulated microtubules and the statistical expectations. Note that the brain MAPs had no effect on the contrast relative to pure tubulin (reproduced with permission from Waterman-Storer and Salmon, 1998, from *Biophys. J.*, 1998, in press, by copyright permission of The Rockefeller University Press).

Storer and Salmon (1997, 1998). Briefly, tubulin is purified from porcine brain by cycles of polymerization and depolymerization followed by phosphocellulose chromatography as described by Walker *et al.* (1998). Tubulin is drop frozen after passage through the phosphocellulose column and stored at −80°C until use. Tubulin is labeled with X-rhodamine succinimidyl ester according to the method of Hyman *et al.* (1991). The final labeled tubulin pellet is resuspended in injection buffer (50 m*M* K glutamate, 0.5 m*M* KCl, pH = 7.0) at a concentration of ~30 mg/ml, drop frozen in liquid N_2, and stored at −80°C. The molar dye : protein ratio can be determined by using the extinction coefficient for X-rhodamine (78,000 M cm^{-1} at a wavelength of 570 nm) and tubulin concentration can be determined using the extinction coefficient for tubulin (115,000 M cm^{-1} at a wavelength of 278 nm). Just prior to an experiment, the labeled tubulin is thawed, diluted in injection buffer to 1 mg/ml, and clarified by centrifugation for 20 min at 4°C, 30,000 rpm, in a TLS-55 rotor in a TLA-100 ultracentrifuge (Beckman).

Following centrifugation, the supernatant is immediately transferred to a fresh chilled tube and used as soon as possible for microinjection. Pure brain tubulin can also be labeled with tetramethylrhodamine by procedures similar to those for X-rhodamine labeling (Sawin and Mitchison, 1991).

B. Tissue Cells

Newt epithelial cells from explants of *Taricha granulosa* lung are cultured in Rose chambers as described by Rieder and Hard (1990). For microinjection, the top coverslip is removed from the Rose chamber, the chamber is filled with media, and the cells are viewed from the bottom with an inverted microscope. Microneedles for injection (Microdot and capillary tubing, Glass Co. of America, Bargaintown, NJ) are pulled to a 0.5- to 1-μm tip diameter with a Kopf (Tujunga, CA) Model 750 needle puller. They are treated to prevent clogging at the needle tips by placing them overnight in a petri dish containing a few drops of HMDS (Pierce). Needles are backloaded with 1 μl of tubulin solution using a 50-μl Hamilton syringe. Labeled tubulin is pressure microinjected into the tissue cells using the apparatus described by Waters *et al.* (1996) at a concentration of about 0.2–0.5% of the total cellular tubulin pool, which is about 20 μM. Tubulin diffuses rapidly and becomes uniformly distributed after several minutes within the cytoplasm in tissue cells. Mitotic cells are injected at either prophase or early prometaphase to allow incorporation along the lengths of the spindle and astal microtubules (Waters *et al.*, 1996).

Coverslips with adhered microinjected cells are then mounted on an ethanol cleaned slide between two strips of double stick tape spaced ~5 mm apart to form a flow chamber. The slide–coverslip chamber is filled with culture media containing 0.3–0.6 units per milliliter of the oxygen-scavenging enzyme oxyrase (Oxyrase, Inc., Mansfield, OH) to retard photobleaching. The chamber is then dried at the edges, sealed with Valap (1:1:1 Vasoline:lanolin:parafin), and placed on the microscope stage at room temperature.

C. *In Vitro* Spindles

Spindles with replicated chromosomes in cytoplasmic extracts are prepared as described in detail by Murray (1991) and Desai *et al.* (1998) from *Xenopus* eggs and sperm. Extracts are supplemented with 4′,6′-diamidino-2-phenylindole (DAPI) at 0.05 μg/ml to make the chromosomes fluorescent blue and 0.1 μM of tetramethylrhodamine-labeled tubulin to give microtubules red fluorescent speckles. Note that in previous studies of spindle dynamics, the extracts were typically supplemented with a 10-fold or higher concentration of fluorescent tubulin to uniformly label the microtubules (Murray *et al.*, 1996). For speckle imaging the procedures for slide–coverslip preparation are similar to those used previously (Murray *et al.*, 1996; Desai *et al.*, 1998). Briefly, about 4 μl of extract containing metaphase spindles is placed on an ethanol cleaned slide, covered

with a cleaned coverslip, sealed on the edges with Valap, and placed on the microscope stage at room temperature.

D. Prevention of Photobleaching

As noted previously, 0.3–0.6 U/ml of oxyrase (Ashland, OH) is added to the tissue culture media in the specimen chamber to retard photobleaching. Oxyrase depletes oxygen in the media, reducing the rate of photobleaching because it is directly dependent on oxygen concentration (Waterman-Storer *et al.,* 1993; Waterman-Storer and Salmon, 1997). The *in vitro* spindles in the *Xenopus* extracts appear less sensitive to photobleaching and no treatments were required.

IV. Microscopy and Image Acquisition

We developed a high-resolution, multimode, multiwavelength, digital fluorescence light microscope for fluorescence imaging of mitosis in living cells or cytoplasmic extracts that has enough sensitivity for fluorescence speckle imaging. The microscope was initially designed to use epifluorescence to obtain images in living cells of individual microtubules or mitotic spindles containing X-rhodamine-conjugated tubulin (red fluorescence) and chromosomes vitally stained with DAPI or Hoescht 33342 (blue fluorescence). Images of chromosomes and cell structure can also be obtained by transmitted light differential interference contrast (DIC) or phase contrast. This instrument is specialized for our microtubule and mitosis studies, but can also be applied to a variety of problems in cellular imaging, including imaging proteins or cellular structures labeled with green fluorescent dyes or fused to the green fluorescent protein (GFP) in live cells or mulitwavelength imaging of immunofluorescently stained cells (Salmon *et al.,* 1998; Shaw *et al.,* 1997; Waters *et al.,* 1998b). Many aspects of the microscope are automated for the time lapse image acquisition needed for analysis of microtubule assembly dynamics and motility. A Pentium-based computer system running MetaMorph software developed by Universal Imaging Corporation controls filter wheels for wavelength selection, transmitted and epiillumination shutters, the camera exposure, and image storage into image stacks corresponding to red, green, and blue fluorescence channels and transmitted light DIC or phase contrast images.

The component parts, construction, and operation of this instrument are described in detail by Shaw *et. al.* (1997) and Salmon *et al.* (1998). Only those features important for speckle imaging will be briefly described here. Other digital imaging microscopes with similar objective NA, magnifications relative to the size of the detector pixels (picture elements), detector quantum efficiency, robotic control of shutters to prevent photobleaching, and ability to acquire and save image stacks larger than 100 MB can also be used.

A. Resolution and Light Sensitivity Are Critical

The microscope utilizes conventional wide field optics and a cooled, slow-scan CCD camera for image detection. The resolution in the CCD images can be diffraction limited and the system was designed to image fluorescence photons as efficiently as possible. The camera detector is placed at the intermediate image plane of the objective lens on the upright microscope with few intervening components to induce loss of light.

For speckle imaging we use a 60X, 1.4 NA objective lens, a 1.25X body tube lens, and a 1.5X intermediate lens to project images to the camera at a total magnification of 112.5X. The CCD chip is composed of pixel element detectors that are 12 μm^2. Using three pixels per optically resolved unit (0.27 μm) satisfies the sampling criteria (Nyquist limit) that the camera is not limiting resolution (Inoué and Spring, 1997). The total magnification (M_{tot}) needed to achieve diffraction-limited resolution is given by

$$M_{tot} = 3 \cdot P_{width}/r \tag{5}$$

where P_{width} is the width of the pixel element in the detector and r is the diffraction-limited resolution from Eq. (1). For P_{width} = 12 μm and r = 0.27 μm, M_{tot} = 133. If the camera had pixels that were 6 μm in size, the total magnification needed for the camera to achieve diffraction-limited resolution in the images would be half this value (67X).

For the TC-215 CCD chip in the camera, there is a 65% chance of converting a "red" photon to an electron (0.65 quantum efficiency) for the X-rhodamine-labeled tubulins used for our spindle speckle imaging and a 35% quantum efficiency for fluorescein or GFP green excitation wavelengths. The CCD camera, which has low noise (about 10 electrons or two gray levels), produces images of microtubules containing X-rhodamine-labeled tubulin with a much higher quantum efficiency and less noise than intensified video cameras, which were previously often used to image fluorescent microtubules in living cells.

B. Microscope Stability Is Critical

The stability of the microscope stand and focus is extremely important. Vibration ruins resolution and a vibration isolation table is required (Salmon *et al.*, 1998). A focus drift of 200–300 nm significantly changes speckle intensity. This is not a major issue for short duration time-lapse recording, but for durations longer than 10 min we still have not solved this problem, in part because of stage mechanical drift or thermal expansion of the microscope body. We have observed that focus stability is much better when the slide is not oiled to the condenser.

C. Wavelength Selection

For fluorescence excitation, a high-efficiency multiple bandpass dichromatic mirror and emission filter (Chroma) in combination with an excitation filter

wheel is used to rapidly switch between red, green, and blue fluorescent imaging. Using this optical method, red, green, and blue fluorescent images are always aligned on the CCD detector. A 570 ± 10-nm filter excites X-rhodamine, a 490 ± 10-nm wavelength bandpass filter is selected for fluorescein and GFP excitation, and a 360 ± 20-nm wavelength filter is selected to excite DAPI or Hoescht 33342 chromosome stains. Neutral density filters in combination with a manual iris diaphragm are used to attenuate the light from the 100 W Hg arc lamp to between 1 and 10% of maximum. For fixed wavelength imaging, some gain in sensitivity can be achieved by using high-efficiency "High Q" filter cubes (Chroma), which have a broader emission bandpass than that available from the multiple bandpass filter.

D. Removal of DIC Imaging Components

For fluorescence speckle imaging, it is important to remove the objective DIC prism and DIC analyzer from the light path. The DIC prism splits point sources of light such as the fluorescent speckles into two lower intensity, slightly overlapping point sources. This reduces resolution and sensitivity in speckle imaging. The analyzer will absorb 70% or more of the incident light. A phase contrast objective and corresponding condenser annulus for illumination can be used to provide images of cell structure in transmitted light imaging, and the same objective can be used for fluorescent speckle imaging without substantial reduction of image quality.

E. Shutters Prevent Photobleaching

The Time-Lapse image acquisition routine in the MetaMorph imaging software controls the epifluorescent shutter so that it is opened just before recording an image and closed after image capture in the camera. This is necessary so that the total illumination time of the specimen is kept to a minimum. Another shutter in the transmitted light path controls illumination for acquisition of phase contrast images.

F. Image Acquisition and Storage Requires a Large Amount of Computer Memory and Disk Space

For speckle imaging of microtubules in tissue spindles, we have recorded 500-pixel (picture element) square images into a MetaMorph image stack at 10-s intervals using a Time-Lapse routine. These images are 12 bits/pixel deep (4096 gray levels). We typically use 1- or 2-s exposures. A "dark" image from the camera for the same amount of time with the shutter closed is also recorded for each image series.

The time-lapse image stacks are often >150 MB. As a result, a fast computer (e.g., 300 MHz or higher Pentium II), substantial computer memory (at least

256 MB RAM), and large storage device are needed. Images are immediately saved onto 1 GB removeable JAZ disks (Iomega Co.) for processing and analysis and later archived onto 650 MB CD-ROMs.

V. Image Processing and Analysis

A. Processing

1. Camera Correction

A dark camera image is obtained by averaging 25 images taken with the camera shutter closed. The dark camera image is subtracted from each image in a stack to correct for the camera dark current in each pixel (Salmon *et al.*, 1998) using the Arithmetic routine in MetaMorph.

2. Image Alignment for Motion Analysis

Often the spindles move around during time-lapse recording, particularly in the tissue cells. This makes the measurment of distances of microtubules relative to the spindle pole or centrosome cumbersome. To minimize this problem, the Align Stack routine in MetaMorph software is used to align the position of the centrosome or spindle pole relative to its position in the first image of a time-lapse stack of images.

3. Background Equalization

Changes in image intensity through the stack occur because of lamp flicker or photobleaching. The Equalize Light routine in MetaMorph is used to make speckle brightness in the images of the time-lapse sequence similar. A reference region is outlined on the first image in the stack and then, for all images in the stack, each image is multiplied by a constant so that the average value of gray level in the reference region is the same for all images.

4. Conversion to Eight-Bit Image Stacks

The processed image stacks are converted from the 12-bit, 4096 gray level images to 8-bit, 256 gray level images using the Scale 16 Bit Image routine to reduce the size of the image stacks by a factor of two. It is not uncommon for 16-bit image stacks of large spindles to be 150 MB; decreasing this to 75 MB results in a better fit with the memory capacity of the computer for making and playing movies and reduces storage requirements. The 8-bit stacks appear satisfactory for speckle motion analysis.

5. Unsharp Mask

To enhance the contrast of the speckles and suppress background intensity variation, an Unsharp Mask routine is used. For each image in a stack, a 9×9 pixel

running average (low pass kernel of 9) generates an image of the background. The background images are multiplied by a constant of 0.5 and subtracted from the original images. The resulting images are multiplied by a scaling factor of 2. The resulting image is contrast enhanced to make the speckles distinctly visible.

6. Movie Viewing

Image stacks can be made into a "movie loop" for viewing speckle motions. This is done using the Movie function in MetaMorph.

B. Analysis of Speckle Motility

1. Distance Calibration

Images of the 10-μm intervals of a stage micrometer (Fisher No. 12-579) are used to calibrate distance in image stacks using the Calibrate Distance routine in MetaMorph. After this calibration is performed for an image stack, subsequent measurements of positions in the image are returned by the software in micrometer units as well as pixel number.

2. Single Speckle Tracking

Movements of individual microtubule speckles can be measured by two methods in the MetaMorph imaging system. One uses the mouse cursor to "point and click" on the position of a speckle. The Measure Pixel routine transfers coordinates of the speckle position to a Microscoft Excel spreadsheet for each frame in an image stack along with the time that the frame was recorded. The position of the spindle pole or centrosome is recorded as a reference. Distance versus time plots are generated in Excel and speckle velocity relative to the pole or centrosome is calculated from the slopes of these plots.

The second method is a "semiautomatic tracking" routine called Single Particle Tracking. A sequence of images containing a speckle in focus is chosen in a stack. A circular cursor is drawn to fit just around this speckle in the first frame. The pixel values within this cursor region are used as a mask to find the speckle in subsequent frames. Then the program incorporates subsequent frames and moves the circular mask one pixel at a time in a search region to find the best correlation with the image. The calculated centriod of the best fit position of the mask is used to define the speckle position. The image stack can be replayed with the measured cursor positions overlayed to check for the accuracy of the tracking. The cursor can be centered over the speckle by hand in an individual frame to correct mistakes made by automatic tracking. The x and y coordinates of the centroid position and the time of each frame are transferred to an Excel spreadsheet for subsequent plotting of distance verses time and velocity analysis.

3. Kymographs

Kymographs allow both a graphic display of speckle motion over time and a means of determining speckle velocity values. There are currently two ways in which MetaMorph makes kymographs of speckle motion in image stacks: One works only for horizontal and vertical directions, whereas the other can follow a line scan in any direction. The first method can only be used if the trajectory of speckle movement is horizontal or vertical. Using this method, a narrow rectangular "slit" region is drawn on the first image in the stack oriented either horizontally or vertically. This rectangle is drawn three to five pixels in width over the distance for motion analysis. The MetaMorph Duplicate Stack routine is used to copy the image within the drawn rectangular slit region to another image stack. The slit stack is converted into a kymograph using the Montage routine, which can convert a stack of images into a montage with the slit images aligned side by side down (horizontal region) or across (vertical region) the montaged image. The width of this montage is the number of pixels in the length of the rectangular slit region, whereas the height is the number of frames in the stack multiplied by the number of pixels in the width of the rectangular region. By eye, the brightest speckles within the slit produce oblique white lines down the kymograph, whose slope yields the velocity of motion.

The second line-scan Kymograph routine in MetaMorph is not restricted to horizontal or vertical kymograph directions. The point-to-point line drawing function in MetaMorph is used to draw a line region in any direction for motion analysis over the first image in a stack, for example, along a kinetochore fiber in a spindle. The advantage of this is that the line can curve with the curvature of the spindle. The Kymograph routine in MetaMorph samples pixel values along this line for each image in a stack and montages these values into an image in which the horizontal axis contains the pixel values measured along line scans aligned side by side in the vertical direction. The width of the resultant kymograph image is the length in pixels of the kymograph line, whereas the height in pixels is the number of images in the stack. In MetaMorph, it is possible to increase the pixel width of the line scan using the Linescan routine, and we typically use a line which samples a three-pixel width because speckles often move or oscillate laterally off of a narrow line. At each position along the line, the average value is returned for the pixels within the width, but the maximum value would provide better visibility.

Velocities are determined by the slopes of the oblique trajectories of speckle movements in kymographs generated by either method. Measurements of distance in the horizontal direction are calibrated in micrometer units using the Calibrate Distances routine. Measurements of distance in the vertical direction must be calibrated to the total time of the number of frames in the stack. For example, if the images are recorded at 10-s intervals and there are 50 frames in the stack, the vertical distance of the kymograph corresponds to 500 s and fractions of this distance are fractions of that time interval. Currently, we draw

a straight line which gives a best fit by eye to a speckle trajectory. This line is then extended to span the height of the kymograph image. Then a rectangular region is drawn so that the line is the diagonal of the region. The Show Region Statistics routine provides the width and the height of this region in micrometers. The width is the distance the speckle would move at the velocity of the trajectory for the total time represented by the height of the kymograph. The ratio of these data is the velocity of the trajectory.

C. Presentation Movies

We have described in detail (Waterman-Storer *et al.*, 1997) the procedures and equipment we use to make videotapes of digital recordings.

VI. Examples

A. Newt Tissue Cell Lamella Micotubules

Figure 3 shows a fluorescence speckle image of microtubules for cells injected with X-rhodamine tubulin at about 0.5% or less of the total cellular tubulin pool. Time-lapse images were recorded for the leading edge and lamella region of migrating newt lung epithelial cells as described by Waterman-Storer and Salmon (1997). The lamella is very thin (<1 μm) and almost all the microtubules are contained within a single focal plane of the microscope. At the very low fractions of X-rhodamine-labeled tubulin in Fig. 3, the brightest speckles occur at 1- to 3-μm intervals along the microtubule lattice, and weaker speckles occur in between. In Fig. 3, note that the background fluorescence is very low compared to speckle intensity. At the lower labeled tubulin concentrations used for speckle imaging the number of microtubules in a linear array of speckles is not obvious. The frequency and relative movements of speckles in time-lapse recordings are clues for detecting the number of microtubules in a bundle.

B. Newt Tissue Cell Mitotic Spindles

Figure 4A shows a fluorescent speckle image of the right half of a newt mitotic spindle in a cell injected with a low (<0.5%) fraction of X-rhodamine-labeled tubulin. The fine stuctural detail of microtubule organization in the spindle is much clearer in the fluorescent speckle image than in images of spindles in cells injected with a higher labeled tubulin concentration (e.g., Waters *et al.*, 1996). Individual astral microtubules are seen in time-lapse movies to exhibit dynamic instability (Inoué and Salmon, 1995; Desai and Mitchison, 1998) by growth and shortening of linear arrays of fluorescent speckles. Within the spindle, individual microtubules are less distinct, but their movements are obvious in time-lapse movies by the motions of their speckles. Figure 4B shows a kymograph along

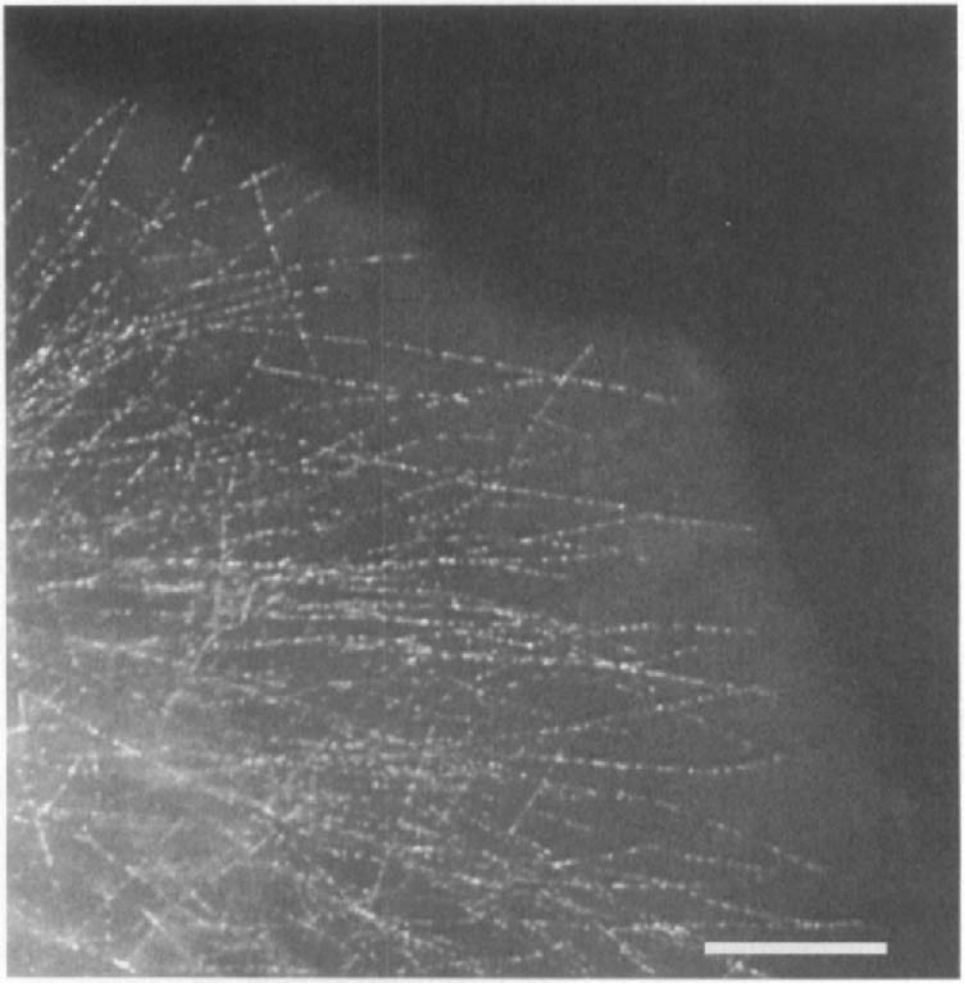

Fig. 3 A fluorescent speckle image of the interphase cytoplasmic microtubule complex in the lamella of a migrating newt lung epithelial cell. See text for details (reproduced with permission from Waterman-Storer, 1998).

Fig. 4 A fluorescent speckle image from a time-lapse series of a mitotic spindle in a newt lung epithelial cell (A) and the corresponding kymograph (B) for the time-lapse stack of images for the narrow horizontal region drawn on the image in A. Only the region of the spindle from the equator to one pole is shown so that the aster is visible. The fluorescence speckle image in A has very low background fluorescence, and individual microtubules in the asters are shown by their linear arrays of fluorescent speckles. The linear arrays of microtubule fluorescent speckles in the spindle are clearly seen with the thicker bundles ending on kinetochore regions of chromosomes (not shown) and thinner bundles extending and moving across the spindle equator. See text for details of kymograph formation. Scale bar = 10 μm (reproduced with permission from Waterman-Storer *et al.*, 1998a, © Current Biology Ltd. Publication).

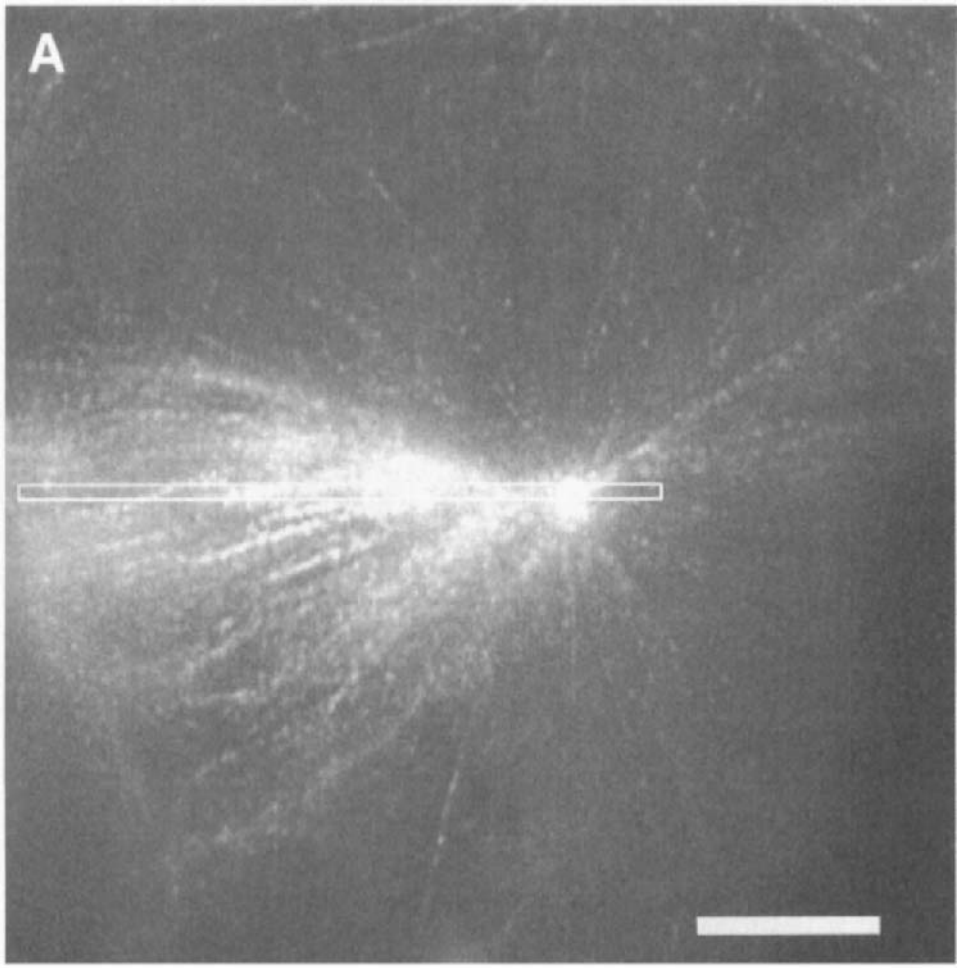
A

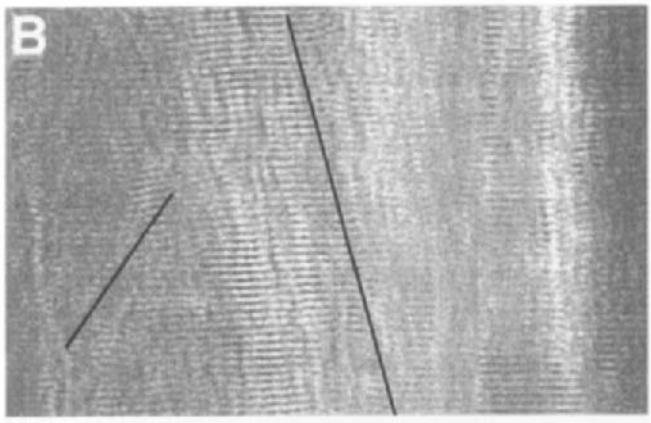
B

the region between the spindle equator superimposed on the spindle in Fig. 4A. The oblique slopes in the kymographs show speckle velocities near the spindle equator of about 1.5 μm/min toward opposite poles and velocities near the kinetochore fiber microtubules of about 0.7 μm/min poleward (Waterman *et al.*, 1988b). The later values are similar to those measured previously for the poleward flux of kinetochore fiber microtubules by fluorescence photoactivation marking experiments (Waters *et al*,. 1996). Speckle imaging has provided the first measurements of nonkinetochore microtubule motility in the tissue cell spindle midzone.

C. *In Vitro* Assembled Spindles in *Xenopus* Egg Cytoplasmic Extracts

Figure 5A shows a fluorescent speckle image of a metaphase–early anaphase spindle assembled in *Xenopus* egg cytoplasmic extracts (Desai *et al.*, 1988). The spindle microtubules are seen as linear arrays of fluorescent speckles. These spindles are known from fluorescence photoactivation marking studies (Sawin and Mitchinson, 1991; Desai *et al.*, 1998) to exhibit poleward flux of microtubules during both metaphase and anaphase at about 2 μm/min velocity. This poleward flux and the movement apart of microtubules during anaphase spindle elongation is obvious in kymographs of time-lapse image stacks of speckle images as shown in Fig. 5B. The slopes of the oblique speckle trajectories in the kymographs demonstrate the substantial amount of continuous microtubule motility in these spindles.

VII. Future Considerations

There are many aspects of speckle microscopy that require further investigation and instrument development. Our experience indicates that stability of the microscope stand is extremely important because a focus drift of 200–300 nm significantly changes speckle intensity. The spindle also moves in the living cell, further complicating this problem. As a result, the focal plane within the spindle changes and the fluorescent speckles of different microtubules come into focus as focus drifts or the spindle moves. Thus, kymographs such as those shown in Figs. 4B and 5B represent several focal planes within the spindles over time. One solution is to take stacks of 0.25-μm optical sections at each time lapse interval (4-D microscopy; Shaw *et al.*, 1997; Straight *et al.*, 1997) so that the microtubules of interest are retained within the stack and image planes can be selected during subsequent image processing. In addition, deconvolution methods should also substantially improve resolution and quality of speckle images (Rizutto *et al.*, 1998). We currently do not understand how photobleaching and other single fluorophore events affect the quantitative aspects of speckle imaging. Potentially, measurements of the intensity of individual speckles can yield lifetimes of fluorescent protein binding to the microtubule lattice or other structures (Waterman-

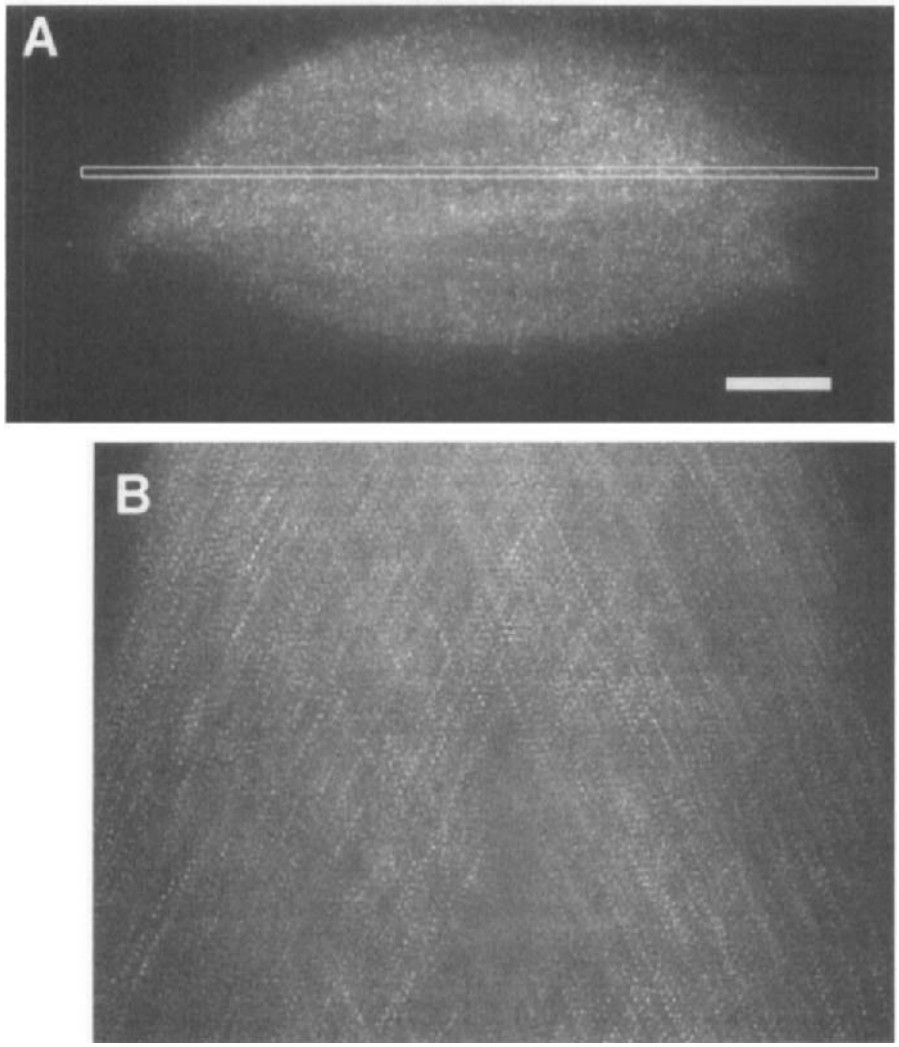

Fig. 5 (A) Fluorescent speckle image from a time-lapse image stack of a metaphase–anaphase spindle assembled in *Xenopus* egg extracts. (B) Kymograph of the narrow horizontal region drawn along the spindle axis in A for the time-lapse stack of images. See Desai *et al.* (1998) for details of spindle assembly and see text for details of kymograph formation and interpretation (reprinted with permission from Waterman-Storer *et al.*, 1998b, © Current Biology Ltd. Publication).

Storer *et al.*, 1998b). Finally, computer-assisted image processing using correlation methods for all the speckles in sequential image stacks should rapidly yield the positions, velocities, and directions of the movement of speckles in a field of view.

References

Desai, A., and Mitchinson, T. J. (1997). Microtubule polymerization dynamics. *Annu. Rev. Cell Dev. Diol.* **13,** 83–117.

Desai, A., Maddox, P. S., Mitchision, T. J., and Salmon, E. D. (1998). Anaphase A chromosome movement and poleward spindle microtubule flux occur at similar rates in *Xenopus* extract spindles. *J. Cell Biol.* **141,** 703–713.

Hyman, A., Dreschsel, D., Kellogg, D., Salser, S., Sawin, K., Stefen, P., Wordeman, L., and Mitchison, T. (1991), Preparation of modified tubulins. *Methods Enzymol.* **196,** 478–485.

Inoué, S. I., and Salmon, E. D. (1995). Force generation by microtubule assembly/disassembly in mitosis and related movements. *Mol. Biol. Cell* **6,** 1619–1640.

Inoué, S., and Spring, K. (1997). "Video Microscopy" 2nd Ed. Plenum, New York.

Khodjakov, A., and Rieder, C. L. (1996). Kinetochores moving away from their associated pole do not exert a significant pushing force on the chromosome. *J. Cell Biol.* **135,** 315–327.

Murray, A. W. (1991), Cell cycle extracts. *Methods Cell Biol.* **36,** 581–605.

Murray, A. W., Desai, A., and Salmon, E. D. (1996). Real time observation of anaphase in vitro. *Proc. Natl. Acad. Sci. USA* **93,** 12327–12332.

Rieder, C. L., and Hard, R. (1990). Newt lung epithelial cells: Cultivation, use and advantages for biomendical research. *Int. Rev. Cytol.* **122,** 153–220.

Rizutto, R., Carrington, W., and Tuft, R. (1998). *Trends Cell Biol.* **8,** 288–292.

Salmon, E. D., Inoue, T., Desai, A., and Murray, A. W. (1994). High resolution multimode digital imaging system for mitosis studies in vivo and in vitro. *Biol. Bull. (Woods Hole, MA)* **187,** 231–232.

Sawin, K. E., and Mitchison, T. J. (1991). Poleward microtubule flux in mitotic spindles assembled in vitro. *J. Cell Biol.* **112,** 941–954.

Shaw, S. L., Yeh, E., Bloom, K., and Salmon, E. D. (1997). Imaging GFP fusion proteins in *Saccharomyces cerevisiae. Curr. Biol.* **7,** 701–704.

Skibbens, R. V., Skeen, V. P., and Salmon, E. D. (1993). The directional instability of kinetochore motility during chromosome congression and segregation in mitotic newt cells: A push–pull mechanism. *J. Cell Biol.* **122,** 859–875.

Straight, A. F., Marshall, W. F., and Murray, A. W. (1997). Mitosis in living budding yeast: Anaphase A but no metaphase plate. *Science* **277,** 574.

Walker, R. A., O'Brien, E. T., Pryer, N. K., Soboeiro, M. F., Voter, W. A., Erickson, H. P., and Salmon, E. D. (1988). Dynamic instability of individual microtubules analyzed by video light microscopy: Rate constants and transition frequencies. *J. Cell Biol.* **107,** 1437–1448.

Waterman-Storer, C. M. (1998). Microtubules and microscopes: How the development of light microscopic imaging technologies has contributed to discoveries about microtubule dynamics in living cells. *Mol. Biol. Cell.* In press.

Waterman-Storer, C. M., and Salmon, E. D. (1997). Actomyosin-based retrograde flow of microtubules in the lamella of migrating epithelial cells influences microtubule dynamic instability and turnover and is associated with microtubule breakage and treadmilling. *J. Cell Biol.* **139,** 417–434.

Waterman-Storer, C. M., and Salmon, E. D. (1998). How microtubules get fluorescent speckles. *Biophys. J.* **75,** 2059–2069.

Waterman-Storer, C. M., Sanger, J. W., and Sanger, J. M. (1993). Dynamics of organelles in the mitotic spindles of living cells: Membrane and microtubule interactions. *Cell Motil. Cytoskel.* **26,** 19–39.

Waterman-Storer, C. M., Shaw, S. L., and Salmon, E. D. (1998a). Production and presentation of digital movies. *Trends Cell Biol.* **7,** 503–506.

Waterman-Storer, C. M., Bulinski, J. C., and Salmon, E. D. (1998b). Fluorescent speckle microscopy, a method to visualize the dynamics of protein assemblies in living cells. *Current Biol.* In press.

Waters, J. C., and Salmon, E. D. (1997). Pathways of spindle assembly. *Curr. Opin. Cell Biol.* **9,** 37–43.

Waters, J. C., Mitchison, T. J., Rieder, C. L., and Salmon, E. D. (1996). The kinetochore microtubule minus-end disassembly associated with poleward flux produces a force that can do work. *Mol. Biol. Cell* **7,** 1547–1558.

Waters, J. C., Chen, R. H., Murray, A. W., and Salmon, E. D. (1998). Mad2 and the spindle assembly checkpoint: The roles of tension and microtubule attachment. *J. Cell Biol.* **141,** 1181–1191.

This Page Intentionally Left Blank

CHAPTER 10

Polarized Light Microscopy of Spindles

Rudolf Oldenbourg
Marine Biological Laboratory
Woods Hole, Massachusetts 02543-1015

I. Introduction

Since the pioneering work of Runnström (1928) and Schmidt (1937), the mitotic figures of many kinds of living cells have been known to be birefringent. Improvements in polarized light microscopic techniques (Swann and Mitchison, 1950; Inoué and Hyde, 1957) made it possible to measure the variation of birefringence within the mitotic apparatus and follow its change during mitosis (Inoué and Dan, 1951; Swann, 1951a,b). Inoué (1953) found by polarization microscopy that the mitotic/meiotic spindle consists of many birefringent fibers and their component fibrils (later identified as microtubules). In subsequent studies Inoué

METHODS IN CELL BIOLOGY, VOL. 61

0091-679X/99 $30.00

and collaborators established the reversible assembly and disassembly of spindle fibers and fibrils in living cells, exposed to cold temperatures (Inoué, 1964), antimitotic drugs (Inoué, 1952), hydrostatic pressure (Salmon, 1975), and exchange of regular water with heavy water (Inoué and Sato, 1967). In each of these studies, polarized light microscopy was the key in observing the submicroscopic fine structure of the spindle. Its dynamic architecture could be followed in real time, at high temporal and spatial resolution, with no staining or labeling required.

The birefringence of the spindle occurs naturally (Fig. 1). In contrast to fluorescence microscopy of the spindle, polarized light imaging does not require invasive preparative techniques such as staining or labeling. Polarized light microscopy, however, lacks the chemical specificity available with fluorescent tag-

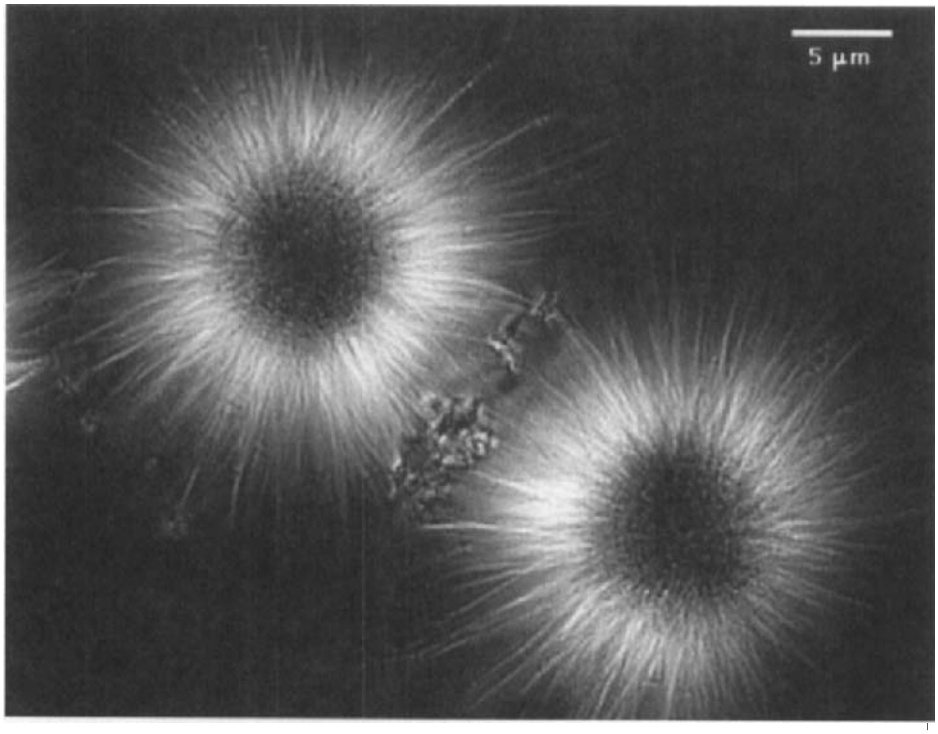

Fig. 1 Mitotic spindle isolated from fertilized sea urchin egg. Microtubule bundles radiate out from two centrosomes which appear dark; chromosomes are visible between the two star formations (preparation by John Murray, University of Pennsylvania). This image of an unstained specimen was recorded using a new type of polarized light microscope called the Pol-Scope. The Pol-Scope is state of the art in polarized light microscopy, combining traditional components with new electrooptic devices, electronic imaging, and image processing algorithms (see Fig. 8). Pol-Scope images rapidly give a wealth of quantitative, submicroscopic information which otherwise can only be gleaned from careful observations with suitably equipped traditional polarizing microscopes, one image point at a time (reproduced from Oldenbourg, 1996. A new view on polarization microscopy. *Nature* **381,** 811–812).

ging of molecular structures. Like other phase-sensitive imaging techniques (Fig. 2), polarizing microscopy is insensitive to the chemical nature of the constituent molecules, except where it involves molecular order, including the alignment of molecular bonds and of submicroscopic fine structures of the material. It is not often recognized, though, that molecular order and its optical byproduct, birefringence, can help identify the chemical nature of materials, such as lipid membranes, linear polymers, and their three-dimensional arrangement. The polarized light microscope provides the advantage of measuring both birefringence

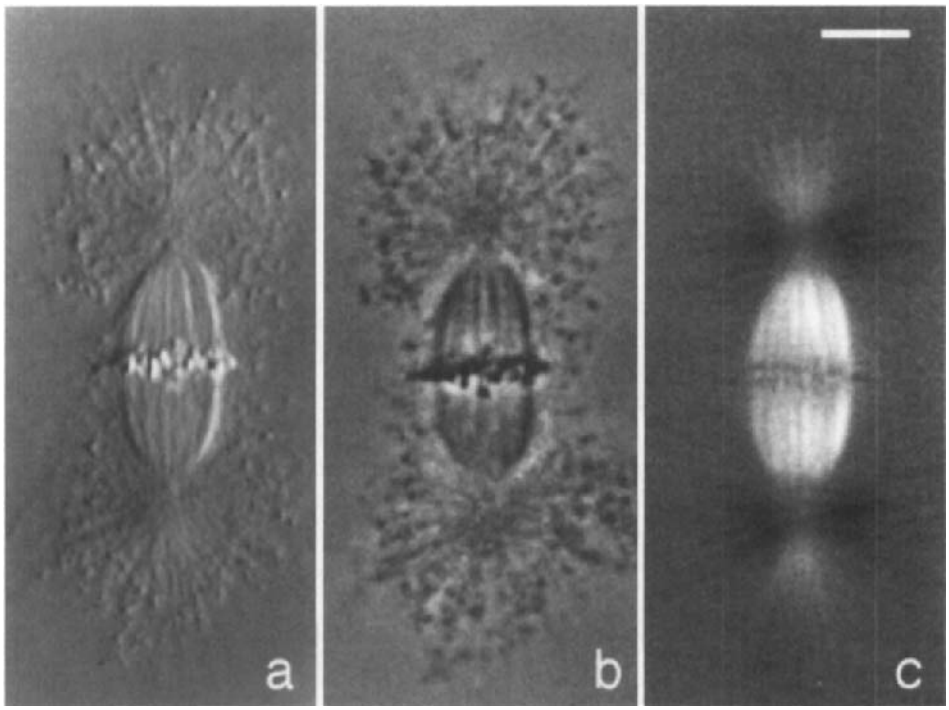

Fig. 2 Isolated spindle at early metaphase viewed with (a) polarization, (b) phase contrast, and (c) differential interference contrast (DIC) microscopy. The polarization micrograph was taken with the compensator set for 3.5-nm positive retardance with respect to the spindle interpolar axis. The micrographs illustrate the complementary information retrieved from these three phase-sensitive contrast methods. Polarization microscopy primarily visualizes, and can measure, the anisotropy or directional change of the refractive index, i.e., the difference in specimen refractive index for two orthogonally polarized light waves. DIC and phase contrast, on the other hand, visualize specimen detail due to the spatial change in refractive index (refractive index gradient), i.e., change of refractive index from point to point in the specimen or relative to the background. As opposed to isolated spindles, the spindle fibers within living cells are difficult to visualize by DIC and phase contrast because the refractive index gradient generated by these fibers against the cytoplasm is exceedingly low. The fibers, however, can definitely be visualized in living cells owing to the form birefringence exhibited by their microtubule bundles. Scale bar-10 μm (Salmon and Segall, 1980, reproduced from *The Journal of Cell Biology*, 1980, **86,** 355–365 by copyright permission of The Rockefeller University Press).

and the morphological arrangement and delineation of birefringent components which give further clues as to the origin and chemical nature of molecular order. In the spindle, for example, the polarizing microscope not only measures spindle birefringence but also delineates regions of high and low birefringence and can even detect individual birefringent fibers, which, early on, gave evidence of the chemical nature of the spindle.

This chapter is divided in three sections: The first is devoted to the technique, starting with the basic setup of the traditional polarized light microscope and ending with state of the art in polarized light microscopy, the Pol-Scope. In this train of technological advances for measuring specimen birefringence we skipped earlier developments which used difficult to use electrooptical devices (Pockels cells; Allen *et al.*, 1963) or an electrically driven mechanical compensator (Hiramoto *et al.*, 1981a) for this purpose. These methods, which were important new developments in their times, are now superseded by techniques that use liquid crystal devices, which we describe briefly. In addition to the instrumentation, we discuss ways to improve sensitivity and achieve high signal to noise ratios in recorded images.

The second section discusses (a) the molecular origin of spindle birefringence, including the distinction between form and intrinsic birefringence, and (b) some analysis tools that can be applied to find, for example, the microtubule density in the spindle based on birefringence measurements.

The third section was contributed by Shinya Inoué of the Marine Biological Laboratory. The section gives a brief introduction to various cell types which are amenable to polarized light microscopy and discusses some preparative techniques such as centrifugation to minimize background birefringence contributed by cell components other than the spindle. At the same time, this section gives a representative overview of the literature describing polarized light imaging of spindles in living cells.

II. Polarized Light Microscopy

A. Basic Setup and Observations

The basic setup of a polarized light microscope (Fig. 3) includes two polarizers, one of which is located in the illumination path before the condenser lens and the other in the imaging path behind the objective lens. The first polarizer is used to polarize the light supplied by a bright halogen or arc lamp. The second polarizer serves to analyze the polarization of the light after it passed through the specimen. This second polarizer is therefore called the analyzer. Usually, the two polars (short for polarizer) are in crossed position so that the analyzer blocks (absorbs) most of the light that has passed through the polarizer. Therefore, the image that is projected by the objective is mostly dark, except for bright specimen parts that are birefringent or otherwise optically anisotropic. When the specimen is rotated on a revolving stage (around the axis of the microscope), the birefringent parts change brightness, from dark to bright and back to dark four times

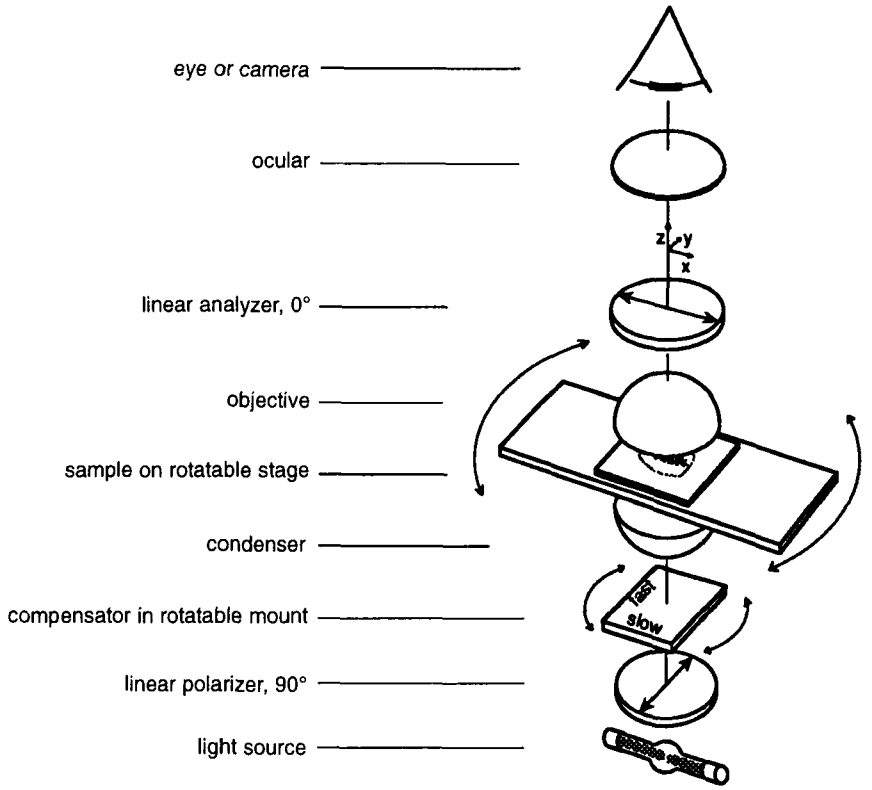

Fig. 3 Optical arrangement of conventional polarized light microscope.

during a full 360° rotation. The systematic variation of brightness when rotating a specimen is a telltale of birefringence in a polarized light microscope. A uniformly birefringent specimen part appears darkest when its birefringence axis is parallel to polarizer and analyzer. This specimen orientation is also called the extinction orientation. Rotating it by 45° away from the extinction orientation makes the birefringent part appear brightest. In general, not all birefringent parts in the field of view will turn dark at the same time because each part has different axis orientations. Hence, in addition to helping recognize birefringent elements, one can also determine the axis orientations by rotating the specimen between crossed polars.

In addition to the polars, the polarized light microscope often includes a compensator in the optical path. While not absolutely necessary for some basic observations, especially of highly birefringent objects, the compensator (a) can significantly improve the detection and visibility of weakly birefringent objects, (b) is required to determine the slow and fast axis of specimen birefringence, and (c) is an indispensable tool for the quantitative measurement of object

birefringence. There are several types of compensators, most of them are named for their original inventors. For the observation of weak specimen birefringences, such as the mitotic spindle, the Brace–Köhler compensator is most widely used. It consists of a thin birefringent plate, often made from mica, with a retardance of a 10th to a 30th of a wavelength ($\lambda/10$ to $\lambda/30$; a definition of retardance is provided later). The birefringent plate is placed in a graduated rotatable mount and inserted either between the polarizer and condenser (as in Fig. 3) or between the objective lens and the analyzer. The location varies between microscope manufacturer and specific microscope type. In either location, the effect of the Brace–Köhler compensator on the observed image is the same and its usage does not depend on location (as long as there is not a third, strongly birefringent element between the polars). In general, the birefringence of the compensator, when inserted into the optical path, causes the image background to become brighter, whereas birefringent specimen parts, such as the mitotic spindle, can turn either brighter or darker than the background (e.g., Figs. 4 and 11–14). We summarize the effects of the compensator on the image and then discuss how these effects can be used to improve contrast, find the slow axis, and measure specimen birefringence.

When viewing a mitotic spindle between crossed polars, one recognizes the array of parallel microtubules (MTs) spanning the two spindle poles. The birefringent microtubule array appears brightest when the spindle orientation is 45° to the polarizer and analyzer. When the array is turned parallel to polarizer or analyzer, it acquires the same brightness as the background and disappears.

Figure 4 shows a series of photographs of an isolated spindle whose long axis is oriented at ca. 45° between crossed polars in the presence of a $\lambda/25$ Brace–Köhler compensator, which is turned to various angles. When the slow axis of the compensator (crystal axis with higher refractive index) is at 0°, it lies parallel to the polarizer or analyzer, and hence 45° to the spindle axis. When the compensator is turned so that its slow axis comes to lie more nearly perpendicular to the spindle axis (negative angles in Fig. 4), the birefringence of the compensator cancels out (part of) the spindle birefringence, the birefringence of these fibers is said to be compensated, and the brightness of the spindle fibers is reduced. When the compensator is turned the other way and its slow axis is made more parallel to the spindle axis (positive angles in Fig. 4), the compensator birefringence adds to the fiber birefringence and the fibers increase in brightness. These observations demonstrate that the slow axis of the spindle fibers runs parallel to the length of the spindle and show at what compensator angles each region of the spindle is fully compensated. They also demonstrate how the contrast between the fibers and their surroundings is changed, which can lead to better visibility of the spindle regions. Before discussing the change in visibility, contrast, and signal to noise ratio (S/N) of the image brought about by the compensator, we first define the word retardance.

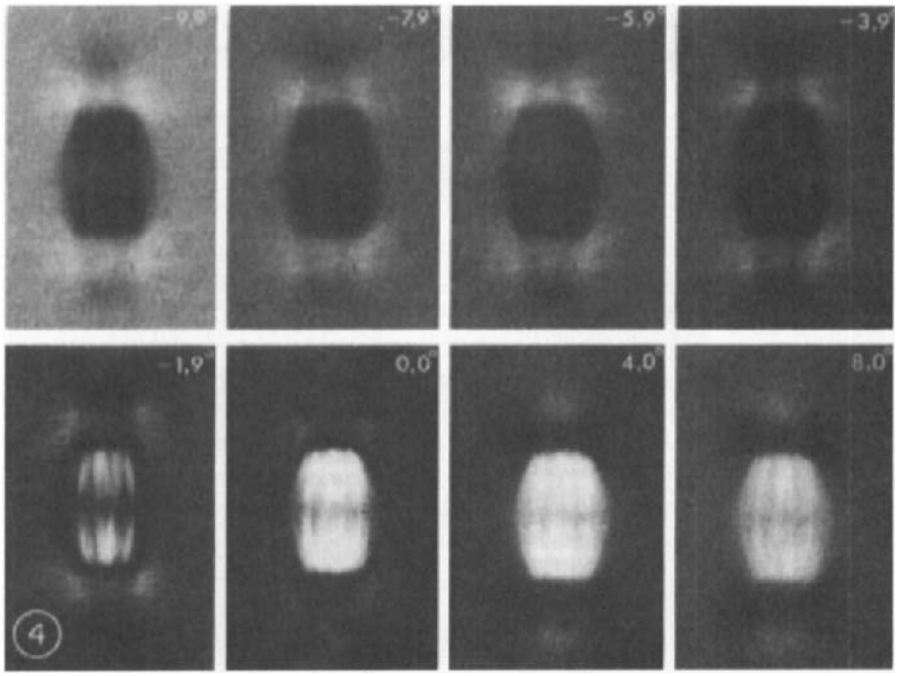

Fig. 4 Appearance of an isolated spindle of the sea star *Pisaster ochraceus* at various angles of the compensator (numbers in top right of each photograph). The angle refers to the orientation between the slow axis of the compensator and the direction of the crossed polars which are at 45° to the vertical spindle axis. Positive angles orient the slow axis more vertically. The compensator angle 0° is called the extinction orientation and the appearance of the spindle is the same as with crossed polars alone. As the $\lambda/25$ Brace–Köhler compensator is turned, the areas with lower retardance are first compensated (−1.9°) leaving the chromosomal spindle fibers (the MT bundles running between the chromosomal kinetochores and the spindle poles; see Fig. 13) shining above the dark, compensated areas. With further rotation of the compensator (−3.9°, −5.9°, and −7.9°) the more highly retarding fibers are compensated, whereas areas of weaker retardance increase in brightness. When the compensator is turned to positive angles the spindle fibers all increase in brightness. Note the difference in appearance of the astral rays around each spindle pole for compensator settings −7.9° and 8.0° (Sato *et al.*, 1975, reproduced from *The Journal of Cell Biology*, 1975, **67,** 501–517 by copyright permission of The Rockefeller University Press).

B. Retardance

When linearly polarized light travels through a birefringent material, it is split into two orthogonally polarized waves that travel with different speeds. The difference in speed of these two waves is determined by the difference in refractive index Δn for the two polarization directions (e.g., Appendix III in Inoué, 1986). Retardance, also called birefringence retardation, expresses the relative phase shift between the two waves after they traversed the birefringent specimen. Hence, when leaving the material, for example, the region of the spindle with

parallel MTs or the birefringent crystal plate of the compensator, the two waves have a different relative phase compared to when they entered the material. The retardance, expressed as distance, is the product between the difference in refractive index, i.e., the birefringence Δn, and the path length d through the material (Hartshorne and Stuart, 1960; Hecht, 1987):

$$R = \Delta n \cdot d \tag{1}$$

Retardance is the primary quantity measured with the compensator in a polarizing microscope. The parallel MT arrays in mitotic spindles can induce a retardance anywhere between a fraction of a nanometer to a few nanometers. The retardance of the birefringent crystal in the Brace–Köhler compensator is typically expressed as a fraction of the wavelength of light λ, assuming a median value of 550 nm for λ. Brace–Köhler compensators with birefringent crystals of $\lambda/30$–$\lambda/10$ (18.3–55 nm) retardance are commonly used.

Figure 4 gives a qualitative impression of the variation of image intensities with compensator angle as well as a means for visually determining the angle of the compensator that extinguishes a particular region of the spindle. Figure 5 illustrates quantitatively the variation of intensity in a single image point that represents a specimen part with uniform retardance (R_{spc}) and its slow axis oriented at 45° to the polars. The graph represents the intensity as a function of

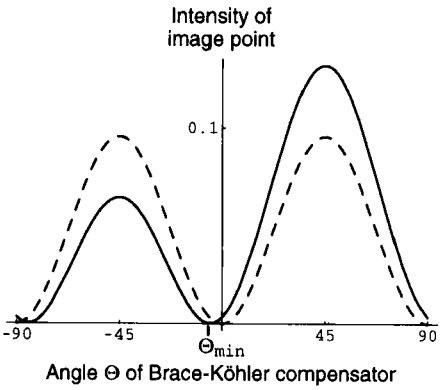

Fig. 5 Intensity detected in a single image point or uniform area of the specimen versus angle of Brace–Köhler compensator. Dashed curve shows the case with no specimen birefringence, whereas the solid curve shows the intensity for a birefringent specimen. The graph illustrates the complex variation of specimen intensity with compensator angle. At angle Θ_{min} the intensity has a minimum, whereas at angles ±45° the specimen shows two unequal maxima. For the higher maximum (Θ = +45°), the birefringence of the compensator adds to the specimen birefringence, hence their birefringence axes are parallel, whereas for the smaller maximum (Θ = −45°), their respective axes are perpendicular to each other. The graph was produced computationally using the Jones calculus and assuming a retardance of $\lambda/10$ for the birefringent compensator crystal and a specimen retardance of 10 nm with slow axis oriented at 45° to polars. The transmitted intensity is given as a fraction of the amount of light I_0 that has passed through the first polarizer.

angle Θ of a Brace–Köhler compensator with a birefringent crystal of retardance R_{cmp}. The graph shows a sinusoidal variation of the intensity with a minimum located at the angle Θ_{min} which directly measures the specimen birefringence R_{spc}:

$$R_{spc} = R_{cmp} \sin(2\Theta_{min}) = -R_{bias} \quad (2)$$

At Θ_{min} the specimen retardance is said to be compensated. The product R_{cmp} sin $(2\,\Theta_{min})$ is considered a bias retardance that is equal in magnitude but opposite in sign to the specimen retardance. The opposite sign means that the orientations of the slow and fast axes of the bias and specimen retardance are exchanged with respect to each other. With Eq. [2] we can determine the specimen retardance using the measured compensation angle Θ_{min} given the compensator retardance R_{cmp}, which is usualy provided by the manufacturer. Specimen retardances larger than R_{cmp} cannot be compensated and hence cannot be measured with this method.

C. Image Contrast

Figures 4 and 5 demonstrate that the compensator can invert image contrast; that is, the specimen can appear brighter or darker than the background. In fact, rotating the compensator and recognizing the contrast reversal is a quick and useful indicator for the presence of birefringence in the field of view of a polarizing microscope. In addition, the intensity difference can vary considerably in magnitude, typically increasing with rotation angles approaching ±45°. Figure 6a shows the intensity difference $(I_{spc} - I_{bg})$ as a fraction of the intensity after the first polar and as a function of the compensator angle. Figure 6b shows similar graphs of the contrast, which is defined as $(I_{spc} - I_{bg})/I_{avr}$, with the average intensity $I_{avr} = (I_{sp} + I_{bg})/2$. While the difference $(I_{spc} - I_{bg})$ increases toward compensator

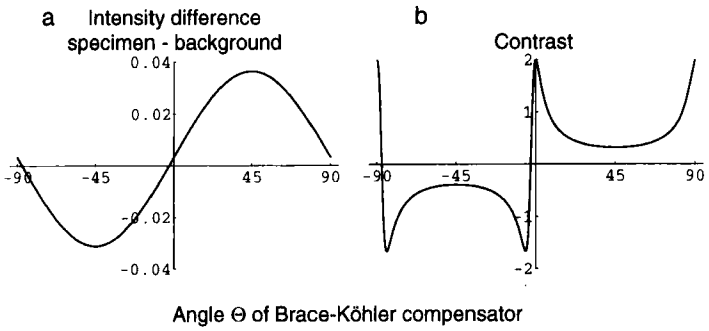

Fig. 6 (a) Intensity difference $[(I_{spc} - I_{bg})/I_0]$ and (b) contrast $[(I_{spc} - I_{bg})/(I_{sp} + I_{bg})/2)]$ versus compensator angle, derived from the specimen and background graphs in Fig. 5. The reversal of the sign of the contrast for a range of negative compensator angles corresponds to the reversed appearance of the spindle contrast in Fig. 4.

angles of ±45°, the contrast, after reaching a maximum, decreases steadily toward compensator angles of ±45° because of the fast increasing background light level (Swann and Mitchison, 1950; Inoué and Dan, 1951). The increase in specimen intensity over background accounts for the better visibility of weakly birefringent parts at small compensator angles inducing low to moderate background intensities. (Note, however, that the intensity difference can also disappear for specific compensator settings.) At large compensator angles, though, the visibility and contrast of weakly birefringent specimen parts is reduced when viewed directly through the eye piece. At these high angles, the gain in intensity difference is rendered useless by the faster increasing background light level. It seems that electronic light detectors such as video cameras or photomultipliers, which can provide means of subtracting the high background light level, can rescue the contrast in the electronically processed image. However, in fact, the more important quantity to consider is the signal to noise ratio.

D. Signal to Noise Ratio

The noise in recorded images has two basic sources; noise due to photon statistics or "shot noise" and noise due to the light detector. Noise leads to a mottled image and to an uncertainty of the detected intensities in each image point (pixel). In cameras with common charge coupled device (CCD) detectors, the total noise in the image is often dominated by the electronics, particularly the read noise of the detector. This can cause apparent intensity fluctuations of from 10% to <0.1% of the maximum detected intensity, depending on the speed of reading out the accumulated charges on the CCD array, the design of the camera circuitry, and the settings of the camera controls, such as amplifier gain.

Low-noise cameras, including chilled CCDs and other sensitive light detectors, when suitably used can achieve low enough electronic noise to give intensity measurements that are shot noise limited. Intensity fluctuations due to shot noise are inherent in the detected light field and cannot be eliminated, but their relative contribution can be reduced by increasing the total amount of light detected because shot noise is proportional to the square root of the detected light intensity. Hence, the absolute amount of intensity fluctuations due to shot noise increases with increasing intensity, whereas the relative amount $\sqrt{I}/I = 1/\sqrt{I}$ decreases. Thus, the amount of noise over the signal can be reduced by increasing the light level of the incoming light (stronger light source or removing attenuator) or by increasing the time over which the signal is accumulated or averaged.

To determine the absolute amount of shot noise we consider the measurement of light intensities as a process of counting photons. If we have counted n photons, then the absolute standard deviation due to shot noise is $\sqrt{n}$ (Taylor, 1997). Many common CCD cameras have pixel arrays that, in one pixel, can store approximately 10,000 electron charges which were created by an equivalent number of absorbed photons. When measuring this electronic charge, the shot

noise will be $\sqrt{10{,}000} = 100$. Hence, $S/N = I/\sqrt{I} = 100$, or the relative standard deviation is $1/100 = 1\%$.

E. Signal to Noise Ratio in Polarizing Microscopy

In our view, the signal to noise ratio of the polarized light microscope should be expressed as follows:

$$S/N = \frac{I_{spc} - I_{bg}}{\sqrt{I_{spc} + I_{bg} + I_{ext} + I_{elc}}} \tag{3}$$

The denominator is the square root of the sum of squares of all pertinent absolute standard deviations, in accordance with the law of standard error propagation of independent noise sources (Taylor, 1997). In addition to the shot noise of the specimen and background intensities, two extra contributions, I_{ext} and I_{elc}, are listed under the square root. I_{elc} is the detector or camera electronic noise (discussed earlier), which we express here as an equivalent intensity noise with a fixed standard deviation. The other quantity, I_{ext}, is the shot noise caused by the light that is detected at extinction. Ideally, I_{ext} is zero, but in reality all optical elements, including the polarizer and analyzer, introduce some polarization aberrations (imperfections) which lead to spurious light that increases image noise. I_{ext} is typically given as the extinction ratio times the light intensity I_0 before the polarizer. Later, we will discuss in more detail the origin of this spurious signal and ways to decrease it. Its reduction will improve not only the signal to noise ratio but also image fidelity.

In evaluating Eq. [3] for different compensator angles we look for realistic assumptions about the signal level and the relative strength of the different noise components. It seems most instructive to consider the case in which detected light levels are constant, i.e., independent of compensator angle. To meet this condition we can assume, for example, that the light intensity of the lamp is changed depending on the compensator angle. For small compensator angles, when transmitted light levels are relatively low (Fig. 5), the lamp intensity is increased, whereas at large compensator angles the lamp intensity is reduced, each time in such a way that the highest detected light level is, for example, 10,000 photons. Instead of changing the lamp power, one can also change the accumulation time on the detector until the highest light level corresponds to 10,000 photons again. Signal to noise ratios computed with the assumption of constant light levels give the maximum attainable values for each compensator angle, given the recorded light level, extinction ratio, and camera noise (Fig. 7). When the number of photon counts is increased, for example, 10-fold from 10,000 to 100,000, all the S/N values increase proportionately by the square root of the increase, or 3.2 times, but the general shapes of the S/N curves remain the same.

From Fig. 7, we conclude that the highest S/N ratios are expected for compensator angles which give a bias retardance that is of the same magnitude as the

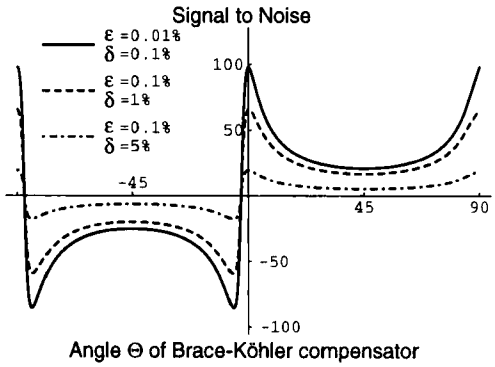

Fig. 7 Signal to noise ratio (S/N) versus compensator angle for a specimen retardance of 10 nm. S/Ns were calculated based on Eq. [3] and the assumption that I_{spc} or I_{bg}, depending on which one is higher, amounts to 10,000 photon counts, independent of compensator angle (to achieve constant detected light levels in these calculations, the incoming light I_0, the intensity before the polarizer, was varied inversely to the graphs in Fig. 5). Three different curves are shown for three different value pairs of the extinction coefficient ε and electronic noise level δ [$I_{ext} = I_0/\varepsilon$; $I_{elc} = (10{,}000\ \delta)^2$, where δ is the relative standard deviation of the electronic noise].

specimen retardance. Higher bias retardances than the specimen retardance, or high compensator angles, reduce S/N because of the increased shot noise of the specimen and background light levels. Hence, to record images of specimens with low retardances such as mitotic/meiotic spindles in living cells, one should use small compensator angles, a bright light source, sufficient exposure time of the detector, and a high extinction optical setup. In practice, this often means finding the right compromise with camera sensitivity and integration time versus specimen movement and light intensity sustained by specimen. In addition, a high extinction optical setup is important.

F. The Importance of High Extinction

The extinction coefficient is the ratio of light intensities detected for parallel and perpendicular arrangement of the polars. With good sheet polarizers one can achieve extinction coefficients of approximately 10^4, assuming no additional elements are present between the polars. In a polarizing microscope using high numerical aperture lenses between the polars, the extinction coefficient decreases considerably due to the differential transmission of s- and p-waves near the periphery of highly curved lens surfaces (Inoué and Hyde, 1957). Between crossed polars, this "light leakage" leads to the Maltese cross-pattern seen in the back focal plane of moderate to high numerical aperture lenses which are free of stress and other sources of birefringence. In the specimen plane, however, the leaked light is distributed more evenly, adding to all image intensities about equally. In a high-resolution polarizing microscope with 1.4 NA condenser and

objective lenses with fully illuminated apertures the detected light intensity at extinction can be approximately 1% of the light transmitted through the first polarizer. This is a significant amount compared to the signal carrying light levels plotted in Fig. 5. The light leakage has two detrimental effects on the image quality in the polarizing microscope: It increases shot noise, as discussed earlier, and it can introduce contrast reversal of specimen structures that lie near the resolution limit of the optical setup. Here, we will briefly discuss the latter effect and describe methods to improve extinction and lessen the effect on image fidelity.

The contrast reversal due to the differential transmission of s- and p-waves near the periphery of highly curved lens surfaces in a high-resolution polarizing microscope was first demonstrated by Inoué and Kubota (1958; also see Appendix III in Inoué, 1986). It is based on the finding that each diffraction spot in the polarizing microscope equipped with high numerical aperture lenses is no longer an Airy disk but is actually a four-leaf clover pattern, similar in appearance to the Maltese cross in the backfocal plane. This four-leaf clover pattern, replacing the Airy disk, can lead to a diffraction anomaly for spacings in the specimen that are close to the resolution limit of the optical setup. The introduction of rectified condenser and objective lenses which can eliminate the four-leaf clover pattern restores a uniform Airy disk and substantially improves the extinction coefficient of the polarizing microscope (Inoué and Hyde, 1957). Unfortunately, no manufacturer offers polarization rectifiers for its modern, highly corrected microscope lenses. However, there are still several measures that can be taken to improve the extinction coefficient of a polarizing microscope.

To achieve high extinction in a polarizing microscope it is most important to select the proper objective and condenser lenses, which are often designated by the manufacturer as Pol objectives with low strain and a minimum of birefringent sources (such as birefringent inclusions or certain types of antireflection coatings) in the lens elements. Hand selecting the best performing combination of objective and condenser from a batch of lenses can improve results. To judge the performance of a lens or lens combination, one should observe the intensity distribution in the back focal plane by using a phase telescope or Bertrand lens and by examining the presence, absence, or distortion of the Maltese cross and contribution of elliptical polarization to the extinction pattern observed at the back aperture (Inoué, 1961). The Maltese cross is less pronounced when using immersion lenses, which perform better than high NA dry lenses, because the differential reflection off the uncoated cover glass and slide are considerably reduced by the index matching of the immersion liquid. Nevertheless, to improve the extinction of high NA lenses it is often advisable to reduce the condenser aperture by closing down its iris diaphragm. Since both the condenser and the objective aperture contribute equally to image resolution, the experimenter has to make the right compromise between closing the condenser aperture to improve extinction and maintaining the required resolution.

G. Liquid Crystal Variable Retarders

In recent years, a variety of liquid crystal (LC) devices became available to precisely control the intensity, spectral composition, and polarization state of light (e.g., Cambridge Research and Instrumentation, Inc., Boston, MA; *http://www.cri-inc.com;* Meadowlark Optics, Longmont, CO; *sales@meadowlark.com*). The devices can be manufactured with high extinction coefficients (10^3 or higher) and exhibit good optical quality with small wave wavefront distortion and large apertures which make them suitable for imaging applications. The LC devices often resemble thin optical flats which can readily be integrated into optical setups. The variable control is accomplished by applying a low voltage to a thin layer of liquid crystaline material sandwiched between two glass windows coated with transparent electrodes (Priestly *et al.*, 1979; Blinov, 1983). The voltage affects the alignment of the liquid crystal molecules, which can have different alignment patterns depending on the symmetry of the molecules themselves (e.g., chiral versus straight) and their anchoring and alignment at the glass surface. One device type uses so-called nematic liquid crystals to build a variable waveplate. At low voltage, the layer is highly birefringent due to the alignment of the liquid crystal molecules parallel to fine textures generated on the glass surface. At voltages of typically 10 V and higher, however, the retardance is reduced due to the realignment of the bulk liquid crystal molecules parallel to the electric field. While the amount of retardance is reduced, the direction of the birefringence axis of the device remains fixed and does not change with voltage. The retardance magnitude of a LC variable waveplate, also called variable retarder, can be adjusted with great precision to retardances between a small fraction of a wavelength to several wavelengths, depending on the design of the specific device.

In a polarizing light microscope, such a variable waveplate can replace a Brace–Köhler compensator for the measurement of specimen retardance. In contrast to mechanically turning crystal plates, the LC device maintains a fixed orientation in the microscope setup. Instead, as mentioned earlier, the retardance of the LC compensator is adjusted by changing the voltage applied to the device. Hence, the LC retarder can compensate and precisely measure a range of specimen retardances without mechanically moving any part of the microscope. These features greatly facilitate automation and allow for direct comparison of image intensities measured with different compensator settings since no shift in image position can occur when changing the compensator settings. By exploiting these advantages, we have developed a new type of polarized light microscope, named the Pol-Scope.

H. The Pol-Scope

The Pol-Scope augments the traditional polarized light microscope by integrating LC variable retarders, electronic imaging, and digital image processing tools to build a birefringence imaging system (Fig. 8; Oldenbourg and Mei, 1995; Oldenbourg, 1996); a commercial version of the Pol-Scope is available from

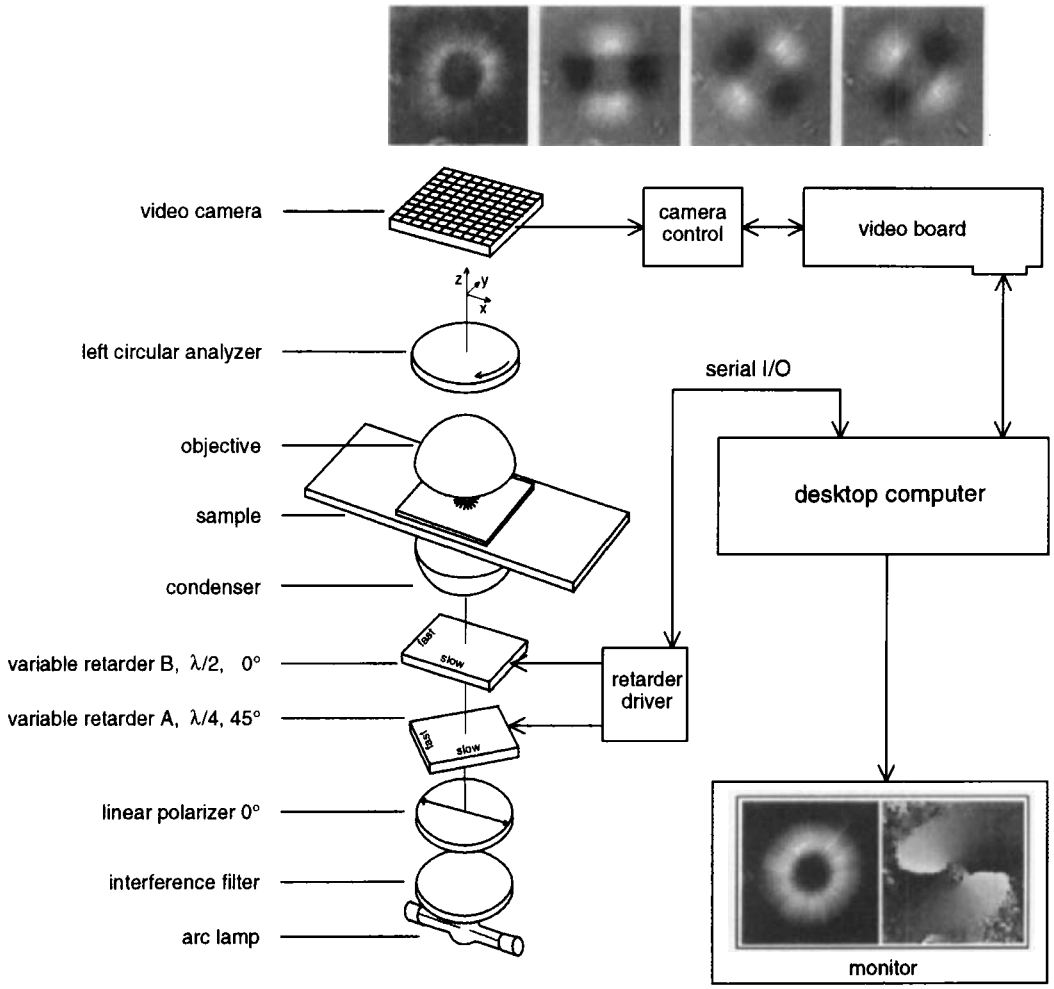

Fig. 8 Schematic of the new Pol-Scope. The optical design (left) builds on the traditional polarized light microscope with the conventional compensator replaced by two variable retarders A and B forming the universal compensator. Images of the specimen (top row, aster isolated from surf clam egg) are captured at four predetermined retarder settings which cause the specimen to be illuminated with circularly polarized light (first left-most image) and with elliptically polarized light of different axis orientations (second to fourth images). The monitor inset shows on the left the retardance magnitude image and on the right the orientation image of the slow axis, both computed from the same four raw image data (reproduce from Oldenbourg, 1996. A new view on polarization microscopy. *Nature* **381,** 811–812).

Cambridge Research and Instrumentation. The two LC variable retarders form a universal compensator which is used to produce, and rapidly switch between, circularly polarized light and elliptically polarized light of different axis orienta-

tions. The polarized light is passed through the specimen and analyzed by a circular analyzer before it is detected by the camera. In rapid succession, the video camera records specimen images for each of the polarization states and transfers the raw image data to a computer. In the computer the image data are combined using specific algorithms to calculate specimen retardances in each image point, typically 640 × 480 pixels. The result of the computation is an image representing the retardance magnitude measured in every pixel independent of specimen orientation (Fig. 1). Hence, the magnitude image is black where there is no birefrignence in the sample and shows a specific shade of gray depending on the retardance of the sample at that point, regardless of its orientation.

In addition to the magnitude of retardance, the Pol-Scope also measures the orientation of the slow axis in every image point, using the same set of raw image data. The orientation is measured as an angle between the horizontal axis and the slow birefringence axis of the specimen at each image point. The orientation values can either be displayed as a separate image or be overlaid on a magnitude image using color or other means of encoding orientation (Fig. 9, see color plate). Thus, computed Pol-Scope images represent material properties rather than light intensities. As a consequence, the magnitude image, for example, displays specimen retardance on a linear scale, in contrast to the quadratic relationship between image intensity and specimen retardance in a traditional polarized light microscope. In the next section, we discuss the physical origin and interpretation of birefringence, including some simple analysis tools for the measurement of three-dimensional birefringent objects, such as the mitotic spindle.

III. Analysis of Spindle Birefringence

The birefringence of the mitotic spindle established the reality of spindle fibers inside living cells long before the molecular composition of the spindle was known (Inoué, 1953). Early on, observations of intact living cells with the polarizing microscope further revealed the labile nature of the spindle, which reversably disassembles by exposing cells, for example, to cold temperatures (Inoué, 1964) or antimitotic drugs such as colchicine (Inoué, 1952). A thorough examination of spindle birefringence inside living cells and of isolated spindles, which were fixed, embedded, and sectioned for electron microscopy, firmly established that spindle birefringence is primarily produced by arrays of parallel microtubules which span the spindle poles and form the associated astral rays (Sato *et al.*, 1975). The labile nature of spindle birefringence in living cells thus predicted the highly dynamic character of steady-state MTs, which are in a thermodynamic equilibrium with their protein subunits (Inoué, 1959; Inoué *et al.*, 1975) and can display stochastic length changes (dynamic instability; Mitchison and Kirschner, 1984; Cassimeris *et al.*, 1988) or preferentially assemble on one end and dissociate at the other (treadmilling; Margolis and Wilson, 1981). The dynamic behavior of individual MTs became the key to understanding the role of spindle fibers in chromosome segregation and the orderly partitioning of organelles during cell

division. With the polarizing microscope we can analyze the dynamics of spindle fibers, noninvasively and quantitatively, by measuring, in real time, the spatial patterns and temporal changes of spindle birefringence. Based on appropriate analysis tools, spindle birefringence can be interpreted in terms of molecular organization of the spindle, such as the local density of aligned MT arrays, the number of MTs in, e.g., kinetochore fibers, and even the detection of individual MTs in regions of low or uniform background birefringence. In the following sections, we discuss the origin of birefringence caused by filamentous structures, using the example of MTs, and develop some analysis tools for the interpretation of spindle birefringence.

A. Molecular Origin of Microtubule Birefringence

Microtubules are stiff rodlets, 25 nm wide and typically several micrometers long. The origin of MT birefringence is based on this highly anisometric shape which leads to an anisotropic polarizability of a single MT subjected to an external electric field. The shape-related birefringence is commonly called form birefringence, which derives from the German word "form" for shape. In addition to form birefringence, MTs are likely to possess some intrinsic birefringence due to the alignment of anisotropic molecular bonds inside the protein material. We discuss the origin of both types of birefringence.

1. Form Birefringence

For a qualitative explanation of form birefringence we consider a rod, in vacuum, that is exposed to an external electric field with the rod axis oriented either parallel or perpendicular to the field. In both cases, the dielectric rod material is polarized by the external field, with the degree of polarization depending on the orientation of the rod axis. When the field is oriented perpendicular to the rod, the resultant polarization is less than when the same field is applied parallel to the rod. This difference in electric polarizability is caused by electric charges induced at the rod surface by the polarization itself. (A uniform displacement of positive and negative charges inside a dielectric material produces surface charges which have opposite signs at opposing surface areas.) The surface charges produce an electric field that, inside the rod, is opposed to the external field and thus weakens the total field polarizing the rod material. Based on simple electrostatics, the strength of the electric field produced by the surface charges decreases with increasing distance of the charges. Therefore, for parallel rod orientation to the external field, the depolarization field inside the rod is weak because the surface charges are located far apart at either end of the rod. In fact, for parallel orientation, the depolarization field is negligibly small for long thin rods with an axial ratio of more than 10, whereas for perpendicular orientation the depolarization field is independent of the length at these axial ratios and is a constant fraction of the external field. Accordingly, the total field, which

is the external field minus the depolarization field, is higher for parallel than for perpendicular orientation, leading to a higher polarizability parallel versus perpendicular and we say that the rod has a positive dielectric anisotropy.

The preceding paragraph describes a qualitative argument which was first treated exactly by J. C. Maxwell, who calculated the depolarization field for simple shapes such as rotational ellipsoids including cylinders and planes (Maxwell, 1881; see also Osborn, 1945). Wiener (1912) considered the properties of arrays of dielectric particles, including the anisotropy of similarly oriented ellipsoids embedded in a dielectric medium. Wiener's results were rederived and made more accessible by Bragg and Pippard (1953) and were further developed and applied to birefringence measurements of biological systems by Oldenbourg and Ruiz (1989). According to these results, the dielectric constant (ε) of an array of alligned rods of dielectric constant ε_2 and volume fraction f, embedded in a medium of ε_1, can be written as follows:

$$\varepsilon_{\parallel} = \varepsilon_2 + f(\varepsilon_2 - \varepsilon_1), \tag{4}$$

$$\varepsilon_{\perp} = \varepsilon_1 + \frac{f(\varepsilon_2 - \varepsilon_1),}{1 + (1-f)\dfrac{(\varepsilon_2 - \varepsilon_1)}{2}} \tag{5}$$

Equations [4] and [5] are the array coefficients for electric field orientations parallel and perpendicular to the rod axes, respectively. The term added to 1 in the denominator of Eq. [5] derives from the depolarization field for perpendicular orientation of the rod axis to the external field. For parallel orientation this term is missing because the depolarization field is negligibly small, assuming long, thin rods. Since we deal with particles of dimensions smaller than the wavelength of light, the refractive index of the array is the square root of its dielectric constant. Hence, the difference of refractive indices for light polarized parallel and perpendicular to the rod axes, the birefringence Δn of the array, is

$$\Delta n = \sqrt{\varepsilon_{\parallel}} - \sqrt{\varepsilon_{\perp}} \tag{6}$$

For small volume fractions, Eq. [6], with Eqs. [4] and [5], can be expanded into a Taylor series around $f = 0$, which leads to

$$\Delta n = \Delta n' f - \left(1 + \frac{\Delta n'}{2\sqrt{\varepsilon_1}}\right) \Delta n' f^2 + \cdots \tag{7}$$

with

$$\Delta n' = \frac{(\varepsilon_2 - \varepsilon_1)^2}{2\sqrt{\varepsilon_1}\,(\varepsilon_1 + \varepsilon_2)} \tag{8a}$$

$\Delta n'$ is the specific birefringence or the birefringence per volume fraction. For biological systems such as the mitotic spindle, the volume fraction f is typically

only a few percent or less, in which case the first term of the Taylor series is sufficient to analyze experimental results. Sato *et al.* (1975) published an extensive study of the spindle birefringence in the sea star *Pisaster ochraceus,* including measurements of the specific birefringence of MTs under physiological conditions ($\Delta n' = 0.025$, with $n_1 = \sqrt{\varepsilon_1} = 1.36$, the refractive index of the cytoplasm). In the same article, careful imbibition measurements on isolated *Pisaster* spindles are reported using solvents of various refractive indices, including a solvent that matched the refractive index of the protein material (Fig. 10). The matching solvent ($n_1 = 1.512$) was recognized when the birefringence of the imbibed spindle nearly disappeared. When the spindle is imbibed with the matching solvent, the dielectric constant, and hence the refractive index, of solvent and rod material are equal and the specific birefringence vanishes, except for the small intrinsic component which is discussed later. [This method measures the refractive index of hydrated proteins ($n \approx 1.51$) which is lower than the index

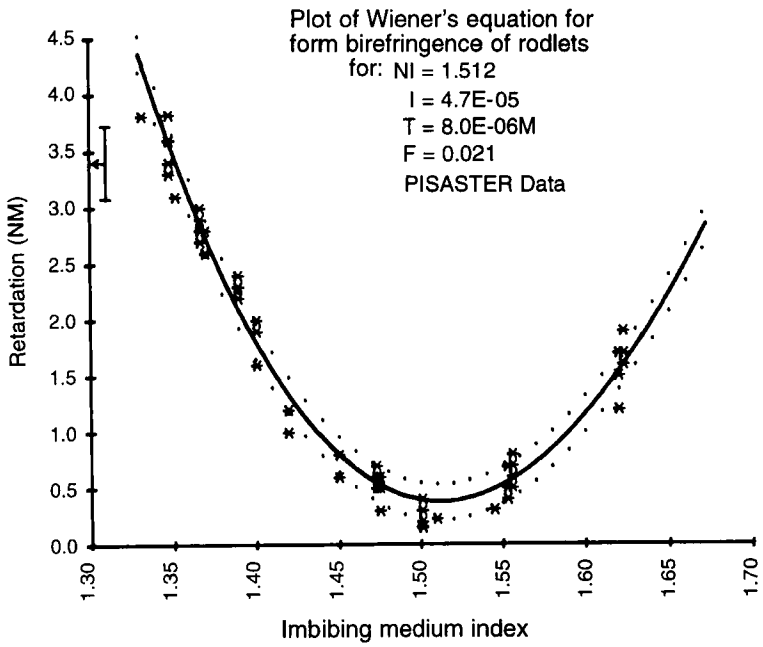

Fig. 10 Birefringence retardation of isolated spindles of the sea star *Pisaster ochraceus* (see Fig. 4) imbibed with media of various refractive indices. The continuous line represents the best fit of the Wiener theory to the data points (89 total, many overlapping) with parameter values for best fit indicated on top (N1 is solvent refractive index which matches rodlet material, I is intrinsic birefringence times volume fraction, T is measured spindle thickness, and F is volume fraction occupied by rodlets). The dotted curves represent the standard deviation of the best fit. The error bar with arrow shown at the ordinate represents the mean and standard deviation of the retardance measured for 30 spindles in intact living *Pisaster* oocytes (Sato *et al.*, 1975, reproduced from *The Journal of Cell Biology,* 1975, **67,** 501–517 by copyright permission of The Rockefeller University Press).

found by refractive index increment measurements which determine the refractive index of dry, dehydrated proteins ($n \approx 1.59$; Perlmann and Longsworth, 1948; Lee *et al.*, 1973).] In addition, for solvents other than the matching one, Sato *et al.* found that spindle birefringence was proportional to the square of the difference between the refractive indices of solvent and rod material. All these findings are in agreement with the previous theoretical expressions and are proof that MT birefringence is caused primarily by form birefringence.

2. Intrinsic Birefringence

To determine the small intrinsic component of spindle birefringence, Sato *et al.* (1975) made imbibition measurements including solvents that nearly matched the protein refractive index. At the match point, spindle birefringence was lowest but did not vanish completely. This nonvanishing contribution to spindle birefringence is thought to be caused by the intrinsic anisotropy of the dielectric constant of the protein material assembling the MTs. The anisotropy can formally be accounted for in Eq. [6] by a relatively small change concerning the dielectric constant ε_2 of the rod material. To account for intrinsic birefringence, ε_2 is replaced by $\varepsilon_{2\parallel}$ and $\varepsilon_{2\perp}$ in Eqs. [4] and [5], respectively. Hence, the average dielectric constant ε_2 is replaced by coefficients specific to the field orientations parallel and perpendicular to the particle axis. The intrinsic birefringence is then $\Delta n_{\text{int}} = \sqrt{\varepsilon_{2\parallel}} - \sqrt{\varepsilon_{2\perp}}$, which can be expanded again in a Taylor series around $f = 0$, leading to a specific birefringence $\Delta n'$ that includes a term for the intrinsic birefringence:

$$\Delta n' = \frac{(\varepsilon_2 - \varepsilon_1)^2}{2\sqrt{\varepsilon_1}\,(\varepsilon_1 + \varepsilon_2)} + \frac{2\,\varepsilon_2^2 + (\varepsilon_2 + \varepsilon_1)^2}{3\sqrt{\varepsilon_1}\,(\varepsilon_2 + \varepsilon_1)^2}\,\Delta\varepsilon_2 \tag{8b}$$

with

$$\Delta\varepsilon_2 = \varepsilon_{2\parallel} - \varepsilon_{2\perp} \text{ and } \varepsilon_2 = (\varepsilon_{2\parallel} + 2\,\varepsilon_{2\perp})/3$$

At the match point ($\varepsilon_1 = \varepsilon_2$), the first term in Eq. (8b) becomes zero and the second term reduces to $\Delta\varepsilon_2/(2\sqrt{\varepsilon_2})$. The second term is an approximate expression for the intrinsic birefringence, in case $\varepsilon_{2\parallel}$ and $\varepsilon_{2\perp}$ do not deviate much from the average dielectric constant ε_2. Using the results of Sato *et al.* for MTs of the *Pisaster* spindle, we arrive at a value of $\Delta n_{\text{int}} = 0.0022$. The intrinsic birefringence of MTs can possibly be interpreted in light of the recent publication of an atomic model of the $\alpha\beta$ tubulin dimer (Nogales *et al.*, 1998).

The molecular origin of intrinsic birefringence is found in the anisotropy of the polarizability of molecular bonds (Applequist *et al.*, 1972). Due to the preferential alignment of molecular bonds in the α-helix, for example, its polarizability is higher parallel to the helix axis than perpendicular to it, leading to the intrinsic birefringence $\Delta n_{\text{int}} = 0.011$ of the tropomyosin molecule (Ruiz and

Oldenbourg, 1988), an α-helical coiled coil which is part of the thin filament in muscle. Aromatic side groups can also contribute to intrinsic birefringence since the aromatic ring is more highly polarizable for electric fields oriented in the plane compared to perpendicular to it. A single strand of DNA, for example, has a negative birefringence because of the many aromatic rings contained in its base pairs (Tsvetkov, 1964). The base pairs are stacked, building the DNA polymer and orienting the aromatic ring planes perpendicular to the polymer axis. Thus, the intrinsic birefringence is negative, overriding the positive form birefringence of the linear polymer. In general, intrinsic birefringence is a sensitive structural parameter which can potentially be used to monitor protein conformation during physiological function.

B. Birefringence of Single and Bundled Microtubules

With a sensitive polarizing microscope one can image not only arrays of parallel fibers but also individual fibers. After improving the performance of the polarizing microscope, for example, Inoué (1953) demonstrated the existence of spindle fibers not only by displaying the birefringence of the fibrous array but also by directly imaging the birefringence of individual fibers and fibrils in the spindle. While it is known that the anisotropy of an individual fiber can be detected, it was not clear until recently how to interpret the measured retardance of the fiber. Can we learn something about the fiber thickness, even though it is below the resolution limit of the light microscope? In answering this question, Tran *et al.* (1995) clearly showed that when measuring a single fiber, consisting of a small number of MTs, the measured peak retardance of the bundle is directly proportional to the number of MTs in the bundle. For a single MT, imaged with a numerical aperture of 1.4, they measured a peak retardance of 0.07 nm, whereas for a bundle of two and three MTs it was two and three times more, namely, 0.14 and 0.21 nm. Axonemes have a 20 times higher peak retardance, in accordance with their nine-doublet and two-singlet MT structure (Oldenbourg *et al.*, 1998). Thus, the measured retardance of a bundle allows one to estimate the number of filaments in a bundle by simply dividing the bundle retardance by the retardance of the single filament.

A detailed analysis of single-fiber retardance was published by Oldenbourg *et al.* (1998), who determined that the peak retardance of a bundle of MTs was proportional to the numerical aperture of the objective and condenser lens of the microscope. More specifically, the bundle, when imaged with low numerical aperture, appeared broad with low peak retardance, whereas with high numerical aperture the image of the same bundle was narrow with high peak retardance. Guided by this observation, the analysis showed that the area of the retardance plot, integrated along a line perpendicular to the bundle axis, was independent of the numerical aperture. The integrated retardance, which we call "retardance cross section," was measured to be 7.5 nm^2 for a single MT.

Oldenbourg *et al.* (1998) also developed a theory for single-fiber birefringence, including the retardance cross section. According to this theory, the cross section is the product of the specific birefringence $\Delta n'$, measured with an array of fibers (see Eqs. [8a] and [8b]), times the volume per unit length of a single fiber. We can use this relationship to independently estimate the retardance cross section of a single MT based on results from bulk measurements. The volume per unit length of a MT can be estimated by multiplying the partial specific volume of tubulin (0.74 cm^3/g; Lee *et al.*, 1973) with the dry mass per unit length of a MT ($2.3\ 10^{-20}$ g/nm; derived from structural data published by Amos, 1979). By combining these estimates with the specific spindle birefringence ($\Delta n' = 0.025$; Sato *et al.*, 1975) we calculate a retardance cross section of 5.5 nm^2, a value that is similar to the one measured directly by imaging single and bundled MTs.

C. Birefringence of Arrays of Parallel Microtubules

We will show that the birefringence of an array of parallel filaments can be related to the number density of the filaments in the array and the retardance cross section of a single filament. Sato *et al.* (1975) have measured the birefringence of isolated spindles which were subsequently fixed, embedded, and sectioned perpendicular to the spindle axis to count the number density of MTs per spindle cross section by electron microscopy. We propose to divide the measured spindle birefringence ($\Delta n = 5.3 \cdot 10^{-4}$) by the density of MTs ($\rho = 106$ MTs/μm^2) in the plane perpendicular to the filament axis, calculating a value ($\Delta n/\rho = 5 \cdot 10^{-6}$ $\mu m^2 = 5\ nm^2$) that is close to the retardance cross section measured directly by imaging single MTs. We believe that this coincidence is based on optical concepts which can be derived rigorously, relating the retardance cross section of a single filament to the birefringence of a filament array of uniform density. Further support for this interpretation comes from the result that the measured spindle birefringence is independent of the numerical aperture of the optical system (Sato *et al.*, 1975; Hiramoto *et al.*, 1981b). This finding corresponds to our result that the retardance cross section of the single filament is independent of the numerical aperture. We will present a more rigorous derivation of this concept in an upcoming publication.

We thus propose a specific procedure to estimate the number density of MTs in the spindle, or parts of it, using the measured retardance. In addition to measuring the spindle retardance, its thickness must be estimated by, e.g., noting the difference in stage position when focusing on the top and bottom of the spindle and/or by relating the thickness to the observed width of the spindle. (For axial distance measurements one needs to consider the foreshortening of the focus level when focusing through media of different refractive indices; see Visser *et al.*, 1992.) The spindle retardance is then divided by the spindle thickness to derive the average birefringence of the MT array. To derive the number density averaged over the thickness of the spindle, the birefringence is divided by the retardance cross section of a single MT. We note that the number density

is the number of individual MTs in a cross section, regardless of the presence of MT bundling. A bundle of three MTs, for example, contributes three MTs to the density count since the retardance cross section of the bundle is three times the single MT cross section.

D. Birefringence of Individual Spindle Components

Images and time-lapse movies of spindles recorded with a sensitive, high-resolution polarizing microscope show fine details of spindle structure, such as kinetochore fibers or highly dynamic spindle regions with fast-changing MT densities (e.g., Figs. 13 and 15). These observations give important and detailed information on the architectural dynamics and physiological function of spindle components. Therefore, it is desirable to be able to analyze quantitatively spindle birefringence at a higher spatial resolution than, e.g., estimating the density of MTs averaged over the spindle cross section. Individual kinetochore fibers, for example, are tight bundles of MTs that can often be recognized by their higher peak retardance in polarized light images (Figs. 4, 13, 15, 17). Their retardance, however, is typically elevated by the MT array surrounding the fibers. To determine the true cross section of an individual fiber, we consider the retardance measured to the left and right of the focused fiber as background representing the birefringence of the surrounding MTs. One can then subtract the background from the fiber retardance to obtain the true retardance cross section of the kinetochore fiber. If the orientation of the fiber and the surrounding array is not parallel, one also needs to consider the mutual orientation of their slow axes (Oldenbourg *et al.*, 1998).

In a traditional polarizing microscope, the slow axis orientations affect the measurement of the specimen retardances, requiring a careful measurement process that includes the correct alignment of the birefringent areas under study with respect to the polarizer and analyzer axes. The requirement of mechanically realigning the specimen is alleviated when using the Pol-Scope, which measures specimen retardances irrespective of their orientation. In fact, the axis orientation anywhere in the plane of focus is included in the measurement and is available for every image point. Thus, Pol-Scope images lend themselves to be analyzed quantitatively at high spatial resolution, including the full three-dimensional analysis of specimen birefringence such as the mitotic spindle. We are currently developing these analysis tools which will greatly extend the information available from polarized light images.

IV. Optimum Cell Types for Polarized Light Microscopy of Spindles

With an appropriate polarizing microscope one can follow the dynamically changing fine structure, assembly states, and morphology of spindle fibers, astral

rays, and phragmoplast fibers that reflect the molecular, physiological, and developmental events taking place in living, dividing cells. Under a sensitive polarizing microscope, the local concentration and assembly states of the MTs that make up these fibers are manifested as a weak (a fraction to a few nanometers of retardance), positive, form birefringence, as described earlier. The birefringence emerges as the astral and spindle MTs assemble in prophase and disappears as the MTs are disassembled in anaphase and early cleavage (Fig. 11). The dynamic assembly states of these MT bundles, changing naturally in the course of mitosis or as experimentally modified pharmacologically or by altering the temperature

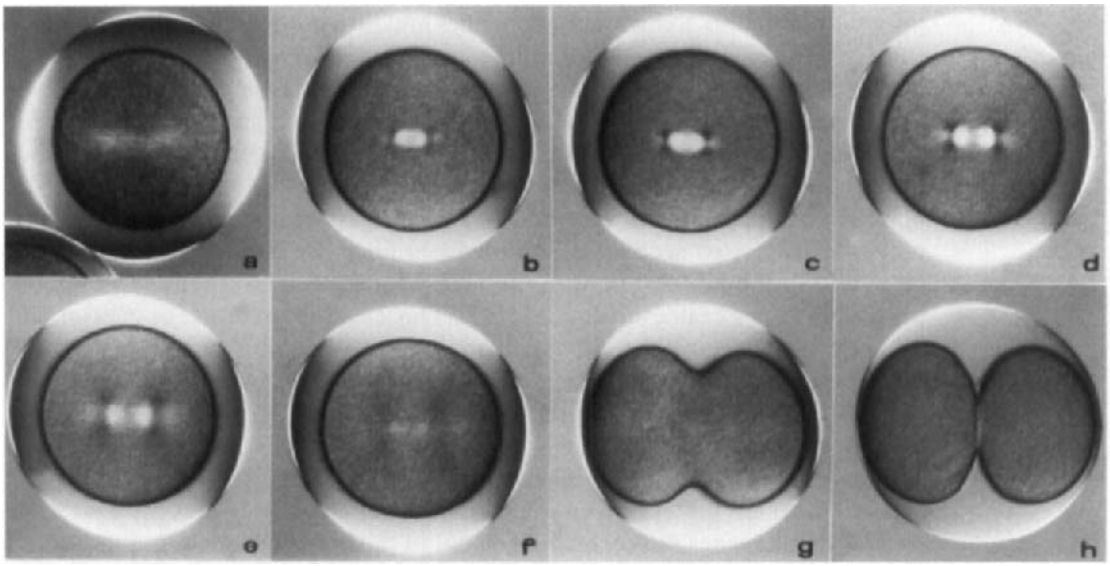

Fig. 11 Birefringence of spindle, asters, and fertilization envelope in the early zygote of a sea urchin, *Lytechinus variegatus*. (a) The "streak stage." After a large monaster with a weak, radially positive birefringence disappears, its midregion turns into a negatively birefringent streak. (b) The streak becomes replaced by a compact, positively birefringent spindle. (c) The spindle and astral birefringence increase as they develop further in prometaphase. (d) In full metaphase to anaphase onset, densely packed microtubules make up the fully formed half spindles and the small but distinct amphiasters. Their birefringence reaches peak values at this stage. (e) The two half spindles lead the chromosomes polewards in midanaphase. The chromosomes are nonbirefringent as explained in the legend to Fig. 13. (f) In telophase, the half spindles and astral rays are made up of longer but less densely packed microtubules, thus exhibiting weaker birefringence. (g) Early cleavage. (h) Late cleavage stage. The strong, tangentially positive birefringence (i.e., slow axis parallel to its tangent) of the fertilization envelope (FE) is visible in all panels. The FE and asters appear brighter or darker in different quadrants due to the action of a compensator that is placed between the crossed polars. Those regions displaying the same contrast as the FE have the same slow axis orientation as that part of the FE. The FE (which acquires a relatively strong, persistent birefringence from a few minutes after fertilization until it is digested many hours later at hatching of the ciliated embryo) thus serves as a useful, built-in contrast reference for determining the slow axis directions of spindle fibers, astral rays, membrane components, etc. (reproduced from Salmon and Wolniak, 1990).

or hydrostatic pressure, etc., can be studied quantitatively in living cells by measuring their birefringence (Inoué, 1952, 1964, 1981b; Inoué and Sato, 1967; Salmon, 1975).

However, some cells are more suited than others for polarization optical studies since the strength of the relevant optical signal (the birefringence retardance), and especially its signal strength over the background, can vary considerably. Even among the same types of cells, there can be considerable variation from species to species as to which is more suitable.

For example, among echinoderm zygotes, those of the sand dollars *Clypeaster japonica* and *Echinarachnius parma* (Fig. 12) contain significantly less birefringent or light scattering particles than those of the sea urchins *Lytechinus pictus* or *Arbacia punctulata* and yield much clearer images of the birefringent spindle fibers as well as of the slightly refractile chromosomes. Also, eggs that are "overripe" tend to contain many small, scintillating, birefringent particles (miniature calcite crystals in vesicles?) that can interfere with polarized light observations of otherwise clear eggs. [Methods for removing the fertilization envelope, whose birefringence can (in compressed eggs) interfere with measurement of

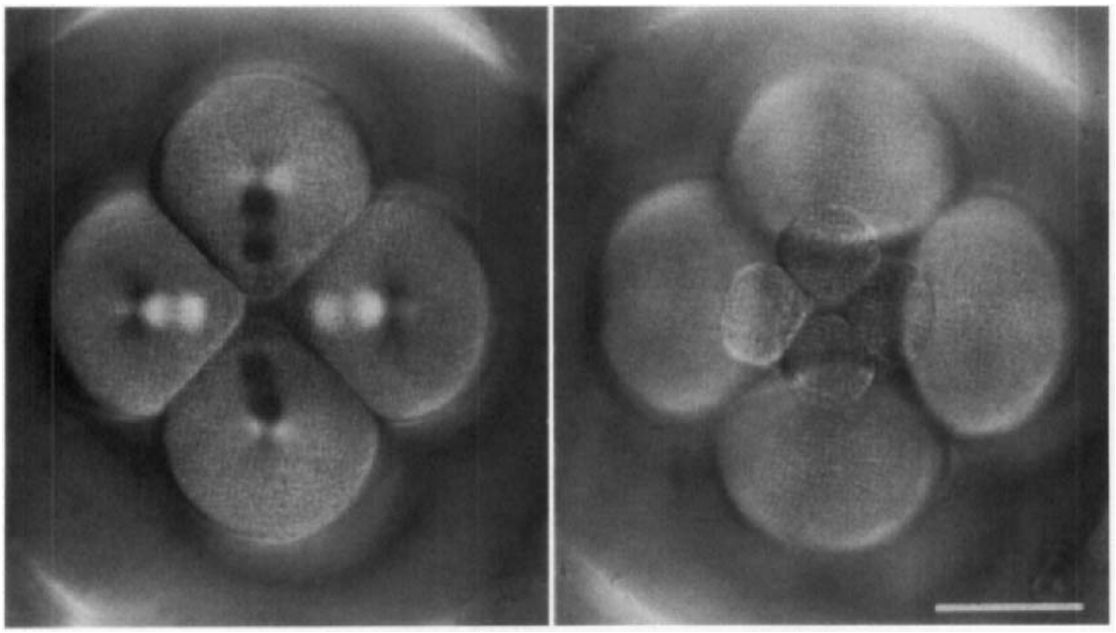

Fig. 12 Fourth division in the zygote of a sand dollar, *Echinarachnius parma.* (Left) The spindles have migrated to, and converge at, the vegetal pole of this eight-cell stage embryo (the four animal-pole cells are out of focus). (Right) Cleavage bisecting the telophase spindle has given rise to four macromeres and four micromeres. These latter four cells form the skeletal spicules and germ cells. Scale bar-50 μm (reproduced from Inoué and Kiehart, 1978).

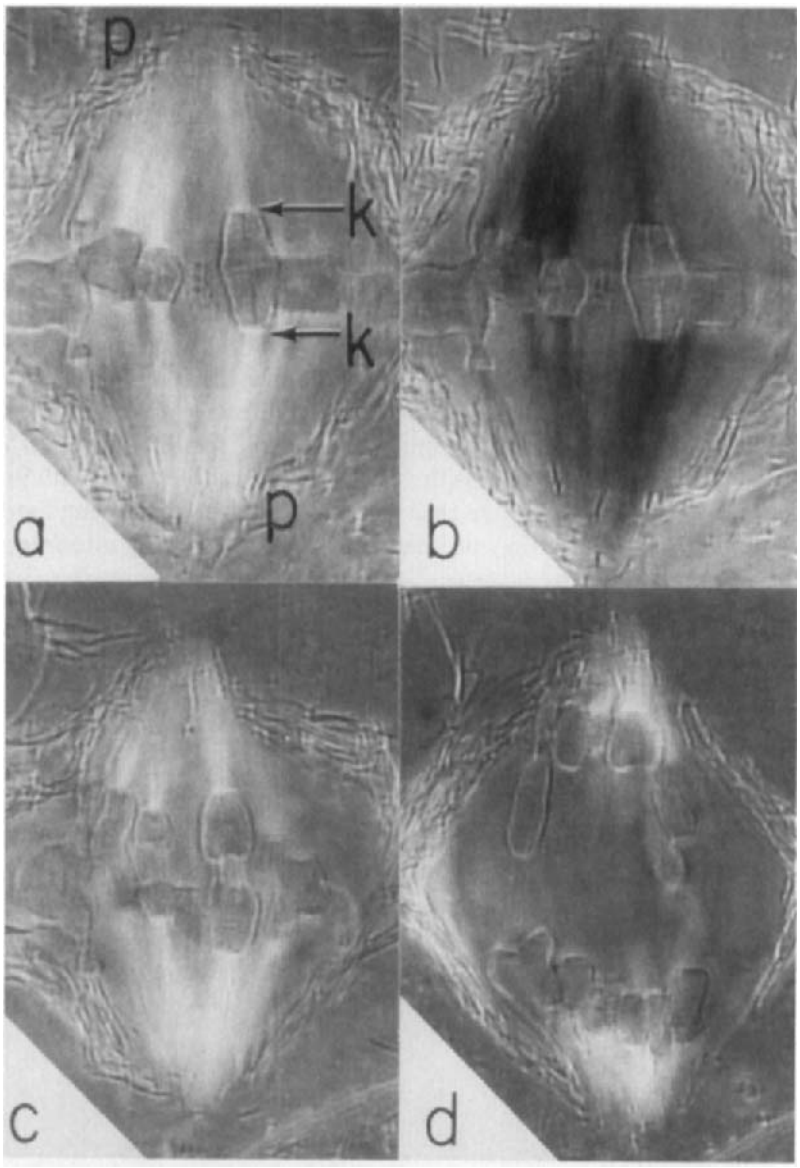

Fig. 13 High-resolution image, obtained using rectified polarization optics, of a primary spermatocyte of a grasshopper, *Pardalophora apiculata.* (a) Metaphase showing chromosomal spindle fibers and their fibrils (microtubules of varying lengths) running from kinetochores (K) on the chromosomes to the spindle poles (p). (b) Metaphase with compensator setting reversed. (c) In early anaphase 22 min after a and b. The microtubules that make up the chromosomal spindle fibers are shortening. The birefringence of the kinetochores appears stronger than at other stages. The chromosomes themselves, as typical for somatic chromosomes (but with the exception of certain dinoflagellate nuclei and late spermatid and mature sperm nuclei; Schmidt, 1937; Inoué and Sato, 1966; Cachon *et al.*, 1989), show virtually no birefringence except at its edges [most likely due to edge birefringence

spindle fiber birefringence, are described, e.g., in Lutz and Inoué (1986) and Roegiers *et al.* (1994).]

Clear eggs of echinoderms have been favored for the study of mitosis and cell division since large populations of zygotes can be fertilized at once and be made to develop synchronously. Also, some insect spermatocytes (Fig. 13; Nicklas, 1971) and mammalian tissue cultured cells (McIntosh, 1994), as well as a number of protozoa (Ritter *et al.*, 1978) and diatoms (Pickett-Heaps and Tippit, 1978), have yielded significant information regarding mitosis and cell division through polarization optical studies made directly in living cells.

In contrast, eggs of many marine molluscs, annelid worms, and tunicates are so full of birefringent yolk granules that, without appropriate treatment, they can completely obscure the image of the more weakly birefringent spindle and asters. Nevertheless, there is considerable interest in following the early development of these species since they represent a group of phyla that show determinate cleavage and tend to develop and differentiate very rapidly. Even among these groups, however, there are some species that yield moderately clear eggs and whose spindle and astral birefringence can be visualized, e.g., *Pectinaria gouldii* (Fig. 14), *Phallusia mamilata* (Sardet *et al.*, 1989), and *Spisula solidissima* (Dan and Inoué, 1987; Palazzo *et al.*, 1992).

Among tissue cultured cells, the giant lung epithelial cells of the newt (*Taricha granulosa*) (Fig. 15), which remain flattened during mitosis and also possess large chromosomes, have allowed greater scrutiny of the behavior of individual spindle fibers and kinetochores with polarization microscopy than the more commonly used, smaller and less flattened, tissue culture cells (Rieder and Hard, 1990).

Some plant tissue cells, such as the endosperm cells (in particular those of *Haemanthus katherinae*), whose mitosis and cytokinesis progress as a wave in space within the cellular endosperm (much as in the formation of the male gamete of many animals, as especially clearly seen in the testicular lobes of orthopteran insects; Bělař, 1929), have also been favorite material for study of

---

Fig. 13 (*Continued*) (Oldenbourg, 1991) caused by its somewhat higher refractive index relative to the surrounding material.] [While chromatin in somatic chromosomes generally exhibits virtually no anisotropy even compared to the weak, positive form birefringence of the spindle fibers, fully oriented chromatin shows a strong, intrinsic birefringence that is characteristic of its DNA moiety which is negative in sign (i.e., its slow axis lies perpendicular to the length of the elongated DNA molecules). For example, the intrinsic birefringence of the DNA protein in mature sperm head is a full order of magnitude greater per unit thickness (Inoué and Sato, 1966) than the form birefringence exhibited by microtubule bundles in spindle fibers (Sato *et al.*, 1975), flagellar axonemes, or axostyles found in hypermastigate protozoa (Langford and Inoué, 1979).] It has not been established whether the birefringence at the kinetochore is due solely to edge birefringence or whether it represents a greater molecular or fine-structural order in that region. (d) In late anaphase 14 min after c. Mitochondria at the periphery of the spindle are beginning to be aligned more nearly parallel to the spindle axis and display a longitudinally positive birefringence similar to the spindle fibers. Magnification, ×1500 (reproduced from Nicklas, 1971).

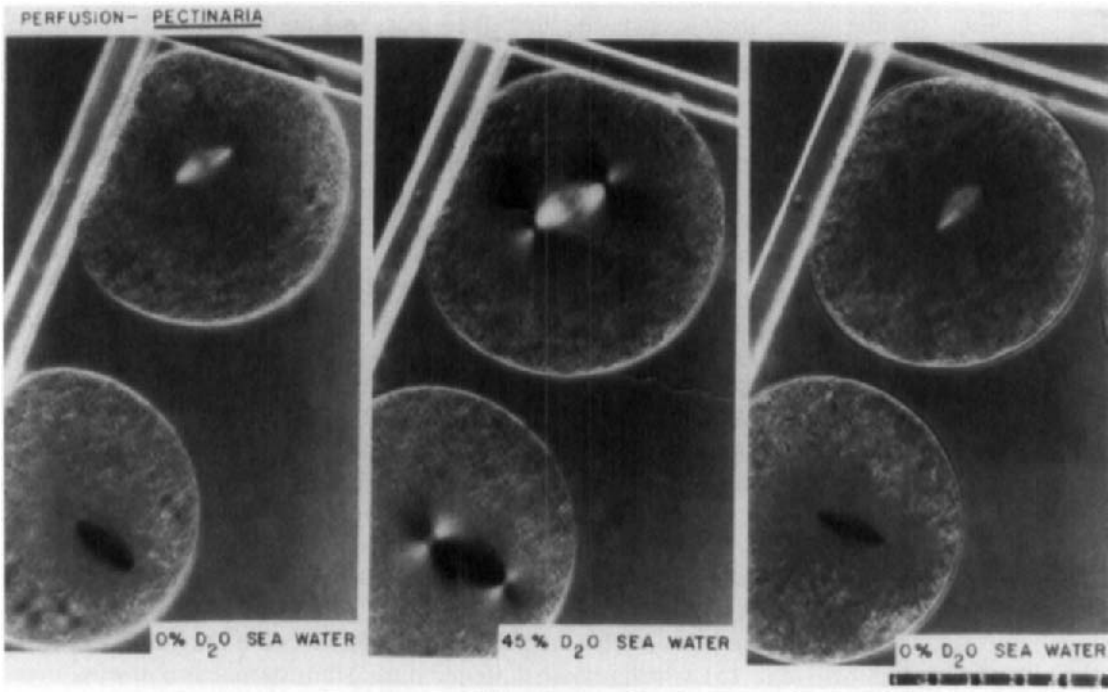

Fig. 14 Reversible assembly of spindle and astral microtubules induced by D_2O in metaphase-arrested oocytes of a marine annelid worm, *Pectinaria gouldii.* (Left) Birefringence and morphology of the normal meiosis I spindle and aster in oocytes perfused with normal seawater. (Middle) After 2 min perfusion with 45% D_2O seawater. The spindle is now ca. 20 μm long. As seen by the striking increase in birefringence and size of the spindle and asters, microtubule assembly rises dramatically in the presence of D_2O (presumably by enhanced hydrophobic interactions since they are reversibly disassembled by cold and by high hydrostatic pressure also). (Right) Microtubule assembly has returned to its normal equilibrium state 3 min after perfusion in normal seawater. The bright double lines in the upper left of these panels are edges of glass wool fibers that were used as a mesh to prevent these somewhat compressed cells from floating away by perfusion (Inoué and Sato, 1967, reproduced from *The Journal of General Physiology* by copyright permission of The Rockefeller University Press).

the details of mitotic organization and movements. The behavior of the large chromosomes, as well as the birefringence of the chromosomal and continuous spindle fibers and phragmoplast fibers, can be clearly seen in these large endosperm cells that continue to divide for many hours as flattened sheets sandwiched between layers of agar (Inoué and Bajer, 1961). The dynamically rocking spindle and cytokinesis in the cellular slime mold *Dictyostelium discoideum,* although very much smaller, can also be studied in polarized light in an agar overlay preparation (Fukui and Inoué, 1991).

Meiosis and mitosis in other plant tissue cells, such as in the pollen mother cells of *Lilium longiflorum,* can be timed precisely by measuring the length of the flower bud (Erickson, 1948). While the *Lilium* pollen mother cells were found to be more suitable for studies of their meiotic mitosis than in several

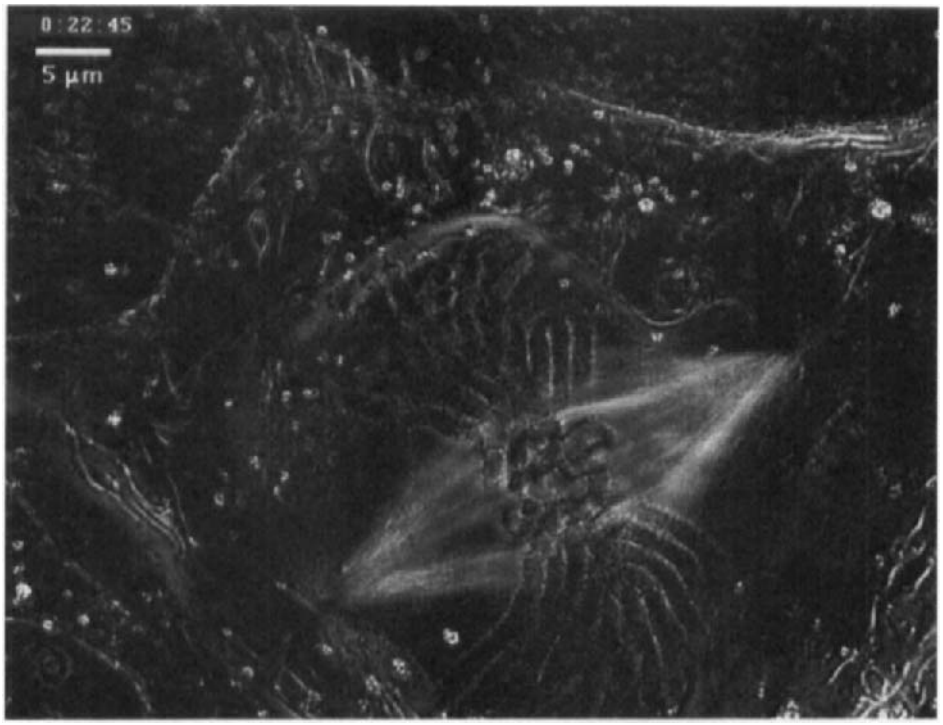

Fig. 15 Pol-Scope image of mitosis in a cultured lung epithelial cell from the newt, *Taricha granulosa.* In this image brightness corresponds to retardance magnitude which is displayed independent of the orientation of the birefringence axes. Bright spindle fibers locate the large chromosomes between the spindle poles. Chromosomes seem to be outlined by birefringence near their edges. In addition, other cell components can be seen, such as mitochondria and stress fibers surrounding the spindle (reproduced from Oldenbourg, 1996. A new view on polarization microscopy. *Nature* **381,** 811–812).

other dicots, the lily cells had to first be centrifuged to displace the large number of birefringent intracellular particles to gain a clear and detailed view of the birefringent spindle and phragmoplast fibers and filaments (Fig. 16; Inoué, 1953). The pollen mother cells were centrifuged within the intact, 22.4-mm-long flower bud at ca. 1800*g* in a clinical centrifuge, after which the anthers were dissected out and the cells were observed in 7/8 concentration frog Ringer's solution.

Likewise, polarization optical studies on oocytes of the annelid worm *Chaetopterus pergamentaceous* (which yielded rich birefringence data on the thermodynamics of the spindle fibers, MT assembly dynamics, and their relation to chromosome movement; for reviews, see Salmon, 1975; Inoué, 1981a; Inoué and Salmon, 1995) would not have been possible without centrifuging and clearing the oocytes of their highly birefringent yolk granules (Fig. 17). These oocytes, when expelled from the body cavity into seawater, progress to metaphase of meiosis I in about 15 min and remain arrested at this stage for many hours unless fertilized or otherwise activated. Clear egg fragments containing intact meiotic spindles and

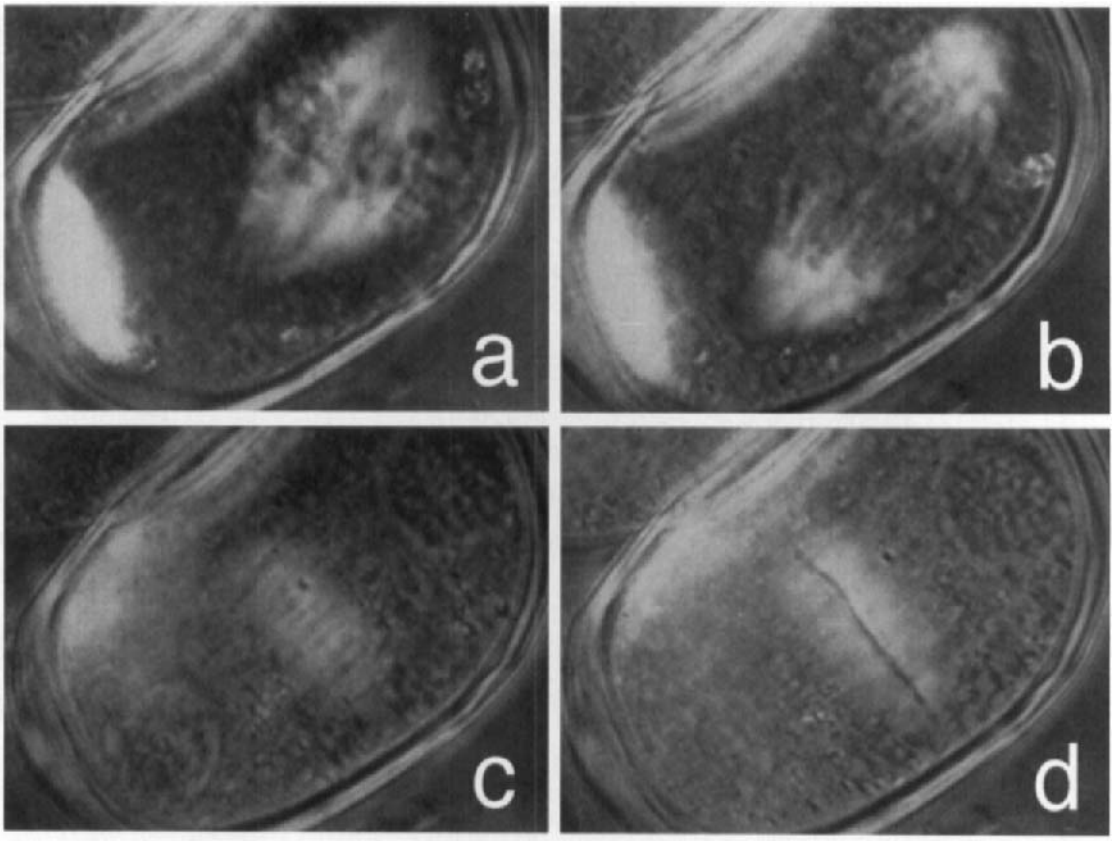

Fig. 16 Mitosis and cell plate formation in a pollen mother cell of the Easter lily, *Lilium longiflorum.* (a) Metaphase. The bright birefringent chromosomal spindle fibers stand out against the nonbirefringent helical chromosomes present on the metaphase plate. (b) Anaphase: The chromosomes are drawn apart by the elongating spindle, which is about to displace the birefringent cell inclusions [which have been centrifuged down (to the lower left) in order to gain a clear view of the spindle birefringence]. (c) Telophase: The chromosomes have been packaged into daughter nuclei at the spindle poles, and microtubule bundles overlapping in the midspindle region are beginning to form the phragmoplast. (d) In the midzone of the phragmoplast, vacuoles have fused to form the cell plate (dark line) (reproduced from Inoué, 1964).

associated asters were obtained by centrifuging the oocytes on a gradient of sucrose or Ficoll at several thousand's times gravity (Inoué, 1953; Lutz *et al.*, 1988).

Some chambers and mounting or manipulation methods appropriate for extended observation and/or experimental manipulation of dividing cells in polarized light microscopy are summarized in the following references: Inoué *et al.* (1975), Hiramoto *et al.* (1981b); and Lutz and Inoué (1986).

As these examples show, for polarization optical studies one should select cell types that provide optical conditions that favor observation and measurement

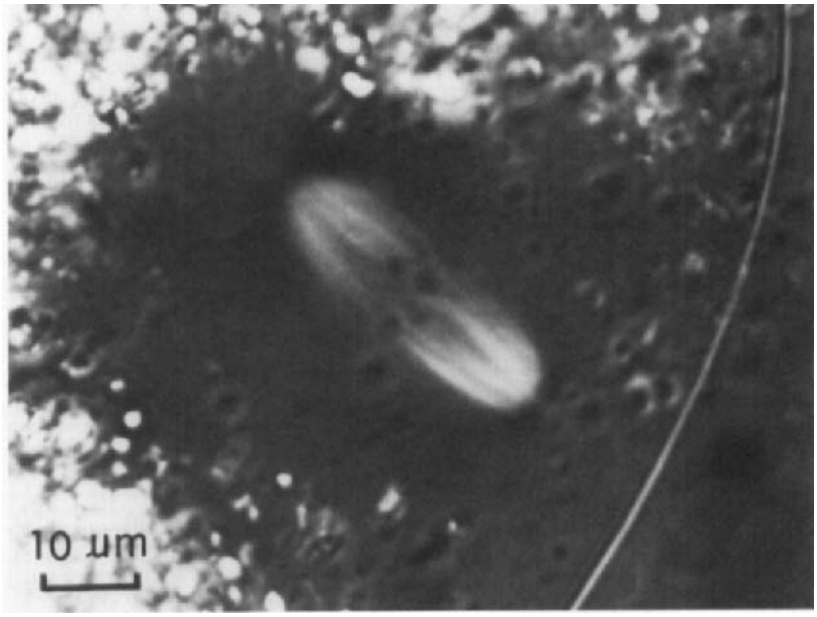

Fig. 17 Metaphase-arrested meiosis I spindle in the oocyte of a marine annelid worm, *Chaetopterus pergamentaceous.* In this centrifuged and somewhat flattened cell fragment, the highly birefringent yolk granules have been displaced from the spindle region, thus making the weakly birefringent chromosomal spindle fibers and asters clearly visible. Micromanipulative displacement of this spindle shows that the microtubules making up the aster at either spindle poles can anchor the 25-µm-long spindle dynamically to the cell cortex specifically at the animal pole of the oocyte (Lutz *et al.*, 1988) (reproduced from Inoué, 1953).

of the weak birefringence and at the same time meet the needed condition for addressing the biological questions to be investigated. Further studies are awaited on the dynamic fine structure underlying mitosis in living cells using polarization microscopy and on material particularly favorable for addressing questions relating to different facets of mitotic mechanisms. Such cell types could well be found among some of the species listed previously or by more widely exploring tissue cells, e.g., among the protists (Bělař, 1926; Schmidt, 1937; Inoué and Ritter, 1978), or hitherto unexplored dissociated tissue cells (Bělař, 1928, 1929).

Acknowledgments

The author is indebted to Shinya Inoué for his inspiration and guidance in exploring and writing about polarized light microscopy of spindles. The technique and its numerous applications to live cell studies owes much to Shinya Inoué's tireless curiosity and ingenuity which I hope shine through in this chapter. Financial support was provided by Grant GM49210 from the National Institute of General Medical Sciences, National Institutes of Health.

References

Allen, R. D., Brault, J., and Moore, R. D. (1963). A new method of polarization microscopic analysis. I. Scanning with a birefringence detection system. *J. Cell Biol.* **18,** 223–235.

Amos, L. A. (1979). Structure of microtubules. *In* "Microtubules" (K. Roberts and J. S. Hyams, Eds.), pp. 1–64. Academic Press, London.

Applequist, J., Carl, J. R., and Fung, K.-K. (1972). An atomic interaction model for molecular polarizability. Application to polyatomic molecules and determination of atom polarizabilities. *J. Am. Chem. Soc.* **94,** 2952–2960.

Bělař, K. (1926). Der Formwechsel der Protistenkerne. *Ergebn. u. Fortschr. Zool.* **6,** 1–420.

Bělař, K. (1928). Die Technik der diskriptiven Cytologie. *In* "Methodik der wissenschaftlichen Biologie," pp. 638–735. Springer-Verlag, Berlin.

Bělař, K. (1929). Beiträje zur kausal analyse der Mitose. II Untersuchungen an den Spermatocyten von Chorthippus (Stenobotrus) Lineatus Pauz. *Wilhelm Roux's Arch. Entwicklungsmech. Org.* **118,** 359–484.

Blinov, L. (1983). "Electro-Optical and Magneto-Optical Properties of Liquid Crystals." Wiley–Interscience, New York.

Bragg, W. L., and Pippard, A. B. (1953). The form birefringence of macromolecules. *Acta Crystall.* **6,** 865–867.

Cachon, J., Sato, H. Cachon, M. and Sato, Y. (1989). Analysis by polarizing microscopy of chromosomal structure among dinoflagellates and its phylogenetic involvement. *Biol. Cell* **65,** 51–60.

Cassimeris, L., Pryer, N. K., and Salmon, E. D. (1988). Real-time observations of microtubule dynamic instability in living cells. *J. Cell Biol.* **107,** 2223–2231.

Dan, K., and Inoué, S. (1987). Studies of unequal cleavage in molluscs. II. Asymmetric nature of the two asters. *Int. J. Invertebr. Reprod. Dev.* **11,** 335–354.

Erickson, R. O. (1948). Cytological and growth correlations in the flower bud and anther of *lilium longiflorum. Am. J. Bot.* **35,** 729–739.

Fukui, Y., and Inoué, S. (1991). Cell division in Dictyostelium with special emphasis on actomyosin organization in cytokinesis. *Cell Motil. Cytoskel.* **18,** 41–54.

Hartshorne, N. H., and Stuart, A. (1960). "Crystals and the Polarising Microscope: A Handbook for Chemists and Others," 3rd ed. Arnold, London.

Hecht, E. (1987). "Optics." Addison-Wesley, Reading, MA.

Hiramoto, Y., Hamaguchi, Y., Shôji, Y., and Shimoda, S. (1981a). Quantitative studies on the polarization optical properties of living cells I. Microphotometric birefringence detection system. *J. Cell Biol.* **89,** 115–120.

Hiramoto, Y., Hamaguchi, Y., Shôji, Y., Schroeder, T. E., Shimoda, S., and Nakamura, S. (1981b). Quantitative studies on the polarization optical properties of living cells II. The role of microtubules in birefringence of the spindle of the sea urchin egg. *J. Cell Biol.* **89,** 121–130.

Inoué, S. (1952). The effect of cholchicine on the microscopic and submicroscopic structure of the mitotic spindle. *Exp. Cell Res. Suppl.* **2,** 305–318.

Inoué, S. (1953). Polarization optical studies of the mitotic spindle. I. The demonstration of spindle fibers in living cells. *Chromosoma* **5,** 487–500.

Inoué, S. (1959). Motility of cilia and the mechanism of mitosis. *In* "Biophysical Science—A Study Program" (J. L. Oncley, F. O. Schmitt, R. C. Williams, M. D. Rosenberg, and R. H. Bolt, Eds.), pp. 402–408. Wiley, New York.

Inoué, S. (1961). Polarizing microscope: Design for maximum sensitivity. *In* "The Encyclopedia of Microscopy." (G. L. Clark, Ed.), Reinhold, New York.

Inoué, S. (1964). Organization and function of the mitotic spindle. *In* "Primitive Motile Systems in Cell Biology." (R. H. Allen and N. Kamiya, Eds.), pp. 549–598. Academic Press, New York.

Inoué, S. (1981a). Cell division and the mitotic spindle. *J. Cell Biol.* **91,** 131s–147s.

Inoué, S. (1981b). Video image processing greatly enhances contrast, quality and speed in polarization-based microscopy. *J. Cell Biol.* **89,** 346–356.

Inoué, S. (1986). "Video Microscopy." Plenum, New York.

Inoué, S., and Bajer, A. (1961). Birefringence in endosperm mitosis. *Chromosoma (Berlin)* **12,** 48–63.

Inoué, S., and Dan, K. (1951). Birefringence of the dividing cell. *J. Morphol.* **89,** 423–456.

Inoué, S., and Hyde, W. L. (1957). Studies on depolarization of light at microscope lens surfaces II. The simultaneous realization of high resolution and high sensitivity with the polarizing microscope. *J. Biophys. Biochem. Cytol.* **3,** 831–838.

Inoué, S., and Kiehart, D. P. (1978). In vivo analysis of mitotic spindle dynamics. *In* "Cell Reproduction: In Honor of Daniel Mazia" (E. R. Dirksen, D. M. Prescott, and C. F. Fox, Eds.), pp. 433–444. Academic Press, New York.

Inoué, S., and Kubota, H. (1958). Diffraction anomaly in polarizing microscopes. *Nature* **182,** 1725–1726.

Inoué, S., and Ritter, H. (1978). Mitosis in *Barbulanympha.* II. Dynamics of a two-stage anaphase, nuclear morphogenesis, and cytokinesis. *J. Cell Biol.* **77,** 655–684.

Inoué, S., and Salmon, E. D. (1995). Force generation by microtubule assembly/disassembly in mitosis and related movements. *Mol. Biol. Cell* **6,** 1619–1640.

Inoué, S., and Sato, H. (1966). Deoxyribonucleic acid arrangement in living sperm. *In* "Molecular Architecture in Cell Physiology." (T. Hayashi and A. G. Szent-Gyorgyi, Eds.), pp. 209–248. Prentice Hall, Englewood Cliffs, NJ.

Inoué, S., and Sato, H. (1967). Cell motility by labile association of molecules: The nature of mitotic spindle fibers and their role in chromosome movement. *J. Gen. Physiol.* **50,** 259–292.

Inoué, S., Fuseler, J. W., Salmon, E. D., and Ellis, G. W. (1975). Functional organization of mitotic microtubules—Physical chemistry of the in vivo equilibrium system. *Biophys. J.* **15,** 725–744.

Langford, G. M., and Inoué, S. (1979). Motility of the microtubular aseostyle in *Pyrsonympha. J. Cell Biol.* **80,** 521–538.

Lee, J. C., Frigon, R. P., and Timasheff, S. N. (1973). The chemical characterization of calf brain microtubule protein subunits. *J. Biol. Chem.* **248,** 7253–7262.

Lewis, W. H., and Lewis, M. R. (1924). Behavior of cells in tissue cultures. *In* "General Cytology." (E. V. Cowdry, Ed.), pp. 385–447. Univ. of Chicago Press, Chicago.

Lutz, D. A., and Inoué, S. (1986). Techniques for observing living gametes and embryos. *In* "Methods in Cell Biology." (L. Wilson, Ed.), pp. 89–110. Academic Press, New York.

Lutz, D. A., Hamaguchi, Y., and Inoué, S. (1988). Micromanipulation studies of the asymmetric positioning of the maturation spindle in Chaetopterus sp. oocytes: I. Anchorage of the spindle to the cortex and migration of a displaced spindle. *Cell Motil. Cytoskel.* **11,** 83–96.

Margolis, R. L., and Wilson, L. (1981). Microtubule treadmills—possible molecular machinery. *Nature* **293,** 705–711.

Maxwell, J. C. (1881). "A Treatise on Electricity and Magnetism," 2nd ed. Clarendon, Oxford.

McIntosh, J. R. (1994). The roles of microtubules in chromosome movements. *In* "Microtubules." (J. Hyams and C. Loyyd, Eds.), pp. 413–434. Wiley–Liss, New York.

Mitchison, T., and Kirschner, M. (1984). Dynamic instability of microtubule growth. *Nature* **312,** 237–242.

Nicklas, R. B. (1971). *In* "Advances in Cell Biology." (D. M. Prescott, L. Goldstein, and E. H. McConkey, Eds.), pp. 225–298. Appelton–Century–Crofts, New York.

Nogales, E., Wolf, S., and Downing, K. (1998). Structure of the $\alpha\beta$ tubulin dimer by electron crystallography. *Nature* **391,** 199–203.

Oldenbourg, R. (1991). Analysis of edge birefringence. *Biophys. J.* **60,** 629–641.

Oldenbourg, R. (1996). A new view on polarization microscopy. *Nature* **381,** 811–812.

Oldenbourg, R., and Mei, G. (1995). New polarized light microscope with precision universal compensator. *J. Microsc.* **180,** 140–147.

Oldenbourg, R., and Ruiz, T. (1989). Birefringence of macromolecules: Wiener's theory revisited, with applications to DNA and Tobacco Mosaic Virus. *Biophys. J.* **56,** 195–205.

Oldenbourg, R., Salmon, E. D., and Tran, P. T. (1989). Birefringence of single and bundled microtubules. *Biophys. J.* **74,** 645–654.

Osborn, J. A. (1945). Demagnetizing factors of the general ellipsoid. *Physiol. Rev.* **67,** 351–357.

Palazzo, R. E., Vaisberg, E., Cole, R. W., and Rieder, C. L. (1992). Centriole duplication in lysates of *Spisula solidissima* oocytes. *Science* **256,** 219–221.

Perlmann, G. E., and Longsworth, L. G. (1948). The specific refractive increment of some purified proteins. *J. Am. Chem. Soc.* **70.**

Pickett-Heaps, J. D., and Tippit, D. H. (1978). The diatom spindle in perspective. *Cell* **14,** 455–467.

Priestly, E. B., Wojtowicz, P. J., and Sheng, P. (1979). "Introduction to Liquid Crystals." Plenum, New York.

Rieder, C. L., and Hard, R. (1990). Newt lung epithelial cells: Cultivation, use, and advantages for biomedical research. *Int. Rev. Cell Biol.* **122,** 153–220.

Ritter, H., Inoué, S. and Kubai, D. (1978). Mitosis in *Barbulanympha.* I. Spindle structure, formation and kinetochore engagement. *J. Cell Biol.* **77,** 638–654.

Roegiers, F., Tran, P., and Inoué, S. (1994). Mitosis, cleavage, and development of highly compressed sea urchin (*Lytechinus variegatus*) zygotes. *Biol. Bull.* **187,** 240–241.

Ruiz, T., and Oldenbourg, R. (1988). Birefringence of tropomyosin crystals. *Biophys. J.* **54,** 17–24.

Runnström, J. (1928). Die Veränderungen der Plasmabolloide bei der Entwicklungs-Erregung des Seeigeleies. *Protoplasma* **4,** 338–514.

Salmon, E. D. (1975). Spindle microtubules: Thermodynamics of in vivo assembly and role in chromosome movement. *Ann. N. Y. Acad. Sci.* **253,** 383–406.

Salmon, E. D., and Segall, R. R. (1980). Calcium-labile mitotic spindles isolated from sea urchin eggs (*Lytechinus variegatus*). *J. Cell Biol.* **86,** 355–365.

Salmon, E. D., and Wolniak, S. M. (1990). Role of microtubules in stimulating cytokinesis in animal cells. *Ann. N. Y. Acad. Sci.* **582,** 88–98.

Sardet, C., Speksnijder, J., Inoué, S., and Jaffe, L. (1989). Fertilization and ooplasmic movements in the ascidian egg. *Development* **105,** 237–249.

Sato, H., Ellis, G. W., and Inoué, S. (1975). Microtubular origin of mitotic spindle form birefringence. Demonstration of the applicability of Wiener's equation. *J. Cell Biol.* **67,** 501–517.

Schmidt, W. J. (1937). "Die Doppelbrechung von Karyoplasma, Zytoplasma und Metaplasma." Bornträger, Berlin.

Swann, M. M. (1951a). Protoplasmic structure and mitosis. I. The birefringence of the metaphase spindle and asters of the living sea urchin egg. *J. Exp. Biol.* **28,** 417–433.

Swann, M. M. (1951b). Protoplasmic structure and mitosis. II. The nature and cause of birefringence changes in the sea urchin egg at anaphase. *J. Exp. Biol.* **28,** 434–444.

Swann, M. M., and Mitchison, J. M. (1950). Refinements in polarized light microscopy. *J. Exp. Biol.* **27,** 226–237.

Taylor, J. R. (1997). "An Introduction to Error Analysis," 2nd ed. University Science Books, Sausalito, CA.

Tran, P., Salmon, E. D. and Oldenbourg, R. (1995). Quantifying single and bundled microtubules with the polarized light microscope. *Biol. Bull.* **189,** 206.

Tsvetkov, V. N. (1964). Flow birefringence. *In* "New Methods of Polymer Characterization." (B. Ke, Ed.). Interscience, New York.

Visser, T. D., Oud, J. L., and Brakenhoff, G. J. (1992). Refractive index and axial distance measurements in 3-D microscopy. *Optik* **90,** 17–19.

Wiener, O. (1912). Die Theorie des Mischkörpers für das Feld der stationären Strömung. *Abh. Math. Phys. Klas. Königl. Sächs. Gesellsch. Wiss.* **32,** 509–604.

CHAPTER 11

Micromanipulation of Chromosomes and Spindles in Insect Spermatocytes

Dahong Zhang[1] and R. Bruce Nicklas

DCMB Zoology
Duke University
Durham, North Carolina 27708-1000

I. Introduction

Micromanipulation is a useful technique for exploring several aspects of cell division, including spindle assembly, the interaction of chromosomes with the spindle, cell cycle regulation, and cytokinesis. The technique is also unbelievably simple. After only a few minutes of instruction, anyone can micromanipulate grasshopper spermatocytes (learning how to make good manipulation needles takes longer, however). The methodology and early findings of micromanipulation studies in cell division have been reviewed in-depth by Ellis and Begg (1981). The focus in this chapter is on the methods we use to manipulate insect

[1] Current address: Department of Zoology, 3029 Cordley Hall, Oregon State University, Corvallis, OR 97331.

METHODS IN CELL BIOLOGY, VOL. 61

0091-679X/99 $30.00

spermatocytes along with some examples of what can be done with a needle in a cell. We provide step-by-step descriptions of how micromanipulation is performed using a video/computer-enhanced polarization microscope in which chromosomes, centrosomes, and microtubules are readily seen. The examples of micromanipulation experiments in spermatocytes should give a general idea of what can be done with this technique in other systems in which cellular mechanics are of interest.

Micromanipulation of chromosomes and spindle components has been done primarily in spermatocytes of insects, such as praying mantids, crickets, crane flies, *Drosophila,* and especially grasshoppers. Grasshopper spermatocytes were among the first cells explored by microdissection (Kite and Chambers, 1912), and they have a number of favorable properties for micromanipulation. First, they have an extremely extensible cell surface that imposes no noticeable restriction on the movement of a microneedle. This property of the cell surface is crucial to easy micromanipulation because it allows free access with a microneedle to the interior of the cell without puncturing the cell. Contrary to what might be expected, the micromanipulation needle in grasshopper spermatocytes is not actually inside the cell, but instead the needle deforms the plasma membrane as it enters, much like a finger poked into a partly inflated balloon. This was long suspected (Carlson, 1952; Nicklas and Staehly, 1967) and finally proven by serial section electron microscopy of cells that were fixed with the needle in place (and then withdrawn after fixation): The space penetrated by the needle is lined by membrane all the way to the final position of the needle tip (unpublished observations on the cell shown in Fig. 2 in Ault and Nicklas, 1989). We suspect that the cell membrane in insect spermatocytes is essentially a naked lipid bilayer that flows around the needle as the needle is moved, relieving elastic stresses. Whatever the explanation, the cells are remarkably undisturbed by micromanipulation. Grasshopper spermatocytes tolerate very invasive manipulations, such as removal of all the chromosomes and centrosomes (Zhang and Nicklas, 1995a,b, 1996). Cells do sometimes die during incautious manipulation, when the needle grinds the membrane against the coverslip and the cell is punctured (seen as a dispersal of cell contents and increased chromosome density within seconds), but cells that survive an operation invariably live as long as unmanipulated control cells in the same preparation (Nicklas and Staehly, 1967). A second set of advantageous properties is that grasshopper spermatocytes remain flat during division, are optically clear, and have large chromosomes and spindles (30–45 μm in length). This makes chromosomes and spindle components exceptionally easy to see and to molest with a microneedle.

II. Preparing for Micromanipulation

A. Equipment

1. Microscope and Imaging System

Micromanipulation is usually carried out in intact, living cells visualized by video microscopy. Chromosome micromanipulations have been done primarily

with phase contrast microscopes (Nicklas and Staehly, 1967; Ellis and Begg, 1981). Polarization microscopy is used to visualize centrosomes and microtubules for micromanipulation (Inoué, 1988a,b; Nicklas and Ward, 1994; Zhang and Nicklas, 1995a,b; Zhang, in press). The video-enhanced, high-extinction/high-resolution polarization microscope we use was inspired by Shinya Inoué's designs (1986, 1988a) and built with his generous help. The microscope is an inverted Zeiss IM-35 stand equipped with an Ellis optical fiber light scrambler (Technical Video, Woods Hole, MA) to provide uniform, high-intensity illumination. The microscope has a rectified achromatic–aplanatic condenser with a numerical aperture (NA) of 1.4 and a 1.4 NA/60× plan apochromatic objective specially selected for high-extinction performance (Nikon, Inc., Melville, NY). A Nikon rectified 0.65 NA/40× objective is also used in micromanipulation of entire spindles. Images from a Newvicon video camera (Model 70, Dage-MTI, Michigan City, IN) are acquired and processed with an Image 1 system (Universal Imaging Corp., West Chester, PA) to adjust the analog video signal and to average several frames to reduce noise. The images are stored either on an optical disk recorder (Model 3038, Panasonic Video Systems, Secaucus, NJ) or on a computer hard disk for further image processing, particularly contrast enhancement and haze removal by unsharp masking.

2. Micromanipulator

The dynamic nature of the spindle and chromosomes in cell division requires micromanipulation with precise and rapid microneedle movement, without any drift or lag and with as little vibration as possible. The piezoelectric micromanipulators designed by Ellis (1962), especially the modified version with ceramic crystal transducers (Ellis and Begg, 1981), perfectly meet these requirements. Ellis manipulators can be constructed by any good instrument shop. A commercially available piezoelectric micromanipulator with a joystick controller is now in production (Model MIS5200, Burleigh Instruments, Inc., Fishers, NY) and is well worth investigating. Hydraulic (Narishige, USA, Inc., Sea Cliff, NY) or pneumatic manipulators (de Fonbrune-type, Technical Products International, Inc., St. Louis, MO) would suffice for some experiments.

In the operating head (Fig. 1a) of a piezoelectric micromanipulator, microneedle movement is controlled by voltage-driven bending of three ceramic crystals (see Ellis and Begg, 1981, for illustrations). Each crystal dictates needle movement on one axis. The voltage to the crystals is controlled by a joystick (Fig. 1b) much like that used for video games. As the joystick is moved, its output is fed to a well-regulated, three-channel power supply (Ellis and Begg, 1981) that determines the voltage at each crystal. The micromanipulator is mounted on a mechanical micropositioner (Fig. 1c) for coarse positioning of the microneedle [of the currently commercially available coarse position controllers, we suggest a ball slide positioning stage from Del-Tron (Bethel, CT) for horizontal control combined with the coarse and fine adjustment from a microscope for vertical control].

3. Vibration Absorption

For years we used foam rubber and steel plates on heavy tables to absorb external vibration. We have since found a better solution in the small and inexpensive, air-damped tables now available, such as the VW series from Newport Corp. (Irvine, CA). The tabletop (Fig. 1, d) "floats" on pneumatic vibration isolators. The micromanipulator and the microscope rest on the tabletop, whereas the manipulator joystick rests on a shelf (Fig. 1, e) mounted on the metal frame of the table, and thus it is not in mechanical contact with the tabletop. Hence, even clumsy operation of the joystick transmits no vibration to the micromanipulation needle.

4. Microforge

The microneedles used for micromanipulation can be made using the widely available de Fonbrune microforge (Technical Products International), but the optics are deficient. The ability to see the needle tip reasonably clearly is important because it is easy to replace a defective tip while at the microforge as opposed to discovering the defect after mounting the needle for micromanipulation. Microforges with satisfactory optics include the commercially available Narishige Model MF-900 (Narishige, USA, Inc.) and an inexpensive, custom-made microforge (Powell, 1952), which we have used. Powell's microforge (Fig. 2) is a modified bright field microscope that is attached to a plate so that the optical axis is horizontal rather than vertical. A platinum heating filament (Fig. 2, f) is mounted in a holder that fits in a centerable condenser holder so that the filament can be centered in the field of view of the microscope and also can be moved back and forth along the optical axis to bring the filament into focus after the tip of the microneedle is in focus. The temperature of the filament is controlled with an adjustable power supply. A holder for the microneedle (Fig. 2, h), mounted on the microscope's mechanical stage, can be rotated to change the angle of the glass tube relative to the heating filament.

B. Microneedle Fabrication

Microneedles for use in micromanipulation of chromosomes and spindle components are made of glass capillary tubes. It is easy to get a fine tip at the end of a long, slender glass fiber, but such a needle will be much too flexible to be of use. Instead, the microneedle must taper abruptly to a very fine tip, 0.1 to 0.2 μm in diameter. Making a proper microneedle requires glass with the right properties as well as skill in fabrication. We find that Pyrex glass tubes with an outer diameter of 0.85 mm and an inner diameter of 0.65 mm (Drummond Scientific, Broomall, PA) work well.

1. Making the First Joint

Before a microneedle can be fabricated in the microforge, one end of a glass tube is pulled by hand into a long and thin region that we call "the first joint."

This region measures ~10 mm long and is ~100 μm in diameter near the tip. The first joint is prepared using a natural gas microburner—simply a hypodermic needle stuck through a cork for support and attached to the gas jet with laboratory tubing; a thumbscrew on the tubing provides fine control of gas flow so that a flame about three times the diameter of the hypodermic needle tip can be produced. A piece of glass tubing is heated near one end, which is pulled straight out with forceps, generating a long, thin region (for use with the ordinary, open-top well slides used for phase contrast microcopy, the first joint is pulled at an angle of approximately 30°); the tubing is then broken in the thin region and the shorter piece is discarded. A few attempts may be needed to get a suitable length and thickness of the pulled-out region. Small adjustments may also be necessary to straighten the joint, which is done by gently heating the region at the flame and prodding it with forceps.

2. Making the Second Joint

The hand-pulled first joint is still much too thick for making a final tip. The end of the first joint is reduced to a diameter of ~10 μm using the microforge. The would-be microneedle is mounted in the microforge and the tip is brought into contact with the warm filament to melt a puddle of glass on the heating filament at the end of the first joint; the microneedle is then moved away from the filament with the stage controls, which pulls a thin glass fiber out from the puddle. The length of the second joint should be <1.5 mm; an excessive length may cause sluggish needle movement due to bending as the needle is dragged through the viscous halocarbon oil over the cells.

3. Shaping the Needle Shaft

Prior to making the final tip, a microneedle tube with a reduced diameter at one end should be bent, if necessary, into a desired shape to adapt to the geometric relations between the micromanipulator and the cell chamber. Only after the shape of the shaft is determined can the final tip be readily made in the correct orientation. The bends of the shaft are made with forceps at the hypodermic needle burner.

4. Making the Final Tip

The final tip is pulled at an angle of 45° to the second joint and should measure ~150 μm long and ~0.1 μm in diameter at the tip (Fig. 3; for microneedles for open-top well slides, the exact length is not critical, but it should be short). The needle holder is rotated so that the tip of the second joint is at an angle of 45° to the microforge heating filament (Fig. 3A). A desirable tip is very fine but stiff; a needle with a somewhat larger tip can be used, though with difficulty, but a long, flexible needle simply cannot be used. Tip diameter and length are

controlled by the filament temperature, the speed of pulling, and the timing of filament cooling. The heating filament should be adjusted to be as "cool" as possible, as long as it can barely melt the very end of the second joint, making a tiny puddle (Fig. 3A, arrow). The tip is pulled out of the puddle by rapidly moving the tubing up from the heating filament (Fig. 3B). Near the end of the pulling, the power supply of the heating filament is switched off to cool the filament so as to break the tip sharply (Fig. 3C), which prevents pulling a long and flexible tip. A slight variation that works better for some is to touch the second joint to the barely warm filament and then to *slowly* pull the tip a slight distance away from the filament until the warm glass forms an hourglass shape of increasingly narrow diameter; at the proper moment, the filament is turned off and its retraction as it cools will pull and break the tip. More often than not, the tip pulled will not be optimal, and then the process is simply repeated, many times if necessary, until an apparently satisfactory tip is obtained (we say "apparently" because the final test of any tip is in a cell, not at the microforge).

5. Microneedle Cleaning

Unlike disposable micropipettes, glass microneedles that are painstakingly made are valuable, and they should and can be used repeatedly. Sometimes they even last for years when special care is taken. Microneedles do get dirty but they are easily cleaned by immersing the tip in a sulfuric acid/dichromate cleaning solution (e.g., "Chromerge," Fisher Scientific, Pittsburgh, PA) for a few seconds. The tip should be rinsed in distilled water and then in acetone before use.

C. Cell Preparation

Laboratory colonies of the grasshopper *Melanoplus sanguinipes* (Fabricius) and *Chortophaga australior* (Rehn and Hebard) are the usual sources of the cells we use. Primary cultures of the spermatocytes are prepared according to the following procedures for polarization microscopy with the manipulation chamber of Ellis and Begg (1981) and Kiehart (1982) (procedures for phase contrast microscopy are described in detail by Nicklas *et al.*, 1979).

1. Dissecting the Testis

A nymph or an adult male grasshopper is cut open with a pair of dissecting scissors on the dorsal side of the abdomen, and the testis (Fig. 4A) is removed with fine forceps and placed in a petri dish containing Pipes-buffered saline (100 m*M* Pipes, 5.4 m*M* KCl, 13.5 m*M* $CaCl_2$, 0.5 m*M* $MgCl_2$, pH 6.8–6.9). The petri dish is then transferred to a dissecting microscope in a closed hood with the relative humidity raised to nearly 100% by boiling water. The fat around the follicles is carefully "combed" away with forceps (Fig. 4B) without tearing follicles away from the group.

2. Preparing Follicles

A group of about four follicles is taken out of the buffered saline by grasping them with forceps at their silvery ends (i.e., the ends that contain sperm and are distal to the free ends of the follicles), and the saline around the follicles and between the tips of the forceps is quickly removed using a wedge-shaped piece of filter paper (Fig. 4C). For ordinary manipulations viewed by phase contrast, the follicles are then transferred to a well slide filled with halocarbon oil (Voltalef 10S; Nicklas *et al.,* 1979). The follicles are cut open and the released cells are spread on the coverslip that forms the bottom of the well slide. For use with the special chamber for polarization microscopy, the follicles are stored briefly by submersion in a few drops of halocarbon oil to prevent evaporation.

3. Preparing Cells in a Chamber for Polarization Microscopy

The follicles are transferred into a puddle of halocarbon oil on a coverslip glued onto one side of a side-opening micromanipulation chamber slide (Ellis and Begg, 1981; Kiehart, 1982). The silvery, sperm-containing ends of the follicles are cut off with the beveled edge of a hypodermic needle (Fig. 4D) and discarded, and the released cells from the tips of the follicles are spread over the center of the coverslip by dragging each follicle tip on the coverslip. The top of the micromanipulation chamber is then covered with a coverslip, and the space (1 mm in thickness) between the two coverslips is completely filled with halocarbon oil. Cells in the chamber can be reached with a micromanipulation needle from the open side of the chamber.

The proper tonicity of cells in preparation is crucial to cell viability and success in micromanipulation. The chromosomes in hypertonic cells are more condensed than normal and are difficult to manipulate because they tend to stick together. In hypotonic cells, the spindle collapses and the chromosomes decondense and are hard to discern. Cell tonicity appears to vary with the temperature and humidity of the grasshopper's environment, the dilution of the buffer solution, and the amount of evaporation during cell preparation. In addition, cell tonicity increases gradually with time after the cell preparation is made. Thus, the final concentration of the buffered saline should be adjusted accordingly to make slightly hypotonic cells (chromosomes are slightly decondensed and appear more or less faint) when they are first prepared.

D. Microneedle Positioning

Insertion of a microneedle into an ordinary, open-top well slide used for phase contrast microscopy requires only a little practice. It is more difficult to insert a needle into the narrow (1 mm or less) opening in the open-sided chamber used for polarization microscopy, but it soon becomes routine if the following steps are carried out. Focus at the level of the cells with a 16 or 20× objective and

then move the chamber out of the field of view with the open side near the center of the field. Insert the microneedle into the micromanipulator and move the coarse vertical control so that the thin region of the needle is level with the stage. Center the needle in the field of view, move the tip downward into focus, and then bring the needle up ~100 μm so that the tip is slightly out of focus (using the width of the out-of-focus image of the tip as a gauge). Move the chamber back into the field of view and lower the needle until the tip is slightly above the cell. Finally, display the image of the cell on the video monitor and lower the needle further until it is seen on the monitor.

III. Manipulating Cell Components

Moving a microneedle in the horizontal plane of focus is very much like moving the cursor of a computer mouse on a monitor since a piezoelectric micromanipulator provides a direct relationship between hand movement on the joystick and microneedle movement. The movement is so natural that within a few minutes a novice stops thinking "OK, so I want to move the needle to touch that chromosome, how must I move my hand?" and simply moves the needle to the chromosome. Vertical movement of the needle moves the needle in and out of focus; the tip of the needle appears blurry and thicker when it is out of focus, either above or below the focal plane. The shank of the needle, however, comes into focus when the tip of the needle is below the focal plane and can be mistaken for the tip, which actually is close to the glass coverslip. To avoid grinding the cell against the coverslip or even breaking the needle when the tip is moved too low, the position of the needle tip needs to be checked frequently. Moving the tip in and out of focus aids in locating a tip that is hard or impossible to see when stationary.

A. Chromosome Micromanipulation

Using a microneedle, chromosomes can be stretched, detached from the spindle, moved wherever desired, or removed from the cell. A recent example of chromosome detachment and removal from grasshopper spermatocytes is diagrammed in Fig. 5A, in which the last chromosome is being removed from the cell (original contents, 11 bivalents plus the X chromosome). The chromosome (Fig. 5A, 1; blue) is detached from the spindle (green) at the kinetochores and then pulled against the cell membrane, generating a minicell that is connected to the original cell by a membrane tube (Fig. 5A, 2). Further pulling of the chromosome breaks the membrane tube and it fuses upon breakage, forming a cell without any chromosomes and a minicell with one chromosome (Fig. 5A, 3; the minicell is not shown). Cells with a reduced number of chromosomes or even no chromosomes can undergo "anaphase" and cytokinesis. Figure 5B shows such a cell undergoing cytokinesis. Notably, spindle microtubules (black fibers),

seen by video-enhanced polarization microscopy, spread toward the cell surface (Fig. 5B, 0- to 35-min images), and the cleavage furrow forms where microtubules come in contact with the cell cortex (Fig. 5B, 35-min image).

B. Centrosome Micromanipulation

Micromanipulation of centrosomes is possible because centrioles and astral microtubules are visible in video-enhanced polarization microscopy. A centrosome can be detached from the spindle as an entity including some associated microtubules, i.e., as an aster. Once detached, an aster can be moved to any desired position in the cell or even extracted from the cell, much as described for a chromosome. Typically, only a few, short astral microtubule are seen attached to the centrosome as it is removed from the cell. In grasshopper spermatocytes, centrosomes are indispensable in spindle assembly (Zhang and Nicklas, 1995a,b): Despite a potent enhancement of spindle microtubule mass by chromosomes, they cannot organize a spindle in the absence of centrosomes.

C. Microtubule Micromanipulation

Single microtubules or groups of a few microtubules can be moved as desired using micromanipulation plus video-enhanced polarization microscopy. For instance, spindle microtubules are known to play an essential role in controlling furrow formation; no furrow forms when the mitotic spindle is chemically or mechanically disrupted (Rappaport, 1996). However, the exact role that microtubules play is poorly understood. By tugging on the microtubules with a micromanipulation needle, physical interactions of microtubules with the cortex are observed in grasshopper spermatocytes (Zhang, in press). This interaction is indispensable for actin contractile ring formation: Mechanically blocking the interaction on one side of the spindle by sweeping microtubules away with a microneedle (Fig. 6A, 1) inhibits formation of the contractile ring on the operated side (Fig. 6A, 2 and 6B).

References

Ault, J. G., and Nicklas, R. B. (1989). Tension, microtubule rearrangements, and the proper distribution of chromosomes in mitosis. *Chromosoma* **98,** 33–39.

Carlson, J. G. (1952). Microdissection studies of the dividing neuroblast of the grasshopper, *Chortophaga viridifasciata* (De Geer). *Chromosoma* **5,** 199–220.

Ellis, G. W. (1962). Piezoelectric micromanipulators. *Science* **138,** 84–91.

Ellis, G. W., and Begg, D. A. (1981). Chromosome micromanipulation studies. *In* "Mitosis/Cytokinesis" (A. M. Zimmermann and A. Forer, Eds), pp. 155–179. Academic Press, New York.

Inoué, S. (1986). "Video Microscopy." Plenum, New York.

Inoué, S. (1988a). Progress in video microscopy. *Cell Motil. Cytoskel.* **10,** 13–17.

Inoué, S. (1988b). Manipulating single microtubules. *Protoplasma Suppl.* **2,** 57–62.

Kiehart, D. P. (1982). Microinjection of echinoderm eggs: Apparatus and procedures. *Methods Cell Biol.* **25,** 13–31.

Kite, G. L., and Chambers, R., Jr. (1912). Vital staining of chromosomes and the function and structure of the nucleus. *Science* **36,** 639–641.

Nicklas, R. B., and Staehly, C. A. (1967). Chromosome micromanipulation. I. The mechanics of chromosome attachment to the spindle. *Chromosoma* **21,** 1–16.

Nicklas, R. B., and Ward, S. C. (1994). Elements of error correction in mitosis: Microtubule capture, release, and tension. *J. Cell Biol.* **126,** 1241–1253.

Nicklas, R. B., Brinkley, B. R., Pepper, D. A., Kubai, D. F., and Rickards, G. K. (1979). Electron microscopy of spermatocytes previously studied in life: Methods and some observations on micromanipulated chromosomes. *J. Cell Sci.* **35,** 87–104.

Powell, E. O. (1952). A microforge attachment for the biological microscope. *J. R. Microsc. Soc.* **72,** 214–217.

Rappaport, R. (1996). "Cytokinesis in Animal Cells." Cambridge Univ. Press, Cambridge, UK.

Zhang, D. Mechanical control of cell cleavage by spindle microtubules. *Proc. Natl. Acad. Sci. USA,* in press.

Zhang, D., and Nicklas, R. B. (1995a). The impact of chromosomes and centrosomes on spindle assembly as observed in living cells. *J. Cell Biol.* **129,** 1287–1300.

Zhang, D., and Nicklas, R. B. (1995b). Chromosomes initiate spindle assembly upon experimental dissolution of the nuclear envelope in grasshopper spermatocytes. *J. Cell Biol.* **131,** 1125–1131.

Zhang, D., and Nicklas, R. B. (1996). "Anaphase" and cytokinesis in the absence of chromosomes. *Nature* **382,** 466–468.

CHAPTER 12

Microinjection of Mitotic Cells

Patricia Wadsworth

Department of Biology
Morrill Science Center
University of Massachusetts
Amherst, Massachusetts 01003

I. Introduction

Direct needle microinjection is a highly precise method that can be utilized to deliver diverse macromolecules into living cells (Celis *et al.*, 1980; Graessmann *et al.*, 1980; Ansorge, 1982; Kreis and Birchmeier, 1982). In this article, I review methods for direct needle microinjection and discuss the application of this method to the study of mitotic cells. Other "injection" methods, including liposome or red blood cell ghost fusion and scrape and bead loading, will not be discussed here (Celis *et al.*, 1980; McNeil, 1989). Because virtually any molecule of interest that can be purified, and obtained at an appropriate concentration, can be injected into the living mitotic cell, this method can be utilized to study how diverse molecules participate in the events of mitosis.

Although remarkable progress has been made in the development of *in vitro* systems to study the events of mitosis (Chapters 3 and 19), in many cases direct analysis of the living cell remains a unique and important approach (see Chapters

METHODS IN CELL BIOLOGY, VOL. 61

0091-679X/99 $30.00

11, 16, and 20). Microinjection of mitotic cells combines high-resolution light microscopic analysis of mitotic events in the living cell with the ability to selectively modify and/or monitor specific molecules. For example, mitotic cells can be injected with function blocking antibodies and various inhibitors or toxins to determine the contribution of the targeted molecules to mitosis (Dinsmore and Sloboda, 1989; Lee, 1989a; Nislow *et al.*, 1990; Vaisberg *et al.*, 1993; Compton and Cleveland, 1994; Tomkiel *et al.*, 1994; Blangy *et al.*, 1995; Campbell and Gorbsky, 1995; Byrd *et al.*, 1996; Lane and Nigg, 1996). A recent report also demonstrates that microinjected mRNA molecules can be translated in mitotic cells, thus providing an additional means to modify the molecular composition of the injected cell (Wheatly *et al.*, 1997).

In addition to inhibiting the normal function of target molecules, it is also possible to monitor the behavior and distribution of various molecules during mitosis. A particularly productive approach has been the microinjection of purified cellular proteins that have been derivatized with fluorescent or caged fluorescent reagents (Kreis and Birchmeier, 1982; Wadsworth and Salmon, 1986a; Gorbsky *et al.*, 1988; Mitchison, 1989; Hepler *et al.*, 1994; Wilding *et al.*, 1995). Photobleaching or photoactivation of the tagged molecules can then provide information regarding the location(s) of assembly and disassembly and the rate of turnover of the marked molecules in living cells. The application of these methods to mitotic cells has provided novel information concerning the location of microtubule disassembly during mitosis, the behavior of marked regions on spindle microtubules, and quantitative information regarding the rate of spindle microtubule turnover (Wadsworth and Salmon, 1986a,b; Gorbsky *et al.*, 1988; Mitchison, 1989; Mitchison and Salmon, 1992; Zhai *et al.*, 1995).

An important and unique advantage of microinjection as a means to introduce various molecules into mitotic cells is that the injection can be precisely timed. Thus, the disruption of a targeted molecule or the behavior of a marked molecule can be tested in the living cell at a particular stage, or stages, of mitosis. The advantage of this precise temporal control is clearly evident from the results of recent experiments. Microinjection of anti-dynein antibodies at prophase blocks spindle formation; injection at later stages of mitosis is without detectable effect on the process of mitosis, thus demonstrating that spindle formation is uniquely sensitive to the injected antibodies (Vaisberg *et al.*, 1993). Similarly, injection of antibodies to a 62-kDa mitotic phosphoprotein at metaphase blocks anaphase; injection after anaphase onset has no effect on chromosome motion and cytokinesis, but the subsequent mitosis is blocked (Dinsmore and Sloboda, 1989). Microinjection experiments have also provided information regarding the regulation of kinetochore fiber disassembly during anaphase. Injection of a high concentration of tubulin during early anaphase induced reversal of chromosome motion and elongation of kinetochore fiber microtubules at their kinetochore proximal plus ends (Shelden and Wadsworth, 1992), demonstrating that during anaphase kinetochores can temporarily switch the direction of motion in response to an elevation in the tubulin concentration.

The precise temporal control afforded by direct needle microinjection can be contrasted with other means of introducing molecules into cells. For example, transfection is widely utilized to express cloned gene products in cells. However, the methods by which DNA is taken up by cells are harsh and cells must be incubated for 24–48 hr before observation to permit cell recovery and to allow the expressed protein to accumulate in the cells. In some cases, transfection has been shown to block cells in mitosis, thus implicating the transfected molecule in the progression of mitosis. For example, transfection with the gene encoding the 50-kDa subunit of the dynactin complex results in an accumulation of cells in a prometaphase-like condition, characterized by condensed, but unaligned, chromosomes and markedly asymmetric spindles; it is possible that the expressed protein functions in later events of mitosis as well, but this cannot be determined by this approach (Echeverri *et al.,* 1996). Note, however, that it is possible to inject plasmids, containing a cDNA of choice, into living cells. However, there is a lag between plasmid injection protein production, so this method may not be suitable for mitotic cells (Mittal *et al.,* 1992). Clearly, a major advantage of direct needle microinjection is that the precise temporal control allows one to determine the contribution of a various molecules to specific stages, or events, of mitosis.

An additional advantage of microinjection is that the concentration of the injectate can be varied, and the minimum concentration necessary to alter particular mitotic events can be.used (Lee, 1989b). The volume that is injected can be determined by several different methods; with practice, injections of relatively constant volume can be achieved. Most important, however, the process of mitosis can be recorded at high resolution following the injection, and any alterations in the mitotic process can be evaluated.

Microinjection of solutions of molecules into mitotic cells should be distinguished from micromanipulation, a method used to apply forces to chromosomes, and other parts of the spindle, during mitosis. In micromanipulation, the microneedle does not perforate the plasma membrane; rather, the membrane is deformed, and the microneedle is used to tug and pull on chromosomes (Nicklas and Staehly, 1967; see Chapter 10).

II. Choice of Cells

Various cells can be used for microinjection during mitosis. A key characteristic is that the cells remain flat throughout mitosis so that the spindle and chromosomes can be visualized (Wadsworth and Salmon, 1986a; Wadsworth *et al.,* 1989; Shelden and Wadsworth, 1990, 1992). The cultured epithelial cell lines, PtK1 and PtK2, are frequently used: the cells are easy to grow, and given the low chromosome number (2n = 12 and 13 for PtK1 and PtK2, respectively), the behavior of individual chromosomes can be monitored. LLCPK cells, an epithelial cell line with morphology similar to PTKs, have also been utilized with

excellent results (Gorbsky *et al.,* 1987, 1988; Zhai *et al.,* 1995). In addition, BSC-1 cells, an epithelial-like kidney cell line, remain flat during mitosis and have a large, clearly visible spindle. However, BSC-1 cells have numerous, small chromosomes, so following the behavior of individual chromosomes is not possible (P. Wadsworth, unpublished observations).

We do not synchronize cultured cells for injection during mitosis. First, most synchronization regimes are very time-consuming and often involve drugs that alter microtubules, the structures that we are interested in examining in injected cells (Telzer and Rosenbaum, 1979). In our hands, it is difficult to adjust the cell density so that optimum synchronization is obtained and so that the cells remain well spread on the coverslip after the synchronization process is complete. In our lab, we have found that if cells are plated at a moderately high density (approximately 10^4 cells/ml) and utilized 36–48 hr after plating, numerous mitotic cells are present and the cells are well spread for injection and subsequent observation (Fig. 1).

Primary cultures of newt lung epithelial cells also remain flat throughout mitosis and have the distinct advantage of exceptionally large cell size (Wadsworth and Salmon, 1986b; Cassimeris and Salmon, 1991; Mitchison and Salmon, 1992; Waters *et al.,* 1996). The procedures for culture of newt lung epithelial cells have been recently reviewed (Rieder and Hard, 1990). Finally, many different kinds of eggs and early embryos are also suitable for microinjection during mitosis. Echinoderm eggs and embryos have been extensively utilized for microinjection

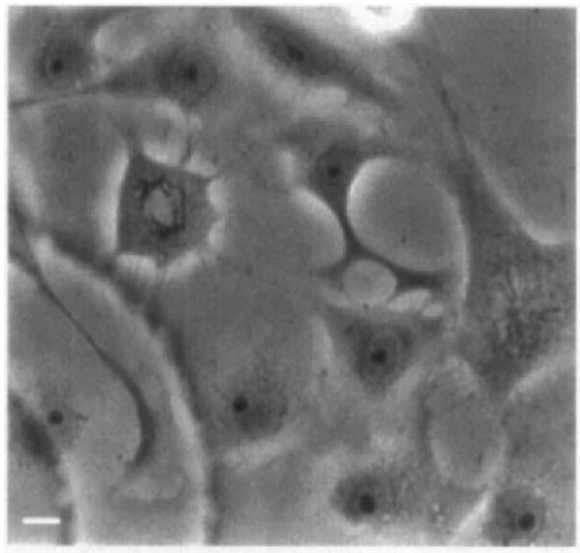

Fig. 1 Phase contrast light micrograph of PtK1 cells plated on a gridded coverslip for injection. The etched number on the coverslip can be seen in the lower left. In this field two mitotic cells can be seen; both are suitable for injection. Scale bar = 50 μm.

studies during mitosis—the natural synchrony of fertilized eggs makes them ideal for such studies. Movement of the spherical egg during injection can be prevented by using an appropriately designed injection chamber and recent advances in confocal microscopy greatly enhance the imaging of fluorescent molecules in these and other spherical cells (Terasaki, 1996). Methods used for the injection of echinoderm eggs have been described in detail by Kiehart (1982). Eggs and/or early embryos of the zebrafish, frog, and fruit fly are also readily injected; the techniques utilized for injections of these cells will not be discussed here (Karess, 1984; Spradling, 1986; Westerfield, 1993; Matten and Vande Woude, 1995). Finally, it has recently become practical to microinject walled plant cells during mitosis; the procedures for plant cell injection are outlined in Chapter 20.

III. Timing of Injection

A major advantage of microinjection experiments during mitosis is that the cell can be injected at a defined point in the mitotic cycle. In our experiments we visually inspect mitotic cells using phase contrast to determine the stage of mitosis; differential interference contrast optics can also be utilized (see Chapters 16 and 20). Cells can be easily microinjected during prometaphase, metaphase, anaphase, and telophase. Prometaphase PtK1 cells are frequently flatter and more well spread than metaphase cells, thus making this stage particularly amenable for injection. Cellular morphology can be recorded before, during, and after injection using a suitable camera and video or digital recording methods. Control experiments demonstrate that injected cells complete mitosis and cytokinesis normally and the rate of chromosome motion is not different from that measured in uninjected control cells (Shelden and Wadsworth, 1992).

We have also injected cells just at or just prior to nuclear envelope breakdown (NEBD). In some cases, injection at or near NEBD delays entry into mitosis, and in some cases injected cells revert to interphase (P. Wadsworth, unpublished results). The reason for this disruption is not known, but it is possible that entry of calcium from the media into the cells at this key transition point may disrupt passage of the cell into mitosis.

IV. Microinjection Procedure

A. Microinjection Chambers

In our laboratory, we subculture cells onto gridded coverslips (Bellco Glass Co., Vineland, NJ) to facilitate subsequent localization of the injected cells. The gridded coverslip is held in one of two types of chamber, depending on experimental design. If the cells are to be monitored by high-resolution light microscopy immediately following injection, the coverslip is mounted in a modi-

fied Rose chamber held on an inverted microscope (Rose *et al.,* 1958). To construct the Rose chamber, we cut two pieces of parafilm to the dimensions of the Rose chamber. The bottom of the chamber is covered with one piece of parafilm, followed by the coverslip containing the cells, the second piece of parafilm, and the top of the chamber, and they are screwed together. The chamber is quickly filled with media and left uncovered during the injection process. Immediately following injection, a 25-mm-diameter round coverslip is added, sealing the top of the chamber (Fig. 2a). Cell culture media without bicarbonate and with 20 m*M* Hepes buffer is used during injection; media that is also lacking phenol red is used for fluorescence microscopy. The Rose chamber is held on the stage of an inverted microsope in a custom machined stage plate (Micro Video Instruments, Inc., Avon, MA) (Fig. 3). When the Rose chamber is held in this way, a cell can be injected at low magnification and subsequently relocalized at high magnification, with no detectable motion of the specimen. If a custom stage holder is not available, then the Rose chamber can be held by the stage clips, for example, on the rotatable stage of the Nikon Diaphot. In our work, we have been extremely satisfied with the Rose chamber for ease of handling, tightness of the seal, cell viability, and, after the initial investment, low cost.

Alternatively, if the cells are to be injected first and examined at a later time, then injection can be performed with the gridded coverslip held either in the plastic petri dish used for cell culture or in a laboratory designed chamber assembled as follows: An 18-mm-diameter hole is drilled in a 51- × 76-mm glass slide, a coverslip is glued over the hole using nail polish, and a layer of Silgard (approximately 5 mm thick) is polymerized on the surface of the slide. The polymerized Silgard is cut, leaving a "frame" with an opening of 25 mm^2 centered over the hole in the slide; the Silgard frame is further sealed to the slide with silicone sealant (Fig. 2b). The chamber, thus formed, is filled with media, and a coverslip of cells can be placed in the bottom for injection. These reusable chambers have the advantages that they are optically superior to the culture

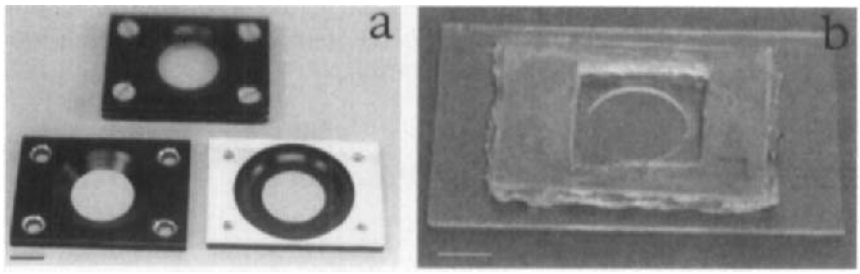

Fig. 2 (a) Rose chambers used for microinjection. An assembled Rose chamber, left open for microinjection, is shown at the top; the top (left) and bottom (right) pieces of the unassembled chamber are shown at the bottom of the photograph. Note that the bottom is machined so that an objective lens does not hit the sloping sides of the bottom plate. Scale bar = 10 mm. (b) A laboratory-constructed injection chamber. See text for details of assembly. Scale bar = 10 mm.

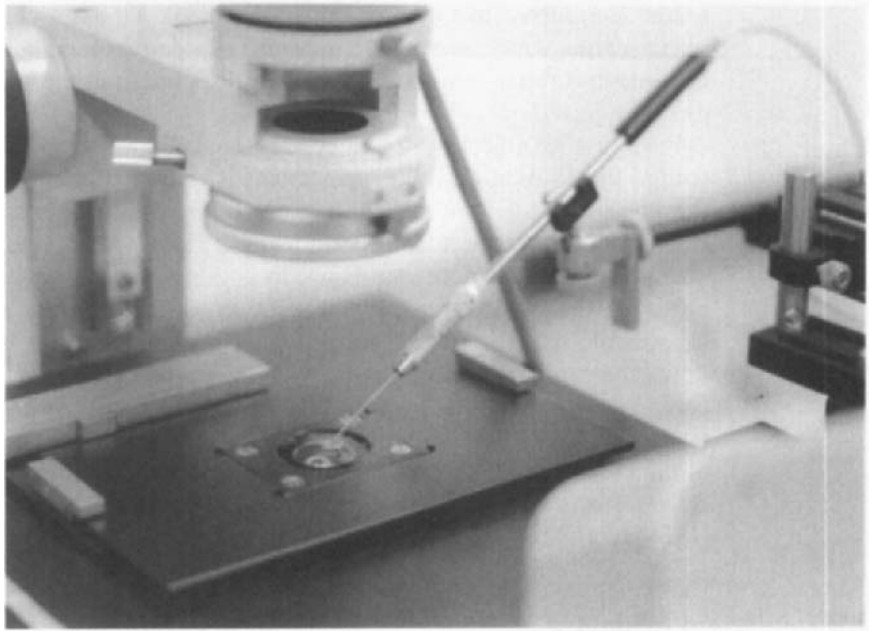

Fig. 3 The modified Rose chamber held in a custom machined stage plate on an inverted microscope. The needle is shown in position for injection.

dishes and the slide on which they are constructed can be held securely on the microscope stage. For subsequent high-resolution work, the coverslip is removed and placed in a Rose chamber as described previously. Finally, it is possible to make or purchase culture dishes that have a coverslip bottom (Mattek, Inc., Ashland, MA); this dish can then be used for both injection and subsequent observation.

B. Micropipettes

Micropipettes are pulled from Omega dot capillary glass (Friedrich and Dimmock, Millville, NJ), of outer diameter 1.2 mm and inner diameter 0.9 mm, containing an internal filament. Pipettes are pulled using a Sutter Instruments (San Raphel, CA) Brown Flaming P-80 micropipette puller. Brown Flaming pipette pullers are equipped with a tank of nitrogen gas that provides a cooling "puff" on the pipette tip just after the pull is complete. With this instrument we can routinely pull needles with inner tip diameter of <1 μm that are ideal for injection of mammalian cells in general and mitotic cells in particular. Micropipettes are pulled the day they are to be utilized and covered prior to use to keep them free of dust. For routine work, we have not found it necessary to clean or coat the glass prior to pulling; for cleaning capillary glass prior to pulling the

reader is referred to Graessmann *et al.* (1980). The size of the opening of the microneedle, which is typically in tenths of micrometers, is far greater than the dimensions of macromolecules and thus does not limit the size of molecules that can be injected.

Prior to microinjection, the injectate is centrifuged at top speed in an microcentrifuge for 15 min, and the supernatant is removed, taking care not to disturb the invisible pellet, and placed in a clean microcentrifuge tube. The solution is back loaded into the micropipette using a Hamilton syringe. Because the glass has an internal filament, the solution is drawn to the tip by capillarity. Note, however, that we deliver the test solution as far down the shaft of the pipette as possible to prevent the collection of contaminants as the solution moves down the capillary wall and to prevent a chromatography effect, wherein buffer components would tend to move faster toward the tip than large macromolecules (Ansorge, 1982). In many cases, it is helpful to include a fluorescent dextran or other inert fluorescent molecule in the injection solution to confirm that the cells were injected or to positively identify the injected cell at a later time (McNeil, 1989).

C. Microinjection Method

To perform microinjection, we utilize a Narishige 3D hydraulic micromanipulator and a coarse, 3D manipulator (Narishige) attached directly to the microscope stage. The pressure for injection is provided by a tank of nitrogen gas regulated by an Eppendorf 5242 Injector. This injector has three pressure settings: a holding pressure to prevent media components from entering the tip of the needle, an injection pressure, and a high pressure for clearing the tip of a clogged microneedle (Ansorge, 1982). All three pressures can be adjusted. To inject cells with tubulin, a dimer of molecular weight 100 kDa, the injection pressure is set to the high end of the allowable range (1500–2000 hPa); for smaller molecules the injection pressure must be greatly reduced. The clearing pressure is set at 6000 hPa; for small molecules this pressure is usually sufficient to clear a clogged needle tip. In the case of tubulin, clogged needles are usually discarded, because the clearing pressure is often insufficient to clear the protein from the tip. The holding pressure is set at a low value (50 hPa), which is insufficient to cause noticeable movement of the injectate out of the needle tip but which prevents movement of media into the needle tip.

The chamber containing the cells to be injected is placed on the microscope stage, and the cells are brought into focus using a 10 or 20× phase objective and a long working distance phase condenser. The loaded pipette is placed in the pipette holder and roughly positioned, using the X and Y controls of the coarse manipulator, so that the needle tip is centered over the objective lens. This is easily accomplished while viewing the preparation from above (i.e., not through the oculars). To avoid drying of the solution at the micropipette tip, the needle tip is lowered into the media above the cells using the Z control of the coarse

manipulator. Note that care must be taken to avoid lowering the needle tip too far toward the cells, thus breaking the needle tip. The image of the out-of-focus pipette is then centered in the field of view using the controls of the micromanipulator. In initial attempts, the needle may not lie within the field of view, even using a 10× objective lens, and a series of adjustments with the X and Y controls of the coarse manipulator may be needed. With practice, however, the needle can be roughly centered in the field of view by the coarse adjustment and quickly brought to into position using the X, Y, and Z controls of the micromanipulator. Note that prior to the injection, the needle is held above the focal plane of the cells and is thus out of focus.

In our lab, we perform microinjection using a 32× phase objective lens that uses the same long working distance phase 1 condensor as the 10 and 20× objectives. Alternatively, needle alignment can be performed at low magnification and injection can be performed at 40×. Note, however, that most 40× phase lenses do not use a phase 1 condensor, so the condensor setting must be adjusted.

For injection, the cell of interest is moved to the center of the field of view using the stage controls, and the focus is checked. Next, the needle is lowered until it is just above the cell using the Z control of the micromanipulator. The injection pressure is activated, usually by means of a foot pedal, and the flowing needle is lowered into the cell. In interphase cells, the flow of the injection solution into the cell can be readily detected as a wave moving from the needle tip due to the change in refractive index of the cytoplasm as the solution flows into the cell. In mitosis, the rounded nature of the cells makes it more difficult to observe the injectate entering the cell. To ensure a successful mitotic injection, an interphase cell adjacent to the selected mitotic cell is injected first so that the flow characteristics of the particular needle can be assessed. Without turning off the injection pressure, the needle is then moved to the mitotic cell of interest, and the mitotic cell is injected. In this way, one can be sure that the rate of flow is appropriate for the injection and that the needle is not clogged.

During the microinjection procedure, it is important that the microscope and micromanipulator be isolated from vibrations, which can injure the cell that is being injected. We find that a 0.5-in. steel plate placed on four tennis balls, or four extra-large rubber stoppers, is sufficient to dampen most vibrations that occur in our building. One source of vibration is the air curtain incubator used to warm the microscope; we have attached our incubator to a movable, wall-mounted arm to reduce this source of vibration. In some cases, however, building vibration cannot be easily removed and a pneumatic vibration isolation table is essential. These tables are "floated" with nitrogen gas, which effectively isolates the microscope and microinjection components from building vibrations. Vibration isolation tables are available from several manufacturers (Technical Manufacturing Co., Peabody, MA; Kinetic Systems, Boston, MA; Newport Corp., Fountain Valley, CA).

Finally, it is essential that the cells are kept healthy during the injection process. For experiments in which the cells will be returned to the 37°C incubator before

analysis at high resolution, we inject the cells at room temperature; this reduces evaporation of the media from the open dish and the cells can tolerate short periods at room temperature. When the cells are later placed in the Rose chamber, it is sealed to prevent evaporation and placed on the warmed microscope. For experiments in which cells are to be injected and observed immediately, the microscope is preheated, and the chamber is opened only for the brief period needed to inject the cell(s). Alternatively, oil can be layered over the media in the dish or chamber (Gorbsky *et al.,* 1988). We use an air curtain incubator and a laboratory-built Plexiglas chamber around the microscope, similar to that described by McKenna and Wang (1989), to maintain the microscope and preparation at 36 ± 1°C.

Several methods are available to measure the volume of a solution injected into the cell. One approach is to microinject radioactively labeled molecules and determine the radioactivity of the injected cells (Stacey, 1976; Graessmann *et al.,* 1980; Zavortink *et al.,* 1983). Alternatively, one can coinject a fluorescent dye and measure the fluorescence of the injected cell. The fluorescence can then be compared with a standard curve of fluorescence of known volumes (Lee, 1989a). Using these methods, the volume injected has been measured and ranges from 0.01 to 2.8 pl (Stacey, 1976; Graessmann *et al.,* 1980; Keith *et al.,* 1983; Zavortink *et al.,* 1983; Lee, 1989a). To determine the percentage of cell volume that is injected, the cell volume must also be determined. This is usually done by measuring the diameter of the detached, rounded cell. For cultured cells, the volume has been estimated as 10–20 pl (Keith *et al.,* 1983; Lee, 1989b). For cases in which both the volume injected and the cell volume have been reported, the percentage of cell volume injected ranges from 1 to 20%. In our experience, cells tolerate microinjection remarkably well, rapidly adjusting cell volume postinjection and maintaining vital cell processes (Shelden and Wadsworth, 1992).

V. Conclusions

In this article, I have briefly reviewed the methods that we utilize to microinject cultured animal cells during mitosis. As stated in the Introduction, direct needle microinjection allows one to introduce virtually any molecule into the dividing cell, at a time that is selected by the experimenter. This approach has provided considerable insight into the contribution of various molecules to mitosis and has allowed the introduction of fluorescently tagged molecules into mitotic cells. It is important to note, however, that many new applications of the method may be forthcoming. For example, the ability to express and purify protein products of wild-type or mutant genes will permit the analysis of the contribution of these molecules to mitosis. In addition, fluorescent probes, which mark specific cell structures or target cellular molecules, and green fluorescent protein fusion proteins, are increasingly available for microinjection studies. These specific probes are likely to provide important new information regarding the role of specific

gene products in the mitotic cell. Perhaps the key advantage of the microinjection method, however, is that it is noninvasive, and the events of mitosis can be observed directly in the living cell.

References

Ansorge, W. (1982). Improved system for capillary microinjection into living cells. *Exp. Cell Res.* **140,** 31–37.

Blangy, A., Lane, H. A., d'Herin, P., Harper, M., Kress, M., and Nigg, E. A. (1995). Phosphorylation by p34cdc2 regulates spindle association of human Eg5, a kinesin related motor essential for bipolar spindle formation in vivo. *Cell* **83,** 1159–1169.

Byrd, P., Wise, D., and Dentler W. L. (1996). Mitotic arrest in PtK2 cells induced by microinjection of a rabbit antiserum and affinity purified antibodies against a 66kDa PtK2 cell polypeptide. *Cell Motil. Cytoskel.* **34,** 57–68.

Campbell, M. S., and Gorbsky, G. J. (1995). Microinjection of mitotic cells with the 3F3/2 anti-phosphoepitope antibody delays the onset of anaphase. *J. Cell Biol.* **129,** 1195–1205.

Cassimeris, L., and Salmon, E. D. (1991). Kinetochore microtubules shorten by loss of subunits at the kinetochores of prometaphase chromosomes. *J. Cell Sci.* **98,** 151–158.

Celis, J. E., Kaltoft, K., and Bravo, R. (1980). Microinjection of somatic cells. *In* "Introduction of macromolecules into Viable Mammalian Cells" (R. Baserga, C. Croce, and G. Rovera, Eds.), pp. 99–123. A. R. Liss, New York.

Compton, D. A., and Cleveland, D. W. (1994). NuMA, a nuclear protein involved in mitosis and nuclear reformation. *Curr. Opin. Cell Biol.* **6,** 343–346.

Dinsmore, J. H., and Sloboda, R. D. (1989). Microinjection of an antibody to a 62kd mitotic apparatus protein arrests mitosis in dividing sea urchin embryos. *Cell* **57,** 127–134.

Echeverri, C. J., Paschal, B. M., Vaughan, K. T., and Vallee, R. B. (1996). Molecular characterization of the 50-kD subunit of dynactin reveals function for the complex in chromosome alignment and spindle organization during mitosis. *J. Cell Biol.* **132,** 617–633.

Gorbsky, G. J., Sammak, P. J., and Borisy, G. G. (1987). Chromosomes move poleward in anaphase along stationary microtubules that coordinately disassemble from their kinetochore ends. *J. Cell Biol.* **104,** 9–18.

Gorbsky, G. J., Sammak, P. J., and Borisy, G. G. (1988). Microtubule dynamics and chromosome motion visualized in living anaphase cells. *J. Cell Biol.* **106,** 1185–1192.

Graessmann, A., Graessman, M., and Muller, C. (1980). Microinjection of early SV40 DNA fragments and T antigen. *Methods Enzymol.* **65,** 816–825.

Hepler, P. K., Sek, F. J., and John, P. C. (1994). Nuclear concentration and mitotic dispersion of the essential cell cycle protein p13suc1, examined in living cells. *Proc. Natl. Acad. Sci. USA* **91,** 2176–2180.

Karess, R. E. (1984). Analysis of P transposable element functions in Drosophilia. *Cell* **38,** 135–146.

Keith, C. H., DiPaola, M., Maxfield, F. R., and Shelanski, M. (1983). Microinjection of Ca-calmodulin causes a localized depolymerization of microtubules. *J. Cell Biol.* **97,** 1918–1924.

Kiehart, D. P. (1982). Microinjection of echinoderm eggs: Apparatus and procedures. *In* "Methods in Cell Biology" (L. Wilson, Ed.), pp. 13–31. Academic Press, New York.

Kreis, T. E., and Birchmeier, W. (1982). Microinjection of fluorescently labeled proteins into living cells with emphasis on cytoskeletal proteins. *Int. Rev. Cytol.* **75,** 209–227.

Lane, H. A., and Nigg, E. A. (1996). Antibody microinjection reveals an essential role for human polo-like kinase 1 in the functional maturation of mitotic centrosomes. *J. Cell Biol.* **135,** 1701–1713.

Lee, G. M. (1989a). Characterization of mitotic motors by their relative sensitivity to AMP-PNP. *J. Cell Sci.* **94,** 425–441.

Lee, G. M. (1989b). Measurement of volume injected into individual cells by quantitative fluorescence microscopy. *J. Cell Sci.* **94,** 443–447.

Matten, W. T., and Vande Woude, G. F. (1995). Microinjection into Xenopus oocytes. *Methods Enzymol.* **254,** 458–466.

McKenna, N. M., and Wang, Y.-L. (1989). Culturing cells on the microscope stage. *In* "Fluorescence Microscopy of Living Cells in Culture" (Y.-L. Wang and D. L. Taylor, Eds.), pp. 195–205. Academic Press, New York.

McNeil, P. L. (1989). Incorporation of macromolecules into living cells. *In* "Fluorescence Microscopy of Living Cells in Culture. Part A" (Y.-L. Wang and D. L. Taylor, Eds.), pp. 153–173. Academic Press, New York.

Mitchison, T. J. (1989). Polewards microtubule flux in the mitotic spindle: Evidence from photoactivation of fluorescence. *J. Cell Biol.* **109,** 637–652.

Mitchison, T. J., and Salmon, E. D. (1992). Poleward kinetochore fiber movement occurs during both metaphase and anaphase-A in newt lung cell mitosis. *J. Cell Biol.* **119,** 569–582.

Mittal, B., Danowski, B. A., Sanger, J. M., and Sanger, J. W. (1992). Expression of desmin cDNA in PtK2 cells results in assembly of desmin filaments from multiple sites throughout the cytoplasm. *Cell Motil. Cytoskel.* **23,** 188–200.

Nicklas, R. B., and Staehly, C. A. (1967). Chromosome micromanipulation I. The mechanics of chromosome attachment to the spindle. *Chromosoma* **21,** 1–16.

Nislow, C., Sellitto, C., Kuriyama, R., and McIntosh, J. R. (1990). A monoclonal antibody to a mitotic microtubule-associated protein blocks mitotic progression. *J. Cell Biol.* **111,** 511–522.

Rieder, C. L., and Hard, R. (1990). Newt lung epithelial cells: Cultivation, use, and advantages for biomedical research. *Int. Rev. Cytol.* **122,** 153–220.

Rose, G. G., Pomerat, C. M., Shindler, T. O., and Trunnel, J. B. (1958). A cellophane strip technique for culturing tissue in multipurpose culture chambers. *J. Biophys. Biochem. Cytol.* **4,** 761–764.

Shelden, E., and Wadsworth, P. (1990). Interzonal microtubules are dynamic during spindle elongation. *J. Cell Sci.* **97,** 273–281.

Shelden, E., and Wadsworth, P. (1992). Injection of biotin–tubulin into anaphase cells induces transient elongation of kinetochore microtubules and reversal of chromosome-to-pole motion. *J. Cell Biol.* **116,** 1409–1420.

Spradling, A. C. (1986). P-element-mediated transformation. *In* "Drosophila a Practical Approach" (D. B. Roberts, Ed.), pp. 175–197. IRL Press, Oxford.

Stacey, D. W. a. V. G. A. (1976). Microinjection studies of duck globin messenger RNA translation in human and avian cells. *Cell* **9,** 725–732.

Telzer, B. R., and Rosenbaum, J. L. (1979). Cell cycle-dependent, in vitro assembly of microtubules onto the pericentriolar material of HeLa cells. *J. Cell Biol.* **81,** 484–497.

Terasaki, M. (1996). Actin filament translocations in sea urchin eggs. *Cell Motil. Cytoskel.* **34,** 48–56.

Tomkiel, J., Cooke, C. A., Saitoh, H., Bernat, R. L., and Earnshaw, W. C. (1994). CENP-C is required for maintaining proper kinetochore size and for a timely transition to anaphase. *J. Cell Biol.* **125,** 531–545.

Vaisberg, E. A., Koonce, M. P., and McIntosh, J. R. (1993). Cytoplasmic dynein plays a role in mammalian mitotic spindle formation. *J. Cell Biol.* **123,** 849–858.

Wadsworth, P., and Salmon, E. D. (1986a). Analysis of the treadmilling model during metaphase of mitosis using fluorescence recovery after photobleaching. *J. Cell Biol.* **102,** 1032–1038.

Wadsworth, P., and Salmon, E. D. (1986b). Microtubule dynamics in mitotic spindles of living cells. *In* "Dynamic Aspects of Microtubule Biology" (D. Soifer, Ed.), pp. 580–592. New York Academy of Sciences, New York.

Wadsworth, P., Shelden, E., Rupp, G., and Rieder, C. L. (1989). Biotin tubulin incorporates into kinetochore fiber microtubules during early but not late anaphase. *J. Cell Biol.* **109,** 2257–2266.

Waters, J. C., Mitchison, T. J., Rieder, C. L., and Salmon, E. D. (1996). The kinetochore microtubule minus-end disassembly associated with poleward flux produces a force that can do work. *Mol. Biol. Cell* **7,** 1547–1558.

Westerfield, M. (1993). The zebrafish book: A guide for the laboratory use of zebrafish danio (Brachydanio) rerio," 3rd ed. Univ. of Oregon Press, Eugene.

Wheatly, S. P., Hinchcliffe, E. H., Glotzer, M., Hyman, A. A., Sluder, G., and Wang, Y. L. (1997). CDK1 inactivation regulates anaphase spindle dynamics and cytokinesis in vivo. *J. Cell Biol.* **138,** 385–393.

Wilding, M., Torok, K., and Whitaker, M. (1995). Activation-dependent and activation-independent localisation of calmodulin to the mitotic apparatus during the first cell cycle of the Lytechinus pictus embryo. *Zygote* **3,** 219–224.

Zavortink, M., Welsh, M. J., and McIntosh J. R. (1983). The distribution of calmodulin in living mitotic cells. *Exp. Cell Res.* **149,** 375–385.

Zhai, Y., Kronebusch, P. J., and Borisy, G. G. (1995). Kinetochore microtubule dynamics and the metaphase–anaphase transition. *J. Cell Biol.* **131,** 721–734.

This Page Intentionally Left Blank

CHAPTER 13

Obtaining Antibodies to Spindle Components

Ryoko Kuriyama and Kathy Ensrud

Department of Cell Biology and Neuroanatomy
University of Minnesota
Minneapolis, Minnesota 55455

I. Introduction

The spindle is a highly dynamic division machine composed of a number of molecular components. To understand how the spindle works and how its function is regulated, it is necessary to identify individual parts of the machine and establish their functional roles in dividing cells. The purpose of this chapter is to outline a basic method for the identification of spindle components by raising monoclonal antibodies specific to proteins included in the isolated mitotic spindle.

The macromolecular composition of the spindle has been analyzed using several experimental approaches, including biochemical characterization of isolated

METHODS IN CELL BIOLOGY, VOL. 61

0091-679X/99 $30.00

spindles and genetic analysis of mutations defective in mitosis and cell division. The hybridoma technology exhibits several advantages over other strategies. First, it is unnecessary to prepare spindle fractions as pure as those required for biochemical analysis since hybridoma clones secreting monoclonal antibodies to nonspindle components can be eliminated during the screening process. In addition, monoclonal antibodies allow us to probe for hitherto unknown molecular components which may not be abundant in the spindle; therefore, it is difficult to identify them with other methods.

Obtaining antibodies to spindle components involves a series of experimental processes: (i) preparation of immunogens and immunization of animals, (ii) cell fusion, (iii) screening of hybridoma supernatants, and (iv) purification and characterization of antibodies (Fig. 1). Although each step is considered labor-intensive and time-consuming, recent progress in hybridoma techniques has made it possible to produce specific antibody probes in a simple and reproducible manner. Following are general descriptions based on our successful experience in generating monoclonal antibodies specific to several microtubule-containing structures, such as mitotic spindles and centrosomes (Kuriyama and Borisy, 1985; Sellitto *et al.*, 1992; Ohta *et al.*, 1994).

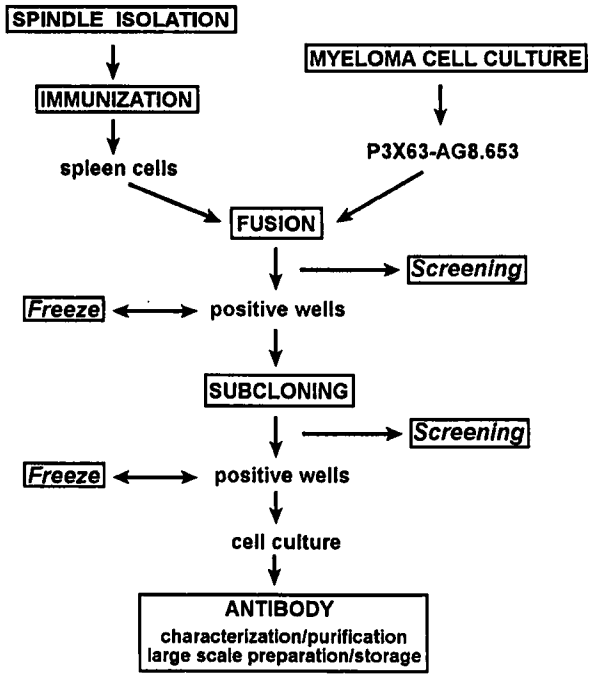

Fig. 1 Monoclonal antibody production.

II. Methods

A. Preparation of Immunogens: Isolation of Mitotic Spindles

The isolation of spindles from dividing cells involves four separate processes: (i) preparation of a homogenous mitotic cell population, (ii) stabilization of spindle microtubules, (iii) lysis of cells, and (iv) separation of the whole stabilized spindle structure from other cellular components. Marine invertebrate eggs, such as sea urchin eggs, have traditionally been an important source of material for spindle isolation since all four steps required for spindle preparation are relatively easy using these cells. The detailed procedure for spindle isolation from sea urchin eggs has been summarized elsewhere (Kuriyama, 1986). Here we provide the protocol for preparation of spindles from cultured mammalian [Chinese hamster ovary (CHO)] cells which, unlike sea urchin eggs, must be synchronized at mitosis (Kuriyama *et al.*, 1984).

Materials

CHO cells cultured in a F-10 medium (ICN Biomedicals) supplemented with antibiotics (100 × penicillin/streptomycin, Sigma Cat. No. A4668), 10% fetal calf serum (FCS; HyClone) and 15 m*M* Hepes at pH 7.2 in a 5–10% CO_2 incubator at 37°C.

Sterilized 100 m*M* thymidine in distilled water.

Nocodazole and taxol stock solutions (~4 mg/ml in DMSO).

Spindle isolation buffer (2 m*M* Pipes at pH 6.9, 0.25% Triton X-100, 20 μg/ml taxol; prepare just before isolation of spindles).

Procedure

1. Add thymidine to a final concentration of 2–5 m*M* onto a monolayer of cells at about 60–70% confluency.
2. Culture cells for 12–16 hr.
3. Remove thymidine and wash cells once with serum-free F-10 medium.
4. Culture cells for an additional 4 or 5 hr in fresh culture medium.
5. Add nocodazole to a final concentration of 0.1 μg/ml, and further culture cells for 4–4.5 hr.
6. Harvest round cells at M phase by gentle shaking and centrifuge them at 1000 rpm for 2 min at 37°C in a clinical centrifuge.

It is important to carry out the following steps at 37°C.

7. Resuspend the cell pellet with 10 ml prewarmed culture medium and transfer into a 15-ml conical tube. Set time zero when nocodazole has been washed away.
8. Resuspend the cell pellet with 2 ml prewarmed culture medium and allow to stand for 15 min.

9. Prepare the spindle isolation buffer by addition of Pipes, Triton X-100, and taxol stock solutions to prewarmed (37°C) distilled water.

10. Add taxol to the cell suspension to a final concentration of 5 μg/ml and stabilize spindle microtubules *in vivo*. Allow to stand for 0.5 min. Note that prolonged incubation of mitotic cells with taxol causes reorganization of microtubule arrays.

11. Spin down cells at 1000 rpm for 1 min and discard the supernatant.

12. Carefully wash the tube by dropping prewarmed distilled water down the side wall of the tube without disturbing the pellet.

13. After removing the washing liquid carefully, resuspend the cell pellet in 100 times volume of the spindle isolation buffer. Disrupt cells by gentle pipetting and/or vortexing.

14. Check the spindle isolation by phase-contrast microscopy. Under these hypotonic conditions, chromosomes become dissociated and the spindle should be free from any cell debris.

15. Sediment spindles at 2000 rpm for 10 min at room temperature in a clinical centrifuge.

B. Immunization of Mice

To increase the chance of success in production of monoclonal antibodies, a number of immunization protocols have been adapted. Two major protocols are outlined as follows.

Procedure I

1. Add equal volume of Freund's complete adjuvant to approximate 10–100 μg of spindle proteins and mix well using glass syringes and a three-way stopcock.

2. Using a 21-gauge needle, inject 0.1–0.5 ml sample into female BALB/c mice (6 weeks old) intraperitoneally.

3. During a 3 or 4-week period, each mouse will receive three additional boosts, which are prepared by mixing 10–100 μg spindles with an equal volume of Freund's incomplete adjuvant. To prepare antibodies reactive to denatured spindle proteins, mice are immunized with spindle proteins resuspend and boiled in SDS sample buffer (10% glycerol, 5% 2-mercaptoethanol, 3% SDS, 62.5 m*M* Tris–HCl at pH 6.8) for 3–5 min. It is important to collect sera and confirm antibody production before cell fusion.

Procedure II

1. Denature antigens by resuspension of spindle pellets in SDS sample buffer, then boil for 3–5 min.

2. Adsorb the denatured antigens on nitrocellulose strips (1 × 1 cm, 0.45-μm pore size).

3. Surgically implant one strip under the skin of one mouse.

4. Animals will be further boosted twice intraperitoneally at 3- or 4-week intervals as above with sonicated native antigens. The final boost should be on the third day before cell fusion.

C. Myeloma Cell Culture

The cells chosen for fusion should not synthesize or secrete any immunoglobulin heavy or light chains. The cell line to be used (clone P3X63-AG8.653) is deficient in hypoxanthine–quanine phosphoribosyltransferase, therefore unless fused with spleen cells they are not able to grow in media such as the HAT medium, which contains aminopterin, an inhibitor of guanosine synthesis.

Materials

Myeloma cells obtained from American Type Culture Collection

HY medium (89% HY, Sigma Cat. No. H9014, supplemented with 10% FCS and 1% 100× antibiotics)

Characterized and heat-denatured FCS (HyClone).

T-75 culture flasks

Procedure

1. Culture cells in suspension in the HY medium in T-75 culture flasks. Cells are incubated at 37°C with 5% CO_2 air–gas mixture.

2. Maintain the cell density at 5×10^4 to 1×10^6 cells/ml by splitting cultures every third day by adding 39 ml fresh culture media to 1 ml cell suspension in T-75 flasks.

3. Check cell viability by phase-contrast microscopy. Healthy cells are rounded up and appear rather opaque under the phase-contrast microscopy, whereas dying cells take on a "granular" appearance and cell lysis begins.

D. Preparation of Spleen Cells from Immunized Mice

Materials

Immunized mice which have received the final boost 3 days before the cell fusion experiment

Sterile surgical instruments such as scissors and forceps

Serum-free HY medium

60-mm petri dishes

Sterilized No. 80 fine wire screen mesh

Red blood cell (RBC) lysis buffer (Sigma Cat. No. R7757)

3 ml disposable syringe

15 and 50-ml sterile centrifuge tubes

Procedures

1. Slightly anesthetize mouse with ether, then dislocate neck.
2. Place mouse on board lying on its back and saturate abdomen with 70% ethanol.
3. Make superficial clip in abdomen and reflect skin.
4. With another sterile scissors, make clip in abdominal wall musculature and retract in both directions exposing the internal organs.
5. Spleen appears as a dark, flat, elongated ovoid structure; remove it and place it in a petri dish with serum-free HY.
6. Transfer spleen to laminar flow hood; rinse twice with serum-free HY.
7. Place spleen on a wire mesh in a petri dish with 10 ml serum-free HY.
8. With plunger from disposable 3-ml syringe, gently mash spleen through screen leaving only organ capsule and connective tissue.
9. Rinse screen with serum-free HY medium to recover spleen cells remaining on the screen mesh.
10. Transfer the spleen cell suspension to a 15-ml centrifuge tube; allow the suspension to settle for 1 or 2 min.
11. Carefully remove cell suspension from the tube and transfer to another 15-ml tube without disturbing the tissue debris at the bottom.
12. Centrifuge for 4 min at 1200 rpm in a clinical centrifuge.
13. Resuspend the pellet in 10 ml RBC lysis buffer and allow to settle for 1 or 2 min. Again, only remove the top cell suspension and transfer to another tube.
14. Centrifuge for 4 min at 1200 rpm and resuspend the pellet in 2-ml serum-free HY.
15. Determine the cell number.

E. Cell Fusion

Materials

Hybridoma-tested, presterilized polyethylene glycol (PEG) (Sigma Cat. No. P7777)

DMSO

HY medium

50X HAT (5 mM hypoxanthine, 20 μM aminopterin, 0.8 mM thymidine; Sigma Cat. No. HO262)

96-well tissue culture plates

Procedure

1. Count myeloma cells in log growth phase and check their viability by phase-contrast microscopy.
2. Prepare 10–20 $\times$ 10^6 spleen cells from immunized mice as previously described and wash three times with serum-free HY.

3. After resuspension of cell pellets in 2 ml serum-free HY, recheck cell count and viability.

4. Prepare the PEG working solution which contains 47% PEG and 7.5% DMSO in 45.5% serum-free HY.

5. Mix myeloma and spleen cells with a ratio of 1:3 in a 50-ml centrifuge tube, then centrifuge at 1200 rpm for 4 min.

6. Remove the supernatant and gently dislodge the cell pellet.

7. Add 1 ml PEG solution to the myeloma/spleen cell pellet over 1 min with stirring.

8. After gentle mixing for an additional 30 sec, add 2 ml serum-free HY over next 2 min.

9. Add 7 ml serum-free HY over the next 2 min.

10. Centrifuge at 1200 rpm over next 2 min.

11. Add 7 ml serum-free HY over the next 2 min.

12. Centrifuge at 1200 rpm for 5 min and discard the supermatant.

13. Resuspend the cell pellet and dilute to 1×10^6 cells/ml with 1X HAT-containing HY medium (HAT medium).

14. Dispense 0.2 ml to each well of 96-well plates.

F. Screening

1. Immunofluorescence Screening

For selection of antibodies capable of labeling spindle structures, screening is carried out by indirect immunofluorescence staining of cells/spindles with hybridoma supermatants. This can be greatly facilitated by employing methanol-fixed cells and/or spindles since the sample on coverslips can be stored in 100% methanol at −20°C for an extended length of time.

1. Prepare CHO cells grown on 22×22 mm^2 coverslips and fix with methanol at −20°C for at least 5 min.

2. Rehydrate cells in PBS–TW20 (0.05% Tween 20 and 0.02% sodium azide in PBS) and cut a coverslip into four pieces with a diamond scribe. Do not dry cells.

3. Collect cell supernatants from semiconfluent hybridoma cultures and add 20–40 μl of each hybridoma supernatant to cells on each coverslip. Incubate coverslips at 37°C for 30 min in a moist chamber.

4. Wash the primary antibody with prewarmed PBS–TW20 by placing coverslips into each well of the 24-well plates.

5. Change the washing medium two or three times every 10 min.

6. Incubate cells with 1/100–1/300 diluted secondary antibodies. Since hybridomas frequently produce IgM molecules, anti-mouse IgM should be included in

the secondary antibody (e.g., FITC-conjugated anti-mouse IgG + IgM; Jackson ImmunoResearch).

7. Wash cells with PBS–TW20 for 30 min at 37°C. Change medium several times.

8. Mount coverslips on a mounting medium and observe by fluorescence microscopy.

2. Immunoblot Screening

If monoclonal antibodies are required that are able to recognize particular protein species on gels, the primary screening of hybridoma clones will be done by immunoblot analysis.

1. Resuspend the spindle pellet in SDS sample buffer and boil for 3–5 min.

2. Run the sample on 7.5% polyacrylamide gels without combs (curtain gels) and transfer proteins to the nitrocellulose membrane.

3. Stain the membrane with Ponceau S. Wet membranes can be stored in a plastic wrap at −20°C.

4. Cut the membrane into small strips (as many as needed) and block with 3% BSA in TBS–TW20 (0.05% Tween 20 containing Tris-buffered saline at pH 7.2) for 30 min at room temperature.

5. Incubate each strip with individual hybridoma supernatant containing 1% BSA on a shaker for several hours to overnight at room temperature.

6. Place nitrocellulose strips in separate dishes and wash them with TBS–TW20 five times for 5 min. It is important to keep individual strips separate during this washing process.

7. Incubate nitrocellulose strips with the secondary antibody (1/2000 to 1/5000 diluted alkaline phosphatase-conjugated anti-mouse IgG + IgM; Jackson ImmunoResearch) for 60 min at room temperature.

8. Wash in TBS–TW20 five times for 5 min.

9. Develop immunoreactive bands using 0.2 mg/ml nitroblue tetrazolium and 0.2 mg/ml 5-bromo-4-chloro-3-indoly phosphate as the enzyme substrates.

G. Subcloning by Limiting Dilution

Materials

Hybridoma Cloning Factor (IGEN, Rockville, MD, Cat. No. 50-0615)

HT medium supplement (50X, Sigma Cat. No. H0137)

96-well plates

Procedures

1. Count hybridoma cells and calculate amount of cell suspension needed to make 1 ml of 1×10^4 cells/ml.

2. Add cell suspension to appropriate amount of the HT medium (HY containing 1X HT medium supplement).

3. Hybridoma cells will be cloned at three different concentrations—0.5, 1, and 2 cells/well in one 96-well plate each. Of 1×10^4 cells/ml suspension, prepare 20 ml solution of 2.5, 5, and 20 cells/ml in HT supplemented with Hybridoma Cloning Factor.

4. Pipet 200 μl into each well of 96-well plates and incubate plates in a CO_2 incubator at 37°C for 1 or 2 weeks.

5. Microscopic colonies should be visible within 1 or 2 weeks. Mark wells with a growing colony, and carefully remove the supernatant from cells for further screening.

6. After identifying positive colonies, repeat the same subcloning process one more time, if necessary.

H. Expansion and Cell Freezing

When positive clones are identified, cell cultures should be expanded as soon as possible. It is highly recommended to prepare freezer stocks for each clone at different stages of antibody production. When freezer stocks become available at later stages, stocks derived from previous steps can be discarded.

Expansion

1. When cells become confluent in a 96-well plate, transfer cell suspension to 24-well plates with 2 ml HT medium.

2. Gradually expand to 6-well plates in 3 ml HT media, to T-25 culture flasks in 10 ml medium, then to T-75 flasks in 20 ml HT.

Freezing cells

1. Centrifuge hybridoma cells to be frozen at 1200 rpm for 5 min.

2. Resuspend cells in serum-free HY.

3. Count the cell number and determine viability of hybridomas using trypan blue dye exclusion method.

4. Prepare freezing media (90% FCS and 10% DMSO) and place on ice.

5. Gently resuspend hybridoma cells in the freezing medium to a final concentration of 10^7 cells/ml.

6. Pipet 1 ml into each freezing cryo vial.

7. Place vials in controlled rate freezing unit and cool at 1°C/min.

8. After a minimum of 4 hr, transfer vials to liquid nitrogen storages. Alternatively, vials will be first placed at −20°C for several hours and then at −80°C overnight before transferring to a liquid nitrogen tank.

I. Large-Scale Antibody Production

Hybridoma supernatant

1. Expand hybridoma cultures which are stable, growing well, and have been checked for antibody production.
2. Prepare saturated $(NH_4)_2SO_4$ solution by adding 75 g to 100 ml distilled water and dissolve at room temperature. Store at 4°C at least overnight.
3. Harvest supernatants from the cell culture in a medium whose color turns yellowish due to overgrowing hybridomas cells.
4. Place the supernatant on ice and add saturated ammonium sulfate in equal volume with continuous stirring on ice.
5. Allow precipitation to occur for 1 hr on ice.
6. Recover the pellet by centrifugation at 48,000*g* for 30 min, and dissolve it in one-tenth the original supernatant volume of PBS.
7. Dialyze against excess volumes of PBS at 4°C for several hours to overnight. Change the dialyzing buffer at least once or twice.
8. Test the antibody's activity by immunofluorescence microscopy and/or immunoblot analysis.
9. Add 0.02% sodium azide and store aliquots in a −80° freezer.

Ascites

1. At least 2 weeks prior to injection of hybridoma cells, pretreat mice (BALB/c mice, minimum of 4 weeks old) by injecting 0.5 ml pristane (2,6,10,14-tetramethypentadecane) per mouse intraperitoneally.
2. Prepare hybridoma cells in log growth phase in the HT medium.
3. Wash cells with serum-free HY at least three times.
4. Determine cell number and inject $2–6 \times 10^6$ cells in serum-free HY or PBS into each mouse.
5. After 10 days, ascites should be ready for first harvest. Gently anesthetize mouse with ether and lay mouse on its back. Using a 10-ml syringe with an 18- or 20-gauge needle, penetrate the abdominal wall and begin withdrawing fluid. Usually one mouse can be tapped at least three times before it is sacrificed.
6. Transfer fluid in centrifuge tubes and spin at 1500 rpm for 10–15 min to remove cells.
7. Add 0.02% sodium azide and make aliquots to store at −80°C.

J. Purification and Characterization

Classification of clones

It is convenient to use commercially available kits, such as Mouse Hybridoma Subtyping Kit (Boehringer-Mannheim Biochemicals, Cat. No. 1-183-117), according to the manufacture's protocol.

Purification

There are well-established purification procedures for IgG molecules (Oi and Herzenberg, 1980; Goding, 1986). For IgM immunoglobulins, ImmunoPure IgM Kit (Pierce) can be utilized. Alternatively, IgM sufficient for microinjection into living cells is prepared using a combined size exclusion and protein A or G column chromatography (Nislow *et al.*, 1990).

1. Precipitate IgM from ascites by the addition of 50% ammonium sulfate (pH 7.4).
2. Resuspend in half its original volume of cold PBS and dialyze against PBS.
3. Load 0.5 ml of ammonium sulfate-precipitated antibody onto a gel filtration column, such as Sephacry S-300 or FPLC on Superdex 200. Elute proteins with PBS.
4. Collect 0.5-ml fractions and locate the position of IgM by SDS–PAGE followed by immunoblotting with goat antibodies specific to the μ chain of mouse IgM (Jackson ImmunoResearch).
5. Pool IgM-containing fractions and precipitate IgM with 40% saturated ammonium sulfate.
6. Apply to a protein A or G column equibulated with PBS.
7. Collect the flow-through fraction which contains IgG-free IgM.

III. Discussion

Monoclonal antibodies generally recognize only a single determinant of a given protein molecule. It has therefore long been noted that they cross-react with essentially nonrelated proteins that nevertheless happen to share the common immunodeterminant site. Since more than one subcellular structure and/or multiple bands are frequently detected by a single monoclonal antibody, it is crucial to evaluate the specificity of individual antibody probes carefully.

There are several factors controlling the production of monoclonal antibodies. First, the antigenicity of mitotic spindle components: If a protein, even if it is substantially low in abundance, displays strong antigenicity, there is a good chance of generating hybridoma clones secreting antibodies specific to the molecule. One such example is putative coiled coil proteins with extensive α-helices (Kuriyama, 1991). Two kinesin-like microtubule motor proteins (CHO1 and CHO2) have been identified by monoclonal antibodies raised against CHO spindles (Sellitto *et al.*, 1992). The determinant site to the antibodies was later shown to reside in the α-helical central stalk domain (Kuriyama *et al.*, 1994, 1995). Second, it is important to take into account the quality of isolated spindles. The mitotic spindle is a dynamic structure, and many components are believed to interact with the spindle in a dynamic way. Thus, a number of spindle components are likely to be released from the structure during sample preparations. In particular, the

spindle isolated in a taxol-containing hypotonic solution described in this chapter is known to be "very clean" and free from chromosomes and any surrounding membranous and filamentous structures (Kuriyama *et al.*, 1984). In order to generate antibodies to a wide range of molecular species, it is useful to immunize mice with spindles and/or dividing cells prepared with different methods.

Acknowledgment

We thank the Minnesota Medical Foundation for grant support.

References

Goding, J. W. (1986). Purification, fragmentation and isotopic labeling of monoclonal antibodies. *In* "Monoclonal Antibodies: Principles and Practice," pp. 104–142. Academic Press, San Diego.

Kuriyama, R. (1986). Isolation of sea urchin spindles and cytasters. *In* "Methods in Enzymology, Structural and Cytoskeletal Proteins, Part D: The Contractile Apparatus and the Cytoskeleton" (R. B. Vallee, ed.). Vol. 134, pp. 190–199. Academic Press, New York.

Kuriyama, R. (1991). Monoclonal antibodies to MTOC-antigens. *In* "Centrosomes" (V. Kalnins, ed.), pp. 131–165. Academic Press, New York.

Kuriyama, R., and Borisy, G. G. (1985). Identification of molecular components of the centrosphere in the mitotic spindle of sea urchin eggs. *J. Cell Biol.* **101,** 524–530.

Kuriyama, R., Keryer, G., and Borisy, G. G. (1984). The mitotic spindle of Chinese hamster ovary cells isolated in taxol-containing medium. *J. Cell Sci.* **66,** 265–275.

Kuriyama, R., Dragas-Granoic, S., Maekawa, T., Vassilev, A., Khodjakov, A., and Kobayashi, H. (1994). Heterogeneity and microtubule interaction of the CHO1 antigen, a mitosis-specific kinesin-like protein. Analysis of subdomains expressed in insect Sf9 cells. *J. Cell Sci.* **107,** 3485–3499.

Kuriyama, R., Kofron, M., Essner, R., Kato, T., Dragas-Granoic, S., Omoto, C. K., and Khodjakov, A. (1995). Characterization of a minus-end-directed kinesin-like motor protein from cultured mammalian cells. *J. Cell Biol.* **129,** 1049–1059.

Nislow, C., Sellitto, C., Kuriyama, R., and McIntosh, J. R. (1990). A monoclonal antibody to a mitotic MAP blocks mitotic progression. *J. Cell Biol.* **111,** 511–522.

Ohta, T., Vogel, J., Peng, G., Palazzo, R., and Kuriyama, R. (1994). Analysis of centrosomal component with monoclonal antibodies. *Mol. Biol. Cell* **5,** 37a.

Oi, V. T., and Herzenberg, L. A. (1980). Immunoglobulin-producing hybrid cell lines. *In* "Selected Methods in Cellular Immunology" (B. B. Mishell and S. M. Shiigi, eds.), pp. 351–372. Freeman, San Francisco.

Sellitto, C., Kimble, M., and Kuriyama, R. (1992). Heterogeneity of MTOC-components as revealed by monoclonal antibodies to mammalian centrosomes and to nucleus associated bodies from *Dictyostelium. Cell Motil. Cytoskel.* **22,** 7–24.

CHAPTER 14

Using Antisense Technology to Study Mitosis

Linda Wordeman and Mike Wagenbach

Department of Physiology and Biophysics
University of Washington School of Medicine
Seattle, Washington 98195

I. Introduction

The strand of double-stranded DNA that has the same base sequence as the mRNA (except for possessing T instead of U) is referred to as the sense strand (or coding strand). The other strand of DNA, which directs the synthesis of the mRNA via complementary base pairing, is called the antisense strand (or template or anticoding strand). The term "antisense" has evolved over time into a general term to describe a sequence of DNA or RNA that is complementary to mRNA. Naturally occurring antisense RNA assists in mRNA processing and in the regulation of gene expression. Recent improvements in cloning, vectors, and DNA and RNA synthesis have made it possible for researchers to use antisense sequences to artificially regulate gene expression. In its conceptually simplest

METHODS IN CELL BIOLOGY, VOL. 61

0091-679X/99 $30.00

form, a short antisense sequence hybridizes to the complementary sequence in an mRNA molecule coding for a particular protein (protein X). The formation of this duplex sterically blocks the progression of the translational machinery and halts protein X synthesis from that strand of mRNA. If all the mRNA molecules coding for protein X are subverted in this manner, then synthesis of all new protein X stops. All proteins turn over in cells with a half-life specific for each protein. If the antisense block of new protein X can be maintained for a sufficient time then all old protein X will eventually be destroyed. This results in a null phenotype for protein X. This also illustrates the challenge of using antisense technology: One must achieve a complete but specific elimination of a gene product of interest over sufficient time to allow for that protein to turn over.

Antisense RNA and DNA have be used to regulate gene expression and to eliminate gene products of interest *in vivo*. This technique can be efficacious in tissue culture systems in which genomic gene disruptions can be difficult and time consuming to accomplish. Antisense-induced protein depletion is also quite useful for studying fundamental processes such as mitosis, in which the elimination of a particular gene product can be lethal and impossible to propagate as a stable cell line. It is the purpose of this chapter to discuss the application of antisense techniques for the study of cell division in tissue culture systems. For this reason, we will not discuss the large body of recent work involving the development of antisense reagents for therapeutic and clinical applications. We hope that this chapter will provide useful guidelines for the practical and cost-effective use of antisense reagents in the small lab as a complimentary technique for the functional analysis of specific gene products. Therefore, we will not discuss the many new and interesting chemical modifications of antisense DNA which can facilitate delivery and potency because these reagents are often difficult to obtain or are not cost-effective for a small lab to prepare.

The application of antisense reagents to a particular problem, such as the study of mitosis, is technically simple but the mechanism by which these reagents operate is exceedingly complex and variable. For this reason, many investigators hesitate to introduce antisense technology into their repertoire of techniques or, having done so, are at a loss to interpret the results. Antisense reagents interfere with the transcriptional and translational regulation of gene expression. For many investigators who study cell division, transcriptional and translational control of gene expression is outside of their field of expertise. Hence, the analysis of antisense-induced data requires an attitude of respect that would be afforded any foray into a new field of research. Some recent reviews in the field of transcriptional and translational control of eukaryotic gene expression (Morris, 1998; Stebbins-Boaz and Richter, 1997) and the regulation of eukaryotic gene expression by naturally occurring antisense (Nellen and Sczakiel, 1996) provide some perspective on some of the cellular mechanisms that can be affected by antisense reagents. Finally, there are some excellent reviews on the practical use of antisense reagents which are of particular interest to those working in *in vitro*

(culture) systems (Denhardt, 1992; Toulme, 1992; Brysch and Schlingensiepen, 1994; Stein and Krieg, 1994).

Denhardt (1992) concluded, "There is no reason at present to conclude that any gene, however, abundant its transcript might be, is inherently recalcitrant to AS-mediated down-regulation of expression" (*Ann. N.Y. Acad. Sci.,* p. 76). If this is the case, why are antisense-based approaches so often viewed with fear and suspicion? One reason is that there are many different mechanisms by which antisense RNA and DNA have been shown to inhibit gene expression. Some mechanisms by which antisense reagents have been demonstrated to inhibit gene expression are listed in the following sections.

II. Antisense Mechanism of Action

A. Events in the Nucleus

Antisense oligonucleotides can be added to the culture medium from which they will accumulate in cells in a receptor-mediated, concentration-dependent manner (Geselowitz and Neckers, 1992; Temsamani *et al.,* 1994; Crooke, 1993). Most of these oligos remain in vesicles, although some can be found free in the cytoplasm (Geselowitz and Neckers, 1992). Cytoplasmic oligonucleotides have been shown to accumulate readily in the nucleus (Leonetti *et al.,* 1991; Geselowitz and Neckers, 1992). In addition, transfected antisense constructs are transcribed into RNA in the nucleus. Whichever the case, it can be assumed that antisense reagents introduced into the cytoplasm of living cells will eventually appear in the nucleus. Antisense oligonucleotides targeted against splice junctions can inhibit mRNA processing and transport of the target mRNA from the nucleus (Hodges and Crooke, 1995; Enjolras and Godinot, 1997). Often the inhibition can be quite potent and RNase insensitive (Moulds *et al.,* 1995). This occurrence can be monitored by Northern blots in which the disappearance of the secondary mRNA transcript is paralleled by the increase in the quantity of primary transcript. However, if the antisense (AS) oligo also triggers RNase-dependent events, then transcripts of unexpected sizes may be detected (Ullu and Tschudi, 1993; Dominski *et al.,* 1996).

Cases have been reported in which mRNA transcripts coding for intronless genes accumulate in the nucleus. In this instance it is solely transport from the nucleus to the cytoplasm rather than splicing which is assumed to be inhibited (Kim and Wold, 1985). A pathologic, naturally occurring antisense transcript may use this mechanism to downregulate myelin basic protein in the myelin-deficient (mld) mouse (Okano *et al.,* 1991).

B. Events in the Cytoplasm

Antisense reagents in the cytoplasm can inhibit gene expression at the level of translation. Antisense oligos targeted to the 5′ cap region of the mRNA can

inhibit formation of the translation initiation complex (Baker *et al.,* 1997). Many researchers have found that antisense reagents directed to the region surrounding the AUG start codon are more effective in blocking translation than those directed against the coding region (Tan *et al.,* 1994; L. Wordeman, unpublished results). A study using peptide nucleic acids (PNAs) directed against the AUG start codon was effective in inhibiting translation *in vitro* due to the steric inhibition of ribosome binding, although once translation had begun it was necessary to employ a triplex-forming PNA to effect the steric inhibition of ribosome elongation (Knudsen and Neilsen, 1996). PNAs do not trigger nuclease activity so the effects of steric hindrance can be assessed without additional complication. Other researchers have reported situations in which the start AUG efficacy rule has been violated. In cases in which a thorough examination of the antisense effect was performed it was often found that stability (Fogel-Petrovic *et al.,* 1996) or *cis*-acting autoregulatory processes (Ostareck-Lederer *et al.,* 1994; Robbie *et al.,* 1995) had been affected by binding to a specific region of the transcript. Therefore, in general, downregulation of specific gene products can be achieved by antisense reagents directed against the AUG start codon but individual messages should be tested empirically for other potent target sequences. Currently, there is no way to predict these regions by sequence analysis, although it is often informative to check the secondary structure of the mRNA transcript of interest using computer software (Jaeger *et al.,* 1989; Hyndman *et al.,* 1996) because regions lacking secondary structure will be more accessible to antisense reagents.

In *Xenopus* and mouse oocytes endogenous RNase H hydrolyzes the RNA moiety of RNA-antisense DNA complexes. This activity can be triggered by either phosphodiester or phosphorothioate (P-S) oligonucleotides binding to their target mRNA. Whether this activity occurs depends on the biological system (*in vitro,* oocytes, and cultured cells), the specific mRNA under study, and the location of the target sequence (Minshull and Hunt, 1986; Shuttleworth and Colman, 1988). Furthermore, other nucleases may mediate antisense-induced cleavage (Dominski *et al.,* 1996). Given the complexity of this mechanism, it is worthwhile to develop a reliable assay system in which to assay for either mRNA or protein product depletion because not all effective antisense reagents will display a nuclease-dependent effect.

III. Choice of Antisense Reagents

Antisense DNA in the form of short oligonucleotides and antisense RNA transcribed from a transfected expression construct are the two most commonly employed antisense reagents. Table I compares transcribed antisense RNA to synthesized antisense DNA with respect to several technical issues of concern to the laboratory researcher. Table I illustrates that both reagents can be equally balanced with respect to pros and cons. The wider prevalence in the literature of successful protein depletion using antisense oligonucleotide suggests that this

Table I
Comparison of Transcribed Antisense RNA to Antisense DNA Oligonucleotides

	Antisense RNA	Antisense DNA
Prerequisite	Cloned coding sequence often required	Can use sequence database
Preparation	Cloned construct	Easily commercially synthesized
Cost (labor excluded)	Cheap in standard molecular biology lab	Can be expensive especially if modified
Controls	Limited by length of transcript; preparation can be time-consuming	Easy to design and prepare several control oligos but costly
Toxicity	Nontoxic	Can be toxic: contaminants of synthesis and backbone modifications
Artifacts	Cellular regulation, cryptic promoters	Toxicity, nonspecific protein-binding-inhibiting translational machinery
Delivery	Transfection, injection	Injection, liposome, uptake from media
Concentration	Depends on promotor strength, RNA stability, transfection method	Variable uptake, limited by toxicity and cost
Persistence	Continuously renewed	P-O oligos, minutes to hours; P-S oligos, hours to days
Detection	Easy to cotransfect markers	Difficult to detect; labels add to cost
Extra bonus	With luck, stable or inducible cell lines can be produced	None
Effectiveness	Variable	Variable

is the easier and more consistently effective reagent to employ. This is because several target sites must often be tested to determine which is most effective in gene silencing. This is more easily done with several synthesized short oligos rather than multiple vector constructs.

The length of an antisense oligo reflects a balance between specificity, which is guaranteed by longer sequence lengths, and nonspecific hybridization inclusive of mismatches, which is also promoted by longer sequence lengths. Helene and Toulme (1989) have calculated that in mammals, if one assumes that only 0.5% of the genome is transcribed, then a minimal length of 11–15 nucleotides is required to guarantee specificity. In practice most researchers employ oligos of between 11 and 25 nucleotides in length. Longer oligos are more likely to partially hybridize to nontarget sequences, to exhibit slower uptake into cells, or to exhibit nonspecific effects especially if they have phosphorothioate-modified backbones. Figure 1 shows some modifications of the phosphate backbone of deoxyoligonucleotides used to enhance stability against naturally occurring nucleases. Phosphorothioate substitutions are the most common commercially available modification.

Attention should be given to the GC content of the antisense oligo. Sequence composition can affect cellular uptake (Peyman *et al.*, 1995), toxicity (Yaswen

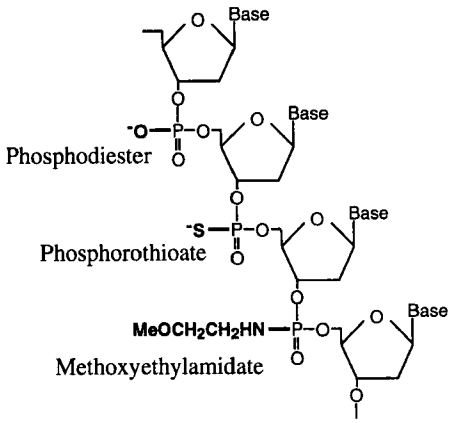

Fig. 1 Examples of DNA phosphate backbone modifications. In phosphorothioates and methoxyethylamidates the nonbridging oxygen atom is replaced, respectively, with a sulfur atom or methoxyethylamine group.

et al., 1992), and binding strength (Stein *et al.*, 1988). Structural features such as hairpins should also be assessed. Composition and structure must also be considered for the design of control oligos. Stein and Krieg (1997) outlined four types of control oligos and suggested that one control oligo from at least two of these categories of oligos be used with each antisense oligo:

1. Sense control: Maintains structural features but not composition.
2. Randomized control: Maintains composition but not structural features.
3. Mismatched control: One or two mismatches in the middle of the oligo control for hybridization selectivity; composition may be preserved.
4. Mismatched target control: Switch to system containing a mutant target gene or rescue with a target transcript containing silent mutations.

Even rigorous and reasonable control oligos may not identify properties such as the antiproliferative effects of a "G-quartet" in the oligo sequence (Yaswen *et al.*, 1992; Burgess *et al.*, 1995).

Phosphorothioate-substituted oligos have been consistently and successfully used to deplete target proteins in a variety of systems. However, these reagents must be carefully controlled because a number of studies have reported nonsequence-specific inhibition of cellular processes (Burgess *et al.*, 1995; Chrisey *et al.*, 1995) by binding to growth factor receptors (Rockwell *et al.*, 1997), activating transcription factors (Perez *et al.*, 1994), or binding to components of the protein translation machinery and other cellular components (Ghosh *et al.*, 1992; Shoeman *et al.*, 1997).

One way to circumvent the problem of phosphorothioate oligo toxicity is to transfect cells with a construct which will express antisense RNA complimentary

to the transcript of interest. Both stable/inducible and transient expression may be tried. Stable/inducible antisense transcripts have the disadvantage that often only one plasmid will stably integrate into the genome in any particular cell [except in the case of calcium phosphate transfection (Toneguzzo *et al.,* 1988)]. Hence, the quantity of antisense transcript produced may be very low in comparison with transiently transfected cells which may take up a number of plasmids at once, depending on the method of transfection employed. Gene amplification (Schimke, 1984) of stable transformants can be employed to increase the amount of antisense transcript.

In some cases, the full-length coding region in the antisense orientation has been found to be the most effective reagent for the inhibition of protein expression (Veres *et al.,* 1996). In these cases, the most simply prepared and widely accepted control is the sense orientation of the coding region which may result in either an increase in the protein of interest in control cells or the downregulation of endogenous protein via decreased endogenous expression (Scherczinger and Knecht, 1993). Another disadvantage of full-length antisense transcript is the rarely reported problem of cryptic sense strand transcription from an antisense construct (Willard *et al.,* 1994). Cryptic promoter activity has been reported with some vectors (Wilson *et al.,* 1993; Rosfjord *et al.,* 1994; Tolentino *et al.,* 1995), and we have seen increased expression of a mitotic centromere-associated kinesin (MCAK; L. Wordeman and M. Wagenbach, unpublished data) in full-length antisense constructs prepared using the pOPRSVICAT mammalian expression vector (Stratagene, La Jolla, CA). When either the 5′ half or the 3′ half of the antisense construct is deleted, cryptic upregulation of MCAK is abolished, similar to the case reported by Willard *et al.* (1994).

Often, however, shorter antisense transcripts are more effective than the full-length transcript in downregulating protein levels (Graessmann *et al.,* 1991). This can be due to faster duplex formation (Rittner *et al.,* 1993), inadvertent unmasking of negative inhibitory elements (Imagawa *et al.,* 1994), or secondary structure-inhibiting duplex formation. When shorter antisense sequences are employed the effective concentration of these sequences can be increased by producing a single transcript of tandem arrays of the sequence. A vector (pGEM-Tan) has been devised that facilitates the production of tandem arrays of identical sequences which can then be subcloned into mammalian expression vectors (Graham and Maio, 1992). Another method which may sometimes increase the potency of antisense sequences is to prepare a hammerhead ribozyme construct from a sequence in the mRNA transcript that contains a ribozyme cleavage site (Haseloff and Gerlach, 1988). The design and facility of hammerhead ribozyme constructs is reviewed by Koizuma and Ohtsuka (1992). Hammerhead ribozymes are a species of catalytic RNA that folds into a characteristic hammerhead tertiary structure. In the presence of divalent cations the ribozyme catalyzes the cleavage of the target sequence XUX′, where X is ACUG and X′ is any ACU. Naturally occurring hammerhead ribozymes are *cis*-operational structures (Buzayan *et al.,* 1986) but antisense hammerhead ribozymes can be targeted to other RNA mole-

cules in a *trans* configuration (Perriman *et al.*, 1993). Theoretically, after cleavage the ribozyme could dissociate and cleave another molecule, but this event is often difficult to document. Furthermore, although ribozyme-mediated cleavage has been observed both *in vivo* and *in vitro,* there are cases in which gene suppression occurs but cleavage cannot be proven (Beck and Nassel, 1995; Sczakiel and Goody, 1994). Figure 2A shows the basic design of the hammerhead ribozyme. Residues important for forming the catalytic core are boxed. Using the pGEM-Tan vector, we have produced a polymerized hammerhead ribozyme directed against the start codon of MCAK. A partial digest of this construct confirms that the vector contains 14 ribozymes in tandem (Fig. 2B).

In Fig. 3, a single anti-MCAK ribozyme has been transcribed *in vitro* and combined with P^{32}-labeled MCAK mRNA. Because cleavage occurs close to the 5′ end of the mRNA, two different gels must be used to quantitate the cleavage products. Figure 3A shows a graph of the extent of cleavage at 50°C in the presence and absence of Mg^{2+}. In an elaborate variation on this scheme, Ohkawa and associates (1993) constructed a polymerized ribozyme consisting of antitarget (*trans*-acting) flanked by self-cleaving (*cis*-acting) ribozymes. The concatameric transcript self-cleaves to release antitarget ribozyme monomers which were more active *in vitro* than a similarly long, non-self-cleaving concatameric transcript (Ohkawa *et al.*, 1993). Several studies have found that greater potency *in vivo* is seen in ribozymes with longer target homology flanking the ribozyme than is optimal for catalysis *in vitro* (Crisell *et al.*, 1993; Sioud, 1997).

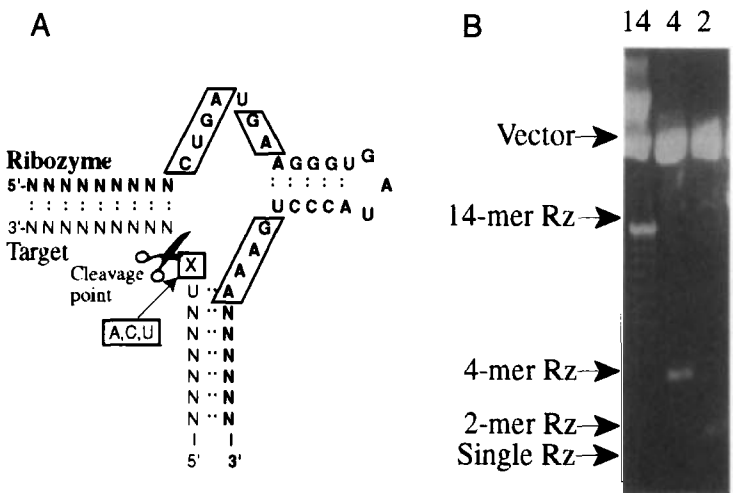

Fig. 2 Synthesis of polymerized ribozyme constructs. (A) The basic design of a hammerhead ribozyme. Boxed residues are critical for the formation of the catalytic core. (B) Partial restriction digest of polymerized ribozyme constructs. A polymer of 14 ribozymes in tandem (14) is shown beside two shorter polymers, a 4-ribozyme construct (4) and a 2-ribozyme construct (2).

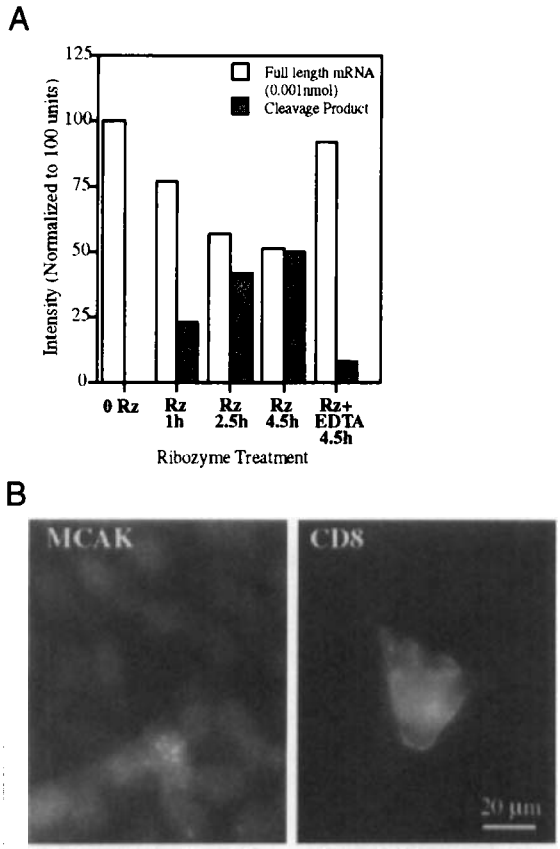

Fig. 3 Analysis of anti-MCAK ribozyme *in vitro* and *in vivo*. (A) Extent of cleavage of radiolabeled full-length MCAK mRNA by anti-MCAK single ribozyme mRNA *in vitro*. Twenty-fold excess ribozyme mRNA was added to MCAK mRNA in the presence and absence of Mg^{2+} and incubated at 50°C. (B) Cotransfection of anti-MCAK ribozyme construct and CD8 construct into CHO cells. The cells are double labeled with anti-MCAK antibodies and anti-CD8 antibodies.

Ribozyme constructs can be cotransfected with marker constructs. Generally, a fivefold excess of antisense construct DNA is combined with marker construct DNA in order to ensure that transfected cells displaying the marker molecule have also taken up the experimental construct. We have used the EBO-pcD-Leu-2 (Margolskee *et al.*, 1988) vector which expresses the human T cell surface marker Leu-2 (CD8). Figure 3B shows a field of chinese hamster ovary (CHO) cells in which an MCAK antisense ribozyme and the EBO-pcD-Leu-2 constructs have been cotransfected. The cells have been double labeled with anti-MCAK antiserum and anti-CD8 antiserum. In this particular cell, MCAK depletion is correlated with CD8 expression. One advantage to this approach is that the CD8-expressing cells can be sorted free of untransfected cells by fluorescence-

activated cell sorting. The uniformly transfected cells can be assayed by Western blots or Northern hybridizations to score target protein depletion. If antisense treatment inhibits cell division then the overgrowth of untransfected cells can be avoided.

IV. Assaying Target Protein Levels

Because the mechanism of action of antisense reagents is complex and variable, it is wise to use antisense in combination with other methods of analysis to functionally characterize a transcript of interest. In addition, it is worth taking some time to design assays to test the efficacy of the antisense reagent of choice. Reported nonspecificity of antisense transcripts and toxicity of oligos makes it essential to correlate defects with depletion of target protein. This is especially true when studying cell division because reduction in overall protein translation has inhibitory effects on cell division. The most obvious assay is to subject antisense and control cells to Western immunoblots and probe for specific loss of the target protein. This has been a standard method to assay for the loss of cytoskeletal proteins and motor proteins in skeletal and nervous tissue (Mangan and Olmsted, 1996; Ferreira *et al.*, 1992; Amaratunga *et al.*, 1993; Morfini *et al.*, 1997). In culture systems target protein levels have also been assayed using quantitative immunofluorescence at the level of the light microscope (Sharp *et al.*, 1997a). It is reassuring to compare target protein levels with selected control proteins to confirm that target protein depletion is sequence specific. In either case, a reagent specific for the target protein is a prerequisite for the antisense study.

In tissue culture cell systems, mRNA is generally not assayed by Northerns because the mechanism of RNA duplex degradation is not well characterized. There are instances in which protein levels are sufficiently depleted even though mRNA for the target protein is still present (Sasaki *et al.*, 1993; Rickman and Rickman, 1996). However, in *Xenopus* oocytes and embryos, the nuclease dependence of antisense-induced mRNA degradation has been well characterized (Woolf *et al.*, 1990; Dagle *et al.*, 1991). For this reason, in this system the analysis of antisense effects with Northern blots (Dagle *et al.*, 1990), or combinations of Northerns and Westerns, is more common (Vernos *et al.*, 1995; Robb *et al.*, 1996).

A simple method for the preliminary analysis of the efficacy of antisense RNA or DNA oligos is to test the reagents in an *in vitro* transcription/translation system (Promega, Madison, WI). The clone coding for the target protein is transcribed from a construct containing a T3 or T7 promoter. Antisense oligos derived from anywhere in the clone can be tested in the system. Different effects may result from using a wheat germ extract-based kit which may contain Rnase H versus commercial reticulocyte lysate kits which are reportedly to be free of nuclease activity (Minshull and Hunt, 1986). This type of assay can be very useful to test for translational inhibition (Walker and Maller, 1991). This assay also

allows for the quantitative assessment of the translational inhibition of a spectrum of antisense oligos since it has been shown that such oligos can exhibit broad variability in efficacy (Milner *et al.*, 1997; Szoka, 1997).

V. Antisense Reagents Used to Study Cell Division

A. Case Studies of Mitotic Kinesin-Related Proteins

Xklp1 is a 139,000 MW kinesin-related protein cloned from a *Xenopus* oocyte cDNA library. The protein is localized to interphase nuclei, mitotic chromosomes, and, additionally, the spindle midzone after the onset of anaphase (Vernos *et al.*, 1995). Unlike genetic systems such as *Drosophila* in which the aberrant phenotype is used to identify and isolate the gene, this protein was identified by virtue of its sequence similarity to kinesin-related proteins which have a broad functional distribution. In the Vernos *et al.* (1995) study antisense oligos were skillfully employed in order to functionally characterize Xklp1. Several 20-mer oligos were prepared with 5′ and 3′ 4-mer methoxyethylphosphoramide ($NHCH_2CH_2OMe$) linkages to enhance oligo stability (Dagle *et al.*, 1991). Because exonuclease activity, especially that of 3′ exonucleases, is thought to be the major nuclease activity in many systems, end-capping is often used as a method to enhance stability while still preserving duplex association kinetics and cutting the cost of oligo synthesis (Cook, 1993). It should be noted, however, that end-capped oligos will eventually be degraded by endonucleases in *Xenopus* oocytes (Dagle *et al.*, 1990, 1991), so if persistence beyond 12 hr is necessary, a fully substituted oligo should be considered. Injection of Xklp1 antisense oligos promoted the formation of multipolar spindles with abnormal chromosome distribution and cleavage was impaired. In this study both sense oligos and rescue by target mRNA with silent mutations rendering it unaffected by antisense oligos were used as controls (Vernos *et al.*, 1995). After successful depletion of the target mitotic protein resulting in the induction of the mutant phenotype, the researcher advances to the most difficult stage of the study: the functional interpretation of the phenotype. Often additional experiments must be used to supplement the antisense-induced gene knockout. In the study by Vernos *et al.* (1995) an Xklp1-immunodepleted spindle assembly extract (Sawin and Mitchison, 1991) was employed to produce a correlative phenotype *in vitro*.

Interestingly, antisense-induced protein depletion has been successfully employed to identify redundant functions for mitotic proteins *in vivo* (Robb *et al.*, 1996). Both methoxyethylphosphoramidate and phosphorothioate end-capped linkages were used to synthesize oligos against Xklp1 and a centrosomal kinesin-related protein Xklp2 (Boleti *et al.*, 1996) and the effectiveness of the two oligos was comparable. In this study Xklp1 sense oligos and antisense oligos directed against Xklp2 were used as a control to indicate that Xklp1 mRNA was not affected by Xklp2 depletion. Robb *et al.*, (1996) found that in addition to the previously reported mitotic defects, germ plasm aggregation was also inhibited by

antisense-induced Xklp1 depletion. Since Xklp-2 depletion also inhibits cleavage, although presumably by a mechanism differing from that of Xklp-1, this control was used to demonstrate that the inhibition of germ plasm aggregation was not a secondary effect of impaired cleavage.

Similarly, antisense-induced depletion has been used to confirm the nonmitotic function of a mitotic midzone motor CHO1/MKLP1 (Yu *et al.*, 1997). Ectopic expression of this motor, which localizes to and can possibly move the antiparallel microtubules of the spindle midzone (Nislow, 1992), inadvertently revealed an alternate role in organizing the dendrite microtubular cytoskeleton which also consists of antiparallel microtubules (Sharp *et al.*, 1996). Incubation of cultures with 1–20 μM of fully substituted P-S oligos complimentary to CHO1 for 24–72 hr inhibited dendrite formation but not axons in hippocampal (Sharp *et al.*, 1997b) and neuroblastoma cells (Yu *et al.*, 1997). In both of these studies the hamster CHO1 nucleotide sequence (Kuriyama *et al.*, 1994) was successfully used to prepare the antisense reagent for use in rat hippocampal or mouse neuroblastoma cells. The successful interspecies use of antisense reagents against kinesin-related proteins has also been reported in other neuronal systems: human sequence : rat cells (Ferreira *et al.*, 1992), rat sequence : rabbit retina (Amaratunga *et al.*, 1993), and mouse sequence : rat cells (Morfini *et al.*, 1997).

B. Uniquely Mitotic Problems

Neuronal cultures are particularly well suited for antisense studies in which oligos are simply added to the culture media. This is partly due to the fact that the cells employed in these types of studies are slow growing and some of the parameters measured, such as neurite outgrowth, occur over the course of several days rather than several minutes or hours. This allows plenty of time for oligo uptake and protein turnover.

Many of the cell lines routinely used for the study of cell division are rapidly dividing cell lines (CHO and HeLa) because such lines produce a large proportion of cells in mitosis during the course of an assay. This property of rapid cell growth has several disadvantages. The cells tend to overgrow during the course of the analysis, especially when the cells are grown to densities optimal for transfection. Oligo uptake can vary from cell to cell, resulting in rapid overgrowth of uninhibited cells even if some cells are exhibiting successful downregulation of the target protein. The transformed characteristics of rapidly dividing cell lines contribute both to variability in oligo uptake and to a basal level of mitotic aberrations that must be controlled.

Shu *et al.* (1995) solved these problems in an antisense study directed against γ-tubulin. In this study, which was performed with a variety of tissue culture cell lines, the group demonstrated that a transient association of γ-tubulin with midbodies may play a role in cytokinesis. Sense and antisense RNA transcribed from the T7 promoter of the pGEM vector (Promega) was transcribed *in vitro* and added in various proportions to a reticulocyte lysate *in vitro* translation

system to confirm that the antisense mRNA was capable of inhibiting the translation of γ-tubulin. Then depletion was confirmed *in vivo* by Western blots of transfected cells. This step is usually difficult to perform because it is difficult to achieve a high enough transfection efficiency. A human kidney cell line (293) exhibiting high transfection efficiencies was employed for this part of the study. The transfection efficiency of CHO and PtK_2 cells can be low to zero, respectively, but these cell lines have prominent midbodies and were superior for the functional analysis of γ-tubulin depletion. Therefore, the antisense and marker constructs were injected into PtK_2 cells or CHO cells cultured at low density on coverslips containing a locator grid (Bellco Glass). This solved the problem of overgrowth and the problem of identifying transfected cells prior to fixation, and it allowed cells to be followed over time through the first cell division. In this way, Shu *et al.* (1995) were able to visualize abortive cytokinesis in living antisense-transfected cells. In an interesting variation, an earlier study by Liu *et al.* (1992) identified, by antisense-induced depletion, a requirement for calmodulin in order to complete cytokinesis in *Dictyostelium.* Giant multinucleate cells were manifested only at high culture densities. At low densities cytokinesis was completed by "traction-mediated cytofission" (Fukui *et al.,* 1990).

MCAK afforded special difficulties as a target protein for depletion. The mRNA coding for MCAK is relatively abundant in CHO cells (Wordeman and Mitchison, 1995), and the protein is fairly stable, exhibiting a half-time of at least 12 hr (L. Wordeman, unpublished results). The level of MCAK is naturally variable in both interphase and mitotic cells (Wordeman and Mitchison, 1995) complicating the quantification of the protein. Addition of oligos to the culture media had little effect on either the level of MCAK or the growth properties of CHO cells over the course of 48 hr. In order to achieve rapid introduction of sufficient oligo to analyze quantitatively a sufficient number of cells we employed scrape loading (McNeil *et al.,* 1984; Bernat *et al.,* 1990). Scrape loading can be an effective means for the introduction of linear DNA into cells with reported transfection efficiencies of 80% (Fechheimer *et al.,* 1987). In our method, we plate cells densely but subconfluent in 35 mm^2 dishes. Loading is best when the cells are dense but not touching each other. The cell monolayer is rinsed twice with serum-free media and then 100 μl of serum-free media containing 100 pmol of oligo is added to the dish and the cells are scraped with a cell scraper (Fisher Scientific, Pittsburgh, PA) for 10 sec. Four milliliters of fresh serum-containing media is added and the cells are plated onto four 12-mm-diameter coverslips. Cells are fixed and assayed immunofluorescently for MCAK depletion 24–48 hr later. Cells scrape-loaded in this way with 100 μl of 2 mg/ml DNP-lysine (Molecular Probes, Eugene, OR), fixed and labeled with anti-DNP antiserum (Molecular Probes), exhibit 80–90% incorporation. The level of marker per cell is unavoidably variable.

Figure 4 shows a field of interphase CHO cells labeled with anti-MCAK antiserum. In Fig. 4A the cells were scrape-loaded 48 hr previously with a fully substituted randomized control oligo in which the 21-base sequence overlaying

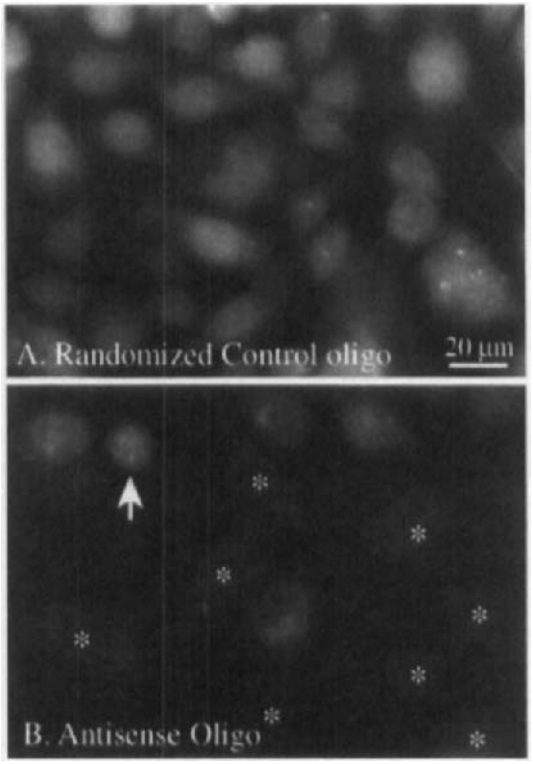

Fig. 4 Scrape loading of phosphorothioate oligos into CHO cells. (A) Fully substituted randomized control phosphorothioate oligo (21-mer). (B) Fully substituted phosphorothioate 21-mer corresponding to the antisense sequence overlying the start AUG for MCAK. Cells were scrape loaded with 100 pmol oligos, cultured for 48 hr, and then fixed and labeled with anti-MCAK antibodies. Asterisks indicate cells with abnormally low levels of MCAK. The arrow shows a cell which has not been effectively depleted of MCAK.

the start codon of MCAK has been randomized using the SHUFFLE program (GCG Inc., Madison, WI). The sequence was tested for accidental identity with sequences in the NBCI database (Bethesda, MD) and then synthesized and purified by high-performance liquid chromatography (Genset Corp., La Jolla, CA). In cells scrape-loaded with the randomized control sequence, the endogenous levels of MCAK were unchanged from that seen in a normal culture of CHO cells. Cells that have been scrape-loaded with fully substituted antisense oligo show a significant number of cells with almost undetectable levels of MCAK label (asterisks in Fig. 4B). However, the arrow in Fig. 4B indicates a cell in which MCAK levels are unchanged or perhaps even slightly high. Such cells make it difficult to perform Western immunoblots to assay for protein levels. Therefore, in the case of MCAK, quantitative immunofluorescence must be

employed to measure protein levels. Figures 5A–5D shows MCAK protein on centromeres of prophase (Figs. 5A and 5B) and prometaphase (Figs. 5C and 5D) CHO cells. At this time the extent of MCAK is at its highest level on mitotic centromeres. However, it is possible to find, in antisense-treated cell cultures, cells that are in prophase (Figs. 5E–5G) or prometaphase (Figs. 5H–5J) which

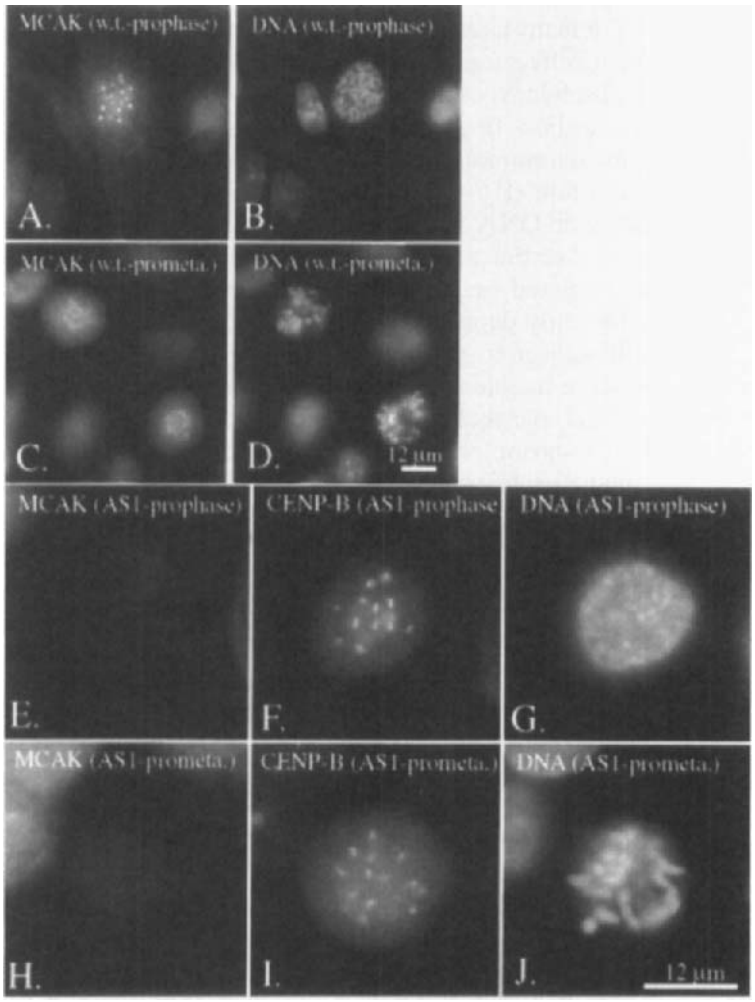

Fig. 5 MCAK-depletion in mitotic CHO cells by scrape-loaded phosphorothioate antisense oligos. Normal (A–D) and antisense-treated (E–J) CHO cells. Anti-MCAK and DNA label of prophase (A, B) and prometaphase (C, D) CHO cells showing the bright centromere-associated MCAK label in cells in these stages of mitosis. In contrast, prophase (E–G) and prometaphase (H–J) cells from a culture treated with antisense oligos directed against MCAK start codon have no discernible centromere-associated MCAK (E, H). The antisense-treated cells have been double labeled with anti-CENP-B antiserum (F, I). Hoechst-labeled DNA is shown in G and J.

lack centromere-associated MCAK label. Despite the abundance of both MCAK protein and mRNA in CHO cells it is easy to obtain a significant proportion of cells in mitosis which lack any detectable MCAK protein. The greater challenge is the analysis of the antisense-induced mitotic phenotype.

C. Utility and Limitations of Antisense Technology for the Study of Mitosis

For many tissue culture systems, antisense-induced gene depletion is the easiest way to effect a gene knockout phenotype. Unfortunately, there are some limits to the usefulness of the antisense approach to study the mechanism of chromosome segregation. In genetic systems such as *Saccharomyces cerevesiae,* temperature-sensitive mutants have been used to disrupt mitotic processes with high temporal resolution (Hoyt and Geiser, 1996). However, protein depletion by antisense RNA or DNA is dependent on the kinetics of turnover of the target protein (and sometimes the target mRNA). This usually requires that the target mRNA be depleted or blocked during interphase to allow protein levels to become sufficiently depleted by the onset of mitosis. Under these conditions the cell is still subject to a series of checkpoint-mediated cell cycle arrests which may obscure the mechanism of function of the mitotic spindle (Rudner and Murray, 1996). Nevertheless, in many systems antisense-mediated depletion has successfully contributed to the functional characterization of many chromosomal and spindle proteins (Vernos *et al.,* 1995; Shu *et al.,* 1995; Robb *et al.,* 1996) and to the general identification of proteins that play a role in cell division (Dagle *et al.,* 1990; Freeman *et al.,* 1990; Haugwitz *et al.,* 1994; Chen *et al.,* 1995; Coats *et al.,* 1996; Khan *et al.,* 1997).

The accumulation of multinucleate and aneuploid cells is a common, practically universal, feature of mitotic disturbances. Therefore, this phenotype alone tells us very little about the mechanism of cell division and the role that the target molecule plays in this process. MCAK depletion leads to multinucleate cells and mitotic cells containing lagging chromosomes. Both of these phenotypes are manifested by a broad array of causes, from microtubule inhibitors such as colchicine (Brues and Jackson, 1937) to asbestos exposure (Hesterberg and Barrett, 1985; Yegles *et al.,* 1993). Binucleate cells appearing after downregulation of γ-tubulin were scored as a defect arising from abortive cytokinesis after antisense-injected cells were observed progressing through cell division in real time (Shu *et al.,* 1995). Also, the participation of a target protein, such as $p27^{Kip1}$, in a checkpoint regulatory pathway is easily scored by flow cytometry if antisense-induced depletion results in the loss of checkpoint arrest (Coats *et al.,* 1996). Nevertheless, it is a sad fact that the mechanism of prometaphase to anaphase progression often requires auxiliary studies in addition to antisense, such as dominant-negative mutants or *in vitro* assays, in order to complete the mechanistic picture for a particular target protein.

As we learn more about the mechanisms of checkpoint arrest during mitosis, however, we will be able to design more effective analyses of antisense-induced

phenotypes. Furthermore, antisense studies are becoming increasingly prevalent, even in the difficult field of mitosis. It is likely that double and triple knockouts may be engineered using a variety of antisense transcripts. Most exciting, gene substitutions may be produced in which antisense depletion is coupled with mutant target protein transcripts rendered insensitive to the antisense by deletions or silent mutations. In such cases, mutant protein may replace endogenous protein in one step, obviating the need for dominant-negative mutants. In any case, antisense-induced target protein depletion is an increasingly useful addition to the experimental arsenal of any laboratory.

Acknowledgments

We are grateful to Dave Coy, Laura Ginkel, Jonathan Howard, Andy Hunter, and Todd Maney for many stimulating discussions. The data presented here were produced with the support of the University of Washington School of Medicine and the Council for Tobacco Research-U.S.A., Inc.

References

Amaratunga, A., Morin, P. J., Kosik, K. S., and Fine, R. E. (1993). Inhibition of kinesin synthesis and rapid anterograde axonal transport *in vivo* by an antisense oligonucleotide. *J. Biol. Chem.* **268,** 17427–17430.

Baker, B. F., Lot, S. S., Condon, T. P., Cheng-Flournoy, S., Lesnik, E. A., Sasmor, H. M., and Bennett, C. F. (1997). 2′-O-(2-Methoxy)ethyl-modified anti-intercellular adhesion molecule 1 (ICAM-1) oligonucleotides selectively increase the ICAM-1 mRNA level and inhibit formation of the ICAM-1 translation initiation complex in human umbilical vein endothelial cells. *J. Biol. Chem.* **272,** 11994–12000.

Beck, J., and Nassal, M. (1995). Efficient hammerhead ribozyme-mediated cleavage of the structured hepatitis B virus encapsidation signal in vitro and in cell extracts, but not in intact cells. *Nucleic Acids Res.* **23,** 4954–4962.

Bernat, R. L., Borisy, G. G., Rothfield, N., and Earnshaw, W. C. (1990). Injection of anticentromere antibodies in interphase disrupts events required for chromosome movement at mitosis. *J. Cell Biol.* **111,** 1519–1533.

Boleti, H., Karsenti, E., and Vernos, I. (1996). Xklp2, a novel Xenopus centrosomal kinesin-like protein required for centrosome separation during mitosis. *Cell* **84,** 49–59.

Brues, A. M., and Jackson, E. B. (1937). Nuclear abnormalities resulting from inhibition of mitosis by colchicine and other substances. *Am. J. Cancer* **30,** 504–511.

Brysch, W., and Schlingensiepen, K.-H. (1994). Design and application of antisense oligonucleotides in cell culture, *in vivo,* and as therapeutic agents. *Cell. Mol. Neurobiol.* **14,** 557–567.

Burgess, T. L., Fisher, E. F., Ross, S. L., Bready, J. V., Qian, Y.-X., Bayewitch, L. A., Cohen, A. M., Herrera, C. J., Hu, S. S.-F., Kramer, T. B., Lott, F. D., Martin, F. H., Pierce, G. F., Simonet, L., and Farrell, C. L. (1995). The antiproliferative activity of c-myb and c-myc antisense oligonucleotides in smooth muscle cells is caused by a nonantisense mechanism. *Proc. Natl. Acad. Sci. USA* **92,** 4051–4055.

Buzayan, J. M., Gerlach, W. L., and Bruening, G. (1986). Non-enzymatic cleavage and ligation of RNAs complementary to a plant virus satellite RNA. *Nature* **323,** 349–353.

Chen, T.-L. L., Kowalczyk, P. A., Ho, G., and Chisholm, R. L. (1995). Targeted disruption of the dictyostelium myosin essential light chain gene produces cells defective in cytokinesis and morphogenesis. *J. Cell Sci.* **108,** 3207–3218.

Chrisey, L. A., Pazirandeh, M., and Liss, H. S. (1995). Nonsequence-specific inhibition of bacterial luminescence by phosphorothioate oligodeoxyribonucleotides. *Antisense Res. Dev.* **5,** 261–269.

Coats, S., Flanagan, W. M., Nourse, J., and Roberts, J. M. (1996). Requirement of $p27^{Kip1}$ for restriction point control of the fibroblast cell cycle. *Science* **272,** 877–880.

Cook, P. D. (1993). Medicinal chemistry strategies for antisense research. *In* "Antisense Research and Applications" (S. T. Crooke and B. Lebleu, eds.), pp. 149–187. CRC Press, Boca Raton, FL.

Crisell, P., Thompson, S., and James, W. (1993). Inhibition of HIV-1 replication by ribozymes that show poor activity *in vitro. Nucleic Acids Res.* **21,** 5251–5255.

Crooke, R. M. (1993). Cellular uptake, distribution and metabolism of phosphorothioate, phosphodiester, and methylphosphonate oligonucleotides. *In* "Antisense Research and Applications" (S. T. Crooke and B. Lebleu, eds.), pp. 427–449. CRC Press, Boca Raton, FL.

Dagle, J. M., Walder, J. A., and Weeks, D. L. (1990). Targeted degredation of mRNA in Xenopus oocytes and embryos directed by modified oligonucleotides: Studies of An2 and cyclin in embryogenesis. *Nucleic Acids Res.* **18,** 4751–4757.

Dagle, J. M., Weeks, D. L., and Walder, J. A. (1991). Pathways of degradation and mechanism of action of antisense oligonucleotides in Xenopus laevis embryos. *Antisense Res. Dev.* **1,** 11–20.

Denhardt, D. (1992). Mechanism of action of antisense RNA. *Ann. N. Y. Acad. Sci.* **660,** 70–76.

Dominski, Z., Ferree, P., and Kole, R. (1996). Antisense 2′-O-methyloligoribonucleotides hybridized to RNA block a nuclear, ATP-dependent 3′-5′ exonuclease. *Antisense Nucleic Acid Drug Dev.* **6,** 37–45.

Enjolras, N., and Godinot, C. (1997). Inhibition of ubiquitous mitochondrial creatine kinase expression in HeLa cells by an antisense oligodeoxynucleotide. *Mol. Cell. Biochem.* **167,** 113–125.

Fechheimer, M., Boylan, J. F., Parker, S., Sisken, J. E., Patel, G. H., and Zimmer, S. G. (1987). Transfection of mammalian cells with plasmid DNA by scrape-loading and sonication loading. *Proc. Natl. Acad. Sci. USA* **84,** 8463–8467.

Ferreira, A., Niclas, J., Vale, R. D., Banker, G., and Kosik, K. S. (1992). Suppression of kinesin expression in cultured hippocampal neurons using antisense oligonucleotides. *J. Cell Biol.* **117,** 595–606.

Fogel-Petrovic, M., Vujcic, S., Haner, R., Regenass, U., Mett, H., and Porter, C. W. (1996). Sequence specific antisense oligonucleotide analog interference with spermidine/spermine N1-acetyltransferase gene expression. *Anticancer Res.* **16,** 2517–2523.

Freeman, R. S., Kanki, J. P., Ballantyne, S. M., Pickham, K. M., and Donoghue, D. J. (1990). Effects of the v-mos oncogene on *Xenopus* development: Meiotic induction in oocytes and mitotic arrest in cleaving embryos. *J. Cell Biol.* **111,** 533–541.

Fukui, Y., DeLozanne, A., and Spudich, J. A. (1990). Structure and function of the cytoskeleton of a *Dictyostelium* myosin-defective mutant. *J Cell Biol.* **110,** 367–378.

Geselowitz, D. A., and Neckers, L. M. (1992). Analysis of oligonucleotide binding, internalization, and intracellular trafficking utilizing a novel radiolabeled crosslinker. *Antisense Res. Dev.* **2,** 17–25.

Ghosh, M. K., Ghosh, K., and Cohen, J. S. (1992). Translation inhibition by phosphorothioate oligodeoxynucleotides in cell-free systems. *Antisense Res. Dev.* **2,** 111–118.

Graessmann, M., Michaels, G., Berg, B., and Graessmann, A. (1991). Inhibition of SV40 gene expression by microinjected small antisense RNA and DNA molecules. *Nucleic Acids Res.* **19,** 53–58.

Graham, G. J., and Maio, J. J. (1992). A rapid and reliable method to create tandem arrays of short DNA sequences. *BioTechniques* **13,** 780–789.

Haseloff, J., and Gerlach, W. L. (1988). Simple RNA enzymes with new and highly specific endoribonuclease activities. *Nature* **334,** 585–591.

Haugwitz, M., Noegel, A. A., Karakesisoglou, J., and Schleicher, M. (1994). Dictyostelium amoebae that lack G-actin-sequenstering profilins show defects in F-actin content, cytokinesis, and development. *Cell* **79,** 303–314.

Helene, C., and Toulme, J. J. (1989). Control of gene expression by oligodeoxynucleotides covalently linked to intercalating reagents and nuclei acid cleaving reagents. *In* "Oligodeoxynucleotides: Antisense Inhibitors of Gene Expression" (J. S. Cohen, ed.), pp. 136–172. Macmillan, London.

Hesterberg, T. W., and Barrett, J. C. (1985). Induction by asbestos fibers of anaphase abnormalities: Mechanism for aneuploidy induction and possibly carcinogenesis. *Carcinogenesis* **6,** 473–475.

Hodges, D., and Crooke, S. T. (1995). Inhibition of splicing of wild-type and mutated luciferase-adenovirus pre-mRNAs by antisense oligonucleotides. *Mol. Pharmacol.* **48,** 905–918.

Hoyt, M. A., and Geiser, J. R. (1996). Genetic analysis of the mitotic spindle. *Annu. Rev. Genet.* **30,** 7–33.

Hyndman, D., Cooper, A., Pruzinsky, S., Coad, D., and Mitsuhashi, M. (1996). Software to determine optimal oligonucleotide sequences based on hybridization simulation data. *BioTechniques* **20,** 1090–1097.

Imagawa, S., Izumi, T., and Miura, Y. (1994). Positive and negative regulation of the erythropoietin gene. *J. Biol. Chem.* **269,** 9038–9044.

Jaeger, J. A., Turner, D. H., and Zuker, M. (1989). Improved predictions of secondary structures for RNA. *Proc. Natl. Acad. Sci. USA* **86,** 7706–7710.

Khan, M. L. A., Gogonea, C. B., Siddiqui, Z. K., Ali, M. Y., Kikuno, R., Nishikawa, K., and Siddiqui, S. S. (1997). Molecular cloning and expression of the Caenorhabditis elegans klp-3, an ortholog of C terminus motor kinesins Kar3 and ncd. *J. Mol. Biol.* **270,** 627–639.

Kim, S. K., and Wold, B. J. (1985). Stable reduction of thymidine kinase activity in cells expressing high levels of anti-sense RNA. *Cell* **42,** 129–138.

Knudsen, H., and Nielsen, P. E. (1996). Antisense properties of duplex- and triplex-forming PNAs. *Nucleic Acids Res.* **24,** 494–500.

Koizumi, M., and Ohtsuka, E. (1992). Design of ribozymes distinguishing a point mutation in c-Ha-ras mRNA. *In* "Antisense RNA and DNA" (J. A. H. Murray, ed.), pp. 373–381. Wiley–Liss, New York.

Kuriyama, R., Dragas-Granoic, S., Maekawa, T., Vassilev, A., Khodjakov, A., and Kobayashi, H. (1994). Heterogeneity and microtubule interaction of the CHO1 antigen, a mitosis-specific kinesin-like protein. *J. Cell Sci.* **107,** 3485–3499.

Leonetti, J. P., Mechti, N., Degols, G., Gagnor, C., and Lebleu, B. (1991). Intracellular distribution of microinjected antisense oligonucleotides. *Proc. Natl. Acad. Sci. USA* **88,** 2702–1206.

Liu, T., Williams, J. G., and Clarke, M. (1992). Inducible expression of calmodulin antisense RNA in *Dictyostelium* cells inhibits the completion of cytokinesis. *Mol. Biol. Cell* **3,** 1403–1413.

Mangan, M. E., and Olmsted, J. B. (1996). A muscle-specific variant of microtubule-associated protein 4 (MAP4) is required in myogenesis. *Development* **122,** 771–781.

Margolskee, R. F., Kavathas, P., and Berg, P. (1988). Epstein–Barr virus shuttle vector for stable episomal replication of cDNA expression libraries in human cells. *Mol. Cell. Biol.* **8,** 2837–2847.

McNeil, P. L., Murphy, R. F., Lanni, F., and Taylor, D. L. (1984). A method for incorporating macromolecules into adherant cells. *J. Cell Biol.* **98,** 1556–1564.

Milner, N., Mir, K. U., and Southern, E. M. (1997). Selecting effective antisense reagents on combinatorial oligonucleotide arrays. *Nat. Biotechnol.* **15,** 537–541.

Minshull, J., and Hunt, T. (1986). The use of single-stranded DNA and RNase-H to promote quantitative "hybrid arrest of translation" of mRNA/DNA hybrids in reticulocyte lysate cell-free translations. *Nucleic Acids Res.* **14,** 6433–6451.

Morfini, G., Quiroga, S., Rosa, A., Kosik, K., and Caceres, A. (1997). Suppression of KIF2 in PC12 cells alters the distribution of a growth cone nonsynaptic membrane receptor and inhibits neurite extension. *J. Cell Biol.* **138,** 657–669.

Morris, D. R. (1998). *Cis*-acting mRNA structures in gene-specific translational control. *In* "Post-Transcriptional Gene Regulation" (D. R. Morris and J. B. Harford, eds.). Wiley, New York.

Moulds, C., Lewis, J. G., Froehler, B. C., Grant, D., Huang, T., Milligan, J. F., Matteucci, M. D., and Wagner, R. W. (1995). Site and mechanism of antisense inhibition by C-5 propyne oligonucleotides. *Biochemistry* **34,** 5044–5053.

Nellen, W., and Sczakiel, G. (1996). *In vitro* and *in vivo* action of antisense RNA. *Mol. Biotechnol.* **6,** 7–15.

Nislow, C., Lombillo, V. A., Kuriyama, R., and McIntosh, J. R. (1992). A plus-end-directed motor that moves anti-parallel microtubules in vitro localizes to the interzone of mitotic spindles. *Nature* **359,** 543–547.

Ohkawa, J., Yuyama, N., Takebe, Y., Nishikawa, S., and Taira, K. (1993). Importance of independence in ribozyme reactions: Kinetic behavior of trimmed and of simply connected multiple ribozymes with potential activity against human immunodeficiency virus. *Proc. Natl. Acad. Sci. USA* **90,** 11302–11306.

Okano, H., Aruga, J., Nakagawa, T., Shiota, C., and Mikoshiba, K. (1991). Myelin basic protein gene and the function of antisense RNA in its repression in myelin-deficient mutant mouse. *J. Neurochem.* **56,** 560–567.

Ostarek-Lederer, A., Ostareck, D. H., Standart, N., and Thiele, B. J. (1994). Translation of 15-lipoxygenase mRNA is inhibited by a protein that binds to a repeated sequence in the 3′ untranslated region. *EMBO J.* **13,** 1476–1481.

Perez, J. R., Li, Y., Stein, C. A., Majumder, S., van-Oorschot, A., and Narayanan, R. (1994). Sequence-independent induction of Sp1 transcription factor activity by phosphorothioate oligodeoxynucleotides. *Proc. Natl. Acad. Sci. USA* **91,** 5957–5961.

Perriman, R., Graf, L., and Gerlach, W. L. (1993). A ribozyme that enhances gene suppression in tobacco protoplasts. *Antisense Res. Dev.* **3,** 253–263.

Peyman, A., Ryte, A., Helsberg, M., Kretzschmar, G., Mag, M., and Uhlman, E. (1995). Enhanced cellular uptake of G-rich oligonucleotides. *Nucleosides Nucleotides* **14,** 3–5.

Rickman, D. W., and Rickman, C. B. (1996). Suppression of trkB expression by antisense oligonucleotides alters a neuronal phenotype in the rod pathway of the developing rat retina. *Proc. Natl. Acad. Sci. USA* **93,** 2564–9256.

Rittner, K., Burmester, C., and Sczakiel, G. (1993). In vitro selection of fast-hybridizing and effective antisense RNAs directed against the human immunodeficiency virus type 1. *Nucleic Acids Res.* **21,** 1381–1387.

Robb, D. L., Heasman, J., Raats, J., and Wylie, C. (1996). A kinesin-like protein is required for germ plasm aggregation in Xenopus. *Cell* **87,** 823–831.

Robbie, E. P., Peterson, M., Amaya, E., and Musci, T. J. (1995). Temporal regulation of the *Xenopus* FGF receptor in development: A translation inhibitory element in the 3' untranslated region. *Development* **121,** 1775–1785.

Rockwell, P., O'Connor, W. J., King, K., Goldstein, N. I., Zhang, L. M., and Stein, C. A. (1997). Cell-surface perturbations of the epidermal growth factor and vascular endothelial growth factor receptors by phosphorothioate oligodeoxynucleotides. *Proc. Natl. Acad. Sci. USA* **94,** 6523–6528.

Rosfjord, E., Lamb, K., and Rizzino, A. (1994). Cryptic promoter activity within the backbone of a plasmid commonly used to prepare promoter/reporter gene constructs. *In Vitro Cell Dev. Biol.* **30A,** 477–481.

Rudner, A. D., and Murray, A. W. (1996). The spindle assembly checkpoint. *Curr. Opin. Cell Biol.* **8,** 773–780.

Sasaki, K., Zak, O., and Aisen, P. (1993). Antisense suppression of transferrin receptor gene expression in a human hepatoma cell (HuH-7) line. *Am. J. Hematol.* **42,** 74–80.

Sawin, K. E., and Mitchison, T. J. (1991). Mitotic spindle assembly by two different pathways in vitro. *J. Cell Biol.* **112,** 925–940.

Scherczinger, C. A., and Knecht, D. A. (1993). Co-suppression of Dictyostelium discoideum myosin II heavy-chain gene expression by a sense orientation transcript. *Antisense Res. Dev.* **3,** 207–217.

Schimke, R. (1984). Gene amplication in cultured animal cells. *Cell* **37,** 705.

Sczakiel, G., and Goody, R. S. (1994). Antisense principle or ribozyme action? *Biol. Chem.* **375,** 745–746.

Sharp, D. J., Kuriyama, R., and Baas, P. W. (1996). Expression of a kinesin-related protein induces Sf9 cells to form dendrite-like processes with nonuniform microtubule polarity orientation. *J. Neurosci.* **16,** 4370–4375.

Sharp, D. J., Yu, W., Ferhat, L., Kuriyama, R., Rueger, D. C., and Baas, P. W. (1997a). Identification of a microtubule-associated motor protein essential for dendritic differentiation. *J. Cell Biol.* **138,** 833–843.

Sharp, D. J., Yu, W. Q., Ferhat, L., Kuriyama, R., Rueger, D. C., and Baas, P. W. (1997b). Identification of a microtubule-associated motor protein essential for dendritic differentiation. *J. Cell Biol.* **138,** 833–843.

Shoeman, R. L., Hartig, R., Huang, Y. P., Grub, S., and Traub, P. (1997). Fluorescence microscopic comparison of the binding of phosphodiester and phosphorothioate (antisense) oligodeoxyribonucleotides to subcellular structures, including intermediate filaments, the endoplasmic reticulum, and the nuclear interior. *Antisense Nucleic Acid Drug Dev.* **7,** 291–308.

Shu, H. B., Li, Z., Palacios, M. J., Li, Q., and Joshi, H. C. (1995). A transient association of gamma-tubulin at the midbody is required for the completion of cytokinesis during the mammalian cell division. *J. Cell Sci.* **108,** 2955–2962.

Shuttleworth, J., and Colman, A. (1988). Antisense oligonucleotide-directed cleavage of mRNA in Xenopus oocytes and eggs. *EMBO J.* **7,** 427–434.

Sioud, M. (1997). Effects of variations in length of hammerhead ribozyme antisense arms upon the cleavage of longer RNA substrates. *Nucleic Acids Res.* **25,** 333–338.

Stebbins-Boaz, B., and Richter, J. D. (1997). Translational control during early development. *Crit. Rev. Euk. Gene Exp.* **7,** 73–94.

Stein, C. A., and Krieg, A. M. (1994). Problems in interpretation of data derived from *in vitro* and *in vivo* use of antisense oligodeoxynucleotides. *Antisense Res. Dev.* **4,** 67–69.

Stein, C. A., Mori, K., Loke, S. L., Subasinghe, C., Shinozuka, K., Cohen, J. S., and Neckers, L. M. (1988). Phosphorothioate and normal oligodeoxyribonucleotides with 5'-linked acridine: Characterization and preliminary kinetics of cellular uptake. *Gene* **72,** 333–341.

Szoka, F. C. (1997). Many are probed, but few are chosen. *Nat. Biotechnol.* **15,** 537–541.

Tan, T. M., Gloss, B., Bernard, H. U., and Ting, R. C. (1994). Mechanism of translation of the bicistronic mRNA encoding human papillomavirus type 16 E6-E7 genes. *J. Gen. Virol.* **75,** 2663–2670.

Temsamani, J., Kubert, M., Tang, J., Padmapriya, A., and Agrawal, S. (1994). Cellular uptake of oligodeoxynucleotide phosphorothioates and their analogs. *Antisense Res. Dev.* **4,** 35–42.

Tolentino, P. J., Dikkes, P., Tsuruda, L., Ebert, K., Fink, J. S., Villa-Komaroff, L., and Lamperti, E. D. (1995). Quantitative analysis of the expression of a VIP transgene. *Mol. Brain Res.* **33,** 47–60.

Toneguzzo, F., Keating, A., Glynn, S., and McDonald, K. (1988). Electric-field-mediated gene transfer: Characterization of DNA transfer and patterns of integration in lymphoid cells. *Nucleic Acids Res.* **16,** 5515–5532.

Toulme, J.-J. (1992). Artificial regulation of gene expression by complimentary oligonucleotides—An overview. *In* "Antisense RNA and DNA" (J. A. Murray, ed.), pp. 175–194. Wiley–Liss, New York.

Ullu, E., and Tschudi, C. (1993). 2'-O-methyl RNA oligonucleotides identify two functional elements in the trypanosome spliced leader ribonucleoprotein particle. *J. Biol. Chem.* **268,** 13068–13073.

Veres, G., Escaich, S., Baker, J., Barske, C., Kalfoglou, C., Ilves, H., Kaneshima, H., and Bohnlein, E. (1996). Intracellular expression of RNA transcripts complementary to the human immunodeficiency virus type 1 gag gene inhibits viral replication in human CD4+ lymphocytes. *J. Virol.* **70,** 8792–8800.

Vernos, I., Raats, J., Hirano, T., Heasman, J., Karsenti, E., and Wylie, C. (1995). Xklp1, a chromosomal Xenopus kinesin-like protein essential for spindle organization and chromosome positioning. *Cell* **81,** 117–127.

Walker, D. H., and Maller, J. L. (1991). Role for cyclin A in the dependence of mitosis on completion of DNA replication. *Nature* **354,** 314–317.

Williard, R., Benz, C. C., Baxter, J. D., Kushner, P., and Hunt, C. A. (1994). Paradoxical production of target protein using antisense RNA expression vectors. *Gene* **149,** 21–44.

Wilson, R. W., Ballantyne, C. M., Smith, C. W., Montgomery, C., Bradley, A., O'Brien, W. E., and Beaudet, A. L. (1993). Gene targeting yields a CD18-mutant mouse for study of inflammation. *J. Immunol.* **151,** 1571–1578.

Woolf, T. M., Jennings, C. G., Rebagliati, M., and Melton, D. A. (1990). The stability, toxicity and effectiveness of unmodified and phosphorothioate antisense oligodeoxynucleotides in Xenopus oocytes and embryos. *Nucleic Acids Res.* **18,** 1763–1769.

Wordeman, L., and Mitchison, T. J. (1995). Identification and partial characterization of mitotic centromere-associated kinesin, a kinesin-related protein that associates with centromeres during mitosis. *J. Cell Biol.* **128,** 95–105.

Yaswen, P., Stampfer, M. R., Ghosh, K., and Cohen, J. S. (1992). Effects of sequence of thioated oligonucleotides on cultured human mammary epithelial cells. *Antisense Res. Dev.* **3,** 67–77.

Yegles, M., Saint-Etienne, L., Renier, A., Janson, X., and Jaurand, M. C. (1993). Induction of metaphase and anaphase/telophase abnormalities by asbestos fibers in rat pleural mesothelial cells in vitro. *Am. J. Respir. Cell Mol. Biol.* **9,** 186–191.

Yu, W., Sharp, D. J., Kuriyama, R., Mallik, P., and Baas, P. W. (1997). Inhibition of a mitotic motor compromises the formation of dendrite-like processes from neuroblastoma cells. *J. Cell Biol.* **136,** 659–668.

CHAPTER 15

The Use and Action of Drugs in Analyzing Mitosis

Mary Ann Jordan and Leslie Wilson

Department of Molecular, Cellular, and Developmental Biology
University of California at Santa Barbara
Santa Barbara, California 93106-0001

I. Introduction: Why Use Drugs?

A large number of chemically diverse compounds, many of which are natural products, bind to tubulin or microtubules, and inhibit mitosis by acting with high selectivity on the microtubules of the mitotic spindle. Several of these drugs, notably colchicine and colcemid, nocodazole, taxol, and vinblastine, have played seminal roles in experiments probing the basic mechanisms of mitosis. In early experiments, they pointed to the importance of microtubules in mitosis. Recently, the discovery that many of these drugs powerfully suppress microtubule dynamics at concentrations below those required to increase or decrease microtubule polymer mass has led to the design of experiments directly testing the roles of

METHODS IN CELL BIOLOGY, VOL. 61

0091-679X/99 $30.00

microtubule dynamics in mitosis, such as in the involvement of microtubule-generated tension during metaphase. These drugs are powerful tools that affect microtubule polymerization and dynamics by interacting with tubulin and microtubules through diverse molecular mechanisms. Their actions on microtubule polymerization and dynamics are highly dependent on drug concentration. To use these probes most effectively to study the roles of microtubules and their dynamics in mitosis (and other cellular processes dependent on microtubules), it is important to understand (i) the mechanisms by which they bind to tubulin and microtubules; (ii) their actions on microtubule polymerization and polymer mass at high concentrations, which increase or decrease cellular microtubule mass; and (iii) their effects on dynamics at relatively low concentrations, which are below those required to affect microtubule mass.

At low concentrations, drugs such as colchicine and vinblastine, which can reduce microtubule mass at high concentrations, actually stabilize microtubule dynamics—actions that would appear to be incompatible with each other. In addition, it is important to understand that many of these antimitotic agents become greatly concentrated in cells, and the intracellular drug concentration achieved under a specific set of experimental conditions with one kind of cell will be different from that in another kind of cell and will likely not be the same as the drug concentration in the growth medium. Therefore, it is often necessary to determine the intracellular drug concentration in a specific cell type under the conditions utilized. It is also important to appreciate that when using drugs to study mitosis, the specific parameters used (e.g., time of incubation and the optimum drug concentration) will be dependent on the kinds of cells or cell models used and the questions asked.

Here we describe how the most commonly used compounds in studies of mitosis work at a biochemical/mechanistic level and present general guidelines for using the drugs as tools. Section II is a brief overview of microtubule assembly dynamics. Section III summarizes our current understanding of (i) the binding of vinblastine, colchicine, nocodazole, and taxol to tubulin and microtubules; (ii) the effects of the drugs on microtubule polymerization and dynamics *in vitro* and in cells; (iii) the levels and kinetics of cellular accumulation and loss of the compounds; (iv) the drug concentration dependence for effects on mitotic spindle organization; and (v) the advantages and disadvantages of using a particular drug for the study of microtubule assembly and dynamics. Section IV describes methods for measuring drug uptake into cultured cells, and Section V summarizes some practical guidelines for drug use.

II. Brief Overview of Microtubule Assembly Dynamics

Microtubules are polymers composed of the protein tubulin (MW 100,000), a heterodimer of two related polypeptides, α and β. Microtubules are intrinsically dynamic polymers, and their dynamic properties are critically involved in their

cellular functions (McIntosh, 1994; Wilson and Jordan, 1994; Wordeman and Mitchison, 1994; Dhamodharan *et al.,* 1995; Liao *et al.,* 1995; Tanaka *et al.,* 1995). They grow and shorten by the reversible noncovalent addition and loss of tubulin dimers at the ends of the microtubules. GTP binds exchangeably to tubulin and is irreversibly hydrolyzed during tubulin dimer addition to microtubule ends, giving rise to two unusual dynamic behaviors. "Treadmilling" is the net growth of microtubules at one end and the net shortening at the opposite end (Margolis and Wilson, 1978). "Dynamic instability" is a stochastic switching between phases of extended growing and shortening at the two ends of individual microtubules (Mitchison and Kirschner, 1984a,b).

The two ends of individual microtubules *in vitro* differ both structurally and kinetically, and the rates and durations of growing and shortening at one end, called the "plus" end, are more extensive than the rates and durations of growing and shortening at the opposite or "minus" end (Horio and Hotani, 1986; Walker *et al.,* 1988). Several important parameters characterize the dynamic behavior of microtubules, both *in vitro* and in cells, including the rates of growing and shortening; the time that a microtubule end spends growing, shortening, or in an attenuated or paused state, when no detectable length change can be detected; the frequencies of transition among the growth, shortening, and attenuation phases; the "dynamicity" (overall rate of microscopically detectable tubulin exchange at the microtubule end); and the treadmilling rate (the flow of tubulin subunits from one microtubule end to the other).

Both treadmilling and dynamic instability occur in living cells (Waterman-Storer and Salmon, 1997; Margolis and Wilson, 1998) and both behaviors appear to be fundamental to the ability of microtubules to function in spindle organization and chromosome movement. In interphase cells, microtubules exchange their tubulin with soluble cytoplasmic tubulin with half-times of ~3 min to several hours (Saxton *et al.,* 1984; Schulze and Kirschner, 1986; Pepperkok *et al.,* 1990). However, at the onset of mitosis, the interphase microtubule network disappears (Karsenti and Maro, 1986; McIntosh and Koonce, 1989; Zhai *et al.,* 1996) and is replaced by a new population of spindle microtubules that are much more dynamic than those in the interphase network. Mitotic spindle microtubules appear to be 10–100 times more dynamic than microtubules in interphase cells and exchange their tubulin with tubulin in the soluble pool with half-times of approximately 15 sec (Saxton *et al.,* 1984; Belmont *et al.,* 1990).

The rapid dynamics of spindle microtubules appear to be especially critical for spindle function. Rapid dynamics are required to build the spindle and to move the chromosomes in an accurate and timely fashion. Dynamic instability appears to be required for establishing the connections between the spindle microtubules and the kinetochores of the chromosomes. Rapid microtubule treadmilling or flux also occurs in spindles, with tubulin addition at the plus ends of microtubules, which interact with the kinetochores, and loss at minus ends, which are organized at the centrosomes, giving rise to a poleward flow of tubulin (Mitchison, 1989). Treadmilling may be important for the poleward flow of signal

molecules, the production of proper tension in the spindle, and/or the poleward transit of the chromosome during anaphase. As will be described, suppression of spindle microtubule treadmilling and dynamic instability may be one of the key actions of antimitotic drugs which have been demonstrated to block mitotic progression at the metaphase/anaphase transition.

III. Mechanisms of Action of Major Antimitotic Drugs: Binding to Tubulin and Microtubules and Effects on Microtubule Polymerization and Dynamics and on Mitosis

A. Vinblastine

The complex actions of antimitotic drugs on microtubule polymerization and dynamics will be illustrated in some detail regarding the drug vinblastine, which has strong potential as a probe of spindle microtubule dynamics. Vinblastine (MW 811; Fig. 1) is a powerful antitumor drug that is widely used in cancer chemotherapy. For many years, cell biologists shied away from using vinblastine to probe mechanisms of mitosis and the roles of microtubule dynamics in mitosis because the drug was thought to act as a "microtubule depolymerizer" and because high concentrations ($\geq 10\ \mu M$), induce formation of vinblastine–tubulin paracrystals in cells (Bensch and Malawista, 1969; Malawista and Sato, 1969; Jordan *et al.*, 1992). However, recent studies revealed that it has potent stabilizing effects on microtubule dynamics at low concentrations without inducing microtubule depolymerization. These studies have shown that vinblastine is a sensitive probe of the roles of dynamics in mitosis that acts, quite surprisingly, in a manner somewhat similar to taxol. Vinblastine (vinblastine sulfate, MW 909, Sigma Chemical Co., St. Louis, MO; ICN Biomedicals, Irvine, CA, and other sources) is readily soluble in aqueous solution (1 mM) in the cold, but more concentrated solutions have the unusual property of precipitating out of solution upon warming to room temperature and above.

1. The Actions of Vinblastine on Tubulin and Microtubules Are Highly Dependent on Drug Concentration

Vinblastine produces a remarkable range of effects on tubulin and microtubules that depends on the drug concentration used. For example, the effects of different concentrations of vinblastine, spanning seven orders of magnitude (10 pM to 100 μM), on the mass of tubulin polymer in cells and on the dynamics and organization of the tubulin polymers formed are shown in Fig. 2. High concentrations of vinblastine ($\geq 10\ \mu M$), both *in vitro* and in cells, inhibit microtubule polymerization and induce aggregation of tubulin into relatively large paracrystalline arrays. Intermediate concentrations of the drug (1 or 2 μM) depolymerize microtubules rapidly (Jordan *et al.*, 1986; Himes, 1991) and, if added to

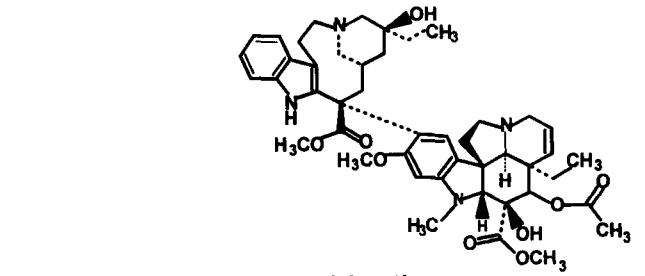

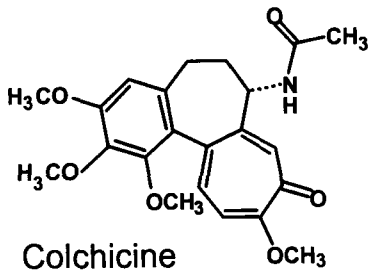

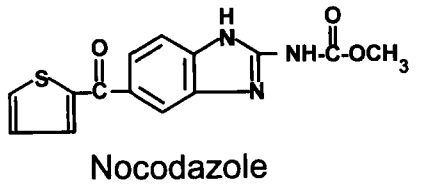

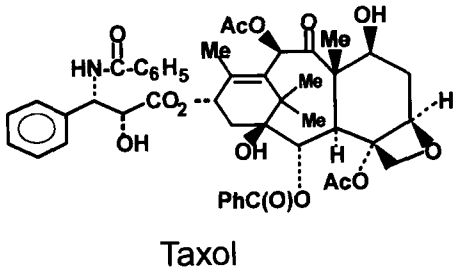

Fig. 1 Structures of antimitotic drugs.

microtubule protein prior to assembly, inhibit polymerization without causing paracrystal formation (Owellen *et al.*, 1976; Wilson *et al.*, 1976). In contrast, at low concentrations (100–200 n*M* *in vitro* and 0.5–30 n*M* added to HeLa cell cultures), vinblastine powerfully suppresses dynamic instability and treadmilling while exerting little or no effect on the microtubule polymer mass (Toso *et al.*, 1993; Dhamodharan *et al.*, 1995; Panda *et al.*, 1996).

Vinblastine binds to tubulin rapidly, and the binding is reversible and independent of temperature between 0 and 37°C. Importantly, the binding of vinblastine to tubulin induces a conformational change in the protein, leading to tubulin self-association (Na and Timasheff, 1980a,b), an action that consequently results

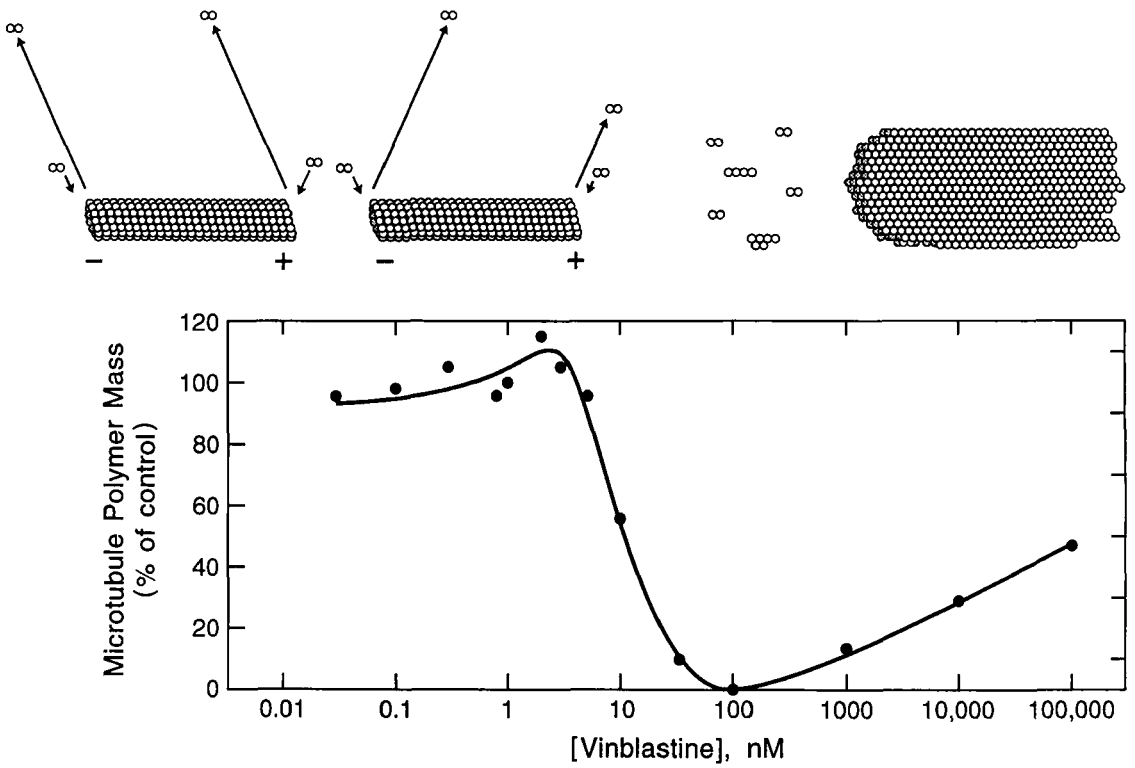

Fig. 2 Effects of vinblastine (10 p*M* to 100 μM) on the mass of tubulin polymer in cells and on the dynamics and organization of the tubulin polymers formed. The graph shows the mass of polymerized tubulin in HeLa cells after incubation for 20 hr with vinblastine over a range of concentrations from 0.03 n*M* to 100 μM. The diagrams above the graph show the effects of vinblastine on microtubule dynamics and tubulin polymers over the same range of vinblastine concentrations. Diagram on far left: In the absence of vinblastine, microtubules undergo episodes of rapid shortening and slow growing at both microtubule ends (the rates are represented quantitatively by the lengths of the arrows). Low nanomolar concentrations of vinblastine (0.1–3 n*M*) suppress dynamic instability preferentially at microtubule plus ends without changing the microtubule polymer mass. The growing and shortening rates at the plus ends are depicted (by shortened arrows) to be reduced by ~50%, whereas the minus end rates are unchanged. Intermediate concentrations of the drug rapidly (30 n*M* to 2 μM) depolymerize microtubules or, if added to microtubule protein, inhibit microtubule assembly. Vinblastine induces self-aggregation of tubulin, thus both tubulin dimers and small oligomers are represented at intermediate concentrations. Very high concentrations of vinblastine *in vitro* and in cells ($\geq$10 μM) inhibit microtubule polymerization and induce aggregation of tubulin into paracrystalline arrays.

in the formation of vinblastine–tubulin paracrystals at high vinblastine concentrations ($\geq$10 μM) (Fujiwara and Tilney, 1975). The ability of vinblastine to increase the affinity of tubulin for itself very likely plays a significant role in the ability of the drug to stabilize microtubules kinetically.

Furthermore, free vinblastine appears to be able to bind directly to microtubules as well, without first forming a complex with soluble tubulin (in contrast to the action of colchicine) (Jordan *et al.*, 1986). Additionally, in contrast to colchicine, the drug does not copolymerize with tubulin into the lattice of the microtubule (Jordan and Wilson, 1990). Vinblastine not only binds to tubulin at microtubule ends with high affinity (K_D, 1 or 2 μM) but also binds with considerably lower affinity to tubulin sites located along the surface of the microtubule cylinder (K_D, 0.25–0.3 mM). Approximately 16 or 17 high-affinity vinblastine-binding sites per microtubule are located at the ends of bovine brain microtubules (Wilson *et al.*, 1982; Jordan *et al.*, 1986; Singer *et al.*, 1989). The binding of vinblastine to these high-affinity sites is undoubtedly responsible for the potent kinetic suppression of tubulin exchange that occurs at low vinblastine concentrations (<1 μM). The binding of the vinca alkaloids to the low-affinity sites along the microtubule surface appears to be responsible for the depolymerization of microtubules *in vitro* and in cells and may also play a role in tubulin paracrystal formation.

2. Low Concentrations of Vinblastine Suppress Treadmilling and Dynamic Instability in the Absence of Significant Microtubule Depolymerization

When approximately one molecule of vinblastine is bound per microtubule *in vitro* (at 0.14 μM vinblastine), treadmilling is inhibited by 50% and the microtubule polymer mass is reduced by less than 5% (Wilson *et al.*, 1982; Jordan and Wilson, 1990). Thus, low concentrations of vinblastine kinetically stabilize treadmilling dynamics without appreciably affecting polymer mass.

The actions of vinblastine on dynamic instability at low concentrations *in vitro* differ at the two microtubule ends; low concentrations of vinblastine (e.g., 0.2–1 μM) strongly inhibit these dynamics at plus ends, whereas they enhance dynamic instability at minus ends. For example, 0.2 μM vinblastine reduces the mass of microtubules assembled from tubulin depleted of microtubule-associated proteins by only 20%, whereas it stabilizes *plus*-end dynamics by suppressing the rate and extent of growth and shortening, decreasing the catastrophe frequency, doubling the rescue frequency, and suppressing dynamicity by 82%. The same vinblastine concentration destabilizes *minus* ends by doubling the catastrophe frequency, decreasing the rescue frequency, and increasing dynamicity by 53%, thus resulting in minus-end depolymerization (Panda *et al.*, 1996). Both the kinetic *destabilization* of microtubules at minus ends and the *stabilization* at plus ends may contribute to mitotic block induced by low concentrations of vinblastine (Jordan *et al.*, 1991, 1992; Wendell *et al.*, 1993).

3. Effects of Vinblastine on the Mass of Tubulin Polymer and on the Dynamics and Organization of Microtubules and Other Tubulin Polymers Formed in Cells

The graph in Fig. 2 shows the effects of vinblastine (10 pM to 100 μM) on the mass of tubulin polymer in HeLa cells, as measured by isolation of stabilized

cytoskeletons and quantitation of polymerized tubulin by ELISA (Jordan *et al.*, 1991). The dynamics of microtubules and the organization of the tubulin polymers formed in cells over the same range of vinblastine concentrations are depicted at the top of Fig. 2. In the absence of vinblastine, microtubules undergo episodes of rapid shortening and slow growing at both microtubule ends (the rates are represented quantitatively by the lengths of the arrows in Fig. 2). Low-nanomolar concentrations of vinblastine suppress dynamic instability preferentially at plus ends without changing the microtubule polymer mass. The growing and shortening rates at plus ends, represented by shortened arrows in Fig. 2, are reduced by 50%, whereas minus-end rates are unchanged. Intermediate concentrations of the drug (1 or 2 μM) rapidly depolymerize microtubules or, if added to unassembled tubulin, inhibit microtubule assembly. Vinblastine induces self-aggregation of tubulin. Thus, both tubulin dimers and small oligomers are formed at intermediate concentrations. Very high concentrations of vinblastine *in vitro* and in cells ($\geq 10\ \mu M$) inhibit microtubule polymerization and induce aggregation of tubulin into paracrystalline arrays.

4. Effects of Vinblastine on Mitosis

Vinblastine potently blocks or slows mitosis at the metaphase/anaphase transition in a number of cell types. At high concentrations (>10 nM added to HeLa cell culture medium; >300 nM added to BSC-1 cell culture medium), mitotic block is accompanied by and most likely results from microtubule depolymerization (Jordan *et al.*, 1991; Dhamodharan *et al.*, 1995). Following nuclear envelope breakdown, no spindle forms. Chromosomes condense but do not congress and remain scattered within the cell. Chromosomes ultimately separate along their lengths but remain attached at the centromeres (Palmer *et al.*, 1960). Cyclin B levels remain high (Gong *et al.*, 1993). Mitotic block can last for more than 50 hr and may result in return to interphase in the absence of anaphase or cytokinesis, accompanied by chromatin decondensation and reformation of multiple nuclei or multilobed nuclei (Palmer *et al.*, 1960).

At low vinblastine concentrations (<10 nM in HeLa cells; <300 nM in BSC-1 kidney cells), mitotic block does not involve microtubule depolymerization (Jordan *et al.*, 1991; Dhamodharan *et al.*, 1995). In HeLa cells, 50% of the cells accumulate in metaphase 20 hr after adding 0.8 nM vinblastine to the culture medium, and anaphase is completely prevented with 1.6 nM vinblastine. The morphological changes in the blocked spindles and the suppression of microtubule dynamics in interphase cells at similar vinblastine concentrations suggest strongly that blockage is due to disruption of spindle microtubule dynamics.

5. Analysis of Spindle Microtubule Dynamics as Probed with Vinblastine

The specific alterations of spindle morphology induced by low concentrations of vinblastine (and other antimitotic drugs) are diagrammed in Fig. 3. At very

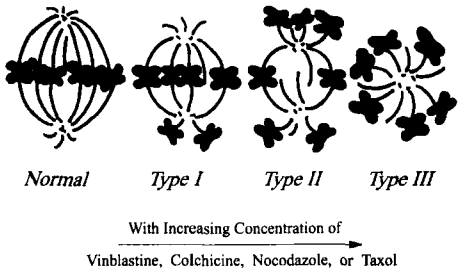

Fig. 3 Changes in spindle organization induced by increasing concentrations of antimitotic drugs. (Left) Normal bipolar spindle blocked in metaphase (with low frequency) in very low drug concentrations. (Middle left and middle right) Bipolar spindles found with high frequency in mitotic block with low concentrations of antimitotic drugs. Astral microtubules are longer and more numerous than in control cells, central spindles are shorter, centriole pairs are often disrupted, and a few chromosomes are found near the spindle poles rather than at the equatorial metaphase plate. (Right) Extremely abnormal monopolar spindles (C mitoses) that predominate at medium concentrations of drugs. Not shown: The absence of spindles in high concentrations of microtubule depolymerizing drugs [reproduced from L. Wilson and M. A. Jordan, Pharmacological probes of microtubule function, *In* "Microtubules" (J. Hyams and C. Lloyd, eds.), 1994, Wiley-Liss, Inc. Reprinted by permission of Wiley-Liss, Inc., a subsidiary of John Wiley and Sons, Inc.].

low vinblastine concentrations, some blocked spindles appear essentially normal; their spindles are bipolar, and their chromosomes are completely congressed. The observation that some spindles are blocked at the metaphase/anaphase transition by vinblastine with no detectable structural alterations provided an important indication that vinblastine might suppress microtubule dynamics thereby reducing the ability of microtubules to produce tension on kinetochores. Thus, these experiments with vinblastine suggested that tension on kinetochores might be an important factor in producing the signal to progress into anaphase (Jordan *et al.*, 1991, 1992; Wendell *et al.*, 1993). This hypothesis has been supported subsequently by the demonstration that increasing tension on relaxed kinetochores can trigger the transition into anaphase (Li and Nicklas, 1995; Nicklas *et al.*, 1995). At slightly higher vinblastine concentrations, some chromosomes fail to congress to the metaphase plate, the astral microtubules become longer and more prominent than in normal spindles, and the kinetochore microtubules become shorter (Fig. 3, middle spindles; Fig. 4: compare Figs. 4A and 4B, microtubules and chromosomes in control BSC-1 cells, with Figs. 4C and 4D, BSC-1 cells incubated with 16 n*M* vinblastine). Several other potentially important spindle abnormalities occur at low vinblastine concentrations. Long-term (20 hr) incubation of HeLa cells with vinblastine induces formation of abnormal centrioles, accumulation of membranous vesicles in the centrosome, separation of mother and daughter centrioles by large distances, and a decrease in the number of microtubules attached to kinetochores of congressed chromosomes (Wendell *et al.*, 1993). Vinblastine also inhibits oscillations or stretching between congressed sister chromatids at metaphase (Shelby *et al.*, 1996). All of these

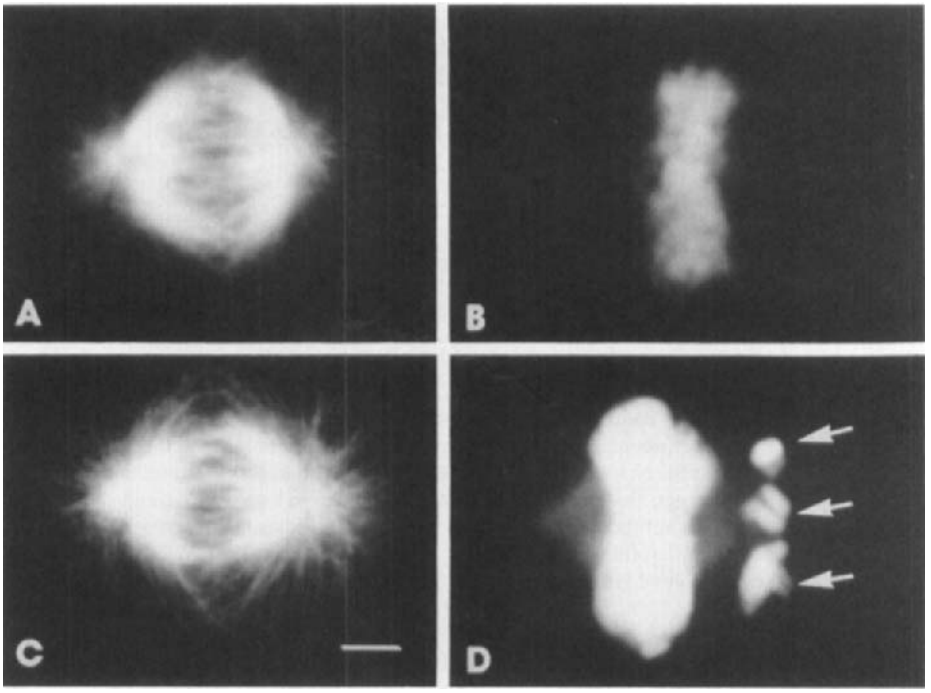

Fig. 4 Effects of vinblastine on mitotic spindle organization in BS-C-1 cells. (A and C) Indirect immunofluorescence with an antibody against tubulin. (B and D) DAPI staining of chromosomes. (A and B) Metaphase spindle of a control cell. Chromosomes have congressed to form a compact metaphase plate. (C and D) Metaphase spindle following incubation with 16 n*M* vinblastine for 22 hr. Astral microtubules (C) appear longer and more prominent than in controls; several chromosomes (arrows) have failed to congress and are located near one spindle pole. Scale bar-5 μm (reprinted with permission from Dhamodharan *et al.*, 1995).

effects on mitosis at low vinblastine concentrations may be due to the binding of a few vinblastine molecules at microtubule ends and suppression of plus-end dynamics.

This suspected action of vinblastine is strongly supported by experiments showing that mitotic block in BSC-1 cells is accompanied by suppression of microtubule dynamics (Dhamodharan *et al.*, 1995). In BSC-1 African green monkey kidney cells, we compared the effects of vinblastine (3–64 n*M* added to the medium) on dynamics of fluorescently labeled microtubules in interphase with its effects on mitotic accumulation. Microtubule dynamics were measured after 4 hr of vinblastine incubation since uptake of vinblastine into the cells attained a maximal and constant level at that time (for methods of determining uptake, see Section IV). Vinblastine (32 n*M* added to medium) significantly suppressed microtubule dynamics in the absence of microtubule depolymerization (Dhamodharan *et al.*, 1995). The extent of microtubule depolymerization was mea-

sured by quantitative ELISA of tubulin in stabilized isolated cytoskeletons (Thrower *et al.*, 1991, 1993). Shortening rates and catastrophe frequencies were reduced, time in pause or attenuation was increased, and dynamicity was reduced by 75%. Cell proliferation was inhibited, mitosis was blocked or slowed significantly, and spindles were abnormal in organization, thus strongly suggesting that these effects resulted from suppression of microtubule dynamics.

As shown in Fig. 3 (right), at higher vinblastine concentrations, microtubules are mostly depolymerized, centrosomes fail to separate, and spindles are essentially monopolar arrays of short microtubules within a sphere of condensed chromosomes.

6. Cells Accumulate Vinblastine to High Concentrations

The concentrations of vinblastine that induce similar effects on dynamics *in vivo* and *in vitro* appear widely disparate. However, intracellular accumulation of vinblastine appears to be responsible for the apparent differences in vinblastine's potency. For example, when 10 n*M* vinblastine was added to the culture medium, it accumulated intracellularly in HeLa cells 40-fold, reaching a concentration of ~400 n*M*. At 100 n*M* vinblastine, the drug accumulated to an intracellular concentration of ~3 μM (Jordan *et al.*, 1991). In BSC-1 cells, 32 n*M* vinblastine accumulated intracellularly to ~9 μM (Dhamodharan *et al.*, 1995). The mechanism(s) responsible for intracellular accumulation of vinblastine is not known but may involve binding to cellular tubulin (Jordan *et al.*, 1991). It is clear that knowing the intracellular drug concentration is important in interpretation of studies using drugs as probes. The degree of vinblastine uptake cannot be predicted and must be determined experimentally. Differential uptake of the drug in different cell types may result from differential expression of tubulin isotypes and/or the presence of different drug import or export mechanisms.

The rate of drug accumulation is also an important parameter that must be considered. For example, the time course for uptake of 2 n*M* vinblastine into HeLa cells is shown in Fig. 5. The intracellular concentration changed rapidly during the first 2 hr after drug addition. It remained relatively constant between 2 and 8 hr after drug addition and diminished gradually to 25% of maximum between 8 and 48 hr. Drug effects on mitosis will vary with the intracellular drug concentration achieved at the time of observation. Determination of intracellular drug concentrations is a relatively easy procedure (see Section IV) and may be extremely critical when using vinblastine to probe microtubule dynamics.

B. Colchicine

1. Colchicine Binding to Tubulin and Microtubules

Colchicine (Fig. 1; MW 399) is available from ICN Biomedicals, Sigma Chemical Co., and other suppliers. It is readily soluble in aqueous solution to 100 m*M*.

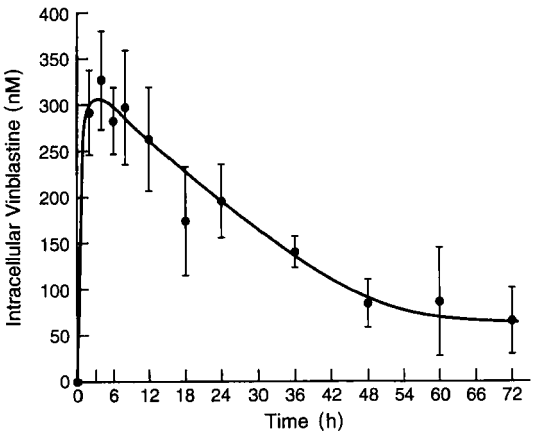

Fig. 5 The time course of uptake of 2 n*M* vinblastine into HeLa cells. [^{3}H]vinblastine (2 n*M*, 11000 Ci/mol) was added to HeLa cells growing exponentially in suspension culture. At timed intervals from 2 to 72 hr, aliquots were sampled for determination of intracellular radioactivity as described in Section IV. Data are means and standard errors derived from four to six individual measurements from three separate experiments.

Colcemid (demecolcine or *N*-deacetyl-*N*-methylcolchicine) is a frequently used analog of colchicine with similar properties. Colchicine has played a fundamental role in studies of mitosis since Levan (1938) coined the term "C-mitosis" to describe the scattered arrangement of condensed chromosomes in colchicine-treated cells, defining it as the "modification in the mitotic behavior characteristic of treatment with colchicine." Shortly thereafter, Ostergren (1944) postulated that colchicine destroyed the mitotic spindle substance by directly binding to its protein molecules. More than 20 years later, colchicine was found to bind to tubulin in cell extracts (Borisy and Taylor, 1967a,b; Wilson and Friedkin, 1967), and tubulin was initially purified using [^{3}H]colchicine binding as a biochemical marker (Weisenberg *et al.*, 1968).

2. Substoichiometric Inhibition of Microtubule Polymerization by Colchicine: Copolymer Formation

The effects of colchicine on microtubule dynamics is dependent on drug concentration. Relatively high colchicine concentrations inhibit microtubule polymerization and depolymerize preformed microtubules. At the lowest effective concentrations, colchicine inhibits microtubule dynamics with no reduction in polymer mass. Colchicine inhibits microtubule polymerization *in vitro* at concentrations well below the concentration of tubulin free in solution (Olmsted and Borisy, 1973; Margolis and Wilson, 1977; Margolis *et al.*, 1980), indicating that colchicine inhibits microtubule polymerization by interacting with the ends of the

microtubules rather than by reducing the concentration of free soluble tubulin. However, in contrast with vinblastine, which binds directly to the ends of the microtubules, colchicine either cannot bind directly to microtubule ends or it does so with very low affinity. Instead, it first binds to soluble tubulin and forms a tubulin–colchicine (TC) complex, which then incorporates at the microtubule ends (Margolis and Wilson, 1977; Skoufias and Wilson, 1992). The binding reaction between colchicine and tubulin is slow, requiring a relatively long time (as long as 2 or 3 hr, depending on concentration) to induce conformational changes in tubulin that result in the formation of the poorly reversible TC complex (Garland, 1978; David-Pfeuty *et al.,* 1979; Andreu and Timasheff, 1981, 1982; Lambeir and Engelborghs, 1981; Detrich *et al.,* 1982).

When tubulin is polymerized into microtubules *in vitro* in the presence of TC complex, the complex becomes incorporated into the microtubules along with unliganded tubulin, resulting in formation of copolymers of tubulin plus TC complex (Sternlicht and Ringel, 1979; Sternlicht *et al.,* 1983; Farrell and Wilson, 1984; Skoufias and Wilson, 1992). Such data indicate that the binding of the complex to microtubule ends does not completely prevent further tubulin addition to the ends but rather the ends remain competent to grow (Sternlicht *et al.,* 1983; Skoufias and Wilson, 1992). Thus, at low TC complex concentrations, incorporation of complexes at the microtubule ends must disrupt the tubulin lattice at or near the end in a way that impairs the efficiency of new tubulin addition but does not completely destroy the ability of tubulin to be incorporated. In contrast, at high concentrations of TC complex tubulin addition at the microtubule ends is blocked completely (Farrell and Wilson, 1980).

3. Suppression of Treadmilling and Dynamic Instability *in Vitro* by Low Concentrations of TC Complex

In vitro, the effects of colchicine on microtubule dynamics have been studied using preformed TC complex rather than free colchicine to eliminate the time required for formation of the final-state complex. Addition of 0.1 μM TC complex to steady-state bovine brain microtubules (with associated proteins) inhibits treadmilling by 50% without depolymerizing the microtubules (Wilson and Farrell, 1986; Skoufias and Wilson, 1992). TC complex kinetically stabilizes plus ends of bovine brain microtubules (Panda *et al.,* 1995) in a manner resembling that of vinblastine. For example, TC complex (0.05–0.4 μM) strongly reduces the growing and shortening rates to similar extents and increases the percentage of time the microtubules remain in an attenuated state, neither growing nor shortening detectably. TC complex strongly decreases the catastrophe frequency and increases the rescue frequency (Panda *et al.,* 1995).

4. The Effects of Colchicine on Mitosis

Like vinblastine, colchicine and colcemid slow or block mitosis at the metaphase/anaphase transition in a number of cell types, inducing accumulation

of blocked spindles in a metaphase-like state. At high colchicine concentrations (*Chaetopterus* oocytes incubated in >10 μM colchicine; ≥30 nM added to HeLa cell culture medium), microtubule polymerization is inhibited and the mitotic spindle dissociates or is not formed (Inoue, 1952; M. A. Jordan, D. Thrower, and L. Wilson, unpublished data). Mitotic block at such high concentrations most likely results from the complete depolymerization of microtubules. Chromosomes condense but do not congress and remain scattered within the cell in a C-mitosis (Levan, 1938).

High concentrations of colcemid (200 nM) [as well as high concentrations of nocodazole (1.5 μM) and taxol (1–10 μM)] induce mitotic block which lasts as long as 72 hr. in many primate cell lines but not in mouse and hamster cell lines, which instead continue the cell cycle in the absence of cytokinesis, producing polyploid cells (Kung *et al.*, 1990). Cyclin B and $p34^{cdc2}$ levels remain high during long-term block in the primate cell lines but undergo periodic degradation in the cycling nonprimate cell lines. These observations suggest that there is a fundamental difference in the stringency of the mitotic checkpoint control mechanism induced by antimitotic drugs in primate versus nonprimate cell lines (Kung *et al.*, 1990). Some plant and animal cells appear to undergo anaphase in the presence of colchicine ("C-anaphase") with disjunction of chromatids along their lengths and at the centromeres, but with no ensuing cytokinesis (Rieder and Palazzo, 1992). Following C-mitosis, chromatids swell and a polyploid restitution nucleus (interphase) is formed. In HeLa cells, mitotic block with high concentrations of colcemid (200 nM) results in apoptosis within 24–48 hr (Sherwood *et al.*, 1994).

In HeLa cells at low colchicine concentrations (<20 nM), mitotic block does not involve significant microtubule depolymerization. For example, with addition of 16 nM colchicine to HeLa cells, mitosis is arrested in 60% of the cells and arrest is accompanied by <20% reduction in microtubule polymer levels (M.A. Jordan, D. Thrower, and L. Wilson, unpublished data). Alterations in spindle organization resemble those induced by low concentrations of vinblastine (Fig. 3), suggesting that blockage occurs as a result of suppression of microtubule dynamics.

5. Cellular Uptake and Loss of Colchicine

Like vinblastine, colchicine accumulates intracellularly many-fold over the concentration added to the culture medium. For example, 7 nM colchicine added to HeLa cells accumulated 25-fold to an intracellular concentration of 178 ± 11 nM (Jordan and Wilson, 1998).

6. Colchicine Is Not Widely Used to Determine the Cellular Effects of Altering Microtubule Assembly Dynamics

The use of colchicine and colcemid in cellular studies (Sluder, 1979; Bamburg *et al.*, 1986; Rieder and Palazzo, 1992; McEwen *et al.*, 1993; Yu and Baas, 1995)

has diminished and these have been replaced by nocodazole. The binding of colchicine to tubulin is slow, which could potentially result in unpredictable levels of TC complex and thus variable effects on polymerization and dynamics. Another disadvantage of colchicine is that its cellular effects are not easily reversible (Zieve *et al.*, 1980).

C. Nocodazole

1. Binding to Tubulin and Rapid Depolymerization of Microtubules in Cells

Nocodazole [methyl (5,2-thienylcarboxyl-1H-benzimidazole-2-YL)-carbamate, MW 301, Janssen Pharmaceutical, Piscataway, NJ; also available from Sigma Chemical and ICN Biomedicals] (Fig. 1) is widely used to study microtubule-dependent processes because, at high concentrations, it rapidly depolymerizes microtubules in cells (DeBrabander *et al.*, 1976). Nocodazole is soluble in dimethyl sulfoxide at 15–30 mM but precipitates in aqueous media at concentrations >30 μM (an information sheet is available from Janssen Pharmaceutical). Nocodazole substoichiometrically inhibits the polymerization of tubulin into microtubules *in vitro* with an IC_{50} of 1 μM (Hoebeke *et al.*, 1976; Lee *et al.*, 1980; DeBrabander *et al.*, 1976). Nocodazole binds in the colchicine-binding domain of tubulin and shares with colchicine the property of increasing the GTPase activity of tubulin in the absence of polymerization (Lin and Hamel, 1981; Carlier and Pantaloni, 1983; Hamel *et al.*, 1988; Lin *et al.*, 1989; Andreu *et al.*, 1991; Mejillano *et al.*, 1996). This property is distinct from that of drugs that bind to the vinblastine domain that in general suppress GTPase activity in parallel with (and probably causally related to) inhibition of microtubule polymerization (David-Pfeuty *et al.*, 1979).

When high concentrations of nocodazole are added to cells, microtubules are rapidly depolymerized, and mitosis is blocked. A number of studies have employed high concentrations of nocodazole (≥200 nM) to examine the effects of partial or complete microtubule depolymerization on the process of mitosis (Ates and Sentein, 1981; Snyder *et al.*, 1983; Paweletz and Lang, 1988; Centonze and Borisy, 1991; Waters *et al.*, 1996). The half-times for microtubule depolymerization with 20 μM nocodazole range from 4 to 72 min, depending on cell type. Complete depolymerization occurs in 4 hr in MDCK cells at 4 μM nocodazole (Wadsworth and McGrail, 1990).

There is good evidence that the rates of uptake and release of nocodazole in cells are relatively rapid. Within 90 min of washing HeLa cells that were blocked in mitosis using 130 nM nocodazole, 80% of the cells had reformed spindles and completed mitosis (Zieve *et al.*, 1980). Nocodazole (165–330 nM) inhibited microtubule dynamic instability in neuronal growth cones within 30 min of application, and the inhibition was reversed within 30 min of washout (Rochlin *et al.*, 1996). Nocodazole is frequently used to examine reformation of microtubules after drug removal; for example, 84% recovery of polymer was reported 2 hr following removal from MDCK cells (Wadsworth and McGrail, 1990). Cell migra-

tion stopped within 10 min of adding 300 n*M* nocodazole and resumed at the control rate within 10 min of washing the cells with nocodazole-free medium (Liao *et al.,* 1995). Mitotic spindles begin to shorten in length within 3 min of adding 250 n*M* nocodazole to LLC-PK cells, and the shortening is partially reversed within 5 min of nocodazole removal (Centonze and Borisy, 1991).

2. Low Concentrations of Nocodazole Inhibit Microtubule Dynamic Instability *in Vitro* and in Cells

Nocodazole inhibits dynamic instability of microtubules *in vitro* (4 n*M*–12 μM) and in cells (4–400 n*M*), suppressing the rates of growing and shortening and greatly increasing the percentage of time in an attenuated or paused state (Wilson *et al.,* 1993; Vasquez *et al.,* 1997). Vasquez *et al.* found that dynamics at both plus and minus ends are suppressed by the drug. The effects on frequencies of catastrophe and rescue appear to be complex and strongly dependent on drug concentration.

3. Effects of Low Nocodazole Concentrations on Mitosis

In HeLa cells, 100 n*M* nocodazole completely blocks mitosis with only 20% loss of microtubule mass (Jordan *et al.,* 1992). Spindle organization is altered in ways that resemble alterations induced by other drugs (vinblastine, taxol, colchicine, and podophyllotoxin) that suppress microtubule dynamics, thus suggesting that the mechanism of mitotic block by low concentrations of nocodazole is suppression of spindle microtubule dynamics. Short-term mitotic block by nocodazole appears to be relatively reversible, and low concentrations of nocodazole have been used to partially synchronize cells (130 n*M* at 4 hr). Following removal of nocodazole, cells completed mitosis and continued to grow with no observed ill effects over the time course of the experiment (Zieve *et al.,* 1980). However, users should be aware that nocodazole, like other antimitotic compounds, can induce apoptosis in some cell lines after prolonged incubation (Yu *et al.,* 1997).

D. Taxol and Related Compounds

Taxol (paclitaxel, MW 854, available from Calbiochem, Sigma Chemical, ICN Biomedicals, and other suppliers) (Fig. 1) arrests cells in mitosis by stabilizing spindle microtubules (Schiff and Horwitz, 1980; Jordan *et al.,* 1993; Derry *et al.,* 1995). Taxol is readily soluble in dimethyl sulfoxide (DMSO) or methanol (>10 m*M*), but it has limited solubility in water. Dilutions of taxol into aqueous solutions from a stock in DMSO are initially clear at concentrations as high as 35 μM (Swindell *et al.,* 1991), but upon standing overnight the drug precipitates and the true solubility in water appears to be no higher than 0.77 μM (Mathew *et al.,* 1992). Taxol adheres avidly to plastics so solutions should be prepared in

glass (R. H. Himes, personal communication). In addition to stabilizing microtubules and greatly increasing the microtubule polymer mass in cells, high concentrations of taxol induce microtubule "bundling" (Schiff and Horwitz, 1980; Turner and Margolis, 1984; Rowinsky *et al.,* 1988; Roberts *et al.,* 1989), a phenomenon which is not well understood.

1. Taxol Binding to Microtubules

Taxol binds directly to microtubules in cells (Manfredi *et al.,* 1982), and it binds reversibly to microtubules *in vitro* with high affinity (K_D, ~10 nM) (Caplow *et al.,* 1994). At high taxol concentrations, 1 mol of taxol binds per mol of tubulin in microtubules (Parness and Horwitz, 1981; Diaz and Andreu, 1993; Caplow *et al.,* 1994). Taxol can also bind to soluble tubulin subunits, but with significantly reduced affinity (Parness and Horwitz, 1981; Takoudju *et al.,* 1988; Diaz *et al.,* 1993; Sengupta *et al.,* 1995). Taxol binding does not inhibit the binding of colchicine, podophyllotoxin, or vinblastine to tubulin (Kumar, 1981; Schiff and Horwitz, 1981). Thus, taxol binds at a site that is distinct from the binding sites of these other drugs. Taxotere (docetaxol; Rhone-Poulenc Rorer, Vitry-sur-Seine, France), a more water-soluble analog of taxol, binds to the same site on microtubules as taxol and is slightly more potent than taxol in its effects on cells and on tubulin polymerization (Ringel and Horwitz, 1991a; Diaz and Andreu, 1993). Recently, three nontaxoid natural product compounds, epothilones A and B and discodermolide, have been found to share a number of properties with taxol and taxotere: They arrest cells in mitosis, cause formation of microtubule bundles in cells, and stabilize microtubule polymers (Bollag *et al.,* 1995; ter Haar *et al.,* 1996; Kowalski *et al.,* 1997).

In contrast to vinblastine, colchicine, podophyllotoxin, and nocodazole, taxol enhances microtubule polymerization *in vitro,* promoting both nucleation and elongation phases of the polymerization reaction and reducing the critical tubulin subunit concentration (*i.e.,* soluble tubulin concentration at steady state) (Kumar, 1981; Schiff and Horwitz, 1981; Howard and Timasheff, 1988). Microtubules polymerized in the presence of high taxol concentrations are extremely stable. They resist depolymerization by cold temperature, calcium ions, dilution, and other antimitotic drugs (Schiff *et al.,* 1979; Kumar, 1981; Howard and Timasheff, 1988). Taxol induces the self-assembly of tubulin into microtubules under unusual conditions: at 0°C (Thompson *et al.,* 1981), in the absence of exogenous GTP (Hamel *et al.,* 1981; Schiff and Horwitz, 1981), without microtubule-associated proteins (Kumar, 1981), and at alkaline pH (Ringel and Horwitz, 1991b).

High concentrations of taxol can induce the formation of morphologically altered tubulin polymers, a phenomenon whose importance in cell function remains to be determined. For example, taxol induces the formation of microtubules with predominantly 12 protofilaments rather than 13, both *in vitro* from pure tubulin (Andreu *et al.,* 1992), and *in vivo* (Mogenson and Tucker, 1990). Taxol also can induce the formation of hoops, ribbons, and other protofilamen-

tous structures *in vitro* (Parness and Horwitz, 1981; Thompson *et al.,* 1981; Bokros *et al.,* 1993).

2. Suppression of Treadmilling and Dynamic Instability by Low Concentrations of Taxol with Little or No Increase in Microtubule Mass *in Vitro* and in Cells

The specific effects of taxol on microtubule polymerization dynamics are complex and vary with the stoichiometry of taxol binding to the microtubule. At low concentrations (10–50 nM), the binding of small numbers of taxol molecules to microtubules reduces the rate and extent of shortening at microtubule plus ends (Derry *et al.,* 1995). For example, when only one taxol molecule is bound for every 270 tubulin dimers in the microtubules, the rate and extent of shortening is reduced by 32%. Under these conditions, taxol may bind at widely spaced sites along the microtubule surface, and the microtubules may shorten until a bound molecule of taxol is reached. Then, either the taxol molecule or the tubulin complexed to taxol may be required to dissociate before the microtubule can shorten further. Low concentrations of taxol (10–100 nM) preferentially suppress dynamics and induce a modest increase in microtubule length at microtubule plus ends while having little or no effect on the dynamics and lengths at microtubule minus ends (Derry *et al.,* 1998). Unlike vinblastine, colchicine, and nocodazole, low concentrations of taxol do not affect catastrophe or rescue frequencies.

At intermediate taxol concentrations (100 nM to 1 μM), the taxol-to-tubulin binding stoichiometry in microtubules increases, growing rates are suppressed to the same degree as shortening rates, and microtubules remain in a state of attenuation or pause most of the time. At very high taxol concentrations (1–20 μM), the binding of taxol to microtubules saturates at a stoichiometry of 1 mol taxol/mol tubulin, and the mass of microtubule polymer increases sharply as tubulin is recruited into the microtubules. Tubulin dissociation is inhibited at both microtubule ends while the ends remain free for normal tubulin addition (Kumar, 1981; Caplow and Zeeberg, 1982; Wilson *et al.,* 1985; Caplow *et al.,* 1994; Derry *et al.,* 1995).

3. Suppression of Dynamic Instability in Cells by Taxol

Low concentrations of taxol induce ~90% mitotic block at the metaphase/anaphase transition in HeLa cells. Spindle abnormalities, and the absence of significant microtubule bundling or of any increase in microtubule polymer mass as measured by quantitative ELISA of isolated cytoskeletons, suggested strongly that the mitotic block results from suppression of microtubule dynamics (Jordan *et al.,* 1993).

Recently, it was found that in human carcinoma cells, taxol suppresses microtubule dynamics in qualitatively the same way as it does with bovine brain microtubules *in vitro* (A.-M. Yvon, P. Wadsworth, and M. A. Jordan, unpublished observations). Human kidney carcinoma and ovarian carcinoma cells were mi-

croinjected with rhodamine-labeled tubulin; the labeled tubulin was allowed to incorporate into cellular microtubules for 90 min prior to addition of taxol to the cells. Cells were incubated with taxol for 4 hr prior to video microscopy to allow the intracellular taxol concentration to reach equilibrium. Suppression of microtubule dynamics by taxol resulted in abnormal spindle organization, some retraction of interphase microtubules from the periphery of the cell, and a slight degree of bundling in interphase.

In an examination of the role of tension on kinetochores in signaling anaphase onset, low concentrations of taxol (0.3–3 n*M*) were used to suppress spindle microtubule dynamics in PtK1 cells (Rieder *et al.*, 1994). Video microscopy revealed that anaphase onset could be delayed in cells containing fully congressed chromosomes by suppressing microtubule dynamics with taxol, demonstrating the importance of microtubule dynamics for cell cycle progression.

4. The Effects of Taxol on Mitosis

Like vinblastine, colchicine, and nocodazole, taxol slows or blocks mitosis at the metaphase/anaphase transition in a number of cell types, inducing accumulation in a metaphase-like state. At low taxol concentrations (≥10 n*M* in HeLa cells), mitosis is blocked with no concomitant change in the mass of intracellular microtubules. Alterations in spindle organization resemble those induced by low concentrations of vinblastine (Fig. 3), suggesting that blockage occurs as a result of suppression of microtubule dynamics. For example, at 33 p*M* to 10 n*M* taxol, many spindles are blocked with a nearly normal spindle configuration. Spindles are bipolar, with a compact metaphase plate and from zero to several chromosomes lagging or becoming "stuck" at the spindle poles. Astral microtubules are more prominent than in control spindles and the central spindle is reduced in length (Jordan *et al.*, 1993). With increasing concentrations of taxol, spindle morphology becomes more abnormal. At high concentrations of taxol (≥100 n*M*), taxol induces massive assembly of microtubules, blocking mitosis in the presence of large and dense asters which contain prominent bundles of stabilized microtubules. Spindles may be monopolar or, depending on the cell type, multipolar and multiastral, and chromosomes condense but do not congress (Schiff and Horwitz, 1980; DeBrabander *et al.*, 1981).

5. Cellular Uptake and Loss of Taxol

Taxol accumulates in HeLa cells to an extraordinary extent—240 to 830-fold over the concentration added in the medium (Table I). A large percentage of taxol is retained following washing; thus, the uptake of taxol is not easily reversible (Jordan *et al.*, 1993, 1996).

Taxol is initially taken up rapidly, but to reach equilibrium requires several hours. The time course of uptake of [^{3}H]taxol into HeLa cells is shown in Fig. 6. Within the first 10 min after addition of 10 n*M* taxol to the medium, the

Table I
Intracellular Levels of Taxol during Taxol Incubation of HeLa Cells and Following Washing with Taxol-Free Medium

Taxol added to medium at time 0 (μM)	Taxol in cells at 20 hr (μM)	Fold uptake	Taxol in cells 24 hr after washing (μM)	Retention (%)
0.003	1.7 ± 0.2	570	0.7 ± 0.04	42
0.01	8.3 ± 2.1	830	4.0 ± 0.7	48
0.1	71.5 ± 6.2	720	27.0 ± 6.7	38
1.0	241.0 ± 27.0	240	38.6 ± 9.9	16

Note. Taxol concentration in HeLa cells after incubation for 20 hr in taxol-containing medium and retention 24 hr after removal of taxol from medium and washing of cells with three changes of taxol-free medium (2 hr total washing). Data were obtained as described in Section IV. Taxol (3 nM–1 μM, 33–11,000 Ci/mol) was a kind gift from the National Cancer Institute (Research Triangle Institute, NC). Values are mean ± SE from three experiments (two in monolayer and one in suspension); n = 4 or 6 total measurements. Data are from Jordan *et al.* (1996).

intracellular concentration rose to 1.4 ± 0.3 μM, a 140-fold increase, and reached half-maximum at ~100 min. By 6 hr, the intracellular concentration approached the maximum (14.6 ± 1.4 μM at 24 hr). After addition of 100 nM taxol to the medium, the intracellular concentration rose to 8.4 ± 1.0 μM within the first 10 min, an 84-fold increase, and reached half-maximum by 25 min. By 2 hr the intracellular concentration approached equilibrium at 41 μM. Thus, experiments performed during the first hours of taxol incubation will reflect the effects of rapidly changing taxol concentrations.

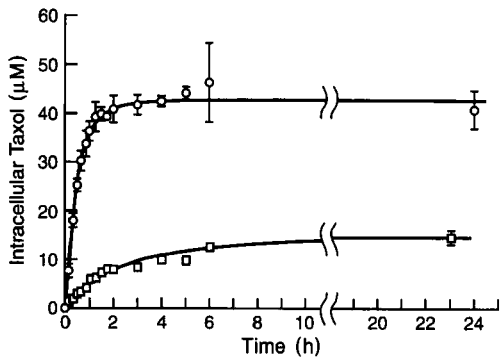

Fig. 6 The time course of uptake of 10 nM (□) and 100 nM (○) taxol into HeLa cells. [^{3}H]taxol (350–3500 Ci/mol), a gift of the National Cancer Institute (NSC 125973), was added to HeLa cells growing exponentially in scintillation vials. At timed intervals from 10 min to 24 hr, samples were prepared for determination of intracellular radioactivity as described in Section IV. Values are means and standard errors of four separate experiments.

IV. Determination of Intracellular Drug Levels

1. Monolayer or suspension culture in flasks (Jordan *et al.,* 1991): Seed cells for suspension culture or into monolayer culture flasks (225 cm^2) at a density such that they will not become superconfluent during the course of the experiment (e.g., for a 20-hr drug incubation with HeLa cells, use 4×10^5 cells/ml). After 1 or 2 days, replace medium with medium containing ^3H-labeled drug (final specific activity can range from 30 to 11,000 Ci/mol). Radiolabeled vinblastine and colchicine can be obtained from Amersham (Arlington Heights, IL), New England Nuclear (Wilmington, DE), and Moravek Biochemicals (Brea, CA). Radiolabeled taxol can be obtained from Research Triangle Institute, North Carolina, and Moravek Biochemicals. Radiolabeled nocodazole is not available commercially. Reserve 2×10 μl aliquots of the final dilution of drug in medium for determination of specific activity. After the desired duration of drug incubation (minutes to days), release cells from monolayer by scraping with a rubber policeman and collect by centrifugation (in 15-ml tubes, ICN clinical centrifuge, 5 min, speed setting 2 or 3). Add [^{14}C]hydroxymethylinulin (Amersham; 0.0156 Ci/ml final concentration) to suspensions immediately prior to centrifugation for determination of extracellular drug trapped in the pellets and for determination of total cell volume in the pellets. Hydroxymethylinulin is not significantly internalized by living cells. Thus, total cell volume can be determined by subtracting extracellular volume (as indicated by trapped hydroxymethylinulin) from the total volume of the pellets of centrifuged cells.

Remove 100-μl aliquots from supernatant for determination of noninternalized drug and add to scintillant for counting. Aspirate remaining supernatant as completely as possible and discard. Remove 100-μl aliquots of the semifluid pellet (by pipetting) and add to scintillant (e.g., Beckman Ready-Protein) for determination of intracellular drug concentration. An alternative method for measuring cell and pellet volumes (using radiolabeled H_20 and radiolabeled hydroxymethylinulin) has been described (Singer and Himes, 1992).

2. Monolayer culture directly in sterilized scintillation vials: Seed cells directly in sterile, autoclaved polylysine-coated (50 μg/ml, 2 hr at 37°C, followed by a rinse with sterile water and a rinse with medium) glass scintillation vials at 3×10^5 cells/ml. Aspirate medium and replace with 2.5 ml of medium containing [^3H]drug at the desired concentration 24 hr later. Remove 2×10 μl aliquots of each suspension for determination of specific activity. Following incubation with [^3H]drug, aspirate medium and wash the cells quickly three times with 2.5 ml buffer [0.1 *M* piperazine-*N,N'*-bis(2-ethanesulfonic acid), 1 m*M* EGTA, 1 m*M* $MgSO_4$, pH 6.9, at 37°C]. Lyse cells by adding 1 ml distilled water and add 10 ml scintillation fluid (Beckman Ready-Protein) for determination of radioactivity. Incubate duplicate vials under the same conditions using nonradiolabeled drug to determine the cell number at each time point and each drug concentration. Determine total cell volume by multiplying the number of cells by the volume

of an average cell (calculated from measurements of cell radius by microscopy after trypsinizing the cells so they become spherical). For example, the average volume of a HeLa cell is 2.4 pl. Similarly, using $[^3H]H_20$, Singer and Himes (1992) found the water volume of a B_{16} melanoma cell to be 1.09 pl. Determine adherence of [^{3}H] drug to scintillation vials; with taxol and vinblastine, we found that it was $< 0.5\%$ of total radioactivity (Jordan *et al.*, 1996).

3. Singer and Himes (1992) measured the uptake of nonradiolabeled vinca alkaloids into B_{16} melanoma cells by high-performance liquid chromatography (HPLC) analysis after extracting the drugs from the cellular protein. Cells were grown in 100-mm culture dishes to a density of $\sim 1 \times 10^7$ cells/dish. Medium was then replaced with 4 ml of fresh medium containing 0.1 or 1 μM of drug. After the desired time of incubation (at 37°C) the medium was removed and the plates were washed quickly three times with phosphate-buffered saline. The cells were detached with trypsin–EDTA, suspended in phosphate-buffered saline, counted, and sonicated. Sonicated samples (1 ml) were cleared of protein by precipitating with 2 ml acetonitrile, followed by centrifugation. Then 2.7 ml of supernatant was evaporated (60°C) under a stream of N_2. The residue was dissolved in 50% methanol in 10 mM KH_2PO_4 (pH 4.5) and the amount of vinca alkaloid present was determined by HPLC.

V. How to Use Antimitotic Drugs: Practical Guidelines

1. It is first necessary to determine the effects of the drug on spindle microtubule organization and mitosis (or any other cell organelle or behavior, such as motility) over a range of concentrations in the cells of choice. It is most useful to examine the effects at 3.3-fold concentration intervals (e.g., 1, 3.3, 10, 33, 100, 330, 1000, and 3300 nM), but 10-fold concentration intervals (0.1, 1, 10, 100, 1000, and 10,000 nM) may also be used. The method of examination will vary and might include immunofluorescence microscopy using an antibody against tubulin to examine spindle structure, examination of chromosomal squashes stained with DAPI, video phase microscopy, cell counting, or determination of frequency of entry into anaphase. The choice will depend on the goal of the study.

2. Ensure the drug is completely solubilized. Cloudy solutions give erratic results, and it is extremely difficult to make accurate serial dilutions of drugs that are only suspended, not dissolved. Some drugs stick to glass, plastic, or serum proteins. Of the drugs we have discussed, taxol adheres to plastics and should be solubilized and diluted in glass vessels (R. H. Himes, personal communication).

3. Determine the effects of varying the duration of drug incubation. As described previously, rates of drug uptake affect the results and require careful consideration. In our experience with HeLa cells, equilibrium concentrations are

approached after 2–4 hr of drug incubation with vinblastine or taxol. Nocodazole is taken up rapidly, but the changes in concentration over time have not been studied.

4. Do not use concentration/time data from one cell type for another cell type. Extrapolations from one cell type to another are extremely dangerous and may invalidate the conclusions reached. The response of different cell types to a given drug varies vastly. (This is frequently the basis of clinical chemotherapeutic selectivity.) The parameters determining response may include such variables as tubulin isotype composition, expression of multidrug resistance proteins, permeability differences, and inherent metabolic characteristics of the cell.

5. Examine a sufficient number of individual cells. The response of individual cells to drugs varies for reasons which are not understood. Individual cells appear to take up some drugs to varying degrees depending on the cell cycle stage of the individual cell (Lopes *et al.*, 1993).

6. Try alternative antimitotic drugs; these may strengthen the validity of the conclusions. All drugs, even all biochemical probes, have multiple effects that may be considered "side effects" depending on the concentrations used. If more than one antimitotic drug probe produces an interesting effect on mitosis, it is more likely that the effect is specific to the effects of the drug on tubulin or microtubules and not to nonspecific effects.

7. Valuable insight can be gained by examining the drug concentration dependence for a given experimental observation. For example, our observation that vinblastine alterated spindle morphology in a concentration-dependent manner initially suggested to us that suppression of microtubule dynamics was involved in the mitotic block (Jordan *et al.*, 1991).

Acknowledgments

We thank Ms. Kim Wendell, Ms. Etsuko Tsuchiya, and Dr. Douglas Thrower for excellent assistance in measuring drug uptake and Dr. Vivian Ngan for critically reading the manuscript. The work was supported by Grants CA 57291 and NS13560 from NIH to MAJ and LW.

References

Andreu, J. M., and Timasheff, S. N. (1981). The ligand and microtubule assembly-induced GTPase activity of purified calf brain tubulin. *Arch. Biochem. Biophys.* **211,** 151–157.

Andreu, J., and Timasheff, S. (1982). Conformational states of tubulin liganded to colchicine, tropolone methyl ether and podophyllotoxin. *Biochemistry* **21,** 6465–6476.

Andreu, J. M., Gorbunoff, M. J., Medrano, F. J., Rossi, M., and Timasheff, S. N. (1991). Mechanism of colchicine binding to tubulin. Tolerance of substituents in ring C' of biphenyl analogs. *Biochemistry* **30,** 3777–3786.

Andreu, J. M., Bordas, J., Diaz, J. F., Garcia de Ancos, J., Gil, R., Medrano, F. J., Nogales, E., Pantos, E., and Towns-Andrews, E. (1992). Low resolution structure of microtubules in solution; Synchrotron x-ray scattering and electron microscopy of taxol-induced microtubules assembled from purified tubulin in comparison with glycerol and map-induced microtubules. *J. Mol. Biol.* **226,** 169–184.

Ates, Y., and Sentein, P. (1981). Action of nocodazole on segmentation mitoses of Triturus helveticus Raz. electron microscopy. *Biol. Cell* **40,** 175–180.

Bamburg, J. R., Bray, D., and Chapman, K. (1986). Assembly of microtubules at the tip of growing axons. *Nature* **321,** 788–790.

Belmont, L., Hyman, A. A., Sawin, K. E., and Mitchison, T. J. (1990). Real-time visualization of cell cycle-dependent changes in microtubule dynamics in cytoplasmic extracts. *Cell* **62,** 579–589.

Bensch, K. G., and Malawista, S. E. (1969). Microtubular crystals in mammalian cells. *J. Cell Biol.* **40,** 95–107.

Bokros, C. L., Hugdahl, J. D., Hanesworth, V. R., Murthy, J. V., and Morejohn, L. C. (1993). Characterization of the reversible taxol-induced polymerization of plant tubulin in microtubules. *Biochemistry* **32,** 3437–3447.

Bollag, D. M., McQueney, P. A., Zhu, J., Hensens, O., Koupal, L., Liesch, J., Goetz, M., Lazarides, E., and Woods, C. M. (1995). *Cancer Res.* **55,** 2325–2333.

Borisy, G. G., and Taylor, E. W. (1967a). The mechanism of action of colchicine. Binding of colchicine-3H to cellular protein. *J. Cell Biol.* **34,** 525–533.

Borisy, G. G., and Taylor, E. W. (1967b). The mechanism of action of colchicine. Colchicine binding to sea urchin eggs and the mitotic apparatus. *J. Cell Biol.* **34,** 535–548.

Caplow, M., and Zeeberg, B. (1982). Dynamic properties of microtubules at steady state in the presence of taxol. *Eur. J. Biochem.* **127,** 319–324.

Caplow, M., Shanks, J., and Ruhlen, R. (1994). How taxol modulates microtubule disassembly. *Biochemistry* **269,** 23399–23402.

Carlier, M.-F., and Pantaloni, D. (1983). Taxol effect of tubulin polymerization and associated guanosine 5'-triphosphate hydrolysis. *Biochemistry* **22,** 4814–4822.

Centonze, V. E., and Borisy, G. G. (1991). Pole-to-chromosome movements induced at metaphase: Sites of microtubule disassembly. *J. Cell Sci.* **100,** 205–211.

David-Pfeuty, T., Simon, C., and Pantaloni, D. (1979). Effect of antimitotic drugs on tubulin GTPase activity and self-assembly. *J. Biol. Chem.* **254,** 11696–11702.

DeBrabander, M., Geuens, G., Nuydens, R., Willebrords, R., and De Mey, J. (1981). Taxol induces the assembly of free microtubules in living cells and blocks the organizing capacity of the centrosomes and kinetochores. *Proc. Natl. Acad. Sci. USA* **78,** 5608–5612.

DeBrabander, M. J., Van de Veire, R. M. L., Aerts, F. E. M., Borgers, M., and Janssen, P. A. J. (1976). The effects of methyl [5-(2-thienylcarbonyl)-1H-benzimadazol-2-yl]carbamate(R 17934; NSC 238159), a new synthetic antitumoral drug interfering with microtubules, on mammalian cells cultured in vitro. *Cancer Res.* **36,** 905–916.

Derry, W. B., Wilson, L., and Jordan, M. A. (1995). Substoichiometric binding of taxol suppresses microtubule dynamics. *Biochemistry* **34,** 2203–2211.

Derry, W. B., Wilson, L., and Jordan, M. A. (1998). Low potency of taxol at microtubule minus ends: Implication for its anti-mitotic and therapeutic mechanism. *Cancer Res.* **58,** 1177–1184.

Detrich, H. W., III, Williams, R. C., Jr., and Wilson, L. (1982). Effect of colchicine binding on the reversible dissociation of the tubulin dimer. *Biochemistry* **21,** 2392–2400.

Dhamodharan, R. I., Jordan, M. A., Thrower, D., Wilson, L., and Wadsworth, P. (1995). Vinblastine suppresses dynamics of individual microtubules in living cells. *Mol. Biol. Cell* **6,** 1215–1229.

Diaz, J. F., and Andreu, J. M. (1993). Assembly of purified GDP-tubulin into microtubules induced by taxol and taxotere: Reversibility, ligand stoichiometry, and competition. *Biochemistry* **32,** 2747–2755.

Diaz, J. F., Menendez, M., and Andreu, J. M. (1993). Thermodynamics of ligand-induced assembly of tubulin. *Biochemistry* **32,** 10067–10077.

Farrell, K. W., and Wilson, L. (1980). Proposed mechanism for colchicine poisoning of microtubules reassembled in vitro from Stronglocentrotus purpuratus sperm tail outer doublet tubulin. *Biochemistry* **19,** 3048–3054.

Farrell, K. W., and Wilson, L. (1984). The differential kinetic stabilization of opposite microtubule ends by tubulin–colchicine complexes. *Biochemistry* **23,** 3741–3748.

Fujiwara, K., and Tilney, L. G. (1975). Substructural analysis of the microtubule and its polymorphic forms. *Ann. N. Y. Acad. Sci.* **253,** 27–50.

Garland, D. L. (1978). Kinetics and mechanism of colchicine binding to tubulin: Evidence for ligand induced conformatinal change. *Biochemistry* **17,** 4266–4272.

Gong, J., Traganos, F., and Darzynkiewicz, Z. (1993). Simultaneous analysis of cell cycle kinetics at two different DNA ploidy levels based on DNA content and cyclin B measurements. *Cancer Res* **53,** 5096–5099.

Hamel, E., del Campos, A. A., Lowe, M. C., and Lin, C. M. (1981). Interactions of taxol, microtubule-associated proteins, and guanine nucleotides in tubulin polymerization. *J. Biol. Chem.* **256**(22), 11887–11894.

Hamel, E., Ho, H. H., Kang, G.-J., and Lin, C. M. (1988). Cornigerine, a potent antimitotic Colchicum alkaloid of unusual structure. Interactions with tubulin. *Biochem. Pharmacol.* **37**(12), 2445–2449.

Himes, R. H. (1991). Interactions of the catharanthus (Vinca) alkaloids with tubulin and microtubules. *Pharmacol. Ther.* **51,** 257–267.

Hoebeke, J., Van Nijen, G., and De Brabander, M. (1976). Interaction of oncodazole (R 17934), a new antitumoral drug, with rat brain tubulin. *Biochem. Biophys. Res. Commun.* **69,** 319–324.

Horio, T., and Hotani, H. (1986). Visualization of the dynamic instability of individual microtubules by dark-field microscopy. *Nature* **321,** 605–607.

Howard, W. D., and Timasheff, S. N. (1988). Linkages between the effects of taxol, colchicine, and GTP on tubulin polymerization. *J. Biol. Chem.* **263**(3), 1342–1346.

Inoue, S. (1952). The effect of colchicine on the microscopic and submicroscopic structure of the mitotic spindle. *Exp. Cell Res. Suppl* **2,** 305–311.

Jordan, M. A., and Wilson, L. (1990). Kinetic analysis of tubulin exchange at microtubule ends at low vinblastine concentrations. *Biochemistry* **29**(11), 2730–2739.

Jordan, M. A., and Wilson, L. (1998). The use of drugs to study the role of microtubule assembly dynamics in living cells. *Methods Enzymol.,* **298,** 252–276.

Jordan, M. A., Margolis, R. L., Himes, R. H., and Wilson, L. (1986). Identification of a distinct class of vinblastine binding sites on microtubules. *J. Mol. Biol.* **187,** 61–73.

Jordan, M. A., Thrower, D., and Wilson, L. (1991). Mechanism of inhibition of cell proliferation by Vinca alkaloids. *Cancer Res.* **51**(8), 2212–2222.

Jordan, M. A., Thrower, D., and Wilson, L. (1992). Effects of vinblastine, podophyllotoxin and nocodazole on mitotic spindles. Implications for the role of microtubule dynamics in mitosis. *J. Cell Sci.* **102,** 401–416.

Jordan, M. A., Toso, R. J., Thrower, D., and Wilson, L. (1993). Mechanism of mitotic block and inhibition of cell proliferation by taxol at low concentrations. *Proc. Natl. Acad. Sci. USA* **90,** 9552–9556.

Jordan, M. A., Wendell, K. L., Gardiner, S., Derry, W. B., Copp, H., and Wilson, L. (1996). Mitotic block induced in HeLa cells by low concentrations of paclitaxel (Taxol) results in abnormal mitotic exit and apoptotic cell death. *Cancer Res.* **56,** 816–825.

Karsenti, E., and Maro, B. (1986). Centrosomes and the spatial distribution of microtubules in animal cells. *Trends Biochem. Sci.* **11,** 460–463.

Kowalski, R., Giannakakou, P., and Hamel, E. (1997). Activities of the microtubule-stabilizing agents epothilones A and B with purified tubulin and in cells resistant to paclitaxel (Taxol(R)). *J. Biol. Chem.* **272,** 2534–2541.

Kumar, N. (1981). Taxol-induced polymerization of purified tubulin. *J. Biol. Chem.* **256**(20), 10435–10441.

Kung, A. L., Sherwood, S. W., and Schimke, R. L. (1990). Cell line-specific differences in the control of cell cycle progression in the absence of mitosis. *Proc. Natl. Acad. Sci. USA* **87,** 9533–9557.

Lambeir, A., and Engelborghs, Y. (1981). A fluorescence stopped-flow study of colchicine binding to tubulin. *J. Biol. Chem.* **256,** 3279–3282.

Lee, J. C., Field, D. J., and Lee, L. L. Y. (1980). Effects of nocadazole on structures of calf brain tubulin. *Biochemistry* **19,** 6209–6215.

Levan, A. (1938). *Hereditas* **24,** 471.

Li, X., and Nicklas, R. B. (1995). Mitotic forces control a cell-cycle checkpoint. *Nature* **373,** 630–632.

Liao, G., Nagasaki, T., and Gundersen, G. G. (1995). Low concentrations of nocodazole interfere with fibroblast locomotion without significantly affecting microtubule level: Implications for the role of dynamic microtubules in cell locomotion. *J. Cell Sci.* **108,** 3473–3483.

Lin, C. M., and Hamel, E. (1981). Effects of inhibitors of tubulin polymerization on GTP hydrolysis. *J. Biol. Chem.* **256,** 9242–9245.

Lin, C. M., Ho, H. H., Pettit, G. R., and Hamel, E. (1989). Antimitotic natural products combrestatin A-4 and combrestatin A-2: Studies on the mechanism of their inhibition of the binding of colchicine to tubulin. *Biochemistry* **28,** 6984–6991.

Lopes, N. M., Adams, E. G., Pitts, T. W., and Bhuyan B. K. (1993). Cell kill kinetics and cell cycle effects of taxol on human and hamster ovarian cell lines. *Cancer Chemother. Pharmacol.* **32,** 235–242.

Malawista, S. E., and Sato, H. (1969). Vinblastine produces uniaxial, birefringent crystals in starfish oocytes. *J. Cell Biol.* **42,** 596–599.

Manfredi, J. J., Parness, J., and Horwitz, S. B. (1982). Taxol binds to cell microtubules. *J Cell Biol.* **94,** 688–696.

Margolis, R. L., and Wilson, L. (1977). Addition of colchicine–tubulin complex to microtubule ends: The mechanism of substoichiometric colchicine poisoning. *J. Biol. Chem.* **252**(20), 7006–7014.

Margolis, R. L., and Wilson, L. (1978). Opposite end assembly and disassembly of microtubules at steady state *in vitro*. *Cell* **13,** 1–8.

Margolis, R. L., and Wilson, L. (1998). Microtubule treadmilling: What goes around comes around. *Bioessays,* in press.

Margolis, R. L., Rauch, C. T., and Wilson, L. (1980). Mechanism of colchicine dimer addition to microtubule ends: Implications for the microtubule polymerization mechanism. *Biochemistry* **19,** 5550–5557.

Mathew, A. E., Mejillano, M. R., Nath, J. P., Himes, R. H., and Stella, V. J. (1992). Synthesis and evaluation of some water-soluble prodrugs and derivatives of taxol with antitumor activity. *J. Med. Chem.* **35,** 145–151.

McEwen, B. F., Arena, J. T., Frank, J., and Rieder, C. L. (1993). Structure of the colcemid-treated PtK1 kinetochore outer plate as determined by high voltage electron microscopic tomography. *J. Cell Biol.* **120,** 301–312.

McIntosh, J. R. (1994). The role of microtubules in chromosome movement. *In* "Microtubules" (J. S. Hyams and C. W. Lloyd, eds.), pp. 413–434. Wiley-Liss, New York.

McIntosh, J. R., and Koonce, M. P. (1989). Mitosis. *Science* **246,** 622–628.

Mejillano, M. R., Shivanna, B. D., and Himes, R. H. (1996). Studies on the nocodazole-induced GTPase activity of tubulin. *Arch. Biochem. Biophys.* **336,** 130–138.

Mitchison, T. J. (1989). Poleward microtubule flux in the mitotic spindle; Evidence from photoactivation of fluorescence. *J. Cell Biol.* **109,** 637–652.

Mitchison, T. J., and Kirschner, M. (1984a). Microtubule assembly nucleated by isolated centrosomes. *Nature* **312,** 232–237.

Mitchison, T. J., and Kirschner, M. (1984b). Dynamic instability of microtubule growth. *Nature* **312,** 237–242.

Mogenson, M. M., and Tucker, J. B. (1990). Taxol influences control of protofilament number at microtubule-nucleating sites in Drosophila. *J. Cell Sci.* **97,** 101–107.

Na, G. C., and Timasheff, S. N. (1980a). Stoichiometry of the vinblastine-induced self-association of calf brain tubulin. *Biochem. Soc. Trans.* **8**(6), 1347–1354.

Na, G. C., and Timasheff, S. N. (1980b). Thermodynamic linkage between tubulin self-association and the binding of vinblastine. *Biochemistry* **19**(7), 1347–1354.

Nicklas, R. B., Ward, S. C., and Gorbsky, G. J. (1995). Kinetochore chemistry is sensitive to tension and may link mitotic forces to a cell cycle checkpoint. *J. Cell Biol.* **130,** 929–939.

Olmsted, J. B., and Borisy, G. G. (1973). Characterization of microtubule assembly in porcine brain extracts by viscometry. *Biochemistry* **12,** 4282–4289.

Ostergren, G. (1944). Colchicine mitosis, chromosome contraction, narcosis and protein chain folding. *Hereditas* **30,** 429–467.

Owellen, R. J., Hartke, C. A., Dickerson, R. M., and Hains, F. O. (1976). Inhibition of tubulin-microtubule polymerization by drugs of the *Vinca* alkaloid class. *Cancer Res.* **36,** 1499–1502.

Palmer, C. G., Livengood, D., Warren, A. K., Simpson, P. J., and Johnson, I. S. (1960). The action of vincaleukoblastine on mitosis in vitro. *Exp. Cell Res.* **20,** 198–265.

Panda, D., Daijo, J. E., Jordan, M. A., and Wilson, L. (1995). Kinetic stabilization of microtubule dynamics at steady state in vitro by substoichiometric concentrations of tubulin–colchicine complex. *Biochemistry* **34,** 9921–9929.

Panda, D., Jordan, M. A., Chin, K., and Wilson, L. (1996). Differential effects of vinblastine on polymerization and dynamics at opposite microtubule ends. *J. Biol. Chem.* **271,** 29807–29812.

Parness, J., and Horwitz, S. B. (1981). Taxol binds to polymerized tubulin in vitro. *J. Cell Biol.* **91,** 479–487.

Paweletz, N., and Lang, U. (1988). Fine structural studies of early mitotic stages in untreated and nocodazole-treated HeLa cells. *Eu. J. Cell Biol.* **47,** 334–345.

Pepperkok, R., Bre, M. H., Davoust, J., and Kreis, T. E. (1990). Microtubules are stabilized in confluent epithelial cells but not in fibroblasts. *J. Cell Biol.* **111,** 3003–3012.

Rieder, C., Schultz, A., Cole, R., and Sluder, G. (1994). Anaphase onset in vertebrate somatic cells is controlled by a checkpoint that monitors sister kinetochore attachment to the spindle. *J. Cell Biol.* **127,** 1301–1310.

Rieder, C. L., and Palazzo, R. E. (1992). Colcemid and the mitotic cycle. *J. Cell Sci.* **102,** 387–392.

Ringel, I., and Horwitz, S. B. (1991a). Studies with RP 56976 (taxotere): A semisynthetic analogue of taxol. *J. Natl. Cancer Inst.* **83**(4), 288–291.

Ringel, I., and Horwitz, S. B. (1991b). Effect of alkaline pH on taxol–microtubule interactions. *J. Pharmacol. Exp. Ther.* **259,** 855–860.

Roberts, J. R., Rowinsky, E. K., Donehower, R. C., Robertson, J., and Allison, D. C. (1989). Demonstration of the cell cycle positions of taxol-induced "asters" and "bundles" by sequential measurements of tubulin immunofluorescence, DNA content, and autoradiographic labeling of taxol-sensitive and resistant cells. *J. Histochem. Cytochem.* **37,** 1659–1665.

Rochlin, M. W., Wickline, K. M., and Bridgman, P. C. (1996). Microtubule stability decreases axon elongation but not axoplasm production. *J. Neurosci.* **16,** 3236–3246.

Rowinsky, E. K., Donehower, R. C., Jones, R. J., and Tucker, R. W. (1988). Microtubule changes and cytotoxicity in leukemic cell lines treated with taxol. *Cancer Res.* **49,** 4093–4100.

Saxton, W. M., Stemple, D. L., Leslie, R. J., Salmon E. D., Zavortnik, M., and McIntosh, J. R. (1984). Tubulin dynamics in cultured mammalian cells. *J. Cell Biol.* **99,** 2175–2186.

Schiff, P. B., and Horwitz, S. B. (1980). Taxol stabilizes microtubules in mouse fibroblast cells. *Proc. Natl. Acad. Sci. USA* **77,** 1561–1565.

Schiff, P. B., and Horwitz, S. B. (1981). Taxol assembles tubulin in the absence of exogenous guanosine 5′-triphosphate or microtubule-associated proteins. *Biochemistry* **20,** 3247–3252.

Schiff, P. B., Fant, J., and Horwitz, S. B. (1979). Promotion of microtubule assembly in vitro by taxol. *Nature* **277,** 665–667.

Schulze, E., and Kirschner, M. (1986). Microtubule dynamics in interphase cells. *J. Cell Biol.* **102,** 1020–1031.

Sengupta, S., Boge, T. C., George, G. I., and Himes, R. H. (1995). Interaction of a fluorescent paclitaxel analogue with tubulin. *Biochemistry* **34,** 11889–11894.

Shelby, R. D., Hahn, K. M., and Sullivan, K. F. (1996). Dynamic elastic behavior of alpha-satellite DNA domains visualized in situ in living human cells. *J. Cell Biol.* **135,** 545–557.

Sherwood, S. W., Sheridan, J. P., and Schimke, R. T. (1994). Induction of apoptosis by the anti-tubulin drug colcemid: Relationship of mitotic checkpoint control to the induction of apoptosis in HeLa S3 cells. *Exp. Cell Res.* **215,** 373–379.

Singer, W. D., and Himes, R. H. (1992). Cellular uptake and tubulin binding properties of four vinca alkaloids. *Biochem. Pharmacol.* **43,** 545–551.

Singer, W. D., Jordan, M. A., Wilson, L., and Himes, R. H. (1989). Binding of vinblastine to stabilized microtubules. *Mol. Pharmacol.* **36**(3), 366–370.

Skoufias, D., and Wilson, L. (1992). Mechanism of inhibition of microtubule polymerization by colchicine: Inhibitory potencies of unliganded colchicine and tubulin–colchicine complexes. *Biochemistry* **31,** 738–746.

Sluder, G. (1979). Role of spindle microtubules in the control of cell cycle timing. *J. Cell Biol.* **80,** 674–691.

Snyder, J. A., Vogt, S. I., and McLelland, S. L. (1983). Nocodazole pretreatment in anaphase selectively reduces anaphase B in PtK1 cells. *Cell Motil.* **3,** 79–91.

Sternlicht, H., and Ringel, I. (1979). Colchicine inhibition of microtubule assembly via copolymer formations. *J. Biol. Chem.* **254,** 10540–10550.

Sternlicht, H., and Ringel, I., and Szasz, J. (1983). Theory for modelling the copolymerization of tubulin and tubulin–colchicine complex. *Biophys. J.* **42,** 255–267.

Swindell, C. S., Krauss, N. E., Horwitz, S. B., and Ringel, I. (1991). Biologically active taxol analogues with deleted A-ring side chain substituents and variable C-2′ configurations. *J. Med. Chem.* **34,** 1176–1184.

Takoudju, M., Wright, M., Chenu, J., Gueritte-Voegelein, F., and Guenard, D. (1988). Absence of 7-acetyl taxol binding to unassembled brain tubulin. *FEBS Lett.* **227,** 96–98.

Tanaka, E., Ho, T., and Kirschner, M. W. (1995). The role of microtubule dynamics in growth cone motility and axonal growth. *J. Cell Biol.* **128,** 139–155.

ter Haar, E., Kowalski, R., Hamel, E., Lin, C., Longley, R., Gunasekera, S., Rosenkranz, H., and Day, B. W. (1996). Discodermolide, a cytotoxic marine agent that stabilizes microtubules more potently than taxol. *Biochemistry* **35,** 243–250.

Thompson, W. C., Wilson, L., and Purich, D. L. (1981). Taxol induces microtubule assembly at low temperature. *Cell Motil.* **1,** 445–454.

Thrower, D., Jordan, M. A., and Wilson, L. (1991). Quantitation of cellular tubulin in microtubules and tubulin pools by a competitive ELISA. *J. Immunol. Methods* **136**(1), 45–51.

Thrower, D., Jordan, M. A., and Wilson, L. (1993). A quantitative solid-phase binding assay for tubulin. *Methods Cell Biol.* 129–145.

Toso, R. J., Jordan, M. A., Farrell, K. W., Matsumoto, B., and Wilson, L. (1993). Kinetic stabilization of microtubule dynamic instability in vitro by vinblastine. *Biochemistry* **32**(5), 1285–1293.

Turner, P. F., and Margolis, R. L. (1984). Taxol-induced bundling of brain-derived microtubules. *J. Cell Biol.* **99,** 940–946.

Vasquez, R. J., Howell, B., Yvon, A.-M. C., Wadsworth, P., and Cassimeris, L. (1997). Nanomolar concentrations of nocodazole alter microtubule dynamic instability in vivo and in vitro. *Mol. Biol. Cell* **8,** 973–985.

Wadsworth, P., and McGrail, M. (1990). Interphase microtubule dynamics are cell type-specific. *J. Cell Sci.* **95,** 23–32.

Walker, R. A., O'Brien, E. T., Pryer, N. K., Soboeiro, M. F., Voter, W. A., Erickson, H., and Salmon, E. D. (1988). Dynamic instability of individual microtubules analyzed by video light microscopy: Rate constants and transition frequencies. *J. Cell Biol.* **107,** 1437–1448.

Waterman-Storer, C., and Salmon, E. D. (1997). Microtubule dynamics: Treadmilling comes around again. *Curr. Biol.* 369–372.

Waters, J. C., Skibbens, R. V., and Salmon, E. D. (1996). Oscillating mitotic newt lung cell kinetochores are, on average, under tension and rarely push. *J. Cell Sci.* **109,** 2823–2831.

Weisenberg, R. C., Borisy, G. G., and Taylor, W. E. (1968). The colchicine-binding protein of mammalian brain and its relation to microtubules. *Biochemistry* **7,** 4466–4478.

Wendell, K. L., Wilson, L., and Jordan, M. A. (1993). Mitotic block in HeLa cells by vinblastine: Ultrastructural changes in kinetochore–microtubule attachment and in centrosomes. *J. Cell Sci.* **104,** 261–274.

Wilson, L., and Farrell, K. W. (1986). Kinetics and steady-state dynamics of tubulin addition and loss at opposite microtubule ends: The mechanism of action of colchicine. *Ann. N. Y. Acad. Sci.* **466,** 690–708.

Wilson, L., and Friedkin, M. (1967). The biochemical events of mitosis II. The *in vivo* and *in vitro* binding of colchicine in grasshopper embryos and its possible relation to inhibition of mitosis. *Biochemistry* **6,** 3126–3135.

Wilson, L., and Jordan, M. A. (1994). Pharmacological probes of microtubule function. *In* "Microtubules" (J. Hyams and C. Lloyd, eds.) pp. 59–84. Wiley, New York.

Wilson, L., Anderson, K., and Chin, D. (1976). Nonstoichiometric poisoning of microtubule polymerization: A model for the mechanism of action of the vinca alkaloids, podophyllotoxin, and colchicine. *In* "Cold Spring Harbor Conferences on Cell Proliferation: Cell Motility" (R. Goldman, T. Pollard, and J. L. Rosenbaum, eds.), pp. 1051–1064. Cold Spring Harbor Laboratory Press, Cold Spring Harbor, NY.

Wilson, L., Jordan, M. A., Morse, A., and Margolis, R. L. (1982). Interaction of vinblastine with steady-state microtubules in vitro. *J. Mol. Biol.* **159,** 129–149.

Wilson, L., Miller, H. P., Farrell, K. W., Snyder, K. B., Thompson, W. C., and Purich, D. L. (1985). Taxol stabilization of microtubules in vitro: Dynamics of tubulin addition and loss at opposite microtubule ends. *Biochemistry* **24,** 5254–5262.

Wilson, L., Toso, R. J., and Jordan, M. A. (1993). Vinblastine, nocodazole, and colchicine suppress the dynamic instability of microtubules: Implications for the mechanism of antimitotic action. *J. Cell Pharmacol.* **1**(Suppl. 1), 35–40.

Wordeman, L., and Mitchison, T. J. (1994). Dynamics of microtubule assembly in vivo. *In* "Microtubules" (J. S. Hyams and C. W. Lloyd, eds.), pp. 287–302. Wiley–Liss, New York.

Yu, K., Ravera, C. P., Chen, Y. N., and McMahon, G. (1997). Regulation of myc-dependent apoptosis by p53, c-Jun N-terminal kinases/stress-activated protein kinases, and Mdm-2. *Cell Growth Differ.* **8,** 731–742.

Yu, W., and Baas, P. W. (1995). The growth of the axon is not dependent upon net microtubule assembly at its distal tip. *J. Neurosci.* **15,** 6827–6833.

Zhai, Y., Kronebusch, P. J., Simon, P. M., and Borisy, G. G. (1996). Microtubule dynamics at the G2/M transition: Abrupt breakdown of cytoplasmic microtubules at nuclear envelope breakdown and implications for spindle morphogenesis. *J. Cell Biol.* **135,** 201–214.

Zieve, G. W., Turnbull, D., Mullins, J. M., and McIntosh, J. R. (1980). Production of large numbers of mitotic mammalian cells by use of the reversible microtubule inhibitor nocodazole. *Exp. Cell Res.* **126,** 397–405.

This Page Intentionally Left Blank

CHAPTER 16

Correlative Light and Electron Microscopy of Mitotic Cells in Monolayer Cultures

Conly L. Rieder*,†,‡ and Grisel Cassels*

* Division of Molecular Medicine
Wadsworth Center
New York State Department of Health
Albany, New York 12201-0509

† Department of Biomedical Sciences
State University of New York
Albany, New York 12222

‡ Marine Biology Laboratory
Woods Hole, Massachusetts 02543-1015

I. Introduction

The goals of mitosis research are to understand how the spindle forms and functions to move the chromosomes and how progress through this stage of the cell cycle is controlled. To achieve these aims the various mechanisms responsible for the dynamic behaviors exhibited by the major spindle components, including the chromosomes, kinetochores, centrosomes (spindle poles), and spindle microtubules (MTs), must be understood in molecular terms. Since these behaviors are defined by observing living cells with the light microscope (LM), and since

METHODS IN CELL BIOLOGY, VOL. 61

0091-679X/99 $30.00

LM technology continues to advance at a rapid pace, models of mitosis must be constantly revised to accommodate the corresponding refined definition of the behaviors they attempt to explain.

The dynamics of chromosome behavior reflect changes in the underlying interactions between the many and varied molecular and macromolecular components involved in spindle formation and function. One approach for defining these interactions is to use indirect immunofluorescent (IMF) LM to determine the positional relationships between spindle-associated proteins in cells fixed at defined stages of mitosis. With this method it can be rapidly determined whether and where a particular gene product is located in the spindle and how its position changes over time relative, e.g., to the spindle MTs, poles, and chromosomes (see, however, the warnings in Melan and Sluder, 1992). Also, the utility of IMF LM can be considerably enhanced by applying it to cells followed in the living state by high-resolution LM until the point of fixation (Rieder and Alexander, 1990; Eckley *et al.,* 1997; Li and Nicklas, 1997). However, because it requires that the cell be fixed, IMF can seldom be used to collect reliable data on the dynamics of mitotic processes. To overcome this problem fluorescently tagged (Gorbsky *et al.,* 1987) or "caged" (Mitchison, 1989; Waters *et al.,* 1995) spindle proteins can be introduced into living cells, which then allow dynamic changes in their distribution to be followed by vital time-lapse fluorescence microscopy. This approach has been used to study the sites of MT assembly/disassembly during spindle function, and it promises to become increasingly useful as more spindle-associated proteins are cloned and then tagged, for example, with green-fluorescent protein [e.g., centromeres (Shelby *et al.,* 1996), MTs (Straight *et al.,* 1997), and centrosomes (Khodjakov *et al.,* 1997b).

By its nature, investigations with the LM are limited to a spatial resolution of >0.20 μm, which means that, although most components comprising the spindle can be detected (e.g., by fluorescence or video-enhanced LM; Hayden *et al.,* 1990; Waters *et al.,* 1993; Nicklas and Ward, 1994), the structural correlates that define their interactions cannot be resolved. Similarly, the complex internal structure of the organelles involved in spindle function, how their various constituent proteins are positioned relative to one another, and how they change during function are not resolvable with the LM. Instead, this information can only be obtained with the electron microscope (EM), which has been (Robbins and Gonatas, 1964; Brinkley and Cartwright, 1966; Bajer and Mole-Bajer, 1969; McIntosh and Landis, 1971) and remains (McDonald *et al.,* 1992; Khodjakov *et al.,* 1997a; Bullitt *et al.,* 1997) the tool of choice for exploring structure–function relationships between spindle components at a high resolution. However, as with IMF studies, the EM can only be used to examine cells after they have been fixed. This means that for an EM study to be informative, the investigator must infer what was occurring at the time of fixation—and such inferences are not always reliable. The only way to minimize this source of error is to follow the cell with the LM until the desired behavior is manifested and then immediately fix it for a subsequent EM analysis. Although labor-intensive, this same-cell

correlative LM/EM technique allows one to determine with confidence the structural interactions that underlie a specific behavior (Sluder and Rieder, 1985; Ault and Nicklas, 1989; Rieder and Alexander, 1990). It is also useful for defining the effect of a localized experimental intervention on the spindle or chromosomes (McNeil and Berns, 1981; Leslie and Pickett-Heaps, 1984; Nicklas *et al.,* 1989; Snyder *et al.,* 1991). The utility of same-cell correlative LM/EM can also be expanded by combining it with immunolabeling methods (Mitchison *et al.,* 1986; Wadsworth *et al.,* 1989).

We have use same-cell correlative LM/EM extensively to explore mitosis in monolayer cultures of vertebrate (PtK_1 and newt) somatic cells (Rieder and Borisy, 1981; Rieder and Alexander, 1990; Rieder *et al.,* 1995; Khodjakov *et al.,* 1997a,b; McEwen *et al.,* 1997). During these studies we developed several shortcuts to facilitate this technique. In this chapter we enumerate some of the issues that should be considered when using same-cell correlative LM/EM and describe the methods that we use to obtain ultrastructural information underlying mitotic events *in vivo.*

II. Light Microscopy

For the most part, the usefulness of the EM data obtained by same-cell correlative LM/EM depends on how accurately the behavior of interest was known up to the point of fixation. For example, because of their minute size and intimate association with the underlying centromeric heterochromatin, the two (sister) kinetochores (regions) on a chromosome are difficult to visualize in living cells even by video-enhanced LM. Moreover, when attached to the spindle each kinetochore undergoes random and rapid (<6 sec) switches in its direction (Khodjakov and Rieder, 1996). Thus, in order to determine the relationship between the number of MTs at a kinetochore and its direction of motion, the behavior of the sister kinetochores must be known at the instant of fixation with the highest possible temporal and spatial resolution (Fig. 1). Similarly, to determine the structural correlates behind the initial stages of kinetochore attachment (Rieder and Alexander, 1990) or chromosome reorientation (Ault and Nicklas, 1989), one must have a constant record of kinetochore behavior through the point in time at which the cell is fixed.

Until the early 1980s the dynamics of mitosis could only be followed by time-lapse cinematography, which required that the cell be periodically photographed onto celluloid ciné film. It was then necessary to develop and print a copy of the film before the success or failure of an experiment could be determined. Since this process took several days, the cell of interest had to be embedded for EM in the interim without knowing the outcome of the experiment. This uncertainty has been eliminated by the development and routine application of video-enhanced LM. Not only does video-enhanced LM produce high-resolution time-lapse sequences that can be manipulated by image processing but it also

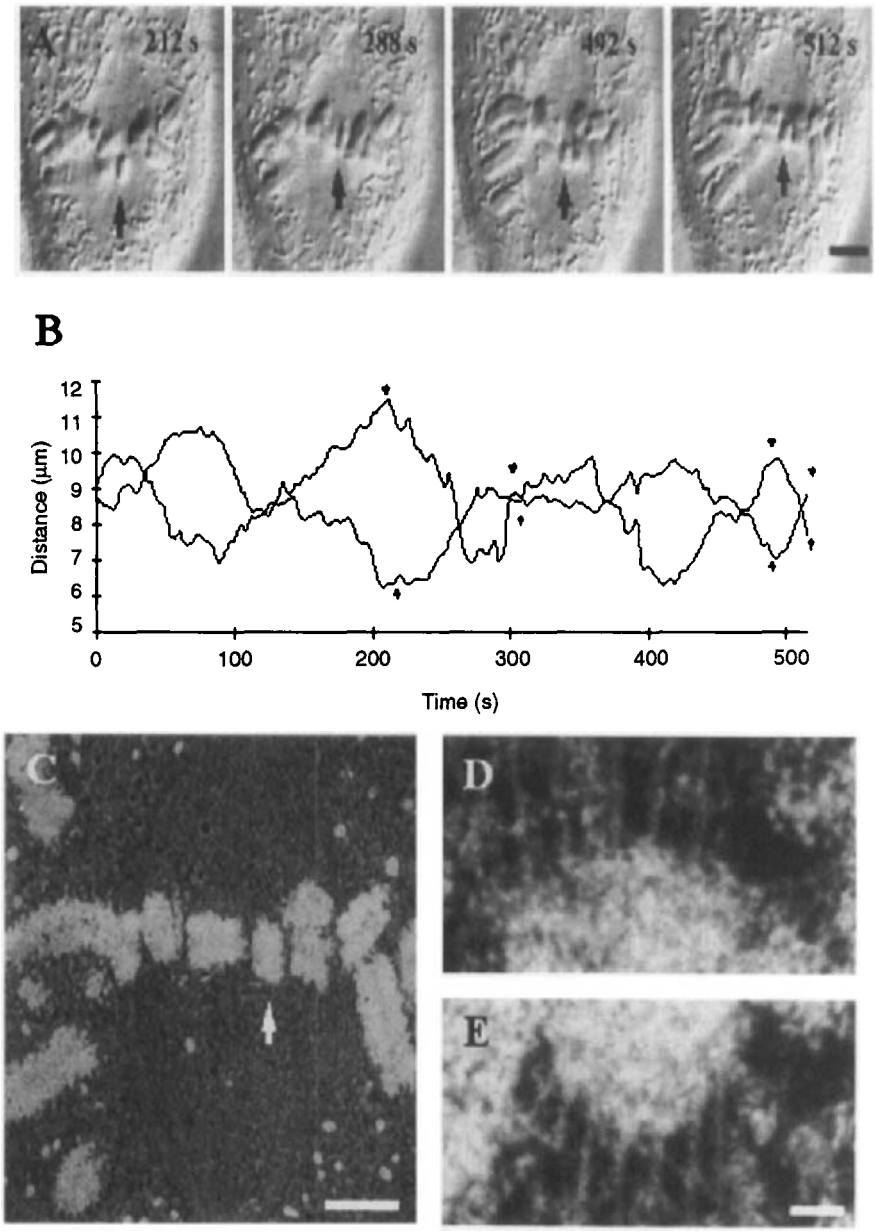

Fig. 1 To determine the relationship between the direction a chromosome moves and the number of microtubules associated with its sister kinetochores, the behavior of the chromosome must be followed at high temporal resolution up to and during fixation. In this example a bioriented and oscillating PtK_1 chromosome (arrow in A) is followed for several cycles before it is fixed (at 512 sec) while moving toward the top pole. A semiautomatic plot of the motion of each sister kinetochore, relative to the pole to which each was attached, is shown in B. The thin line represents motion of the top kinetochore toward and away from its pole, whereas the thick line similarly plots

allows these sequences to be viewed immediately after (and even during) the experiment. Corresponding advances in software development also make it possible, e.g., to semiautomatically track the motion of a mitotic organelle, which provides a clear and nonbiased record of its behavior until the point of fixation (Fig. 1).

Ideally, the optical system used to follow an event should be matched to the goals of the experiment. Studies concerned with changes in the behavior and/or distribution of spindle MTs benefit most by polarization LM, which allows the otherwise invisible spindle MTs to be visualized in the living cell (Leslie and Pickett-Heaps, 1984; Sluder *et al.,* 1986; Snyder *et al.,* 1991). Alternatively, those concerned with centrosome and kinetochore motion should employ differential interference contrast (DIC) LM, which benefits most from the image processing associated with video enhancement. Indeed, with the appropriate objective, camera, and software, lateral displacements of 60–80 nm can be detected within the spindle by DIC LM (Skibbens *et al.,* 1993; Khodjakov and Rieder, 1996; Fig. 1). However, a high-quality phase-contrast LM that is coupled to a video camera and image processing/recording system is often adequate for documenting the behavior of mitotic events with a spatial resolution sufficient for the study (McNeil and Berns, 1981; Wadsworth *et al.,* 1989; Ault and Nicklas, 1989; Hays and Salmon, 1990).

The frequency with which a cell should be photographed (*i.e.,* the framing rate) will define the temporal resolution of the study, and again should be set by goals of the study. In our work on vertebrate cells 2 to 4-sec intervals (15–30 frames/min) are optimal for following the motion of kinetochores and centrosomes, which move at rates of 1–3 μm/min. At these framing rates the moving organelle undergoes just enough of a lateral displacement in each frame (1 pixel) to be detected by our tracking programs (Skibbens *et al.,* 1993; Khodjakov and Rieder, 1996). Alternatively, if a cell needs to be followed for a long period of time, and it will be fixed at any point after a particular event has occurred, much slower framing rates (e.g., 1 or 2 per minute) can be used (Brenner *et al.,* 1977; Jensen *et al.,* 1994). In addition to saving disk (or tape) space, slower framing rates limit the sequence to a reasonable viewing length. Regardless of the framing

---

Fig. 1 (*Continued*) the motion of the lower kinetochore with respect to its pole. Note that when the cell was fixed (512 sec) the bottom kinetochore was moving away from its pole (distance increasing) while the top kinetochore was moving poleward. (C) A low-magnification electron micrograph of one section from a serial series through this cell. The chromosome followed *in vivo* is noted with an arrow. (D and E) Micrographs of individual sections through the poleward-moving (D) and away-from-the-pole moving (E) kinetochores. The results of such studies reveal that the direction a chromosome moves is not related to the number of microtubules on its sister kinetochores. Bar in A, 4 μm; C, 2.2 μm; D and E, 0.12 μm (reproduced from *The Journal of Cell Biology,* 1997, **137**, 1567–1580, by copyright permission of the Rockefeller University Press).

rate, it is important to shutter the light source between exposures to minimize specimen irradiation.

In order to "freeze" a dynamic process at a specific time point, the cell must be fixed rapidly after the decision is made to do so and with minimal changes in focus. This requires the use of a perfusion chamber, of which many designs are described in the literature. We use one of our own design, detailed in Rieder and Cole (1997), that allows cells grown on 25-mm^2 glass coverslips (we used No. 1.5) to be followed *in vivo* at the highest spatial resolution with either an inverted or upright LM. In addition to having excellent optical properties, our chamber keeps cells healthy for hours to days, depending on the type of specimen. (Mammalian cells, which must be maintained well above ambient temperature, require a perfusion with fresh media every 30 min, whereas amphibian cultures, which thrive at room temperature, remain healthy without a change of media for over a day; Jensen *et al.,* 1994.) There are a number of considerations when constructing and using perfusion chambers that are beyond the scope of this chapter. For a detailed discussion of this topic see Rieder and Cole (1997).

After the culture has been perfused with the primary (glutaraldehyde) fixative the specimen-containing coverslip must be detached from the chamber for further processing. However, prior to this step the experimental cell must be marked so that it can be subsequently relocated after embedding. For this task we use an objective marker with a diamond tip (approx. $1200 from Zeiss, Cat. No. 462960) which, like an objective lens, mounts on the microscope nosepiece adjacent to the objective used for the study. This scribe is designed to scratch a circle of a variable but definable diameter (20 μm to 3 mm) onto the surface of the coverslip above the cell so that the center of the circle contains the center of the field of view (Figs. 2A–2C). After the cell has been circled it should be photographed by DIC or phase-contrast optics (Fig. 2C). This photograph will be used to help relocate the cell within the embedment.

III. Flat Embedding

After circling and photographing the experimental cell, the perfusion chamber is disassembled so that the cell-containing coverslip can be further processed and flat-embedded. The object of the latter is to embed the cell in a thin wafer of epoxy plastic in a manner that allows it to be easily and routinely recovered for serial sectioning. Through the years many methods have been described for accomplishing this task (Borysko and Roslansky, 1959; Brinkley *et al.,* 1967; Mole-Bajer and Bajer, 1968; Nicklas *et al.,* 1979). However, as for many EM procedures, most laboratories have developed their own methods for flat-embedding cells.

We routinely postfix coverslip cultures of vertebrate cell monolayers in 2% aqueous OsO_4 at 4°C under a fume hood, rinse, en bloc stain, and otherwise

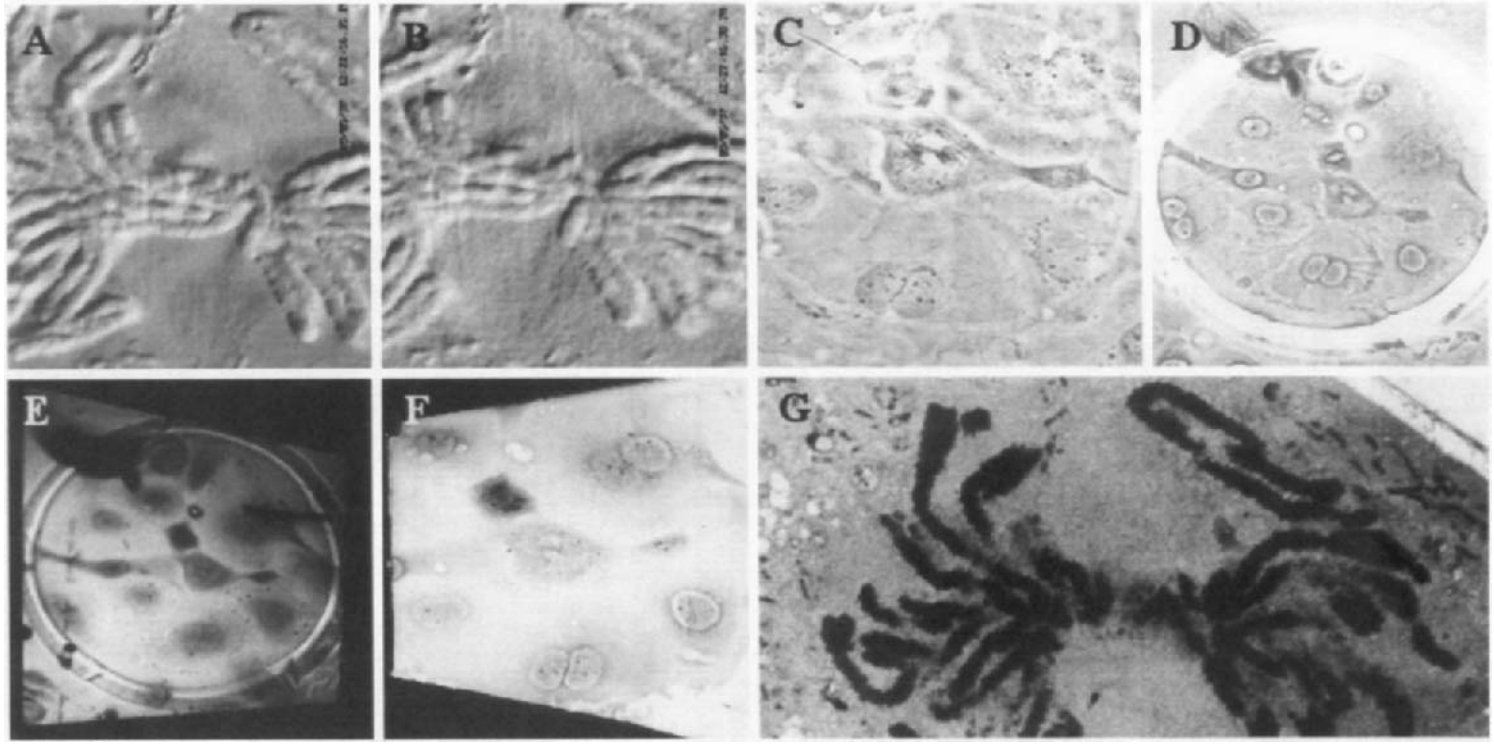

Fig. 2 Some of the steps that we use to obtain ultrastructural information from a cell followed *in vivo* until fixation. Using a perfusion chamber (detailed in Rieder and Cole, 1997) a mitotic cell is followed by high-resolution DIC light microscopy (A) through fixation (B). After fixation a circle is scratched around the cell, on the surface of its glass coverslip growth substrate, with a diamond-tipped objective scribe. The perfusion chamber is then dismantled and the circled cell is rephotographed at a low magnification with phase-contrast LM (C). After flat embedding, the coverslip is removed and the cell is again relocated and circled (D; see text for details). A rectangular or trapezoidal block that contains the cell is then cut from the embedment (E) and mounted on an Epon peg with superglue. The block is then trimmed to remove all parts of the circle, leaving the cell of interest near the middle of the block face (F). (G) An electron micrograph of the cell followed *in vivo* until fixation that was cut from this block face.

treat the culture in small Coplin jars with lids (Fischer Scientific, Cat. No. 08-815). Although designed to hold up to eight standard 12 × 32-in. microscope slides back to back, they can be modified to conveniently hold the same number of 25-mm^2 coverslips by simply shortening them to about 1.5 in. with a diamond cutoff wheel. However, in lieu of Coplin jars all of the previous steps can be carried out in small plastic petri dishes, but under these conditions it is important that the coverslip surface containing the cells be maintained face-up in the bottom of the dish, and that fluids be exchanged by pouring or pipetting at the peripheral edges.

Because cell monolayers are exceedingly thin, the dehydrating steps (we use 20, 30, 40, 60, 80, 95, and 100% ethanol) can be abbreviated to 5 min each with three changes at 100%. (It is interesting to note that chromosomes shrink up to 9% of their original length during dehydration, and that maximum shrinkage occurs in 95% ethanol; Jensen and Bajer, 1969). After the coverslip culture has been fully dehydrated, it is incubated in a 50:50 solution of 100% ethanol:propylene oxide for 5 min and then in three changes of 100% propylene oxide for 5 min each. These steps "clear" or remove all the ethanol from the preparation, which, if left in the cells, can deleteriously affect the polymerization of our Polybed/Araldite resin formulae (detailed in Rieder *et al.*, 1985). Since propylene oxide is very volatile and reactive this step must be conducted under a fume hood. Again, we use glass Coplin jars with lids for this task, which should not be conducted in plastic petri dishes that melt in propylene oxide. Extreme care must be taken at this stage so that the cells do not dry out during the solution exchanges.

After clearing, the culture-containing coverslip is removed with forceps from its last change of propylene oxide and placed cell-side up on a support platform that will hold it in a horizontal position during the infiltration process. For reasons outlined later, it is important that the surface area of this platform be smaller than that of the coverslip. Our support platform consists of a cylindrical Teflon tower (22-mm diameter; 70 mm high) that has been glued onto a larger stainless-steel stage. Once the coverslip culture is placed on this peg, a freshly made 50:50 mixture of propylene oxide:uncatalyzed resin is quickly pipetted onto its cell-side surface until it forms a 1 or 2-mm-high meniscus due to surface tension. This whole operation must be conducted very rapidly so that the culture does not dry between the time when it is removed from the propylene oxide and when it is covered with the Epoxy:propylene oxide mixture. Similarly, extreme care must also be taken so that the meniscus of the Epoxy mixture does not become excessively high (in which case it will run over the sides of the coverslip edges). After adjusting the height of the meniscus the preparation is then covered with a beaker to protect it from dust.

At this stage it must be stressed that the processes of dehydration, clearing, and infiltration must be conducted in a relatively dry atmosphere because the condensation of any water onto the specimen, at any stage of its processing for EM, will ruin it.

Over the next 8–12 hr the propylene oxide slowly evaporates from the 50:50 mixture and the cells progressively experience a higher concentration of the resin mixture. After this time the noncatalyzed resin mixture is drained from the coverslip surface by holding it vertically against tissue or filter paper. Next, the coverslip is returned to the support platform and 10–15 drops of fresh uncatalyzed resin, degassed of air bubbles by a brief vacuum treatment, are placed on its cell-containing surface. Over the next several minutes the resin will spread evenly over the coverslip surface and form a meniscus at its edges. We then cover this preparation with a beaker and leave it undisturbed at room temperature for 1 or 2 hr. After this time the uncatalyzed resin is again drained from the coverslip and replaced with fresh catalyzed resin. After 1 hr the preparation is drained for the final time and a fresh coat of catalyzed resin is applied. At this point the preparation is incubated on its support platform and on a flat surface in a 60°C oven until the resin has polymerized.

The end product of this flat-embedding operation is a 25-mm^2 glass coverslip with a monolayer of cells on one side that are embedded in a clear, thin (1–3 mm) wafer of plastic. At this point the cell-free glass side of the embedment should be cleaned of stray plastic debris, first with a razor blade and then with acetone or ether. Here, care must be exercised to avoid contacting the plastic wafer with the solvent since it will cloud the surface of the embedment and hamper subsequent LM. After cleaning, the embedded preparation should be taped along its sides onto a glass slide, coverslip-side up. This side contains the score marking the experimental specimen which can be easily located under a dissecting microscope. Once located we use an extra-fine-tip black Sharpie pen to draw a small indelible circle around the score mark so that its position can be more easily determined on the coverslip with the unaided eye. At this point the preparation can be mounted on an upright or inverted microscope so that the experimental cell can be rephotographed within the embedment by phase-contrast optics (Fig. 2D). When using oil-immersion objectives for this task, we first pipette a small amount of glycerol between the surface of the glass slide and plastic embedment to remove any air interface.

IV. Preparing the Cell for Sectioning

This section describes how to prepare the cell that was followed *in vivo* in the easiest way possible for serial sectioning. To do this the glass coverslip must first be removed from the preparation without damaging the experimental cell. Over the years a number of methods have been described to accomplish this goal (Chang, 1971) but the best by far is the technique described by Moore (1975), which needs to be conducted under a fume hood. In this procedure the flat embedment is placed into a plastic beaker of concentrated 4°C hydrofluoric acid. Over a 20 to 30-min period the hydrofluoric acid (HF) completely etches the (No. 1.5) glass coverslip from the plastic wafer without deleteriously affecting

the underlying cells. However, this step also removes the fiduciary scribe that was made earlier to relocate the experimental cell within the embedment. Therefore, prior to removing the coverslip we invert the embedment so that the plastic side is up and place it under a dissecting microscope. We then use the tip of a scalpel or razor blade to score a deep square in the plastic which coincides with the underlying scribe circle on the opposing (glass) surface.

The etching of glass by HF is an exothermic reaction which, if conducted at room temperature, softens the embedding resin to the point where the razor blade score marks are removed. Fortunately, this can be avoided by simply placing the beaker of HF in an ice bucket so that etching occurs at 4°C. With our resin formula, etching is complete when the plastic wafer floats to the top of the HF. At this point the newly exposed plastic surface is perfectly smooth, flat, and sometimes mirrored, and the ventral surface of the cell monolayer is on this surface. After HF treatment the embedment must be thoroughly washed to remove any residual acid. To do this we place the wafer on top of a thin layer of 5-mm glass beads that rest in the bottom of a 250-ml glass Erlenmeyer flask with a side arm. This flask is then attached to a continuous stream of filtered (Millipore) water that slowly removes any residual HF from the wafer. Water flows into the top of the flask through a glass tube embedded in a rubber stopper, and it exists the flask through the side arm. The glass beads keep the embedment from sticking to the bottom of the flask. After washing in water for about 60 min, the preparation should then be placed on a flat surface, cell side up, covered, and allowed to dry for several hours. It should not be dried in an oven, which will soften the plastic and remove the score marks.

After it is dry the plastic wafer is again taped to a microscope slide cell-side up. Next, the experimental cell is relocated by phase-contrast LM using the underlying razor score marks and the low-magnification photograph of the cell taken after fixation. In the absence of a coverslip the contrast of the cell on the surface of the plastic is generally weak but it is usually sufficient to easily visualize the denser chromosomes and the neighboring nuclei/nucleoli (Fig. 2E). When necessary, the contrast can be enhanced slightly by placing a drop a glycerol between the glass slide and the plastic wafer. If this is not sufficient, contrast can be further boosted by placing a drop of glycerol on the cell surface along with a coverslip shard. However, this is a last resort position because, although it boosts contrast sufficient for cell recognition, it does not allow the cell to be marked for trimming until the coverslip and glycerol have been removed by a water rinse.

After the experimental cell has been relocated on the surface of the embedment, it should again be circled with the diamond objective scribe, and during this step it is important to make sure that it lies directly in the center of the circle (Fig. 2E). Centering can be ensured by first using the scribe to draw a circle in a remote part of the embedment, well removed from the cell of interest. Then, without translating the microscope stage (which will change the position of the circle), the circle should be viewed with a 20–40X objective. At this time

one of the microscope eyepieces should be rotated until a conspicuous piece of dirt on the eyepiece is positioned in the center of the circle, and then the eyepiece should be secured in place. In essence this "calibrates" the scribe for the surface of the embedment so that whenever the cell of interest is positioned under the dirt on the eyepiece it will be centered within the circle subsequently etched by the scribe.

Once the experimental cell has been circled, the embedment should be solidly stuck by double-stick tape, cell-side up, into the bottom of a plastic petri dish. Using a dissecting microscope, and a cleaned single-edge razor blade, a small block containing the circled cell should be cut from the embedment (Fig. 2F). The double-stick tape is important because it keeps the small chunk of plastic containing the experimental cell immobilized during the "blocking" process. (Few things are more frustrating than to lose the cell at this stage because it becomes ejected from the field of view as it is being cut from the embedment).

We then superglue the block containing the circled cell, circle-side up, onto the center of a blank Epon peg that is sized to fit into our microtome chuck. After drying, the block can then be trimmed into a pyramid with a short vertical height for subsequent serial sectioning. We do this by making cuts under a stereomicroscope with a new single-edge (GEM Super Stainless Steel) razor blade that has been cleaned of oil by storing in acetone. In essence, we trim all the surface of the block away, leaving only a trapezoid-shaped cell-containing region that formerly occupied the center of our fiduciary circle (Fig. 2F). To facilitate this process we have designed a Silastic elastomer block holder that immobilizes the support peg while allowing the specimen to be illuminated from the bottom and/or side. With this holder it is often possible to actually see the cell of interest on the surface of the plastic throughout the trimming process. The Silastic holder, and our method for trimming blocks containing cells followed *in vivo,* has been thoroughly described previously (Rieder, 1981; Rieder and Bowser, 1984) and will not be detailed here. Rieder (1981) also discusses many of the factors that must be considered when trimming a flat-embedded cell for serial sectioning and outlines how the trimmed block can be aligned in the microtome so that a complete section of desired thickness is obtained the first time the knife makes contact with the face of the specimen.

V. Obtaining the Required Ultrastructural Information

The three-dimensional (3D) ultrastructural information needed for a same-cell correlative LM/EM project can be derived by two methods, both of which require that the specimen be serially sectioned. In the first and still most popular method, the necessary information is obtained by examining a consecutive series of thin or semithick (0.25–0.50 μm) sections that totally encompass the area of interest. In the second method, which has only recently become available, the information is obtained from one thick section by high or intermediate-voltage

EM tomography. Each of these approaches has its own benefits and shortcomings, which are discussed in the following sections.

A. From Sequential Sections

The most popular method for obtaining 3D ultrastructural information on the mitotic apparatus is to serially thin section the specimen and then extract the required information from those consecutive sections that contain the areas (events) of interest. Depending on the goals of the study, the required information can sometimes be obtained by simply examining sequential photomicrographs of the serial series. For example, to determine how the centrioles are distributed during an unusual mitosis (Brenner *et al.*, 1977; Sluder and Rieder, 1985) or to confirm that a kinetochore targeted by laser microsurgery has been destroyed (McNeil and Berns, 1981), serial sections are required, but the conclusion can be reached by examining the sections without stacking them into a 3D format. Similarly, the number of MTs on a kinetochore moving in a known direction at fixation can be determined directly from sequential sections without a need to stack the information into a 3D display (McEwen *et al.*, 1997).

In other serial section studies the relevant information from each section must be stacked into a continuous 3D volume in order to conduct the analysis. This is especially true if one is trying to determine where MTs start and end within the spindle and/or their relationship to one another (Nicklas *et al.*, 1989; Snyder *et al.*, 1991; McDonald *et al.*, 1992). Over the years this task has been greatly simplified by the development of computer software and hardware that not only facilitate data entry but also align and stack data into a highly manipulatable 3D voxel volume density map (McDonald *et al.*, 1991; Marko and Leith, 1996). The sophistication of these programs varies considerably, but depending on the problem even simple PC-based systems (Young *et al.*, 1987) can sometimes be used to generate useful 3D displays (Snyder *et al.*, 1991).

The z-axis resolution of most computer-aided serial section reconstructions is defined by the section thickness because the input data for each section usually consist of a single 2D surface tracing, even though there is 3D information throughout the section thickness. As a result the z-axis resolution from a reconstruction employing serial 75-nm-thick sections will be no better than 75 nm. This problem can be eliminated by using the Sterecon system (Marko and Leith, 1996), which allows objects viewed in stereo micrographs to be traced throughout the depth of the section.

Most modern EMs can generate a high-quality negative from sections as thick as 0.25 μm, whereas intermediate- and high-voltage EMs can utilize sections well over 0.5 μm. When compared with thin sections, the use of thick sections can greatly facilitate a same-cell correlative LM and EM study. First, it significantly reduces the time needed to cut and examine a specimen because it reduces the number of sections needed to reconstruct the region of interest by 5–10 times. Second, the thicker sections can be prescreened for content under the light

microscope so that only those containing the area of interest need be examined in the EM (Rieder and Bowser, 1983; Sluder *et al.,* 1990). These time-saving benefits allow certain types of same-cell correlative LM/EM studies to be conducted that would otherwise be shunned. For example, during the past decade we have been studying the replication and function of centrosomes and centrioles in echinoderm (sea urchin and starfish) and mollusc (surf clam) oocytes and zygotes at a same-cell correlative LM/EM level. The major technical difficulty inherent in these studies is the fact that oocytes are large cells (about 100 μm in diameter) and centrosomes with their associated centrioles are exceedingly small (the centriole to egg volume ratio is $1:1X\,10^6$). A conventional thin-section study requires that 1000–1500 serial sections be cut and then examined in the EM. By contrast, the same study using 0.25- to 0.50-μm-thick sections requires that only 200–400 serial sections be cut from each egg and, of these, only those containing centrosomes/centrioles need be examined in the EM (Rieder *et al.,* 1985).

Useful 3D information can also be obtained by viewing thick sections through the region of interest in stereo. Although seldom used in same-cell LM/EM studies, this approach has proven useful for examining the structure of unattached kinetochores (Ris and Witt, 1981). Unfortunately, the utility of this stereo-viewing approach is constrained by the fact that the overlapping of cell constituents in sections thicker than 0.5 μm usually hides or obscures the structure of complex cell components. For example, near the kinetochore the density of kinetochore fiber MTs is so high that it is impossible to accurately count them by viewing a 0.50-μm-thick section containing the whole kinetochore in stereo. In order to overcome the confusion generated by the overlapping of constituents in a thick section, thinner sections must be used or tomography must be employed.

B. From Tomography of Thick Sections

EM tomography allows all the structural information within a section to be extracted with a z-axis resolution approaching 3–5 nm. In this method (McEwen and Heagle, 1997) a 0.20- to 0.50-μm-thick section containing the region of interest is photographed in the electron microscope over a wide variety of tilt angles. The information from each of these views is then digitized and aligned into a 3D voxel volume density map that accurately reflects the distribution of stain throughout the section thickness. This volume can then be analyzed by "stepping" through consecutive 3-nm-thick slices, and the pertinent structure can then be followed and traced throughout the volume at high resolution.

Thick-section tomography has proven especially useful for defining the structure of kinetochores *in situ* (McEwen *et al.,* 1993; McEwen and Heagle, 1997) and isolated centrosomes (Moritz *et al.,* 1995; Vogel *et al.,* 1997). (The methods used in tomography, and the utility of this approach for examining

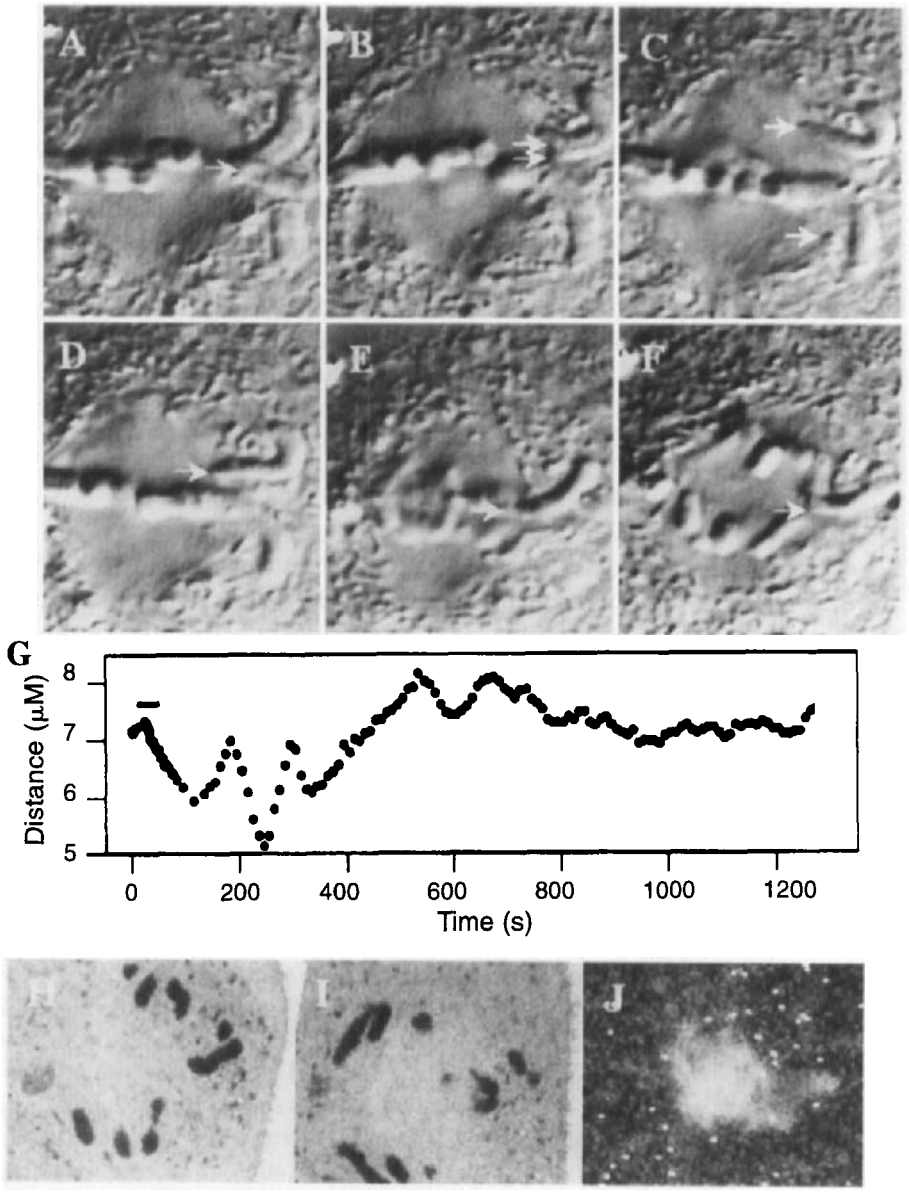

Fig. 3 In A–H, a 0.25-μm-diameter laser microbeam is used to sever a bioriented chromosome between its two sister kinetochore regions (arrow in A) to produce two chromosome fragments (arrow in B), each of which contains a single kinetochore. After moving toward its associated (top) pole, the larger fragment (top arrow in C) "congressed" to the spindle equator (arrow in D), where it remained stably positioned during the ensuing anaphase (arrows in E and F). The cell was fixed immediately after F. The motion of this chromosome fragment relative to the top pole, from the time it was formed until fixation, is graphed in G. (H and I) Low-magnification electron micrographs, from a serial series of 0.25-μm-thick sections, through the chromosome fragment noted by the arrows

the structure of mitosis-related organelles, are outlined in Chapter 5.) Its value for same-cell LM/EM studies has also recently been demonstrated. Using this method Khodjakov *et al.* (1997a) were able to determine the numbers and distribution of spindle MT plus ends near and on the centromere region of congressing chromosomes that contained a single kinetochore (Figs. 3 and 4). McEwen and Heagle (1997) similarly used tomography to determine where the plus ends of kinetochore MTs terminated, relative to the kinetochore outer plate, on kinetochores moving in a known direction at the time of fixation. These recent studies demonstrate that tomography is particularly useful for defining the interactions that occur between spindle MTs and where the ends of these MTS are located relative to the kinetochores and centrosomes.

The major difficulty in combining tomography with the same-cell LM/EM approach is that the region underlying the event of interest can seldom be captured in a single thick section. Rather, either the volume of the region is too large or, more commonly, even if it is small enough to be contained in a single thick section, it is bisected during the sectioning process. This is not a problem for some studies, but it can become a major problem for others. For example, because of its ability to unambiguously map the distribution of MTs ends, tomography would appear to be the method of choice for determining the number of MTs on kinetochores moving in a known direction upon fixation. However, in practice it is seldom possible to capture the entire kinetochore of interest in a single section, which is a requirement for obtaining the desired result by tomography. As a result, the more reliable method of serial thin sectioning was employed for this study (McEwen *et al.*, 1997). However, methods are currently being developed to allow tomographic reconstructions from consecutive thick sections to be fused within the computer with little loss of data (Soto *et al.*, 1994).

Acknowledgments

C. L. R. thanks Drs. Robert Palazzo, Roger Sloboda, and Melvin Spiegel for helpful discussions, Ms. Marion Howard for her assistance with library work, and Mr. R. Cole for his help with the content and figures. The original work described in this chapter was supported by NIH Grant GMS 40198 to C. L. R. and by NIH Grant RR 01219, awarded by the Biomedical Research Technology Program (NCRR/DHHR-PHS) to support the Wadsworth Center's Biological Microscopy and Image Reconstruction facility as a National Biotechnological Resource.

Fig. 3 (*Continued*) in C–F. Almost all of the kinetochore region (arrow in I) was contained in one section and is pictured at a higher magnification in J. The small white spheres on the surface of the section are gold fiduciary particles used to align the multiple views required during IVEM tomography (see Fig. 4), (reproduced from *The Journal of Cell Biology*, 1997, **136**, 229–240, by copyright permission of The Rockefeller University Press).

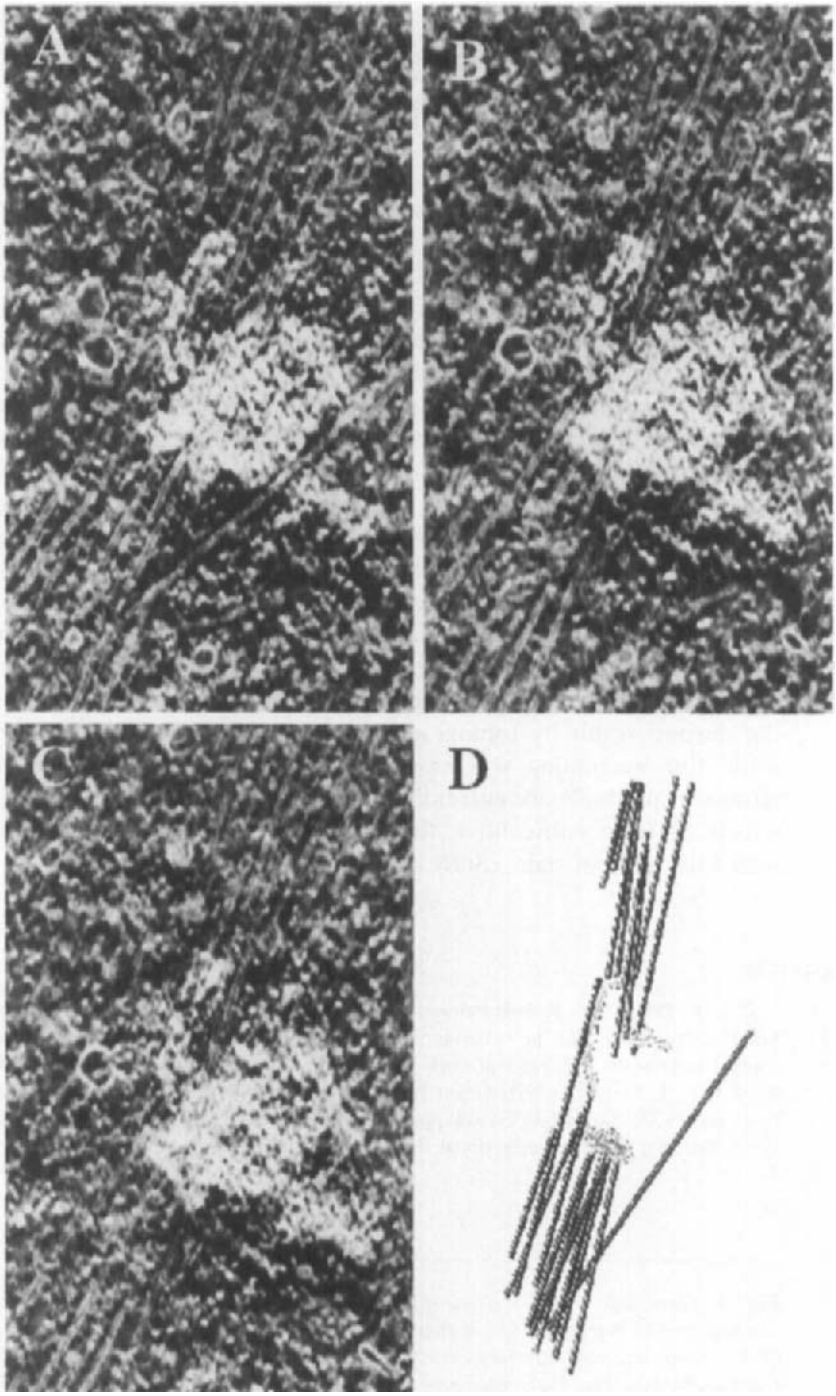
A
B
C
D

References

Ault, J. G., and Nicklas, R. B. (1989). Tension, microtubule rearrangements, and the proper distribution of chromosomes in mitosis. *Chromosoma* **98,** 33–39.

Bajer, A., and Mole-Bajer, J. (1969). Formation of spindle fibers, kinetochore orientation, and behavior of the nuclear envelope during mitosis in endosperm. *Chromosoma* **27,** 448–484.

Borysko, E., and Roslansky, J. (1959). Methods for correlated optical and electron microscopic studies of amoebae. *Ann. N. Y. Acad. Sci.* **78,** 432–477.

Brenner, S., Branch, A., Meredith, S., and Berns, M. W. (1977). The absence of centrioles from spindle poles of rat kangaroo (PtK_2) cells undergoing meiotic-like reduction division in vitro. *J. Cell Biol.* **72,** 368–379.

Brinkley, B. R., and Cartwright, J. (1966). Ultrastructural analysis of mitotic spindle elongation in mammalian cells in vitro. *J. Cell Biol.* **50,** 416–431.

Brinkley, B. R., Murphy, P., and Richardson, L. C. (1967). Procedure for embedding in situ selected cells cultured in vitro. *J. Cell Biol.* **35,** 279–283.

Bullitt, E., Rout, M. P., Kilmartin, J. V., and Akey, C. W. (1997). The yeast spindle pole body is assembled around a central crystal of Spc42p. *Cell* **89,** 1077–1086.

Chang, J. P. (1971). A new technique for separation of coverglass substrate from epoxy-embedded specimens for electron microscopy. *J. Ultrastruct. Res.* **37,** 370–377.

Eckley, D. M., Ainsztein, A. M., Mackay, A. M., Goldberg, I. G., and Earnshaw, W. C. (1997). Chromosomal proteins and cytokinesis: Patterns of cleavage furrow formation and inner centromere protein positioning in mitotic heterokaryons and mid-anaphase cells. *J. Cell Biol.* **136,** 1169–1183.

Gorbsky, G. J., Sammak, P. J., and Borisy, G. G. (1987). Chromosomes move poleward in anaphase along stationary microtubules that coordinately disassemble from their kinetochore ends. *J. Cell Biol.* **104,** 9–18.

Hayden, J. H., Bowser, S. S., and Rieder, C. L. (1990). Kinetochores capture astral microtubules during chromosome attachment to the mitotic spindle: Direct visualization in live newt lung cells. *J. Cell Biol.* **111,** 1039–1045.

Hays, T. S., and Salmon, E. D. (1990). Poleward force at the kinetochore in metaphase depends on the number of kinetochore microtubules. *J. Cell Biol.* **110,** 391–404.

Jensen, C., and Bajer, A. (1969). Effects of dehydration on the microtubules of the mitotic spindle. *J. Ultrastruct. Res.* **26,** 367–386.

Jensen, C. G., Jensen, L. C. W., Ault, J. G., Osorio, G., Cole, R. W., and Rieder, C. L. (1994). Time-lapse video light microscopic and electron microscopic observations of vertebrate epithelial cells exposed to crocidolite asbestos. *In* "Cellular and Molecular Effects of Mineral and Synthetic Dusts and Fibers" (J. M. G., Davis, and M.-C. Jurand, eds.), ASI Series, H85, 63–78. Springer-Verlag, New York.

Khodjakov, A., and Rieder, C. L. (1996). Kinetochores moving away from their associated pole do not exert a significant pushing force on the chromosome. *J. Cell Biol.* **135,** 315–327.

Fig. 4 (A–C) Selected 3-nm-thick "slices" through the tomographic volume calculated for the single kinetochore on the chromosome fragment followed in Fig. 3 and pictured in a thick section in Fig. 3J. Note the clarity with which the associated microtubules can be visualized and followed. A Sterecon (Marko and Leith, 1996) reconstruction of the pertinent structural information within the tomogram is shown in D. It is evident from this reconstruction that at the time of fixation the single kinetochore was connected to the opposing spindle poles by bundles of MTs and that its structure was highly distorted/fragmented (reproduced from *The Journal of Cell Biology,* 1997, **136,** 229–240, by copyright permission of The Rockefeller University Press).

Khodjakov, A., Cole, R. W., McEwen, B. F., Buttle, K. F., and Rieder, C. L. (1997a). Chromosome fragments possessing only one kinetochore can congress to the spindle equator. *J. Cell Biol.* **136,** 229–240.

Khodjakov, A., Cole, R. W., and Rieder, C. L. (1997b). A synergy of technologies: Combining laser microsurgery with green fluorescent protein (GFP)-tagging. *Cell Motil. Cytoskel.* **38,** 1–8.

Leslie, R. J., and Pickett-Heaps, J. D. (1984). Spindle microtubule dynamics following ultraviolet microbeam irradiations of mitotic diatoms. *Cell* **36,** 717–727.

Li, X., and Nicklas, R. B. (1997). Tension-sensitive kinetochore phosphorylation and the chromosome distribution checkpoint in praying mantid spermatocytes. *J. Cell Sci.* **110,** 537–545.

Marko, M., and Leith, A. (1996). Sterecon: Three-dimensional reconstructions from stereoscopic contouring. *J. Struct. Biol.* **116,** 93–98.

McDonald, K., Mastronarde, D., O'Toole, E., Ding, R., and McIntosh, J. R. (1991). Computer-based tools for morphometric analysis of mitotic spindles and other microtubule systems. *EMSA Bull.* **21,** 47–53.

McDonald, K. L., O'Toole, E. T., Mastronarde, D. N., and McIntosh, J. R. (1992). Kinetochore microtubules in PtK cells. *J. Cell Biol.* **118,** 369–383.

McEwen, B. F., and Heagle, A. B. (1997). Electron microscopic tomography: A tool for probing the structure and function of subcellular components. *J. Imaging Syst. Technol.* **8,** 175–187.

McEwen, B. F., Arena, J., Liu, Y. U., Frank, J., and Rieder, C. L. (1993). Three dimensional ultrastructure of the colcemid-treated PtK_1 kinetochore outer plate as determined by high voltage electron microscopic tomography. *J. Cell Biol.* **120,** 301–312.

McEwen, B. F., Heagle, A. B., Cassels, G. O., Buttle, K. F., and Rieder, C. L. (1997). Kinetochore fiber maturation in PtK_1 cells and its implications for the mechanisms of chromosome congression and anaphase onset. *J. Cell Biol.* **137,** 1567–1580.

McIntosh, J. R., and Landis, S. C. (1971). The distribution of spindle microtubules during mitosis in cultured human cells. *J. Cell Biol.* **49,** 468–497.

McNeil, P. A., and Berns, M. W. (1981). Chromosome behavior after laser microirradiation of a single kinetochore in mitotic PtK_2 cells. *J. Cell Biol.* **88,** 543–553.

Melan, M. A., and Sluder, G. (1992). Redistribution and differential extraction of soluble proteins in permeabilized cultured cells. *J. Cell Sci.* **101,** 731–743.

Mitchison, T. J. (1989). Polewards microtubule flux in the mitotic spindle: Evidence from photoactivation of fluorescence. *J. Cell Biol.* **109,** 637–652.

Mitchison, T. J., Evans, L., Schultz, E., and Kirschner, M. W. (1986). Sites of microtubule assembly and disassembly in the mitotic spindle. *Cell* **45,** 515–527.

Mole-Bajer, J., and Bajer, A. S. (1968). Studies of selected endosperm cells with the light and electron microscope. The technique. *Cellule* **67,** 257–265.

Moore, M. J. (1975). Removal of glass coverslips from cultures flat embedded in epoxy resins using hydrofluoric acid. *J. Microsc.* **104,** 205–207.

Moritz, M., Baumfeld, B., Sedat, J. W., Alberts, B., and Agard, D. A. (1995). Microtubule nucleation by gamma-tubulin containing rings in the centrosome. *Nature* **378,** 638–640.

Nicklas, R. B., and Ward, S. C. (1994). Elements of error correction in mitosis: Microtubule capture, release and tension. *J. Cell Biol.* **126,** 1241–1253.

Nicklas, R. B., Brinkley, B. R., Pepper, D. A., Kubai, D. F., and Rickards, G. K. (1979). Electron microscopy of spermatocytes previously studied in life: Methods and some observations on micromanipulated chromosomes. *J. Cell Sci.* **35,** 87–104.

Nicklas, R. B., Lee, G. M., Rieder, C. L., and Rupp, G. (1989). Mechanically cut mitotic spindles: Clean cuts and stable microtubules. *J. Cell Sci.* **94,** 415–423.

Rieder, C. L., and Alexander, S. P. (1990). Kinetochores are transported poleward along a single astral microtubule during chromosome attachment to the spindle in newt lung cells. *J. Cell Biol.* **110,** 81–95.

Rieder, C. L. (1981). Thick and thin serial sectioning for the three-dimensional reconstruction of biological ultrastructure. *Methods Cell Biol.* **22,** 215–249.

Rieder, C. L., and Borisy, G. G. (1981). The attachment of kinetochores to the prometaphase spindle in PtK_1 cells: *Chromosoma* **82,** 693–716.

Rieder, C. L., and Bowser, S. S. (1983). Factors which influence the light microscopic visualization of biological material in sections prepared for electron microscopy. *J. Microsc.* **132,** 71–80.

Rieder, C. L., and Bowser, S. S. (1984). A versatile system for illuminating flat-embedded specimens during block trimming. *J. Electron Microsc. Tech.* **1,** 207–208.

Rieder, C. L., and Cole, R. W. (1997). Perfusion chambers for high-resolution video light microscopic studies of vertebrate cell monolayers: Some considerations and a design. *Methods Cell Biol.* **56,** 253–275.

Rieder, C. L., Rupp, G., and Bowser, S. S. (1985). Electron microscopy of semithick sections: Advantages for biomedical research. *J. Electron Microsc. Tech.* **2,** 11–28.

Rieder, C. L., Cole, R. W., Khodjakov, A., and Sluder, G. (1995). The checkpoint delaying anaphase in response to chromosome monoorientation is mediated by an inhibitory signal produced by unattached kinetochores. *J. Cell Biol.* **130,** 941–948.

Ris, H., and Witt, P. L. (1981). Structure of the mammalian kinetochore. *Chromosoma* **82,** 153–170.

Robbins, E., and Gonatas, N. K. (1964). The ultrastructure of a mammalian cell during the mitotic cycle. *J. Cell Biol.* **21,** 429.

Shelby, R. D., Hahn, K. M., and Sullivan, K. F. (1996). Dynamic elastic-behavior of alpha-satellite DNA domains visualized in situ in living human cells. *J. Cell Biol.* **135,** 545–557.

Skibbens, R. V., Skeen, V. P., and Salmon, E. D. (1993). Directional instability of kinetochore motility during chromosome congression and segregation in mitotic newt lung cells: A push–pull mechanism. *J. Cell Biol.* **122,** 859–876.

Sluder, G., and Rieder, C. L. (1985). Centriole number and the reproductive capacity of spindle poles. *J. Cell Biol.* **100,** 887–896.

Sluder, G., Miller, F. J., and Rieder, C. L. (1986). The reproduction of centrosomes: Nuclear versus cytoplasmic controls. *J. Cell Biol.* **103,** 1873–1881.

Sluder, G., Miller, F. J., Cole, R., and Rieder, C. L. (1990). Protein synthesis and the cell cycle: Centrosome reproduction in sea urchin eggs is not under translational control. *J. Cell Biol.* **110,** 2025–2032.

Snyder, J. A., Armstrong, L., Stonington, O. G., Spurck, T. P., and Pickett-Heaps, J. D. (1991). UV-microbeam irradiations of the mitotic spindle: Spindle forces and structural analysis of lesions. *Eur. J. Cell Biol.* **55,** 122–132.

Soto, G. E., Young, S. J., Martone, M. E., Deerinck, T. J., Lamont, S., Carragher, B. O., Hama, K., and Ellisman, M. H. (1994). Serial section electron tomography: A method for three-dimensional reconstruction of large structures. *Neuroimage* **1,** 230–243.

Straight, A. F., Marshall, W. F., Sedat, J. W., and Murray, A. W. (1997). Mitosis in living budding yeast: Anaphase A but no metaphase plate. *Science* **277,** 574–578.

Vogel, J. M., Stearns, T., Rieder, C. L., and Palazzo, R. E. (1997). Centrosomes isolated from *Spisula solidissima* oocytes contain rings and an unusual stoichiometric ratio of alpha and beta tubulin. *J. Cell Biol.* **137,** 193–202.

Wadsworth, P., Shelden, E., Rupp, G., and Rieder, C. L. (1989). Biotin–tubulin incorporates into kinetochore fiber microtubules during early but not late anaphase. *J. Cell Biol.* **109,** 2257–2265.

Waters, J. C., Cole, R. W., and Rieder, C. L. (1993). The force producing mechanism for centrosome separation during spindle formation in vertebrates is intrinsic to each aster. *J. Cell Biol.* **122,** 361–372.

Waters, J. C., Mitchison, T. J., Rieder, C. L., and Salmon, E. D. (1995). The kinetochore microtubule minus-end disassembly associated with poleward flux produces a force that can do work. *Mol. Biol. Cell* **7,** 1547–1558.

Young, S., Royer, S. M., Groves, P. M., and Kinnamon, J. C. (1987). Three-dimensional reconstructions from serial micrographs using the IMB PC. *J. Electron Microsc. Tech.* **6,** 207–217.

This Page Intentionally Left Blank

CHAPTER 17

Identification and Characterization of Mitotic Mutations in *Drosophila*

William E. Theurkauf* **and Margarete M. S. Heck†**

* Department of Biochemistry and Cell Biology
State University of New York at Stony Brook
Stony Brook, New York 11794-5215

† Institute of Cell and Molecular Biology
University of Edinburgh
Edinburgh EH9 3JR, United Kingdom

METHODS IN CELL BIOLOGY, VOL. 61

0091-679X/99 $30.00

I. Introduction

The fruit fly *Drosophila melanogaster* has emerged as an important experimental system for the genetic analysis of mitosis. A large number of mitotic mutations have been characterized in *Drosophila,* and the proteins identified by these mutations include structural components of the mitotic spindle and cleavage furrow, regulatory kinases and phosphatases important for the dynamic reorganization of microtubules and actin filaments, and components of the cell cycle machinery. A detailed review of mitotic mutants in *Drosophila* is beyond the scope of this chapter but can be found elsewhere (Gatti and Goldberg, 1991; Foe *et al.,* 1993; Sullivan and Theurkauf, 1995). We include a basic overview of *Drosophila* genetics and mutagenesis protocols, but these topics are more extensively covered in several handbooks and other chapters from this series (Ashburner, 1989; Wolfner and Goldberg, 1994; Hamilton and Zinn, 1994; Greenspan, 1997). Specifically, we focus on the particular technical and biological factors that should be considered in designing screens for mitotic mutations in *Drosophila* and provide protocols for the cytological analysis of mitosis at various stages of the life cycle.

Designing a screen for mitotic mutants requires an understanding of the basic biology of the experimental system that will be used, and this is particularly important for multicellular organisms, such as *Drosophila,* in which mitosis must be viewed within a developmental context. This context strongly influences both experimental design and the genes that a specific mutant screen will identify. We therefore begin with a review of the *Drosophila* life cycle and brief descriptions of the ways in which the life cycle influences the isolation and characterization of mitotic mutants.

A. The *Drosophila* Life Cycle and the Genetics of Mitosis

Figure 1 diagrams the main features of the *Drosophila* life cycle. Oogenesis is ongoing within adult females, and eggs are produced continuously (Spradling, 1993). Females store mature eggs, which are arrested in metaphase of the first meiotic division. As eggs enter the oviduct, they are activated and the two meiotic divisions are completed. If the female has mated, the developmental program is initiated by fertilization and fusion of the male and female pronuclei. Pronuclear fusion is immediately followed by 13 very rapid and synchronous mitotic divisions that proceed without cytokinesis. Each of the first 10 nuclear division cycles takes only 8–10 min. The cell cycle begins to slow following division 9 and is approximately 25 min by syncytial division 13 (Foe and Alberts, 1983). As the syncytial mitoses proceed, the nuclei are redistributed in a cell cycle number-specific manner (Foe and Alberts, 1983; Baker *et al.,* 1993). During the first 4 syncytial divisions, nuclei form a spherical mass in the interior of the egg, near the anterior pole. The nuclei redistribute along the anterior–posterior axis during divisions 5–7, and this axial expansion forms a nuclear ellipse that mirrors the

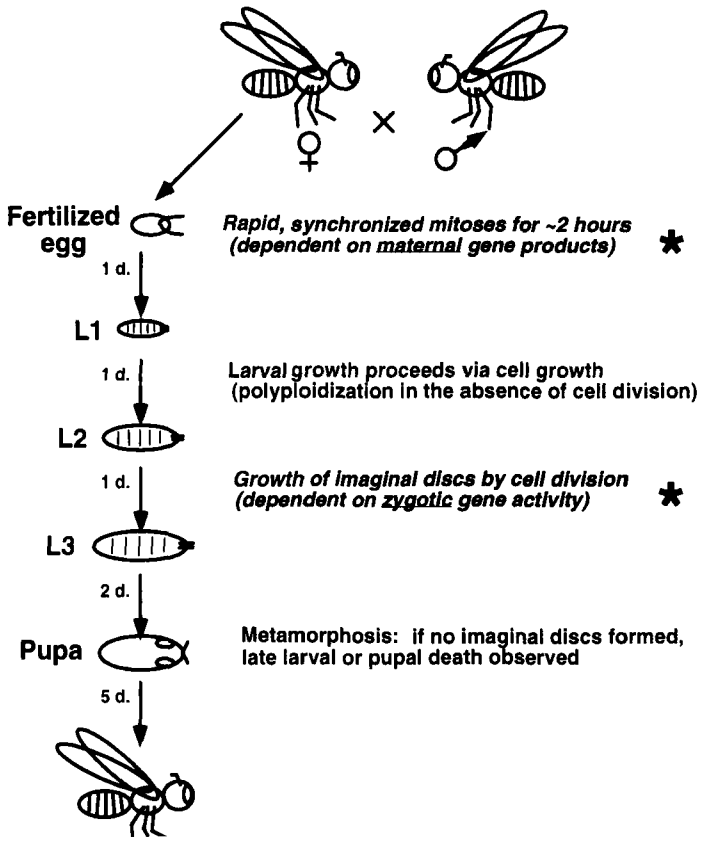

Fig. 1 The life cycle of *Drosophila melanogaster.* Adult females mate and produce fertilized eggs that initiate development with a series of rapid mitotic divisions under maternal control. Growth through the three larval instar stages (L1–L3) is driven by cell growth rather than mitotic cell division. Mitosis is required for growth of the brain and imaginal discs, which form adult structures during papal development. Defects in imaginal disc development thus lead to late larval and pupal death. The length of each stage, in days, is indicated.

shape of the embryo surface. Most of the nuclei migrate to the cortex during divisions 8 and 9, and a syncytial blastoderm with a uniform monolayer of surface nuclei is thus established at interphase of the 10th division. Four syncytial blastoderm stage divisions (10–13) follow completion of nuclear migration. After the 13th syncytial division, membranes invaginate and surround the cortical nuclei to form a cellular blastoderm. The morphogenetic movements of gastrulation are initiated shortly after completion of cellularization.

After cellularization, the cell cycle slows dramatically and begins to increase in complexity. During the syncytial divisions, the cell cycle is composed of synthesis (S) and mitosis (M) phases alone. Following cellularization, a G_2 phase is

first observed. Later, a subset of cells show a full cell cycle composed of G_1, S, G_2, and M phases, whereas other cells proceed through endoreduplication cell cycles in which multiple rounds of S phase without mitosis are observed (Foe *et al.*, 1993; Orr-Weaver, 1994; Edgar, 1995).

The segmental body plan and major organ systems develop during embryogenesis, and first-instar larvae hatch and begin to feed approximately 1 day after fertilization. Larvae proceed through three instars punctuated by molts, and growth during these stages reflects increases in cell size with endomitotic DNA replication rather than cell proliferation. The exceptions to this pattern of cell growth and endoreduplication are found in the brain, imaginal discs, and abdominal histoblasts. Mitotic cell division continues in these tissues, which reorganize to form adult structures during pupation, when most polyploid larval tissues degenerate. Flies eclose from the pupal cases approximately 10 days post-egg laying, completing the life cycle (Fig. 1).

Within the context of this life cycle, genetic control of mitosis can be divided into three stages. The rapid syncytial divisions that initiate embryonic development comprise the first of these stages. This initial period of mitotic activity does not require zygotic gene activity and is driven entirely by material that is deposited in the oocyte during oogenesis (Foe *et al.*, 1993). The syncytial mitoses are therefore under the genetic control of the female and not the embryo itself. Mutations affecting these divisions therefore target genes that are expressed during oogenesis in the adult female. Zygotic gene function is first required at blastoderm cellularization and is essential for subsequent mitotic divisions (Wieschaus and Sweeton, 1988; Merrill *et al.*, 1988; Foe *et al.*, 1993). However, many maternally deposited proteins and RNAs have long half-lives and continue to function well into the larval stages. As a result, genetic control of the postcellularization divisions is not strictly zygotic but depends on both maternal and zygotic genotypes (stage 2). Thus, embryos that are homozygous for null mutations in essential mitotic factors often survive embryogenesis and early larval development due to perdurance of maternal gene products. These embryos do not show clear mitotic defects until the larval stages, when maternal stores are finally depleted and zygotic gene activity becomes essential. Late larval development thus defines the third stage in the genetic control of mitosis. During this stage, maternally deposited material is depleted, and control of mitosis switches completely to the zygotic genome. As indicated previously, larval growth is driven almost exclusively by increases in cell size, and mitosis during these stages is primarily in the imaginal discs and brain. As a result, mutations affecting zygotic activity of essential mitotic genes generally produce late larval or pupal lethality. These animals are unable to proceed through metamorphosis because the precursors for adult structures have not been formed. Prior to death, the affected larvae are characterized by small brains and imaginal discs.

As the previous discussion indicates, control of the mitoses that occur after cellularization and before late larval stages is genetically complex. As a result, mutational analyses of mitosis in *Drosophila* generally focus on either maternal

control of the early embryonic divisions or zygotic control of mitosis in imaginal discs and larval brain tissues. Genetic and cytological techniques for the analysis of mitosis during these stages are described in detail later.

B. A Brief Note on Choosing a Mutagen

Ultimately, genes identified by mutational analyses will be candidates for molecular characterization. A number of approaches can be used to move from a *Drosophila* mutation to a cloned gene, and these approaches have been discussed in detail by other authors (Wolfner and Goldberg, 1994). In this section, we briefly discuss the factors that should be considered in choosing a mutagen, which is influenced by the specific goal of the screen and determines the strategy that will be used to clone the genes that are identified.

Chemical mutagens such as ethyl methane sulfonate are commonly used and generally produce single base changes or small deletions. These chemical agents are very efficient mutagens and generally random in action and are therefore the choice for "saturation" screens designed to genetically define entire cellular or developmental pathways (Greenspan, 1997). For example, this approach has been spectacularly successful in elucidating the pathways that control embryonic patterning (St. Johnston and Nüsslein-Volhard, 1992). The primary disadvantage to chemical mutagenesis is that the changes in DNA sequence are small and do not provide a clear marker for the mutated gene. However, these small changes may create complete genetic null mutations. As a result, mapping and cloning procedures are fairly involved and can take months to years to complete, depending on the physical location of the gene.

Transposon mutagenesis, by contrast, is inefficient but significantly simplifies subsequent molecular cloning by structurally tagging the mutated gene. Current transposon mutagenesis protocols generally produce stocks that carry a single transposon insertion (usually a derivative of the P element) so that the resulting mutations are linked to a unique molecular marker (Cooley *et al.*, 1988). Furthermore, the engineered transposons used in these screens generally harbor several unique restriction sites, a bacterial antibiotic resistance gene, and origin of replication. Sequences flanking the insertions can therefore be recovered directly by "plasmid rescue": Genomic DNA is subjected to restriction digestion, ligation, and transformation directly into bacteria. Bacteria carrying plasmids containing genomic sequences are recovered by selection for antibiotic-resistant colonies (Cooley *et al.*, 1988; Bier *et al.*, 1989). The recovered flanking sequences can then be used to identify additional genomic and cDNA clones by hybridizing to appropriate libraries. Unfortunately, the P element as mutagen frequently prefers to insert into 5′ regulatory sequences, thereby often resulting in only a decrease of a particular gene's expression (whether this creates a detectable phenotype is dependent on the particular gene). In addition, "hot spots" for transposon insertion mean that a random sampling of genes important to a particular process

is often not possible. Therefore, in designing a genetic screen, the advantages of efficient mutagenesis must be weighed against ease of molecular characterization.

II. Maternal-Effect Mutations That Disrupt the Syncytial Mitotic Divisions

A. Advantages and Limitations of Screens for Maternal Mutations

The early *Drosophila* embryo is a remarkable mitotic system. The first 10 divisions are only 8–10 min long. Cell cycle time increases during the three divisions that follow, but cycle 13 is still only 25 min in length. In addition, these rapid nuclear divisions are nearly synchronous and proceed without cytokinesis. The early embryo is therefore a large syncytium filled with rapidly dividing nuclei. During divisions 10–13, the majority of the syncytial nuclei are found in a monolayer at the cortex of the embryo, and both standard immunocytochemical procedures and *in vivo* imaging techniques can be used to analyze these cortical divisions. In addition to this cytological accessibility, mutations affecting the early embryonic division are relatively easy to identify. Furthermore, the genetics of early embryogenesis allows recovery of pure populations of mutant embryos, which facilitates phenotypic analyses at both cytological and biochemical levels. The early embryo thus allows a unique combination of cytological, genetic, and biochemical approaches to mitosis.

The primary disadvantage to screens for maternal mutations affecting early embryogenesis is that strong loss-of-function alleles of essential mitotic genes generally will not be recovered. This reflects the fact that these screens require homozygous mutant females to develop to the adult stage and produce embryos that can be scored, whereas severe loss-of-function mutations in genes required for mitosis throughout the life cycle will generally lead to zygotic lethality during preadult stages. Several factors partially compensate for this serious limitation. For example, partial loss-of-function mutations in essential mitotic genes are often recovered as maternal alleles that disrupt the early embryonic mitoses (Gonzalez *et al.*, 1990; Llamazares *et al.*, 1991; Glover *et al.*, 1995). This likely reflects the extraordinary rate of division in the early embryo, which puts extra stress on the mitotic machinery. As a result, weak mutations that reduce the level of an essential mitotic gene product may support the relatively slow zygotic divisions that are required for development to the adult stage but produce severe defects during the 8- to 10-min divisions that initiate embryogenesis. Another ameliorating factor is that essential mitotic proteins are sometimes encoded by multiple genes, and oocyte-specific forms provide maternal function, whereas zygotic isoforms provide gene function through the remainder of the life cycle. Screens for maternal mitotic factors can therefore identify strong loss-of-function mutations in a maternal isoform because the zygotic gene supports development to adult stage (Matthews *et al.*, 1993). Finally, conditional alleles and germline

clones of lethal mutations may allow generation of embryos mutant for zygotically active mitotic factors (Chou and Perrimon, 1996).

B. Basic Genetic Strategy

As noted previously, a number of handbooks and methods chapters describe *Drosophila* mutagenesis and maintenance of mutant stocks (Greenspan, 1997; Ashburner, 1989). We therefore begin our discussion of the genetic strategy used to identify maternal mitotic mutations with an established mutant stock that is to be analyzed. Mutations in *Drosophila* are maintained with a homologous balancer chromosome. Balancer chromosomes have multiple inversions and generally carry both recessive lethal and dominant visible mutations. As a result of the multiple inversions, meiotic pairing and recombination with normal sequence homologs is suppressed, and recombination events that could revert a mutant allele or uncouple it from a second marker are inhibited. The dominant visible marker allows identification of heterozygous individuals, which can then be separated from the homozygous mutants that are usually the subject of investigation. Finally, the recessive lethal mutation eliminates homozygous balancer animals from the stock. The properties of commonly used balancer chromosome and associated marker mutations are described in "The Red Book" (Lindsley and Zimm, 1992). This essential reference work, and the on-line *Drosophila* resource FlyBase (http://www.ebi.ac.uk/flybase/), provides detailed information on the genetics and molecular biology of *Drosophila.*

The utility of a balanced stock is shown by the example outlined in Fig. 2. In this instance, the mutation under investigation (designated m) is on the second chromosome and is "balanced" with the In(2LR)O,Cy balancer chromosome (abbreviated CyO). This chromosome carries the Cy marker, which causes the wings to curve upward in heterozygotes. The Cy mutation is also a recessive lethal, so homozygous balancer adults are not recovered. Our analysis begins with a cross of heterozygous males and females, which have easily scored curly wings. The offspring from this cross fall into two classes: Homozygous mutants (m/m) which do not carry the Cy marker and have straight wings and heterozygous animals (m/CyO) with curly wings. To score for maternal mutations affecting the early embryonic mitoses, homozygous mutant females (straight wings) are crossed to wild-type males and the resulting embryos are analyzed cytologically for division errors. We generally perform an initial screen in which embryos from mutant females are fixed in methanol and labeled for DNA with 4,6-diamino-2-phenylindole (DAPI, protocol 3). Methanol fixation is simple and efficient, and DAPI staining and standard epifluorescence microscopy reveal nuclear organization and thus allow identification of candidates for further investigation. Additional cytological characterization generally includes time-lapse analysis of mitosis in living embryos, which provides high spatial and temporal resolution data on the embryonic mitoses (protocol 6), and immunofluorescence analysis of the distributions of specific cytoskeletal elements.

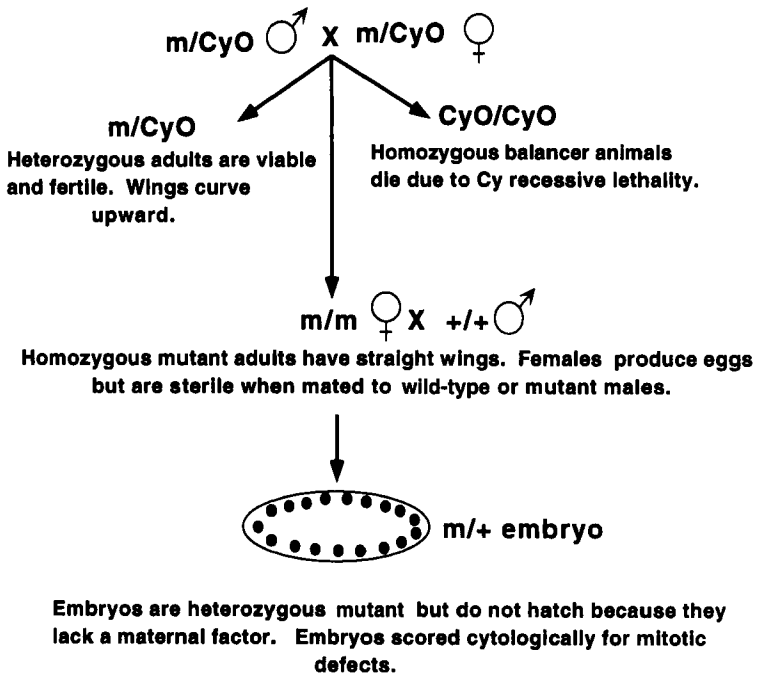

Fig. 2 Identifying maternal-effect mitotic mutations on the second chromosome. Flies carrying the mutant chromosome (m) in combination with the CyO second chromosome balancer (m/CyO) are mated and produce three classes of offspring: viable and fertile heterozygotes that have curly wings (m/CyO), CyO homozygotes (CyO/CyO) that die prior to the adult stage due to a recessive lethal on the balancer, and homozygous mutants (m/m) that develop to the adult stage. Homozygous mutant females are mated to wild-type males and the resulting embryos are cytologically examined for mitotic defects.

III. Cytological Analysis of the Syncytial Mitoses

Versions of the fixation and immunolabeling protocols in this section have been published previously (Theurkauf, 1994). For convenience, these protocols are repeated here, with recent modifications and notes on fluorescent probes that were not available earlier.

A. Formaldehyde/Methanol Fixation

This simple variation on the embryonic fixation protocol of Mitchison and Sedat (1983) preserves microtubule and actin organization and works well with antibodies to a number of nuclear and cytoskeletal proteins. We believe that this is the best general-purpose fixation protocol for most cytoskeletal applications, although it is not appropriate in all circumstances.

The most significant difference between this protocol and most others is that an undiluted 37% formaldehyde solution is used to fix the embryos. Lower concentrations of formaldehyde do not preserve microtubule structures during the rapid syncytial divisions, which has prompted the use of the microtubule-stabilizing drug taxol (Karr and Alberts, 1986). However, taxol often induces abnormal microtubule assembly and should be avoided (Kellogg *et al.,* 1989).

1. Procedure

1. Collect embryos on apple juice agar plates (Ashburner, 1989).

2. Rinse the embryos from the plates with Triton/NaCl (0.05% Triton X-100 and 0.7% NaCl) and collect on a fine nylon mesh supported in a filter assembly (prepared as shown in Fig. 3). For small-scale fixation of mutants, in which a few dozen to a few hundred embryos are recovered, it is best to use the smaller filtration assembly show in Fig. 3.

3. Dip the entire filter assembly with embryos into a beaker containing a solution of 50% commercial bleach and 50% Triton/NaCl. Incubate 2 or 3 min to dissolve the chorion.

4. Remove the filter assembly from the bleach solution and rinse the dechorionated embryos with Triton/NaCl and then with distilled water.

5. Draw water away from the embryos by placing paper towels against the nylon mesh. Dry the inside walls of the filter assembly with a tissue.

6. Rinse the embryos into a 50-ml Erlenmeyer flask with 10 ml of 100% octane. Gently swirl the embryos in the octane for 20–30 sec to permeabilize the vitelline membranes. Embryos can also be picked from the filter and transferred to the octane with a fine brush.

7. Add 10 ml of 37% formaldehyde to the embryo/octane mixture and incubate for 3–5 min. The embryos float at the interface between the formaldehyde (lower phase) and the octane (upper phase).

8. Draw off most of the lower formaldehyde phase, leaving the octane and fixed embryos in the flask.

9. Add 10 ml 100% methanol, stopper the flask, and shake vigorously for 30 sec to 1 min. The vitelline membranes will rupture, and embryos without vitelline membranes sink to the bottom of the methanol phase. Embryos that have not lost their vitelline membranes remain trapped at the methanol/octane interface.

10. Draw off the octane, any embryos remaining at the interface, and most of the methanol.

11. Resuspend the remaining embryos in 100% methanol and incubate for 1 or 2 hr at room temperature.

12. Rehydrate the embryos by passage through a methanol series. Start with 90% methanol/10% dH_2O and follow with 75% methanol/25% dH_2O, 50% metha-

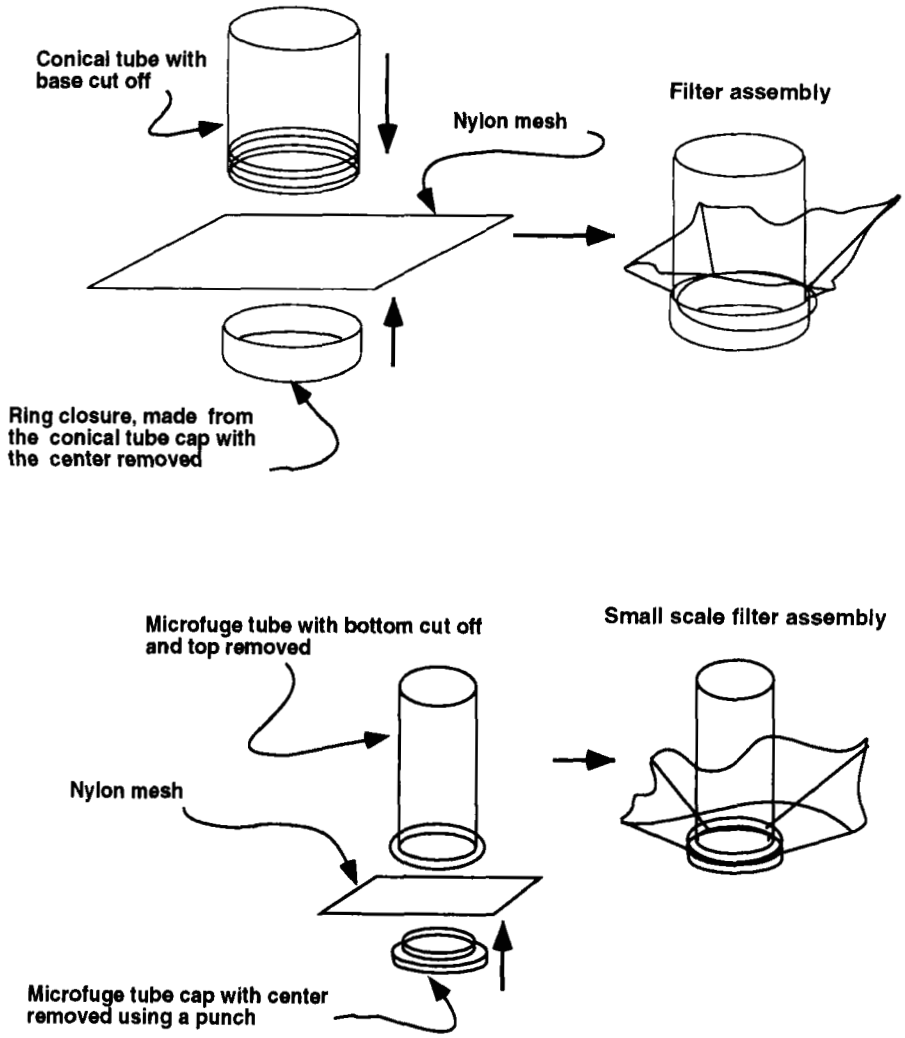

Fig. 3 Assembly of medium and small-scale embryo collection filters.

nol/50% phosphate-buffered saline (PBS; Karr and Alberts, 1986), and 100% PBS. At each solution change, allow the embryos to settle to the bottom of the flask, then immediately draw off the supernatant and resuspend in the next solution. Prolonged incubation at each methanol solution change is not required.

13. Draw off the PBS, add PBST (PBS containing 0.05% Triton X-100), and incubate for 30 min.

The embryos are now ready for antibody labeling (see Section III,D).

2. Comments

1. The most common artifacts encountered in this technique are the result of anoxia, which can develop when small containers are used during dechorionation and/or fixation. Under these conditions, the tightly packed embryos appear to rapidly deplete the oxygen supply in the bleach and wash buffers. Anoxia leads to interphase chromosome condensation and anaphase chromosome bridging, which are easily observed in DAPI-stained preparations. Many examples of artifactual anaphase bridges have been published. To avoid anoxia, the nylon filter apparatus should be large enough so that the embryos form a sparse monolayer during dechorionation. Similarly, the fixation vessel should be wide enough so that the embryos form a monolayer at the octane/formaldehyde interface. An Erlenmeyer flask is an ideal fixation container because a relatively large octane/formaldehyde interface forms within the wide base. In general, narrow dechorionation and fixation containers should be avoided.

2. The syncytial mitoses are very rapid, and analysis of living embryos suggest that the microtubule cytoskeleton turns over quickly (Kellogg *et al.*, 1988; Matthies *et al.*, 1996). Rapid fixation is therefore essential to microtubule preservation. Octane prepermeabilization, combined with the very high concentrations of fixative, may allow rapid formaldehyde penetration and fixation. When embryos are added directly to an octane/formaldehyde mixture, microtubule preservation is poor. We speculate that this is because the vitelline membranes are permeabilized in the presence of fixative, and penetration of fixative during the initial stages of permeabilization is relatively slow.

3. Because of the high concentration of formaldehyde used in this protocol, relatively short fixation times are required. If fixation is allowed to proceed too long, methanol removal of the vitelline membranes is inefficient and antibody penetration is poor. Formaldehyde fixation for as little as 2.5 min works well, and shorter times may be sufficient.

4. Incubating the fixed embryos in methanol (step 11) helps clear the cytoplasm. However, immediate rehydration also works well, particularly when cortical structures are the focus of the experiment. Fixed embryos can be stored in 100% methanol at −20°C for at least 2 weeks, and more extended storage is probably fine.

B. Formaldehyde Fixation

Much of the actin in a typical cell is not filamentous, and antiactin immunolabeling thus produces significant cytoplasmic signal that can obscure details of filament organization. Fluorescent conjugates of phalloidin specifically bind to filamentous actin (Cooper, 1987) and are therefore extremely useful reagents for cytological analysis of actin filament organization. However, these powerful reagents cannot be used to label tissues that have been treated with methanol. The formaldehyde fixation protocol presented here preserves microtubules and

allows phalloidin staining, although the vitelline membranes must be mechanically removed before labeling.

1. Procedure

1. Collect embryos on apple juice agar plates (Ashburner, 1989).
2. Rinse the embryos from the plates with Triton/NaCl (0.05% Triton X-100 and 0.7% NaCl) and collect on a fine nylon mesh supported in a filter assembly (prepared as shown in Fig. 3).
3. Transfer the filter assembly to a beaker containing a solution of 50% commercial bleach and 50% Triton/NaCl. Incubate 2 or 3 min.
4. Remove the filter assembly from the bleach and rinse the embryos with Triton/NaCl and then with distilled water.
5. Draw water away from the embryos by placing paper towels against the nylon filter. Dry the inside walls of the filter assembly with a tissue.
6. Rinse the embryos into a 50-ml Erlenmeyer flask with 10 ml of 100% octane. Gently swirl the embryos in the octane for 20–30 sec to permeabilize the vitelline membranes.
7. Add 10 ml of 37% formaldehyde to the embryo/octane mixture, and incubate for 3–5 min. The embryos float at the interface between the formaldehyde (lower phase) and the octane (upper phase).
8. Draw off the formaldehyde phase, leaving the octane and fixed embryos in the flask.
9. Add 10 ml PBS, swirl, and draw off the PBS. To remove residual formaldehyde, repeat this PBS wash two more times.
10. Add 10 ml of fresh PBS.
11. Draw the fixed embryos from the octane–PBS interface using a Pasteur pipette, and transfer to the frosted portion of a slide. Remove most of the transfer liquid.
12. To remove the vitelline membranes, draw the edge of a 22 × 40-mm cover glass across the embryos and then roll the embryos between the slide and cover glass, using a circular motion (Theurkauf, 1994). Alternate between these two disrupting techniques, while monitoring vitelline membrane removal with a dissecting microscope.
13. Rinse the "rolled" embryos into a test tube with PBST and allow them to gravity settle.
14. Remove the supernatant and add 1% Triton X-100 in PBS. Incubate with gentle rocking for 1 or 2 hr at room temperature.
15. Let the rolled embryos settle to the bottom of the tube, remove the 1% Triton solution, and resuspend in PBST.

The embryos are now ready to label as described in Section III,D.

2. Comments

Small numbers of embryos can be fixed using this protocol, but the procedure for mass removal of vitelline membranes described here does not work well when only a few embryos are on the slide. In this circumstance, the vitelline membranes may need to be manually removed from individual embryos as described by Schubiger and Edgar (1994).

C. Methanol Fixation

Some antibody–antigen combinations are sensitive to formaldehyde fixation. The following Methanol fixation protocol is a useful alternative to the formaldehyde-based procedure described previous. The overall organization of the microtubules and actin filaments is preserved with this method (Kellogg *et al.,* 1988), but individual microtubules are not as well-defined as in formaldehyde-fixed material. In addition, phalloidin labeling is not possible.

1. Procedure

1. Collect embryos on apple juice agar plates (Ashburner, 1989).

2. Rinse the embryos from the plates with Triton/NaCl (0.05% Triton X-100 and 0.7% NaCl) and collect on a fine nylon mesh supported in a filter assembly (prepared as shown in Fig. 3).

3. Transfer the filter assembly to a beaker containing a solution of 50% commercial bleach and 50% Triton/NaCl. Incubate 2 or 3 min.

4. Remove the filter assembly from the bleach and rinse the embryos with Triton/NaCl and then with distilled water.

5. Draw water away from the embryos by placing paper towels against the nylon filter. Dry the inside walls of the filter assembly with a tissue.

6. Rinse the embryos into a 50-ml Erlenmeyer flask with 10 ml of 100% octane. Gently swirl the embryos in the octane for 20–30 sec to permeabilize the vitelline membranes.

7. Add 10 ml 100% methanol, stopper tightly, and shake vigorously for 30 sec to 1 min.

8. Remove the octane and most of the methanol, leaving the embryos that have settled to the bottom of the flask in a minimal volume of methanol.

9. Add 100% methanol and incubate for 1 or 2 hr.

10. Rehydrate the embryos through a methanol series, starting with 90% methanol (in water), followed by 75% methanol, 50% methanol, and 100% PBS. During each solution change, allow the embryos to settle to the bottom of the flask

and immediately draw off the supernatant and resuspend in the next solution. Prolonged incubation at each step is not required.

11. Draw off the PBS, add PBST, and incubate for 30 min.

Label the fixed embryos as described in Section III,D.

2. Comments

Vitelline membrane removal is very efficient with this simple technique. It is therefore a good choice for mutant screens in which small-scale embryo collections are used. It is also a good method for preparation of embryos that will be used to preabsorb secondary antibodies (Karr and Alberts, 1986).

D. Labeling Cytoskeletal Elements and Nuclei in Fixed Embryos

The following protocol works for embryos fixed by any of the previous procedures. For laser confocal analyses, we now routinely label nuclei with Oli-green (Molecular Probes, Inc.). This nucleic acid-binding reagent has excitation and emission spectra similar to those of fluorescein, making it useful for double-label applications with rhodamine. Oli-green (like propidium iodide) binds to both DNA and RNA, so an RNase A treatment should be done prior to labeling if this reagent will be used. As described in the following protocol, we usually include RNase A during the secondary antibody incubation. If Oli-green will not be used, the RNase A treatment can be omitted.

1. Procedure

1. Transfer the fixed embryos to a 0.5- or 1.5-ml tube. After the embryos have settled to the bottom of the tube, remove the supernatant and resuspend in 0.2–0.5 ml fresh PBST.

2. Add an appropriate dilution of primary antibody and incubate overnight at 4°C with constant gentle mixing. A rotator set up in a cold room works well. Antibody dilution must be determined empirically. For dual-label applications using antibodies from different species, both primary antibodies can be added to the sample at the same time.

3. Remove the primary antibody solution and wash the embryos in four changes of PBST, incubating for 15 min after each solution change.

4. After the final PBST wash, resuspend the embryos in 200 μl PBST and add fluorescently conjugated secondary antibodies that have been preabsorbed against fixed *Drosophila* embryos (Karr and Alberts, 1986). If nuclei are to be labeled with Oli-green, add RNase A to 5 μg/ml. Incubate embryos/egg chambers in secondary antibody for 2 hr at room temperature or overnight at 4°C.

5. Remove the secondary antibody solution and wash the embryos in four changes of PBST, incubating for 15 min at each solution change.

6. Add fresh PBST. Fluorescently conjugated phalloidin (1 μg/ml) and DAPI (1 μg/ml) or Oli-green (1 : 5000 dilution) can be added at this time. Incubate for 10 min at room temperature.

7. Wash the embryos in four changes of PBST for 15 min each. Follow these washes with two rinses in PBS.

8. Let the labeled embryos settle and remove the PBS supernatant. Add a few drops of mounting medium (1 mg/ml *p*-phenylene diamine, 90% glycerol, in PBS) to the labeled material, gently stir with a pipette tip, and transfer to a slide. Place a cover glass over the mixture and seal with nail polish. Alternatively, labeled egg chambers can be cleared as described later.

2. Comments

1. When monoclonal or affinity-purified primary antibodies are used, blocking with nonspecific protein is generally not required. If background is a problem, 1% bovine serum albumin or powdered milk can be added to the antibody solution. Secondary antibodies should be preabsorbed against fixed embryos (Karr and Alberts, 1986).

2. The appropriate dilution of primary antibody must be determined empirically. Strong microtubule labeling is obtained using a 1:1000 dilution of the monoclonal anti-α-tubulin antibody DM1α (Sigma Chemical Co., St. Louis, MO).

3. Fluorescently conjugated anti-tubulin antibodies penetrate and label the interior of the embryo more efficiently than primary antibody–secondary antibody combinations (Theurkauf, 1992; Theurkauf *et al.*, 1993). Direct primary antibody conjugates may therefore help reveal internal structures.

E. Clearing Immunolabeled Embryos

Embryos are relatively large, and internal structures can be difficult to image, even with the aid of a confocal microscope. Light scattering and diffraction by yolk, lipid droplets, and membrane-bound organelles lead to loss of fluorescent signal, and this limits the depth of the optical sections that can be obtained. To overcome this limitation, immunofluorescently labeled embryos can be cleared as described in the following procedure.

1. Procedure

1. Remove as much of the PBS wash as possible from immunolabeled embryos.

2. Add 100% methanol and resuspend the embryos by inverting the tube several times.

3. Remove the methanol supernatant and add fresh methanol. Incubate 1 or 2 min.

4. Draw off as much of the methanol as possible and add a few drops of clearing solution (benzyl benzoate:benzyl alcohol, 2:1). Stir gently with a pipette tip.

5. Transfer the cleared material, in the clearing solution, to a slide. Place a cover glass over the sample and seal with nail polish. Slides last for several weeks if stored at −20°C but are best viewed immediately after mounting.

2. Comments

1. Cleared embryos are almost impossible to detect in the benzyl benzoate: benzyl alcohol solution and do not rapidly settle to the bottom of the tube. To avoid losing your sample in this mixture, use a minimum volume of clearing solution to resuspend the embryos and transfer everything to slides.

2. Both fluorescein and rhodamine bleach very rapidly in this clearing solution. It is therefore essential to photograph or electronically capture images as quickly as possible. If you stare at your embryos for too long, they may bleach to the point that subsequent photography is not possible.

3. Phalloidin labeling does not survive methanol dehydration and clearing and cannot be used with this protocol.

F. Analysis of Cytoskeletal and Nuclear Reorganization in Living Embryos

The ability to image cytoskeletal elements and chromatin *in vivo,* using commonly available tools and reagents, is one of the primary advantages to studying mitosis in the early *Drosophila* embryo. Syncytial *Drosophila* embryos can be microinjected with fluorescent probes using very simple microinjection equipment, and the embryo tolerates fairly intense illumination. In addition, the syncytial blastoderm-stage mitoses are rapid, synchronous, and restricted to a monolayer a few micrometers below the plasma membrane. As a result, high numerical aperture oil immersion lenses with short working distances can used. This combination of factors makes the early embryo an ideal system for high-resolution time-lapse microscopic study.

A variety of microscopic techniques have been used to image cytoskeletal and nuclear reorganization in syncytial blastoderm-stage embryos (Kellogg *et al.,* 1988; Minden *et al.,* 1989; Matthies *et al.,* 1996). We use laser scanning confocal microscopy for all our analyses. This technique is now widely available and is well suited to analyses of thick embryonic samples. However, the sample preparation procedure described here can be adapted to essentially any imaging technique.

1. Procedure

1. Prepare cover slips for microinjection as follows: Place several sections of double-stick tape in a small (50–100 ml) beaker containing 10–20 ml of octane and swirl to help dissolve the adhesive. Draw 100–200 μl of solution into a

Pasteur pipette and paint a stripe of adhesive down the center of a 22 × 40-mm cover glass. As the octane evaporates, a thin film of adhesive is left on the cover glass.

2. Collect embryos on apple juice agar plates (Ashburner, 1989). Use a fine brush to transfer embryos from the plates to double-stick tape on a slide.

3. Manually remove the chorion (eggshell) as follows: Gather a small ball of double-stick tape adhesive with the tips of No. 5 Dumont forceps. Using the ball of adhesive, gently stroke the surface of the embryo until the chorion is ruptured and the embryo is partially freed. Pick up the embryo by touching the ball of adhesive to a portion of the embryo that is free of shell. This procedure and step 4 are best done using a stereo microscope.

4. Transfer the dechorionated embryo to the adhesive strip on the 22 × 40-mm cover glass. To facilitate microinjection at midembryo, align the embryos end to end. Injection into the middle of the egg best allows spreading of probe throughout the syncytium.

5. Briefly dry the embryos by placing them over dessicant in a covered container. A petri dish works well for this. Usually, 5–10 min over dessicant is sufficient. The ideal time must be determined empirically, and time varies with temperature and relative humidity.

6. Cover the embryos with halocarbon oil and transfer the slide to the stage of an inverted microscope. For microinjection, we use a Narishige manual micromanipulator to position the micropipette and an air-filled line attached to a 20-cc syringe to control fluid flow. This simple setup is inexpensive and works well but does not allow delivery of fixed volumes.

7. Break off the pipette tip on the edge of the coverslip. Place a 1-μl drop of probe solution in the oil, and front-fill the pipette by placing the tip in the probe solution and applying vacuum with the syringe. Pipettes can also be backfilled prior to mounting in the manipulator, although we have found that some protein conjugates bind to the glass and are therefore lost as the solution flows to the tip. Microinject the embryos with probe.

8. The embryos are now ready to image. We use a BioRad MRC 600 attachment on a Nikon Diaphot inverted microscope for confocal imaging. Time-lapse images are initially stored on the hard drive of the computer that controls the confocal head. For video rate playback, sequences are transferred to optical disks using a Sony LVN3000R video system.

2. Comments

1. We have used many commercially available fluorescent probes for time-lapse studies in early embryos. To image microtubule reorganization, we generally use rhodamine-conjugated bovine brain tubulin obtained from Molecular Probes. This reagent is supplied in 10-μl aliquots and should be rapidly thawed, divided into 1-μl aliquots, rapidly frozen in liquid nitrogen, and stored at −70°C.

Prior to use, the aliquots are thawed, diluted 1:1 in dH_2O, and centrifuged for 10 min at maximum speed in a 4°C tabletop microfuge. Samples should be kept on ice until use because the tubulin will polymerize at room temperature and clog the micropipette. We also have used rhodamine and fluorescein-conjugated actin obtained from Cytoskeleton Inc. Sample handling is essentially the same as that for tubulin, although polymerization and clogging are less of a problem. To label chromatin, we use Oli-green (Molecular Probes) diluted 1:10 to 1:20 in dH_2O. Prior to use, Oli-green dilutions should be centrifuged for 10 min as described for the protein conjugates.

2. *In vivo* imaging techniques, though powerful, are not immune to artifacts. In general, these artifacts are cause by photodamage and can be reduced by limiting the amount of light to which the sample is exposed. As a rule, the light source should be attenuated as much as possible without compromising image quality. The rate of image capture should also be kept to a minimum. Using the BioRad confocal to analyze embryos injected with rhodamine tubulin, we generally capture a single full-frame image (512 lines, slow scan rate) every 10 sec, with the laser attenuated by 1.0 or 1.5 OD neutral density filters. Using these conditions, we have captured up to 1000 images without affecting subsequent development (cellularization and gastrulation). When imaging embryos injected with nuclear labels, by contrast, it is often difficult to obtain sequences of 100 images without inducing some artifacts, including anaphase chromosome bridges and complete segregation failures. To gain familiarity with these artifacts, embryos should be intentionally analyzed using minimal laser attenuation. Buffer components can also cause artifacts. Because it is usually necessary to introduce a probe in a specific buffer, these artifacts can be difficult to rigorously control. In general, the results of *in vivo* imaging should be confirmed by immunofluorescence analyses. For example, abnormal spindle structures that are observed in mutant embryos injected with rhodamine tubulin should also be observed in fixed samples stained with anti-tubulin antibodies. Structures that are seen exclusively in injected embryos are suspect.

IV. Zygotic Mutations That Disrupt Mitosis in Larval Tissues

A. Advantages and Limitations of Screens for Zygotic Mutations

The advantages and limitations of screens for zygotic mutations outlined here complement those of screens for maternal mutations. Zygotic mutations, in contrast to maternal mutations, should include strong loss-of-function alleles of most essential mitotic genes. In addition, the early embryo does not undergo true cytokinesis and has a simplified cell cycle of alternating S and M phases. Thus, cell cleavage and progression through G_1 and G_2 phases cannot be genetically analyzed during early embryogenesis but are potential targets of zygotic screens. These genetic advantages come at the expense of cytological and biochemical

tractability. Although high-resolution cytological analysis of mitosis is relatively simple in the early embryo, there are technical and biological challenges to this during larval development. Also, while the *Drosophila* embryo is characterized by synchronized divisions and a mitotic index of 30–40%, mitosis in larval tissues is asynchronous and the mitotic index in a wild-type brain may only be on the order of 1%. In addition, though not difficult, homozygous mutant animals must be separated from heterozygous siblings and the dividing tissues manually dissected from individual larvae. For maternal mutations, on the other hand, large numbers of pure mutant embryos can be collected directly on agar plates. Because of these contrasting advantages and limitations, there is no clear "best" genetic approach to mitosis in *Drosophila.*

For a number of reasons, zygotic screens have been particularly useful in the genetic examination of chromosome architecture (perhaps because the chromosomes of early embryos lack some levels of complexity given that there is little or no transcription and no obvious heterochromatin). Chromosome condensation and segregation are readily apparent in the mitotically active cells of larval tissues, and the level of mitotic chromosome condensation in these tissues (about 5000-fold in length) approaches that observed in other higher eukaryotic cells. Therefore, flies remain a good model for higher eukaryotic chromosome structure; it is much more difficult to visualize chromosome behavior in yeast cells. In addition, the *Drosophila* genome is compact (~165 Mb), there are only four chromosomes, and these chromosomes are readily distinguishable by DAPI staining. The karyotype is composed of three autosomes: two large metacentric chromosomes (II and III), a very small IV (~4 Mb) chromosome which appears as a dot, and the sex chromosomes (two X's or an X and Y). This very simple karyotype allows one to determine whether particular chromosomes or regions of chromosomes are affected by a specific mutation. For example, mutations have been identified that affect condensation of only the Y chromosome or condensation of all centromeric heterochromatin. Other mutations lead to telomere to telomere fusion (Cenci *et al.,* 1997). It may be possible to identify maternal mutations causing similar defects. However, the cytological techniques used to study mitosis in larval brain and discs appear to be particularly well suited to these studies. For example, the hypotonic treatments that are used to enhance mitotic chromosome spreading in larval tissues are not possible in early embryos because they are surrounded by a vitelline membrane.

B. Basic Genetic Strategy

As explained previously, maternal gene products allow progression through the rapid early syncytial divisions in the absence of zygotic transcription. Because the majority of the larval tissues grow through increases in cell size and endoreduplication, mitotic activity is not necessary for the production of mature third-instar larvae. Only the brain, imaginal discs, and histoblasts (which survive into the adult) continue normal diploid cell cycles during larval development. As a

result, mitotic mutations specifically affect these tissues and thus prevent metamorphosis of the adult fly. This led Gatti and Baker (1989) to speculate that late larval and pupal lethal mutations that also affect development of imaginal discs will be enriched for lesions in genes affecting mitosis. Indeed, in panning through existing collections of lethal mutations, they identified defects in (i) interphase progression, (ii) chromosome integrity, (iii) chromosome condensation, (iv) spindle formation and/or function, and (v) completion of chromosome segregation or cytokinesis. These results demonstrated that genetic analysis of mitotic chromosome behavior in a higher eukaryote was possible.

The basic strategy for identifying recessive zygotic mutations affecting mitosis involves crossing heterozygous fly stocks and collecting and analyzing the resulting homozygous mutant larvae for defects in disc development/mitosis (Fig. 4). The main technical problems lies in distinguishing heterozygous wild-type larvae from homozygous mutant siblings (Fig. 4). This is actually straightforward because balancer chromosomes with dominant visible larval markers are available. The most commonly used third-chromosome larval marker is *Tubby* (*Tb*), which causes heterozygous larvae to appear short and fat in comparison to their long and thin (lacking *Tb*) homozygous mutant siblings. As described previously, the balancer homozygotes are embryonic lethal. Animals carrying *Tb* are not reliably distinguishable from wild type during the early larval or adult stages, so this marker can only be used to separate genotypes during the third-larval instar

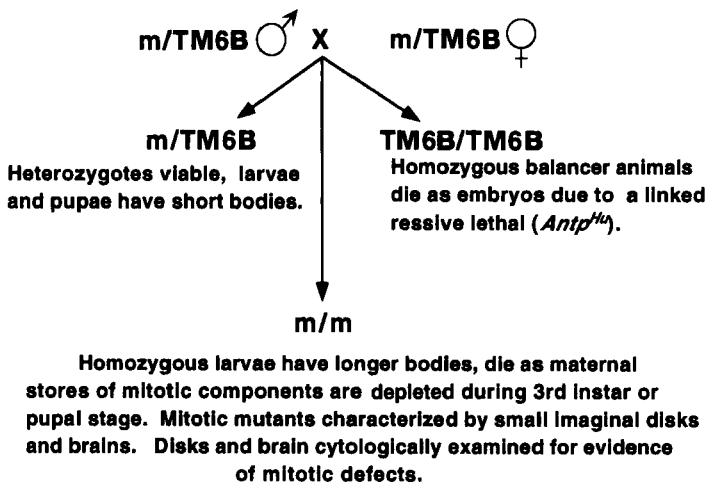

Fig. 4 Identifying third-chromosome zygotic mutations that disrupt mitosis. Flies carrying the mutant chromosome (m) in combination with the TM6B third-chromosome balancer (m/TM6B) are mated and produce two classes of offspring: viable and fertile heterozygotes with shorter than wild-type larvae due to the Tubby (Tb) mutation (m/TM6B) and homozygous mutants (m/m) that show wild-type larval size but die during L3 or the pupal stage. Homozygous balancer larvae (TM6B/TM6B) are not recovered due to a recessive embryonic lethal on the TM6B chromosome.

when they are wandering on the vial walls or in the food. This is not a serious limitation for mitotic mutant screens since most of these mutations allow development to late larval stages. Though Tb is on the third chromosome, a T(2;3) translocation balancer can be used to analyze mitotic mutations on the second chromosome. Because double balancers are not easy to work with, a preferable alternative would be to use a second chromosome balancer carrying *Black Cells* (*Bc*) which results in the deposition of black crystals in the hemolymph of heterozygous larvae. The mutation of interest can also be linked to a recessive visible mutation. For example, the recessive *red* mutation (on the third chromosome), which turns the Malphigian tubules of homozygous animals red, can be recombined onto the mutant chromosome (or present to begin with in the stock to be mutagenized). Homozygous mutant larvae can then be identified by the presence of red Malphigian tubules. Once the mutant larvae are identified, the cytological techniques described later can be used to determine if the imaginal discs and brain are small and to more specifically score for defects in chromosome behavior, spindle function, or cytokinesis.

V. Cytological Analysis of Larval Brain and Imaginal Discs

A. Dissecting Larval Brain and Imaginal Discs

Having identified a mutation that leads to late larval lethality, and with homozygous mutant larvae in hand, the next step is to examine brain and imaginal disc morphology. Third-instar larvae can be collected from culture vials when they are crawling on the walls. If most of the third instars are in the food, they can be recovered by squirting a small amount of water into the culture, which will encourage them to crawl up on the vial walls. Pick the larvae from the vial with forceps and rinse in "Ephrussi–Beadle" Ringer's solution (129 m*M* NaCl, 4.7 m*M* KCl, 1.9 m*M* $CaCl_2$, 10 m*M* Hepes, pH 6.9) and transfer to a drop of this solution on a slide or in a dissecting dish for dissection.

Using two very fine "Biologie"-grade Dumont No. 5 forceps, grab the larva just posterior to the black mouth hooks and at a position about one-half to two-thirds back along the length of the body. The larval body is then pulled apart. The translucent brain is usually attached to the anterior portion and is recognizable by its characteristic morphology of two spherical brain hemispheres connected with a long ventral ganglion (Fig. 5). These tissues bear a striking resemblance to the human male reproductive system. Many of the imaginal discs will be attached to the wild-type brain. In most mitotic mutants, the brain hemispheres will be small, the ventral ganglion thin, and the imaginal discs small or absent. It is not necessary to remove the imaginal discs prior to squashing. The polytene salivary glands are the paired long tubes (containing a lumenal space) with easily visible nuclei (Fig. 5).

If desired, male and female larvae can also be distinguished by examination of the gonad through the body wall. The testes are two clear ovals within sheets

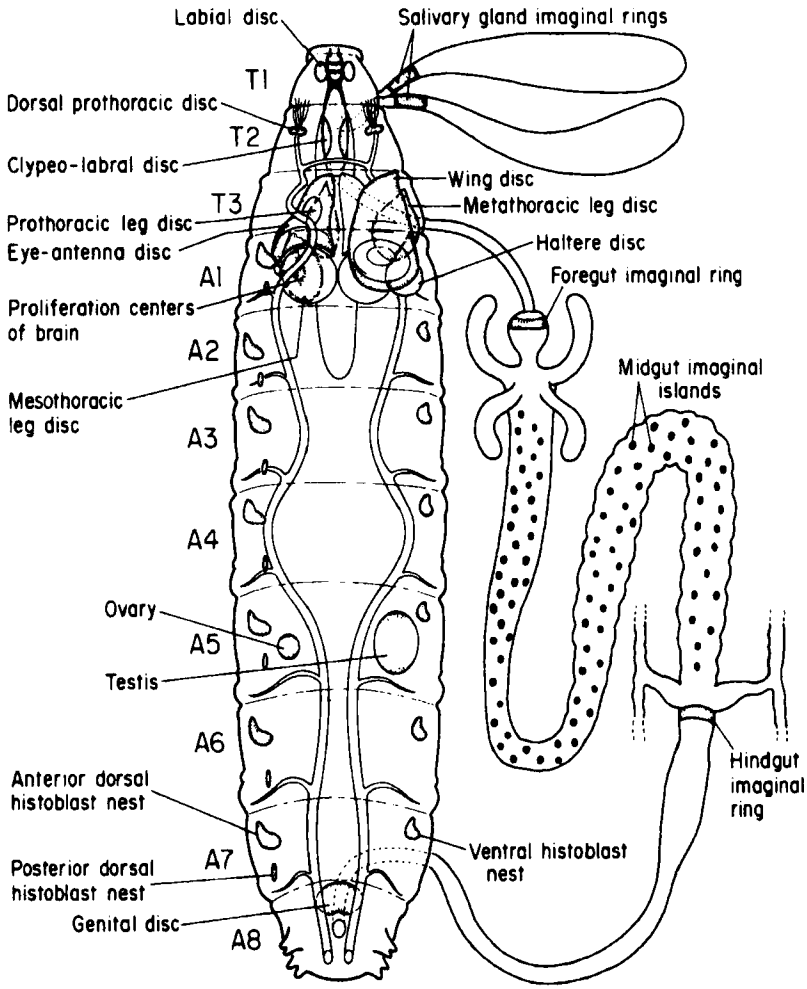

Fig. 5 Imaginal discs, salivary glands, and gut of a third-instar (L3) larva (reproduced with permission from Bryant and Levinson, 1985).

of fat body located about two-thirds of the way along the larvae; the ovaries are much smaller than the testes (Fig. 5). The meiotic divisions can be cytologically examined in larval testes, which have particularly large and elaborate spindles.

B. Orcein Staining of Neuroblast Squashes

Traditionally, neuroblasts and the polytene chromosomes of salivary glands have been examined after orcein staining. While this is not state-of-the-art technology, the stained chromosome are visible using bright field optics, allowing

direct examination of chromatin organization relative to other cellular structures. This can be an advantage when examining some mutations. However, this technique may not reveal subtle defects in chromosome structure.

1. Procedure

1. Remove brain as detailed previously and fix in a drop of 45% acetic acid for 15–20 sec.

2. Transfer brain to a drop of 4% orcein (Gurr's synthetic) in 45% acetic acid in the top of a plastic petri dish and stain for 5 min. Use the bottom of the petri dish as a cover to prevent evaporation.

3. Wash brains in a drop of 60% acetic acid for about 15 sec (until the tissue becomes slightly pink).

4. Place a small drop (5 μl) of 4% orcein in 45% acetic acid on a clean coverslip. Put the brain in this drop, and then place a clean slide on top and pick up the coverslip.

5. Place a folded Kim-Wipe over the cover slip and squash for 5 sec.

6. After a few minutes, the stained tissue is ready for examination.

2. Comments

1. Before preparing the stain, the orcein needs to be refluxed in the acetic acid for 30 min, cooled, and then filtered (Ashburner, 1989). Note that orcein can be quite variable from batch to batch.

2. Orcein-stained slides cannot be saved unless the coverslips are frozen off (see Section V,C) and the sample is dehydrated in 95% ethanol and mounted in Euparal (Ashburner, 1989). Glycerol or Mowiol mounting cannot be used because the dye is soluble in these solutions.

C. DAPI Staining of Neuroblast Squashes

In order to detect subtle changes in chromosome structure, DAPI staining of neuroblast squashes is advised. In our hands, one mutation that was initially characterized as giving rise to fragmented chromosomes by orcein staining actually showed thin strands of chromatin interconnecting more condensed regions by DAPI staining and fluorescence microscopy. In other words, the "signal to noise" ratio is higher with DAPI staining, and this can be advantageous if a mutation has subtle effects on chromatin.

1. Procedure

1. Remove brains (one to four) as detailed previously and transfer each brain to a separate 5-μl drop of 45% acetic acid and then transfer to second drop.

Start timing the fixation from transfer to the first drop, and incubate for 3 min total. The 5-μl drops should be on an ethanol-washed and siliconized coverslip (one brain/drop), which should be on top of a folded Kim-Wipe.

2. When the 3-min fix is finished, place a polylysine-treated slide on top of coverslip and squash gently for about 5 min, letting some of the excess acetic acid blot away on the Kim-Wipe. Using alcohol-proof black lab marker, encircle the barely visible squashed brains. This will help you keep track of the tissue during subsequent steps.

3. Freeze the slides by (i) dipping in liquid nitrogen and waiting until the bubbling stops, (ii) placing on a block of dry ice for 10 min with the coverslip facing up, or (iii) storing at −80°C for at least 10 min.

4. Breathe on the coverslip to quickly warm, and remove the coverslip using a razor blade. To wash off acetic acid, immerse the slide immediately in a Coplin jar filled with PBS.

5. Stain for 5–10 min by transferring to PBST containing 0.1 μg/ml DAPI.

6. To remove excess DAPI, dip the slide a few times in a third Coplin jar containing PBST.

7. To mount, put 25 μl Mowiol 4–88 (Calbiochem; prepared as described later) in PBS on a coverslip, invert the slide (drained but not dry), and place the area with the brains on the coverslip. The location of the brains should be obvious from the marker. The Mowiol will harden in 5–10 min. The squashes are now ready to examine.

2. Comments

1. DAPI staining may fail if the acetic acid fix is not completely rinsed from the slide.

2. DAPI-stained preparations can be stored for months in a cardboard slide folder, preferably kept at 4°C and protected from light.

3. To help visualize chromosome arms, a cytogeneticist's trick is to hypotonically swell the brains in 0.5% sodium citrate for 5–10 min prior to squashing. This has the effect of separating the mitotic chromosome arms but not the centromeres (unless allowed to proceed for too long). This may make it easier to detect abnormalities in chromosome condensation or integrity. However, interphase nuclear morphology is disrupted by this technique; the nucleus becomes very homogeneous in appearance and does not show a characteristic DAPI-bright heterochromatic spot (observed without hypotonic swelling). Hypotonic swelling also disrupts anaphase figures, so nonhypotonically treated controls should always be done.

4. For the preparation of Mowiol:

   1. Mix the following in a 15-ml round-bottom tube:

      1 g analytical-grade glycerol

0.4 g Mowiol

1 ml H_2O

2. Incubate at room temperature for a few hours.

3. Add an equal volume of 2× PBS (2 ml) and incubate overnight at 50°C with intermittent mixing.

4. Spin at 5000*g* 10 min and aliquot (250 μl/tube) into glass tubes. Store at −20°C.

D. Immunofluorescence in Whole Mounts of Larval Brains

The very characteristic patterns of cell division and growth of the larval brain are particularly useful for analyzing mitotic mutants (Truman and Bate, 1988). Areas that should have particular proliferation patterns can be identified in whole mount preparations at low magnification, whereas high-magnification analyses reveal considerable subcellular detail with respect to mitotic chromosome arrangement and spindle organization. For the best high-magnification images, however, confocal or deconvolution microscopy may be necessary. Unless the confocal is equipped with a UV laser, the chromatin will have to be stained with propidium iodide or Oli-green.

1. Procedure

1. Dissect larval brains in PBS.

2. Incubate in PBS + 4% formaldehyde (diluted from an ampoule of 16% stock) for 15–20 min (you can process a number of brains at a time, but put them straight into the fix as they are dissected).

3. Rinse twice in PBS.

4. Block in PBS + 10% normal goat serum for 60 min.

5. Permeabilize 3 × 15 min in PBST.

6. Incubate overnight at 4°C in PBST containing the appropriate dilution of primary antibody. If you are going to use propidium iodide to stain the DNA, add RNase A to 100 μg/ml.

7. Wash 3 × 15 min in PBST. If you are going to stain the chromatin with DAPI, include it at 0.1 μg/ml in the second wash.

8. Block by incubating in PBS with 10% normal goat serum.

9. Incubate for 60 min in PBST containing the appropriate dilutions of secondary antibodies.

10. Wash 3 × 15 min in PBS. (If using a tertiary streptavidin or avidin conjugate, repeat steps 7–9.) The middle wash should contain 1 μg/ml propidium iodide (not necessary if you are staining with DAPI).

11. Put the brains in a drop of 90% glycerol in PBS on a coverslip (2.5% propylgallate or 1 mg/ml paraphenylenediamine as an antifade agent can be used).

12. Mount by placing a glass slide on top of the coverslip, turning over the slide, and sealing the coverslip in place with nail polish.

2. Comments

Some investigators report including 2 μM taxol in a 5-min prefix incubation to stabilize microtubules. However, as described previously, this should be carefully monitored because taxol may induce abnormal microtubule assembly.

E. Immunofluorescence in "Semisquashed" Preparations

In the absence of a confocal microscope, it is possible to get good micrographs of subcellular structures in semisquashed preparations, which preserve quite a bit of tissue organization while facilitating penetration of light by mechanically flattening of the sample. This protocol has been successfully used to examine centrosomes and mitotic spindles in KLP61F mutant larvae (Heck *et al.*, 1993). In this protocol, rather than adding taxol to stabilize microtubules, a microtubule-stabilizing buffer is used.

1. Procedure

1. Wash wandering third-instar larvae in EBR and pull apart as for usual brain squashes.

2. Dissect brain/discs from rest of tissue in PHEM (60 mM Pipes, 25 mM Hepes, 10 mM EGTA and 2 mM $MgCl_2$).

3. Place 20-μl drops of PHEM + 4% paraformaldehyde (diluted from an ampoule of 16% stock) on a square sheet of parafilm.

4. Transfer one brain to one drop and invert concanavalin A-treated coverslip onto brains. Tap gently with the back end of your forceps and leave in the fix for 6 min.

5. Peel off parafilm and place coverslip in one well of 6-well dish containing 4 ml PBSB (PBS + 0.1% BSA).

6. When all coverslips are done, replace the solution with 3 ml PBSBT (PBS + 0.1% BSA + 0.1% Triton X-100) for 5 min.

7. Permeabilize for another 5 min in second rinse of PBSBT, then rinse once with PBSB.

8. Remove PBSB by aspiration and add primary antibody diluted in same buffer (60 μl). Incubate for 30 min at 37°C. Put moistened paper towel on the inside of the 6-well dish lid to prevent evaporation.

9. Wash 3 × 5 min in PBSB.

10. Add secondary antibody (biotinylated or fluorescent conjugate) in PBSB and incubate for 30 min at 37°C.

11. Wash 3 × 5 min in PBSB.

12. If needed, add tertiary reagent (e.g., streptavidin: Texas red) and incubate for 30 min at 37°C.

13. Wash 4 × 5 min in PBSB. The second of these washes should contain DAPI at 0.5 μg/ml.

14. Clean the back side of the coverslip using a cotton swab and water. Blot dry with Kim-Wipe. Put 20 μl mountant with antifade (e.g., Slowfade from Molecular Probes) on the sample and place a cleaned microscope slide on top of the coverslip. Invert and seal the coverslip in place with nail polish.

2. Comments

Platero *et al.* (1998) reported the successful localization of chromosomal proteins on acetic acid/formaldehyde neuroblast squashes. However, in our hands, the success of this protocol is quite antigen dependent because we have observed mislocalization of a nuclear component to the cytoplasm and poor labeling of the nuclear lamins (usually a "positive" control).

F. *In Vitro* Drug Treatments of Neuroblasts

For some applications, it is useful to arrest the cell cycle at specific phases prior to sample fixation. This can be achieved by treating isolated brains with various inhibitors in culture prior to analysis. To promote oxygen exchange (and avoid anoxia) during these treatments, it is important to use a relatively small volume of culture solution. In addition, appropriate drug carrier controls should always be done with the drug treatments because day-to-day variations in the response of neuroblasts to the treatment are not uncommon.

1. Procedure

1. Wash larvae and dissect brains in Schneider's medium (Sigma Chemical Co.).

2. Place dissected brains into 50- to 100-μl drops of Schneider's medium (with and without drug) and incubate for 2 hr.

3. (Optional) Hypotonically swell the brains in 0.5% sodium citrate for 5–10 min.

4. Fix and process for immunofluorescence as described in Sections V,D and V,E.

2. Comments

1. For mitotic arrest, colchicine works quite well at concentrations of 1 μg/ml in Schneider's medium (diluted from a stock solution at 100 μg/ml). Though

colcemid is less toxic than colchicine to most animal cells, it does not work as well as colchicine to achieve mitotic arrest in *Drosophila.*

2. For S-phase arrest, hydroxyurea can be used at 10 μg/ml (stock solution at 1 mg/ml).

3. To cytologically detect cells undergoing S phase, 5-bromo-deoxyuridine (BrdU) can be included in the culture medium at 10 μg/ml (Ashburner, 1989). Incorporated BrdU can only be detected if the DNA is first nicked with 2N HCl for 30 min.

G. *In Vivo* Drug Treatments of Neuroblasts

Drug treatments can also be done *in vivo* by feeding larvae instant fly food (Sigma Chemical Co.) supplemented with the appropriate agent. Food coloring is also added to help distinguish larvae that have ingested the food and drug mixture. To save on potentially expensive inhibitors, a small amount of food can be made and the feedings can be done in small weigh boats or multiwell plates. However, the larvae have to be watched or they may crawl away.

1. Procedure

1. Wash larvae in Schneider's medium.

2. Place larvae in the instant fly food containing food coloring with and without drug. Let the larvae feed for 2 or 3 hr.

3. Dissect brains from larvae with colored guts and proceed with cytological analyses as discussed previously.

2. Comments

For *in vivo* treatment of larval tissues, the concentrations of drugs must be increased 10-fold over that used for *in vitro* treatment. Stocks of hydroxyurea (1 mg/ml) or colchicine (100 μg/ml) can be diluted with the water to make up the food. Since the BrdU must be prepared fresh, 100 mg BrdU/g of powdered food should be added when preparing the instant food.

References

Ashburner, M. (1989). "*Drosophila:* A Laboratory Manual." Cold Spring Harbor Laboratory Press, Cold Spring Harbor, NY.

Baker, J., Theurkauf, W. E., and Schubiger, G. (1993). Dynamic changes in microtubule configuration correlate with nuclear migration in the preblastoderm *Drosophila* embryo. *J. Cell. Biol.* **122,** 113–121.

Bier, E., Vaessin, H., Shepherd, S., Lee, K., McCall, S., Barbel, S., Ackerman, L., Carretto, R., Uemura, T., Grell, E., Jan, L. Y., and Jan, Y. N. (1989). Searching for pattern and mutation in the *Drosophila* genome with a P-lacZ vector. *Genes Dev.* **3,** 1273–1287.

Bryant, P. J., and Levinson, P. (1985). Intrinsic growth control in the imaginal primordia of *Drosophila,* and the autonomous actions of a lethal mutation causing overgrowth. *Dev. Biol.* **107,** 355–363.

Cenci, G., Rawson R. B., Belloni, G., Castrillon, D. H., Tudor, M., Petrucci, R., Goldberg, M. L., Wasserman, S. A., and Gatti, M. (1997). UbcD1, a *Drosophila* ubiquitin-conjugating enzyme required for proper telomere behavior. *Genes Dev.* **11,** 863–875.

Chou, T. B., and Perrimon, N. (1996). The autosomal FLP-DFS technique for generating germline mosaics in *Drosophila melanogaster. Genetics* **144,** 1673–1679.

Cooley, L., Kelley, R., and Spradling, A. (1988). Insertional mutagenesis of the *Drosophila* genome with single P elements. *Science* **239,** 1121–1129.

Cooper, J. A. (1987). Effects of cytochalasin and phalloidin on actin. *J. Cell Biol.* **105,** 1473–1478.

Edgar, B. (1995). Diversification of cell cycle controls in developing embryos. *Curr. Opin. Cell Biol.* **7,** 815–824.

Foe, V. E., and Alberts, B. M. (1983). Studies of nuclear and cytoplasmic behavior during the five mitotic cycles that precede gastrulation in *Drosophila* embryogenesis. *J. Cell Sci.* **61,** 31–70.

Foe, V. E., Odell, G., and Edgar, B. A. (1993). Mitosis and morphogenesis in the *Drosophila* embryo: Point and counterpoint. *In* "The Development of *Drosophila melanogaster*" (M. Bate and A. Martinez Arias, eds.). Cold Spring Harbor Laboratory Press, Cold Spring Harbor, NY.

Gatti, M., and Baker, B. (1989). Genes controlling essential cell-cycle functions in Drosophila melanogaster. *Genes Dev.* **3,** 438–453.

Gatti, M., and Goldberg, M., L. (1991). Mutations affecting cell division in *Drosophila. Methods Cell Biol.* **35,** 543–586.

Glover, D. M., Leibowitz, M. H., McLean, D. A., and Parry, H. (1995). Mutations in *aurora* prevent centrosome separation leading to the formation of monopolar spindles. *Cell* **81,** 95–105.

Gonzalez, C., Saunders, R. D., Casal, J., Molina, I., Carmena, M., Ripoll, P., and Glover, D. M. (1990). Mutations at the asp locus of *Drosophila* lead to multiple free centrosomes in syncytial embryos, but restrict centrosome duplication in larval neuroblasts *J. Cell Sci.* **96,** 605–616.

Greenspan, R. J. (1997). "Fly Pushing." Cold Spring Harbor Laboratory Press, Cold Spring Harbor, NY.

Hamilton, B. A., and Zinn, K. (1994). From clone to mutant gene. *Methods Cell Biol.* **44,** 81–98.

Heck, M. M. S., Pereira, A., Pesavento, P., Yannoni, Y., Spradling, A. C., and Goldstein, L. S. B. (1993). The kinesin-like protein KLP61F is essential for mitosis in Drosophila. *J. Cell Biol.* **123,** 665–679.

Karr, T. L., and Alberts, B. M. (1986). Organization of the cytoskeleton in early *Drosophila* embryos. *J. Cell Biol.* **102,** 1494–1509.

Kellogg, D. R., Mitchison, T. J., and Alberts, B. M. (1988). Behavior of microtubules and actin filaments in living *Drosophila* embryos. *Development* **103,** 675–686.

Lindsley, D. L., and Zimm, G. G. (1992). "The Genome of *Drosophila melanogaster.*" Academic Press, New York.

Llamazares, S., Moreira, A., Tavares, A., Girdham, C., Spruce, B. A., Gonzalez, C., Karess, R. E., Glover, D. M., and Sunkel, C. E. (1991) *polo* encodes a protein kinase homolog required for mitosis in *Drosophila. Genes Dev.* **5,** 2153–2165.

Matthews, K. A., Rees, D., and Kaufman, T. C. (1993). A functionally specialized alpha-tubulin is required for oocyte meiosis and cleavage mitoses in Drosophila. *Development* **117,** 977–991.

Matthies, H., McDonald, H., Goldstein, L. S. B., and Theurkauf, W. E. (1996). Meiotic spindle morphogenesis in living *Drosophila* oocytes: Role of the ncd kinesin-like protein. *J. Cell Biol.* **134,** 455–464.

Merrill, P. T., Sweeton, D., and Wieschaus, E. (1988). Requirements for autosomal gene activity during precellular stages of Drosophila melanogaster. *Development* **104,** 495–509.

Minden, J. S., Agard, D. A., Sedat, J. W., and Alberts, B. M. (1989). Direct cell lineage analysis in *Drosophila melanogaster* by time lapse three dimensional optical microscopy of living embryos. *J. Cell Biol.* **109,** 505–516.

Mitchison, T. J., and Sedat, J. W. (1983). Localization of antigenic determinants in whole *Drosophila* embryos. *Dev. Biol.* **99,** 261–264.

Orr-Weaver, T. L. (1994). Developmental modification of the Drosophila cell cycle. *Trends Genet.* **10,** 321–327.

Platero, S. J., Csink, A. K., Quintanilla, A., and Henikoff, S. (1998). Changes in chromosomal localization of heterochromatin-binding proteins during the cell cycle in Drosophila. *J. Cell Biol.* **140,** 1297–1306.

Saunders, R. D., Avides, M. C., Howard, T., Gonzalez, C., and Glover, D. M. (1997). The Drosophila gene abnormal spindle encodes a novel microtubule-associated protein that associates with the polar regions of the mitotic spindle. *J. Cell Biol.* **137,** 881–890.

Schubiger, G., and Edgar, B. (1994). Using inhibitors to study embryogenesis. *Methods Cell Biol.* **44,** 697–713.

Spradling, A. C. (1993). Developmental genetics of oogenesis. *In* "The Development of *Drosophila melanogaster*" (M. Bate and A. Martinez Arias, eds.). Cold Spring Harbor Laboratory Press, Cold Spring Harbor, NY.

St. Johnston, D., and Nüsslein-Volhard, C. (1992). The origin of pattern and polarity in the *Drosophila* embryo. *Cell* **68,** 201–219.

Sullivan, W., and Theurkauf, W. E. (1995). The cytoskeleton and morphogenesis of the early *Drosophila* embryo. *Curr. Opin. Cell Biol.* **7,** 18–22.

Sullivan, W., Fogarty, P., and Theurkauf, W. (1993). Mutations affecting the cytoskeletal organization of syncytial *Drosophila* embryos. *Development* **118,** 1245–1254.

Theurkauf, W. (1992). Behavior of structurally divergent alpha-tubulin isotypes during *Drosophila* embryogenesis: Evidence for post-translational regulation of isotype abundance. *Dev. Biol.* **154,** 204–217.

Theurkauf, W. E. (1994). Immunofluorescence analysis of the cytoskeleton during oogenesis and embryogenesis. *Methods Cell Biol.* **44,** 489–505.

Theurkauf, W. E., Alberts, B. M., Jan, Y. N., and Jongens, T. A. (1993). A central role for microtubules in the differentiation of Drosophila oocytes. *Development* **118,** 1169–1180.

Truman, J. W., and Bate, M. (1988). Spatial and temporal patterns of neurogenesis in the central nervous system of *Drosophila melanogaster. Dev. Biol.* **125,** 145–157.

Wieschaus, E., and Sweeton, D. (1988). Requirements for X-linked zygotic activity during cellularization of early Drosophila embryos. *Development* **104,** 483–493.

Wolfner, M. F., and Goldberg, M. L. (1994). Harnessing the power of *Drosophila* genetics. *Methods Cell Biol.* **44,** 34–80.

CHAPTER 18

Methods for Isolating and Analyzing Mitotic Mutants in *Aspergillus nidulans*

Berl R. Oakley

Department of Molecular Genetics
Ohio State University
Columbus, Ohio 43210

METHODS IN CELL BIOLOGY, VOL. 61

0091-679X/99 $30.00

I. Introduction

Mitosis is one of the most important, fascinating, and perplexing process in nature. Although much remains unknown, the past decade has seen great progress in our understanding of mitosis. Much of this progress has been made through the use of mutants that affect mitosis and much of the most important work with mitotic mutants has been carried out in the filamentous fungus *Aspergillus nidulans.* Indeed, a small fraction of the findings made with this organism include the discovery that a kinesin-like protein is essential for mitosis (Enos and Morris, 1990), that a phosphatase is essential for the completion of mitosis (Doonan and Morris, 1989), the discovery of a mitotic regulator that now seems to be ubiquitous in eukaryotes (Engle *et al.,* 1990), and the discovery of γ-tubulin (Oakley and Oakley, 1989). The findings made with *A. nidulans* are particularly impressive when one considers that a relatively small number of labs are using this organism to study mitosis and the cell cycle. Clearly, *A. nidulans* is a particularly good organism for studying mitosis.

Many methods come into play in isolating and studying mitotic mutants in *A. nidulans* and I will not be able to discuss them all in detail. Rather, I will try to give an overview of how mitotic mutants can be isolated and studied in this organism. I will discuss some methods in detail but, in areas in which good methodological reviews exist, I will discuss the methods briefly and refer readers to those reviews.

II. Characteristics of *Aspergillus nidulans*

Aspergillus nidulans is a filamentous ascomycete fungus. It grows well over a wide range of temperatures from below 20°C to about 43°C and this facilitates searches for temperature-sensitive mutations. At its optimum growth temperature of 37°C, its doubling time is only about 75 min (Bergen and Morris, 1983). This allows tests of growth rates to be carried out quickly, and it facilitates the rapid production of large quantities of hyphae for biochemical studies.

Aspergillus nidulans is very amenable to classic genetic studies. Since it is normally haploid, mutations can be isolated easily, and stable diploids can be constructed for complementation tests and mapping mutations to linkage groups. Both meiotic and mitotic mapping are relatively easy in *A. nidulans,* and it has one of the largest and most complete genetic maps. It has eight genetic linkage groups or chromosomes and a relatively small genome (about 2.6×10^7 base pairs) (Timberlake, 1978). It also has a very good molecular genetic system. It is possible to transform *A. nidulans,* to clone genes by complementation, to disrupt genes, and to replace genes. A number of vectors with selectable markers are available, as are good genomic, cDNA, and other libraries, and there is an *A. nidulans* genome project which promises to further facilitate molecular genetic

studies. In addition, cloned promoters are available which allow one to regulate the expression of cloned genes.

A. The *A. nidulans* Life Cycle

To understand how mutations are generated and studied in *A. nidulans,* it is important to understand the life cycle and cell cycle of this organism. *Aspergillus nidulans* can reproduce both asexually (vegetatively) and sexually. A diagram of its life cycle is shown in Fig. 1. Vegetative reproduction occurs through asexual spores called conidospores or conidia. Conidia are quite small (3–3.5 μm) in size and each contains a single nucleus. On appropriate solid media or in appropriate liquid media, conidia swell and germinate, sending out germ tubes which eventually lengthen to form hyphae. The time required for germination depends on strain, medium, temperature, and the age of the conidia but will generally be 4 or 5 hr for a healthy strain at 37°C.

At about the time of germination the single nucleus divides. Additional rounds of division occur without cell division, which in *A. nidulans* involves the formation of a septum. Within a single cell, or hyphal segment, mitosis is more or less synchronous although there may be small differences in mitotic stage from one end of a hyphal segment to the other. After the third or fourth nuclear divisions (8 or 16 nuclei) the first septum forms (Harris *et al.,* 1994) and additional septations occur with subsequent divisions. Growth is primarily at the hyphal tip

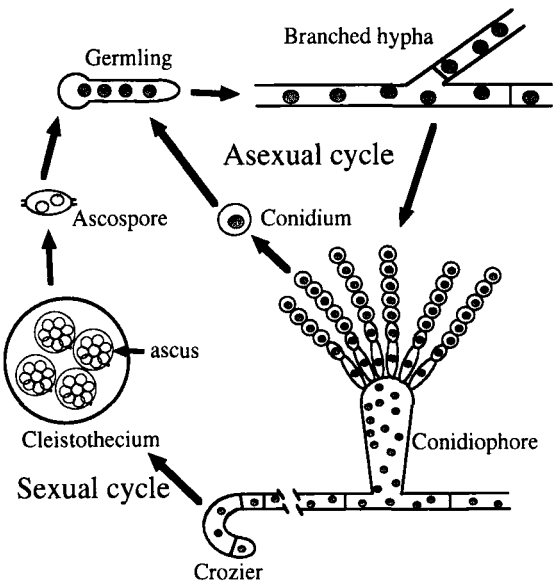

Fig. 1 The life cycle of *Aspergillus nidulans.*

and, as growth continues, hyphal branching occurs and an intertwined mass of hyphae eventually forms.

Aspergillus nidulans does not normally undergo sexual or asexual reproduction in liquid culture, but on solid media both types of reproduction occur. In the asexual cycle, multicellular structures called conidiophores develop after less than 2 days of growth at 37°C and produce long chains of conidia. The sexual cycle involves the formation of complex structures called cleistothecia or perithecia. These contain specialized hyphal tips called croziers. As reported by Elliot (1960), croziers consist of a uninucleate tip cell, a binucleate penultimate cell, and a uninucleate basal cell. The two nuclei in the penultimate cell fuse to form a zygote, and the zygote immediately undergoes meiosis and two mitotic divisions to form eight binucleate ascospores, positioned randomly in an ascus derived from the penultimate cell. As many as 100,000 asci may eventually form within a single cleistothecium. The ascus walls generally break, however, releasing spores into the lumen of the cleistothecium. Ascospores are discoidal, 3.5–4 μm in diameter, and have two distinctive raised rings around them. They germinate in appropriate media and form germ tubes and hyphae.

B. The Cell Cycle of *A. nidulans*

The cell cycle of *A. nidulans* is similar to that of higher organisms. There are discrete G_1, S, G_2, and M phases and at 37°C G_1 requires approximately 15 min, S requires 25 min, G_2 requires 30 min, and mitosis requires 5 min or slightly less (Bergen and Morris, 1983). Cytoplasmic microtubules are present in interphase and, as judged by immunofluorescence microscopy, these disassemble at the onset of mitosis (Fig. 2; Osmani *et al.*, 1988; Oakley *et al.*, 1990; Martin *et al.*, 1997). Microtubules are absent from the nucleus in interphase and the mitotic spindle assembles at the onset of mitosis from spindle pole bodies (SPBs), a type of microtubule-organizing center (Fig. 3) (Oakley and Morris, 1981, 1983; Osmani

---

Fig. 2 Microtubules in interphase and mitotic hyphae. (a) Phase-contrast micrograph of a field containing two hyphae. (b) Immunofluorescence micrograph of the same field. Microtubules have been stained with an anti-α-tubulin antibody and are visible as thin lines. Portions of the microtubules are out of the plane of focus making the microtubules look discontinuous. (c–e) A mitotic hypha. (c) Phase-contrast micrograph. (d) Immunofluorescence micrograph in which mitotic spindles (arrows) have been stained with an anti-α-tubulin antibody. The cytoplasmic microtubule network has disassembled but a few regrowing cytoplasmic microtubules are visible at the upper ends of both spindles and at the bottom of the spindle at the left. (e) Chromatin stained with DAPI. The nucleus at the left (arrowhead) is in anaphase. The chromosomes have moved to the poles of the spindle but the spindle will elongate additionally before mitosis is complete. The nucleus at the right is in a slightly earlier stage. Chromosomes are condensed and arranged along the length of the spindle. Since no metaphase plate is formed in *A. nidulans*, it is not possible to know whether anaphase has begun in this nucleus. Faintly staining mitochondrial genomes are visible between the two nuclei. Scale bar = 10 μm. (reproduced with permission from Oakley *et al.*, 1990; copyright the Cell Press).

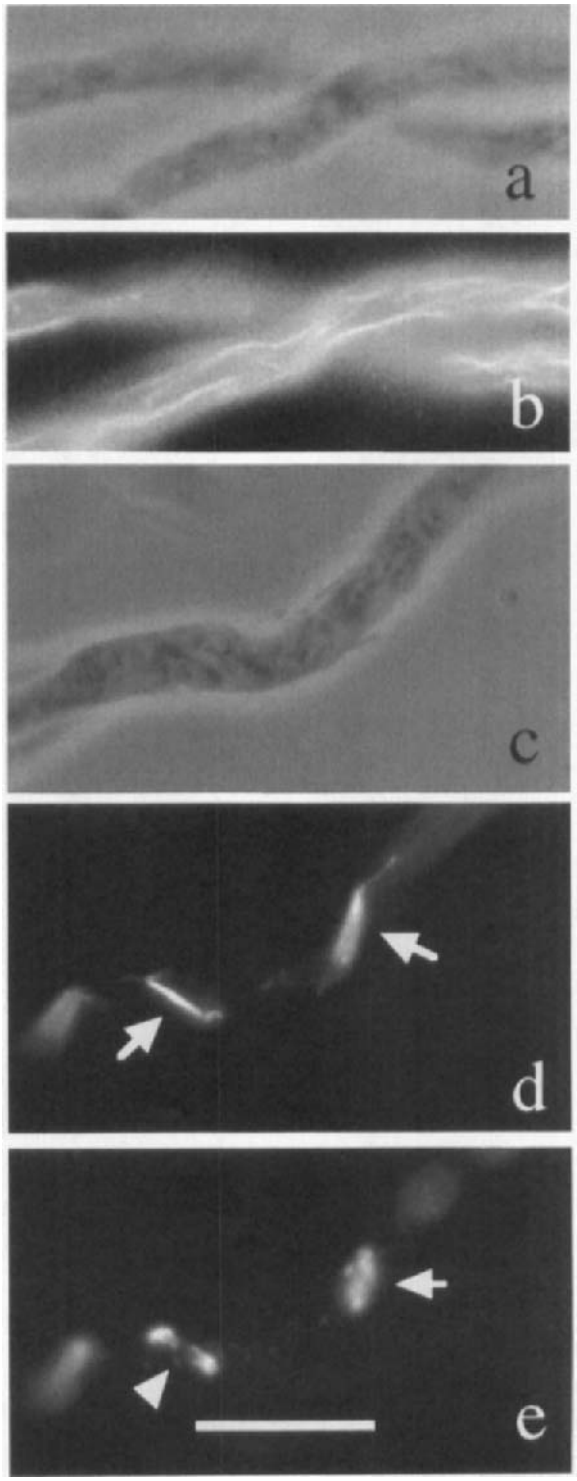
a
b
c
d
e

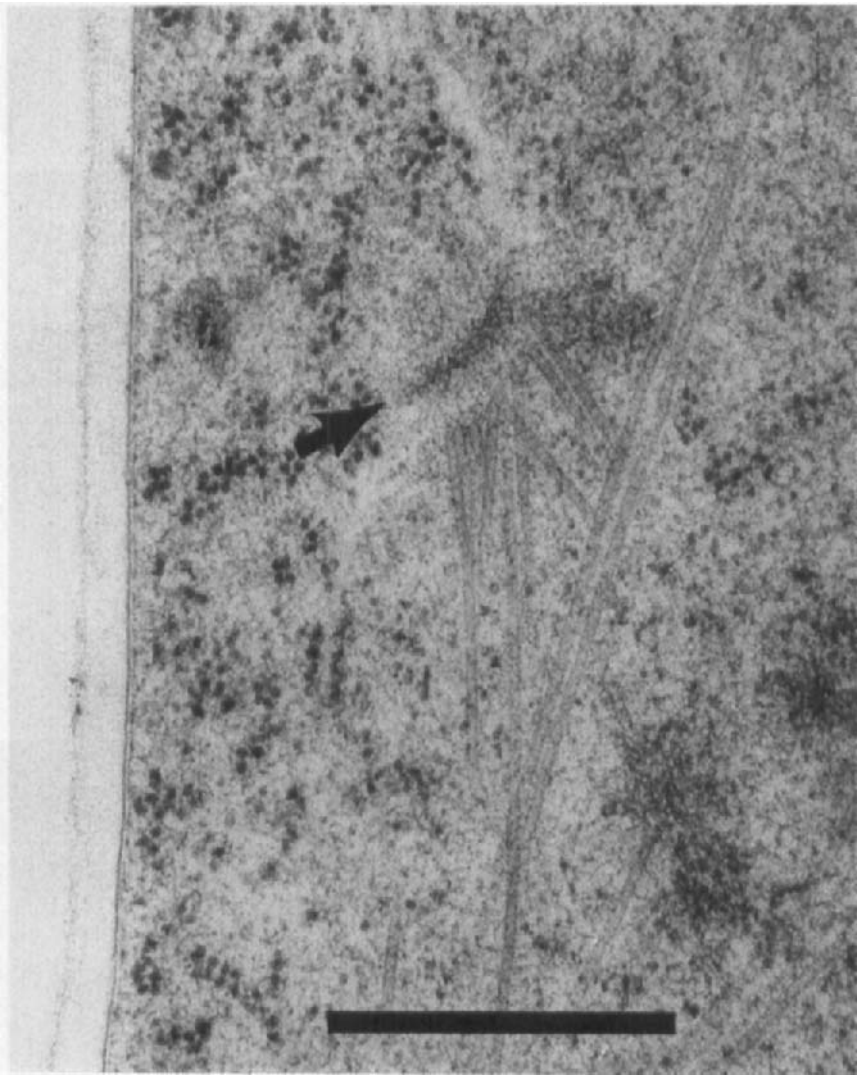

Fig. 3 An electron micrograph of a portion of a mitotic spindle of *A. nidulans* prepared by freeze substitution. The nuclear membrane is lost in freeze substitution but the spindle pole body is visible (arrow) as are microtubules and darkly staining fibrous chromatin. Scale bar = 0.5 μm (micrograph courtesy of Dr. I. Brent Heath and Dr. Gregory S. May).

et al., 1988; Oakley *et al.*, 1990; Martin *et al.*, 1997). The mitotic apparatus contains 35–50 microtubules, and this number decreases as the spindle elongates in the late stages of anaphase (Oakley and Morris, 1981, 1983, unpublished observations). Cytoplasmic microtubules begin to reassemble in the latter stages of mitosis (Osmani *et al.*, 1988; Oakley *et al.*, 1990) and can be seen extending into the

cytoplasm from the region of the spindle pole body (Fig. 2). *Aspergillus nidulans* is thus similar to higher organisms in that the cytoplasmic microtubule network disassembles as cells enter mitosis and the mitotic spindle is present only in mitosis. This is in contrast to some other fungi in which mitotic microtubules begin to assemble in the nucleus in G_1 [e.g., the budding yeast *Saccharomyces cerevisiae* (Byers and Goetsch, 1975)]. Also as in higher organisms, chromosomal condensation is evident in mitosis (Robinow and Caten, 1969) and interphase and mitotic nuclei are clearly distinguishable by a number of DNA or chromatin staining methods (Fig. 4; see Section VII,A,1).

III. Strains and Media

The Fungal Genetics Stock Center (FGSC, Department of Microbiology, University of Kansas Medical Center) is a wonderful resource for anyone working

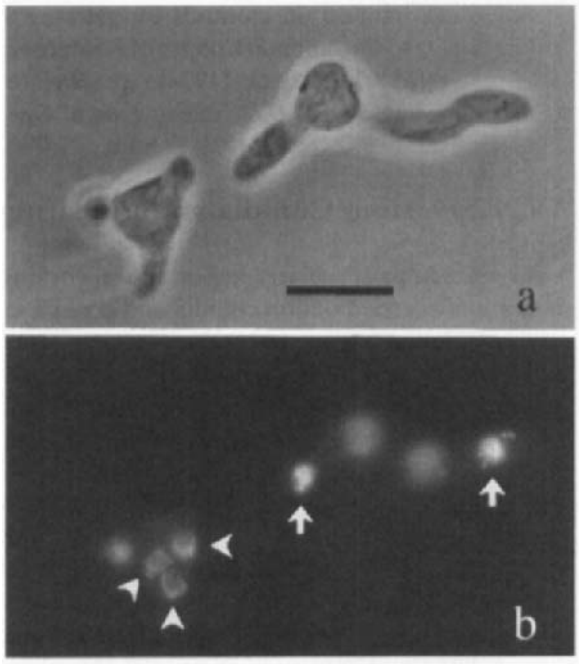

Fig. 4 Interphase and mitotic chromatin of *A. nidulans*. (a) A phase-contrast micrograph of a field containing two germlings. Much of the germling at the left is out of the plane of focus. (b) A fluorescence micrograph of the same field. DNA has been stained with DAPI. The nuclei in the germling at the left (arrowheads) are in interphase. Chromatin is smooth and a faintly staining region in the nuclei corresponding to the nucleolus is visible. Nuclei in the germling at the right are in mitosis. Two nuclei are in the plane of focus (arrows). The chromatin has condensed giving a characteristic lumpy appearance and nucleoli are no longer apparent. Scale bar = 10 μm.

with *A. nidulans.* The FGSC maintains and makes available hundreds of strains of *A. nidulans* as well as libraries, cloned genes, and bibliographic references.

Aspergillus nidulans grows well on simple media. YG medium (5 g/liter yeast extract and 20 g/liter *d*-glucose) is a good complete medium for most strains. A few nutritional mutations are not fully supplemented by yeast extract and in these cases additional nutrients must be added. YAG (YG medium plus 15 g/liter agar) is a good solid complete medium for most strains, although some strains grow and/or form conidia better on MAG medium (20 g/liter malt extract, 1 g/liter peptone, 20 g/liter *d*-glucose, and 15 g/liter agar). *Aspergillus nidulans* also grows well on simple defined media. Such media are important for testing nutritional markers and for selecting transformants when certain selectable markers are used. We generally use a minimal medium derived from that of Pontecorvo *et al.* (1953) [6 g/liter $NaNO_3$, 0.52 g/liter KCl, 0.52 g/liter $MgSO_4 \cdot 7H_2O$, 1.52 g/liter KH_2PO_4, 10 g/liter *d*-glucose, and 1 ml/liter of a trace metal solution (Cove, 1966), adjust pH to 6.5 with NaOH before autoclaving]. For a solid minimal medium, 15 g/liter of agar can be added. Appropriate nutrients must be added, of course, for growth of strains with nutritional markers. For more detailed information on methods for growing and working with *A. nidulans,* I refer readers to the landmark paper of Pontecorvo *et al.* (1953), to the comprehensive review of Clutterbuck (1974), to *Genetics and Physiology of Aspergillus* (Smith and Pateman, 1977), and to *Fungal Genetics* (Fincham *et al.,* 1979).

IV. Harvesting Conidia and Preparing Conidial Suspensions

Conidia are particularly important in working with *A. nidulans.* Mutagenesis is normally carried out on conidia and conidia are normally the starting material for most morphological or biochemical studies of *A. nidulans.* In addition, strains may be maintained for years at room temperature as conidial suspensions dried on silica gel (Ogata, 1962). To prepare a conidial suspension, conidia from a colony of the strain of interest can be harvested with a sterile, wetted loop and suspended in 1 ml of sterile distilled water or Tween–saline solution (0.1% Tween 80 and 0.85% NaCl). Two or three drops of this solution can be spread onto each of several plates of complete medium. After 3 or 4 days at 37°C or somewhat longer at other temperatures, the colonies should be covered with conidia. They can be harvested by adding 3- or 4-mm glass beads to each plate and shaking gently for a few seconds. Tween–saline solution (5–10 ml) can then be added to a standard 85-mm petri plate and the plate can be swirled gently and the conidial suspension removed with a sterile pipet. Alternatively, the surface of the colonies can be rubbed gently with a sterile, bent glass rod to dislodge conidia which can then be harvested in Tween–saline solution as previously described. With each approach, if care is taken to harvest the conidia gently, few hyphae or conidiophores will be present in the spore suspensions. If such structures are present, they can be removed by low-speed centrifugation of the suspension.

The concentration of conidia in the suspension can be determined with a hemacytometer and the suspension can be stored at 4°C. The conidia remain viable for weeks under these conditions but the synchrony of germination declines with time.

V. Mutagenesis

Mutagenesis is carried out on a conidial suspension from the parental strain. A number of mutagens can be used with *A. nidulans* (Clutterbuck, 1974). Two mutagens that have been used successfully to create mitotic and related mutations are ultraviolet light (Morris, 1976) and 4-nitroquinoline 1-oxide (Harris *et al.*, 1994). The extent of mutagenesis is always important and, as I will discuss subsequently, some types of genetic screens require higher levels of mutagenesis than others. A convenient indication of the extent of mutagenesis is the percentage of conidia that are killed by the process.

For ultraviolet mutagenesis, it is convenient to mutagenize a suspension of conidia in an open, gently shaking petri dish with a germicidal lamp. We have found it convenient to irradiate at an intensity of 200 $\mu W/cm^2$ and to take samples before mutagenesis and at 30-sec intervals during mutagenesis. Serial dilutions are made of the samples and the dilutions are plated on solid media. They are incubated to determine the number colonies that form and, thus, the number of conidia that have survived mutagenesis. A plot of the percentage of viable conidia with respect to time is called a kill curve and it allows one to determine the time of mutagenesis that gives the desired rate of conidial survival.

VI. Methods for Isolating Mitotic Mutants in *A. nidulans*

Three approaches have been used to isolate mitotic mutants in *A. nidulans:* (i) the isolation of randomly mutagenized temperature-sensitive mutants which are subsequently screened microscopically for mitotic blockage, (ii) the isolation of tubulin mutations that block microtubule function and mitosis by isolating antimicrotubule drug-resistant mutants and screening for temperature sensitivity, and (iii) the isolation of conditionally lethal revertants of existing mitotic or tubulin mutants. In addition, mutant alleles of cloned genes that are essential for mitosis can be created at will in *A. nidulans.*

A. Isolation of Conditionally Lethal Mutations and Screening for Mutations That Affect Mitosis

I use the term "conditionally lethal" to refer to all mutations that inhibit growth sufficiently to prevent colony formation under some conditions but allow growth under other conditions. The most commonly used conditionally lethal

mutations are temperature-sensitive (ts^-) mutations. These allow growth at some temperatures but not at other temperatures. Among ts^- mutations, those that allow growth at low temperatures but prevent growth at high temperatures are "heat-sensitive" (hs^-). Those that permit growth at high temperatures but prevent growth at low temperatures are "cold-sensitive" (cs^-). It should be noted that the term "temperature sensitive" is often used for mutations that I term heat sensitive, but I will reserve temperature sensitive as a general term for temperature-dependent, conditionally lethal mutations.

The rationale behind isolating mitotic mutants by screening temperature-sensitive mutants is as follows. Mutagenesis of conidia will, under the right conditions, result in the majority of mutagenized spores carrying one or more mutations. Many of these mutations will be silent, but others will have clear phenotypic effects. Some of the mutations will prevent an essential protein from functioning and conidia carrying such mutations will not grow large enough to form colonies. A fraction of the remaining conidia will carry mutations that alter proteins such that they function properly at some temperatures (permissive temperatures) but not at other temperatures (restrictive temperatures). When such mutations occur in essential genes, conidia will grow to form colonies at permissive temperatures but not at restrictive temperatures. If a temperature-sensitive mutation occurs in a gene that is essential for the successful completion of mitosis, mitosis will not occur normally at the restrictive temperature. Strains carrying mutations that affect mitosis can thus be identified by looking microscopically for mitotic blockage or other mitotic abnormalities at the restrictive temperature.

Morris' (1976) screen for temperature-sensitive mutants is a landmark in the study of mitosis and the cell cycle. He isolated approximately 1000 hs^- mutants and found among them 9 that were blocked in mitosis at restrictive temperatures, 26 that were blocked in interphase at restrictive temperatures, 5 in which nuclear movement was blocked at restrictive temperatures, and 5 in which septation was blocked. Among the many important findings that came from these mutants was the first demonstration that a member of the kinesin superfamily of proteins is essential for mitosis (Enos and Morris, 1990), the discovery of the *bimE* mitotic regulator (Engle *et al.*, 1990), the discovery of the *nimA* kinase that is involved in the G_2–M transition (Oakley and Morris, 1983; Osmani *et al.*, 1987), and the demonstration that the cytoplasmic dynein heavy chain is essential for nuclear movement but not mitosis (Xiang *et al.*, 1994). The breadth of these findings illustrates one of the great advantages of this approach: One not only obtains mutants that affect mitosis but also mutants that affect many other important cellular processes.

1. Isolation of Temperature-Sensitive Mutants

One must first choose a strain to mutagenize, a parental strain. An ideal parental strain should carry a conidial color marker mutation and one or two nutritional marker mutations. Such markers facilitate subsequent crosses and

analyses. A greater number of mutations may reduce the vigor of the strain or complicate subsequent analyses.

The extent of mutagenesis is important. If conidia are heavily mutagenized, it is relatively easy to find temperature-sensitive mutants, but many of the mutant strains will carry multiple mutations that make phenotypic and genetic analysis difficult. Lower mutagenesis levels result in fewer multiply mutant strains but temperature-sensitive strains will be a lower percentage of the colonies that form after mutagenesis. Past screens (Morris, 1976; Harris *et al.*, 1994) used mutagenesis levels in which 10–39% of conidia remain viable after mutagenesis.

Mutagenized spores are diluted and spread onto plates such that 100 colonies or fewer are present on each plate. The plates are then incubated at a temperature that one wishes to be the permissive temperature for the mutants. For example, if one were attempting to obtain hs^- mutants, one would incubate the plates at a low temperature (25–32°C). After sufficient time to allow colony formation and conidiation, colonies are tested for temperature sensitivity by replica plating. Strains that do not grow at the restrictive temperature but do grow at the permissive temperature are putative ts^- mutants. They are normally streaked to single colony to eliminate any possibility of two strains being present in the same colony. They are then retested for temperature sensitivity and analyzed for phenotype.

Replica plating of *A. nidulans* colonies is less convenient than for yeasts because the colonies are larger, hyphae do not transfer readily, and conidia, which do transfer readily, do not form until colonies have reached a size of 0.5–1 cm. If 0.8% sodium deoxycholate is added to the medium, colony growth is inhibited and conidiation occurs at smaller colony diameter (Mackintosh and Pritchard, 1963). It is then possible to replica plate with sterile felts or filter paper as is done for yeasts. It is often more convenient, however, to simply stab conidia onto two test plates using sterile toothpicks. The colonies are typically stabbed in a grid pattern which facilitates keeping track of the colonies and subsequent testing.

2. Microscopic Screens for Mitotic Mutants

Only a small fraction of randomly isolated ts^- mutants are likely to have mitotic defects. As a consequence, one must screen the mutant collection microscopically to identify those with mutations that affect mitosis. A rapid initial screen is to look for inhibition of nuclear division at a restrictive temperature. This can be done easily by germinating conidia from parental and mutant strains at a restrictive temperature for long enough to allow two or three rounds of nuclear division in the parent. The time of incubation will be a few hours and will vary with temperature of incubation. Such experiments are most conveniently carried out in small-volume (e.g., 1 ml) liquid cultures. The parent and mutants are then fixed and stained with a DNA-binding dye such as 4′, 6-diamidino-2-phenylindole (DAPI) or mithramycin (see Section VII,A,1) and examined by

fluorescence microscopy. If conidia have germinated but a single nucleus is present, the mutation must interfere with the nuclear division cycle at the restrictive temperature. Strains that simply do not germinate or that form germlings with normal numbers of nuclei are not likely to carry mutations that affect mitosis or the cell cycle.

Strains that appear to be promising after this initial screen may be screened further with temperature-shift experiments. In these experiments, conidia are germinated at a permissive temperature and then shifted to a restrictive temperature. Samples are taken just before the shift and at 30-min intervals after the shift. Samples are fixed and stained with DAPI or mithramycin and chromosome mitotic indices (CMIs) determined. The CMI is the percentage of germlings in which the nuclei have condensed chromatin. Ts^- mutations in genes required for mitosis should block or slow the progress of mitosis and will thus give an increase in the CMI over time relative to the parental strain. If mitotic checkpoints are overcome, the CMI may eventually drop, but there should be at least a significant transient increase. An important point in such screens is that shifts to high temperatures (>40°C) may result in heat shock which causes a transient reduction in mitotic index. The period of CMI reduction due to heat shock depends on the temperature and can be determined easily by measuring the CMI of the parental strain treated in the same way as the mutants (i.e., the parental control). The CMI in wild-type strains is normally about 5% at all temperatures but will decrease to zero during heat shock and rise to 5% again after the effects of the heat shock have passed. After the heat shock period, the CMI in mitotic mutants should increase to levels significantly greater than the 5% found in wild-type strains.

Ts^- mutants that show elevated mitotic indices when shifted to a restrictive temperature can be analyzed by immunofluorescence microscopy (see Section VII,A,2) with anti-tubulin antibodies to determine if the percentage of germlings with mitotic spindles [spindle mitotic index (SMI)] increases in concert with the CMI. Careful examination of mitotic spindles at this point may be particularly instructive in that it can reveal whether, at the restrictive temperature, mitosis is blocked at a single point (e.g., all mitotic nuclei have short spindles) and whether spindles demonstrate obvious abnormalities that would account for the mitotic blockage and, perhaps, provide a clue as to the function of the protein produced by the mutant gene.

Irrelevant mutations that occur during mutagenesis can be detected and eliminated by crossing the mutant strain to a wild-type strain. When more than two mutations are present, they should segregate from each other in crosses to a wild-type strain and the progeny of such a cross should have two phenotypes in addition to the wild type. The real mitotic mutant can be determined by examining each of the two classes of mutants for mitotic defects at restrictive temperatures. Methods for crossing *A. nidulans* strains have been summarized previously (Clutterbuck, 1974; Morris *et al.*, 1982).

B. Isolation of Mutations Resistant to Antimicrotubule Agents

Most antimicrotubule agents bind to β-tubulin and most mutations that confer resistance to such agents occur in β-tubulin genes. A fraction of the mutations that confer resistance to antimicrotubule agents also confer conditional lethality (Morris *et al.*, 1979; Oakley and Morris, 1981) and some of these mutations have proven to be very useful mitotic mutants (Oakley and Morris, 1981).

Mutations that confer resistance to an antimicrotubule agent can be selected easily. One can simply mutagenize conidia and plate them out onto solid medium containing a concentration of the antimicrotubule agent that prevents growth of wild-type conidia. Mutations that confer resistance to the antimicrotubule agent are rare, but they can be selected easily because only conidia carrying such mutations will be able to grow to form colonies on plates containing the antimicrotubule agent. Because there is generally a strong selection, it is not necessary to mutagenize as vigorously as when attempting to obtain random ts^- mutations. Mutagenizing less vigorously so that a greater percentage of conidia are alive after mutagenesis will reduce the chance of obtaining irrelevant conditionally lethal mutations. Mutagenesis such that 50% of the conidia survive should be more than sufficient. In addition, because the selection for mutants is strong, conidia can be plated out at high densities (e.g., 1×10^7 conidia per 85-mm petri dish).

Once selected, the antimicrotubule agent-resistant mutants can be screened for temperature sensitivity by replica plating at various temperatures. If ts^- mutants are found, they should be crossed to existing β-tubulin mutants to determine if the mutation that confers temperature sensitivity is indeed a β-tubulin mutation. If the mutation is in another gene, wild-type progeny will result from such a cross, but if the mutation is in the β-tubulin gene, wild-type progeny will be exceedingly rare (i.e., they would be due to intragenic recombination which would occur at a very low frequency). Since most antimicrotubule agents investigated to date bind to β-tubulin, logic (and previous results) indicates that β-tubulin mutations are likely to be the majority of antimicrotubule agent-resistance mutations. Mutations in other genes, however, would be particularly interesting because they might be located in novel genes required for microtubule function or they might be useful alleles of previously identified genes (α-tubulin or γ-tubulin?). Any interesting ts^- mutants obtained can be studied morphologically (see Section VII) to determine what effects the mutations have on mitosis.

If ts^- mutations are found, it is important to determine if the temperature sensitivity is caused by the mutation that causes drug resistance rather than a random, irrelevant mutation. This can be done by crossing the mutant to a wild-type strain. The presence of temperature-sensitive, drug-sensitive progeny from such a cross would indicate that temperature sensitivity is caused by a mutation irrelevant to drug resistance.

C. Isolation of Mitotic Mutations as Revertants of Existing Mutations

As mentioned previously, ts^- mutations in genes essential for mitosis prevent the growth of conidia into colonies. If conidia carrying such a mutation are mutagenized, new mutations may occur that reverse the effect of the original ts^- mutation. It is very easy to select for such mutations, which are called revertants, because if one plates out millions of mutagenized conidia from a ts^- strain and incubates them at a restrictive temperature, only revertants will be able to grow. One can easily plate 1×10^7 conidia on a standard 85-mm plate and if the reversion frequency is 1×10^{-6}, 10 revertants will be present on the plate and will grow to form colonies. Revertants can be tested for conditional lethality and mitotic blockage as discussed in Section VI.A.

Reversions can be of three sorts and the terminology for these types of reversions varies among authors. Reversion can be due to a mutation that simply reverses the mutation that caused the original conditional lethality. I term this a "back mutation." Reversion can be due to a second mutation within the same gene as the mutation that caused the original conditional lethality. In such cases the mutation that causes the reversion causes a second alteration that compensates for the original mutation. I term this an "intragenic suppressor." Finally, a reversion can be in another gene, the product of which interacts, directly or indirectly, with the product of the original mutant gene. In such cases, an alteration in a second protein compensates for the original mutation. I term this an "intergenic suppressor."

If one is fortunate, a fraction of the intragenic and intergenic suppressor mutations may cause some form of conditional lethality. For example, some fraction of the intragenic or intergenic suppressors of hs^- mutations might cause cold sensitivity. Conditionally lethal intragenic and intergenic suppressors can be extremely useful. Conditionally lethal intragenic suppressors may have different and informative phenotypes from the original mutation and conditionally lethal intergenic suppressors may be located in previously undiscovered genes that are important for the process under study (in this case mitosis).

Tubulin genes provide an excellent example of this approach. Mutations in the *benA* gene, which we now know encodes the major β-tubulin expressed in hyphae, were originally discovered as mutations that confer resistance to the antifungal, antimicrotubule agent benomyl (Van Tuyl, 1977; Sheir-Neiss *et al.*, 1978). It was subsequently discovered that a fraction of the *benA* mutations that confer benomyl resistance also cause heat sensitivity (Morris *et al.*, 1979; Oakley and Morris, 1981). Revertants of hs^- *benA* mutations were isolated and among the revertants were some useful cs^- β-tubulin mutations (Oakley *et al.*, 1985), the first α-tubulin mutation identified in any organism (Morris *et al.*, 1979), the first conditionally lethal α-tubulin mutations identified (Oakley *et al.*, 1987), and, perhaps most important, the first γ-tubulin mutations (Weil *et al.*, 1986; Oakley and Oakley, 1989). Indeed, this approach was responsible for the discovery of γ-tubulin.

It is important to remember, however, that the number and nature of the revertants one obtains depends on the nature of the original mutant allele and the

function of the protein encoded by the original mutant gene. As a consequence, reversion of some alleles can be quite fruitful, whereas reversion of other alleles may yield nothing of value. It is often a good idea to isolate revertants of several conditionally lethal mutant alleles of a gene if they are available and to simply determine which allele gives rise to the most interesting and useful revertants.

For revertants to be of value, they must be analyzed genetically. One can determine if reversion is due to an intragenic or extragenic suppressor by crossing the revertant to a wild-type strain. I use a cs^- revertant of an hs^- strain as an example. In a cross of such a revertant to a wild-type strain, if reversion is due to an intragenic suppressor mutation, the mutation that causes reversion should be closely linked to the original hs^- mutation and there should little or no crossing over between the original hs^- mutation and the suppressor and there will be few or no hs^- progeny. If there are hs^- progeny, suppression of heat sensitivity must be due to an intragenic suppressor. Such a cross will not establish, however, that cold sensitivity is caused by the same mutation that causes reversion. One could have an irrelevant cs^- mutation as well as a separate mutation that suppresses heat sensitivity but does not cause cold sensitivity. Demonstrating that cold sensitivity is due to the same mutation that causes reversion for either an intragenic suppressor or an extragenic suppressor may not be trivial. If appropriate conditions can be found, however, the cs^- revertant can be crossed to the original hs^- strain. If any cs^+, hs^+ progeny are found, cold sensitivity must be caused by a mutation irrelevant to suppression.

VII. Morphological Analysis of Mutants

A. Light Microscopy

1. Visualization of Chromatin and Determination of Chromosome Mitotic Indices

Nuclei of *A. nidulans* are quite small. Haploid hyphae are only about 2 or 3 μm in diameter and nuclei are even smaller. Nevertheless, *A. nidulans* chromosomes clearly condense and some mitotic stages can be discerned. Traditional staining procedures such as acetoorcein and Feulgen staining are quite effective for staining *A. nidulans* chromatin and these have been discussed thoroughly by Robinow and Caten (1969) and Morris *et al.*, (1982). Procedures using fluorescent DNA-binding dyes, such as mithramycin (Morris *et al.*, 1982) and, particularly, DAPI (Oakley and Rinehart, 1985), have become the methods of choice, however, because they are easier to perform and more rapid than traditional methods. DAPI staining works with a variety of fixation regimes but different regimes may require different concentrations of DAPI to obtain optimal staining. A detailed DAPI staining protocol has been published recently (Oakley and Osmani, 1993).

Interphase nuclei have relatively smooth chromatin. The chromatin partially envelopes the nucleolus which is visible as an unstained region (Fig. 4). When

cells enter mitosis, chromosomes condense and the chromatin assumes a lumpy appearance and the nucleolar region is no longer apparent. Early stages of mitosis are difficult to distinguish but late anaphase and telophase nuclei are easily identified (Fig. 2). There are several nuclei in each hyphal segment of *A. nidulans* and they generally enter mitosis synchronously. As a consequence, the mitotic index is generally considered to be the percentage of hyphal segments in which nuclei are in mitosis rather than simply the percentage of nuclei that are in mitosis. Finally, since *A. nidulans* undergoes tip growth, the hyphal tip cells are the most rapidly dividing and cells not on the hyphal tips may not be undergoing mitosis at all. As a consequence, mitotic indices are generally determined from hyphal tip cells or germlings which are a single cell.

2. Immunofluorescence Microscopy

Immunofluorescence microscopy in *A. nidulans* has presented challenges but, fortunately, they can be overcome and excellent results are possible (Fig. 2). One challenge is antibody specificity. Many mice and rabbits have antibodies against fungal epitopes (presumably because they have had fungal infections) and polyclonal antibodies often must be affinity purified to obtain adequate specificity. Fortunately, for studying mitosis, two monoclonal anti-α-tubulin antibodies that work well in *A. nidulans,* YOL1/34 (Sera Labs) and DM1A (Sigma) are commercially available.

Secondary antibodies also present challenges. Commercially available secondary antibody preparations, even those that are affinity purified, often react with one or more *A. nidulans* proteins. This problem can be overcome by preadsorbing the secondary antibodies with an *A. nidulans* acetone powder (Oakley *et al.,* 1990).

A third problem is that the *A. nidulans* cell wall is impermeable to antibodies. The wall can be digested with a crude enzyme preparation, Novozym 234, but this is high in protease activity and varies a great deal in activity from lot to lot. As a consequence, much effort must be expended to inhibit protease activity and cell wall digestion conditions must be determined experimentally for each lot of Novozym 234. Details of immunofluorescence procedures have been discussed at length recently (Oakley and Osmani, 1993) and readers are referred to this source for a detailed immunofluorescence protocol.

B. Electron Microscopy

Analysis of the structure of mitotic spindles of mutants blocked in mitosis at a restrictive temperature can provide important clues regarding the role of the mutant protein in mitosis. Adequate preservation of spindle structure can be obtained with conventional aldehyde fixatives and fixation procedures have been discussed (Morris *et al.,* 1982). An alternative approach that appears to provide better preservation of intracellular structures in fungi in general (Howard and

Aist, 1979; Heath and Rethoret, 1982; Howard and O'Donnell, 1987), and in *A. nidulans* in particular (Osmani *et al.,* 1987), is freeze substitution (Fig. 3). This is a specialized technique, however, that requires specialized equipment. Detailed instructions in carrying out this technique have been published by Howard and O'Donnell (1987), but those wishing to use the technique with *A. nidulans* would be well advised to collaborate with a lab that uses the technique routinely.

VIII. Genetic Analysis of Mutants

Once strains carrying mutations that block or otherwise alter mitosis are identified, it is important to analyze the strains genetically for several reasons. First, it is important to remember that after a mutagenesis, some of the strains carrying mutations that affect mitosis may carry other mutations as well, and these may complicate further analyses. I have already discussed how one can use crosses to detect and eliminate such irrelevant mutations. Second, by creating diploids heterozygous for a newly isolated mitotic mutation, it is possible to determine if the mutation is dominant or recessive. Third, by performing complementation tests, it is possible to determine if the newly isolated mitotic mutations are allelic with (i.e., are in the same gene as) other newly or previously isolated mitotic mutations. Fourth, mapping mutations to linkage group and subsequently to locus can be very helpful in cloning and working with the mutant genes.

A. Determining Whether Mutations Are Dominant or Recessive

It is important to know if mutations are dominant or recessive. In particular, complementation of mutant alleles with a library of wild-type sequences has been one of the most important approaches for cloning genes involved in mitosis, and it is not possible to complement dominant mutant alleles with libraries of wild-type sequences. To determine if a mutant allele is dominant, one can construct a stable diploid between the mutant strain and a wild-type strain for the mutant gene. If the mutation is dominant, of course, the diploid will have the mutant phenotype, and if it is recessive the diploid will have the wild-type phenotype. Partially dominant alleles will produce phenotypes intermediate between the wild type and the mutant.

Diploid formation in *A. nidulans* is quite different from diploid formation in yeasts. Diploids form prior to meiosis in *A. nidulans,* as in yeasts and all other sexually reproducing haploid organisms. These diploids are transient, however, and cannot be used for complementation tests. The stable diploids used for complementation tests form vegetatively and at a relatively low rate. The formation of these diploids requires two steps, the formation of a heterokaryon between the two strains being tested and the spontaneous formation of a diploid from the heterokaryon. Methods for constructing heterokaryons and diploids have been discussed by Morris *et al.* (1982).

It is important to note that while *A. nidulans* diploids are generally quite stable, nondisjunction can occur and can result in aneuploids which tend to break down further to haploids. Unlike yeast diploids, the stable, vegetative diploids produced by *A. nidulans* do not readily undergo meiosis and are essentially sterile.

B. Complementation Tests

Complementation tests are used to determine if two mutations are alleles of the same gene. If, for example, one isolates several mutations that affect mitosis, it is useful to know whether the mutations are in one, two, or several genes. In addition, it is useful to know if any or all of the mutations are alleles of previously identified genes. To determine if two mutations are alleles of the same gene, they must each be recessive. One must create a stable diploid between two strains, each carrying one of the mutations. If the two mutations are allelic, there will be no wild-type copy of the mutant gene in the diploid and the diploid will almost always have a mutant phenotype. (Complementation by two alleles of the same gene can occur but such complementation is rare.) If the two mutations are in different genes, a wild-type copy of each gene will be present and, if the mtuant alleles are recessive, the diploid will have a wild-type phenotype.

C. Mapping Genes

Mapping genes to a chromosomal locus is a prerequisite for positional cloning, and when, in the future, ordered cosmid libraries are correlated with genetic maps, cloning genes for which map locations are known will become trivially easy. Genetic mapping in *A. nidulans* is a two-step process. Genes are first mapped to linkage group and then to the locus on the linkage group.

1. Mapping Genes to Linkage Groups

Mapping genes to linkage groups is a two-step process. First, a diploid is constructed from a strain carrying the mutation of interest and a mitotic mapping strain. Mitotic mapping strains carry a genetic marker on each of the eight chromosomes or linkage groups and a number of them are available from the FGSC. Second, the diploid is forced to undergo haploidization and haploids are tested for the mutation of interest and for each of the genetic markers in the mitotic mapping strain. If one is mapping an hs^- mutation, heat sensitivity should segregate randomly with respect to the markers on seven linkage groups and in opposition to the marker(s) on one linkage group. For example, if the mutation is on linkage group V, heat sensitivity would segregate randomly with respect the markers on all linkage groups except linkage group V. Heat-sensitive haploids would never have the linkage group V marker from the mitotic mapping strain and haploids that have the linkage group V marker from the mitotic mapping strain would never be heat sensitive.

Diploids are generally induced to undergo haploidization by agents, such as antimicrotubule agents, that cause nondisjunction. Detailed procedures for haploidization have been given by Morris *et al.* (1982).

2. Mapping Genes to Chromosomal Locus by Meiotic Crosses

Once the mutation of interest has been mapped to a linkage group, its map position on the linkage group can be determined by meiotic crosses to one or more strains that carry multiple genetic markers on the linkage group to which the mutation has been mapped. Progeny of the crosses are then tested for the mutation of interest and each of the genetic markers on the same linkage group. This allows one to determine recombination frequencies between the mutation of interest and each of the genetic markers and, thus, the map position of the mutation of interest. Strains that carry multiple genetic markers on specific linkage groups (meiotic mapping strains) are available from the FGSC.

IX. Molecular Genetic Methods for Working with *A. nidulans*

A. Cloning of Genes Involved in Mitosis

For mitotic mutants to be maximally useful in understanding mitosis, the genes must be cloned, and in *A. nidulans* such genes are usually cloned by complementation of a mutant allele with a library of wild-type sequences. Using the example of a hs^- mitotic mutation, one would transform a strain carrying the mutation with a plasmid library of wild-type sequences and incubate transformed cells at a restrictive temperature. Those rare cells that were transformed with the wild-type allele of the hs^- mutation would be able to grow at the restrictive temperature and could be easily selected. This approach requires, of course, that the hs^- mutation is recessive and it requires an efficient transformation system. Efficient transformation is possible in *A. nidulans,* and although there is some variation among procedures, transformation generally involves the use of cell wall lytic enzymes to create protoplasts and the use of Ca^{2+} and polyethylene glycol to facilitate entry of DNA into the protoplasts. It is beyond the scope of this chapter to review transformation procedures in detail, but readers are referred to Oakley and Osmani (1993).

Transformation in *A. nidulans* generally occurs by integration of transforming sequences into the chromosome, often by homologous recombination. Recovering plasmids containing the wild-type allele from a transformant is more difficult than doing so in organisms in which transforming vectors replicate autonomously. It is possible to recover genes, however, by taking advantage of the fact that all commonly used plasmids carry one or more antibiotic resistance genes selectable in *Escherichia coli.*

DNA from transformants can be digested with restriction endonucleases and ligated to produce circular fragments. Circularization is facilitated by dilution of

the DNA before ligation to reduce the frequency of intermolecular interactions. An appropriate strain of *E. coli* can be transformed with the ligation mixture and the transformants should contain plasmids that carry all or part of the gene of interest. Depending on the nature of the integration of the transforming sequences into the *A. nidulans* chromosome, plasmids may carry all of the wild-type allele, all of the mutant allele, or portions of one or both of these alleles. Southern hybridizations of restriction digests of *A. nidulans* transformant DNA using the library plasmid as a probe can help to clarify the nature of the insertion into the chromosome and help one choose the restriction enzymes that are most likely to allow the recovery of the entire gene. Recovered plasmids carrying the entire wild-type allele of the gene of interest can easily be identified because, when used in transformations, they will complement the hs^- mutation very efficiently.

Since ordered and chromosome-specific cosmid libraries are available for *A. nidulans,* it is possible to clone by complementation using a sib-selection approach. If one has mapped a mutation to a linkage group, one can obtain, from the FGSC, a set of cosmids that contain inserts spanning that linkage group. One can then transform with DNA from groups of cosmids and determine which groups complement the mutation. One can break a group of cosmids that complements the mutation into subgroups or individual cosmids and determine which complement the mutation. A cosmid carrying the gene of interest can be identified in two or three steps using this approach.

This approach has been greatly facilitated by the identification of sequences that increase transformation frequencies (Gems and Clutterbuck, 1993). These sequences on helper plasmids can be cotransformed with cosmids and greatly increase the transformation frequencies of the cosmids. Unfortunately, the helper plasmids recombine frequently with other sequences, including transforming cosmids, so they present problems if one is trying to recover sequences from transformants. With the sib-selection approach, however, recovery is not necessary.

Other approaches for cloning genes involved in mitosis have also been useful. For example, if one has an interesting mutation that is not selectable under any condition (e.g., is not sufficiently ts^- to prevent growth at any temperature) one can map the gene to locus, clone a selectable gene nearby, and chromosome walk to the gene of interest. This approach was used, for example, to clone the γ-tubulin gene of *A. nidulans* (Oakley and Oakley, 1989) and should be even easier to use now that ordered cosmid libraries are available.

B. Creating Mutant Alleles of Cloned Genes

Temperature-sensitive mutations are valuable for determining the functions of genes, but in some instances ts^- alleles may retain some function and in other instances ts^+ alleles may not be available. In *A. nidulans* it is possible to disrupt genes or delete genes, as is possible in many other organisms. In *A. nidulans,*

however, it is possible to maintain nuclei carrying a disruption or deletion of an essential gene in a heterokaryon. The phenotype caused by the disruption can be determined in conidia produced by the heterokaryon (Osmani *et al.*, 1988; Oakley *et al.*, 1990). It is even possible to disrupt genes in strains carrying cell cycle mutations that allow synchronization of germlings carrying a disruption of an essential gene (Martin *et al.*, 1997). This is a powerful tool for rapid examination of gene function and detailed procedures for heterokaryon gene disruptions have been described by Oakley and Osmani (1993).

Finally, one-step and two-step gene replacement procedures have been described for *A. nidulans* (Miller *et al.*, 1985; Dunne and Oakley, 1988). Thus, it is possible to create mutant alleles *in vitro* and replace wild-type alleles with the mutant alleles. This should allow one to create strains carrying mutant alleles of any cloned gene involved in mitosis.

Acknowledgments

I thank C. Elizabeth Oakley for discussions and for reading the manuscript and Dr. MaryAnn Martin for assistance with Fig. 1. This work was supported by Grant GM31837 from the NIH.

References

Bergen, L. G., and Morris, N. R. (1983). Kinetics of the nuclear division cycle of *Aspergillus nidulans*. *J. Bacteriol.* **156,** 155–160.

Byers, B., and Goetsch, L. (1975). Behavior of spindles and spindle plaques in the cell cycle and conjugation of *Saccharomyces cerevisiae*. *J. Bacteriol.* **124,** 511–523.

Clutterbuck, A. J. (1974). *In* "Handbook of Genetics" (R. C. King, ed.), Vol. 1, pp. 447–510. Plenum, New York.

Cove, D. J. (1966). The induction and repression of nitrate reductase in the fungus *Aspergillus nidulans*. *Biochim. Biophys. Acta* **113,** 51–56.

Doonan, J. H., and Morris, N. R. (1989). The *bim*G gene of Aspergillus nidulans, required for completion of anaphase, encodes a homolog of mammalian phosphatase 1. *Cell* **57,** 987–996.

Dunne, P. W., and Oakley, B. R. (1989). Mitotic gene conversion, reciprocal recombination and gene replacement at the *benA*, β-tubulin locus of *Aspergillus nidulans*. *Mol. Gen. Genet.* **213,** 339–345.

Elliot, C. G. (1960). The cytology of *Aspergillus nidulans*. *Genet. Res.* **1,** 462–476.

Engle, D. B., Osmani, S. A., Osmani, A. H., Rosborough, S., Xiang, X., and Morris, N. R. (1990). A negative regulator of mitosis in *Aspergillus* is a putative membrane spanning protein. *J. Biol. Chem.* **256,** 16132–16137.

Enos, A. P. and Morris, N. R. (1990). Mutation of a gene that encodes a kinesin-like protein blocks nuclear division in A. nidulans. *Cell* **60,** 1019–1027.

Fincham, J. R. S., Day, P. R., and Radford, A. (1979). "Fungal Genetics." Univ. of California Press, Berkeley.

Gems, D. H., and Clutterbuck, A. J. (1993). Co-transformation with autonomously-replicating helper plasmids facilitates gene cloning from an *Aspergillus nidulans* gene library. *Curr. Genet.* **24,** 520–524.

Harris, S. D., Morrell, J. L., and Hamer, J. E. (1994). Identification and characterization of *Aspergillus nidulans* mutants defective in cytokinesis. *Genetics* **136,** 517–532.

Heath, I. B., and Rethoret, K. (1982). Mitosis in the fungus Zygorhynchus moelleri: Evidence for stage specific enhancement of microtubule preservation by freeze substitution. *Eur. J. Cell Biol.* **28,** 180–189.

Howard, R. J., and Aist, J. R. (1979). Hyphal tip cell ultrastructure of the fungus *Fusarium:* Improved preservation by freeze-substitution. *J. Ultrastruct. Res.* **66,** 224–234.

Howard, R. J., and O'Donnell, K. L. (1987). Freeze substitution of fungi for cytological analysis. *Exp. Mycol.* **11,** 250–269.

Mackintosh, M. E., and Pritchard, R. H. (1963). The production and replica plating of micro-colonies of *Aspergillus nidulans. Genet. Res.* **4,** 320–322.

Martin, M. A., Osmani, S. A., and Oakley, B. R. (1997). The role of γ-tubulin in mitotic spindle formation and cell cycle progression in *Aspergillus nidulans. J. Cell Sci.* **110,** 623–633.

Miller, B. L., Miller, K. Y., and Timberlake, W. E. (1985). Direct and indirect gene replacements in *Aspergillus nidulans. Mol. Cell Biol.* **5,** 1714–1721.

Morris, N. R. (1976). Mitotic mutants of *Aspergillus nidulans. Genet. Res.* **26,** 237–254.

Morris, N. R., Lai, M. H., and Oakley, C. E. (1979). Identification of a gene for α-tubulin in Aspergillus nidulans. *Cell* **16,** 437–442.

Morris, N. R., Kirsch, D. R., and Oakley, B. R. (1982). *Methods Cell Biol.* **25,** 107–130.

Oakley, B. R., and Morris, N. R. (1980). Nuclear movement is β-tubulin-dependent in Aspergillus nidulans. *Cell* **19,** 255–262.

Oakley, B. R., and Morris, N. R. (1981). A β-tubulin mutation in Aspergillus nidulans that blocks microtubule function without blocking assembly. *Cell* **24,** 837–845.

Oakley, B. R., and Morris, N. R. (1983). A mutation in *Aspergillus nidulans* that blocks the transition from interphase to prophase. *J. Cell Biol.* **96,** 1155–1158.

Oakley, C. E., and Oakley, B. R. (1989). Identification of γ-tubulin, a new member of the tubulin superfamily encoded by *mip*A gene of *Aspergillus nidulans. Nature* **338,** 662–664.

Oakley, B. R., and Osmani, S. A. (1993). *In* "The Cell Cycle. A Practical Approach" (P. Fantes and R. Brooks, eds.), pp. 127–142. IRL Oxford Univ. Press, Oxford.

Oakley, B. R., and Rinehart, J. E. (1985). Mitochondria and nuclei move by different mechanisms in *Aspergillus nidulans. J. Cell Biol.* **101,** 2392–2397.

Oakley, B. R., Oakley, C. E., Kniepkamp, K. S., and Rinehart, J. E. (1985). Isolation and characterization of cold-sensitive mutations at the *benA,* β-tubulin, locus of *Aspergillus nidulans. Mol. Gen. Genet.* **201,** 56–64.

Oakley, B. R., Oakley, C. E., and Rinehart, J. E. (1987). Conditionally lethal *tubA* α-tubulin mutations in *Aspergillus nidulans. Mol. Gen. Genet.* **208,** 135–144.

Oakley, B. R., Oakley, C. E., Yoon, Y., and Jung, M. K. (1990). γ Tubulin is a component of the spindle-pole-body that is essential for microtubule function in Aspergillus nidulans. *Cell* **61,** 1289–1301.

Ogata, W. N. (1962). Preservation of *Neurospora* stock cultures with anhydrous silica gel. *Neurospora Newslett.* **1,** 13.

Osmani, S. A., May, G. S., and Morris, N. R. (1987). Regulation of the mRNA levels of *nimA,* a gene required for the G2-M transition in *Aspergillus nidulans. J. Cell Biol.* **104,** 1495–1504.

Osmani, S. A., Engle, D. B., Doonan, J. H., and Morris, N. R. (1988). Spindle formation and chromatin condensation in cells blocked at interphase by mutation of a negative cell cycle control gene. *Cell* **52,** 241–251.

Pontecorvo, G., Roper, J. A., Hemmons, D. W., Macdonald, K. D., and Bufton, A. W. (1953). The genetics of *Aspergillus nidulans. Adv. Genet.* **52,** 141–238.

Robinow, C. F., and Caten, C. E. (1969). Mitosis in *Aspergillus nidulans. J. Cell Sci.* **5,** 403–431.

Sheir-Neiss, G., Lai, M. H., and Morris, N. R. (1978). Identification of a gene for β-tubulin in Aspergillus nidulans. *Cell* **15,** 639–647.

Smith, J. E., and Pateman, J. A. (1977). "Genetics and Physiology of *Aspergillus.*" Academic Press, London.

Timberlake, W. E. (1978). Low repetitive DNA content in *Aspergillus nidulans. Science* **202,** 973–975.

Van Tuyl, J. M. (1977). Genetics of fungal resistance to systemic fungicides. *Meded. Landbouwhogesch. Wageningen* **2,** 1–137.

Weil, C. F., Oakley, C. E., and Oakley, B. R. (1986). Isolation of *mip* (microtubule-interacting protein) mutations of *Aspergillus nidulans. Mol. Cell. Biol.* **6,** 2963–2968.

Xiang, X., Beckwith, S. M., and Morris, N. R. (1994). Cytoplasmic dynein is involved in nuclear migration in *Aspergillus nidulans. Proc. Natl. Acad. Sci. USA* **91,** 2100–2104.

CHAPTER 19

Using Green Fluorescent Protein Fusion Proteins to Quantitate Microtubule and Spindle Dynamics in Budding Yeast

Kerry S. Bloom, Dale L. Beach, Paul Maddox, Sidney L. Shaw,* Elaine Yeh, and Edward D. Salmon

Department of Biology
University of North Carolina at Chapel Hill
Chapel Hill, North Carolina 27599-3280

* HHMI Long Laboratory
Department of Biology
Stanford University
Stanford, California 94305

I. Introduction

The small cell size and susceptibility to photodamage complicate imaging live budding yeast. The haploid yeast cell measures only 5–8 μm in diameter, requiring

METHODS IN CELL BIOLOGY, VOL. 61

0091-679X/99 $30.00

that high magnification and high numerical aperture lenses be used for resolution of intracellular structures. Furthermore, yeast have little intrinsic contrast, requiring the use of differential interference contrast (DIC) optic for brightfield imaging. Fluorescence studies of Green fluorescent protein (GFP) fusion proteins are difficult because high-intensity excitation at 470 nm or shorter wavelengths for more than 2 or 3 min dramatically impairs cell growth and results in GFP photobleaching.

The previous conditions present a serious problem for the microscopist. Fluorescence excitation must be of low intensity to prevent phototoxicity and photobleaching during the course of a time-lapse experiment. Also, the level of GFP fusion protein expression must be kept low so that excess protein does not adversely affect the cell. Under these conditions, the total light from GFP fluorescence emmission is extremely small. Compounding the problem is the requirement for high magnification. As total magnification increases, the amount of light collected at the microscope decreases as a product of the square of the magnification. Gathering sufficient fluorescence signal for imaging without damaging the cells requires that the efficiency of the optical system be maximized and necessitates balancing temporal and spatial resolution with the need for light sensitivity.

One project that illustrates both the difficulties and the potential benefits of imaging GFP fusion proteins in live yeast cells is the problem of how microtubules contribute to the positioning of the nucleus. The astral microtubules in budding yeast are very labile and have been difficult to preserve by fixation methods for either immunofluorescence or electron microscopy. We have developed a C-terminal dynein–GFP probe (Shaw *et al.*, 1997b) containing an N-terminal 300-amino acid deletion, which partially complements dynein null mutants. This probe labels the astral microtubules, which have a role in moving the nucleus to the nascent bud. Characterizing the astral microtubule assembly dynamics using the dynein–GFP probe required that we optimize our handling of GFP expressing cells and dictated several microscopy enhancements to allow imaging over the 90+ min cell cycle. In addition, it was imperative to examine cells with similar amounts of the dynein–GFP fusion protein, necessitating a quantitative measurement of fluorescence in single cells.

The multimode instrumentation we developed for time-lapse GFP, DIC, and DAPI imaging has been presented in detail elsewhere (Salmon *et al.*, 1998; Shaw *et al.*, 1997a). This article focuses on aspects of cloning, with regard to promoter choice for GFP fusion proteins, methods to quantitate the fluorescence signal in single cells, and quantitative solutions to the imaging problem. Examples of cells expressing excess levels of dynein–GFP are provided to illustrate (i) how overexpression is documented and (ii) phenotypes resulting from severe protein overexpression.

II. Construction of Protein–GFP Fusion and Promoter Selection

Several modules for construction of GFP fusion proteins have been reported that allow very rapid one-step manipulation without requiring plasmid clones of

the gene of interest. These modules utilize the regulatable HIS3 (Straight *et al.*, 1996, 1997), MET25 (Mumberg *et al.*, 1994; Niedenthal *et al.*, 1996), or GAL1–10 (Longtine *et al.*, 1998) promoters. Endogenous promoters that drive sufficient quantities for visualization include Nuf2p (Kahana *et al.*, 1995), Myo1p (Bi *et al.*, 1998; Lippincott and Li, 1998), Sec3p (Finger *et al.*, 1998), Tub3p (S. Shaw and K. Bloom, unpublished results), and Tublp (A. Straight, personal communication). However, many GFP–protein fusions (i.e., dynein) have not been visualized with endogenous promoters and therefore require methods to enhance mRNA transcription.

A. Choice of Vector Cassette

Levels of GFP fusion proteins are dependent in part on the plasmid vector containing the expression cassette. Integrative vectors offer the benefit of a single copy in every cell. Advantages include uniform copy number and the presence of the clone throughout the population. Plasmids maintained with centromere DNA are present in 2–5 copies per cell (Futcher and Carbon, 1986; Resnick *et al.*, 1990). Centromere plasmids are present in a very large fraction of the population (>80% depending on the growth conditions). Using the 2μ vector can increase copy number to 40–60 copies per cell, with concomitant increases in expression levels (Mumberg *et al.*, 1994). Variation in the copy number of these plasmids from cell to cell may contribute to the heterogeneity in expression levels seen in single cells of a population.

B. Choice of Promoter

The ability to regulate the quantity of GFP–fusion protein in individual cells is paramount to obtaining an accurate assessment of protein function. Saturation of binding sites by excess levels of the fusion protein may contribute to background fluorescence or lead to aberrant positioning of the fusion protein *in vivo*. The level of mRNA transcription, and thus protein level, is greatly influenced by the strength of the promoter. Low-level constitutive promoters, such as the actin promoter, can produce sufficient amounts of protein without the need for induction (Amberg *et al.*, 1997). Transcription from many regulatable promoters ranges from low to titratable and extremely high levels. The HIS3 promoter exhibits very low levels of transcription in the presence of histidine, basal levels of expression during histidine starvation, and enhanced expression with addition of 3-aminotriazole (3-AT), a competitive inhibitor of histidine (Straight *et al.*, 1996). Bimodal expression levels from the HIS3 promoter derive from amino acid starvation (about 10-fold increase) and global amino acid derepression (triggered by 3-aminotriazole as well as amino acid imbalances) increasing transcription an additional 2.5- to 4-fold (Hinnebusch, 1992; Jones and Fink, 1982).

The MET promoter can be titrated with methionine to produce a linear gradient of expression. Below a threshold of 500 μM methionine, the MET25 promoter increases protein amounts nearly linearly to fourfold baseline levels as methio-

nine concentration decreases in the media (Mumberg *et al.*, 1994). Thus, levels of GFP fusion protein can be adjusted to optimize levels of signal over background fluorescence. Additionally, varying the methionine concentration of the media during imaging maintains induction over the course of the experiment. Appropriate levels of induction during imaging must be determined empirically. This may be critical for proteins with short half-lives or to replenish photobleached GFP molecules to endogenous levels. The MET promoter is comparable to other variably active promoters, such as CUP1 (Etcheverry, 1990; Resnick *et al.*, 1990), in its ability to regulate levels of gene product. The MET25 promoter, and the use of amino acid starvation to regulate gene activity, compares favorably to heavy metal salts, which may further stress cells during imaging.

The divergent GAL1–10 promoter is one of the most highly active promoters, generating a level of expression on the order of 1000 times more than the uninduced state. In addition, catabolite repression in cells grown on glucose renders the promoter virtually incapacitated. In this way, high levels of expression on galactose and tight repression on glucose can be attained. A consequence of the catabolite repression is that stores of glucose must be depleted prior to activation by galactose. A temporal lag in induction occurs following addition of galactose to a glucose-grown culture. This can be avioded by growing cells on carbon sources that do not induce catabolite repression, such as raffinose or sucrose.

It has been reported that levels of expression from GAL1 promoter can be regulated by altering the ratio of galactose : glucose in the medium (Moreland *et al.*, 1987). This provides another option in the repertoire of induction strategies. It is likely that a small amount of glucose in the presence of galactose delays induction from the GAL1 promoter. It is of interest to determine the levels of induction in single cells grown in varying galactose : glucose cultures. Once an individual cell is induced, the levels of induction might be comparable to and independent of the galactose : glucose ratio in the medium. In any case, induction for extended periods of time is not recommended because overexpression and excess accumulation of fusion protein is likely to be detrimental.

C. Inducing Production of the GFP Fusion Protein

The induction regime for visualizing GFP fusion proteins is critical for success in subsequent analysis. It is essential for cells to be in midlogarithmic growth phase because this will increase the likelihood of survival during the imaging process. In our experience, very short induction times have been sufficient (and are optimal) in obtaining visible levels of a GFP fusion protein. Addition of galactose to raffinose-grown cultures results in very rapid (15 min) induction from the GAL1 promoter. Thirty-minute induction from the HIS3 promoter (following addition of 3-AT) leads to detectable levels of signal with low background (Straight *et al.*, 1996, 1997). Expression from the MET25 promoter requires 1.5–3 hr of induction to obtain renderable levels of fluorescence. Typically,

cells grown to early or midlogarithmic growth phase can be switched into inducing conditions without a significant lag in growth and then harvested after an appropriate time for microscopy.

III. Quantifying Fluorescence in Cell Populations

Quantification of fluorescence intensity by flow cytometry of cells expressing GFP from the GAL1, GAL4, and URA3 promoters produced bell-shaped curves representing the distribution of fluorescence in a population of cells (Niedenthal *et al.*, 1996). Cells not expressing GFP also displayed a bell-shaped curve reflecting the distribution of autofluorescence in uninduced populations. Induction levels were evident by the peaks of separation in the autofluorescence versus induced fluorescence. GFP production from the strong GAL1 promoter increased the peak of fluorescent intensity 10-fold over autofluorescence, therefore reducing the overlap between the two curves. Expression from the GAL4 or URA3 promoters provided minimal separation between induced and uninduced levels of fluorescence. Such differences provide clear indications of promoter strength and illustrate the gains in expression when "strong" promoters are used to drive expression of the fusion protein. Production of GFP fusion protein above autofluorescence is fundamental to one's ability to resolve localized protein in the cell; however, the trade-offs of overexpression are potentially detrimental side effects for certain proteins.

The fluorescence measurements provide an accurate assessment of protein concentration. When a GFP fusion to a TATA-binding protein was imaged by quantitative laser scanning confocal microscopy (LSCM), the levels measured by LSCM correlated with the levels determined by immunoblot of whole cell extract protein (Patterson and Piston, 1998). Thus, the live cell analysis provides a new dimension in this genetic system. However, it is imperative that precise fluorescence measurements be made to ensure that individual cells being examined express similar amounts of the fusion protein. Imaging GFP fusion proteins not only offers a method of measurement equivalent to a more conventional technique but also provides real-time quantitation.

A. Quantitative Image Analysis of Fluorescence Intensity in Single Cells

Changes in expression level of tubulin and/or microtubule motors have significant consequences on microtubule dynamics. Altered stoichiometry of tubulin has dire effects on cell growth (Solomon, 1991). Likewise, alterations in motor proteins may adversely affect microtubule dynamics, such as changes in growth or shortening velocities, or frequency of rescue (Shaw *et al.*, 1997b). As shown in Fig. 1, the heterogeneity in single cells expressing a bacteriophage MS2–GFP fusion protein is quite significant. For accurate kinetic measurements, it is critical that one examines cells expressing similar concentrations of the fusion protein.

A

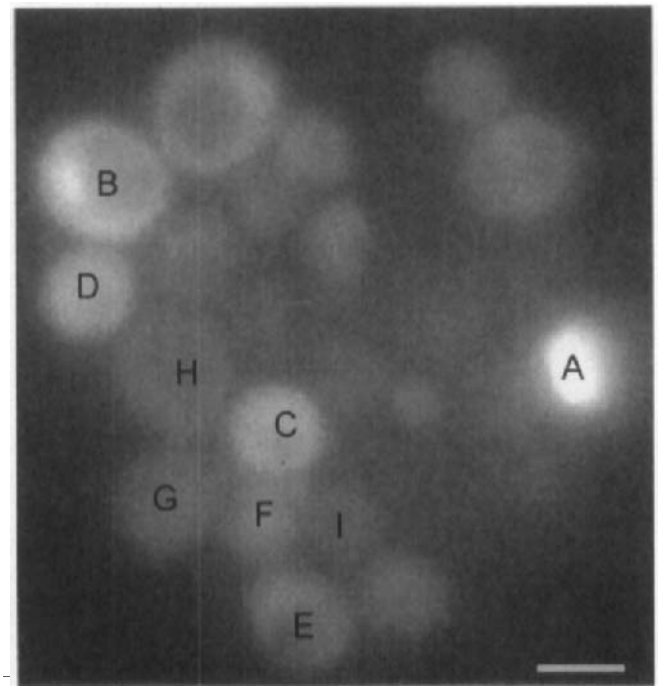

B

CELL	RF	CELL	RF
A	>4095	F	2544
B	3904	G	2768
C	3152	H	2784
D	3120	I	2384
E	2480	BG	1872

Fig. 1 Individual cells in large population may exhibit heterogeneity in protein levels. (A) Expression from the MET25 promoter (2 hr of induction) of a cytoplasmic protein (the bacteriophage MS2 coat protein) fused to GFP leads to a virtually continuous range of fluorescent intensities in individual cells. The cells with no fluorescence most likely represent plasmid loss (the fraction of cells lacking fluorescence correlates to the fraction of cells without plasmid). (B) Measurements of the relative fluorescence (RF) for each labeled cell. The arbitrary units correspond to pixel values also known as gray level. Cell A exceeds the maximum gray level in this exposure. A background reading (BG) was taken from the lower right corner of the image. Variation of fluorescence in the population is likely to be related to plasmid copy number and variations in transcriptional activity. Scale bar = 5 μm.

To measure the protein levels in single cells, all images should be unenhanced since enhancement of contrast or brightness changes the intensity value. The maximum, minimum, and average intensity of the fluorescence should be recorded as well as the imaging conditions (exposure time, excitation intensity,

camera settings, and lens elements used), making sure that maximum intensity is less than the saturation level of the camera. These measurements result in a range of intensity, which correlates directly with expression levels.

Once the range has been established, the level of protein expression in which the kinetic phenotype is complemented can be deduced. For our purposes, dynein–GFP is expressed in cells lacking the endogenous dynein gene (a dynein null background). Exogenous expression of dynein–GFP results in three major phenotypes. The first is underexpression, i.e., the expression of dynein–GFP is insufficient to complement the mutant phenotype. The second is overexpression, resulting in growth defects and malpositioning of the mitotic spindle (Shaw *et al.*, 1997b). Finally, there is a range of expression between these two phenotypes that provides sufficient dynein to restore wild-type spindle movement and kinetic progression through mitosis. Since expression is heterogeneous within a given population of cells, we posit that complementation in individual cells expressing specified level of protein expression be the standard for such experiments.

By comparing the relative fluorescence within various cells and observing the doubling time of these cells, a standard can be determined for the amount of GFP fusion protein that does not perturb the kinetics of cell cycle progression. The relative amount of GFP fusion protein can be determined by measuring the mean and maximum pixel value (gray level or fluorescence intensity in arbitrary units) within a given cell as seen in unenhanced images. Various points of fluorescence, such as spindle poles and microtubules, should be measured and compared throughout the population to ensure accuracy. Cells observed by time-lapse microscopy can then be analyzed for growth rate versus expression level. Using the expression standard allows a high level of assurance that the reported experimental observations are derived from cells with wild-type growth rates (Shaw *et al.*, 1997b). Cells that are expressing a level of GFP fusion protein determined to be deleterious to the cell (such as slowed cell cycle time) can be excluded from further study.

IV. The Imaging System

Our digital imaging microscope utilizes conventional wide-field optics and a cooled, slow-scan charge couple device (CCD) camera for image detection (Fig. 2). Because we require both DIC and fluorescence images, a filter wheel containing an analyzer and a glass blank (to equalize the light path for DIC and fluorescence modes) has been placed in front of the CCD camera to assist in switching between DIC and fluorescence modes. Filters and shutters have been added to the microscope to control light intensity for both DIC and fluorescence illumination pathways. A multiple bandpass dichromatic mirror in combination with an excitation filter wheel is used to rapidly switch between GFP and DAPI imaging. Focus is controlled by hand or by using an electronic focus motor. Most aspects (shutters, filter wheels, and focus) of the microscope have been automated and are con-

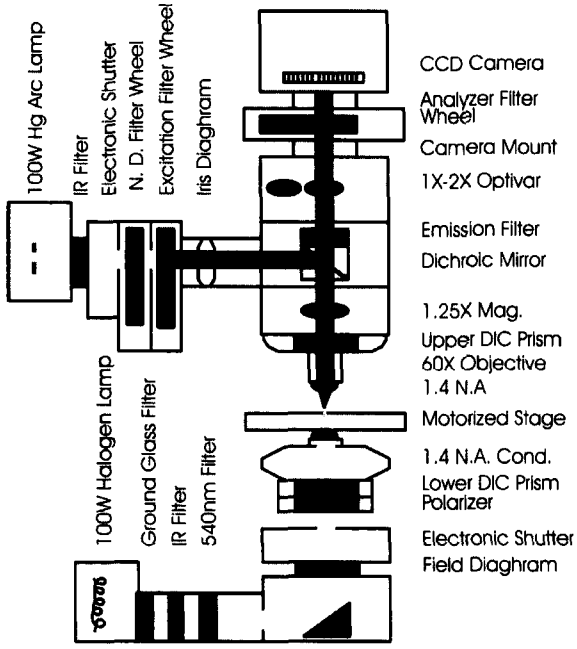

Fig. 2 Multimode optical microscope. Modification of our original imaging system (for component list, see Salmon *et al.*, 1994) by the addition of a filter wheel containing the DIC analyzer allowed automated switching between DIC and fluorescent modes (Salmon *et al.*, 1998). NA, numerical aperture; ND, neutral density.

trolled by Pentium-based computer system running MetaMorph software developed by Universal Imaging Corporation. The system is explained in detail elsewhere (Shaw *et al.*, 1997a).

V. Quantitative Solution to the Imaging Problem

A. Signal and Noise

Production of an image requires that more photoelectrons be collected from the specimen (signal) than from other sources (noise). Signal acquisition is a product of the number of fluorochromes (GFP molecules), the fluorescence excitation intensity, the quantum efficiency of the detector, and the duration of the exposure. GFP fusion concentration and fluorescence excitation must be very low to approach normal cell growth. The quantum efficiency of the CCD detector is fixed, leaving only the duration of the exposure as a variable for acquiring signal.

Noise in the imaging system derives from three major sources: autofluorescence and scattered light in the microscope system, the random nature of photon

generation, and the camera. Noise from scattered light in the microscope and from out of focus fluorescence in the media is substantially reduced by closing the epifluorescence field diaphragm to exclude all but the cell of interest. Noise is also reduced by placing the microscope in a dark room with minimal exposure to light from computer monitors.

Photons from the GFP molecule are emitted in a stochastic manner, not a steady stream, giving rise to "shot noise" or "photon noise" (Salmon *et al.,* 1998). This phenomena, measured as the square root of the total number of photons emitted, results in a variation on gray level values for the same pixel position from image to image. For example, if 100 photoelectrons are collected on average in one pixel well, the noise associated with that pixel is ± 10 electrons. In our system, 5 electrons correspond to 1 gray level, a difference of ± 2 gray levels of 20 between subsequent images for the same number of GFP molecules. When 1000 photoelectrons are collected, there is a ± 31 electron variability. Hence, as a percentage of signal, photon noise constitutes a maximum of 6% at 1000 photons (12 of 200 gray levels) but represents 20% at 100 photons (4 of 20 gray levels).

Camera noise comes from the amplifiers, which force the electrons out of the CCD wells into the computer (readout noise), and electrons arising from the silicon chip due to heat (dark current or thermal noise). Since the average camera noise for any given exposure time is generally a constant, we can later subtract this from our image using background subtraction. The standard deviation of the average represents the number of random electrons contributed to each well. The gray levels representing these electrons cannot be removed by background subtraction and appear as a variation in gray level for each image. Readout noise from the CCD chip is reduced by using "slow-scan" readout amplifiers. Dark current noise can be nearly eliminated by physically cooling the CCD chip. In our camera cooled to $-40°C$, the camera noise derives mainly from readout (about 10 electrons/pixel).

B. Resolution and Magnification

A 1.4 numerical aperture (NA) lens has a theoretical lateral resolving power for 540 nm light of about 235 nm. Hence, an 8-μm yeast cell divides into about 34 resolvable points along a line. Our CCD chip is composed of wells, or pixels, that are physically 12 μm square. By using $150\times$ magnification, we project an 8-mm long yeast cell at a size of 1200 μm onto the CCD chip that, given the 12-μm pixel size, samples 100 points across the cell. Having 3 pixels per resolved unit satisfies the sampling criteria (Nyquist limit) for ensuring that we are accurately sampling all the resolvable information (Inoué and Spring, 1997).

In order to gain sensitivity for our fluorescence images we binned (grouped) the pixels on the chip 2×2 during readout, giving a pixel size of 24 μm square. The GFP or DAPI image is now sampled by only 50 pixels, whereas, the bright field image is still sampled by 100 pixels. The resolution of the fluorescence images is now limited by the camera and not by the microscope. Given that we

need two or three sample points for every unit of the resolution, our effective resolution is now between 320 and 480 nm for the fluorescence images. By binning the wells in the CCD chip, we sacrificed half of the spatial resolution in fluorescence for a fourfold increase in light sensitivity.

C. Imaging GFP in Live Cells with a CCD Camera

The main advantage of the CCD camera for imaging GFP fusion proteins in yeast cells is sensitivity. The CCD camera, with high-efficiency detectors, proper cooling, and slow-scan readout, can accumulate light from the wide field microscope over long exposure periods without building up significant noise to degrade the image. Taking 3-s exposures with 2 × 2 binning at 1–10% of maximum excitation generates 50–250 gray levels above the noise floor of 20–30 gray levels. The major noise components, after background subtraction, are autofluorescence from the cell and media and the photon counting noise. A signal-to-noise ratio of between 1.5 : 1 and 5 : 1 produces an acceptable image of microtubules. Growth was not impaired by this level of shuttered 490-nm excitation and imaging was limited by eventual photobleaching. Shorter (1-s) exposures, using maximum fluorescence excitation, killed the cells within 15 min but indicated that there is little movement of the dynein–GFP–labeled microtubules during the 3-s exposure. Hence, we use low levels of irradiance, which are not harmful to the cell, and gain sensitivity by "on-chip integration" of the signal for 3 s.

Confocal microscopy has been successfully used to image larger cells having higher total concentrations of GFP fusion protein. Confocal imaging requires very strong illumination, usually a laser, because the majority of the fluorescence emission is discarded and because the efficiency of the photomultiplier tubes used as detectors is low (often 10%). The high level of excitation is phototoxic to yeast and photobleaches the GFP rapidly. Confocal microscopy, however, is useful for immunofluorescence studies in yeast because of the tremendous signal amplification derived from having many fluorochrome-containing antibodies bound to a single copy of the protein of interest.

VI. Image Acquisition and Processing

Given that the haploid yeast approximates a sphere of about 5–8 μm in diameter, and the depth of field of one fluorescence image from a wide-field microscope is about 1 μm, we developed a routine to image the entire cell. Using a computer controlled Z-motor, five images of 3-s exposure are taken for each time point (usually 1-min intervals). Briefly, the stage is moved up 2 μm and then moves down in 1-μm steps to -2 μm, taking a fluorescence image at each step. A single DIC image is taken when the state is at the zero position. The stage then returns to the zero (starting) position. The background (average of 25 3-s exposures taken with the camera shutter closed) is subsequently subtracted

from the fluorescence images. A maximum projection is then made from each set of five fluorescence images. The DIC and fluorescence images can now be montaged or overlaid for display. It should be noted that measurements are done by using the nonprojected images to preserve accuracy in three dimensions (Shaw *et al.*, 1997a).

VII. Applications and Examples: Expression of Dynein–GFP *in Vivo*

The dynein–GFP fusion protein allowed us to visualize the dynamic behavior of the microtubule cytoskeleton and the spindle poles. TEM descriptions of cellular physiology and anatomy (Byers, 1981; Byers and Goetsch, 1975) were unable to clearly define the ultrastructure of budding yeast astral microtubules. Antitubulin immunostaining and DAPI on fixed cells greatly enhanced observation, but fixation methods still left astral microtubules incomplete (Adams and Pringle, 1984; Pringle *et al.*, 1989). Expression of a GFP-tagged dynein within the yeast cell (Shaw *et al.*, 1997b), as well as GFP-tagged tubulin (Carminati and Stearns, 1997), produced the first view of the dynamic and physiological role for astral microtubules *in vivo*. Though the single images of astral microtubules and the nucleus look very similar to fixed cell photographs, putting the images into motion provides critical new information, especially with regard to dynamic processes such as mitosis.

Early forays into kinetic studies of *in vivo* processes in *Saccharomyces cerevisiae* used only DIC (Jones *et al.*, 1993; Koning *et al.*, 1993; Yang *et al.*, 1997; Yeh *et al.*, 1995). The addition of multimode time-lapse imaging of GFP fusion proteins (Kahana *et al.*, 1995; Salmon *et al.*, 1998; Shaw *et al.*, 1997a) enabled kinetic analysis at the molecular level. The addition of multimode, time-lapse images of spindle elongation reveals that the transition from a sausage-shaped to a bilobed-shape nucleus, observed in DIC (Yeh *et al.*, 1995), is accompanied by the separation of the chromatin, observed using the DNA intercalating dye, DAPI (see Fig. 4 in Shaw *et al.*, 1997a). We also see that in the heart-shaped stage, observed in DIC (lower cell at 15 min, Shaw *et al.*, 1997a, Fig. 4), the spindle pole fits into the cleft of the heart shape. Additionally, astral microtubules emanating from the spindle poles at either end of the nucleus exhibit dynamic instability throughout anaphase. Astral microtubules >2 μm in length are occasionally observed but do not maintain this length for more that the 1-min interval of the original time-lapse series (Shaw *et al.*, 1997b).

Altering protein complex stoichiometry can reveal information about protein function not apparent from traditional genetic analysis. Extreme overexpression of the dynein–GFP (8 hr of induction) had unexpected consequences for the integrity of the spindle pole. In 2 of the 14 cells we imaged that had dynein–GFP levels 15- to 20-fold higher than normal, we observed a fragmentation of the

spindle pole body (Fig. 3). MTOC fragmentation did not occur in cells expressing other GFP fusion proteins, regardless of expression level [tubulin–GFP, cyclin–GFP, and nuf2–GFP (S. Shaw and K. Bloom, unpublished results)]. Time-lapse imaging revealed that the astral microtubules attached to the new fragment were dynamic and that the fragment center remained in proximity to the nucleus, represented by the dark area in the cell in Fig. 3. Spindle elongation occurs between the two original spindle poles oriented along the mother bud axis, with no apparent regard for the new fragment.

A role for dynein in spindle pole organization has been demonstrated for animal cells by reconstitution of spindle components in an *in vitro* extract system (Walters and Salmon, 1997) and *in vivo* by injection of components of the dynein

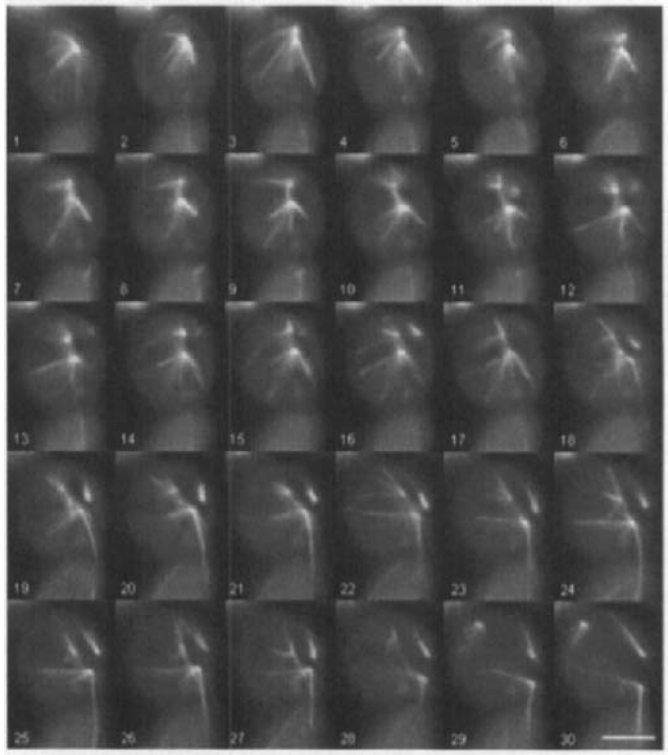

Fig. 3 Fragmentation of the spindle pole body in a cell overexpressing dynein–GFP. A time-lapsed series (3-min intervals shown) of a large budded cells, with bud facing down and out of the micrograph, containing extremely high dynein–GFP levels. Astral microtubules are hyperelongated but remain dynamic. Separation of spindle poles (1–6) is followed by the fragmentation of the pole distal to the bud with the fragment appearing to the right (11–16). Note that the astral microtubules emanating from the new spindle pole remain dynamic. Astral microtubules from the bud-proximal pole remain oriented into the bud (19–30) as the nucleus undergoes anaphase in the mother cell (28–30). Spindle elongation appears to involve only the two original spindle poles and not the new fragment. Scale bar = 5 μm.

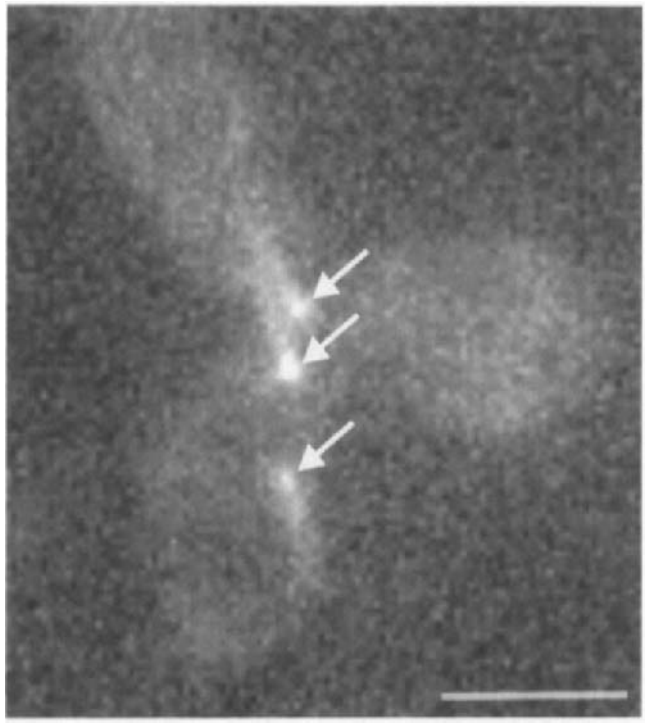

Fig. 4 Dynein–GFP overexpression during mating in *S. cerevisiae.* Zygote and first bud after mating are shown. The bud extends toward the upper left corner. Arrows mark three spindle pole bodies where only two are expected. Scale bar = 5 μm.

or dynactin complexes (p50; Echeverri *et al.,* 1996). A complex of proteins, including dynein and dynactin, has been postulated to organize the pole. Multiple proteins tether a large number of microtubules to the relatively small centrosomes (Waters and Salmon, 1997). No function for dynein at the spindle pole has been found in yeast even though dynein decorates each pole (Eshel *et al.,* 1993; Li *et al.,* 1993; Shaw *et al.,* 1997b) (Fig. 4). The occasional fragmentation of the MTOC in the presence of a vast excess of dynein–GFP may suggest a role for dynein in maintaining MTOC cohesion in yeast as well as mammalian cells.

Early attempts to image the kinetics of cell cycle progression with DIC microscopy led to the establishment of critical kinetic parameters of the cell division process and to mitosis in particular. The advent of multimode imaging together with the utility of the GFP allow *in vivo* analysis and kinetic parameters to be explored for the entirety of proteins comprising the yeast genome.

References

Adams, A. E. M., and Pringle, J. R. (1984). Relationship of actin and tubulin distribution to bud growth in wild-type and morphogenetic-mutant *Saccharomyces cerevisiae. J. Cell Biol.* **98,** 934–945.

Amberg, D. C., Zahner, J. E., Mulholland, J. W., Pringle, J. R., and Botstein, D. (1997). Aip3p/Bud6p, yeast actin-interacting protein that is involved in morphogenesis and the selection of bipolar budding sites. *Mol. Biol. Cell* **8,** 729–753.

Bi, E., Maddox, P., Lew, D. J., Salmon, E. D., McMillan, J. H., Yeh, E., and Pringle, J. R. (1998). Roles of a nonessential actomyosin contractile ring and of the septins in *Saccharomyces cerevisiae* cytokinesis. Submitted for publication.

Byers, B. (1981). *In* "The Molecular Biology of the Yeast *Saccharomyces:* Life Cycle and Inheritance" (J. N. Strathern, E. W. Jones, and J. R. Broch, eds.), pp. 59–96. Cold Spring Harbor Laboratory Press, Cold Spring Harbor, NY.

Byers, B., and Goetsch, L. (1975). Behavior of spindles and spindle plaques in the cell cycle and conjugation of *Saccharomyces cerevisiae. J. Bacteriol.* **124,** 511–523.

Carminati, J. L., and Stearns, T. (1997). Microtubules orient the mitotic spindle in yeast through dynein-dependent interactions with the cell cortex. *J. Cell Biol.* **138,** 629-641.

Cottingham, F. R., and Hoyt, M. A. (1997). Mitotic spindle positioning in *Saccharomyces cerevisiae* is accomplished by antagonistically acting microtubule motor proteins. *J. Cell Biol.* **138,** 1041–1053.

Dezwaan, T. M., Ellingson, E., Pellman, D., and Roof, D. M. (1997). Kinesin-related KIP3 of *Sacchromyces cerevisiae* is required for a distinct step in nuclear migration. *J. Cell Biol.* **138,** 1023–1040.

Echeverri, C. J., Paschal, B. M., Vaughan, K. T., and Vallee, R. B. (1996). Molecular characterization of the 50-kD subunit of dynactin reveals function for the complex in chromosome alignment and spindle organization during mitosis. *J. Cell Biol.* **132,** 617–633.

Eshel, D., Urrestarazu, L. A., Vissers, S., Jauniaux, J. C., van Vliet-Reedijk, J. C., Planta, R. J., and Gibbons, I. R. (1993). Cytoplasmic dynein is required for normal nuclear segregation in yeast. *Proc. Natl. Acad. Sci. USA* **90,** 11172–11176.

Etcheverry, T. (1990). *Methods Enzymol.* **185,** 319–329.

Finger, F. P., Hughes, T. E., and Novick, P. (1998). Sec3p is a spactial landmark for polarized secretion in budding yeast. *Cell* **92,** 559–571.

Futcher, B., and Carbon, J. (1986). Toxic effects of excess cloned centromeres. *Mol. Cell. Biol.* **6,** 2213–2222.

Hinnebusch, A. G. (1992). *In* "The Molecular and Celluar Biology of the Yeast *Saccharomyces*" (E. W. Jones, J. R. Pringle, and J. R. Broach, eds.), pp. 319–414. Cold Spring Harbor Laboratory Press, Cold Spring Harbor, NY.

Inoué, S., and Spring, K. (1997). *Video Microscopy,* 2nd ed. Plenum, New York.

Jones, E. W., and Fink, G. R. (1982). *In* "The Molecular Biology of the Yeast *Saccharomyces:* Metabolism and Gene Expression" (J. N. Strathern, E. W. Jones, and J. R. Broach, eds.), pp. 181–299. Cold Spring Harbor Laboratory Press, Cold Spring Harbor, NY.

Jones, H. D., Schliwa, M., and Drubin, D. G. (1993). Video microscopy of organelle inheritance and motility in budding yeast. *Cell Motil.* **25,** 129–142.

Kahana, J. A., Schnapp, B. J., and Silver, P. A. (1995). Kinetics of spindle pole body separation in budding yeast. *Proc. Natl. Acad. Sci. USA* **92,** 9707–9711.

Koning, A. J., Lum, P. Y., William, J. M., and Wright, R. (1993). DiOC6 staining reveals organelle structure and dynamics in living cells. *Cell Motil. Cytoskel.* **25,** 111–128.

Li, Y. Y., Yeh, E., Hays, T., and Bloom, K. (1993). Disruption of mitotic spindle orientation in a yeast dynein mutant. *Proc. Natl. Acad. Sci. USA* **90,** 10096–10100.

Lippincott, J., and Li, R. (1998). Sequential assembly of myosin II, an IQGAP-like protein, and filamentous actin to a ring structure involved in budding yeast cytokinesis. *J. Cell Biol.* **140,** 355–366.

Longtine, M. S., McKenzie, A., III, Demarini, D. J., Shah, N. G., Wach, A., Brachat, A., Philippsen, P., and Pringle, J. R. (1998). Additional modules for versatile and economical PCR-based gene deletion and modification in *Saccharomyces cerevisiae. Yeast* **14,** 953–961.

Moreland, R. B., Langevin, L. L., Singer, R. H., Garcea, R. L., and Hereford, L. M. (1987). Amino acid sequences that determine the nuclear localization of yeast histone 2B. *Mol. Cell. Biol.* **7,** 4048–4057.

Mumberg, D., Muller, R., and Funk, M. (1994). Regulatable promoters of *Saccharomyces cerevisiae:* Comparison of transcriptional activity and their use for heterologous expression. *Nucleic. Acids Res.* **22,** 5767–5768.

Niedenthal, R. K., Riles, L., and Hegeman, J. H. (1996). Green fluorescent protein as a marker for gene expression and subcelluar localization in budding yeast. *Yeast* **12,** 773–786.

Patterson, G., and Piston, D. (1998). Quantitative imaging of TATA-binding protein (TBP) in living yeast cells. Submitted for publication.

Pringle, J. R., Preston, R. A., Adams, A. E. M., Stearns, T., Drubin, D. G., Haarer, B. K., and Jones, E. W. (1989). Fluorescence microscopy methods for yeast. *Methods Cell Biol.* **31,** 338–437.

Resnick, M. A., Westmoreland, J., and Bloom, K. (1990). Heterogeneity and maintenance of centromere plasmid copy number in *Saccharomyces cerevisiae. Chromosoma* **99,** 281–288.

Salmon, E. D., Inoué, T., Desai, A., and Murray, A. W. (1994). High resolution multimode digital imaging system for mitosis studies in vivo and in vitro. *Biol. Bull.* **187,** 231–232.

Salmon, E. D., Shaw, S. L., Waters, J., Waterman-Storer, C. M., Maddox, P. S., Yeh, E., and Bloom, K. (1998). *In* "Methods in Cell Biology: Video Microscopy" (G. Sluder and D. D. Wolf, eds.), Vol. 56. Academic Press, London.

Shaw, S. L., Yeh, E., Bloom, K., and Salmon, E. D. (1997a). Imaging green fluorescent protein fusion proteins in *Saccharomyces cerevisiae. Curr. Biol.* **7,** 701–704.

Shaw, S. L., Yeh, E., Maddox, P., Salmon, E. D., and Bloom, K. (1997b). Astral microtubule dynamics in yeast: A microtubule-based searching mechanism for spindle orientation and nuclear migration into the bud. *J. Cell Biol. 139,* 985-994.

Solomon, F., (1991). *Annu. Rev. Cell Biol.* **7,** 633–662.

Straight, A. F., Belmont, A. S., Robinett, C. C., and Murray, A. W. (1996). GFP tagging of budding yeast chromosomes reveals that protein–protein interactions can mediate sister chromatid cohesion. *Curr. Biol.* **6,** 1599–1608.

Straight, A. F., Marshall, W. F., and Murray. A. W. (1997). Mitosis in living budding yeast: Anaphase a but no metaphase plate. *Science* **277,** 574.

Waters, J. C., and Salmon, E. D. (1997). Pathways of spindle assembly. *Curr. Opin. Cell Biol.* **9,** 37–43.

Yang, S. S., Yeh, E., Salmon, E. D., and Bloom, K. S. (1997). Identification of a mid-anaphase checkpoint in budding yeast. *J. Cell Biol.* **136,** 345–354.

Yeh, E., Skibbens, R. V., Cheng, J. W. Salmon, E. D., and Bloom, K. (1995). Spindle dynamics and cell cycle regulation of dynein in the budding yeast, *Saccharomyces cerevisiae. J. Cell Biol.* **103,** 687–700.

This Page Intentionally Left Blank

CHAPTER 20

The Use of *Xenopus* Egg Extracts to Study Mitotic Spindle Assembly and Function *in Vitro*

Arshad Desai,[*] Andrew Murray,[†] Timothy J. Mitchison,[‡] and Claire E. Walczak[‡]

[*] Department of Biochemistry and Biophysics,[†] Department of Physiology, and [‡]Department of Cellular and Molecular Pharmacology
University of California at San Francisco
San Francisco, California 94143-0450

METHODS IN CELL BIOLOGY, VOL. 61

0091-679X/99 $30.00

I. Introduction

Since Flemming first described mitosis more than a century ago, understanding the mechanisms underlying cell division has been a major focus in cell biology (Flemming, 1965). Over the years, the study of cell division has evolved from a detailed description of mitosis by the early cytologists to a modern molecular investigation. Essential for this evolution has been the development of experimental systems in which molecular and observational studies can be linked. Extracts from unfertilized *Xenopus* eggs provide one such system. These extracts are capable of maintaining specific cell cycle states and carrying out many of the events associated with cell division *in vitro* (Lohka and Masui, 1983; Blow and Laskey, 1986; Hutchison *et al.*, 1988; Murray and Kirschner, 1989). In addition to providing fundamental insights into the nature of the cell cycle, these extracts have been very useful for dissecting downstream mitotic processes, such as regulation of microtubule dynamics, chromosome condensation, mitotic spindle assembly, sister chromatid separation, anaphase chromosome movement, and kinetochore assembly (Lohka and Maller, 1985; Belmont *et al.*, 1990; Verde *et al.*, 1990; Hirano and Mitchison, 1991; Sawin and Mitchison, 1991; Shamu and Murray, 1992; Murray *et al.*, 1996; Desai *et al.*, 1997, 1998). A hallmark of studies in *Xenopus* extracts has been the combination of detailed structural and functional analysis of complex macromolecular assemblies such as the mitotic spindle with the manipulation of selected components. Similar feats have been difficult to accomplish in genetic systems such as budding yeast because the cytology is limiting and the biochemistry is difficult. Furthermore, *Xenopus* extracts also provide insight into the mechanisms of vertebrate mitosis, the details of which may not be revealed from studies in lower eukaryotes.

The two most useful attributes of *Xenopus* extracts are their ability to maintain specific cell cycle states and to recapitulate many of the detailed morphological changes associated with mitosis. Both of these features depend on the natural cell cycle arrest of the frog egg and on the ability to make concentrated extracts that retain many of the properties of intact cytoplasm. Mature *Xenopus* eggs are arrested in metaphase of meiosis II by an activity termed cytostatic factor (CSF), which is thought to be the product of the c-*mos* protooncogene (Sagata *et al.*, 1989). Sperm entry triggers a calcium spike that initiates a series of events leading to the destruction of CSF and exit from the meiosis II metaphase arrest. This calcium sensitivity of the CSF arrest is exploited in the preparation of extracts by use of the calcium chelator EGTA. The presence of EGTA in buffers results in extracts that maintain the CSF arrest (referred to as CSF extracts) but can be induced to exit the CSF arrest by addition of calcium (Lohka and Maller,

1985). This convenient control of cell cycle state allows one to easily obtain *in vitro* spindles with replicated chromosomes as described later in detail. It should be noted that CSF extracts are meiotic (meiosis II) and not mitotic cytoplasm, a distinction that has not generally been made in the literature. However, given the mechanistic similarity of meiosis II and mitosis, studies using CSF extracts should be generally relevant to the study of mitosis, and several phenotypes of depletion of spindle assembly components in CSF extracts have also been observed in antibody-injection experiments in somatic cells (Sawin *et al.,* 1992; Blangy *et al.,* 1995; Gaglio *et al.,* 1995, 1996, 1997; Merdes *et al.,* 1996; Heald *et al.,* 1997) as well as with genetic analysis of mitotic mutants (Enos and Morris, 1990; Hagan and Yanagida, 1990; Hoyt *et al.,* 1992; Roof *et al.,* 1992).

In this chapter, we will present detailed methods for the preparation of CSF extracts and for performing spindle assembly reactions. We will also describe methods for depleting specific components from extracts, an approach that has been used successfully to determine the contributions of both motor and nonmotor components to spindle assembly (Sawin *et al.,* 1992; Merdes *et al.,* 1996; Walczak *et al.,* 1996, 1997). Finally, we will describe methods for analyzing anaphase *in vitro* (Murray *et al.,* 1996). We recommend that anyone interested in using *Xenopus* egg extracts as an experimental system should first consult Murray (1991) who provides an introduction to the early stages of the *Xenopus* life cycle, documents the history of cell cycle extracts, provides detailed technical descriptions on the preparation of different types of extracts, and gives advice on troubleshooting problems with extracts; Murray's article serves as the basis for several of the procedures described here.

II. Preparation of CSF Extracts for Spindle Assembly

A. Requirements for Extract Preparation

1. Buffer and Reagent Stocks

10× MMR
- 50 m*M* Na–Hepes, pH to 7.8 with NaOH
- 1 m*M* EDTA
- 1 *M* NaCl
- 20 m*M* KCl
- 10 m*M* $MgCl_2$
- 20 m*M* $CaCl_2$
- Autoclave and store at room temperature (RT); if desired, MMR can also be prepared as a 25× stock

20X XB salts
- 2 *M* KCl
- 20 m*M* $MgCl_2$

2 m*M* $CaCl_2$
Sterile filter and store at 4°C

2 M Sucrose
Sterile filter or autoclave and store at 4°C or in aliquots at −20°C

1 M K-Hepes
pH to 7.7 with KOH, sterile filter and store at 4°C or in aliquots at −20°C

0.5 M K-EGTA
pH to 7.7 with KOH, sterile filter and store at RT

1 M $MgCl_2$
Sterile filter and store at RT

20X energy mix
150 m*M* creatine phosphate
20 m*M* ATP
20 m*M* $MgCl_2$
Store in 100-μl aliquots at −20°C

Protease inhibitors (LPC)
10 mg/ml each of leupeptin, pepstatin A, and chymostatin dissolved in DMSO; store in 100-μl aliquots at −20°C

Cytochalasin B or D
10 mg/ml in DMSO; store in 10- or 50-μl aliquots at −20°C
(Note: Both protease inhibitors and cytochalasin stocks can be frozen and thawed multiple times without detriment)

5% Gelatin (w/v)
Dissolved in water; autoclave and store in aliquots at −20°C

Cysteine, free base
Sigma No. C-7755

Versilube F-50
ANDPAK-EMA

Hormone stocks for priming frogs and inducing ovulation
Pregnant mare serum gonadotropin (PMSG): 100 U/ml (Calbiochem No. 367222) made up in water and stored at −20°C
Human chorionic gonadotropin (hCG): 1000 U/ml (Sigma No. CG-10) made up in water and stored at 4°C
(Hormones are injected into the dorsal lymph sac using a 27-gauge needle)

2. Equipment

Glass petri dishes
60-, 100-, 150-mm-diameter regular and 150-mm-diameter high-sided, i.e., 150-mm diameter and 75-mm height

13 X 51-mm Ultraclear tubes (Beckman No. 344057)

Ultracentrifuge and SW50.1/SW55.1 rotor
Clinical centrifuge

3. Primed Frogs

Frogs for extract preparation are primed using progesterone (present in PMSG) which induces maturation of oocytes. Priming is performed in two steps by injection with 50 U of PMSG (0.5 ml of 100 U/ml stock) on Day 1 and 25 U of PMSG (0.25 ml) on Day 3. Primed frogs are stored in dechlorinated water containing 2 g/liter rock salt in a cool room (ambient temperature of 16–20°C) and can be induced to lay eggs for up to 2 weeks after the second priming.

B. Protocol for Extract Preparation

1. Day before Extract Preparation

Sixteen to 18 h before extract preparation, four to six primed frogs are induced to ovulate by injection with 500 U (0.5 ml) of hCG. After injection, frogs are rinsed well in distilled water, put individually into plastic buckets (Fisher No. 03-484-21) containing two liters MMR, and stored overnight in a 16°C incubator.

2. Setup for Extract Preparation

For a four to six frog prep, you will need the following prior to beginning the prep:

a. Buffers

Prepare just before use unless indicated otherwise; all graduated cylinders and glassware should be rinsed well with double-distilled water (dd H_2O) prior to use.

Two or three liters 1X MMR (the MMR can be made the night before and stored in a plastic carboy in the 16°C incubator)

200 ml dejellying solution: 2% (w/v) cysteine in 1X XB salts; pH to 7.8 by adding 0.9 ml of 10 *N* NaOH

750 ml XB: 10 m*M* K-Hepes (pH 7.7), 100 m*M* KCl, 1 m*M* $MgCl_2$, 0.1 m*M* $CaCl_2$, and 50 m*M* sucrose; prepare using 20X XB salts, 2 *M* sucrose, and 1 *M* K-Hepes (pH 7.7) stocks; to maintain a pH of 7.7 at 10 m*M* Hepes, add 11 μl 10 *N* KOH per 100 ml XB

250 ml CSF-XB: XB + 1 m*M* $MgCl_2$ + 5 m*M* EGTA; to prepare, transfer 250 ml of XB (from the 750 ml prepared previously) to a separate graduated cylinder and add EGTA to 5 m*M* and $MgCl_2$ to 1 m*M* final

100 ml CSF-XB + PIs: CSF-XB + 10 μg/ml LPC; to prepare, transfer 100 ml of CSF-XB (from the 250 ml prepared previously) to a separate graduated cylinder and add LPC to 10 μg/ml (mix immediately after adding LPC)

b. Equipment, etc.

SW55.1 or SW50.1 rotor at 16°C in ultracentrifuge

Two Pasteur pipettes with tips broken and fire polished to ~3 or 4-mm diameter

Four to six 13 × 51-mm Ultraclear tubes

Two 150-mm regular petri dishes, one high-sided 150-mm petri dish; rinse well with dd H_2O and coat with 100 μg/ml gelatin (thaw gelatin at 37°C, pour ~30 ml MMR into petri dish, pipet in 60 μl of gelatin and swirl well for ~30 sec, and pour out MMR and replace with XB); if making a squeezed egg extract in parallel (see Section VII,A) gelatin coat four 60-mm petri dishes (15 ml MMR and 30 μl gelatin) and fill with MMR for squeezing frogs into dishes, and coat one 100-mm petri dish for processing the squeezed eggs after dejellying

600-ml glass beaker (rinsed well with dd H_2O)

C. General Considerations for Preparing Spindle Assembly Extracts

Spindle assembly is best performed using freshly prepared extracts because freezing extracts considerably decrease their ability to form bipolar spindles. For spindle assembly extracts, egg quality must take precedence over egg quantity. Because 1 or 2 ml of extract is more than sufficient for most experiments, it is best not to use any batches of eggs containing significant numbers (>10%) of lysed eggs, activated eggs (detected by contraction of dark pigment at the animal pole), or "puffballs" (eggs which are swollen and often white and puffy). Strings of eggs which do not have fully separated jelly coats can be used as a last resort unless they contain a high percentage of deformed or activated eggs. Any batches of eggs which are distinguishable in quality should be processed separately. Although the best spindle assembly extracts are often made from freshly squeezed eggs, we have had good success with laid eggs and will focus here on their use. Further discussion of squeezed egg extracts is presented in Section VII,A.

For laid eggs, extract preparation should begin 16–18 hr after hCG injection. We recommend that the temperature of the buffers and the room in which eggs will be manipulated not exceed 23°C (ideally 18–20°C). Warmer temperatures will almost certainly result in lower quality extracts. Rinsing of eggs after dejellying is best performed in gelatin-coated petri dishes by swirling the dishes a couple of times and pouring out the buffer. Never pour solutions directly onto the dejellied eggs because they are quite fragile. Pour the solutions down the side of the wash vessel, and then gently swirl the eggs. Maximal buffer exchange in petri dishes can be achieved by turning the dish away from you and quickly removing buffer at the edge of the egg mass using a wide-bore Pasteur pipet prior to pouring in the next wash buffer. During the washes, the eggs should be "gardened," i.e., visibly deformed eggs, activated eggs, puffballs, and large pieces of debris should be removed using the wide-bore Pasteur pipets. However, one should not get so caught up in removing bad eggs and debris that this slows the preparation of

the extract. Time is another important variable. Generally it should be possible to go from collecting of eggs to the crushing spin in 45 min to 1 hr.

D. Procedure for Extract Preparation

1. Combine batches of good laid eggs and remove as much MMR as possible.
2. Wash eggs in 2 or 3 liter of MMR until all of the debris is removed. Combine good egg batches in a frog bucket, rinse a couple of times with MMR, and pour the eggs into a 600-ml beaker for the rest of the MMR washes. Since eggs settle quickly, pouring out the MMR immediately after the eggs have settled allows easy removal of debris. Eggs should be gardened during this step and during washes after dejellying.
3. Remove as much MMR as possible and rinse eggs into dejellying solution.
4. Swirl gently and intermittently in the dejellying solution. While the eggs are dejellying, pipet 1 ml of CSF-XB + PIs to each 13 × 51-mm Ultraclear centrifuge tube and add 10 μl of 10 mg/ml cytochalasin B/D per tube (flick the tube well immediately after pipeting in the cytochalasin or it will precipitate).
5. After eggs are dejellied (this will take 7–10 min and the volume will decrease approximately five-fold; eggs will pack tightly and orient with their vegetal poles down), remove as much dejellying solution as possible, rinse eggs with residual dejellying solution and once with XB, then transfer eggs to gelatin-coated petri dishes. Wash dejellied eggs three or four times with XB in the petri dish as described in Section II,C. For larger batches of eggs, we recommend using the high-sided 150-mm petri dishes.
6. Wash eggs two or three times in CSF-XB. Remove as much buffer as possible.
7. Wash eggs twice in CSF-XB + PIs. Leave eggs in a small volume of CSF-XB + PIs after the second wash.
8. Draw eggs up into the wide-bore Pasteur pipet and slowly drop them into the 1-ml CSF-XB + PIs + 100 μg/ml cytochalasin solution in the ultraclear tube. Insert the pipet below the meniscus to break the surface tension and gently release eggs into the solution. Minimize transfer of buffer along with the eggs.
9. Aspirate excess buffer from the top of the eggs.
10. Put the ultraclear tubes into 14-ml polypropylene round-bottom culture tubes (Falcon No. 2059) and spin for 10 sec at setting No. 4 (approx. 1500 rpm) in a clinical centrifuge.
11. Gently aspirate buffer from top of the eggs and layer on 0.75–1 ml of Versilube F-50. Use of versilube minimizes dilution during extract preparation. The density of versilube is intermediate between that of buffer and cytoplasm; thus, versiluble displaces buffer between the eggs during the packing spin but floats to the top of the cytoplasmic layer during the crushing spin.

12. Pack the eggs by spinning at setting No. 5 for 30 sec (2000 rpm) and full speed (No. 7) for 15 sec (2500–3000 rpm) in the clinical centrifuge.

13. Aspirate all buffer and versilube from the top of the packed eggs.

14. Transfer the tubes containing the packed eggs to the SW55.1 rotor in the ultracentrifuge. Crush the eggs by centrifugation at 10,000 rpm for 15 min at 16°C (full brake).

15. Store tubes with crushed eggs on ice. The light yellow layer on top represents the lipid droplets and the dark layer on the bottom contains the yolk and nuclei. The cytoplasmic layer is the muddy or straw-colored layer in the middle of the tube. Prior to collecting the cytoplasmic layer, wipe the sides of the tubes with 95% ethanol. Puncture the tube near the bottom of the cytoplasmic layer with an 18-gauge needle (on a 1-cc syringe), and gently draw out the extract. [See Fig. 3 of Murray (1991) for a picture of an extract.] We find it best to use a new needle for each centrifuge tube. Transfer the collected extract to a 5-ml snap cap tube and estimate its volume.

16. Add 1/1000 volume of protease inhibitor (LPC) and cytochalasin stocks, 1/20 volume of 20× energy mix, and 1/40 volume of 2 *M* sucrose. Note that some people do not add additional sucrose to the extract after preparation, but we find that it often helps stabilize the extract during immunodepletions (see Section V,A).

E. Preparation and Use of Sperm Nuclei and Fluorescent Tubulin

Sperm nuclei are prepared exactly as described by Murray (1991) and stored in small aliquots at −80°C at a density of $1–5 \times 10^7$/ml. Sperm nuclei can be frozen and thawed multiple times without apparent loss of activity, but we prefer to store them in small aliquots and only freeze–thaw once for spindle assembly reactions. Sperm nuclei are added to extracts at a 1/100–1/200 dilution yielding a final concentration of 100–300 nuclei/μl.

Fluorescent tubulin is used to monitor microtubule distributions during spindle assembly and is prepared by the high pH labeling protocol described by Hyman *et al.,* (1991). Fluorescein, tetramethyl rhodamine, or X-rhodamine-labeled tubulin can be used to monitor spindle assembly. We generally use X-rhodamine-labeled tubulin because it has better spectral separation from fluorescein than does tetramethyl rhodamine, allowing double-label immunofluorescence studies with fluorescein-conjugated secondary antibodies (see Section IV). Our X-rhodamine-labeled tubulin preps have final concentrations varying between 15 and 25 mg/ml with labeling stoichiometries between 0.5 and 1. For monitoring spindle assembly, we add X-rhodamine tubulin to the extract at a final concentration of 20–50 μg/ml (generally a 1/400 dilution). Although tubulin by itself is highly unstable, it appears to be very stable in the extract and can be added immediately after extract preparation.

III. Spindle Assembly Reactions

Three types of spindle assembly reactions have been described in the literature (Sawin and Mitchison, 1991; Heald *et al.,* 1996). In the first type of reaction, termed CSF spindle assembly, each sperm nucleus added to the extract drives the formation of a half spindle. Two such half spindles then fuse to form a bipolar mitotic spindle (Fig. 1, top) (Sawin and Mitchison, 1991). Thus, two haploid sperm nuclei drive the formation of a single bipolar spindle. In the second type of reaction, termed cycled spindle assembly or interphase-to-mitosis spindle assembly, calcium is added to a CSF extract containing sperm nuclei, inactivating the CSF arrest and driving the extract into interphase. As the nuclei in the extract cycle through interphase their DNA is replicated once (Sawin and Mitchison, 1991). Fresh CSF extract without any sperm nuclei is then added to drive the extract containing replicated sperm nuclei into metaphase. In this type of spindle assembly reaction, each sperm nucleus undergoes one round of replication and drives the formation of a bipolar mitotic spindle (Fig. 1, bottom). Cycled spindles containing replicated chromosomes are arrested in metaphase by CSF; addition of calcium for a second time results in inactivation of CSF and anaphase chromosome segregation (Shamu and Murray, 1992). Heald and coworkers (1996) described the assembly of spindles around DNA-coated beads in extracts. These studies demonstrated that chromatin-coated beads are sufficient to generate a bipolar mitotic spindle in the absence of centrosomes and kinetochores. A study describing the use of DNA-coated beads for studying spindle assembly has been presented recently (Heald *et al.,* 1998).

A. General Considerations for Spindle Assembly Reactions

Xenopus extracts are a powerful tool for studying mitosis but their use can be very frustrating because of high variability. These extracts are very sensitive to physical perturbations and must be treated gently to ensure the best results. Avoid pipeting up and down vigorously with narrow-bore pipet tips or dropping tubes containing extract reactions since either of these can sufficiently perturb the extract to disrupt the spindle assembly process. We recommend pipeting with either commercially available wide-bore P-200 tips (Rainin HR-250W) or regular P-200 tips that have been cut off to an opening of ~2 mm diameter and mixing by either gently tapping the bottom of the tube or inverting the tube two or three times. Use a fresh pipet tip for each aliquot, especially for experiments requiring quantitation because these extracts are very viscous. Never vortex a tube containing extract because this will surely destroy the extract. Finally, avoid diluting the extract with buffer or other reagents because this can also inhibit spindle assembly (see Section V,B).

To set up spindle assembly reactions, add sperm nuclei and labeled tubulin to a large volume of extract and then aliquot it into individual reactions. The extract is very viscous and difficult to pipet accurately. Use a fresh pipet tip for

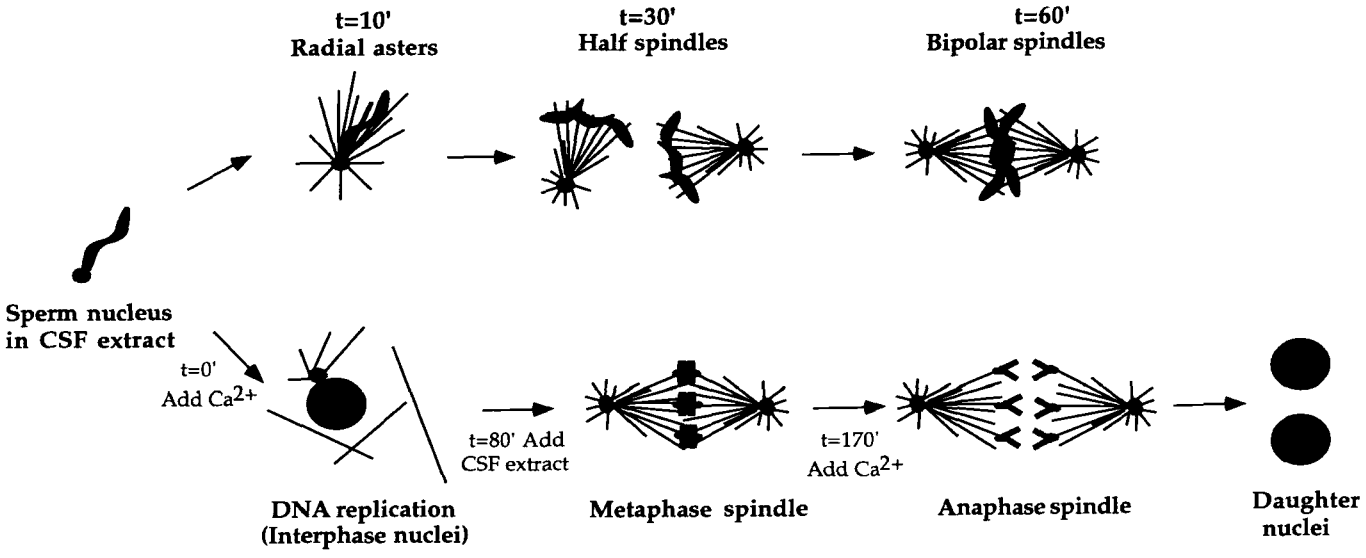

Fig. 1 The *in vitro* spindle assembly pathways. (Top) CSF spindle assembly. (Bottom) Cycled spindle assembly.

each aliquot to ensure reproducibility and allow for a 20% volume loss upon aliquoting. Do not exceed a reaction volume of >50 μl/1.5 ml Eppendorf tube since larger reaction volumes tend to inhibit spindle assembly. We recommend incubating reactions at 20°C in a cooled water bath (a home-made one can be a plastic tray containing water with some ice to maintain 20°C). However, if the room temperature is stable from day to day and does not exceed 24 or 25°C, then the reactions can be incubated on the bench top.

B. Reagents Required for Spindle Assembly

Sperm nuclei at 1–5 × 10^7/ml

Fluorescently labeled tubulin

Extract fix: 60% (v/v) glycerol, 1× MMR, 1 μg/ml Hoechst 33342/33258, 10% formaldehyde [from 37% (w/v) stock]

Sperm dilution buffer (1×): 10 m*M* Hepes (pH 7.7), 1 m*M* $MgCl_2$, 100 m*M* KCl, 150 m*M* sucrose, 10 μg/ml cytochalasin B/D; can be prepared as a 5× stock; both 1× buffer and 5× stock should be stored at −20°C

10× calcium: 4 m*M* $CaCl_2$ in 1× sperm dilution buffer

C. CSF Spindle Assembly

To CSF extract containing labeled tubulin add sperm nuclei to a final concentration of 100–300/μl. Mix gently, aliquot 25 μl/tube, and incubate at 20°C. At 15, 30, 45, and 60 min take samples to test the progress of the reaction as follows: pipet a 1-μl aliquot of the reaction on a microscope slide, overlay with 3 μl of extract fix, cover gently with an 18 × 18-mm coverslip, and view by fluorescence microscopy. At the 15-min time point, small microtubule asters emanate from the sperm centrosome (Fig. 2, top); these often have a very dense core of microtubules. By 30 min the chromatin has migrated away from the centrosome, and the microtubules are polarized toward the chromatin: These structures are termed half spindles (Fig. 2, middle). Between 30 and 60 min, half spindles begin to fuse to form bipolar spindles (Fig. 2, bottom). During CSF spindle assembly, the percentage of total structures that are bipolar spindles varies considerably from extract to extract. In a typical extract, 40–60% of the total structures are bipolar spindles by the 60-min time point. This number can range from <10% in very poor extracts to >90% in the best extracts.

D. Cycled Spindle Assembly

For cycled spindle assembly the extract is divided into two tubes after the addition of labeled tubulin. One tube is supplemented with sperm nuclei and cycled into interphase by the addition of calcium, whereas the second tube is held on ice until it is needed to drive the extract with replicated sperm nu-

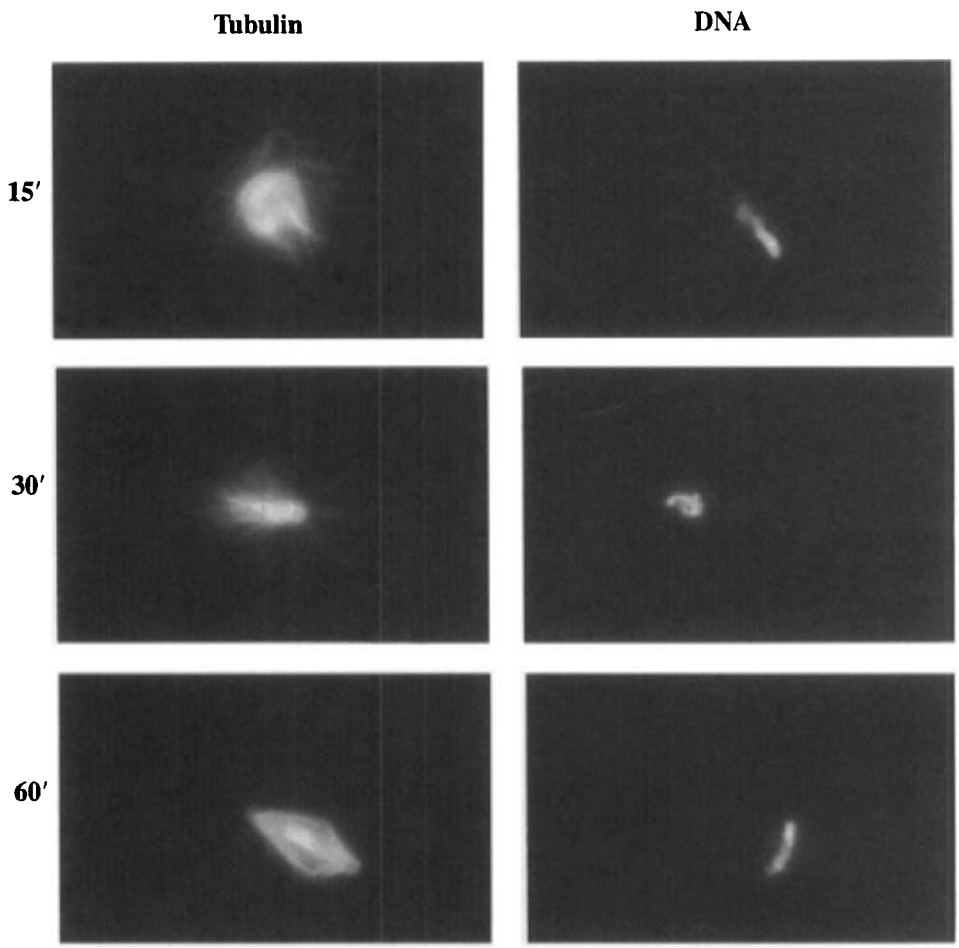

Fig. 2 Reaction intermediates of CSF spindle assembly reaction. Samples were removed from the reaction and sedimented onto coverslips as described in the text. The microtubules and chromatin structures formed during the reaction are shown for 15-, 30-, and 60-min time points.

clei back into metaphase. Specifically, to one-half of the extract containing labeled tubulin add sperm nuclei. Withdraw a small amount as a negative control (~20 μl), and to the rest add 1/10 volume of 10× calcium solution. Mix the calcium into the extract gently but thoroughly, aliquot 20-μl/tube, and incubate both the aliquot withdrawn prior to calcium addition and the reaction tubes supplemented with calcium at 20°C for 80 min. During this incubation the extract is monitored by taking samples at 30-, 45-, and 60-min time points as described in Section III,C. Reactions to which calcium was added should exit the CSF arrest and cycle through interphase; negative control sample (withdrawn before calcium addition) should remain in CSF (mitotic) arrest. Morphology of the

mitotic arrest was described in Section III,C. The reactions with calcium should appear as follows: after 30 min, the sperm nucleus should be swollen and many free microtubules should be present in the extract; after 45 min, the sperm nucleus should be large and round and resemble a typical mammalian cell interphase nucleus; after 60 min, the sperm nucleus should appear large and reticular much like an early prophase nucleus, suggesting that the extract may be starting to cycle back into metaphase. In our experience, extracts that have irregularly shaped interphase nuclei at the 45-min time point tend to be less robust in generating mitotic spindles. After 80 min at RT, 20 μl of CSF extract containing labeled tubulin but not sperm nuclei is added to each reaction (this represents an equal volume of extract added to the initial reaction), mixed in gently and incubated at 20°C for 60–90 min to allow establishment of the metaphase CSF arrest and formation of bipolar spindles. The reactions containing bipolar spindles can be held at RT for many hours without detriment, although with increased time the number of single bipolar spindles drops significantly because the spindles tend to aggregate laterally, forming large multipolar structures.

In general, cycled spindle assembly results in a more uniform distribution of structures than CSF spindle assembly and yields a higher proportion of bipolar spindles (80–90% of total structures at 60 min). Cycled spindles have chromosomes aligned in an equatorial plane, highly reminiscent of a metaphase plate in somatic cells (Fig. 3, top). However, the tightness of the metaphase plate in cycled spindles can vary significantly between extracts. In good extracts, the chromosomes are tightly focused at the spindle equator, whereas in less robust extracts, the chromosomes tend to be both at the spindle equator and scattered on either side of the equator. These less robust extracts generally do not work well for anaphase chromosome segregation (see Section VII).

The morphological pathway by which cycled spindles assemble remains to be clarified. Sawin and Mitchison (1991) first described the pathway as being chromatin driven, i.e., microtubules assembled in the region of the chromatin and with time organized into a bipolar structure with morphologically distinguishable poles. This pathway is similar to that described recently using chromatin-coated magnetic beads, with the exception that spindles assembled from sperm nuclei contain centrosomes. However, Boleti and coworkers (1996) reported that two distinct centrosomal arrays of microtubules are separated to opposite sides of the nucleus in a more classical somatic cell-type spindle assembly pathway. A clear picture of the cycled spindle assembly pathway awaits a thorough real-time study of this reaction using fluorescence video microscopy.

IV. Monitoring Spindle Assembly Reactions

A. Methods for Pelleting Spindles onto Coverslips

Spindle assembly reactions are routinely monitored using fixed squashes as described in Section III,C. However, for quantitative analysis we prefer to sedi-

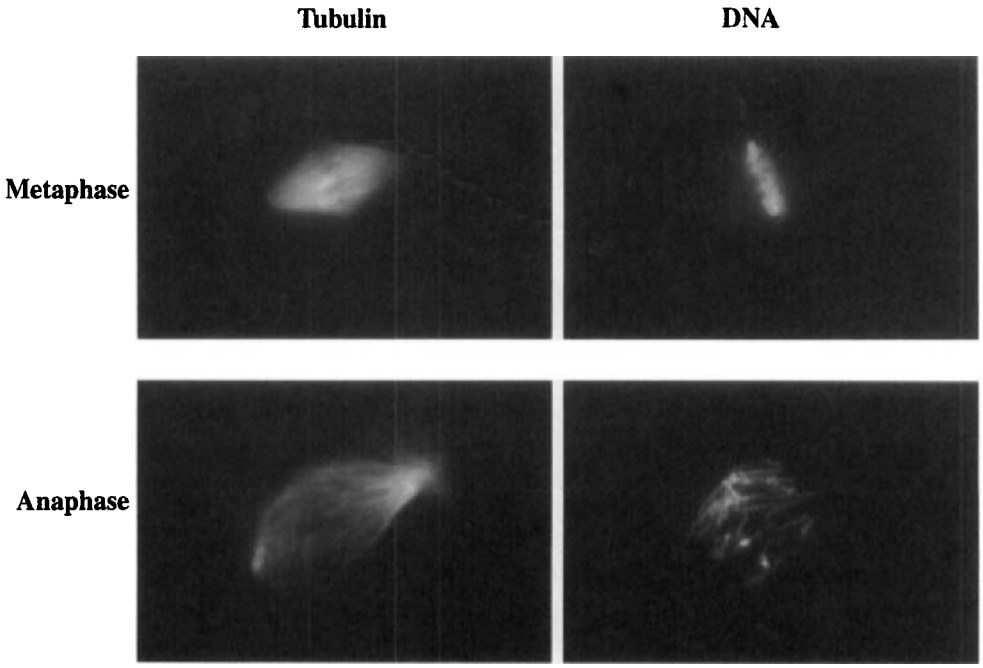

Fig. 3 Optimal fixation of spindle structures. Using the optimized fixation conditions it is possible to preserve chromosome structure and microtubule structure. (Top) Metaphase spindles assembled by the cycled spindle pathway. (Bottom) Spindles that have been induced to enter anaphase following calcium addition.

ment the spindles from a large volume (20 μl) of extract onto a coverslip. The advantages of sedimenting spindles onto coverslips are threefold. First, spindles from 20 μl of reaction are concentrated onto a 12-mm coverslip, providing a dense, relatively homogenous sample for quantitative analysis. Second, having the spindles fixed on coverslips allows one to perform immunofluorescence to analyze the localization of specific antigens on the *in vitro* spindles. Third, unlike squashes, the pelleted samples are very stable when stored at −20°C. This allows one to prepare many samples at once but analyze them when convenient and store them for any future reanalysis. We use two procedures for pelleting spindles onto coverslips. In the first (method 1), reactions are diluted extensively into a microtubule-stabilizing buffer, pelleted unfixed onto coverslips, and fixed onto the coverslips using methanol. Two limitations of this method are an extreme disruption of chromosome structure and day-to-day variability. Recently, we have developed an alternative method (method 2) that involves first diluting the spindles into a microtubule-stabilizing buffer and then fixing the spindles in solution using formaldehyde, pelleting the spindles onto coverslips, and postfixing using methanol. Using method 2 we have satisfied the demanding requirement

of retaining the fine structure of chromosomes as they are undergoing anaphase without causing significant disruption of spindle structure (Fig. 3, bottom).

1. Requirements for Pelleting Spindles onto Coverslips

BRB80
80 m*M* K-Pipes, pH 6.8
1 m*M* $MgCl_2$
1 m*M* EGTA
Make as 5X stock, sterile filter and store at 4°C

5-ml snap cap tubes (Sarstedt No. 55.526.006)

Dilution buffer
BRB-80
+ 30% (v/v) glycerol
+ 0.5% Triton X-100

Fixation buffer
BRB80
+ 30% (v/v) glycerol
+ 0.5% Triton X-100
+ 4% formaldehyde, added just before use from 37% stock

Cushion
BRB80
+ 40% (v/v) glycerol

Spindown tubes (Evans *et al.*, 1985)
With 12-mm coverslips and 4-ml cushion at room temperature

Coverslip holders
For 12-mm round coverslips; we like to use Thomas Scientific No. 8542-E40

−20°C methanol

TBS-TX
1X TBS [10 m*M* Tris (pH 7.4) and 150 m*M* NaCl]
0.1% Triton X-100

Mounting medium
0.5% *p*-phenelynediamine (free base) in 90% glycerol and 20 m*M* Tris–Cl, pH 9.0

2. Method 1

1. Prior to beginning the spindown procedure, prepare spindown tubes with coverslips and cushion and 5-ml snap cap tubes with 2 ml of dilution buffer. All buffers should be at RT.

2. Pipet 20 μl of spindle assembly reaction into the dilution buffer. Prior to transferring the extract into the dilution buffer, we often pipet up and down two or three times with a regular yellow tip to break any large aggregates.

3. Immediately cap the tube and mix by gently inverting four or five times.

4. Using a disposable plastic transfer pipet, layer the diluted sample onto the cushion in the spindown tube. After dilution, the spindles are stable; therefore, if a large number of samples are being pelleted, first do the dilution and mixing for all samples and then layer them sequentially onto cushions.

5. Centrifuge the tubes in an HS-4 rotor at 18°C for 20 min at 5500 rpm (6000*g*). We use the HS-4 because it can hold 16 tubes; an HB-4, HB-6, or equivalent rotor can be used for smaller numbers of tubes.

6. Aspirate until just below the sample–cushion interface, rinse with BRB80, aspirate off the rinse and the cushion, and transfer the coverslips to a coverslip holder.

7. After all coverslips are in the holder, fix by immersion in −20°C methanol for 3 min.

8. Rehydrate using two sequential 5-min incubations in TBS-TX.

9. Label DNA by rinsing coverslips with 1 μg/ml Hoechst in TBS-TX for 30 sec, mount in mounting medium, and seal with nail polish. Rinse top surface of coverslip with water prior to observation.

3. Method 2

Method 2 is different from method 1 as follows:

1. Dilute 20 μl of sample into 1 ml of dilution buffer as in step 2 of method 1.

2. Dilute all samples first, then add 1 ml of fixation buffer and mix well by inversion.

3. Fix for 5 min at RT prior to layering onto cushion.

4. After pelleting fixed spindles onto coverslips and aspirating the cushion after rinsing (step 6 in method 2) postfix the coverslips in −20°C methanol.

Using this method we have successfully preserved the fine structure of chromosomes (Fig. 3) without significantly compromising spindle structure.

Spindles pelleted onto coverslips using either method can be processed for immunofluorescence using antibodies to specific spindle components (Walczak *et al.*, 1996). After rehydrating in TBS-TX, coverslips are blocked in TBS-TX + 2% BSA (antibody dilution buffer or AbDil) for 15–30 min, incubated sequentially with primary and secondary antibodies diluted in AbDil, rinsed in TBS-TX containing 1 μg/ml Hoechst, and mounted as described previously. For localizing antibodies added to inhibit function of a particular component, only incubation with the appropriate secondary is necessary (Walczak *et al.*, 1997).

B. Time-Course Experiments

While characterizing the functions of spindle components using the CSF spindle assembly reaction, it is often desirable to monitor the intermediates in the path-

way. In order to set up time-course experiments for this purpose, it is important that samples for all time points are derived from a single pool of reaction mix and that they are sedimented onto coverslips at the same time. Specifically, to a volume of extract sufficient for all time points, add sperm nuclei and any other reagents, such as antibodies or dominant-negative fusion proteins, and store on ice. At various intervals beginning with $t = 0$ min, remove 25 μl and transfer to a tube at 20°C. At the end of the time course, pellet all samples onto coverslips using either of the methods described in Section IV,A.

V. Manipulation of Extracts

The ability to manipulate specific components in the extract by either immunodepletion or reagent addition and to assay the effects of these manipulations on spindle assembly is one of the main advantages of *Xenopus* egg extracts. A recent flurry of publications applying this strategy to dissect the role of both motor and nonmotor components during spindle assembly demonstrates the value of this approach (Sawin *et al.*, 1992; Vernos *et al.*, 1995; Boleti *et al.*, 1996; Heald *et al.*, 1996, 1997; Merdes *et al.*, 1996; Walczak *et al.*, 1996, 1997).

A. Immunodepletion of Extracts

The main difficulty with immunodepletion of CSF extracts is that they lose the CSF arrest during or soon after immunodepletion. In our experience, the following actions seem to aid in immunodepleting proteins without losing the CSF arrest:

1. During the CSF extract prep, after washing with XB, the eggs are washed thoroughly with CSF-XB without protease inhibitors (step 6 in Section II,D). This CSF-XB wash ensures that there is sufficient EGTA in the final extract to maintain a tight CSF arrest.

2. Eggs are crushed at 10,000 rpm (full brake) in a SW55 rotor at 16°C. Even a slightly faster spin (12,500 rpm) does not work well—one does not obtain robust spindle assembly after immunodepletion.

3. Antibodies are coated on BioRad Affi-Prep Protein A beads (BR No. 156-0006). Unlike regular protein A agarose beads, these high-density beads sediment readily through the viscous extract at speeds gentle enough to not perturb the extract.

4. Remove as much buffer as possible after coating the beads with antibody to avoid diluting the extract, which will inhibit spindle assembly.

5. Extracts are handled extremely gently during manipulations such as resuspending beads or sedimenting beads.

The ability to deplete a specific protein from the extract is dependent on both the quality of the antibody used for depletion and the abundance of the protein

being depleted. Regarding antibody quality, for reasons we do not understand, we have had much better success with antibodies prepared by immunizing with native proteins as opposed to antibodies generated against denatured proteins, e.g., proteins excised from acrylamide gels.

The following protocol is for depleting a protein present at ~10–20 μg/ml in the extract using high-affinity polyclonal antibodies. While this presents a good starting point, exact conditions must be optimized for each new antibody, particularly the amount of antibody needed for maximal depletion. As a control, we use an equivalent amount of random IgG from the same species; given the extreme perturbation of the extract by the immunodepletion procedure all interpretations of depletion phenotypes must be restricted to comparison with random IgG depletion performed at the same time and processed identically. The procedure for depletion is as follows:

1. Pipet 25 μl of Affi-Prep protein A beads (50 μl of slurry) into a 0.5-ml Eppendorf tube.
2. Wash beads three times with 0.5 ml TBS-TX [20 m*M* Tris (pH 7.4), 150 m*M* NaCl, and 0.1% Triton-X 100].
3. Add 4 μg of antibody and bring total volume to 200 μl using TBS-TX.
4. Bind antibody to beads at 4°C for 1 hr on rotator. Make sure beads are rolling around during the incubation.
5. Pellet beads in a microfuge for 20 sec, wash one time with TBS-TX and three times with CSFXB + PIs using 200 μl/wash. Remove as much buffer as possible to avoid diluting the extract.
6. Add 200 μl of extract to each tube and resuspend beads in extract very gently using a wide-bore P-200 tip; Do not pipet up and down more than three times and avoid tapping the tube or any other type of vigorous agitation.
7. Before the beads settle, rapidly place the tube on the rotator and rotate for 1 hr at 4°C. Make sure that the beads are mixing well with the extract during this period.
8. Pellet the beads for 20 sec in a microfuge and transfer the supernatant to a fresh tube—this is the depleted extract. It is difficult to recover more than 175 μl from a 200-μl depletion without contaminating the extract with the beads. Save a small amount of depleted extract to test the extent of depletion by immunoblotting.
9. To analyze what is bound to the beads, wash the beads two times with CSF-XB + PIs, three times with TBS-TX, and one time with TBS. Resuspend the beads in 50 μl SDS–PAGE sample buffer and boil to release the IgG–antigen complexes from the beads. Analyze the sample by SDS–PAGE and Coomassie brilliant blue staining.

Extracts that have been immunodepleted are far less robust than nondepleted extracts. A good CSF extract will remain mitotic for at least 6–10 hr on ice,

whereas a depleted extract will remain mitotic for a few hours at most. We find that with depleted extracts CSF spindle assembly proceeds normally, although the extent of bipolar spindle formation is reduced by twofold compared to the undepleted extract (Walczak *et al.*, 1997). At a frequency lower than that for CSF spindle assembly, we have successfully used immunodepleted extracts for cycled spindle assembly. We have yet to attempt anaphase chromosome segregation in depleted extracts.

We have tried to optimize the immunodepletion procedure to minimize perturbation of the extract but have yet to find the perfect conditions. We believe that the primary problem with immunodepletions is the physical perturbation of the extract by the beads as they are sloshing through the extract. Our most successful manipulation to minimize extract perturbation has been to reduce the time of depletion to 30–45 min instead of 1 hr. However, with lowered times we also see a reduced efficiency of depletion; we have yet to systematically investigate this issue. We have also wondered whether doing the depletions at RT might be better since calcium uptake machinery would sequester released calcium more efficiently at RT than at 4°C and also whether adding antibody directly to extracts and collecting the antibody–antigen complexes later might be faster and less disruptive than using antibody-coated beads. Addition of excess EGTA to sequester released calcium never gave reproducible improvements. Given the logical importance of immunodepletion experiments, technical improvements to immunodepletion procedures are eagerly awaited by many researchers.

B. Reagent Addition to Extracts

A complementary approach to immunodepletions is to assay the effect of adding either inhibitory antibodies or dominant-negative proteins on spindle assembly. This approach is useful because it is less perturbing to the extract than immunodepletion. In addition, it allows one to perturb protein function both before and after spindle assembly, thus allowing one to address the requirement of protein function in both the establishment and maintenance of spindle structure.

One concern with respect to addition of reagents to extracts is dilution of the extract. We recommend not adding reagents to >10% of extract volume since greater dilution results in poor extract performance. For antibodies, we recommend dialyzing into a buffer that is compatible with extracts, such as 10 m*M* Hepes (pH 7.2) and 100 m*M* KCl. In this buffer, several antibodies that we generated are stable at −80°C and working stocks are stable for several months at 4°C. Also compatible with extracts is 50 m*M* K-glutamate (pH 7.0) and 0.5 m*M* $MgCl_2$, and this can also be used for storage of antibodies. We avoid the use of CSF-XB or sperm dilution buffer for storing antibodies since both these buffers contain sucrose, making them highly susceptible to bacterial contamination at 4°C. We also avoid adding azide to our antibody stocks. Dominant-

negative fusion proteins can be dialyzed into CSF-XB and stored at −80°C prior to addition to extracts.

The amount of antibody that must be added to perturb function depends on the quality of the antibody being used and on the abundance of the target protein in the extract. We have found that as little as 25–50 μg/ml of a very potent antibody, such as the polyclonal anti-XKCM1 antibody, completely inhibits XKCM1 function, whereas 1 mg/ml of a monoclonal antibody to the intermediate chain of dynein is required to inhibit dynein function. We suggest that each new antibody be titrated to determine the amount necessary for full inhibition. Since the mode of action of dominant-negative proteins is presumably to compete with the endogenous protein, the amount of fusion protein that must be added to perturb function depends on the endogenous concentration of the target protein. We recommend a 10-fold molar excess of fusion protein as a starting point but the concentration for optimal inhibition must be empirically determined for each protein.

VI. Data Analysis and Interpretation

Xenopus extracts are very powerful for analyzing protein function in spindle assembly, but all extract workers admit that their use is plagued by variability. It is not uncommon to go through periods in which several concurrent extracts will not assemble good spindles or in which immunodepletions consistently lead to extract activation. This is perfectly normal and can only be overcome by persistence. However, the extreme variability does necessitate care in performing and interpreting experiments, and we discuss how we approach the analysis of protein function in spindle assembly.

To analyze spindle assembly defects, we recommend starting with technically simpler antibody addition experiments, varying the concentration of added antibody and analyzing the effect using spindowns to facilitate detailed analysis. We quantitatively characterize the phenotype in at least three different experiments on three different extracts, often preparing duplicate samples on a single extract to increase the sample size. Once the effect of antibody addition is clear, the next step is to determine the effect of protein depletion. The immunodepletion procedure itself perturbs the extract significantly, making it difficult to discern subtle phenotypes. Furthermore, immunodepletion is technically much more difficult to execute than antibody addition. However, the results of antibody addition experiments must be interpreted cautiously in the absence of a confirmation of the observed effects by immunodepletion. In the absence of immunodepletions, combining antibody inhibition with a dominant-negative approach might help strengthen conclusions with respect to the role of a specific protein in spindle assembly. In addition, determining the effect of manipulating a particular protein on all three types of spindle assembly reactions—CSF spindle assembly, cycled spindle assembly, and DNA bead spindle assembly—can also provide greater

insight into its role in spindle assembly (Heald *et al.*, 1997). Performing identical manipulations on different types of spindle assembly reactions can also provide new insights into the process of spindle assembly itself, as demonstrated by recent work characterizing the role of centrosomes during spindle assembly (Heald *et al.*, 1997). Finally, the most desirable extension of the manipulation of specific components during spindle assembly is to reconstitute spindle assembly by adding back purified protein to immunodepleted extract—the logical equivalent of a genetic complementation. However, as might be expected, this has proven to be quite difficult and has only been partially achieved (Merdes *et al.*, 1996; Walczak *et al.*, 1996). Future technical improvements in immunodepletion procedures will be necessary to achieve this goal.

The extreme variability between extracts makes identifying the effect of manipulating specific components heavily dependent on the strength of the observed phenotype. Certain phenotypes, such as the one induced by inhibition of XKCM1, are extremely dramatic and can be easily defined in the first extract analyzed (Walczak *et al.*, 1996). Others, such as the one induced by inhibition of the spindle motor XCTK2, are much more subtle and difficult to detect without careful inspection of many extracts (Walczak *et al.*, 1997). Reproducibility and quantitative analysis become critical in determining the nature of subtler phenotypes.

VII. Anaphase *in Vitro*

Cycled spindles assembled in *Xenopus* egg extracts are capable of undergoing anaphase chromosome segregation (Shamu and Murray, 1992). This *in vitro* anaphase reaction has proven valuable for dissecting both the mechanism of sister chromatid separation and the mechanism of chromosome movement (Murray *et al.*, 1996; Desai *et al.*, 1998). However, successful anaphase *in vitro* requires considerably higher quality extracts than those used for spindle assembly and this has significantly limited the use of this reaction. In the following sections we provide some hints to facilitate successful preparation of anaphase-competent extracts. We also describe methods to set up and monitor an anaphase reaction using either fixed time points or time-lapse fluorescence microscopy.

A. Preparation of Anaphase-Competent Extracts

Extracts for monitoring anaphase are prepared exactly as described for CSF extracts (see Section II). Anaphase extracts require high-quality eggs, and frogs which lay even small amounts of puffballs or stringy eggs should not be used. Note that the absolute volume of extract required for these experiments is very small and quality should always take precedence over quantity. One factor, which should be minimized in the preparation of anaphase-competent extracts, is the time between egg-laying and extract preparation. Often the best extracts are

prepared from freshly squeezed eggs since they have not been floating for several hours in "frog-conditioned" MMR. However, laid egg extracts, which are easier to prepare, can also be fully competent for anaphase. We routinely collect laid eggs from four to six frogs about 12–14 hr after injection with hCG (frogs are stored at 16°C in 1X MMR as described previously, generally two to four of the frogs lay eggs of sufficient quality for extract preparation) and prepare extracts from the laid eggs and freshly squeezed eggs in parallel. While squeezing the frogs, it is extremely important to avoid getting any frog skin secretions ("frog slime") into the squeezed eggs or the eggs will activate. Frog slime can be avoided by frequently dipping the frog into a bucket of clean distilled water during the squeezing process. Squeezed eggs from different frogs should be kept separate initially but can be pooled after dejellying if they do not exhibit signs of activation. It is difficult to obtain large quantities of squeezed eggs, but from four frogs we generally get enough to fill one-half to three-fourths of a 13 × 51-mm Ultraclear tube. The laid eggs and squeezed eggs are separately processed as described previously for the CSF extract prep. It is important to thoroughly wash out residual jelly coat after the dejellying step and to crush the eggs at 10,000 rpm for 15 min at 16°C (full brake). This speed spin results in highly turbid muddy-colored extracts. Faster spins result in clearer extracts that often suffer from extensive and rapid spindle aggregation, resulting in very limited time of manipulation and precluding any significant analysis. We also note that newer frogs that have not been through multiple rounds of ovulation tend to be better for anaphase experiments, although, as with many other aspects of frog egg extracts, this is by no means definitive. Using frogs that have been through less than two cycles of ovulation (with at least a 3-month rest between ovulations) after being obtained from a distributor and taking great care in preparing the extracts, we have been able to successfully obtain anaphase extracts on a routine basis (70% of the time).

B. Setting Up and Monitoring Anaphase Reactions

Anaphase reactions require spindles obtained by cycled spindle assembly as described in Section III,D. It is essential that the cycled spindles have tight metaphase plates; often, chromosomes on the spindles are not confined to a tight metaphase plate but stray over the entire spindle, and these extracts are not useful for anaphase. To perform an anaphase reaction, 9 μl of a cycled spindle assembly reaction is mixed with 1 μl of the 10X calcium stock (see Section III,B) and monitored by taking fixed time points every 5 min for 30 min. The added calcium should be mixed well with the extract, either by gently flicking the bottom of the tube or by gently pipeting up and down. The addition of calcium results in the destruction of CSF and exit from the metaphase arrest. Between 5 and 15 min after calcium addition, clear evidence for anaphase should be evident in the chromosome morphology as depicted in Fig. 3. In addition to anaphase chromosome movement, changes in spindle structure, particularly thinning out of spindle MT density and expulsion of asters, should be evident (Murray *et al.,* 1996). By

25–30 min, rounded interphase nuclei should be visible in the reaction. In a good anaphase extract, 40–80% of the spindles show clear evidence of anaphase. However, it is not unusual to have an extract whose spindles have tight metaphase plates but do not exhibit anaphase. In addition, the percentage of spindles that exhibit anaphase often decreases dramatically with aging of the extract.

C. Real-Time Analysis of Anaphase *in Vitro*

1. Lengthening Extract Life Span

Although technically challenging, it is possible to observe anaphase *in vitro* in real time allowing detailed analysis of chromosome movement and spindle dynamics (Murray *et al.*, 1996; Desai *et al.*, 1998). Since there is no reliable procedure for freezing extracts while maintaining anaphase competency, and since each anaphase reaction takes approximately 30 min, during which only one spindle can be observed per field of view (of which <50% will provide analyzable data), it is essential to maximize the life span of the extract to perform real-time analysis. We have found it best to stagger the entire spindle assembly reaction by 3.5–4 hr, storing the original extract on ice during the interim, to maximize the amount of time that observational studies can be performed. We find this to be better than storing the extract on ice after cycling through interphase and have been able to use extracts routinely for 12–16 hr after preparation. We have also had some success with storing the cycled spindles at 10–12°C and warming them up to room temperature for 10–15 min prior to their use. We note, however, that with increased time spindles will be present in larger aggregates and the percentage of spindles capable of undergoing anaphase will decline.

2. Slide and Coverslip Cleaning

Requirements

Water, acetone, ethanol, slides, and coverslips (22 × 22 mm; No. 1), hotplate, slide storage box, 100-mm tissue culture dish, and coverslip spinner (optional).

It is essential to obtain homogenous sample films to avoid problems derived from air bubbles—we have often watched a spindle just beginning or in the middle of anaphase, only to have a bubble roll into view and wipe it out of existence. The key to good sample films is clean particulate-free slide and coverslip surfaces.

Cleaning Slides

1. Set up three 50-ml conical tubes filled with water, acetone, and ethanol and have a hotplate with a clean surface set such that the top feels hot to the touch (50–60°C).

2. Holding the frosted end, dip the slide several times in water and then in acetone and finally in ethanol. Transfer to the hotplate surface to rapidly dry

off the ethanol and store in a covered slide box. It is best to use a reasonably new box of slides to minimize particulates on the slides. If problems with bubbles persist, clean slides in a cup sonicator filled with warm water containing a small amount of detergent and rinse off the detergent prior to cleaning with acetone and ethanol.

Cleaning Coverslips

Coverslips are cleaned exactly as slides, except that coverslip holders are used for rinsing 12 coverslips at a time and the coverslips are dried using a homemade coverslip spinner. If no spinner is available, the coverslips can be dried by gently wiping both surfaces using lens paper (wear gloves while doing this). Clean coverslips can be stored in a plastic 100-mm tissue culture dish for several weeks.

3. Sample Preparation

Requirements

Valap, hotplate (for melting Valap), clean slides and coverslips, 10X calcium/DAPI stock (4 m*M* calcium chloride, 750 ng/ml DAPI in 1X sperm dilution buffer), extract reactions with cycled spindles.

Spindle microtubules are visualized using X-rhodamine tubulin added to the extract just after preparation. Chromosomes are visualized using DAPI and it is most convenient (and least perturbing) to add the DAPI to the calcium stock used for triggering anaphase. The 10X calcium/DAPI stock can be stored indefinitely at −20°C and is not sensitive to freezing and thawing. Prior to sample preparation, make sure that melted Valap is available to seal the sample. Valap is a 1:1:1 mixture of vaseline:lanolin:paraffin prepared by weighing equal amounts of the three components into a beaker and melting and mixing them on a hotplate.

Preparation of Sample

1. Transfer 9 μl of the cycled spindle assembly reaction to an Eppendorf tube.
2. Add 1 μl of the 10X calcium/DAPI stock. Mix gently but thoroughly by flicking and pipeting up and down.
3. Pipet 8 μl onto a clean slide. Cover gently with a clean 22 × 22-mm No. 1 coverslip. It is essential not to squash the sample film too vigorously. If there are many bubbles in the film, the sample should be discarded and a new sample should be prepared; however, it is often impossible to avoid one or two small bubbles near the center of the coverslip.
4. Seal the edges with Valap and start observation (a Q-tip works well as a Valap applicator).

We have experimented with more elaborate schemes to prevent distortion of spindles during sample preparation, such as coating of the slide surface with spacer latex beads, and also with alternative means of sealing the sample that avoid any local heating problems associated with the use of Valap (Murray *et*

al., 1996). However, we find that the simple procedure outlined previously is sufficient for observing anaphase and considerably reduces the complexity of sample preparation.

4. Sample Observation

Given the variable composition of products in a spindle assembly reaction, it is essential to pick the correct type of spindle for observation. We find it best to scan the sample in the DAPI channel using a 20× dry objective lens (with a 25% transmission neutral density filter in the light path) and to select medium-sized spindles with tight metaphase plates for time lapsing. Often, small spindles are too sensitive to flows under the coverslip (which are highly variable from extract to extract) that cause them to either spin around or float out of the field of view (both of which make analysis nearly impossible). Larger aggregates, while they do exhibit good anaphase, tend to be very messy and difficult to analyze. With a little practice, one can begin to pick spindles good for time lapsing anaphase with a frequency of 60–80%.

For acquiring images, we use low-power dry objectives (20×, 0.5 or 0.75 NA) and a cooled charged-coupled device camera. The minimal additional requirements for the real-time observation are the ability to acquire images at two different wavelengths (X-rhodamine and DAPI), to store the acquired images, and to shutter the illuminating light to minimize photodamage. A detailed description of the microscope setup used to acquire the images shown in Fig. 4 has

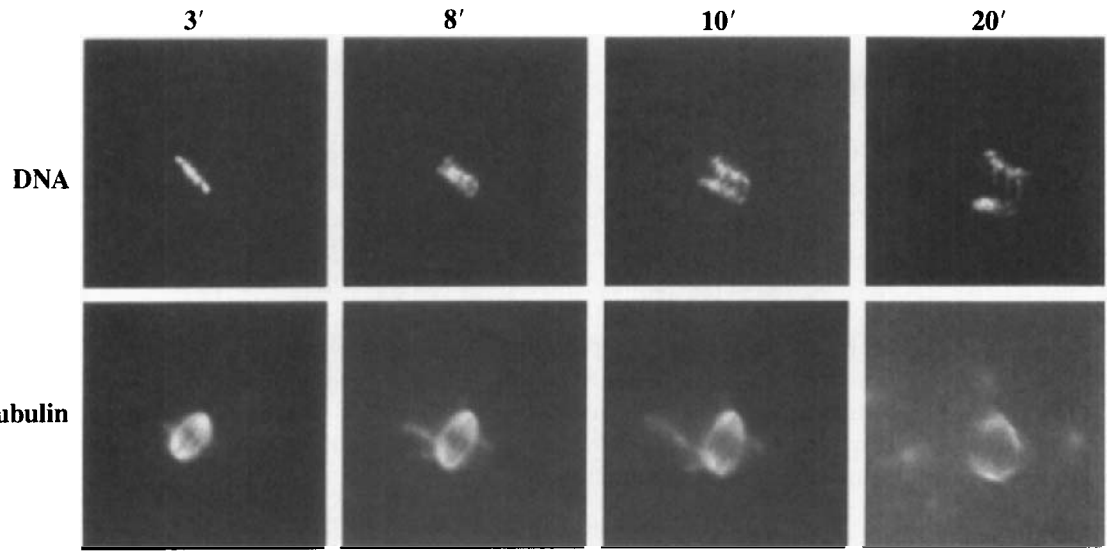

Fig. 4 Time course of anaphase chromosome movement. Individual frames are presented from a time-lapse recording of anaphase *in vitro*.

been published (Salmon *et al.*, 1994). Analysis of chromosome movement and spindle microtubule density can be performed on the collected images using one of several commercially available image analysis software packages.

D. Manipulation of Anaphase *in Vitro*

Manipulation of anaphase reactions has been restricted to addition of either nondegradable cyclin (cyclin Δ90) or pharmacological agents. For addition of cyclin Δ90, titrate the cyclin concentration such that physiological levels of H1 kinase are attained (Murray *et al.*, 1989). For optimal results, the cyclin Δ90 must be added to the extract for 20–30 min prior to triggering anaphase by addition of calcium. In the presence of cyclin Δ90 sister separation appears normal, although spindle microtubule density near the spindle poles does not decline and chromosome decondensation and formation of nuclei does not occur. For addition of pharmacological agents, trigger anaphase by adding 1/10 vol of a 10× calcium/agent stock and monitor as described previously. If anaphase is being monitored in real time, then add the agent from a 10× calcium/DAPI/agent stock. We have successfully used real-time analysis to monitor the effects of cyclin Δ90, AMPPNP, taxol, and vanadate on anaphase (Murray *et al.*, 1996; Desai *et al.*, 1998).

The more ambitious manipulation of depleting specific components and assaying the effect on chromosome segregation remains a technical challenge for the future. However, addition of reagents to anaphase reactions has been very useful, leading to the important discoveries that activation of the cyclin destruction machinery is sufficient to promote sister chromatid separation and that topoisomerase II activity is required for sister separation (Shamu and Murray, 1992; Holloway *et al.*, 1993).

VIII. Conclusions

In this chapter we have described detailed procedures for the preparation of spindle assembly extracts, for manipulation of extracts to define the function of specific proteins in spindle assembly, and for the analysis of anaphase chromosome movement *in vitro*. The importance of *Xenopus* extracts for analyzing spindle assembly and function is evident from their increasing use in recent years. However, many technical advances need to be made to allow a realization of the full potential of *Xenopus* extracts, particularly with respect to the manipulation and storage of extracts. We hope that the methods described here will serve as a starting point for future studies on spindle assembly and function and will stimulate technical innovations that will expand the types of analyses possible using *Xenopus* egg extracts.

Acknowledgments

We thank Manfred Lohka and Yoshio Masui, whose pioneering work led to the use of *Xenopus* egg extracts for studying spindle assembly and function; Manfred Lohka and James Maller, whose

early observations on *in vitro* spindles led to the development of the spindle assembly reactions described here; Ken Sawin, who characterized the pathways of spindle assembly and performed the first immunodepletions; and Caroline Shamu, who developed the *in vitro* anaphase reaction. We also thank Ted Salmon for his contributions to the analysis of anaphase *in vitro* and for many stimulating discussions on spindle assembly and chromosome movement. Finally, we thank our colleagues in the *Xenopus* extract field and members of our laboratories for many technical discussions on performing extract experiments. This work was supported by an HHMI predoctoral fellowship to A. D., grants from the NIH and Packard Foundation to A. M., grants from the NIH and HFSP to T. J. M. and postdoctoral fellowships from the NIH and the DOD Breast Cancer Research Program to C. E. W.

References

Belmont, L. D., Hyman, A. A., Sawin, K. E., and Mitchison, T. J. (1990). Real-time visualization of cell cycle dependent changes in microtubule dynamics in cytoplasmic extracts. *Cell* **62,** 579–589.

Blangy, A., Lane, H. A., d'Hérin, P., Harper, M., Kress, M., and Nigg, E. A. (1995). Phosphorylation by p34cdc2 regulates spindle association of human Eg5, a kinesin-related motor essential for bipolar spindle formation in vivo. *Cell* **83,** 1159–1169.

Blow, J. J., and Laskey, R. A. (1986). Initiation of DNA replication in nuclei and purified DNA by a cell-free extract of Xenopus eggs. *Cell* **47,** 577–587.

Boleti, H., Karsenti, E., and Vernos, I. (1996). Xklp2, a novel Xenopus centrosomal kinesin-like protein required for centrosome separation during mitosis. *Cell* **84,** 49–59.

Desai, A., Deacon, H. W., Walczak, C. E., and Mitchison, T. J. (1997). A method that allows the assembly of kinetochore components onto chromosomes condensed in clarified Xenopus egg extracts. *Proc. Natl. Acad. Sci. USA* **94,** 12378–12383.

Desai, A., Maddox, P., Mitchison, T. J., and Salmon, E. D. (1998). Anaphase A chromosome movement and poleward microtubule flux occur at similar rates in *Xenopus* extract spindles. *J. Cell Biol.* **141,** 703–713.

Enos, A. P., and Morris, N. R. (1990). Mutation of a gene that encodes a kinesin-like protein blocks nuclear division in A. nidulans. *Cell* **60,** 1019–1027.

Evans, L., Mitchison, T. J., and Kirschner, M. W. (1985). Influence of the centrosome on the structure of nucleated microtubules. *J. Cell Biol.* **100,** 1185–1191.

Flemming, W. (1965). Contributions to the knowledge of the cell and its vital processes. Part II. *J. Cell Biol.* **25,** 3–69.

Gaglio, T., Saredi, A., and Compton, D. A. (1995). NuMA is required for the organization of microtubules into aster-like mitotic arrays. *J. Cell Biol.* **131,** 693–708.

Gaglio, T., Saredi, A., Bingham, J., Hasbani, J., Gill, S. R., Schroer, T. A., and Compton D. A. (1996). Opposing motor activities are required for the organization of the mammalian mitotic spindle pole. *J. Cell Biol.* **135,** 399–414.

Gaglio, T., Dionne, M. A., and Compton, D. A. (1997). Mitotic spindle poles are organized by structural and motor proteins in addition to centrosomes. *J. Cell Biol.* **138,** 1055–1066.

Hagan, I., and Yanagida, M. (1990). Novel potential mitotic motor protein encoded by the fission yeast cut7 + gene. *Nature* **347,** 563–566.

Heald, R., Tournebize, R., Blank, T., Sandaltzopoulos, R., Becker, P., Hyman, A., and W. Karsenti, W. (1996). Self-organization of microtubules into bipolar spindles around artificial chromosomes in *Xenopus* egg extracts. *Nature* **382,** 420–425.

Heald, R., Tournebize, R., Habermann, A., Karsenti, E., and Hyman, A. (1997). Spindle assembly in Xenopus egg extracts: Respective roles of centrosomes and microtubule self-organization. *J. Cell Biol.* **138,** 615–628.

Heald, R., Tournebize, R., Vernos, I., Murray, A., Hyman, A., and Karsenti, E. (1998). In vitro assays for mitotic spindle assembly and function. *In* "Cell Biology: A Laboratory Handbook" (J. Celis, ed.).

Hirano, T., and Mitchison, T. J. (1991). Cell cycle control of higher-order chromatin assembly around naked DNA in vitro. *J. Cell Biol.* **115,** 1479–1489.

Holloway, S. L., Glotzer, M., King, R. W., and Murray, A. W. (1993). Anaphase is initiated by proteolysis rather than by the inactivation of MPF. *Cell* **73,** 1393–1402.

Hoyt, M. A., He, L., Loo, K. K., and Saunders, W. S. (1992). Two Saccharomyces cerevisiae kinesin-related gene products required for mitotic spindle assembly. *J. Cell Biol.* **118,** 109–120.

Hutchison, C. J., Cox, R., and Ford, C. C. (1988). Periodic DNA synthesis in cell-free extracts of Xenopus eggs. *EMBO J.* **6,** 2003–2010.

Hyman, A., Drechsel, D., Kellogg, D., Salser, S., Sawin, K., Steffen, P., Wordeman, L., and Mitchison, T. (1991). Preparation of modified tubulins. *Methods Enzymol.* **196,** 478–485.

Lohka, M. J., and Maller, J. L. (1985). Induction of nuclear envelope breakdown, chromosome condensation, and spindle formation in cell-free extracts. *J. Cell Biol.* **101,** 518–523.

Lohka, M. J., and Masui, Y. (1983). Formation in vitro of sperm pronuclei and mitotic chromosomes induced by amphibian ooplasmic components. *Science* **220,** 719–721.

Merdes, A., Ramyar, K., Vechio, J. D., and Cleveland, D. W. (1996). A complex of NuMA and cytoplasmic dynein is essential for mitotic spindle assembly. *Cell* **87,** 447–458.

Murray, A. W. (1991). Cell cycle extracts. *Methods Cell Biol.* **36,** 581–605.

Murray, A. W., and Kirschner, M. W. (1989). Cyclin synthesis drives the early embryonic cell cycle. *Nature* **339,** 275–280.

Murray, A. W., Desai, A. B., and Salmon, E. D. (1996). Real time observation of anaphase in vitro. *Proc. Natl. Acad. Sci. USA* **93,** 12327–12332.

Murray, A. W., Solomon, M., and Kirschner, M. W. (1989). The role of cyclin synthesis in the control of maturation promoting factor activity. *Nature (London)* **339,** 280–286.

Roof, D. M., Meluh, P. B., and Rose, M. D. (1992). Kinesin-related proteins required for assembly of the mitotic spindle. *J. Cell Biol.* **118,** 95–108.

Sagata, N., Watanabe, N., Vande Woude, G. F., and Ikawa, Y. (1989). The c-mos protooncogene is a cytostatic factor responsible for meiotic arrest in vertebrate eggs. *Nature* **342,** 512–518.

Salmon, E. D., Inoue, T., Desai, A., and Murray, A. W. (1994). High resolution multimode digital imaging system for mitosis studies in vivo and in vitro. *Biol. Bull.* **187,** 231–232.

Sawin, K. E., and Mitchison, T. J. (1991). Mitotic spindle assembly by two different pathways in vitro. *J. Cell Biol.* **112,** 925–940.

Sawin, K. E., LeGuellec, K., Philippe, M., and Mitchison, T. J. (1992). Mitotic spindle organization by a plus-end directed microtubule motor. *Nature* **359,** 540–543.

Shamu, C. E., and Murray, A. W. (1992). Sister chromatid separation in frog egg extracts requires DNA topoisomerase II activity during anaphase. *J. Cell Biol.* **117,** 921–934.

Verde, F., Labbe, J.-C., Doree, M., and Karsenti, E. (1990). Regulation of microtubule dynamics by cdc2 protein kinase in cell-free extracts of Xenopus eggs. *Nature* **343,** 233–238.

Vernos, I., Raats, J., Hirano, T., Heasman, J., Karsenti, E., and Wylie, C. (1995). Xklp1, a chromosomal Xenopus kinesin-like protein essential for spindle organization and chromosome positioning. *Cell* **81,** 117–127.

Walczak, C. E., Mitchison, T. J., and Desai, A. (1996). XKCM1: A Xenopus kinesin-related protein that regulates microtubule dynamics during mitotic spindle assembly. *Cell* **84,** 37–47.

Walczak, C. E., Verma, S., and Mitchinson, T. J. (1997). XCTK2: A kinesin-related protein that promotes mitotic spindle assembly in Xenopus laevis egg extracts. *J. Cell Biol.* **136,** 859–870.

CHAPTER 21

Methods for Studying Cell Division in Higher Plants

Jan W. Vos, Aline H. Valster, and Peter K. Hepler

Department of Biology and the Plant Biology Graduate Program
University of Massachusetts
Amherst, Massachusetts 01003

I. Introduction

The study of mitosis and cytokinesis in cells of higher plants has a long and distinguished history (Wilson, 1928). From the outset the distinct parallels in mitotic processes between plant and animal cells have been apparent, leading to the conclusion that a similar substructure and mechanism underlies both. However, it was also recognized early that there are notable differences. Mitotic plant cells, for example, generally do not possess a centrosome or a highly focused spindle apparatus at the mitotic poles. During anaphase they also generally exhibit chromosome to pole motion (anaphase A) but with little pole separation (anaphase B) when compared to animal cells. Finally, they accomplish cytokinesis

METHODS IN CELL BIOLOGY, VOL. 61

0091-679X/99 $30.00

by forming a phragmoplast and cell plate within the cell interior, which then grows outward, rather than by inward furrowing as occurs typically in animal cells. Indeed, the process of cytokinesis and cell plate formation determines the plane of division and thus plays a crucial role in defining cell shape and tissue morphogenesis for which a parallel event is not so evident in animal cells. It is for these and all the other obvious reasons that the study of cell division in plants is both interesting and important.

Given the wide scope of the subject and the limited space for this article, we have focused on the study of mitotic processes as revealed by examination of living cells or permeabilized cell models. We specifically draw attention to five different cell types as follows: tobacco culture cells (BY-2), endosperm (*Haemanthus/Clivia*), stamen hair cells (*Tradescantia*), epidermal slices/peels (*Allium/Tradescantia*), and pollen mother cells (*Iris, Tradescantia,* and *Lilium*). We recognize that other cell types could be considered but believe that these five provide the investigator with a wide variety of systems favorable for the study of both mitosis and meiosis. We also give special attention to the method of intracellular microinjection as a way to introduce agents or reporter molecules, which then allows the experimenter to observe and/or modulate a vital process. While microinjection of animal cells is considered by Wadsworth (see Chapter 12), the technique she describes is not suitable for plant cells, which because of their rigid walls and high turgor pressure require different strategies.

II. Cell Types of the Study of Cell Division

A. Tobacco BY-2 Culture Cells

1. Overview

There are several cell culture lines that offer possibilities for studies on mitosis in higher plant cells. However, for different reasons, the BY-2 cell line, which has been established from a callus of *Nicotiana tabacum* cv. Bright Yellow 2 in 1972 (Nagata *et al.,* 1992), seems particular advantageous. The cell line is distinctive because of its extremely high growth rates and its homogeneity, in which cells of relatively uniform size occur singly or as small clusters, sometimes organized in files. In contrast to carrot cell cultures, the BY-2 cell culture does not contain proembryogenic masses. The cells are about 40–50 μm in diameter and are highly vacuolated. Transvacuolar cytoplasmic strands, exhibiting active cytoplasmic streaming, connect the centrally located nucleus with the cell periphery. For visualization and observation of living mitotic and interphase cells, differential interference contrast (DIC) microscopy is preferred.

Under proper culture conditions BY-2 cells multiply 80- to 100-fold in 1 week wherein the generation time is approximately 13 hr: M phase takes about 2 hr, S phase about 5 hr, and G_1 and G_2 respectively, take about 2.5 and 4 hr. Typically,

a mitotic index of 5–8% can be observed in the first 4 days after transfer; however, through synchronization this can be increased to 70–90% (Nagata *et al.,* 1992).

2. Culture Methods

The tobacco BY-2 cell line was initiated by Japan Tobacco, Inc., and can be obtained for scientific use from Nagata's lab under an agreement with Japan Tobacco, Inc. (Nagata *et al.,* 1992). The cells are cultured in modified Linsmaier and Skoog's medium containing the following: Murashige/Skoog salt mixture (4.3 mg/liter), KH_2 PO_4 (370 mg/liter), thiamine–HCl (1 mg/liter), 2,4-D (0.2 mg/liter), inositol (100 mg/liter), and 3% sucrose at pH 5.7 (adjusted using KOH). Cells are subcultured every 7 days by diluting 1.5 ml of stationary-phase cells into 95 ml of fresh medium in a 300-ml flask. Cells are cultured on a rotary shaker at 130–150 rpm in the dark at approximately 26°C.

A high percentage of synchronization of the BY-2 cell culture is achieved in a two-step process (Nagata *et al.,* 1992). A fast-growing culture is first treated with the specific DNA polymerase-α inhibitor, aphidicolin, which causes minimal chromosome aberration compared to hydroxyurea, another synchronization agent. Six hours after removal from aphidicolin, and shortly before entry into M phase, the partly synchronized cell culture is further treated with propyzamide, an antimicrotubule (MT) drug that induces mitotic arrest. Release from propyzamide results in an immediate progression of the cell cycle. Using this method, Nagata *et al.* (1992) were able to increase the mitotic index up to 70–90%. However, other investigators (L. A. Staehelin, personal communication) have not been able to achieve mitotic indices exceeding 50%.

3. Principal Findings

The use of tobacco BY-2 cells has contributed some important findings, especially in our understanding of mitotic motor proteins and in the process of cell plate formation. For example, Asada *et al.* (1991) permeabilized telophase tobacco BY-2 cells with glycerin in the presence of fluorescently labeled tubulin and GTP or ATP. Fluorescence was first observed at the equatorial plane, suggesting that tubulin dimers had incorporated at the plus ends of preexisting phragmoplast MTs. If, after 30 min, the fluorescently labeled tubulin dimers were replaced by nonlabeled tubulin dimers, two fluorescent bands appeared, each moving away from the equatorial plane in opposite directions. These results provided evidence that, while polymerizing at their plus ends, the phragmoplast MTs are translocated in the direction of their minus ends (Asada *et al.,* 1991).

Kakimoto and Shibaoka (1988) developed a method to isolate phragmoplasts and developing cell plates of tobacco BY-2 cells, and by using autoradiography, they revealed that the synthesis of the polysaccharide 1,3-β-glucan (callose) occurs at the cell plate and not in the Golgi apparatus (Kakimoto and Shibaoka, 1992). Later, Asada and Shibaoka (1994) isolated two MT-based motor proteins

with plus-end-directed activities from these isolated phragmoplasts. After cDNA analysis, one of these proteins was characterized as a novel member of the kinesin superfamily and was named TKRP125 (tobacco kinesin-related polypeptide of 125 kDa) (Asada *et al.,* 1997). This protein is suggested to play a role in MT translocation that is thought to be important in the formation and maintenance of the structural integrity of the phragmoplast (Asada *et al.,* 1997).

Liu *et al.,* (1996) observed the dynamic changes of another plant kinesin-like protein (KatAp from *Arabidopsis*) during mitosis in BY-2 cells. BY-2 protoplasts were lysed in the presence of taxol and ATP, and after different incubation times (1, 5, or 15 min) the lysed protoplasts were immunostained with anti-KatAp. Observations revealed that the antibody staining "moved" rapidly away from the equatorial region with increased incubation time in lysis buffer, providing evidence that KatAp is a minus-end-directed MT motor protein which requires ATP (Liu *et al.,* 1996).

Gu and Verma (1997) studied the dynamics of phragmoplastin in living tobacco BY-2 cells. Phragmoplastin, which is a dynamin-like protein from soybean, is thought to be associated with exocytotic vesicles that are responsible for the deposition of cell plate material (Gu and Verma, 1996). A GFP–phragmoplastin construct was introduced into tobacco BY-2 cells using *Agrobacterium* transformation. Observation of the transformed live cells revealed that GFP–phragmoplastin is mainly associated with early stages of cell plate formation at areas of active vesicle fusion (Gu and Verma, 1997). Overexpression of the GFP–phragmoplastin construct resulted in an elongated early phase of cell plate formation giving rise to "S"-shaped and obliquely oriented cell plates.

In addition to gene delivery with the aid of *Agrobacterium,* it is possible to introduce genes into BY-2 cells using liposomes and polyethylene glycol or polyvinyl alcohol and by electroporation (Nagata *et al.,* 1992). Indeed, with its rapid growth, ease of synchronization, and the ability to be transformed, the tobacco BY-2 cell culture emerges as an important system for future studies that will address a wide variety of questions surrounding the mechanism and control of cell division in plants.

B. Endosperm

1. Overview

Of all dividing plant cells, those derived from the liquid endosperm of certain species are probably the most visually elegant and captivating to study. Recognizing the potential of these tissues for studies of cell division, Bajer and Molè-Bajer (1954), in a landmark study, explored the utility and culture methods for endosperm from approximately 30 different species, providing evidence on all phases of mitosis. A key feature of these cells is that they do not possess a cell wall, and thus when cultured, they flatten substantially, becoming essentially two-dimensional objects. In addition, some of the species have large chromosomes, making their visualization easy. When taken together, it can be appreci-

ated that endosperm cells are nearly ideal objects for virtually all microscopic methods, but especially so for phase contrast, polarized light, DIC, and conventional epifluorescence microscopy.

In evaluating various plant species for their suitability as sources for endosperm cells, Bajer and Molè-Bajer (1954) considered the following general characteristics: the length of the flowering period, the number of flowers, the ease of preparation, the number of endosperm cells in the embryo sac, and their viability after preparation. They also considered the size and number of chromosomes, noting that since endosperm is triploid it is possible to have a large number of small chromosomes that will make careful analysis of movement, condensation, and kinetochore function difficult. Large chromosomes are easier to examine but in general mitosis in these cells takes longer. The four most popular species are *Haemanthus, Clivia, Iris,* and *Leucojum,* but *Ornithogalum, Asparagus, Zephyranthes, Pisum, Helianthus* (Bajer and Molè-Bajer, 1954), and *Tilia* (Fuseler, 1975) are also useful. The most widely used source of endosperm cells, *Haemanthus katherinae* Baker, the African blood lily, has inflorescences with about 100 flowers that contain seeds of the proper stage 3–5 weeks after flowering (for details on plant growth see Molè-Bajer and Bajer, 1963). Each embryo sac contains hundreds of endosperm cells, with many dividing, that in preparation will flatten to 5–7 μm within 20 min. The chromosomes ($3n = 27$) are large (2–4 μm in diameter and up to 100 μm long) and are spread out so that the kinetochores do not overlap in *in vitro* preparations.

2. Culture Methods

The right stage for mitotic endosperm cells can be found by carefully examining the phases of fruit and embryo sac development. For *Haemanthus* the proper size of ovule is 4–6 mm long, and seeds can be isolated from the young fruit and kept under moist conditions for several days. The substance of the embryo sac should be colorless with a delicate whitish suspension of endosperm cells. For culturing, cells are spread on a thin agar surface (0.5% agar containing 3.0–4.5% glucose) in a culture chamber since contact with glass or fatty substances such as petroleum jelly leads to cell death. To make a preparation, a Vaseline ring is made on a clean coverslip, within which a thin agar layer is spread. Then, the immature seed is cut at one end and the second drop of liquid endosperm is gently spread out over the agar. A second coverslip covered with agar is placed on top of the Vaseline ring to keep the chamber moist and to prevent condensation. The whole preparation is then mounted in a holder and placed at a 45° angle to allow cells to flatten. After 5–25 min excess fluid is wicked away and the preparation is placed under an upright or inverted microscope. A detailed description with photos and drawings of this technique can be found in Molè-Bajer and Bajer (1963). A recent variation of this chamber technique, which allows for microinjection of the cells, is one in which the top coverslip is replaced by a film of 1% Gelrite with 3.5% glucose on a metal loop that isdropped

over the cells. Using this method, the endosperm cells become immobilized but are still accessible for microinjection (Bajer and Molè-Bajer, 1986). Since endosperm cells lack a cell wall, the suitable microinjection technique is similar to the one used for animal cells (Bajer *et al.*, 1986; Wadsworth, Chapter 12, this volume).

3. Principal Findings

From the early 1950s on, Bajer and coworkers have established the principal organization and behavior of the mitotic apparatus and chromosomes using phase contrast, DIC microscopy, cinematography, and, later, time-lapse video-enhanced microscopy (Bajer and Molè-Bajer, 1956; Bajer, 1958, 1965). With polarizing microscopy, Inoué and Bajer (1961) demonstrated the existence of spindle fibers during mitosis, which later were found to consist of MTs (Bajer, 1990). Further studies showed that temperature shock could reversibly arrest anaphase (Lambert and Bajer, 1977), and that the correlation between the velocity of anaphase chromosomes and temperature was associated with MT disassembly rates (Fuseler, 1975). In addition to their role in separating the chromosomes, MTs were found to be important in the phragmoplast for transporting Golgi vesicles to the growing cell plate (Bajer and Allen, 1966). Many drugs have been used to alter the events of mitosis and show the importance of MTs in mitosis; the MT-stabilizing drug taxol was found to reverse anaphase by inhibiting MTs from shortening (Bajer *et al.*, 1982), whereas the MT depolymerizing drugs, e.g., colchicine, amiprophos-methyl (APM), and oryzalin, were shown to reversibly stop anaphase (Molè-Bajer, 1958; Bajer and Molè-Bajer, 1986; Morejohn *et al.*, 1987). Heterologous tubulin has been shown to incorporate into the mitotic arrays of *Haemanthus* endosperm cells after lysis and immunolabeling or microinjection (Vantard *et al.*, 1990).

Endosperm cells have also been used in studies on the organization of the actin network and its relation to the MT cytoskeleton, especially in cells injected with rhodamine-phalloidin (Schmit and Lambert, 1990), actin antibodies, and through the use of actin-binding drugs, such as cytochalasin-D (Molè-Bajer and Bajer, 1988). From these studies the importance of actin microfilaments (MFs) in mitosis was shown. Cells have also been injected with lipid-coated colloidal gold particles (Bajer *et al.*, 1986, 1987), revealing that the particles moved toward the forming cell plate at the end of anaphase and during telophase similar to phragmoplast vesicles.

Endosperm cells have also been probed with ultraviolet microbeam irradiation and laser surgery, wherein MTs and chromosomes can be broken and kinetochores disabled (Bajer and Molè-Bajer, 1961). In recent studies, Czaban *et al.* (1993) showed that the two pieces of a UV-severed kinetochore bundle responded differently, indicating that both kinetochores and the spindle poles influence the behavior of kinetochore MTs. The production of chromosomal fragments with laser microsurgery has provided evidence for the presence of nonkinetochore

poleward forces and midanaphase equatorial forces, both of which have not been observed in similar studies of dividing vertebrate cells (Khodjakov *et al.,* 1996).

Calcium (Ca^{2+}) measurements during cell division have been reported on *Haemanthus* endosperm cells by ratio imaging with quin-2 (Keith *et al.,* 1985); however, it now seems evident that elevated calcium levels observed during anaphase in the area of the spindle poles resulted from the sequestration of the dye into membrane compartments. Examination of membrane-associated Ca^{2+} with chlortetracycline showed an increase of fluorescence associated with the spindle poles and with birefringent kinetochore fibers (Wolniak and Hepler, 1981). However, reductions in fluorescence were noted before the onset of anaphase, suggesting an efflux of Ca^{2+} from membrane compartments into the spindle (Wolniak *et al.,* 1980, 1983).

Despite the many studies and significant progress that has been made with endosperm, these cells still offer many opportunities for the future. For example, the use of fluorescent analogs, which can be introduced by microinjection, has received relatively little attention thus far but could be used to great advantage, e.g., to directly observe the turnover and flux of cytoskeletal components. Studies such as these are encouraged since endosperm remains one of the most favorable model systems, plant or animal, for observing spatial organization of components and structural elements as they relate to cell division.

C. Stamen Hair Cells

1. Overview

Stamen hair cells of *Tradescantia* have been used for the study of mitosis and cytokinesis for over 100 years. From the classic studies of Strasburger (1880) and Bělař (1929), the elegance of these cells has been recognized and exploited widely. However, they were relatively infrequently used from the 1930s to the 1980s, perhaps because they are not well portrayed by phase-contrast microscopy, especially in comparison with endosperm cells (see Section II,B). With the introduction of newer microscopic methods, e.g., DIC and confocal microscopy, that allow the observer to optically section these cylindrical cells, the stamen hair once again emerged as an extremely favorable object for studies of cell division (Hepler *et al.,* 1993; Hepler and Gunning, 1997).

When compared with other cell types, there are several important advantages that accrue with the use of stamen hair cells. First, the plants from which the cells are derived, including *Tradescantia* and some other members of the Commelinaceae, are extremely easy to grow. Under long-day conditions *Tradescantia virginiana* produces flowers continuously, ensuring that potential dividing cells are available at any time throughout the entire year. Second, the stamen hairs are easily isolated from young flower buds and can be cultured in a simple, defined medium or even distilled water, within which the cells will continue to divide for 3 or 4 hr. Third, the dividing cells are extremely robust and can readily withstand a variety of insults, including the process of microinjection,

even multiple times, without showing abnormalities in the mitotic processes. Fourth, from a developmental point of view the dividing stamen hair cells are typical for a higher plant; in marked contrast to endosperm, they possess preprophase bands and display orientation mechanisms for cell plate alignment. Finally, as mentioned previously, stamen hair cells can be analyzed in great detail especially with DIC and confocal fluorescence microscopy.

2. Culture Methods

Tradescantia virginiana plants are grown under long-day (16 hr light/8 hr dark) conditions at 20–25°C in growth chambers. Inflorescences, harvested just prior to use, are dissected until the bud that is fifth or sixth from the open flower is exposed. This young bud, which is about 5–8 mm in length, is first sliced transversely at the basal end and the contents are gently squeezed out into a drop of culture medium consisting of 1 m*M* KCl, 1 m*M* $MgCl_2$, 0.1 m*M* $CaCl_2$, and 5 m*M* Hepes buffer at pH 7.0. Among the contents of the bud are six stamens and anthers, with numerous hairs still attached to the stamen filament. The hairs can be trimmed off by cutting with a sharp razor blade or scalpel parallel to the stamen filament. At this stage a cursory inspection with a dissection microscope can determine if potential dividing cells are present. If the terminal cells in the hair are swollen like beads, then these stamen hairs are generally too old and should be discarded in favor of hairs that have cylindrical cells at their apical termini. Although the hairs can be examined directly, we normally embed the cells in a thin layer of 1% agarose (Type VII, Sigma chemical Co., St. Louis, MO) in culture medium in order to adhere them tightly to the coverslip and to immobilize them for microinjection (see Section III).

Yet another step that can be useful before observation is treatment of the hairs with cutinase. Because the stamen hair cells are coated by a waxy cuticle, often various pharmacological agents do not readily enter the cell. To alleviate this situation the cells can be treated with cutinase (InterSpex Products, Foster City, CA) at 0.1% (pH 8.0) for 30 min. This procedure apparently etches the cuticle and permits agents such as dinitrophenol, azide (Hepler and Palevitz, 1985), lanthanum, deoxyverapamil (Hepler, 1985), and okadaic acid (Larsen and Wolniak, 1993) to enter the cell much more readily when compared to nontreated cells. However, it must be kept in mind that once the cells are removed from the cutinase, the continued vital activities of the cell will repair the etched cuticle and again render the cell less permeable to external agents.

3. Principal Findings

Historically, the stamen hair cell has been a prime object in which to observe the events of mitosis from early prophase to the completion of cytokinesis and cell plate formation (Fig. 1). Experimental modulation of these events has utilized primarily pharmacological agents (Hepler, 1985; Wolniak, 1991) but also physical

forces such as centrifugation to displace the nucleus and mitotic apparatus relative to the predetermined plane of division (Ôta, 1961). Among the pharmacological studies, those with caffeine and related methylxanthines have been particularly interesting since they specifically inhibit cell plate formation. However, it has been observed from live stamen hair cells that the cell plate always arises in the presence of caffeine, and even expands to about 70% of its projected final size, before finally dispersing until no trace is evident (Sawamura, 1952; Bonsignore and Hepler, 1985). Somewhat similar findings, obtained through injection of the Ca^{2+}-specific buffer, BAPTA, lend support to the idea that caffeine might act through modulation of local Ca^{2+} gradients associated with the developing cell plate (Jügens *et al.*, 1994).

Several studies have used various pharmacological agents that have taken advantage of the high degree of regularity in the timing of mitotic events, e.g., nuclear envelope breakdown to anaphase onset (metaphase transit time; ~33 min), anaphase onset to cell plate vesicle aggregation (~19 min), and the rate of chromosome motion (~1 μm/min) (Hepler, 1985). For example, it has been found that different Ca^{2+} antagonists markedly retard metaphase transit time without affecting rate of motion in anaphase or time of cell plate formation in cytokinesis (Hepler, 1985). Wolniak and coworkers performed a series of carefully timed studies to uncover unique points in the progression of mitosis in which the cell is sensitive to agents that modulate Ca^{2+} and/or related kinases. Thus, they used calcium chelators (quin-2 and EGTA), phosphoinositide cycle inhibitors (Li^{+} and neomysin), inhibitors of Ca^{2+} transport (rutheneum red and Bay K-8644), protein kinase C inhibitors (H-7), protein phosphatase inhibitors (α-naphthyl phosphate, okadaic acid, and microcystin), and general protein kinase inhibitors (K-252a, staurosporine, and protein kinase substrate peptide VRKRTLRRL). The results indicated that metaphase, anaphase, or telophase transit times were either lengthened or shortened, and that these effects could often be reversed by adding counteractive molecules (Wolniak, 1991). A further interesting result obtained with okadaic acid was the induction of asynchronous entry into anaphase (Wolniak and Larsen, 1992; Larsen and Wolniak, 1993).

A particularly exciting development has been the application of methods for the microinjection of macromolecules into dividing stamen hair cells (Zhang *et al.*, 1990a). Thus, it has been possible to introduce heterologous tubulin (isolated from pig or sheep brain and derivatized with fluorescein or rhodamine) and, with the use of the confocal fluorescence microscope, to witness the incorporation of the probe into all the plant mitotic arrays, including the preprophase band, kinetochore fibers, the spindle interzone, and the phragmoplast, and to observe their dynamic transformation (Zhang *et al.*, 1990a). While these observations agree closely with those previously obtained by immunofluorescence microscopy, they provide a direct record from the living cell and thus permit additional experiments, which were not possible heretofore. For example, noting that elevation of internal $[Ca^{2+}]$ to 1 μM accelerated chromosome motion during anaphase,

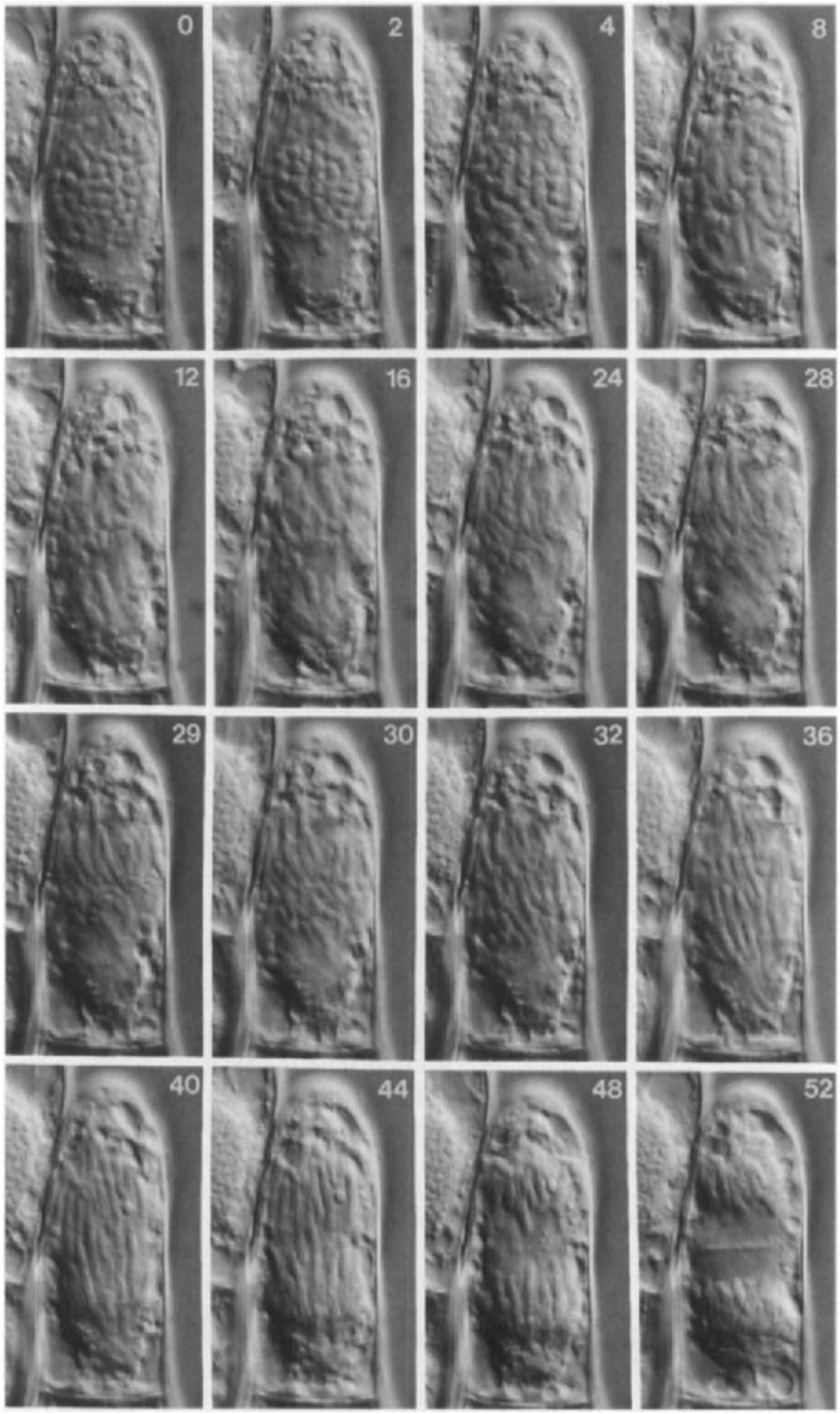
0
2
4
8
12
16
24
28
29
30
32
36
40
44
48
52

Zhang *et al.* (1990b, 1992) were able to correlate this with a 30% decrease in fluorescence from the kinetochore fibers, establishing that Ca^{2+} modulates chromosome motion, presumably through the facilitated depolymerization of kinetochore MTs (Zhang *et al.*, 1992). Beyond this, through the application of localized photobleaching, it has been possible to observe the turnover of MTs in all the principal arrays and to discover that the mitotic MTs show kinetics ($t_{1/2}$ = 31 sec) similar to those of dividing animal cells (Hush *et al.*, 1994).

Actin microfilaments have also been observed in the living, dividing stamen hair cell using the F-actin-specific, fungal toxin, phalloidin, which has been injected into the cell. Some notable observations include the demonstration of the actin-depleted zone in the cell cortex at the site of the preprophase band, which arises at late prophase and persists throughout division (Cleary *et al.*, 1992); the rich array of MFs among the MTs in the phragmoplast (Zhang *et al.*, 1993); and the apparent connection between the MFs of the phragmoplast with those in the cell cortex, possibly representing the structures that cause cell plate alignment (Valster and Hepler, 1997). Combining fluorescence labeling of the cytoskeleton with pharmacology, it has been shown that caffeine permits the initial formation and early expansion of the phragmoplast but completely blocks the later stages of phragmoplast expansion (Valster and Hepler, 1997). Further evidence supporting the idea that the actin MFs in the phragmoplast have an important function derives from a recent study showing that the actin monomer binding protein, profilin, when microinjected into the dividing cell retards or even blocks cell plate formation (Valster *et al.*, 1997).

The use of microinjection to introduce different cell cycle factors has also provided new information about the location and activity of these factors. The suc1 gene product, p13, an essential cell cycle factor, accumulates in the nucleus during interphase but disperses into the spindle and nonspindle cytoplasm following nuclear envelope breakdown (Hepler *et al.*, 1994). Injection of stamen hair cells with extracts, from a mutant of *Chlamydomonas* possessing high $p34^{cdc2}$ kinase activity, reveals that the process of chromatin condensation and timing of nuclear envelope breakdown can be markedly advanced over cells injected with inactive extracts (Hush *et al.*, 1996). An additional exciting observation obtained from cells injected with both active $p34^{cdc2}$ kinase and fluorescent tubulin reveals that the kinase causes the breakdown of the preprophase band of MTs while having no apparent effect on the other MT arrays (Hush *et al.*, 1996).

Fig. 1 Mitosis in *Tradescantia*. The time-lapse sequence shows the successive stages of division as revealed by DIC optics, with the time interval in minutes from nuclear envelope breakdown being indicated in the upper right corner of each panel. In this cell metaphase transit time, the interval from nuclear envelope breakdown to the onset of anaphase takes 29 min, whereas anaphase motion and the start of cytokinesis occupies an additional 23 min, with cell plate initiation occurring at 52 min from nuclear envelope breakdown (reproduced from *The Journal of Cell Biology*, 1985, **100**, 1363–1368, by copyright permission of The Rockefeller University Press).

Finally, the fluorescent analog approach has been used to monitor the distribution of calmodulin during cell division (Vos and Hepler, 1998). In contrast to previous studies, largely on fixed cells, recent work on live stamen hair cells injected with fluorescent calmodulin clearly shows that the protein is uniformly distributed throughout the cell and possesses no evident localization with MTs or any structure. Further work regarding why there is such a marked difference between the observations from live cells and those from fixed preparations provides compelling evidence that the process of fixation and permeabilization, necessary for immunofluorescence labeling, causes a massive redistribution of the calmodulin (Vos and Hepler, 1998).

From this sampling it should be evident that the stamen hair cells are remarkably versatile and cooperative and can be used for a wide variety of studies on mitosis and cell division.

D. Epidermal Cells

1. Overview

It is possible to make epidermal peels or paradermal slices from the young leaves of different plants in which the cells are still undergoing nuclear migration and cell division. Here it is possible to focus on those divisions giving rise to the formation of the stomatal complex, including the guard cell and its subsidiaries. Briefly, the formation of the stomatal complex entails a series of precisely orchestrated symmetrical and asymmetrical divisions, together with marked changes in division plane alignment. These orientation events are crucial for proper development since, due to the presence of the rigid cell wall, the subsequent stages of cell differentiation are dependent on the alignment and spatial orientation of the preceding division. A simple example, found in onion leaves, involves first the migration of the nucleus to the distal end of an elongating protodermal cell where it divides transversely, but asymmetrically, to produce two cells of very different sizes. The smaller of the two is the guard mother cell, and it subsequently divides longitudinally to produce two guard cell initials (Palevitz and Hepler, 1974a). A more complicated developmental program occurs in *Tradescantia,* in which longitudinal files of cells arise in which the small guard mother cells are separated from one another by large intervening epidermal cells. Subsequently, these neighboring epidermal cells divide asymmetrically to yield subsidiary cells that surround the guard mother cell. Finally, the guard mother cell divides longitudinally, but symmetrically, to produce the guard cell initials, which subsequently differentiate to produce the stoma (Cleary, 1995). Impressively, these nuclear migrations and divisions can be observed directly in living preparations requiring only simple preparative and culture procedures.

2. Culture Methods

For onions, seedlings are grown in vermiculite for 5–7 days. Paradermal slices, made with a sharp scalpel between the seedling hook and the terminally attached

seed coat, produces a preparation that is rich in dividing guard mother cells (Palevitz and Hepler, 1974a,b). The slices are then simply cultured in water. To stabilize the preparation for microinjection it is possible to adhere it with low gelling agarose (type VII, Sigma; Hepler and Palevitz, 1985), as used for stamen hairs (see Section III). Cells thus prepared can be readily examined using DIC.

The preparation of epidermal cells from *Tradescantia* involves discarding the old leaves from a young meristem until the second or third youngest leaves are exposed (Cleary, 1995). Peels are then made from the basal 5- to 10-mm portions of these leaves and cultured in 1% mannitol and 1% agarose (type VII), although distilled water may be adequate (Cleary, 1995). Under these conditions the peels remain alive for 24 hr, during which time nuclear migration and cell divisions can be observed for the first 3 or 4 hr. These cells can be successfully microinjected, and although the events of cell division may be slowed, the cells recover quickly and display normal vital processes.

3. Principle Findings

Several exciting and important results have emerged from studies of these systems that increase our understanding of cell division in plants. In onion guard mother cells it became evident that the mitotic apparatus was often not aligned properly to generate the correct longitudinal plane of division. Direct observation led to the discovery of a process of spindle reorientation during anaphase and early telophase that caused the entire mitotic spindle apparatus, including the daughter nuclei and nascent cell plate, to move to the correct longitudinal alignment (Palevitz and Hepler, 1974a). Subsequent studies with pharmacological agents, notably cytochalasin (Palevitz and Hepler, 1974b) and phalloidin (Palevitz, 1980), indicated that the reorientation motions are dependent on an actomyosin system.

In studies of epidermal peels of *Tradescantia,* Cleary (1995) and Kennard and Cleary (1997) examined the relationship between nuclear migration and cell division. Cleary (1995) has been able to microinject rhodamine-phalloidin and observe MFs in living, dividing cells and to establish that the actin-depleted zone, previously observed at the preprophase band site in symmetrically dividing cells, is also present in asymmetrically dividing cells, where it similarly occupies the position where the cell plate will fuse with the parental wall. Kennard and Cleary (1997) focused on the control of the nuclear migration that precedes asymmetric division of the subsidiary cells. Through centrifugation they caused the displacement of polarized nuclei (nuclei that had already moved to asymmetric position), permitting them to examine the process of repolarization. The results indicate that MFs, but not MTs, are involved. An additional interesting result is the observation that mechanical deformation of the plasma membrane at a distal point can cause a polarized nucleus to move away from its preferred location to the site of deformation. These studies provide evidence for a rearrangement in

the MFs in response to mechanical perturbation of the plasma membrane (Kennard and Cleary, 1997).

Despite these insightful studies, these systems are quite underutilized. Given their ease of preparation and culture, and the ability to apply modern microscopical methods as well as intracellular microinjection, many exciting and potentially revealing studies can be undertaken, especially those that address the relationship of nuclear migration to division and the control of asymmetric division.

E. Pollen Mother Cells

1. Overview

Whereas the meiotic events leading to the formation of the egg in higher plants are difficult to examine directly, owing to the encasement of the relevant cells deep within the ovary, by contrast the meiotic divisions that lead to the formation of the male gametes occur in the exposed anthers and are extremely accessible. Importantly, these meiotic cells, referred to as pollen mother cells (PMCs), can be isolated from several different flowering species and examined in culture as they progress through meiosis, which, however, is usually restricted to the stages from late meiotic prophase or metaphase I through to the formation of the tetrad. Most success has been achieved with PMCs of monocots, including species of *Lilium, Iris, Allium,* and *Tradescantia.* While PMCs from other species might perform well under culture conditions, it must be noted that these cells in general are reasonably fragile and thus care is required to achieve a successful culture.

2. Culture Method

Lilium PMCs have been favorite objects for many studies in part because of their large size and the fact that by simply measuring bud length one can ascertain the stage of meiosis in the anthers (Erickson, 1948). PMCs can be excised from the anther loculi and expressed into sucrose solution or isotonic Ringer's solution (Inoué, 1953). Inoué found it expedient to centrifuge the cells (3 min at 1800*g*), thus displacing the refractile oil bodies to one side so that microscopic inspection would be improved. Ryan (1983), who summarizes several earlier studies, provides comparative culture methods for PMCs of *Iris, Allium,* and *Tradescantia.* Using slide chambers, particularly suitable for an inverted microscope, PMCs were expressed onto the coverslip, which had previously been coated with a thin layer of agar. Ryan emphasizes that if the PMC breaks through the agar layer and contacts the glass surface, the cell wall often puckers. The isolated cells are typically cultured in a solution of 0.22 *M* sucrose for *Iris* and *Tradescantia* or 0.28 *M* sucrose for *Allium,* plus 0.15% yeast extract, adjusted to pH 6.0–6.2 and covered with an inert halocarbon or paraffin oil to prevent drying.

Under these conditions PMCs of *Iris* can be cultured for 20 hr, during which time they have been observed to progress from metaphase I to the tetrad stage. Also, even when the sucrose solution is carefully adjusted for a particular PMC, the requirement can change during the process of meiosis. For example, at metaphase I in *Allium* the PMC requires 0.28 *M* sucrose, whereas somewhat later at metaphase II it requires 0.32 *M* sucrose.

3. Principal Findings

In contrast to most plant cell walls, those of the PMC do not contain cellulose but rather are composed of callose, which is nonbirefringent. Taking advantage of this condition, Inoué (1953, 1964), using polarized light microscopy, observed birefringent elements in the meiotic apparatus and phragmoplast in lily PMCs, providing the first evidence that living plant cells contained spindle fibers. These observations have been repeated in studies on the phragmoplast during telophase I in PMCs of *Tradescantia* (Schopfer and Hepler, 1991). In addition to polarized light it has also been possible to observe and quantitate chromosome motion and cell plate formation using phase contrast (Ryan, 1983), although much greater clarity in the images is provided by DIC (Schopfer and Hepler, 1991).

Fluorescence microscopic studies on PMCs have recently benefited substantially from the introduction of methods that allow the observer to optically section the cell. The problem of out-of-focus blur is probably more acute with PMCs than any other plant cell because they are essentially spherical (Hepler and Gunning, 1997). Therefore, the application of fluorescence confocal microscopy (Schopfer and Hepler, 1991), or deconvolution (Dawe *et al.,* 1994), yielding crisp planes of focus, has greatly increased the ability to visualize fine details. Although Dawe *et al.* (1994) applied the deconvolution procedure to fixed cells, it is nevertheless important to note the remarkable detail they observed in the structure and organization of the chromosomes during meiotic prophase in PMCs of *Zea mays.* In a similar manner, the confocal microscope together with the application of appropriate dyes has permitted the visualization of endoplasmic reticulum and MFs in PMCs of *Tradescantia* (Schopfer and Hepler, 1991). During anaphase, membranes, stained with $DiOC_6(3)$, were observed in association with the aggregating vesicle. MFs, stained with rhodamine-phalloidin under conditions in which the cells were lightly fixed or stabilized with m-maleimidobenzoyl N-hydroxysuccinimide ester (MBS), were found in two groups on each side of the cell plate.

Similar to the situation in many other dividing plant cell systems, PMCs have been underutilized. It seems clear, however, that the culture requirements are more acute for these cells when compared to other plant cells, e.g., stamen hairs. Nevertheless, there are many important questions about meiosis that deserve attention and that can be approached through the analysis of the living cell; for these reasons the study of PMCs is encouraged.

III. Microinjection of Plant Cells

A. Overview

The process of intracellular microinjection, as with animal cells (Wadsworth, Chapter 12, this volume), permits many experiments that otherwise have not been possible. In essence, it allows one to introduce virtually any molecule, e.g., analog, inhibitor, and indicator dye, into the living, dividing cell at any selected moment in the cell cycle, vastly increasing the precision with which the target cell can be probed and dissected. Because plant cells usually possess a rigid cell wall, and also because these cells are usually under substantial turgor pressure, the techniques required for successful microinjection are different than those that work well for animal cells (see Chapter 12). During the past decade considerable progress has been made in establishing the optimal methods that permit dividing plant cells to be routinely microinjected. These methods have been developed in studies on the dividing stamen hair cells of *Tradescantia,* but they apply equally well to other plant cells.

B. Microinjection Methods

1. Microscope Slide Chamber

Since work is best carried out on an inverted microscope with a rotatable stage, the chambers are designed for this format. There are two methods that we commonly use to mount stamen hairs. In the first method we use poly-L-lysine-coated microscope slide chambers, consisting of a microscope slide (75 × 50 mm) in which a 16-mm-diameter hole is drilled with a diamond drill. A poly-L-lysine-coated coverslip (22 × 22 mm) is glued to the slide with nail polish to create a poly-L-lysine-coated well. The coated coverslips are prepared as follows: Coverslips are soaked in 96% ethanol for about 30 min, after which they are air-dried. They are then incubated with a high-molecular-weight (150–300 kDa) poly-L-lysine hydrobromide solution (Sigma) by placing each coverslip, under a small weight, directly on a small (±15 μl) drop of poly-L-lysine solution on a strip of parafilm. The coverslips are allowed to incubate for about 2 hr at room temperature, after which they are washed thoroughly with distilled water and baked at 70°C for at least 20 min. Poly-L-lysine-coated coverslips can be stored at 4°C for a couple of weeks.

A second procedure employs etching of the glass surface with 5% hydrofluoric acid (HF) after the ethanol-cleaned coverslips are glued to the microscope slide. Following a 30-sec incubation in HF the well is washed by dipping in a beaker filled with water, followed by a 10-min wash under streaming tap water. After a final rinse with distilled water the etched microscope slide chambers are air-dried and can be stored indefinitely at room temperature.

2. Preparation of Stamen Hair Cells for Microinjection

Using the methods discussed in Section II,C, the stamen hair cells are isolated and prepared for mounting in agarose in a poly-L-lysine-coated or HF-etched microscope slide chamber. The hairs are carefully cut from the stamen filaments with a sharp scalpel or double-edged razor blade and transferred to a small drop of culture medium. At this point a dissecting microscope with a heated stage (35–40°C) is used to keep a drop of low-gelling temperature agarose (type VII, Sigma) in the microscope slide chamber molten. The isolated stamen hairs are then transferred to the drop of melted agarose and spread carefully, and the excess agarose is removed with a piece of filter paper to make the layer of agarose as thin as possible. The preparation is then placed at 4°C for about 15 sec to solidify the agarose and immobilize the stamen hairs. The growth chamber is then flooded with culture medium. During the course of extended observation, distilled water is added to replace evaporated water from the culture medium. If after microinjection one intends to examine the preparation for an hour or longer, the chamber can be covered with a second coverslip and sealed with VALAP (1:1:1, Vaseline, lanolin, and paraffin).

3. Microinjection Needles for Plant Cells

For injection, 1-mm-diameter borosilicate glass capillaries containing a filament are normally used (Fig. 2). The tip of the needle should be sharp enough to penetrate the cell wall easily, but the opening should be large enough to allow the passage of the experimental solution into the cell. We also note that the shank should be about 5 mm since longer ones tend to be too flexible to allow easy penetration of the cell wall. We use a Kopf (Tujunga, CA) vertical pipette puller (Model 700 D) on which adjustments of the heat allow us to influence the time it takes to pull a micropipette and thus the diameter of the tip orifice. It is our impression that the increased heat and shorter pull time (~10 sec) produces a sharper needle than lower heat and a longer pull time (~25 sec). To test this idea we have determined the electrical resistance of the needles in 3 *M* KCl. Although we find that there is substantial variation between two pipettes prepared under the same conditions, in general the 10-sec needles exhibit a high resistance (up to ~40 $M\Omega$), which for a 15-sec needle drops exponentially to ~10 $M\Omega$. Direct measurements of the tips with the scanning electron microscope indicate that the outer diameter for needles between 10- and 25-sec pull time is between 0.4 and 1.2 μm, and the inner diameter is between 0.1 and 0.6 μm. These preliminary observations may provide assistance for the preparation of suitable pipettes.

The size of the needle opening is particularly important for the microinjection of proteins, which because of their size and tendency to aggregate can clog the needle. The molecular weight of the protein seems to be important, with larger proteins generally requiring a larger diameter of tip opening. For example, microinjection of profilin (~15 kDa) requires a needle pull time (on pipette puller

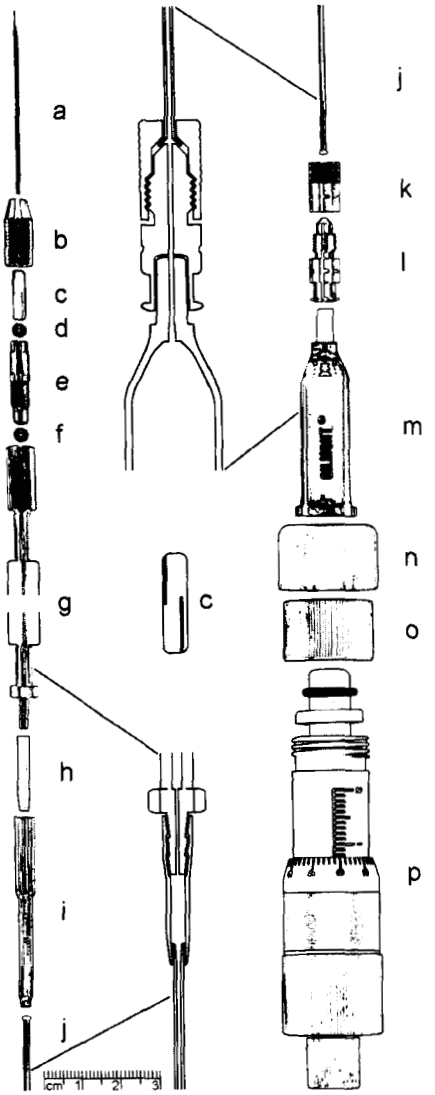

Fig. 2 Microinjector. For plant cell pressure injection a system composed of parts of various companies is assembled as shown. The needle (a) (1.0-mm diameter, with filament; World Precision Instruments, Sarasota, FL, Cat. No. 1B100F-4) is loaded and placed in the capillary grip head (b and e) (Eppendorf, Madison, WI, Cat. No. 5242-023-007) of which the original inner part is replaced with a custom-made Delrin insert (c) (Small Parts Inc., Miami Lakes, FL, Cat. No. E-ZRD-2-12), a slightly beveled 12.5-mm-long hollow cylinder with an outer diameter of 3.2 mm, an inner diameter of 1.0 mm, and two 6-mm-long, 0.25-mm-wide slits at either end, oriented at 90° from each other. The inside of the apical part (b) of the capillary grip head has also been slightly beveled in order to tighten the needle in the Delrin insert. Two O-rings (d and f) (Eppendorf, Cat. No. 5242-020-008 or Small Parts Inc., Cat. No. E-ORV-002) make a tight seal between the needle, capillary grip head, and capillary grip holder (g) (Eppendorf, Cat. No. 5242-150-009). The end of the holder

Kopf Model 700 D) of about ~16 sec, whereas microinjection of tubulin dimers (~100 kDa) requires a needle with pull time of ~20 sec. Smaller molecules such as carboxyfluorescein, by contrast, can readily pass through very sharp needles, requiring only 10–12 sec pull time.

It is possible to load needles by capillary action simply by placing the base of the needle shaft in the appropriate test solution. However, this procedure can be problematic for proteins; due to a chromatographic effect separation of the protein from its solvent can occur, with the result that only the latter will fill the needle tip. For this reason, needles are usually back filled using a fine plastic syringe or commercially available micropipette tip. After loading the needle tip with the experimental solution, the remainder of the capillary is filled with distilled water before mounting the needle into the microinjection device. Because of the small diameter of the needle, especially toward the tip, there is very little mixing between the water in the shaft of the pipette and the test solution, and thus essentially no dilution of the fraction will be microinjected.

4. Microinjector

A water-based microinjection system is used to microinject plant cells. The device is an assembly of parts of different manufacturers, which are listed in the Fig. 2 legend. The loaded microinjection needle (Fig. 2a) is mounted in a capillary grip head (Figs. 2b–2e) of which the internal metal cylinder is replaced by a Delrin insert (Fig. 2c). The capillary grip head screws into a capillary holder (Fig. 2g), which is connected to a 2-ml or 0.2-ml micrometer burette (Fig. 2m) by plastic tubing (Fig. 2i) and an adapter luer lock (Figs. 2k and 2l). We connect the tubing and the metal capillary holder using a cutoff pipette tip (Fig. 2h). First, the plastic tubing is pulled through the cutoff pipette tip after which the end of the tubing is heated with a small flame that will cause it to become flared. Taking care not to seal the end of the tubing, superglue is applied to the flared end of the tubing, and the tubing is then pulled back through the cutoff pipette tip until it is

---

is connected to about 50 cm polyethylene tubing (j) (inner diameter, 0.76 mm; outer diameter, 1.22 mm; Clay Adams, Becton–Dickinson, Sparks, MD, Cat. No. 427415) through a cutoff pipette tip (h) (Barky, Folkestone, UK). The end of the tubing is pulled through the cut of pipette tip, flared by heating, and glued inside the pipette tip with Instant Krazy Glue (Borden, Columbus, OH, Cat. No. KG-824). On the other end of the tubing a connection is made with a 2.0-ml micrometer syringe: glass syringe (m), nut (o), and micrometer (p) (Gilmont, Barrington, IL, Cat. No. GS-1200). The tubing is pulled through the outer part (k) of a luer-lock (Perfektum, Popper and Sons, Inc., New Hyde Park, NY, Cat. No. 6190) and flared and screwed onto the second part (l) that has been glued with Instant Krazy Glue (Borden) to the glass syringe (m). The glass syringe is mounted to the micrometer with a nut (o) that has been covered with a custom-made copper cap (n) (outer diameter, 23 mm; inner diameter, 21 mm; 15 mm long, with a 12-mm hole drilled in the top where the glass syringe sticks through). Cross sections and Delrin insert (c) at center of figure are at double magnification of the scale bar.

snugly sealed. After heating the back end of the capillary holder with a flame, the other end of the plastic cutoff pipette tip can be mounted. A cutoff plastic transfer pipette sleeve is placed over the connection for protection (Fig. 2i).

A second connection is made between the plastic tubing (Fig. 2j) and the luer lock (Figs. 2k and 2l). To make a proper fit, the tubing is pulled through the unscrewed part of the luer lock (Fig. 2k) and heated with a small flame as described previously. When the tubing is pulled back, the conical shape of the heated end ensures a tight seal between the tubing and the luer lock. To protect the neck of the glass syringe, a cutoff 5-ml pipette tip can be slid over the glass syringe (Fig. 2m). Recently, we adapted a copper cap (Fig. 2n) to tightly fit over the plastic threaded nut (Fig. 2o) that mounts the glass syringe on the plastic micrometer (Fig. 2p); this helps to keep the nut from cracking.

If too much pressure is applied to the injection system, leakages can occur in the connections with the plastic tubing; however, usually this is an indication that the needle tip is clogged rather than an inherent problem with the construction of the system.

5. Injection Procedure

A typical sequence of operation would include the positioning of the needle tip so it touches the cell wall at the chosen injection site, followed by the application of a positive hydraulic pressure within the microinjection system. The site of injection is mostly chosen at one of the "corners" of the cell since there is usually more cytoplasm. Also, it has been found that microinjection at these sites does not interfere with the site of cell plate connection to the parental cell wall. Thereafter, the needle is brought forward with the manipulator, causing a slight indentation of the cell wall of maximal 2 μm. Finally, by carefully tapping the microscope, the vibrations will cause the needle to impale the cell; the positive pressure in the microinjection system will simultaneously deliver the test solution into the cytoplasm. The delivery of the injected solution causes a visible pressure wave. In addition, the end walls (in the case of *Tradescantia* stamen hair cells) are usually curved outward due to the increased volume of the cell after a successful microinjection. Because many plant cells are highly vacuolated, successfully loading the test solution in the cytoplasm may be a problem. If the probe is fluorescent, a quick inspection can determine the location of the molecule. If, however, the probe is unlabeled, it helps to add an inert fluorescent tracer to serve as a marker for the compartment into which injection has occurred.

A particular problem with the use of large-bore needles and the injection of proteins is the requirement for the cell to heal the needle wound site before withdrawing the pipette from the cell. If the needle is immediately withdrawn after injection, due to the internal turgor pressure, cytoplasm will be driven out of the cell, quickly leading to death. Fortunately, plant cells have an active wound healing mechanism; soon after impalement, callose wall material and a new plasma membrane are deposited over the needle tip, creating a new cell boundary

with the needle being on the outside. This process may take 10–20 min, during which time it is essential that there is no drift in the micropositioner or the microscope stage. When the healing process is completed, the needle can be withdrawn without loss of cytoplasm, and although a refractile wound plug is present, the cell behaves normally.

For small, charged molecules it is possible to use iontophoresis, wherein current, rather than hydraulic pressure, is used to carry the species of interest into the cell. These methods are the same as those routinely used for animal cells (Purves, 1981).

Among the problems with microinjection, clogged needles are foremost. This problem can occur with virtually any molecule, small or large, but is most troublesome with proteins. Using larger needles, as noted previously, can help solve certain problems. However, especially with proteins there are other problems, notably aggregation/clumping or its adherence to the glass surface, that markedly affect the ease of injection. For example, in working with tubulin the protein is suspended in an assembly buffer and thus a certain amount of dimer/dimer interaction is inevitable. Centrifugation (14,000*g*) of the protein solution for at least 10 min will pellet protein aggregates and reduce the problem of clogged needles. To prevent protein denaturation, which can cause aggregation, the protein solution should be kept on ice and the time between loading the needle tip and actual impalement of the cell should be minimal.

Needle blockage can also be caused by a turgor-dependent flow of cytoplasmic organelles into the needle tip immediately after impalement. This problem can be avoided by applying an anticipatory counterpressure in the injector system, which prevents the flow into the needle. In addition, needle clogging can be caused by the inadvertent scooping of agarose into the pipette tip prior to impalement of the cell. This matter can be solved by keeping the agarose layer very thin during cell culture preparation and by controlling the lowering of the needle so that is contacts the cell before encountering a pool of agarose.

IV. Conclusions

There are many excellent systems among the higher plants for the study of division and related events in living cells. To date, endosperm cells, especially those of the African blood lily, *Haemanthus,* have received the most attention and are nearly unparalleled among all organisms, plant or animal, for the direct examination of chromosome motion from prophase through anaphase. However, with the development of improved optical methods, e.g., DIC and confocal fluorescence microscopy or deconvolution, other cell types, which heretofore had been considered less favorable, are emerging as excellent objects. Not only can chromosome motion be noted with clarity but also particularly the relationship of mitosis and cytokinesis to division plane determination and tissue morphogenesis can be directly examined and experimentally probed, permitting levels

and types of analysis that are not possible with endosperm. It is indeed a propitious time in which to explore these underutilized systems and take advantage of modern technical developments to make impressive advances.

In this article we also emphasized the procedure of microinjection, which has only relatively recently become routine for plant cells with walls. It permits the experimenter to introduce virtually any sort of molecule or probe, at any given moment, into the dividing cell and thus greatly expands the numbers and kinds of experiments that can be undertaken. Regardless of the cellular system or the experimental program that is selected, we emphasize that there is no substitute for sitting at the microscope and actually witnessing the dramatic events of cell division as they unfold before your eyes. Through direct observation of the vital processes it seems evident that important new information and insight about cell division will emerge.

Acknowledgements

We thank our colleagues, especially Dr. Patricia Wadsworth, for helpful comments, and Dr. Terena Holdaway-Clarke, Luke Hepler, and Mr. Dale Callaham, for technical assistance, during the preparation of this article. Support has been provided by Grant 94-37304-1180 from the United States Department of Agriculture to P. K. H. and by Grant NSF BBS 8714235 to the Central Microscopy Facility of the University of Massachusetts at Amherst from the National Science Foundation.

References

Asada, T., and Shibaoka, H. (1994). Isolation of polypeptides with microtubule translocating activity from phragmoplasts of tobacco BY-2 cells. *J. Cell Sci.* **107,** 2249–2257.

Asada, T., Sonobe, S., and Shibaoka, H. (1991). Microtubule translocation in the cytokinetic apparatus of cultured tobacco cells. *Nature* **350,** 238–241.

Asada, T., Kuriyama, R., and Shibaoka, H. (1997). TKRP125, a kinesin-related protein involved in the centrosome-independent organization of the cytokinetic apparatus in tobacco BY-2 cells. *J. Cell Sci.* **110,** 179–189.

Bajer, A. S. (1958). Ciné-micrographic studies on mitosis in endosperm. V. Formation of the metaphase plate. *Exp. Cell Res.* **15,** 370–383.

Bajer, A. S. (1965). Ciné-micrographic analysis of cell plate formation in endosperm. *Exp. Cell Res.* **37,** 376–398.

Bajer, A. S. (1990). The elusive organization of the spindle and the kinetochore fiber: A conceptual retrospect. *Adv. Cell Biol.* **3,** 65–93.

Bajer, A. S., and Allen, R. D. (1966). Role of phragmoplast filaments in cell-plate formation. *J. Cell Sci.* **1,** 455–462.

Bajer, A. S., and Molè-Bajer, J. (1954). Endosperm, material for study on the physiology of cell division. *Acta Soc. Bot. Poloniae* **23,** 69–98.

Bajer, A. S., and Molè-Bajer, J. (1954). Endosperm, material for study on the physiology of cell division. *Acta Soc. Bot. Polonia* **23,** 69–98.

Bajer, A. S., and Molè-Bajer, J. (1956). Ciné-micrographic studies on mitosis in endosperm. II. Chromosome, cytoplasmic and Brownian movements. *Chromosoma* **7,** 558–607.

Bajer, A. S., and Molè-Bajer, J. (1961). UV microbeam irradiation of chromosomes during mitosis in endosperm. *Exp. Cell Res.* **25,** 251–267.

Bajer, A. S., and Molè-Bajer, J. (1986). Drugs with colchicine-like effects that specifically disassemble plant but not animal microtubules. *Ann. N. Y. Acad. Sci.* **466,** 7767–784.

Bajer, A. S., Cypher, C., Molè-Bajer, J., and Howard, H. M. (1982). Taxol-induced anaphase reversal: Evidence that elongating microtubules can exert a pushing force in living cells. *Proc. Natl. Acad. Sci. USA* **79,** 6569–6573.

Bajer, A. S., Sato, H., and Molè-Bajer, J. (1986). Video microscopy of colloidal gold particles and immuno-gold labeled microtubules in improved rectified DIC and epi-illumination. *Cell Struct. Funct.* **11,** 317–330.

Bajer, A. S., Vantard, M., and Molè-Bajer, J. (1987). Multiple mitotic transports expressed by chromosome and particle movement. *Fortschritte Zool.* **34,** 171–186.

Bělař, K. (1929). Beiträge zur Kausalanalyse der Mitose. III. Untersuchungen an den Staubfadenhaarzellen und Blattmeristemzellen von *Tradescantia virginica. Z. Zellforsch. Mikrosk. Anat.* **10,** 73–134.

Bonsignore, C. L., and Hepler, P. K. (1985). Caffeine inhibition of cytokinesis: Dynamics of cell plate formation–deformation *in vivo. Protoplasma* **129,** 28–35.

Cleary, A. L. (1995). F-actin redistributions at the division site in living *Tradescantia* stomatal complexes as revealed by microinjection of rhodamine-phalloidin. *Protoplasma* **185,** 152–165.

Cleary, A. L., Gunning, B. E. S., Wasteneys, G. O., and Hepler, P. K. (1992). Microtubule and F-actin dynamics at the division site in living *Tradescantia* stamen hair cells. *J. Cell Sci.* **103,** 977–988.

Czaban, B. B., Forer, A., and Bajer, A. S. (1993). Ultraviolet microbeam irradiation of chromosomal spindle fibers in *Haemanthus katherinae* endosperm. *J. Cell Biol.* **105,** 571–578.

Dawe, R. K., Sedat, J. W., Agard, D. A., and Cande, W. Z. (1994). Meiotic chromosome pairing in *Maize* is associated with a novel chromatin organization. *Cell* **76,** 901–912.

Erickson, R. O. (1948). Cytological and growth correlations in the flower bud of *Lilium longiflorum. Am. J. Bot.* **35,** 729–739.

Fuseler, J. W. (1975). Temperature dependence of anaphase chromosome velocity and microtubule depolymerization. *J. Cell Biol.* **67,** 789–800.

Gu, X., and Verma, D. P. S. (1996). Phragmoplastin, a dynamin-like protein associated with cell plate formation in plants. *EMBO J.* **15,** 695–704.

Gu, X., and Verma, D. P. S. (1997). Dynamics of phragmoplastin in living cells during cell plate formation and uncoupling of cell elongation from the plane of cell division. *Plant Cell* **9,** 157–169.

Hepler, P. K. (1985). Calcium restriction prolongs metaphase in dividing *Tradescantia* stamen hair cells. *J. Cell Biol.* **100,** 1363–1368.

Hepler, P. K., and Gunning, B. E. S. (1997). Confocal fluorescence microscopy of plant cells. *Protoplasma,* in press.

Hepler, P. K., and Palevitz, B. A. (1985). Metabolic inhibitors block anaphase A *in vivo. J. Cell Biol.* **102,** 1995–2005.

Hepler, P. K., Cleary, A. L., Gunning, B. E. S., Wadsworth, P., Wasteneys, G. O., and Zhang, D. H. (1993). Cytoskeletal dynamics in living plant cells. *Cell Biol. Int.* **17,** 127–142.

Hepler, P. K., Sek, F. J., and John, P. C. L. (1994). Nuclear concentration and mitotic dispersion of the essential cell cycle protein, $p13^{suc1}$ examined in living cells. *Proc. Natl. Acad. Sci. USA* **91,** 2176–2180.

Hush, J. M., Wadsworth, P., Callaham, D. A., and Hepler, P. K. (1994). Quantification of microtubule dynamics in living plant cells using fluorescence redistribution after photobleaching. *J. Cell Sci.* **107,** 775–784.

Hush, J., Liping, W., John, P. C. L., Hepler, L. H., and Hepler, P. K. (1996). Plant mitosis promoting factor disassembles the microtubule preprophase band and accelerates prophase progression in *Tradescantia. Cell Biol. Int.* **20,** 275–287.

Inoué, S. (1953). Polarization optical studies of the mitotic spindle. I. The demonstration of spindle fibers in living cells. *Chromosoma* **5,** 487–500.

Inoué, S. (1964). Organization and function of the mitotic spindle. *In* "Primitive Motile Systems in Cell Biology" (R. D. Allen and N. Kamiya, eds.), pp. 549–598. Academic Press, New York.

Inoué, S., and Bajer, A. S. (1961). Birefringence in endosperm mitosis. *Chromosoma* **12,** 48–63.

Jürgens, M., Hepler, L. H., Rivers, B. A., and Hepler, P. K. (1994). BAPTA-calcium buffers modulate cell plate formation in stamen hairs of *Tradescantia:* Evidence for calcium gradients. *Protoplasma* **183,** 86–99.

Kakimoto, T., and Shibaoka, H. (1988). Cytoskeletal ultrastructure of phragmoplast–nuclei complexes isolated from cultured tobacco cells. *Protoplasma* (Suppl. 2), 95–103.

Kakimoto, T., and Shibaoka, H. (1992). Synthesis of polysaccharides in phragmoplasts isolated from tobacco BY-2 Cells. *Plant Cell Phys.* **33,** 353–361.

Keith, C. H., Ratan, R., Maxfield, F. R., Bajer, A., and Shelanski, M. L. (1985). Local cytoplasmic calcium gradients in living mitotic cells. *Nature* **316,** 848–850.

Kennard, J. L., and Cleary, A. L. (1997). Pre-mitotic nuclear migration in subsidiary mother cells of *Tradescantia* occurs in G1 of the cell cycle and requires F-actin. *Cell Motil. Cytoskel.* **36,** 55–67.

Khodjakov, A., Cole, R. W., Bajer, A. S., and Rieder, C. L. (1996). The force for poleward chromosome motion in *Haemanthus* cells acts along the length of the chromosome during metaphase but only at the kinetochore during anaphase. *J. Cell Biol.* **132,** 1093–1104.

Lambert, A. M., and Bajer, A. S. (1977). Microtubule distribution and reversible arrest of chromosome movements induced by low temperature. *Eur. J. Cell Biol.* **15,** 1–23.

Larsen, P. M., and Wolniak, S. M. (1993). Asynchronous entry into anaphase induced by okadaic acid: Spindle microtubule organization and microtubule/kinetochore attachments. *Protoplasma* **177,** 53–65.

Liu, B., Cyr, R. J., and Palevitz, B. A. (1996). A kinesin-like protein, KatAp, in the cells of arabidopsis and other plants. *Plant Cell* **8,** 119–132.

Molè-Bajer, J. (1958). Ciné-micrographic analysis of C-mitosis in endosperm. *Chromosoma* **9,** 332–358.

Molè-Bajer, J., and Bajer, A. S. (1963). Mitosis in endosperm, techniques of studies in vitro. *La Cellule* **63,** 399–407.

Molè-Bajer, J., and Bajer, A. S. (1988). "Relation of F-actin organization to microtubules in drug treated *Haemanthus* mitosis. *Protoplasma* (Suppl. 1), 99–112.

Morejohn, L. C., Bureau, T. E., Molè-Bajer, J., Bajer, A. S., and Fosket, D. E. (1987). Oryzalin, a dinitroaniline herbicide, binds to plant tubulin and inhibits microtubule polymerization in vitro. *Planta* **172,** 252–264.

Nagata, T., Nemoto, Y., and Hasezawa, S. (1992). Tobacco BY-2 cell line as the "Hela" cell in the cell biology of higher plants. *Int. Rev. Cytol. Biology.* **132,** 1–30.

Ôta, T. (1961). The role of cytoplasm in cytokinesis of plant cells. *Cytologia* **26,** 428–447.

Palevitz, B. A. (1980). Comparative effects of phalloidin and cytochalasin B on motility and morphogenesis in *Allium*. *Can. J. Bot.* **58,** 773–785.

Palevitz, B. A., and Hepler, P. K. (1974a). The control of the plane of division during stomatal differentiation in *Allium*. I. Spindle reorientation. *Chromosoma* **46,** 297–326.

Palevitz, B. A., and Hepler, P. K. (1974b). The control of the plane of division during stomatal differentiation in *Allium*. II. Drug studies. *Chromosoma* **46,** 327–341.

Purves, R. D. (1981). Microelectrode methods for intracellular recording and ionophoresis. *In* "Biological Techniques Series" (J. E. Treherne and P. H. Rubery, eds.). Academic Press, London.

Ryan, K. (1983). Chromosome movements in pollen mother cells: Techniques for living cell ciné-microscopy and for electron microscopy. *Mikroskopie* **40,** 67–78.

Sawamura, S. (1952). The effect of caffeine and 8-oxyquinoline on the mitosis of *Tradescantia* cell *in vivo*. *Bull. Utsunomiya Univ.* **2,** 167–175.

Schmit, A. C., and Lambert, A. M. (1990). Microinjected fluorescent phalloidin *in vivo* reveals the F-actin dynamics and assembly in higher plant mitotic cells. *Plant Cell* **2,** 129–138.

Schopfer, C. R., and Hepler, P. K. (1991). Distribution of membranes and the cytoskeleton during cell plate formation in pollen mother cells of *Tradescantia*. *J. Cell Sci.* **100,** 717–728.

Strasburger, E. (1880). "Zellbildung und Zelltheilung," 3rd Ed. Fischer, Jena.

Valster, A. H., and Hepler, P. K. (1997). Caffeine inhibition of cytokinesis: Effect on the phragmoplast cytoskeleton in living *Tradescantia* stamen hair cells. *Protoplasma* **196,** 155–166.

Valster, A. H., Pierson, E. S., Valenta, R., Hepler, P. K., and Emons, A. M. C. (1997). Probing the plant actin cytoskeleton during cytokinesis and interphase by profilin microinjection. *Plant Cell* **9,** 1815–1824.

Vantard, M., Levilleirs, N., Hill, A. M., Adoutte, A., and Lambert, A. M. (1990). Incorporation of *Paramecium* axonemal tubulin into higher plant cells reveals functional sites of microtubule assembly. *Proc. Natl. Acad. Sci. USA* **87,** 8825–8829.

Vos, J. W., and Hepler, P. K. (1998). Calmodulin is uniformly distributed during cell division in living stamen hair cells of *Tradescantia virginiana.* Submitted for publication.

Wilson, E. B. (1928). "The cell in development and heredity," 3rd Ed. Macmillan, New York.

Wolniak, S. M. (1991). Patterns of regulation during mitosis. *In* "The Cytoskeletal Basis of Plant Growth and Form" (C. W. Lloyd, ed.), pp. 209–226. Academic Press, London.

Wolniak, S. M., and Hepler, P. K. (1981). The coincident distribution of calcium-rich membranes and kinetochore fibers at metaphase in living endosperm cells of *Haemanthus. Eur. J. Cell Biol.* **25,** 171–174.

Wolniak, S. M., and Larsen, P. M. (1992). Changes in the metaphase transit times and the pattern of sister chromatid separation in stamen hair cells of *Tradescantia* after treatment with protein phosphatase inhibitors. *J. Cell Sci.* **102,** 691–715.

Wolniak, S. M., Hepler, P. K., and Jackson, W. T. (1980). Detection of the membrane-calcium distribution during mitosis in *Haemanthus* endosperm with chlorotetracycline. *J. Cell Biol.* **87,** 23–32.

Wolniak, S. M., Hepler, P. K., and Jackson, W. T. (1983). Ionic changes in the mitotic apparatus at the metaphase/anaphase transition. *J. Cell Biol.* **96,** 598–605.

Zhang, D., Wadsworth, P., and Hepler, P. K. (1990a). Microtubule dynamics in living plant cells: Confocal imaging of microinjected fluorescent brain tubulin. *Proc. Natl. Acad. Sci. USA* **87,** 8820–8824.

Zhang, D. H., Callaham, D. A., and Hepler, P. K. (1990b). Regulation of anaphase chromosome motion in *Tradescantia* stamen hair cells by calcium and related signalling agents. *J. Cell Biol.* **111,** 171–182.

Zhang, D. H., Wadsworth, P., and Hepler, P. K. (1992). Modulation of anaphase spindle microtubule structure in stamen hair cells of *Tradescantia* by calcium and related agents. *J. Cell Sci.* **102,** 79–89.

Zhang, D. H., Wadsworth, P., and Hepler, P. K. (1993). Dynamics of microfilaments are similar, but distinct from microtubules during cytokinesis in living, dividing plant cells. *Cell Motil. Cytoskel.* **24,** 151–155.

This Page Intentionally Left Blank

CHAPTER 22

Using Sea Urchin Gametes for the Study of Mitosis

Greenfield Sluder, Frederick J. Miller, and Edward H. Hinchcliffe

Department of Cell Biology
University of Massachusetts Medical Center
Shrewsbury Campus
Shrewsbury, Massachusetts 01655

METHODS IN CELL BIOLOGY, VOL. 61

0091-679X/99 $30.00

I. Introduction

In this chapter we describe the methods we have found useful for the study of cell division in early cleavage stage sea urchin zygotes. We have not provided an inclusive review of procedures developed over the past 100 years by the many investigators who have used this experimental system. To partially mitigate our omissions we have included at the end of this chapter an annotated bibliography of papers and reviews covering techniques developed by a number of contemporary workers.

II. The Experimental System

Why use sea urchin zygotes as a model system for the study of mitosis? The answer is simple: One can conduct many sorts of experiments more easily and at a substantially lower cost with zygotes than with cultured cells. In fact, there are certain experiments of general relevance that would, for practical reasons, be impossible to conduct with somatic cells. Some of the advantages of the sea urchin zygote system include the following:

1. Quantity of gametes and zygotes: One can obtain large numbers/volumes of cells at a reasonable cost for studies that require the isolation of macromolecules or organelles. Also, sea urchin zygotes are easier to work with than somatic cells because they do not need to be cultured under sterile conditions.

2. Rapid cell cycle: Sea urchin zygotes have a fast cell cycle relative to the 18- to 24-hr cell cycle of cultured somatic cells. Depending on the species, the time from fertilization to first division ranges from 1 to 1.5 hr, with succeeding divisions occurring at 45- to 60-min intervals. If one is working with cells at first or second division, this means that multiple experiments can be conducted in a single day, especially when the next batch of eggs is fertilized before the completion of the prior experiment. For much of our work we need to follow the behavior of live cells through three cell cycles; this would take days with cultured cells if one could keep them healthy that long on the microscope.

3. Synchronous Cell Cycles: Synchronization of the cell cycle is possible with only some cultured cell types and can be a time-consuming, problematic procedure. Obtaining large quantities of essentially synchronous cells for the first three cell cycles is simple with the sea urchin system since unfertilized eggs are all

arrested at the same point in development (first mitotic G_1) and their cell cycles start in unison at fertilization.

4. Cell size and optical characteristics: Sea urchin eggs, by the standards of most cultured cells, are large. For the commonly used species in the United States the eggs range from 70 to 100 μm in diameter with negligible size variation between eggs of the same species. As a consequence, the mitotic spindles are large and relatively easy to follow with microscope objectives of moderate magnification (20–40×). In addition, the size of these zygotes make them relatively easy to microinject or micromanipulate. Also, in some species of sea urchins and starfish the eggs are optically clear, which makes them ideal for studies that require following nuclear and cytoplasmic events *in vivo.* We routinely use the clear eggs of the sea urchins *Lytechinus pictus* and *L. variegatus* and the starfish *Pisaster ocraceus, P. gigantea,* and *Asterias forbesi.*

5. Zygotes do not grow between divisions: One can study the control of cell cycle events using approaches that are not possible to use on cultured cells. Since somatic cells need to grow before dividing, experimental perturbations that block macromolecular synthesis or other "housekeeping" functions stop the cell cycle. Thus, one cannot determine if the event in question is directly dependent on the blocked process or if the event fails to occur because the cell cycle is arrested at a point prior to its scheduled execution. Eggs, on the other hand, store almost all the substances necessary for early development and the rapid progression of the cell cycle. Thus, one can assay for the importance of various metabolic pathways in the regulation of particular events without the concern that the cell cycle is stopped for trivial reasons unrelated to the function of the natural control mechanisms.

III. Maintenance of the Organisms

Although it is beyond the scope of this article to provide a comprehensive review of the care and maintenance of marine organisms, we list a few commonsense items and concerns. First, we emphasize that even though it is not hard to maintain echinoderms in recirculating seawater tanks, one should pay attention to their care. Organisms in poor health do not provide gametes of optimal viability, which leads to undesirable variability in the response of individual zygotes to experimental perturbations.

A. Organisms

Most established suppliers have evolved good methods to pack and ship echinoderms. However, since shipping is invariably stressful for the animals, be willing to pay for the fastest form of shipment. Also, be certain to arrange for prompt notification of their arrival at your institution and unpack them just after they

arrive. If the organisms are shipped in water of a significantly different temperature than that of your aquarium, float the plastic bags or containers holding individual animals in your tank for 30 min to prevent temperature shock that can lead to spawning. Importantly, never put spawning individuals into the tank; spawners, be they male or female, can trigger spawning of the whole population, a reproductive strategy used by echinoderms in the wild.

B. Tanks

In maintaining seawater tanks the only practical philosophy is to be proactive and stay ahead of problems before they arise. Tanks should have reliable temperature control and a redundant supply of air sources for the bubblers since air stones can clog or disintegrate over time. The seawater should be changed on a regular schedule even if it looks clean; by the time the water looks obviously dirty the organisms are at serious risk and usually will be unhealthy. Experience has shown us that when the tank "goes bad" organisms start spawning and then dying at a remarkable rate. We normally change one-third of the water volume every week. Obtain good quality sea salts or clean natural seawater. For the past 10 years we have made seawater using Morton brand noniodized food-grade NaCl and Fritz SuperSalt Concentrate (Fritz Aquaculture, Dallas, TX) to provide the trace ions. Be careful to prepare salts in distilled or reverse osmosis water; tap water in metropolitan areas contains chlorine and building plumbing can add metal ions, typically copper, to the water. Do not overload a tank with animals for any length of time. For each gallon of seawater we typically maintain approximately two or three small sea urchins (*L. pictus*) or one large sea urchin (*L. variegatus* and *S. purpuratus*). For large starfish (*Pisaster ocraceus*) we allow 10 gallons of seawater per animal. Normally sea urchins like to climb the walls of the tank. There is clearly a problem if all animals are sitting on the bottom of the tank for any length of time and/or their spines "droop."

It is of real importance to have a thick bed of dolomite, crushed coral, or porous gravel in the bottom of the tank and use a tank design that continuously circulates the water though this gravel layer, not just over it. The ammonia produced as a metabolic by-product by the animals is toxic. The gravel layer should be inoculated with nitrobacter which turns the ammonia into nitrite and nitrate, which are relatively benign. Dolomite is a favorable substrate for these bacteria because its microcrystalline structure provides a large surface area for the bacteria to attach. In this regard, it is of obvious importance not to overclean or sterilize the gravel bed when cleaning the tank. In setting up a tank for the first time we normally put in a lobster or two for a week to start the bacterial colony.

It is possible and desirable to feed echinoderms for their long-term maintenance. We feed sea urchins fish food (e.g., "Tetramin") either sprinkled on the water surface or cast into chunks of agar. Starfish are fed bits of fish or clam. It is of utmost importance to remove unused food and to not overfeed. Addition of significant amounts of food puts a real load on the tank and, if continued too

long without water changes, will lead to the death of the animals. If one has a laboratory near a coast, the best food is living seaweed because the plants remain alive until eaten.

IV. Obtaining Gametes

Fuseler (1973) provides a good description of how to obtain gametes from sea urchins and starfish. To this we add the following items taken from our experience:

1. Spawning: Use the minimum amount of 0.5 *M* KCl to induce spawning of sea urchins and use only a single injection to minimize the number of punctures to the membrane surrounding the oral apparatus. If spawned judiciously, the animals can be returned to the tank, fed, and used again. Be careful not to leave the sea urchins out of water on the laboratory bench for prolonged periods of time. We normally keep the spawned animals (particularly the males) in a bucket of seawater for an hour or two to ensure that they have completed spawning before they are returned to the aquarium. To control temperature in the bucket, on warm days we add a capped plastic soft drink bottle containing frozen water. Although this does not represent precise temperature control, the method works well.

2. Sperm: Spawn the males onto a clean, dry plastic petri dish and cover the "dry sperm" for storage in the refrigerator. The sperm are viable for several days in this condition. We dilute dry sperm into seawater at the start of each experiment.

3. Eggs: We spawn eggs fresh for each day's experiments. When storing eggs for that day's experiment, plate them out as a monolayer in the bottom of a beaker; do not leave them as a pellet in a test tube or as a thick layer in a small beaker. Beakers should always be covered to prevent evaporation. We find that unfertilized eggs can be stored for 8 hr at the physiological temperature for the organism. Beyond that one runs the risk of loss of egg viability. Promising strategies for the long-term storage of spawned eggs are being developed (D. Epel, unpublished results). We do not recommend the storage of eggs in the refrigerator (unless this represents the physiological temperature for the species you are using). It is important to maintain the seawater to be used with gametes at the physiological temperature for that species of echinoderm. Novices will sometimes add warm seawater to eggs and then put the culture onto the colder water bath. Later they wonder why the "toasted" gametes are of poor quality. For obvious reasons, avoid accidentally dripping bath water clinging to the bottom of tubes and beakers into the zygote cultures during the movement of tubes and beakers.

4. Seawater: We are careful to use the best quality seawater when handling gametes. When mixing seawater from salts be certain that the specific gravity and pH are correct and keep the stored batches of salt water covered. Normally

we maintain the organisms in seawater made from bulk salts and handle the gametes/zygotes in natural seawater. If natural seawater is to be used for experiments involving the uptake of radiolabeled tracers it should be filtered through a 0.2-μm filter to remove microorganisms that also take up the tracer.

V. Zygotes

A. Fertilization

Successful and reliable fertilization of sea urchin eggs is simple if a few precautions are kept in mind. First, use only clean glassware that has not been exposed to fixatives or metal ions. If the glassware is washed in a central facility, be certain that there is no residual detergent present. We also have had good results with the use of "conditioned" glassware that is dedicated to use with live cells. At the end of the day we rinse the glassware with distilled water and store it filled with distilled water. The glassware should be thoroughly washed if it is exposed to drugs.

To conduct routine fertilizations we first prepare a sperm solution adding just enough sperm to the test tube to make the water barely opalescent. If the sperm are too concentrated, there is the risk of polyspermy. We then prepare a dilute solution of eggs and add a small amount of sperm solution. There is no precise ratio that needs to be attained, but the water around the eggs appears clear to the eye. For some species, eggs will not fertilize well if they are too concentrated.

Sea urchin eggs have a jelly coat that plays a role in sperm–egg recognition. We have found no need to strip the jelly coats off the eggs, as some advocate. In fact, when we thoroughly strip the jelly coats with acidified seawater, we find that the eggs fertilize slowly and asynchronously.

B. Fertilization Envelopes

Upon fertilization echinoderm eggs elevate a tough fertilization membrane, or envelope, as the cortical granules exocytose (Fig. 1). For routine work we leave the fertilization envelopes intact because this minimizes mechanical damage to the zygotes during handling. However, for some experiments, such as micromanipulation, microinjection, and organelle isolation, it is necessary to remove fertilization envelopes. There are many methods that have been used for this purpose and we will not review them. The method we use works well, does not use exotic chemical treatments, and produces zygotes with excellent viability. However, a good sense of timing and efficient handling of the zygotes are helpful.

First we fertilize the diluted eggs in a beaker with approximately 0.5–1 cm of natural seawater in the bottom. After 1 min (when the fertilization envelopes are just coming up and still fragile) we add a large volume of calcium-free seawater and immediately pass the eggs though a nylon screen (Tetco, Inc.,

Fig. 1 Sea urchin zygote with fertilization envelope indicated. The zygote nucleus can be seen in the center of the 100-μm-diameter cell. Differential interference contrast microscopy.

Elmsford, NY) with a mesh size of 102 μm. We use at most two passes to minimize egg fragmentation and use two separate screens to ensure that we have a clean screen for each pass. After use the screens are immediately washed with distilled water to prevent the buildup of proteinaceous deposits that clog the openings. The screen holder is made by cutting the bottom (rounded or pointed end) off a 30- to 50-ml plastic test tube and cutting the center out of the screw cap. The screw cap is then used to hold the screen to the tube (Fig. 2). Should proteinaceous deposits accumulate on the screen, one can either discard it or clean it with a 1 or 2 mg/ml solution of pronase in distilled water.

We initially fertilize the eggs in natural seawater because they will not fertilize in calcium-free seawater. The calcium-free seawater is added to help prevent the fertilization envelopes from hardening. We typically store the zygotes in the resulting low-calcium seawater. Although it is possible to wash the eggs back into natural seawater, they tend to be sticky and may clump when pelleted.

C. Storing Zygotes

Zygotes in modest quantities, with or without fertilization envelopes, are stored as loose monolayers in covered beakers containing at most 1 cm of seawater. Agitation is not necessary or desirable. We are careful to limit the water depth to 1 cm because the zygotes are metabolically active and depend on the diffusion of oxygen from the water surface. Overloading the beaker with zygotes or leaving the water too deep will noticeably affect development time and cell cycle synchrony.

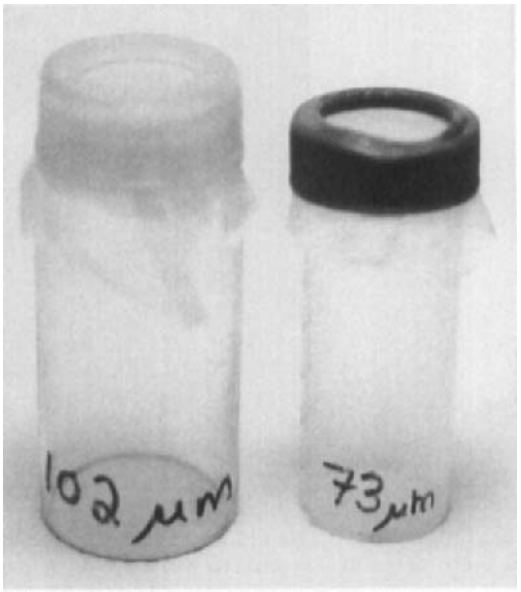

Fig. 2 Screw cap plastic centrifuge tubes modified to hold nylon screening.

When working with large quantities of zygotes, for example, in experiments of a biochemical nature, we maintain the zygotes at a concentration of approximately 1% (v/v) in 1- or 2-liter beakers that are stirred with paddles at approximately 60 rpm. For this purpose we mount a small electric "clock" motor on a Plexiglas rectangle (Fig. 3a) and rest it on the top of the beaker or hold it above the beaker with a clamp on a ring stand. It is useful to have a hole drilled in the Plexiglas to facilitate sampling with a pipette. The paddle is a rod of glass inserted through two slits in a flat piece of polyethylene that we cut from flat-sided reagent bottles. We hold the glass rod to the shaft of the motor with a short piece of rubber tubing (Fig. 3b). To prevent a shearing action on the zygotes the paddle should not contact the bottom of the beaker. We specifically recommend against the use of magnetic stir bars because they fragment or kill the zygotes and the stir plate can warm the beaker.

D. Centrifuges

It is of great importance when pelleting eggs and zygotes to be as gentle as possible. It is possible to use motorized tabletop centrifuges or low-speed floor centrifuges for routine work if one is careful. However, for routine handling of small volumes of zygotes in cytological work we find motorized centrifuges to be inconvenient due to the time required for them to come up to speed and slow down at the end of the run. Often, time is of the essence, for example,

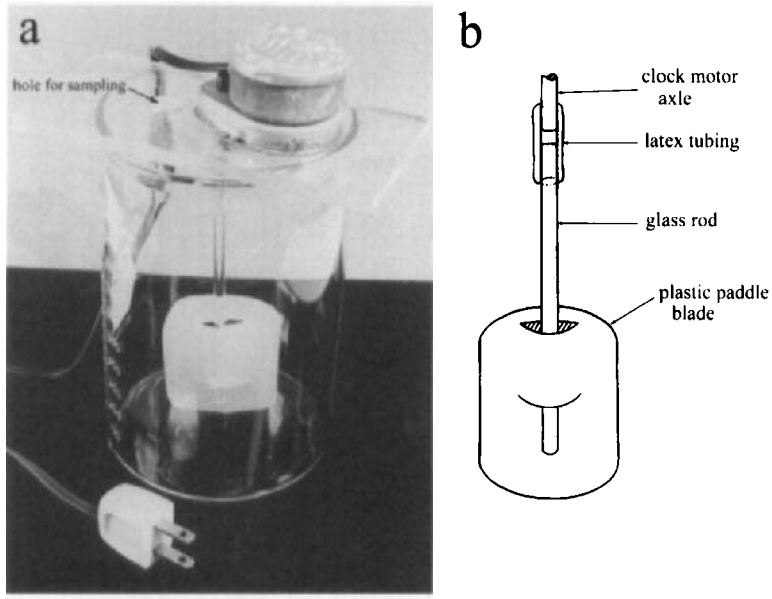

Fig. 3 Stir paddle apparatus for maintaining large volumes of zygotes in suspension. (a) "Clock" motor is mounted on a Plexiglas rectangle that has an access hole for sampling with a pipette. Plexiglas can rest on top of the beaker or can be held with a clamp attached to a ring stand. (b) Diagram of the stir paddle assembly.

when terminating a drug treatment, and modern centrifuges with safety locks on the lids can prove to be irritatingly slow. We use hand centrifuges of the sort shown in Fig. 4 that hold 12- to 15-ml conical glass centrifuge tubes. These centrifuges allow one to work quickly, allow good control over how tightly the zygotes are pelleted, and are gentle to the cells when used properly. For a laboratory extensively using echinoderm zygotes, such centrifuges are an essential piece of equipment. Unfortunately, they are not common laboratory apparatus and can be difficult to locate. We suggest ordering "Hand Centrifuge" Model 1160-2-15 (Boekel Scientific, Feastervill, PA, 1-800-336-6929). We also suggest the purchase of 12-ml heavy walled conical glass tubes for use in these centrifuges. The speeds commonly used do not preclude the use of the cheaper thin-walled tubes but we have found that there is a significant attrition rate for such tubes due to handling by glassware washers. Finally, be certain to put a small amount of cotton in the bottom of the buckets to cushion the tips of the tubes and facilitate tube removal from the holders.

When handling large volumes of eggs or zygotes, the hand centrifuge is often not practical. For such work we use a low-speed refrigerated floor centrifuge with a swing bucket rotor capable of taking 15- or 30-ml conical tubes. Empirically work out the minimal speed and time required to form loose pellets of zygotes.

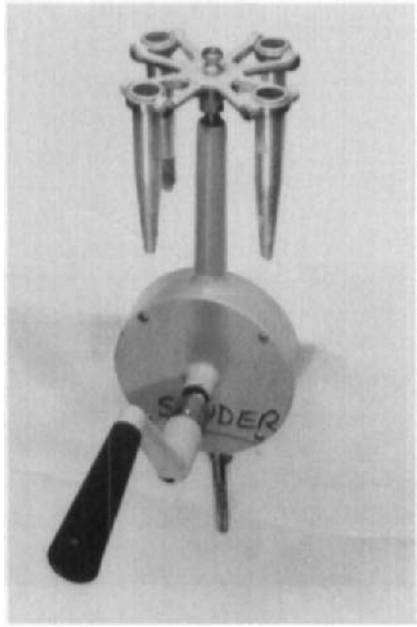

Fig. 4 Hand centrifuge.

E. Pipettes

In principle, any sort of pipetting method can be used to transfer zygotes as long as it does not shear the cells. We routinely use 5.75-in. Pasteur pipettes with a latex bulb. It is possible to use an adjustable pipetter with plastic tips, especially when one wants to control the volume of packed cells used. However, one should pay attention to the diameter of the tip orifice and the rate at which the cells are drawn into the tip. Careless use of such tips can lead to the killing or fragmentation of zygotes, especially when the fertilization envelopes have been removed.

VI. Mounting Cells for Observation

The strategy used to mount zygotes for observation is determined by whether one wants to conduct short-term observation, in essence a "snapshot" assay, or one needs to follow the longer term development of the zygotes. In the latter application, bear in mind that reliable maintenance of cell viability is of paramount importance. Echinoderm zygotes are metabolically very active and will quickly deplete the oxygen in a simple seawater slide preparation and cease dividing. In addition, long-term observations require the cleaning of the slides and coverslips.

A. Tools of the Trade

For making preparations of all sorts we have found it useful to use a black Lucite work surface (Fig. 5). This can be easily cleaned with alcohol and provides a dark background to optimize the contrast of the glass surfaces and zygotes. For handling coverslips we use fine blunt-tipped curved forceps. To handle and peel the adhesive tapes used in the preparation of chambers described later we use a pair of sharp-tipped curved forceps of the sort used by electron microscopists. As part of our "kit" we also have a narrow 6-in. precision steel ruler (machine shop supply), a curved-tip scalpel, a small tapered stainless reagent spatula, a diamond scribe, a small alcohol lamp, and a lighter. We also keep on hand small petri dishes containing Vaseline and silicone vacuum grease. For sealing slides we use VALAP, which is a 1:1:1 mixture of Vaseline, lanolin, and paraffin wax. A long-term supply of this sealant can be prepared and stored indefinitely in a number of plastic petri dishes.

To remove supernatants from test tubes or to clear excess fluids from slide preparations we use a Pasteur pipette connected by clear plastic tubing to a vacuum source. Although a vacuum source consisting of a venturi apparatus mounted on a water faucet suffices, we have found this to be impractical for routine work. Unless one can waste enormous amounts of water, it is inconvenient to turn the faucet on and off for each operation; also, we find this apparatus to

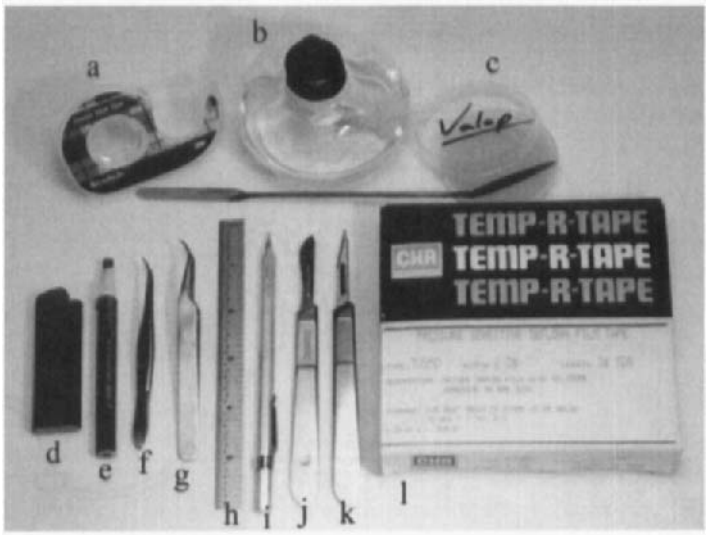

Fig. 5 Tool kit for making slide preparations to follow living zygotes on the microscope. a, doublestick tape; b, alcohol lamp; c, petri dish filled with VALAP and the bent spatula used to apply it; d, disposable lighter; e, wax pencil with tip tapered on two sides; f, blunt-tipped curved forceps; g, sharp-tipped curved forceps; h, 6-in metal ruler; i, diamond scribe; j and k, scalpels; l, Teflon tape.

be irritatingly noisy. Instead, we use "house" vacuum hooked up to a 2- to 4-liter vessel with a 0.5- to 1-liter sidearm Erlenmeyer flask between the vacuum source and the larger vessel to serve as an overflow trap (Fig. 6). Be certain to use heavy-walled vacuum flasks. When preparing the two-hole stopper at the top of the primary collection vessel, be certain to make the glass delivery tube longer than the vacuum source tube to prevent water from going directly into the overflow trap. Also, note the sidearm tube at the bottom of the primary collection vessel. This has a corked piece of plastic tubing attached to it to serve as a drain when the vacuum is turned off. This drain is optional but is convenient when there is a bench drain in close proximity to the suction apparatus. If house vacuum is not available, one can use a quiet electrically driven vacuum pump placed in an out-of-the-way place and allowed to run continuously.

B. Microscopes

In order to check fertilization rates, cell cycle stages, divisions, etc., an upright bright field microscope dedicated for use with "wet" (i.e., unsealed) preparations is useful. Our experience has shown that, as a shared instrument in heavy use, such microscopes often become dirty and encrusted with sea salt crystals. If not used carefully and maintained regularly, such microscopes can degrade to the point of being useless. As a consequence, we recommend the use of older microscopes of little value. In regard to the expensive research-grade microscopes of

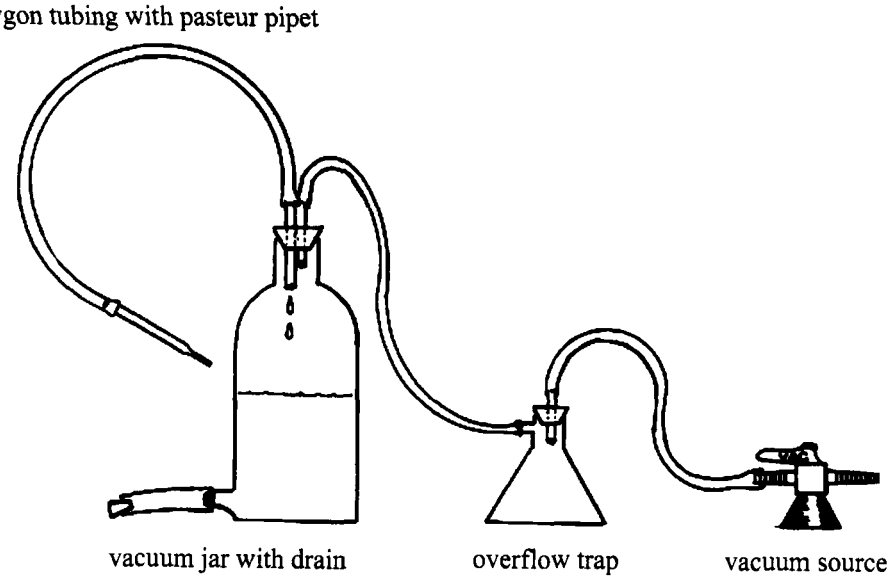

Fig. 6 Diagram of suction apparatus used to aspirate seawater from test tubes containing zygotes.

the laboratory, we emphasize the importance of being fastidious in keeping seawater off of them. In the presence of seawater an electrolytic couple is established between the steel, aluminum, and the brass components of the microscope, resulting in catastrophic corrosion. This is especially relevant to inverted microscopes on which seawater can run down into the nosepiece.

C. Preparations for Short-Term Observations

When we want to determine the status of a culture of zygotes at a point in time with no intent of following them, we use a simple wedge chamber. We use standard 1 × 3-in. slides and 22-mm square coverslips straight from the "box," without cleaning. With a slide ready on the work surface, we gently "scoop" a tiny amount of Vaseline onto two corners of the coverslip using the corners of the coverslip to pick up the Vaseline. We then put a drop of egg suspension on the slide and place the coverslip over the drop of water. Normally the volume of water is determined by eye and after some experience this can be easily delivered with a Pasteur pipette. One wants a preparation in which the water just fills the space between the glass surfaces without excess that could run over onto the microscope.

The great value of these chambers is that the zygotes range along the wedge from free floating (completely unflattened) to homogenized at the thin end. By choosing a position along the wedge, one can find zygotes flattened to the extent desired. We emphasize that these preparations are not suitable for following the development of zygotes.

D. Cleaning of Slides and Coverslips

For long-term observations of living zygotes, we never use slides and coverslips straight from the box. There are enough variables to deal with in an experiment without having to worry about what effect dirty glass surfaces may have in reducing zygote viability. We describe the methods we use for coverslips with the understanding that the same procedures apply for slides. Although this procedure may sound time consuming, it is the sort of chore that needs be done infrequently and can be done in parallel with other laboratory jobs.

1. Prepare a clean 1-liter beaker with warm distilled water to which a small amount of detergent has been added (we use "Liquinox for Critical Cleaning" purchased from VWR Scientific, Inc.). We add just enough detergent to make a few suds when the water is agitated.
2. Introduce coverslips one at a time or in small groups so that all glass surfaces contact the detergent solution.
3. Sonicate the beaker in a bath sonicator for approximately 5 min. Often we will gently rearrange the pile of coverslips with a blunt plastic probe.

4. Decant the detergent solution and wash 5–10 times with copious amounts of house-distilled water, rearranging the coverslips between washes to ensure that all glass surfaces contact the distilled water.

5. Add the best grade distilled water available and sonicate again for 5 min.

6. Rinse five times with this "best grade" distilled water, being certain to rearrange the coverslips during the washes.

7. Decant the water and store the coverslips in screw cap jars containing 95–100% reagent-grade ethanol.

8. When later removing slides and coverslips from ethanol-filled jars, be careful to handle the glassware only with forceps or clean gloved hands. Glassware covered with ethanol will extract oil and other contaminants from bare hands; the return of unused glassware to the jar will eventually lead to a buildup of contaminants in the alcohol that will leave a film on dried glass surfaces.

E. Preparations for Long-Term Observations

For long-term observations we use fluorocarbon preparations that provide not only for mild flattening of the zygotes but also for excellent viability over a period of 24 hr or more (Sluder *et al.*, 1989). The principle of this preparation is to sandwich the zygotes between the coverslip and a layer of fluorocarbon oil that is heavier than seawater. Importantly, the oils recommended here have high gas solubilities (see product manual for 3M Fluorinert liquids; 3M Specialty Chemicals Division, St. Paul, MN). We normally use these preparations with zygotes that have fertilization envelopes because the envelopes restrict the extent of flattening. When used with zygotes that are stripped of fertilization envelopes, care must be exercised to not overflatten the cells, which for unknown reasons limits their viability. The extent of flattening is to some degree controllable by varying how much seawater is drained from around the zygotes during the assembly of the preparations.

We make these preparations from 1 × 3-in. glass slides and 18 × 18- or 22 × 22-mm coverslips. Be sure to use only No. 1.5 coverslips because this is the thickness for which all objectives are designed. This applies not only to "dry" objectives but also to oil and water immersion optics. Both the slides and coverslips are taken from previously cleaned stocks stored in ethanol. First, on the slide we make a hollow square of Teflon tape that is just slightly smaller than the coverslip to be used. We use "Temp-R-Tape" pressure-sensitive Teflon film tape No. TV350, 1-in. wide (purchased from CHR Industries, 407 East Street, New Haven, CT 06509). Probably any tape will suffice if it is over 100 μm thick. We lay the tape across one or more cleaned slides and cut out hollow squares with the tip of a curved or pointed scalpel. The sharp-curved forceps are used to pull off excess tape. Generally, we make several slides at once and store them in covered petri dishes.

To make this preparation (Fig. 7), smooth the cut edges of the tape with the back of the curved forceps and apply three or four drops of fluorocarbon oil to the center of the hollow tape square. The oil should not contact the tape and the number of drops should be sufficient to fully fill the chamber when the coverslip is applied but not result in excess oil. Coverslips are prepared individually at the time needed by first exposing them to the alcohol lamp flame to burn off the alcohol in which they are stored. Then, we quickly flame both sides of the coverslip to provide a hydrophilic surface. If the coverslip cracks upon cooling, it has been flamed too long. Important: Be certain to let the coverslip cool completely before applying the egg suspension. Then apply one or more drops of the zygote suspension to the coverslip sufficient to cover the central portion of the glass. Typically we take zygotes from the top of a loose pellet in the bottom of a conical centrifuge tube. If the zygotes are too concentrated the preparation will not be satisfactory. Next, blot off excess water by applying the edge of the coverslip to absorbent paper and immediately place the coverslip over the drop of oil. It is important to do this quickly to avoid dehydration of the zygotes. The tips of the blunt-curved forceps can be used to gently translate the coverslip to center it over the tape square. Excess oil can be aspirated carefully with the Pasteur pipette on the suction hose. Finally, seal the preparation with molten VALAP using the tip of the tapered reagent spatula heated over the alcohol lamp. Be careful to use the lowest temperatures needed to melt the VALAP and apply only the minimum necessary. Too much or too hot VALAP will heat the preparation. Also, large aggregates of this waxy substance will get caught on objective lenses; VALAP is hard to clean off lens surfaces.

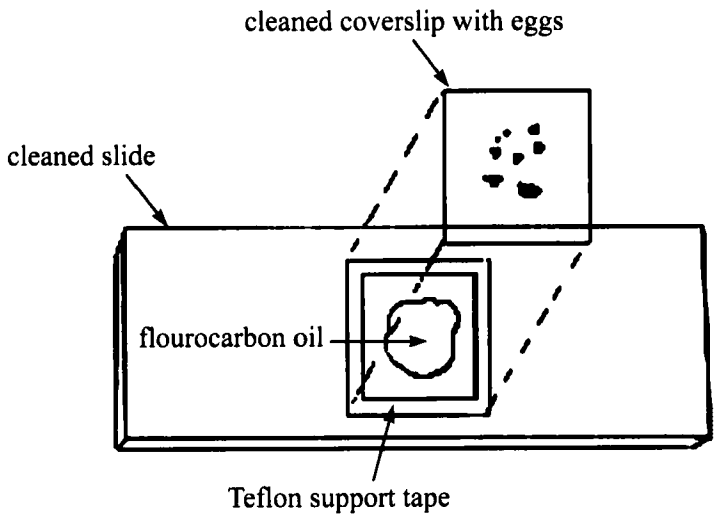

Fig. 7 Diagram of fluorocarbon preparation as it would appear just before the coverslip is dropped onto the oil. Later, the preparation is sealed with a thin bead of melted VALAP.

Some of the zygotes will appear as singles or as small islands of zygotes flattened against the coverslip. Other zygotes will be present in pools of water that span between the coverslip and slide. It is important to follow only those zygotes that are sandwiched between the oil and glass; zygotes in the pools of water will not develop and are unreliable for even short-term observations. With practice one can easily distinguish between these populations with the naked eye; the pools of water have sharp refractile edges that the flattened zygote islands do not. When following zygotes we normally observe those around the margins of the islands and we avoid islands that are adjacent to a pool of water or an air bubble. Over several hours the air bubbles may move and displace the zygotes one is following; water pools have an irritating habit of incorporating just the zygotes one is interested in. Also, it is worthwhile to draw a map of the cells one is following because over time loosely packed zygotes will sometimes rearrange into a denser configuration.

We normally use these preparations on upright microscopes; we have also had good luck using them on inverted microscopes with no tendency for the zygotes to "float" away from the coverslip. When using these preparations on an inverted microscope it is of obvious importance to put spacers on each end of the slide to keep the coverslip and VALAP from dragging on the stage.

Perfluorocarbon liquids (fluorocarbon oils) are fully fluorinated fluids that are nonflammable, nontoxic, and essentially nonreactive chemically. We use Fluorinert Brand Electronic Liquids made by the Minnesota Mining and Manufacturing Corporation (3M Specialty Chemicals Division). Currently, we work with a vintage stock of 3M Medifluor oil (FC-47), which, unfortunately, is no longer available. However, two of the Flourinert liquids currently produced by 3M Corp., FC-40 and FC-43, have the same physical properties as FC-47 and work well for applications involving living zygotes.

F. Adhering Zygotes to Slides or Coverslips

For some procedures, such as micromanipulation or microinjection, it may be necessary to adhere zygotes to the glass surface to keep them from rolling about when engaged by the microtool. The cationic agents described later work well for unfertilized eggs and zygotes from which the fertilization envelopes have been removed; zygotes with fertilization envelopes are only weakly held by these agents to glass surfaces.

The best known agent for this application is high-molecular-weight poly-L-lysine (Mazia *et al.,* 1975). Although this polycation strongly adheres eggs or demembranated zygotes to glass, we have found that the zygotes are not healthy when followed for more than a short time. As a consequence we have abandoned its use in favor of protamine sulfate as used in the manner described later. However, we do not exclude the possible efficacy of poly-L-lysine for short-term applications, such as holding zygotes during fixation and extraction for immunofluorescence (Hinchcliffe and Linck, 1998).

1. We use Herring grade III protamine sulfate (Sigma) because this grade is relatively inexpensive and zygotes remain viable when it is used judiciously.

2. We make a 0.5–3% (w/v) solution of protamine sulfate in distilled water fresh each day; we have found that the use of old protamine solutions leads to reduced viability of the zygotes. The concentration of protamine sulfate is adjusted to the minimum that will support the application.

3. Take a cleaned and flamed coverslip and apply a drop of the protamine solution to just the area in which one wants zygotes to adhere. If the water drop does not wet the area and form a "bead," the coverslip has not been adequately flamed. After one or more minutes rinse the area with sea water using a Pasteur pipette. Then apply a drop of diluted zygotes to the treated area and let them settle (<1 min). Drain the seawater by applying the edge of the coverslip to an absorbent surface and immediately apply the coverslip to the chamber one is using. It is important to complete these last steps quickly to avoid dehydration of the zygotes. When working in a low-humidity environment or in making preparations that expose zygotes for more than a moment, we have sought to minimize dehydration in the following way. Just before making the preparations we put the zygotes in seawater made approximately 5% hypotonic with distilled water. This degree of hypotonicity does not appear to influence zygote development and we assume that the slight degree of dehydration inherent in making preparations under these conditions will return the cells to near normal conditions.

G. Micromanipulation Preparations

To micromanipulate sea urchin zygotes we use chambers that combine several of the methods just described. Our applications include the experimental movement of nuclei, the cutting of mitotic spindles, detachment of meiotic spindles from the egg cortex, and the amputation of specific regions of cytoplasm. Basically, we use an open-faced fluorocarbon preparation that is capped with mineral oil. The microtool is brought in just slightly below horizontal to engage the zygotes. Since the particulars of the experiments and the microtools needed will vary, we will describe only the construction of the chamber.

These preparations are built upon an aluminum or stainless-steel support slide diagrammed in Fig. 8. Note that this particular configuration is for upright microscopes, which we favor. For use on inverted microscopes, the surface facing the objective must have thin standoffs or shoulders to keep the coverslip from dragging on the stage. Several layers of tape work well or 0.5- to 1-mm shoulders can be incorporated into the design of the chamber.

Also note that the lower coverslip is slightly above the level of the stage. For some upright microscopes the condenser cannot be brought above the level of the stage and Kohler illumination cannot be achieved. Should this be the case, the support slide can be redesigned to bring the lower coverslip closer to the

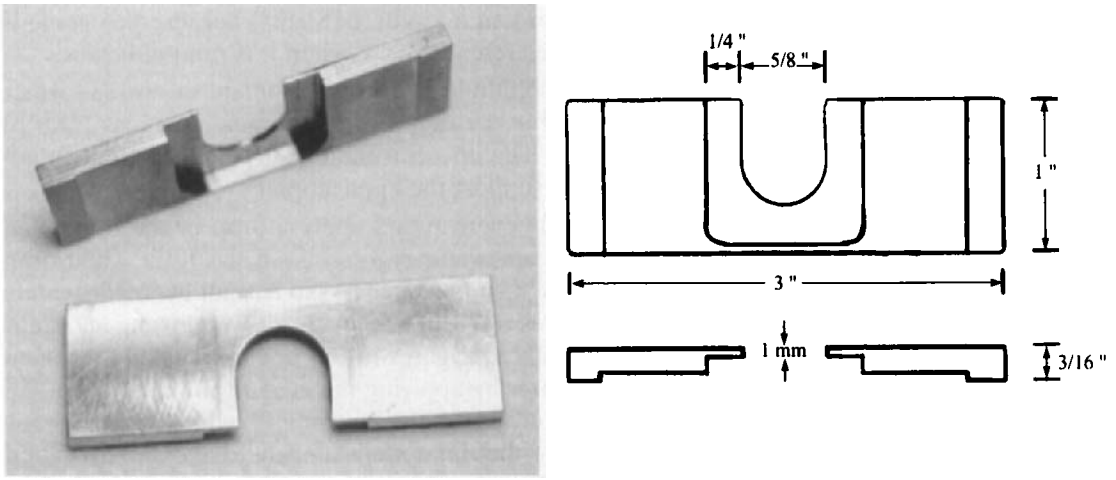

Fig. 8 Photograph and diagram of metal support slide used to hold microinjection and micromanipulation preparation. The support slide shown here is configured for use on an upright microscope. For use on an inverted microscope, the standoffs or shoulders at the ends of the slide would be built onto the "top." These support slides can be made from aluminum or stainless steel.

stage. Since we know of no commercial supplier of these support slides, we have them made by our institutional machine shop.

The chamber is constructed of two cleaned and freshly flamed 22 × 22-mm coverslips that cover the top and the bottom of the oval window in the support slide (Fig. 9). We first scribe a wax pencil line across one side of each coverslip approximately 2 or 3 mm from the edge. To ensure uniformity we line up several

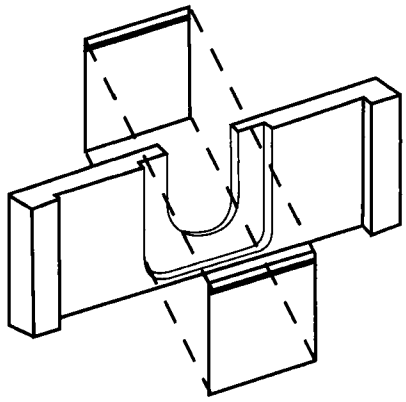

Fig. 9 Exploded view of coverslip placement on the metal support slide. The coverslips are adhered by thin beads of silicone grease applied to both sides of the support slide. The dark lines on the coverslips represent wax pencil lines which face the interior of the preparation.

coverslips and lay the small metal ruler across them to guide the sharpened wax pencil. In the completed chamber these wax pencil lines will both be facing the inside of the chamber at the exposed or "open" side and serve to keep the seawater around the zygotes from creeping up under the mineral oil cap. Importantly, the wax line on the coverslip closest to the objective lens serves as a reference to indicate when the microscope is focused in the inner surface of the cell-bearing coverslip.

Next we use a small spatula to put a thin bead of silicone grease on the upper and lower surfaces of the support slide to adhere and seal the coverslips to the metal. The lower coverslip is adhered to the support slide with the wax pencil line on the exposed edge and on the inside of the future chamber.

The zygotes, with fertilization envelopes removed, are then applied to a small portion of the coverslip adjacent to the wax pencil line and the excess seawater is removed with the suction apparatus. The zygotes should be on the same coverslip surface as the wax pencil line. As quickly as possible the upper coverslip should be placed on the support slide and gently pressed down against the bead of silicone grease with curved blunt forceps.

Next, we fill the chamber to the wax pencil lines with fluorocarbon oil using a 1-ml syringe fitted with a fine-gauge needle (Fig. 10a). Then we cap the preparation with mineral oil using another 1-ml syringe. Drops of mineral oil are first applied to both margins and then the center is filled in (Fig. 10b). This keeps the mineral oil from displacing the fluorocarbon oil resulting in a filled but incompletely capped preparation. All operations from the spreading of the zygotes on the coverslip to the filling of the chamber with fluorocarbon oil must be completed quickly to minimize dehydration of the zygotes. To this end, we

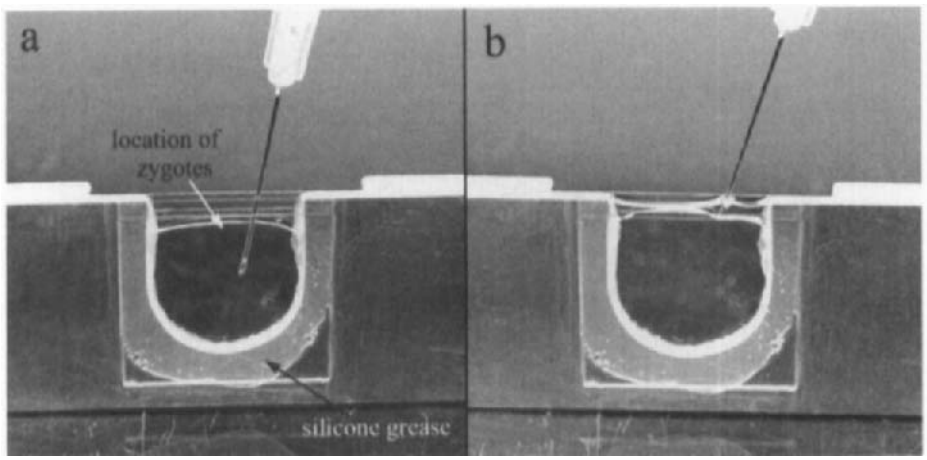

Fig. 10 (a) Filling the preparation with seawater or fluorocarbon oil using a 1-ml syringe. (b) Capping the preparation with mineral oil. Drops of oil are placed at the two corners and then the center is filled in. This preparation would be used for micromanipulation.

have all materials prepared ahead of time and often have the zygotes in seawater made 5% hypotonic. If possible, one can make these preparations in an environment with high humidity.

For micromanipulations the necessary anchorage of the zygotes is provided by the flattening action of the fluorocarbon oil. If this anchorage proves to be insufficient we treat the upper coverslip with protamine sulfate at the minimal concentration that provides adequate adherence of the zygotes. We do not seek to "weld" the zygotes to the coverslip but rather adapt the movements of the microtool to minimize the movement and rolling of the cells during the micromanipulation. To minimize sticking of the microtool to the hyaline layer on the outside of the zygotes we siliconize the tips of the glass tools.

The micromanipulation preparations, when filled with fluorocarbon oil, present the investigator with zygotes that are somewhat flattened, which can be an advantage for some applications. However, if one does not desire to have the cells flattened the chamber can be filled with seawater and capped with mineral oil. In such cases it is important to adhere the zygotes to the coverslip with protamine sulfate.

H. Microinjection Preparations

A complete description of microinjection methods for sea urchin zygotes is provided by Kiehart (1982). Here we describe the variations we have made to his chamber design. Basically this is a micromanipulation preparation with a modified top coverslip that provides mechanical anchorage of the zygotes (Fig. 11). First, we prepare the support slide with silicone grease and affix a bottom

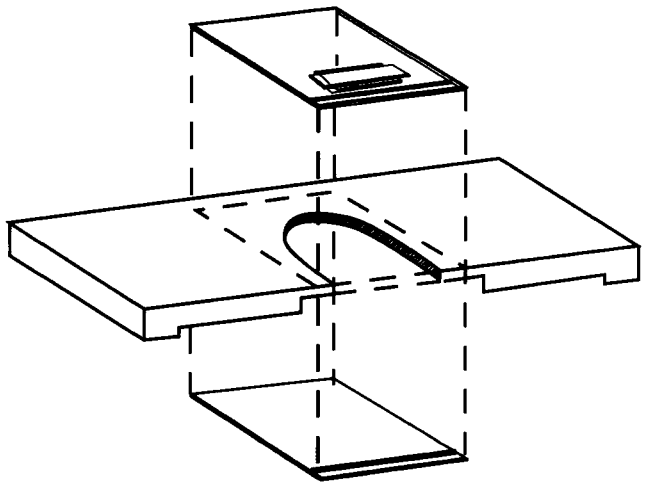

Fig. 11 Exploded view of a microinjection preparation. The holding chamber for the zygote is diagrammed just inside the wax pencil line on the top coverslip.

coverslip that has a wax pencil line close to the exposed margin. To prepare the zygote holding chamber on the top coverslip (sequence of steps shown in Fig. 12), we start with a cleaned and flamed coverslip on which a wax pencil line has been scribed. Then 2 or 3 mm inside the wax pencil line and on center we adhere a 4 × 12-mm piece of Scotch brand "Double Stick Tape" (3M Corp.). These small rectangles of tape are prepared by lightly adhering a piece of double-stick tape to a slide and then cutting it with a scalpel. The pieces are then transferred to the coverslips with curved sharp-tipped forceps. It is important to firmly adhere the entire rectangle of tape to the coverslip using the curved shoulder of the forceps. Then we adhere firmly to the tape a 6 × 10-mm piece of glass coverslip so that one of the longer sides extends into the space between the tape and the wax line. The top coverslip with zygote holding chamber is then adhered to the support slide with silicone grease.

The zygotes, with fertilization envelopes removed, are then introduced into the zygote holding chamber using an adjustable pipettor with a yellow tip that has been cut back to provide a larger opening. The zygotes are applied to one end and capillary action is normally sufficient to draw them across. The preparation is then immediately filled with seawater to the wax pencil lines and capped with mineral oil. As with the micromanipulation preparations, we apply drops of oil to both margins before filling in the center. The completed preparation is diagrammed in cross section in Fig. 13. The Double Stick Tape is approximately 85 μm thick and thus slightly flattens the 100-μm-diameter zygotes. Normally this flattening provides sufficient anchorage of the zygotes for insertion of the micropipette. If the anchorage proves to be poor, the micropipette will push the zygote back against the Double Stick Tape, at which point it can no longer avoid microinjection. These preparations allow zygote development until at least the ciliated blastula stage, when the embryos hatch from the fertilization envelopes and swim away.

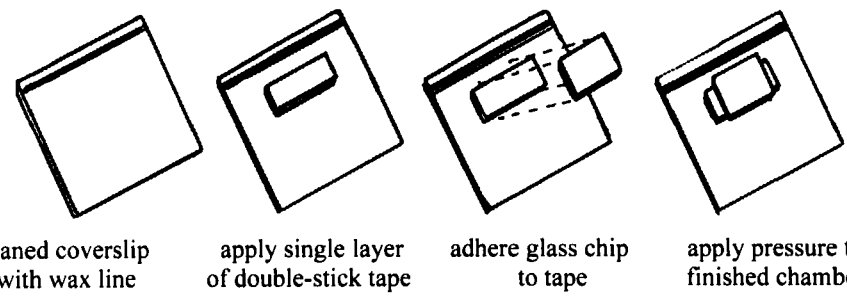

Fig. 12 Sequence of steps used to make a zygote holding chamber on the top coverslip. Note that the small rectangle of coverslip should be firmly adhered to the double-stick tape and its forward edge does not extend as far as the wax pencil line.

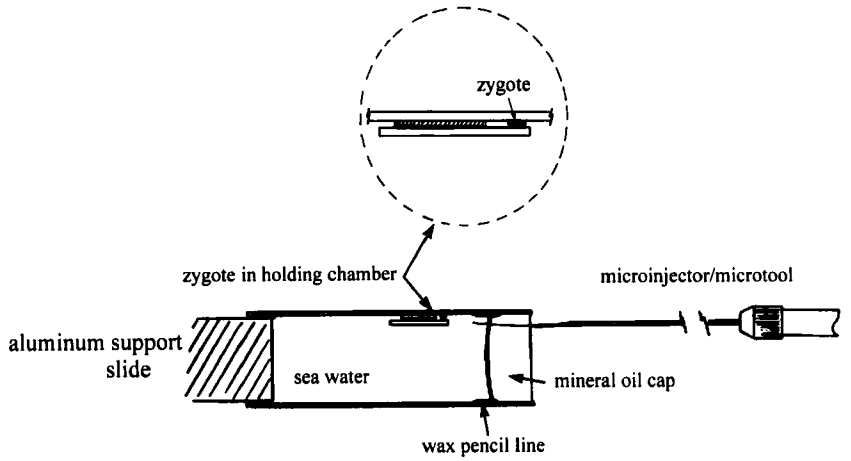

Fig. 13 Diagram showing a cross section of a microinjection preparation.

I. Micropipettes

Since the preparation and use of micropipettes for sea urchin zygote injections is well described by Kiehart (1982), we will add only a few items drawn from our experience.

1. Micropipettes are made from 50–ul Drummond (Drummond Scientific, Broomall, PA) "Microcaps" pulled on a Kopf Model 700C vertical pipette puller (David Kopf Instruments). We use relatively high filament heat to produce a long taper. Often the axis of the drawn portion is at a very slight angle to the axis of the unmodified pipette. We use this to our advantage by orienting the pipette in the tool holder so that the pipette tip curves upward so as to engage the zygotes slightly from below (for an upright microscope). This minimizes surface tension effects at the water–oil interface that push the pipette onto the upper coverslip and impede easy movement.

2. In attaching luer lock fittings to the ends of the small-bore polyethylene tubing, which connects the 2-ml syringe to the Leica tool holder, we insert 3- or 4-mm pieces of fine-gauge syringe needle into the tubing before assembling the units. This prevents distortion of the tubing at the tip of the flare fitting that sometimes blocks the lumen.

3. Kiehart (1982) describes the use of a short segment of oil-capped capillary tubing to hold the test solution for front-end loading the micropipette. Using such a loading chamber on a fixed-stage microscope requires a focus change for the microscope, a z axis change for the micropipette, and repositioning the preparation every time one needs to load the pipette. In addition, the cylindrical surfaces of the capillary tube compromise the image of the micropipette tip.

We have found it easier to use a loading chamber mounted to another metal support slide (Fig. 14). We start with two cleaned coverslips that have a wax pencil line scribed along one side. One of them has an approximately 4 × 12-mm rectangle of multiple layer double-stick tape adhered approximately 3 or 4 mm inside the wax pencil line. Typically we use two layers of tape cut with a scalpel from a multilayer strip of tape on a glass slide. The second coverslip is cut into 8 × 6-mm rectangles, with the wax line running across one of the smaller ends. One such rectangle is adhered to the double-stick tape so that the wax lines superimpose and face each other (Fig. 14). This assembly is then adhered to the top surface of a metal support slide using silicone grease. The test solution is introduced into the back of the chamber and the space between the wax lines and the front edges of the coverslips is filled with mineral oil. The sides of the loading chamber can be sealed with silicone grease if evaporation of the test solution is a concern. The volume of test solution held in the loading chamber can be controlled by varying the size of the chip of coverslip and the number of layers of double-stick tape.

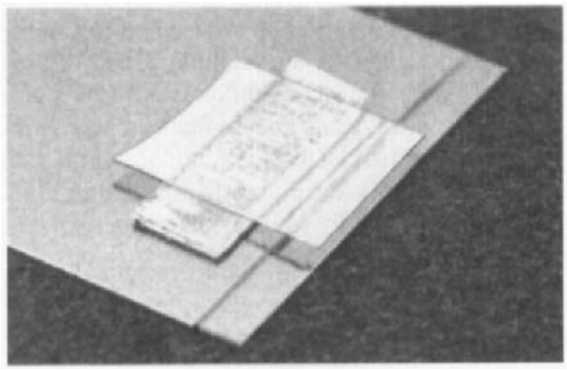

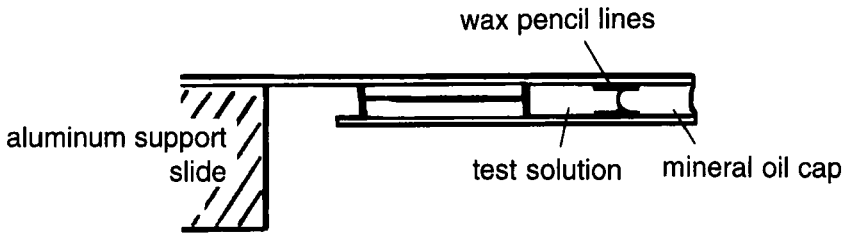

Fig. 14 Photograph and diagram of a chamber used to load the test solution into micropipettes. The loading chamber shown in the photograph would be inverted when placed on the metal support slide, as is indicated in the diagram. Note the use of two layers of double-stick tape, the presence of wax pencil lines on both the top coverslip and the glass rectangle, and the placement of the glass rectangle so that its front edge is even with that of the coverslip. The mineral oil serves both as a seal for the preparation and as a source of oil to cap the micropipette. A bottom coverslip on the metal support slide is not necessary.

This loading chamber is then put on the microscope and the pipette is front loaded as described by Kiehart (1982) using the mineral oil at the front of the preparation as a source of oil to cap the loads in the micropipette. The loaded micropipette is then pulled out of the field of view with the micromanipulator and the loading preparation replaced with the zygote preparation. The zygotes are brought into the field using the mechanical stage and then the micropipette is brought into the field with the micromanipulator. The advantage of using this sort of loading chamber on a fixed-stage microscope is that the image of the needle/test solution is substantially better; one does not need to substantially refocus the microscope or significantly reposition the micropipette along the z axis if the metal support slides have been uniformly machined.

VII. Other Methods

A. Buffers That Mimic the Intracellular Conditions of Sea Urchin Zygotes

We routinely use the buffers described here in test solutions for microinjections and to extract zygotes to better visualize microtubule distributions with the polarization or differential interference microscopes. These buffers, designed to mimic the intracellular conditions of echinoderm eggs, better preserve cell viability than conventional buffers such as phosphate-buffered saline or TRIS. We specifically recommend *against* the use of PIPES-based buffers for live echinoderm cell work. Although zygotes may tolerate small injected doses of this buffer, they are frequently not healthy; higher doses kill zygotes.

The first buffer, developed by Daniel Mazia, has the following formulation:

300 m*M* K *d*-gluconic acid (K gluconate)
300 m*M* glycine
10 m*M* NaCl
2 m*M* $MgSO_4$
2–5 m*M* EGTA
pH 7.2–7.5 (adjusted with KOH or HCl)

For microinjections we usually omit the EGTA because the zygotes do not seem to be bothered by the residual calcium in the buffer.

The second buffer, developed by Frank Suprynowicz (Suprynowicz *et al.*, 1994), has the following formulation:

250 m*M* *d*-gluconic acid, K-salt (K gluconate)
250 m*M* *N*-methyl-D-glucamine
50 m*M* HEPES
10 m*M* EGTA
6.7 m*M* MgCl
pH 7.2 (adjusted with glacial acetic acid)
(This solution has 40 n*M* free Ca^{2+})

B. Enhanced Visualization of Cytoskeletal Details

Some zygotes are relatively clear and thus well suited for *in vivo* light microscopy (especially *Lytechinus* sea urchins and *Pisaster* and *Asterias* starfish). However, the presence of densely packed yolk granules can make sparse microtubule arrays or male pronuclear morphology shortly after fertilization difficult to visualize with the polarization or differential interference contrast microscopes. As a consequence we sometimes extract the zygotes to clear the yolk granules (Sluder *et al.*, 1990). The procedure outlined below works well for zygotes that have fertilization envelopes which serve to contain the fragile cell remnants. "Demembranated" zygotes can also be used if care is exercised to minimize agitation and mechanical shear that will fragment the cell remnants (unless this is desired).

First, the zygotes are pelleted and resuspended gently once or twice in one of the buffers described previously (with EGTA). The washes should be done quickly to minimize the time the live zygotes are out of seawater. Then the zygotes are resuspended in buffer containing detergent; we normally use 1% Triton X-100 although its concentration is not critical. Once in the detergent-containing buffer we gently agitate with a Pasteur pipette without bubbling air. Lastly, a drop of the extracted zygotes is placed on a slide and covered with a coverslip and observed. There is no need to use spacers because the flattening provided by the coverslip enhances the visualization of the desired detail. By varying the volume of the drop relative to the size of the coverslip used, one can control the extent of flattening. When doing a timed series of extractions we observe the zygotes soon after extraction and do not seek to store them for later observation.

For experiments in which we want to count or photograph asters in zygotes at a stage of the cell cycle during which astral birefringence is normally low, we sometimes augment microtubule assembly by treating the zygotes for a few minutes in seawater containing 3% hexylene glycol (2-methyl-2,4-pentanediol; J. T. Baker Chemical Co., Phillipsburg, NJ) (Hinchcliffe *et al.*, 1998). We either immediately observe the zygotes *in vivo* or extract them as described previously. When working with hexylene glycol it is important to bear in mind that this agent arrests development and eventually will diminish cell viability. Thus, it is not to be used for long-term observations. Also, since hexylene glycol at concentrations above 5% can cause the assembly of supernumerary asters (Endo *et al.*, 1990), we are always careful to limit its concentration and duration of exposure before observations are made. When we extract such zygotes, hexylene glycol is added to the washes and the extraction buffer.

C. Fragmentation of Zygotes

For studies of microtubule-organizing center activity around female pronuclei we developed a simple method to fragment zygotes soon after fertilization (Sluder *et al.*, 1989). The advantage of this method is that one can produce viable nucleated and enucleated fragments whose cell cycle has been activated in a normal

way (i.e., fertilization). Also, the distribution of cytoplasmic constituents is normal, unlike eggs fragmented by centrifugation (Harvey, 1956).

First, we strip off the fertilization envelopes as previously described. Then we pass the zygotes twice through a nylon screen (Fig. 2) with a mesh size of 35–70 μm, sometimes applying modest pressure by mouth on the open end of the tube holding the screening. Although further fragmentation may be achieved by additional passes through the fine mesh screen, the incidence of egg lysis increases.

The resultant culture has a mixture of cell fragment types (e.g., some with no nuclei, some with just the male pronucleus, some with just the female pronucleus, and some with both pronuclei). It is simple to differentiate between fragments containing just a male pronucleus from those with just a female pronucleus based on the noticeably smaller size of the male pronucleus. At mitosis, the "paternal" fragments assemble a functional haploid bipolar spindle, whereas the "maternal" fragments assemble a monaster, seen as a radial array of microtubules with a more diffuse focus than an aster of paternal origin. If it is of importance to differentiate between fragments containing just a female pronucleus and those containing both pronuclei, observations on individual cells should begin as soon as possible. Fragments containing both pronuclei will undergo syngamy within 30 min of fertilization and then appear mononucleated. This experimental system is well suited for cytology when one is prepared to follow individual cells starting soon after fragmentation. The applicability of this system to biochemical studies is questionable since we have not found a way to separate and purify the different classes of fragments.

VIII. Annotated List of References

The following partial bibliography is offered as a resource to those searching for techniques not described in this chapter. Since there are undoubtedly important references that we have missed, we apologize for any omission.

1. Classic texts

Chambers, R., and Chambers, E. L. (1961). "Explorations into the Nature of the Living Cell." Harvard Univ. Press, Cambridge, MA.

Czihak, G. (1975). "The Sea Urchin Embryo: Biochemistry and Morphogenesis." Springer-Verlag, Berlin.

Giudice, G. (1973). "Developmental Biology of the Sea Urchin Embryo." Academic Press, New York.

Giudice, G. (1986). "The Sea Urchin Embryo: A Developmental Biological System." Springer-Verlag, Berlin.

Harvey, E. B. (1956). "The American Arbacia and Other Sea Urchins." Princeton Univ. Press, Princeton, NJ.

Schroeder, T. E. (ed.). (1986). Echinoderm gametes and embryos. *In* "Methods in Cell Biology, Volume 27." Academic Press, San Diego.

Terman, S. A., Berg, W. E., and Infante, A. A. (1973). "The Sea Urchin III: Molecular Biology." MSS Information, New York.

Wilson, E. B. (1896). "The Cell in Development and Inheritance." Columbia Univ. Press, New York.

Wilson, E. B. (1928). "The Cell in Development and Heredity," Vol. 3. MacMillian, New York.

2. Use of colcemid for the reversible Control of Microtubule Assembly during mitosis

Aronson, J., and Inoué, S. (1970). Reversal by light of the action of N-methyl N-desacetyl colchicine on mitosis. *J. Cell Biol.* **45,** 470–477.

Sluder, G. (1976). Experimental manipulation of the amount of tubulin available for assembly into the spindle of dividing sea urchin eggs. *J. Cell Biol.* **70,** 75–85.

Sluder, G. (1990). The practical use of colchicine and colcemid to reversibly block microtubule assembly in living cells. *In* "Advanced Techniques in Chromosome Research" (K. Adolph, ed.), pp. 427–447. Dekker, New York.

Sluder, G., Miller, F. J., and Spanjian, K. (1986). The role of spindle microtubules in the timing of the cell cycle in echinoderm eggs. *J. Exp. Zool.* **238,** 325–336.

3. Enucleation of zygotes

Lorch, I. J. (1952). Enucleation of sea urchin blastomeres with or without removal of asters. *Q. J. Microsc. Sci.* **93,** 475–486.

Sluder, G., Miller, F. J., and Rieder, C. L. (1986). The reproduction of centrosomes: Nuclear vs. cytoplasmic control. *J. Cell Biol.* **103,** 1873–1881.

Sluder, G., Miller, F. J., and Rieder, C. L. (1989). Reproductive capacity of sea urchin centrosomes without centrioles. *Cell Motil. Cytoskel.* **13,** 264–273.

Sluder, G., Miller, F. J., and Lewis, K. (1993). Centrosome inheritance in starfish zygotes II: Selective suppression of the maternal centrosome during meiosis. *Dev. Biol.* **155,** 58–67.

4. Isolation of nuclei

Fansler, B., and Loeb, L. A. (1972). Sea urchin nuclear DNA polymerase. IV. Reversible association of DNA polymerase with nuclei during the cell cycle. *Exp. Cell Res.* **75,** 433–441.

Goran, P., and Ljiljana, S. (1980). The isolation and characterisation of the nuclear matrix from sea urchin embryos. *Cell Biol. Int. Rep.* **4,** 701–709.

Marzluff, W. F. (1990). Preparation of active nuclei. *Methods Enzymol.* **181,** 30–36.

Poccia, D. L., and Green, G. R. (1986). Nuclei and chromosomal proteins. *Methods Cell Biol.* **27,** 153–174.

Thaler, M. M., Cox, M. C., and Villee, C. A., Jr. (1969). Isolation of nuclei from sea urchin eggs and embryos. *J. Cell Biol.* **42,** 846–850.

5. Visualization of chromosome dynamics in living zygotes

Sluder, G., Miller, F. J., Thompson, E. A., and Wolf, D. E. (1994). Feedback control of the metaphase–anaphase transition in sea urchin zygotes: Role of maloriented chromosomes. *J. Cell Biol.* **126,** 189–198.

6. Isolation and *in vitro* assembly of cytoskeletal elements

Bryan, J., and Sato, H. (1970). The isolation of the meiosis I spindles from the mature oocyte of *Pisaster ochraceus*. *Exp. Cell Res.* **59,** 371–378.

Dessev, G. N., Iovcheva-Dessev, C. and Goldman, R. D. (1990). Lamin dimers. Presence in the nuclear lamina of surf clam oocytes and release during nuclear envelope breakdown. *J. Biol. Chem.* **265,** 12636–12641.

Forer, A., and Zimmerman, A. M. (1975). Isolation of sea urchin mitotic apparatus using glycerol-dimethyl sulfoxide. *Ann. N. Y. Acad. Sci.* **253,** 378–382.

Gibbons, B. H., and Gibbons, I. R. (1972). Flagellar movement and adenosine triphosphate activity in sea urchin sperm extracted with Triton X-100. *J. Cell Biol.* **54,** 75–97.

Harris, P. and Shaw, G. (1984). Intermediate filaments, microtubules and microfilaments in epidermis of sea urchin tube foot. *Cell Tissue Res.* **236,** 27–33.

Hinchcliffe, E. H., and Linck, R. W. (1998). Two proteins isolated from sea urchin sperm flagella: Structural components common to the stable microtubules of axonemes and centrioles. *J. Cell Sci.* **111,** 585–595.

Hisanaga, S., and Sakai, H. (1986). Purification of cytoplasmic dynein from sea urchin eggs. *Methods Enzymol.* **134,** 337–351.

Holy, J., Wessel, G., Berg, L., Gregg, R. G., and Schatten, G. (1995). Molecular characterization and expression patterns of a B-type nuclear lamin during sea urchin embryogenesis. *Dev. Biol.* **168,** 464–478.

Kane, R. E. (1986). Components of the actin-based cytoskeleton. *Methods Cell Biol.* **27,** 229–242.

Keller, T. C. D., and Rebhun, L. I. (1982). Strongylocentrotus purpuratus spindle tubulin. I. Characteristics of its polymerization and depolymerization *in vitro*. *J. Cell Biol.* **93,** 788–796.

Kuriyama, R. (1976). *In vitro* polymerization of flagellar and ciliary outer fiber tubulin into microtubules. *J. Biochem. (Tokyo)* **80,** 153–165.

Kuriyama, R., and Borisy, G. G. (1983). Cytasters induced within unfertilized sea urchin eggs. *J. Cell Sci.* **61,** 175–189.

Kuriyama, R., and Kanatani, H. (1981). The centriolar complex isolated from starfish spermatozoa. *J. Cell Sci.* **49,** 33–49.

Leslie, R. J., and Wilson, L. (1989). Preparation and characterization of mitotic cytoskeletons from embryos of the sea urchin *Stronglyocentrotus francisanus*. *Anal. Biochem.* **181,** 51–58.

Linck, R. W., and Langevin, G. L. (1981). Reassembly of flagellar B ($\alpha\beta$) tubulin into singlet microtubules: Consequences for cytoplasmic microtubule structure and assembly. *J. Cell Biol.* **89,** 323–337.

Mabuchi, I. (1973). A myosin-like protein in the cortical layer of the sea urchin egg. *J. Cell Biol.* **59,** 542–547.

Pirner, M. A., and Linck, R. W. (1995). Methods for the isolation of tektins and sarkosyl-insoluble protofilament ribbons. *Methods Cell Biol.* **47,** 373–380.

Pratt, M. M. (1986). Purification of cytoplasmic dynein from Strongylocentrotus sea urchin eggs. *Methods Enzymol.* **134,** 325–373.

Salmon, E. D. (1982). Mitotic spindles isolated from sea urchin eggs with EGTA lysis buffers. *Methods Cell Biol.* **25** (Part B), 69–105.

Spudich, A., and Spudich, J. A. (1979). Actin in Triton-treated cortical preparations of unfertilized and fertilized sea urchin eggs. *J. Cell Biol.* **82,** 212–226.

Stephens, R. E. (1970). Isolation of nexin—The linkage protein responsible for maintenance of the nine-fold configuration of flagellar axonemes. *Biol. Bull.* **139,** 438.

Stephens, R. E. (1970). Thermal fractionation of outer doublet microtubules into A and B-subfiber components: α and β-tubulin. *J. Mol. Biol.* **47,** 353–363.

Stephens, R. E. (1986). Isolation of embryonic cilia and sperm flagella. *Methods Cell Biol.* **27,** 217–227.

Suprenant, K. A., and Marsh, J. C. (1987). Temperature and pH govern the assembly of microtubules from unfertilized sea urchin egg extracts. *J. Cell. Sci.* **87,** 71–84.

Suprenant, K. A., Tempero, L. B., and Hammer, L. E. (1989). Association of ribosomes with *in vitro* assembled microtubules. *Cell. Motil. Cytoskel.* **14,** 401–415.

Terasaki, A. G., Ohnuma, M., and Mabuchi, I. (1997). Identification of actin-binding proteins from sea urchin eggs by F-actin affinity column chromatography. *J. Biochem. (Tokyo)* **122,** 226–236.

Thompson-Coffe, C., Coffe, G., Schatten, H., Mazia, D., and Schatten, G. (1996). Cold-treated centrosome: Isolation of centrosomes from mitotic sea urchin eggs, production of an anticentrosomal antibody, and novel ultrastructural imaging. *Cell Motil. Cytoskel.* **33,** 197–207.

Tilney, L. G., and Jaffe, L. A. (1980). Actin, microvilli, and the fertilization cone of sea urchin eggs. *J. Cell Biol.* **87,** 771–782.

Vacquier, V. D. (1986). Handling, labeling, and fractionating sea urchin spermatozoa. *Methods Cell Biol.* **27,** 15–40.

Vallee, R. B. (1982). A taxol-dependent procedure for the isolation of microtubules and microtubule-associated proteins (MAPs). *J. Cell Biol.* **92,** 435–442.

Walker, G. R., Kane, R., and Burgess, D. R. (1994). Isolation and characterization of a sea urchin zygote cortex that supports *in vitro* contraction and reactivation of furrowing. *J. Cell. Sci.* **107,** 2239–2248.

Wright, B. D., Henson, J. H., Wedaman, K. P. Willy, P. J., Morand, J. N., and Scholey, J. M. (1991). Subcellular localization and sequence of sea urchin kinesin heavy chain: Evidence for its association with membranes in the mitotic apparatus and interphase cytoplasm. *J. Cell Biol.* **113,** 817–833.

7. Molecular biology of development

Akasaka, K., Frudakis, T. N., Killian, C. E., George, N. C., Yamasu, K., Khaner, O., and Wilt, F. H. (1994). Genomic organization of a gene encoding the spicule matrix protein SM30 in the sea urchin Strongylocentrotus purpuratus. *J. Biol. Chem.* **269,** 20592–20598.

Hardin, P. E., and Klein, W. H. (1987). Unusual sequence conservation in the 5' and 3' untranslated regions of the sea urchin spec mRNAs. *J. Mol. Evol.* **25,** 126–133.

Hardin, S. H., Keast, M. J., Hardin, P. E., and Klein, W. H. (1987). Use of consensus oligonucleotides for detecting and isolating nucleic acids encoding calcium binding domains of the troponin C superfamily. *Biochemistry* **26,** 3518–3523.

Killian, C. E., and Wilt, F. H. (1989). The accumulation and translation of a spicule matrix protein mRNA during sea urchin embryo development. *Dev. Biol.* **133,** 148–156.

Kuhn, O., and Wilt, F. H. (1981). Chromatin proteins of sea urchin embryos: Dual origin from an oogenetic reservoir and new synthesis. *Dev. Biol.* **85,** 416–424.

Livingston, B. T., and Wilt, F. H. (1990). Determination of cell fate in sea urchin embryos. *Bioessays* **12,** 115–119.

Livingston, B. T., and Wilt, F. H. (1990). Range and stability of cell fate determination in isolated sea urchin blastomeres. *Development* **108,** 403–410.

Loeb, L. A. (1969). Purification and properties of deoxyribonucleic acid polymerase from nuclei of sea urchin embryos. *J. Biol. Chem.* **244,** 1672–1681.

Mao, C. A., Wikramanayake, A. H., Gan L., Chuang, C. K., Summers, R. G., and Klein W. H. (1996). Altering cell fates in sea urchin embryos by overexpressing SpOtx, an orthodenticle-related protein. *Development* **122,** 1489–1498.

Maxson, R. E., Jr., and Wilt, F. H. (1981). The rate of synthesis of histone mRNA during the development of sea urchin embryos (*Strongylocentrotus purpuratus*). *Dev. Biol.* **83,** 380–386.

Nash, M. A., Kozak, S. E., Angerer, L. M., Angerer, R. C., Schatten, H., Schatten, G., and Marzluff, W. F. (1987). Sea urchin maternal and embryonic U1 RNAs are spatially segregated in early embryos. *J. Cell. Biol.* **104,** 1133–1142.

Nemer, M. (1986). An altered series of ectodermal gene expressions accompanying the reversible suspension of differentiation in the zinc-animalized sea urchin embryo. *Dev. Biol.* **114,** 214–224.

Norrander, J. M., Linck, R. W., and Stephens, R. E. (1995). Transcriptional control of tektin A mRNA correlates with cilia development and length determination during sea urchin embryogenesis. *Development* **121,** 1615–1623.

Venuti, J. M., Gan, L., Kozlowski, M. T., and Klein, W. H. (1993). Developmental potential of muscle cell progenitors and the myogenic factor SUM-1 in the sea urchin embryo. *Mech Dev.* **41,** 3–14.

Wang, W., Wikramanayake, A. H., Gonzalez-Rimbau, M., Vlahou, A., Flytzanis, C. N., and Klein, W. H. (1996). Very early and transient vegetal-plate expression of SpKrox1, a Kruppel/Krox gene from Strongiyocentrotus purpuratus. *Mech. Dev.* **60,** 185–195.

Wells, D. E., Showman, R. M., Klein, W. H., and Raffy, R. A. (1981). Delayed recruitment of maternal histone H3 mRNA in sea urchin embryos. *Nature* **292,** 477–478.

Wikramanayake, A. H., and Klein, W. H. (1997). Multiple signaling events specify ectoderm and pattern the oral–aboral axis in the sea urchin embryo. *Development* **124,** 13–20.

Wikramanayake, A. H., Brandhorst, B. P., and Klein, W. H. (1995). Autonomous and non-autonomous differentiation of ectoderm in different sea urchin species. *Development* **121,** 1497–1505.

Wilt, F. H. (1987). Determination and morphogenesis in the sea urchin embryo. *Development* **100,** 559–576.

8. Electron microscopy

Amos, W. B., Amos, L. A., and Linck, R. W. (1986). Studies of tektin filaments from flagellar microtubules by immunoelectron microscopy. *J. Cell Sci. Suppl.* **5,** 55–68.

Gibbons, I. R., and Grimstone, A. V. (1960). On flagellar structure of certain flagellates. *J. Biophys. Biochem. Cytol.* **7,** 697–716.

Harris, P. (1962). Some structural and functional aspects of the mitotic apparatus in sea urchin embryos. *J. Cell Biol.* **14,** 475–487.

Mazia, D., Schatten, G., and Sale, W. S. (1975). Adhesion of cells to surfaces coated with polylysine: Applications to electron microscopy. *J. Cell Biol.* **66,** 198–200.

Mazia, D., Paweletz, N., Sluder, G., and Finze, E. M. (1981). Cooperation of kinetochores and pole in the establishment of monopolar mitotic apparatus. *Proc. Natl. Acad. Sci. USA* **78,** 377–381.

Rieder, C. L., Bowser, S., Nowogrodzki, R., Ross, K., and Sluder, G. (1983). Probing the ultrastructure of the mitotic and meiotic spindle in eggs: An expeditious approach based on semi-thin (0.25 μm) serial sections. *In* "Proceedings of the 41st Annual Meeting of the Electron Microscopy Society of America" (G. W. Baily, ed). San Francisco Press, San Francisco.

Rieder, C. L., Miller, F. J., Davison, E., Bowser, S. S., Lewis, K., and Sluder, G. (1987). Quantitative ultrastructural reconstruction of small regions within large volumes by correlative light and high voltage electron microscopy of serial 0.25–0.50 μm sections. *In* "Proceedings of the 45th Annual Meeting of the Electron Microscopy Society of America" (G. W. Baily, ed). San Francisco Press, San Francisco.

Schatten, G., and Mazia D. (1976). The penetration of the spermatozoon through the sea urchin egg surface at fertilization. Observations from the outside on whole eggs and from the inside on isolated surfaces. *Exp. Cell Res.* **98,** 325–337.

Sluder, G., and Miller, F. J. (1993). Correlative light and electron microscopy: Counting centrioles in individual sea urchin zygotes previously followed *in vivo*. *In* "Proceedings of the 51st Annual Meeting of the Microscopy Society of America" (G. W. Baily and C. L. Rieder, eds.). San Francisco Press, San Francisco.

Sluder, G., and Rieder, C. (1985). Centriole number and the reproductive capacity of spindle poles. *J. Cell Biol.* **100,** 887–896.

9. Cytology and cytochemistry

Amos, W. B., Amos, L. A., and Linck, R. W. (1985). Proteins closely similar to flagellar tektins are detected in cilia but not in cytoplasmic microtubules. *Cell Motil.* **5,** 239–249.

Boyle, J. A., and Ernst, S. G. (1989). Sea urchin oocytes possess elaborate cortical arrays of microfilaments, microtubules, and intermediate filaments. *Dev. Biol.* **134,** 72–84.

Burke, R. D., and Gibson, A. W. (1986). Cytological techniques for the study of larval echinoids with notes on methods for inducing metamorphosis. *Methods Cell Biol.* **27,** 295–308.

Collas, P., Pinto-Correia, C., and Poccia, D. L. (1995). Lamin dynamics during sea urchin male pronuclear formation *in vitro*. *Exp. Cell Res.* **219,** 687–698.

Fishkind, D. J., Bonder, E. M., and Begg, D. A. (1990). Subcellular localization of sea urchin egg spectrin: Evidence for assembly of the membrane-skeleton on unique classes of vesicles in eggs and embryos. *Dev. Biol.* **142,** 439–452.

Foltz, K. R., and Lennarz, W. J. (1992). Identification of the sea urchin egg receptor for sperm using an antiserum raised against a fragment of its extracellular domain. *J. Cell Biol.* **116,** 647–658.

Harris, P., Osborn, M., and Weber, K. (1980). Distribution of tubulin-containing structures in the egg of the sea urchin *Stronglyocentrotus purpuratus* from fertilization through first cleavage. *J. Cell Biol.* **84,** 668–679.

Harris, P. J. (1986). Cytology and immunocytochemistry. *Methods Cell Biol.* **27,** 243–262.

Henson, J. H., and Begg, D. A. (1988). Filamentous actin organization in the unfertilized sea urchin egg cortex. *Dev. Biol.* **127,** 338–348.

Horwitz, B., Kupper, H., Eshhar, Z. and Geiger, B. (1981). Reorganization of arrays of prekeratin filaments during mitosis. *Exp. Cell Res.* **134,** 281–290.

Kubo, H., and Hoshi, M. (1990). Immunocytochemical study of the distribution of a ganglioside in sea urchin eggs. *J. Biochem. (Tokyo)* **108,** 193–199.

Kuriyama, R., Levin, A., Nelson, D., Madl, J., Frankfurter, A., and Kimble, M. (1995). Monoclonal anti-dipeptide antibodies cross-react with detyrosinated and glutamylated forms of tubulins. *Cell Motil. Cytoskel.* **30,** 171–182.

Long, F. J. (1989). Incorporation and dispersal of sperm surface antigens in plasma membranes of inseminated sea urchin (*Arbacia punctulata*) eggs and oocytes. *Dev. Biol.* **131,** 37–43.

Oka, M. T., Arai, T., and Hamaguchi, Y. (1994). Different reactivity with monoclonal anti-tubulin antibodies between native and fixed mitotic microtubules in sea urchin eggs. *Cell Motil. Cytoskel.* **29,** 241–249.

Pehrson, J. R., and Cohen, L. H. (1985). Distribution of histone H1 alpha among cells of the sea urchin embryo. *Dev. Biol.* **111,** 530–533.

Simerly, C., and Schatten, G. (1993). Techniques for localization of specific molecules in oocytes and embryos. *Methods Enzymol.* **225,** 516–552.

Steffen, W., Fajer, E. A., and Linck, R. W. (1994). Centrosomal components immunologically related to tektins from ciliary and flagellar microtubules. *J. Cell Sci.* **107,** 2095–2105.

Terasaki, M. (1995). Visualization of exocytosis during sea urchin fertilization using confocal microscopy. *J. Cell Sci.* **108,** 2293–2300.

Terasaki, M., and Jaffe, L. A. (1993). Imaging endoplasmic reticulum in living sea urchin eggs. *Methods Cell Biol.* **38,** 211–220.

Vater, C. A., and Jackson, R. C. (1990). Immunolocalization of hyalin in sea urchin eggs and embryos using an antihyalin-specific monoclonal antibody. *Mol. Reprod. Dev.* **25,** 215–226.

Wang, Y.-L., and Taylor, D. L. (1979). Distribution of fluorescently labeled actin in living sea urchin eggs during early development. *J. Cell Biol.* **82,** 672–679.

Wessel, G. M., and McClay, D. R. (1986). Two embryonic, tissue-specific molecules identified by a double-label immunofluorescence technique for monoclonal antibodies. *J. Histochem. Cytochem.* **34,** 703–706.

Wright, B. D., and Scholey, J. M. (1993). Nonfluorescent immunolocalization of antigens in mitotic sea urchin blastomeres. *Methods Cell Biol.* **37,** 223–240.

10. Electrical and magnetic fields

Cameron, I. L., Hardman, W. E., Winters, W. D., Zimmerman, S., and Zimmerman, A. M. (1993). Environmental magnetic fields: Influences on early embryogenesis. *J. Cell Biochem.* **51,** 417–425.

Levin, M., and Ernst, S. G. (1995). Applied AC and DC magnetic fields cause alterations in the mitotic cycle of early sea urchin embryos. *Bioelectromagnetics* **16,** 231–240.

Zimmerman, S., Zimmerman, A. M., Winters, W. D., and Cameron, I. L. (1990). Influence of 60-Hz magnetic fields on sea urchin development. *Bioelectromagnetics* **11,** 37–45.

11. Cell–free extracts

Dessev, G., Palazzo, R., Rebhun, L., and Goldman, R. (1989). Disassembly of the nuclear envelope of spisula oocytes in a cell-free system. *Dev. Biol.* **131,** 496–504.

Gliksman, N. R., and Salmon, E. D. (1993). Microtubule-associated motility in cytoplasmic extracts of sea urchin eggs. *Cell Motil. Cytoskel.* **24,** 167–178.

Gliksman, N. R., Parsons, S. F., and Salmon, E. D. (1993). Cytoplasmic extracts from the eggs of sea urchins and clams for the study of microtubule-associated motility and bundling. *Methods Cell Biol.* **39,** 237–251.

Luca, F. C., and Ruderman, J. V. (1989). Control of programmed cyclin destruction in a cell-free system. *J. Cell Biol.* **109,** 1895–1909.

Palazzo, R. E., Lutz, D. A., and Rebhun, L. I. (1991). Reactivation of isolated mitotic apparatus: Metaphase versus anaphase spindles. *Cell Motil. Cytoskel.* **18,** 304–318.

Palazzo, R. E., Vaisberg, E., Cole, R. W., and Rieder, C. L. (1992). Centriole duplication in lysates of *Spisula solidissima* oocytes. *Science* **256,** 219–221.

Rebhun, L. I., and Palazzo, R. E. (1988). *In vitro* reactivation of anaphase B in isolated spindles of the sea urchin egg. *Cell Motil. Cytoskel.* **10,** 197–209.

Suprynowicz, F. A. (1993). Inactivation of cdc2 kinase during mitosis requires regulated and constitutive proteins in a cell-free system. *J. Cell Sci.* **104,** 873–818.

Suprynowicz, F. A., Prusmack, C., and Whalley, T. (1994). Ca2+ triggers premature inactivation of the cdc2 protein kinase in permeabilized sea urchin embryos. *Proc. Natl. Acad. Sci. USA* **91,** 6176–6180.

Winkler, M. M., and Steinhardt, R. A. (1981). Activation of protein synthesis in a sea urchin cell-free system. *Dev. Biol.* **84,** 432–439.

Xu, Z., and Hille, M. B. (1990). Cell-free translation systems prepared from starfish oocytes faithfully reflect *in vivo* activity: mRNA and initiation factors stimulate supernatants from immature oocytes. *Cell Regul.* **1,** 1057–1067.

Zhang, H., and Ruderman, J. V. (1993). Differential replication capacities of G_1 and S-phase extracts from sea urchin eggs. *J. Cell Sci.* **104,** 565–572.

12. Micromanipulation, microinjection, and microtechniques

Bennett, J., and Mazia, D. (1981). Fusion of fertilized and unfertilized sea urchin eggs. Maintenance of cell surface integrity. *Exp. Cell Res.* **134,** 494–498.

Colin, A. M. (1985). Rapid repetitive microinjection. *Methods Cell Biol.* **27,** 395–406.

Hiramoto, Y. (1971). Analysis of cleavage stimulus by means of micromanipulation of sea urchin eggs. *Exp. Cell Res.* **68,** 291–298.

Hiramoto, Y., and Nakano, Y. (1988). Micromanipulation studies of the mitotic apparatus in sand dollar eggs. *Cell Motil. Cytoskel.* **10,** 172–184.

Hiramoto, Y., and Yoneda, M. (1986). Determination of mechanical properties of the egg by the sessile drop method. *Methods Cell Biol.* **27,** 443–456.

Kiehart, D. P. (1982). Microinjection of echinoderm eggs: Apparatus and procedures. *Methods Cell Biol.* **25,** 13–31.

Kubota, L. F., and Carroll, E. J., Jr. (1988). Refertilization in eggs of the sea urchin Stronglyocentrotus purpuratus. *Gamete Res.* **21,** 29–40.

Mazia, D., and Ruby, A. (1967). A chamber for the prolonged observation of cells under compression. *Exp. Cell Res.* **45,** 505–506.

Mazia, D., Harris, P., and Bibring, T. (1960). The multiplicity of the mitotic centers and the time-course of their duplication and separation. *Biophys. Biochem. Cytol.* **7,** 1–20.

McCulloh, D. H., and Chambers, E. L. (1992). Fusion of membranes during fertilization: Increases of the sea urchin egg's membrane capacitance and membrane conductance at the site of contact with the sperm. *J. Gen. Physiol.* **99,** 137–175.

Mohri, T., and Hamaguchi, Y. (1991). Propagation of transient Ca^{2+} increase in sea urchin eggs upon fertilization and its regulation by microinjecting EGTA solution. *Cell Struct. Funct.* **16,** 157–165.

Ransick, A., and Davidson, E. H. (1993). A complete second gut induced by transplanted micromeres in the sea urchin embryo. *Science* **259,** 1134–1138.

Rappaport, R. (1967). Cell division: Direct measurement of maximum tension exerted by furrow of echinoderm eggs. *Science* **156,** 1241–1243.

Rappaport, R. (1977). Tensiometric studies of cytokinesis in cleaving sand dollar eggs. *J. Exp. Zool.* **201,** 375–378.

Rappaport, R. (1986). Simple methods and devices for handling echinoderm eggs. *Methods Cell Biol.* **27,** 345–358.

Rappaport, R., and Rappaport, B. N. (1984). Division of constricted and urethane-treated sand dollar eggs: A test of the polar stimulation hypothesis. *J. Exp. Zool.* **231,** 81–92.

Sluder, G., Miller, F. J., and Lewis, K. (1993). Centrosome inheritance in starfish zygotes II: Selective suppression of the maternal centrosome during meiosis. *Dev. Biol.* **155,** 58–67.

Sluder, G., Miller, F. J., and Rieder, C. L. (1989). Reproductive capacity of sea urchin centrosomes without centrioles. *Cell Motil. Cytoskel.* **13,** 264–273.

Vacquier, V. D., and Mazia, D. (1968). Twinning of sea urchin embryos by treatment with dithiothreitol. Roles of cell surface interactions and of the hyaline layer. *Exp. Cell Res.* **52,** 459–468.

Wadsworth, P., and Sloboda, R. D. (1983). Microinjection of fluorescent tubulin into dividing sea urchin cells. *J. Cell Biol.* **97,** 1249–1254.

Yoneda, M. (1986). The compression method for determining the surface force. *Methods Cell Biol.* **27,** 421–434.

Acknowledgments

The authors thank Ms. Susan Decker and Mr. George Kelly for continuously supplying us with the most excellent echinoderms and Mr. Dan Krueger (3M Specialty Chemicals Division, St. Paul, MN) for generously providing us with perfluorocarbon liquids and the relevant literature detailing their use. We also acknowledge those researchers who supplied us with lists of their methods publications for inclusion in the annotated bibliography. I (G. S.) acknowledge those who have

introduced me to the sea urchin zygote as an experimental system and have shaped the way in which I use it. Dr. Hidemi Sato first taught me how to handle and use these zygotes while I was a graduate student in his laboratory; his skill, patience, and ability to communicate his enthusiasm for the practice of cell biology are a model for laboratory instruction. Dr. Daniel Mazia, my mentor for my years as a postdoctoral fellow, furthered my education in the use of echinoderm zygotes in many important ways. He also had a contagious enthusiasm for this experimental system and, beyond that, a rare ability to step away from established procedures to establish novel, imaginative approaches to the study of these zygotes. The influence of these mentors on my development has been so fundamental that it is not possible for me to know where their instruction has left off and my own contributions have begun. I thank them for providing me with not only a core library of techniques but, more important, the ability to think independently about how to manipulate the system to develop new approaches. I am pleased to dedicate this chapter to them.

References

Endo, S., Toriyama, M., Ohta, K., and Sakai, H. (1990). Formation of miniasters in the cytoplasm of hexyleneglycol-treated sea urchin eggs. *Cell Motil. Cytoskel.* **15,** 23–33.

Fuseler, J. W. (1973). Repetitive procurement of mature gametes from individual sea stars and sea urchins. *J. Cell Biol.* **57,** 879–881.

Hinchcliffe, E. H., and Linck, R. W. (1998). Two proteins isolated from sea urchin sperm flagella: Structural components common to the stable microtubules of axonemes and centrioles. *J. Cell Sci.* **111,** 585–595.

Hinchcliffe, E. H., Cassels, G. O., Rieder, C. L., and Sluder, G. (1998). The coordination of centrosome reproduction with nuclear events during the cell cycle in the sea urchin zygote. *J. Cell Biol.* **140,** 1417–1426.

Kiehart, D. P. (1982). Microinjection of echinoderm eggs: Apparatus and procedures. *Methods Cell Biol.* **25,** 13–31.

Mazia, D., Schatten, G., and Sale, W. (1975). Adhesion of cells to surfaces coated with polylysine. Applications to electron microscopy. *J. Cell Biol.* **66**(1), 198–200.

Sluder, G., and Begg, D. (1983). Control mechanisms of the cell cycle: Role of the spatial arrangement of spindle components in the timing of mitotic events. *J. Cell Biol.* **97,** 877–886.

Sluder, G., Miller, F. J., and Rieder, C. L. (1989). Reproductive capacity of sea urchin centrosomes without centrioles. *Cell Motil. Cytoskel.* **13,** 264–273.

Sluder, G., Miller, F. J., Cole, R., and Rieder, C. L. (1990). Protein synthesis and the cell cycle: Centrosome reproduction in sea urchin eggs is not under translational control. *J. Cell Biol.* **110,** 2025–2032.

Suprynowicz, F. A., Prusmack, C., and Whalley, T. (1994). Ca^{+2} triggers premature inactivation of the cdc2 protein kinase in permeabilized sea urchin embryos. *Proc. Natl. Acad. Sci. USA* **91,** 6176–6180.

INDEX

This Page Intentionally Left Blank